

THE PLASTIC BEHAVIOUR OF COMPOSITE
FLOOR SYSTEMS IN RELATION TO
MULTI - STOREY STRUCTURES

RAJIH IBRAHIM MAJED

A THESIS SUBMITTED FOR THE DEGREE OF
DOCTOR OF PHILOSOPHY

DEPARTMENT OF CIVIL ENGINEERING
UNIVERSITY OF ASTON IN BIRMINGHAM

23.NOV.72 156504

THESIS
624.042
MAJ

JULY 1972

SYNOPSIS

The work described in this thesis is concerned with the ultimate load behaviour of beam and slab floor systems, using steel beams and reinforced concrete slabs. Three main areas of study have been attempted within this general heading.

Firstly, upper-bound plastic solutions were developed for floor systems, involving either non-composite design or composite design. These solutions were then used to design model beam and slab floor systems to fail by a pre-chosen mode. The agreement with experimental results confirmed the validity of the theoretical methods for both composite and non-composite design.

Subsequently, five different sets of assumption on degree of composite action were taken. These were shown theoretically to give very significant differences in structural and economic efficiency. An experimental program was then used to establish which of the five sets of theoretical assumptions on degree of composite action gave the best agreement with the results of the experiments.

Finally, a theoretical investigation was made of the advantage to be gained by including the composite floor system, rather than just the steel beams, when designing a multi-storey steel frame. The inclusion of the floor system was found to be particularly significant as the stiffness of the beam or floor system plays a significant part in the stability criteria for a multi-storey building.

A C K N O W L E D G E M E N T S

The Author wishes to express his particular gratitude to Professor M. Holmes, B.Sc., Ph.D., C.Eng., F.I.C.E., F.I.Struct.E., F.I.Mun.E., the Head of the Department of Civil Engineering of the University of Aston in Birmingham, for his generous help, encouragement and valuable advice throughout this research project. The Author has benefited immensely by the long hours of discussion he enjoyed with Professor Holmes.

The Author also wishes to thank Professor K.I. Majid, B.Sc., Ph.D., C.Eng., M.I.C.E., M.I.Struct.E., Professor of Civil Engineering of the University of Aston for his help and advice on computer matters; also to Mr. W. Parsons, the Chief Technician in the Civil Engineering Department at the University of Aston and to his assistants, particularly Mr. M.D. Rowberry, for their willing help and invaluable advice during the experimental work.

In the preparation of this thesis, the Author would like to thank Miss P. Sage for reproducing the drawings with such good care and to Miss C. Martin for her typing of the script.

Finally, the Author is indebted to the Ministry of Oil of the Republic of Iraq for their financial support during the course of this work.

C O N T E N T S

	<u>Page</u>
Synopsis	(i)
Acknowledgements	(ii)
Contents	(iii)
Notation	(viii)
CHAPTER 1. Introduction.	1
1.1 Aims of the present work.	1
1.2 Proposed design method.	3
1.3 Limitations of simple plastic design.	5
1.4 Basic assumptions.	7
CHAPTER 2. Historical review of related work.	8
2.1 Introduction.	8
2.2 Irrationality of elastic design methods.	10
2.3 Development of the simple plastic theory.	12
2.4 The instability problem.	15
2.5 Composite action.	19
2.6 Plastic collapse of slabs and continuous structures.	24
2.7 Use of computers.	27
CHAPTER 3. Introduction to upper-bound solutions.	29
3.1 Introduction.	29
3.2 Plastic theory.	29
3.3 Theorems of plastic collapse.	31
3.4 Upper and lower-bound solutions to non-composite and composite structures.	33
3.5 Introduction to upper-bound collapse solutions.	34
CHAPTER 4. Determination of collapse loads by upper-bound solutions of continuous beam and slab floor systems with non-composite action.	39
4.1 Introduction.	39
4.2 Beam and slab floor systems continuous in four directions.	40
4.2.1 Mode A.	41
4.2.2 Mode B.	42
4.2.3 Independent collapse of the slab	43
4.3 Beam and slab floor systems continuous in three directions.	44
4.3.1 Mode A.	45
4.3.2 Mode B.	45
4.3.3 Independent collapse of the slab	46
4.4 Beam and slab floor systems continuous in two directions.	47

	<u>Page</u>	
4.4.1	Mode A.	47
4.4.2	Mode B.	47
4.4.3	Independent collapse of the slab.	48
4.5	Beam and slab floor system for test M_1 .	48
4.5.1	Mode A.	49
4.5.2	Mode B.	49
4.5.3	Independent collapse of the slab.	50
4.6	Beam and slab floor system for test M_2 .	50
4.6.1	Mode A.	51
4.6.2	Mode B.	51
4.6.3	Independent collapse of the slab.	51
4.7	Comparison of collapse modes of the internal bay.	52
4.7.1	Comparison of modes A and C.	52
4.7.2	Comparison of modes A and D.	53
4.7.3	Comparison of modes B and C.	53
4.7.4	Comparison of modes B and D.	54
4.7.5	Comparison of modes A and B.	54
4.8	Change over from mode C to mode D.	55
4.9	Design procedure for the slab moment and beam sizes using charts.	57
4.10	Example.	57
CHAPTER 5.	Determination of collapse loads by upper-bound solutions for continuous beam and slab floor systems where composite action of type (2) or (3) is present.	59
5.1	Introduction.	59
5.2	Beam and slab floor systems continuous in four directions.	59
5.2.1	Type (2) - ignoring the effect of slab reinforcement.	60
5.2.2	Type (3) - including the effect of slab reinforcement.	63
5.2.3	Effective width of slab compression flange.	65
5.2.4	Determination of number of shear connectors required.	66
5.2.5	Basic modes of failure for internal bay.	68
5.3	Beam and slab floor systems continuous in three directions.	71
5.4	Beam and slab floor systems continuous in two directions.	71
5.5	Beam and slab floor system for test M_1 .	72
5.6	Beam and slab floor system for test M_2 .	73
5.7	Comparison of collapse modes of the internal bay.	73
5.8	Design procedure for the slab moment and beam sizes using charts.	75
5.9	Example.	76
CHAPTER 6.	Determination of collapse loads by upper-bound solutions for continuous beam and slab floor systems where composite action of type (4) or (5) is present.	79
6.1	Introduction.	79
6.2	Beam and slab floor systems continuous in four directions.	80
6.2.1	Effective width of hogging concrete flange at supports.	83

	<u>Page</u>	
6.2.2	Determination of number of shear connectors required.	84
6.2.3	Basic modes of failure for internal bay.	85
6.3	Beam and slab floor systems continuous in three directions.	87
6.4	Beam and slab floor systems continuous in two directions.	88
6.5	Beam and slab floor system for test M_1 .	89
6.6	Beam and slab floor system for test M_2 .	89
6.7	Comparison of collapse modes of the internal bay.	90
6.8	Design procedure for slab moment and beam sizes.	92
6.9	Example.	93
CHAPTER 7.	The design of beam and slab floor systems by computer and the comparison and evaluation of relative economy of the various design solutions.	96
7.1	Introduction.	96
7.2	Design procedure.	97
7.3	Arrangement of the data tape.	99
7.4	Explanation.	101
7.4.1	Section data.	101
7.4.2	Yield stresses and sizes of slab reinforcement data.	103
7.4.3	Frame data.	104
7.5	Typical output of the computer program.	106
7.6	Design examples.	110
7.7	Effect of variation of slab thickness on the weight of beam and slab floor systems.	113
7.8	Effect of variation of cube strength on the weight of beam and slab floor systems.	116
7.9	Deflection of non-composite and composite beam and slab floor systems.	118
7.10	Effect of the sides ratio (ρ) on the weight of beam and slab floor systems.	119
7.11	Effect of increasing the applied live load on the weight of beam and slab floor systems.	122
7.12	Comparison between the various assumptions on degree of composite action.	123
CHAPTER 8.	The significance of composite action between beams and floor slabs in the design of multi-storey building frames.	130
8.1	Introduction.	130
8.2	Plastic design of multi-storey buildings.	130
8.3	Simple plastic design.	132
8.3.1	Failure under vertical loading.	133
8.3.2	Failure under combined mechanism.	134
8.3.3	Selection of the critical equations.	135
8.4	Modifications to the simple plastic design procedure.	136
8.4.1	P δ effect (without joint rotation).	137
8.4.2	Other effects.	137
8.5	Introduction of composite action into the design of multi-storey frames.	139
8.6	Direct moment distribution.	142
8.7	Derivation of the magnification factors.	143

	<u>Page</u>	
8.7.1	Zone I.	144
8.7.2	Zone II.	144
8.7.2(a)	Zone II(i).	145
8.7.2(b)	Zone II(ii).	148
8.7.3	Zone III.	150
8.7.4	Summary of the magnification factors.	151
8.8	The effect of composite action on the stiffness of the beams.	152
8.8.1	Equivalent uniform beam.	154
8.8.1(a)	The far end pinned.	154
8.8.1(b)	The beam is fully elastic under the factored vertical load λ_2 .	155
8.9	The effect of the beam stiffness on the magnification factor.	156
CHAPTER 9. Description of experimental work.		160
9.1	Introduction.	160
9.2	Materials for models.	161
9.2.1	Cement.	161
9.2.2	Aggregates.	161
9.2.3	Concrete mixes.	161
9.2.4	Concrete control specimens.	161
9.2.5	Slab reinforcement.	162
9.2.6	Supporting beams.	162
9.3	Test M_1 .	163
9.3.1	Collapse load for type (1) assumption.	166
9.3.2	Collapse load for type (2) assumption.	166
9.3.3	Collapse load for type (3) assumption.	167
9.3.4	Collapse load for type (4) assumption.	167
9.3.5	Collapse load for type (5) assumption.	168
9.3.6	Total moment at the supports of model M_1 .	169
9.4	Test M_2 .	170
9.4.1	Collapse load for type (1) assumption.	170
9.4.2	Collapse load for type (2) assumption.	171
9.4.3	Collapse load for type (3) assumption.	171
9.4.4	Collapse load for type (4) assumption.	172
9.4.5	Collapse load for type (5) assumption.	172
9.5	Design of the shear connectors.	173
9.6	Construction of the models.	175
9.7	Setting up of the apparatus for tests M_1 and M_2 .	176
9.8	Experimental values of beam and slab strengths.	180
9.8.1	Test M_3 .	180
9.8.1(i)	Test C_1 .	180
9.8.1(ii)	Tests C_2 and C_3 .	181
9.8.2	Slab strips S_1 and S_2 .	182
9.9	Instrumentation.	183
9.9.1	Strain measurements.	183
9.9.1(i)	Supporting beams strains.	183
9.9.1(ii)	Reinforcement strains.	184
9.9.1(iii)	Concrete strains.	184
9.9.2	Deflection measurement.	185
9.9.3	Slip measurement.	185
9.9.4	Load measurement.	186
9.9.5	Moment measurement.	186
9.9.6	Gauge positions.	186

	<u>Page</u>
CHAPTER 10. The experimental behaviour of composite beam and slab floor systems.	188
10.1 Introduction.	188
10.2 Test M ₁ .	188
10.3 Test M ₂ .	194
10.4 Control tests.	200
10.4.1 Test C ₁ .	200
10.4.2 Tests C ₂ and C ₃ .	203
10.4.3 Slab strips S ₁ and S ₂ .	204
 CHAPTER 11. Comparison of experimental and theoretical results.	 206
11.1 Introduction.	206
11.2 Control tests.	206
11.3 Test M ₁ .	208
11.4 Test M ₂ .	209
 CHAPTER 12. Conclusions.	 215
12.1 Introduction.	215
12.2 Conclusions.	215
12.3 Suggestions for future research.	221
 APPENDIX 1	 224
APPENDIX 2	227
REFERENCES	
PLATES	

NOTATION

A	beam magnification factor;
A _c	column magnification factor;
A _f	area of top flange of steel beam = b _f × t _f ;
$\frac{A(mHh)av}{WL}$	wind load ratio;
A _s	area of steel I-section beam;
A _t	area of slab reinforcement per unit run;
A _{t1} , A _{t2}	area of slab reinforcement per unit run in longitudinal and transverse directions (i.e. X-direction and Y-direction) respectively;
a ₁₂ [∞]	real distribution factor in the elastic range for member 12, under horizontal load ∞ H;
a ₁₂ ^Δ	real distribution factor in the plastic range for member 12, under horizontal load (λ ₂ - ∞) H;
a	lever arm of a composite section = $\frac{d}{2} + t - \frac{d_n}{2}$;
a ₁ , a ₂	constants;
b	width of compression flange (slab) of a composite section;
b _f	breadth of top flange of steel beam;
C _E	required plastic moment for an external column;
C _I	required plastic moment for an internal column;
c	= (t - d ₁) for longitudinal reinforcement or = (t - d ₂) for transverse reinforcement; reduction factor for calculating the plastic modulus of an I-section in the presence of axial load;
d	overall depth of steel beam;
d _c	= $\frac{d + t}{2}$;
d _n	depth of plastic neutral axis below top of slab;
d' _n	depth of plastic neutral axis below top of slab of a composite beam at support;
d ₁ , d ₂	effective depth of slab in longitudinal and transverse directions (i.e. X-direction and Y-direction) respectively;
E	Young's Modulus of Elasticity for steel;
E _c	modulus of elasticity of concrete;

F_{cc}	compressive force in the concrete slab at ultimate load;
F_e	equivalent tensile force;
F_{rc}	compressive force in the slab reinforcement at ultimate load;
F_{rt}	tensile force in the slab reinforcement at ultimate load;
F_{sc}	compressive force in the steel beam at ultimate load;
F_{st}	tensile force in the steel beam at ultimate load;
$F.E.M._2$	total fixed end moment or initial sway moment at joint 2;
F_1	$= \frac{(19\beta + 13)}{(7\beta + 1)}$;
F_2	$= \frac{(5\beta + 11)}{(7\beta + 1)}$;
f_w	working stress of the steel I-section;
f_y	yield stress of the steel I-section;
H	horizontal wind shear force per bay acting in any storey at floor level;
ΣH	total shear force in any storey;
h	storey height;
$(mHh)_{av}$	average value of (mHh) for two consecutive storeys;
I_b	second moment of area of a beam section;
I_c	second moment of area of a column section; second moment of area of a composite section;
I_e	second moment of area of an equivalent uniform composite section;
I'	$= \frac{\beta I_b}{(\beta + 1)}$;
K_b	$\frac{E I_b}{L}$ for a beam;
K_b^e	flexural rigidity of an equivalent uniform composite beam $= \frac{E I_e}{L}$, for non-composite design $K_b^e = K_b$;
K_c	$\frac{E I_c}{h}$ for a column;
\bar{K}	ratio of the flexural rigidities of the two columns at a joint $= \frac{K_{c1}}{K_{c2}}$, where suffixes 1 and 2 refer to the columns above and below the joint, respectively;

K_2	ratio of the flexural rigidities of the lower column and the beam at a joint = $\frac{K_{c2}}{K_{b2}}$
L, l	dimensions of bay in X-direction and Y-direction respectively;
$L_x(1)$	beam spanning in X-direction bay No. 1;
$L_y(2)$	beam spanning in Y-direction bay No. 2;
M_b	fully plastic moment of the secondary beam (in Y-direction);
M_B	fully plastic moment of the main beam (in X-direction);
M_c	fully plastic composite moment of the slab and the secondary beam at mid-span;
M_c'	fully plastic composite moment of the effective width of the slab and the secondary beam at mid-span;
M_e	fully plastic composite moment of the slab and the main beam at mid-span;
M_n	fully plastic composite moment of the slab and the secondary beam at support;
M_N	fully plastic composite moment of the slab and the main beam at support;
M_s	fully plastic moment of the slab;
M_x	sum of fully plastic moments at mid-span and support of the main composite beam, in case of non-composite design (type (1) assumption) $M_x = M_B$;
M_y	sum of fully plastic moments at mid-span and support of the secondary composite beam, for type (1) assumption $M_y = M_b$;
M_{12}	bending moment at end 1 of member 12;
m	Merchant's ⁽³²⁾ magnification factor, allowing for the eccentricity of axial load in a member $= \frac{2s(1+c)}{2s(1+c) - \pi^2 \rho}$;
n	stability function ⁽⁵⁾ = $s \left[1 - \frac{m(1+c)}{2} \right]$;
o	stability function ⁽⁵⁾ = $s \left[-c + \frac{m(1+c)}{2} \right]$;
P	axial load in a member;
P_c	design value ⁽⁴⁰⁾ of one shear connector;
P_c'	80% ⁽⁴⁸⁾ of design value of one shear connector;
P_e	Euler load = $\frac{\pi^2 EI_c}{h^2}$

p	uniform loading per unit area;
P_1, P_2	ratios $\frac{(mHh)_{av}}{m_1H_1h_1}$ and $\frac{(mHh)_{av}}{m_2H_2h_2}$ respectively, where suffixes 1 and 2 refer to the storeys above and below the beam;
q	total number of storeys in a frame;
R_3	ratio of joint rotations at the ends of member 23 = $\frac{\theta_3}{\theta_2}$;
r	total number of bays in a frame;
S_{12}^r	real rotational stiffness at end 1 of member 12;
ES_2^r	sum of the real stiffnesses of all members meeting at joint 2;
t	slab thickness;
t_f	thickness of top flange of steel beam;
t_w	thickness of web of steel beam;
t_y	yield stress of slab reinforcement;
U	internal work done in a system;
U_c	assumed stress in the concrete at ultimate load = $\frac{4U_w}{9}$, for experimental work $U_c = \frac{2U_w}{3}$;
U_w	cube strength for concrete;
U.D.L.	uniformly distributed load;
V	external work done in a system; combined stability function for the two columns meeting at a joint = $(n_1 - o_1) \bar{K} + (n_2 - o_2)$;
W	total load on any beam;
W_B	total weight of the supporting beams of a floor system;
W_C	total weight of the concrete of a floor system;
W_F	total weight of the whole floor system;
W_R	total weight of the slab reinforcement of a floor system;
α	the load factor for wind loading at which the first plastic hinge forms in a beam; = $\frac{f_v}{U_c}$;
β	= $\frac{I_c}{I_b}$, where I_c is the second moment of area of a composite section;
δ	sway deflection of a single storey;

ρ	ratio of the sides of a slab = $\frac{l}{L}$;
ρ	Euler ratio, axial load : Euler load = $\frac{P}{P_e}$;
$\bar{\rho}$	relative Euler ratios = $\frac{\rho_1}{\rho_2}$;
ρ_1	= $\frac{A_{t1}}{12d_1}$;
θ	rotation of a plastic hinge;
λ_1	design load factor for vertical load alone;
λ_2	design load factor for combined loading;
γ_B	= $\frac{M_B}{M_s \cdot l/2}$
γ_b	= $\frac{M_b}{M_s \cdot l/2}$
γ_c	= $\frac{M_c + M_b}{M_s \cdot l/2}$
γ_e	= $\frac{M_e + M_B}{M_s \cdot l/2}$
γ_N	= $\frac{M_e + M_N}{M_s \cdot l/2}$
γ_n	= $\frac{M_e + M_n}{M_s \cdot l/2}$

C H A P T E R 1

INTRODUCTION

The impetus for the development of the multi-storey building frame came after the disastrous fire in Chicago in 1871, where the majority of the buildings were of wooden construction. During the rebuilding of Chicago, site values rose considerably, leading to a desire for taller and taller buildings. The traditional construction method of load bearing brickwork was exploited to its limit, leading to fourteen storey buildings with external walls up to nine feet thick. Eventually the gain in floor area arising from additional storeys was almost offset by the floor area lost in thickening the walls of the lower storeys. In addition, the weight of such buildings was beginning to pose serious foundation problems. These difficulties led to the investigation of methods of supporting tall building loads by using framed structures rather than load bearing masonry. By 1885 the first iron frame building was completed in Chicago, in which the frame carried all the loads and the walls were reduced to panel infilling between the frames. By the 1890's buildings of this type, by using steel rather than iron for the frames, were common in Chicago. Nowadays, multi-storey building frames are commonly used all over the world.

1.1 AIMS OF THE PRESENT WORK

During the last 100 years, therefore, there have been many ideas and methods of design suggested, discussed, modified, improved, and finally accepted or rejected. The main requisite is simplicity and rapidity of design of multi-storey buildings, as well as producing an economical and structurally efficient design.

The work presented in this thesis consists of the development of a method of structural design suitable for multi-storey buildings, originally proposed by Steel⁽¹⁾, where composite action is present in a continuous beam and slab floor system. The slab is connected to the I beam by mechanical shear connectors fastened to the I beam and embedded in the slab floor. The proposed plastic design method produces a more economical and structurally efficient design, as for simplicity and rapidity of design the use of design charts or the computer make the proposed method satisfy these criteria.

The prime aim of this work is to extend, corroborate and support the proposed design method by an experimental study of collapse loads and deflections of composite beam and slab floor systems, representing bays of multi-storey buildings with various boundary conditions. The load applied to the beam and slab floor systems is considered uniformly distributed and is represented by a system of interconnected hydraulic jacks.

Designs were prepared by the proposed plastic method for various assumptions on degree of composite action. These designs were compared with each other and with the plastic collapse approach with no composite action, from the point of view of weight saving and deflection. All these comparisons were made on a series of design examples of beam and slab floor systems of multi-storey buildings. In these examples, different cube strengths and slab thicknesses were used to investigate their effect on weight saving and deflection in composite and non-composite construction. A computer program was written to carry out the considerable amount of computation required for these comparative design studies.

1.2 PROPOSED DESIGN METHOD

For a continuous beam and slab floor system, using an upper-bound solution for predicting collapse load proved by Prager⁽²⁾, the proposed design method used here takes into consideration three basic modes of failure.

- (1) Secondary beam and slab failure (Mode A).
- (2) Main "edge" beam and slab failure (Mode B).
- (3) Slab alone failure (Mode C or D).

In deriving equations for the collapse loads of the three mechanisms given above, the kinematic or work equation was used making one or other of the assumptions given below regarding the degree of composite action:-

- (1) Type(1)- ignoring composite action altogether.
- (2) Considering composite action at the centres of main and secondary beams (i.e. regions of sagging bending moments) and ignoring composite action at the supports (i.e. regions of hogging bending moments).
In calculating the value of composite sagging moments the two following variations were also considered:-
 - (a) Type(2)- when calculating the plastic composite moments at the centres of main and secondary beams M_e and M_c , the effect of slab reinforcement is ignored.
 - (b) Type(3)- when calculating M_e and M_c , the effect of slab reinforcement is taken into consideration.
- (3) Considering composite action at the centre and the supports of main and secondary beams, (i.e. regions of both sagging and hogging bending), again this was divided into two possible variations:-

- (a) Type (4) - ignoring the effect of slab reinforcement when calculating M_e and M_c .
- (b) Type (5) - taking the effect of slab reinforcement into consideration when calculating M_e and M_c .

The various assumptions regarding the degree of composite action of the proposed design method were investigated by an experimental study of collapse load and deflection of composite beam and slab floor models for the different failure mechanisms. It proved possible to use a system of interconnected hydraulic jacks to represent uniformly distributed loading on the models.

A computer program was developed in Atlas Autocode for the Atlas Computer to design single and multi-bay beam and slab floor systems of multi-storey buildings. The computer program was so written that structural sections were chosen to give collapse loads by the three basic mechanisms which were identical. In this way, the most economical design was obtained. With regard to the above assumptions on the degree of composite action the validity of these was investigated in the experimental program, and their relevant significance in design economy was studied in the design examples carried out by computer.

For given data supplied to the computer such as the number of bays, whether or not the bays are of equal length, length of each bay, width of bay, live load, yield stresses of the beams and reinforcement, size of the reinforcing bars to be used in the slab and which of the assumptions regarding degree of composite action is to be adopted, the computer program automatically designed the main and secondary beams and printed out their sizes, together with

their composite and non-composite fully plastic moments. The ultimate slab moment M_s was also calculated, together with the amount of reinforcement per foot run required in each direction for each bay. Other useful information was also printed, such as the depth of plastic neutral axis at the centre and supports of the main and secondary beams, the total horizontal shear force between the concrete slab and the supporting beams, this helps in finding the number of shear connections required on each beam. Deflections of the designed main and secondary beams at working load were also printed for the alternative cases when each beam is considered fixed ended and simply supported, the true deflection, which will depend on column stiffness, lies between these two limits. The weights of the main beams, secondary beams, slab reinforcement, concrete and of the whole beam and slab floor system were also calculated. These various quantities were determined for different values of cube strength and slab thickness.

Comparison of theoretical, experimental and computer design results are made in a later chapter.

1.3 LIMITATIONS OF SIMPLE PLASTIC DESIGN

The simple plastic method cannot be safely applied to the design of tall multi-storey frames because of the limitations imposed by the assumptions on which the plastic theory is based. The plastic theory is based on several assumptions, but the following two are of particular importance here:-

- (a) the equilibrium equations can be based on the undeformed structure, i.e. deflections are small;

- (b) instability of an individual member or of the frame as a whole does not occur.

Both these assumptions are quite valid when dealing with comparatively small structures. However, for multi-storey frame-works, neither of them may be assumed to be true, particularly if the members of the frame carry large axial forces or if the frame itself is subjected to heavy applied wind loading.

Instability of the frame as a whole has been discussed by Wood⁽³⁾ who showed the stability of a frame deteriorates owing to the formation of plastic hinges as the load goes on increasing. It is, therefore, possible for a frame to become unstable, after the formation of a number of plastic hinges, before the complete plastic collapse mechanism is attained.

A plastic design method originally proposed by Gandhi⁽⁴⁾ takes due account of instability and sway deflection under wind load by introducing a correction factor to the simple plastic theory; this has been termed the "magnification factor". This factor is a function of the stability functions derived by Livesley and Chandlar⁽⁵⁾, Euler ratio (Axial load/Euler load) and relative stiffness of the selected members.

The design procedure of this method consists of two stages, in the first stage the beams and columns are designed and sections selected by simple plastic theory in a way similar to that suggested by Calladine⁽⁶⁾. In the second stage these selected sections are checked and increased if necessary to allow for instability and sway deflection effects by the introduction of the magnification factor to the simple plastic design equations.

Tabulated values of the magnification factor were given by Gandhi⁽⁴⁾ to be used for hand computation; later a computer program was developed by Clough⁽⁷⁾ to design frames of any number of storeys and bays automatically using the plastic design method proposed by Gandhi⁽⁴⁾.

The effect of composite action between slab floors and supporting beams on the plastic design method proposed by Gandhi⁽⁴⁾ will be discussed in Chapter 8.

1.4 BASIC ASSUMPTIONS

In the plastic design method presented in this thesis, the basic hypotheses of plastic behaviour of the steel beams and slab reinforcement are as follows:-

- (1) The idealised stress-strain curve for steel as shown in Figure 1 is assumed to apply.
- (2) Strain hardening effects are neglected.
- (3) There is no resulting axial force on the total composite beam section.
- (4) Effects due to spread of the plastic zone are neglected.
- (5) The steel material is homogeneous and isotropic in both elastic and plastic regions.
- (6) Plane transverse sections remain plane and normal to the longitudinal axis after bending, the effect of shear on the fully plastic moment of the section is neglected.

The general theory of the composite design of beam and slab floor systems is developed in Chapters 5 and 6. The following chapter consists of an historical review of associated work in the fields of plastic design and composite actions of structures.

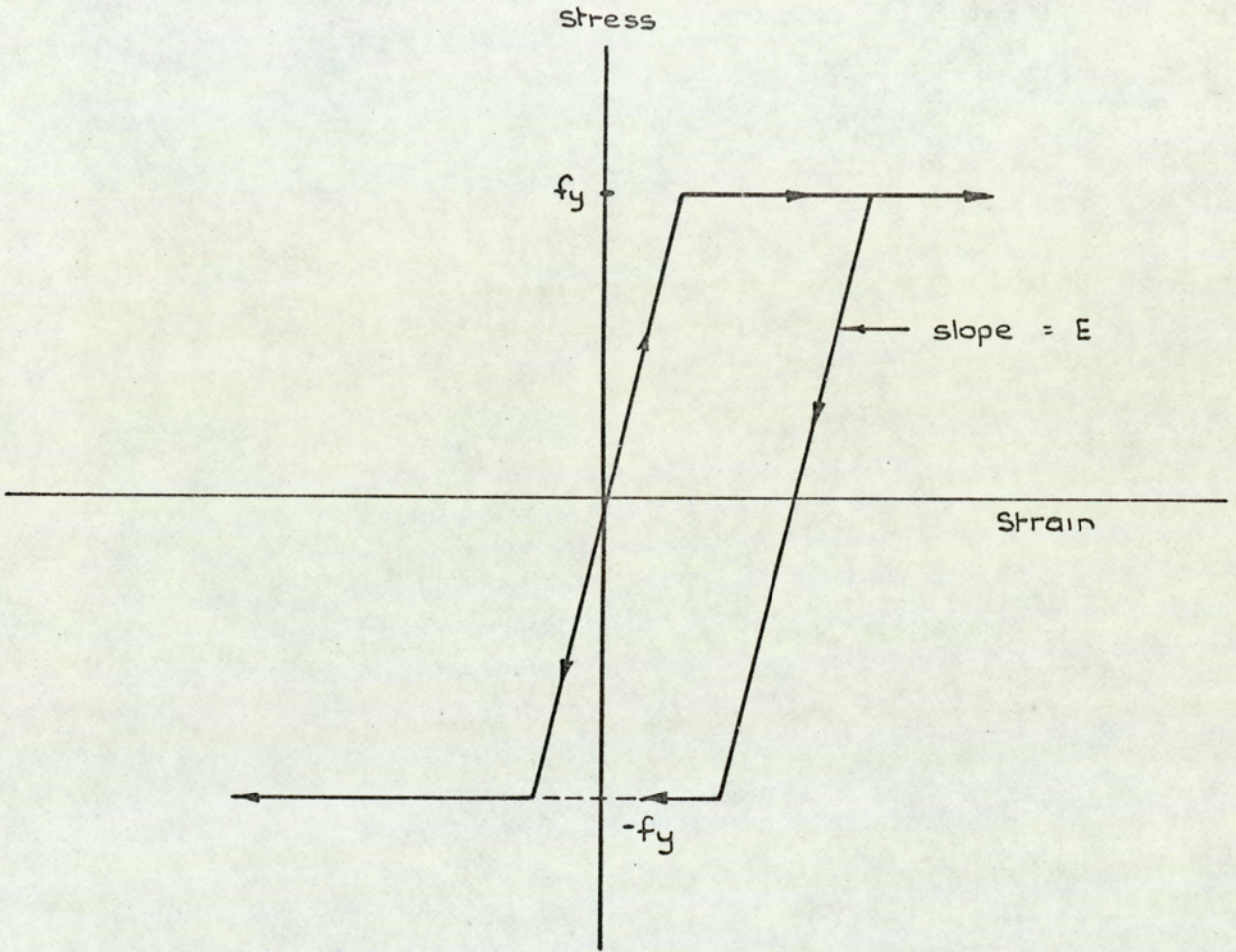


Fig. 1.1. Ideal plastic stress strain relation.

HISTORICAL REVIEW OF RELATED WORK

2.1 INTRODUCTION

During the last three decades the plastic behaviour of structures has attracted the interest of design engineers and research workers. This may partly be due to the realisation of the irrationality of the elastic method.

Prior to the development of the plastic theory in a form which was suitable for design purposes, all multi-storey frameworks were designed using modifications of the traditional elastic methods. Directly or indirectly, these frames were generally safe, but uneconomical and inefficient in their structural behaviour as shown later.

In the late twenties in this country, the reinforced concrete construction industry was beginning to offer serious competition to the steel industry. In 1929 a joint venture between the industry and the Department of Scientific and Industrial Research set up the Steel Structures Research Committee to investigate the design methods of steel structures, and to draft a more efficient, economical and rational elastic design method. It was, in fact, realised by the members of the Steel Structures Research Committee as they passed a riveted steel framework of a cinema undergoing construction in Bristol at that time that the elastic methods of design were far from reality.

Furthermore, with the use of reliable strain gauges on existing buildings, they found that the elastic behaviour of a structure such as the cinema frame was exceedingly complex and variable. These actual tests on existing structures showed that even with the lightest connections possible, the joints of a framed building resembled a rigid

framework much closer than a pin-jointed framework. Obviously the redundant nature of the frame, and the loading conditions of the stanchion lengths could not be ignored. After seven years work in 1936⁽⁸⁾, the Committee published their final report which proposed a design procedure which utilized the additional stiffness contributed to the ends of a member by those members connected to it. This was in contrast with the previous methods, from which a deliberately safe design has been obtained by underestimating the stiffness of the connections, for example by designing the beams in a framework as pin-ended. The Committee produced two sets of design curves⁽⁸⁾, one for a single curvature, and one for double curvature, but these proved to have serious limitations. Many people considered them extremely complicated to use, even though every simplifying assumption possible was made, and they did not take into account what effects wind loading would have on the design method. Baker and Williams⁽⁹⁾ remedied the latter objection, but the Committee itself still considered this as far too complicated.

Several years later steps were taken to improve the elastic method of design. Wood⁽¹⁰⁾ managed to produce charts giving a speedier and more economical design. Other improvements in technique and speed of design using substitute frames were made by Lightfoot⁽¹¹⁾ and Naylor⁽¹²⁾, which helped to reduce the design office work considerably.

The assumptions of the elastic method are far from reality, whilst the exact elastic methods are too complicated for routine use in the design office. The introduction of the electronic computer into civil engineering design has given new impulse to the elastic methods, but apart from all this the irrationality of the method still remains.

2.2 IRRATIONALITY OF ELASTIC DESIGN METHODS

One of the principle reasons for the development of the plastic theory was the realisation that most structures designed by elastic method are necessarily uneconomical. The basis of elastic design is that the stresses developed in any part of a structure under normal working loads shall not exceed certain allowable stresses, as laid down in the British Standard Specification No. 449⁽¹³⁾.

Working loads represent the normal loads likely to arise in the everyday use of the structure, and the working stresses are intended to provide an adequate safety margin to guard against unpredictable situations such as poor materials and workmanship.

The irrational nature of the elastic design method may be clearly demonstrated⁽¹⁴⁾ by comparing the relative strengths of a simply supported beam and an encastred beam when both are designed elastically.

B.S. 449 allows a maximum stress at working loads of 10.5 tons per sq.in. for a material with a guaranteed yield stress of 16 tons per sq.in. It followed that the loads could be increased by a factor of $\frac{16}{10.5}$ or 1.524, before yielding could occur in the extreme fibres at the most critical cross-section in the structure. This is true for any structure designed in this way. Elastic analysis does not take account of the effect in increase of loads and thus there is a safety factor of 1.524 against the occurrence of yield.

Analysis due to further loading can be made by plastic theory as the structure will support additional load after yielding first occurs. This is due to the fact that the plastic modulus of a cross-section is greater than the corresponding elastic modulus. The ratio of the two is called the shape factor, and for an I-section is approximately equal to 1.15. Accordingly this implies that the fully plastic moment of the section is 1.15 times as great as the moment at which yield first occurs.

Therefore, for any elastically designed statically determinate structure the safety factor against the occurrence of a plastic collapse mechanism is 1.15×1.524 , or 1.75 times the working loads.

Thus, in the case of a simply supported beam carrying a uniformly distributed load, where only one plastic hinge is required to cause collapse, the load factor (i.e. the ratio of collapse load to working load) has the same value as the safety factor against a plastic hinge, both being equal to 1.75.

However, in the case of an encastré beam more than one plastic hinge is required to produce collapse. As for the simply supported beam the first plastic hinges occur at 1.75 times the working loads at the ends of the beams. In this case, however, collapse does not occur until a third plastic hinge forms at the centre of the beam at 2.34 times the working loads, and yet both elastically designed beams have a safety factor of 1.524. The real strength of the two beams is therefore different. Obviously for steel economy the section of the encastré member could be reduced until its load factor against collapse was 1.75 and there can be no reason for providing the encastré beam with a greater margin of safety.

Any framed structure which consists of a number of beams and columns with different end conditions and applied loads will exhibit similar behaviour. The safety factor for every member of the frame is likely to be different. This is clearly undesirable since it implies that the majority of the members in the frame are stronger than they are required to be.

To be more precise, this means that any member designed elastically which is not pinned at both ends is over-designed. This will be true for every single member in a rigid jointed frame.

With the increasing competition from reinforced and pre-stressed

concrete, the steel designers must provide a simple, economical and rational design method. Quite clearly the rational and considerably more economical method of design for steel frames is to select the members in such a way that the complete framework has some definite load factor against collapse. In addition, it would be desirable for every single member to have a similar strength, although this is seldom possible. This is the basis of plastic design, of which the proposed method in the subsequent chapters is a modified form.

Plastic design methods have the additional advantage that the analysis techniques involved are generally considerably less demanding than those required for an accurate elastic design, due to the fact that the framework under consideration has far fewer redundancies than the corresponding fully elastic structure. Neal⁽¹⁴⁾ pointed out that the accuracy of the plastic methods is very little affected by the presence of residual stresses due to welding and rolling of steel sections, flexibility of joints, i.e. joints assumed to be rigid are in fact flexible, the relative settlement of the supports of a structure and stress concentrations, whereas they should be considered when using the allowable stress approach of elastic design.

2.3 DEVELOPMENT OF THE SIMPLE PLASTIC THEORY

The principle reason for the introduction of mild steel in preference to other structural materials such as cast iron was its marked ductility. It had been appreciated that stress concentrations in the regions of rivet and bolt holes and at sudden change of cross-sections could be easily absorbed with a material such as this without the occurrence of local failure due to brittle fracture. Nevertheless, this ductility, which is associated with behaviour outside the elastic range, was completely disregarded in the conventional elastic design of the

major structural components.

The first published work on the plastic behaviour of steel appeared in Hungary in 1914, describing what has now come to be known as the formation of plastic collapse mechanisms. In this paper⁽¹⁵⁾ Kazinczy noted that if a load on an encastré beam was steadily increased "failure" was found to occur when three independent cross-sections of the beam had yielded completely. Similar observations were made by Kist⁽¹⁶⁾ in Holland in 1917.

Following the publications of these two papers a German named Grunig⁽¹⁷⁾ published a small book in 1926, but the analysis leading to theories on the failure conditions of pin-jointed trusses were complicated and lacked experimental confirmation.

At the same time as the Steel Structures Research Committee was sitting, Maier-Leibnitz⁽¹⁸⁾ investigated experimentally the loading of simple and continuous beams into the plastic range. In addition, he was the first to show that the collapse load of a continuous beam is unaffected by settlement of the supports. This one fact has remained a powerful argument in favour of ultimate load methods of analysis. It is well known by engineers that considerable difficulties are introduced in elastic analysis by differential movement of supports. Thus it was recognised in 1936 that many of the inherent difficulties encountered in the elastic design of redundant structures would disappear if their behaviour in the plastic range was similar to that of continuous beams. Maier-Leibnitz was also largely responsible for the stimulation of interest in plastic methods in Britain, by the publication of his paper in Berlin in 1936⁽¹⁹⁾, in which he summarized much of the relevant work in the previous ten years in Europe. Following that he was invited to a meeting with members of the Steel Structures Research Committee, who became increasingly critical of elastic design whilst

preparing their final report⁽⁸⁾.

In the past three decades, there have been many investigations into different aspects of plasticity in design. In America, the concepts of plastic theory were restated^(20,21) in 1940 - the technique of design using plastic methods, being there termed Limit Design. Baker⁽²²⁾ was the first to realise that plastic theory was the answer to finding a simple and rational method of designing complex frames. Plastic theory, however, was not immediately accepted and it was not until 1948 that a clause allowing the members of a frame to be proportioned so that the frame had some definite load factor against collapse was introduced into B.S. 449⁽²³⁾. This was modified in the 1959 edition of B.S. 449⁽¹³⁾ as follows:-

Clause 9b(iii) "fully rigid design". This method, as compared with the method for simple and semi-rigid design, will give the greatest rigidity and economy in weight of steel used when applied to appropriate cases. For this purpose, the design shall be carried out in accordance with accurate methods of elastic analysis and to the limiting stresses permitted in this British Standard. Alternatively, it shall be based on the principles of plastic design so as to provide an adequate load factor, and with the deflections under working loads not in excess of the limits implied in this British Standard."

This Clause does not consider a value of load factor (although in the 1948⁽²³⁾ edition, it was specified as 2). However, in this country a load factor of 1.75 as shown earlier, is accepted as providing an adequate safety margin. Furthermore, as B.S. 449⁽¹³⁾ permits an increase in elastic working stresses for increased stresses owing to wind forces, the load factor is reduced to 1.4 for such cases.

Various approaches have helped to establish plastic design as a better alternative than elastic methods. In 1950, the first

comprehensive definition of the general principles of simple plastic behaviour, later to be known as the kinematical, statical and uniqueness theorems, was given by Horne⁽²⁴⁾, this paper preceding a similar publication in America by Greenberg and Prager⁽²⁵⁾. Subsequently, the most important developments came from firstly Neal and Symonds^(26 27 28), who extended the basic philosophy of simple plastic theory in producing several rapid methods of analysis, in particular the method of "combination of elementary mechanisms", and secondly from Horne⁽²⁹⁾, who devised the "plastic moment distribution" technique. In 1956, all these suggestions were correlated by the publication of the second volume of "The Steel Skeleton"⁽³⁰⁾, which deals exclusively with the plastic behaviour of steel structures.

Many satisfactory structures have been designed on the simple plastic method, but in the case of multi-storey buildings, it has not always been possible to satisfy the deflection and instability conditions.

2.4 THE INSTABILITY PROBLEM

A real understanding of the instability problem was delayed, since any tendency towards reduction in stiffness in complete structures owing to axial loads was disguised by the nature of the commonly used design methods. The majority of frameworks were restrained against sway and were therefore less susceptible to instability failure and the fact that the majority of structures had a large reserve of strength, owing to the lack of economy in their design by traditional elastic methods.

The dangers of buckling and instability of individual members were appreciated long before the concept of overall frame instability was recognised, and several recommendations already existed in the codes of practice to counteract failure to individual members. A stanchion length will have a reduced load carrying capacity whenever a hinge is formed within its length. The instability problem of a member is

related to the reduction of its carrying capacity, owing to the deformation within its length. Heyman⁽³¹⁾ pointed out that a column designed to take both a large axial force and a wind load will be of such a heavy section that its slenderness ratio for usual storey heights will be small, and hence the likelihood of the instability of an individual member is remote. There are, therefore, only a few exceptions to be catered for when unusually long columns have been used for some reason or perhaps in the uppermost storeys of a tall building.

Overall frame instability is a far more complex problem than that of individual member instability, since it becomes necessary to consider the interaction of every single member in the structure. Most of the work designed to obviate this type of failure has been carried out in the past fifteen years.

Merchant⁽³²⁾ gave a detailed account of the instability problem in both the elastic and plastic⁽³³⁾ range. This, together with the work developed by Livesley and Chandler⁽⁵⁾, who have developed a wide range of readily applicable stability functions, helped towards a clearer understanding of the instability problem.

The first detailed account of the complete frame instability problem was given by Merchant⁽³⁴⁾ in 1954. As an approximate method for the evaluation of the elastic-plastic failure load, he suggested a relationship based on the Rankine formula, as applied to struts. This relationship is known as the "Merchant-Rankine formula". This formula, which is an empirical relationship between the real failure load, the elastic critical load, and the (rigid) plastic collapse load, was thought to check conservatively the plastically designed structure against stability. In the majority of cases, it did give a conservative estimate of the failure load, but its generality has been disproved by Low⁽³⁵⁾, who carried out a comprehensive series of tests on multi-storey model frames at Cambridge in 1959. Wood⁽³⁾, although supporting

Merchant's formula, indicated that the formation of plastic hinges would have a more profound effect than that assumed by Merchant⁽³²⁾.

The real significance of the elastic critical load was first demonstrated conclusively by Wood⁽³⁾ in 1958. He showed that despite the fact that the critical load may initially appear to be deceptively high, a serious deterioration in the overall stiffness of a frame may occur whenever a fully plastic hinge develops in a member. Using the hypothesis that a plastic hinge contributes no more stiffness to a structure than a real hinge, provided that rotation continues in the same direction as before, Wood suggested that a new reduced critical load may be obtained for the modified structure by effectively substituting a real hinge for the plastic hinge. Furthermore, as successive plastic hinges form this "deteriorated critical load" becomes so low that failure may occur, owing to elastic-plastic instability well before the attainment of the rigid plastic collapse load factor, and with far fewer plastic hinges than are required for a complete collapse mechanism.

Wood⁽³⁾ demonstrated very clearly the danger of instability in plastic design. He showed, by taking practical illustrations, that a structure designed on the simple plastic method, neglecting the effect of instability, could fail at a much lower load than the plastic collapse load when instability is taken into consideration. This premature failure was sometimes applicable even to relatively simple structures, such as a single bay four storey frame.

Heyman⁽³¹⁾ suggested that the stiffening effect of cladding would generally be sufficient to eliminate the stability problem, although in the discussion on his paper⁽⁶⁾, some doubt was expressed concerning the effectiveness of this safeguard. In fact, the method he proposes generally produces a conservative design, and this lack of economy contributes towards the safety of the frame. This method may however be criticised for its lack of direct consideration of instability, and

in the discussion⁽⁶⁾ it was Calladine who suggested a possible procedure for developing a rational design allowing for the instability effects. This was investigated further by Holmes and Gandhi^(4 36), who proposed a design method for tall, rigidly-jointed steel building frames where suitable beam and column section sizes were selected, given the geometry, loading and required load factor, based on simple plastic theory with the introduction of a magnification factor to allow for instability effects. An experimental research program designed to substantiate their work was later conducted by Clough⁽⁷⁾, who also developed a computer program for the Holmes and Gandhi method^(4 36) which was intended to reduce the quantity of repetitive work. This method was developed further by Holmes and Sinclair-Jones^(37 38) by introducing an improved and more accurate method of dealing with the boundary regions (i.e. upper storey, lower storey, and external bays) of a frame, and with the prediction of values of the magnification factors which greatly reduces the number of iterations or eliminates the need for iteration entirely. In addition, the limitations and advantages of this method were critically assessed by accurate elastic-plastic computer analysis⁽³⁹⁾ of a series of design examples and by comparison with other design methods.

The design methods that have been discussed so far all rely to some extent on the individual judgement of the engineer, and are based on a variety of assumptions and approximations. An alternative approach is that of automatic design by computer. The most sophisticated method available is that suggested by Majid and Anderson⁽³⁹⁾. This involves the iterative use of a non-linear elastic-plastic analysis procedure which is based on the matrix displacement method. This method traces the actual load-deflection behaviour of a frame up to collapse. Overall instability of the frame is taken into consideration as the effects of axial loads on stiffness are allowed by the introduction of stability

functions, while the loss of stiffness owing to the formation of plastic hinges is automatically recorded by successive alteration to the overall stiffness matrix as each hinge forms. The design method depends on first of all analysing the frame with an initially assumed set of sections, and then altering these sections which are either inadequate or oversafe. The frame is then re-analysed and the procedure is repeated until the method converges to a unique set of sections which economically satisfy the design criteria. Although the method does not pretend to provide the minimum weight solution, it undoubtedly produces a very economical design and may be applied to large frameworks of extremely irregular shape.

2.5 COMPOSITE ACTION

There are many advantages to be obtained by considering a structure as a composite system rather than a series of individual components. Whenever any continuity exists between two components, there is bound to be a certain degree of structural interaction, and the basic philosophy of composite design is that this interaction should be both recognised and allowed for during the design process.

The most obvious way to produce a more economical design is to allow for composite action between the concrete floor slabs and the supporting steel beams. The intrinsic merit of this design is the rational disposition of the concrete slab and the steel beam materials in respect of their compressive and tensile strengths. Thus the steel beams are designed primarily as tension members of the framework, the slab acting as a compression member. It will be appreciated then that if such a method were devised of designing a steel framework, with the steel beams mainly in tension and concrete slab in compression, it would lead to a very economical design.

Although the concrete slab is usually connected to the I-beam through natural bond, such a connection is unreliable and may not provide composite action throughout the life of the structure. Thus, if the design calls for a composite structure, it is necessary to connect the slab to the I-beam by mechanical shear connections fastened to the I-beam and embedded in the slab. This connection transmits the shear between the I-beam and the slab and prevents the slab lifting away from the beam. The root of the shear connector transmits the horizontal shear, whilst the head is provided for holding down. Breakdown of shear connection can occur by failure of the shear connector or by crushing of the concrete or both. Various types of shear connectors are recommended in C.P.117 part 1(40), these are illustrated in Figure 2.1.

The shear connectors are usually connected to the I-beams by welding. Although welding shear connectors presents no technical difficulties, it is ordinarily time consuming and complicates fabrication of beams. It is desirable, therefore, to devise a shear connector which can be fastened rapidly to I-beams both in the shop and at the construction site. A rapid process known as electric arc stud welding is available. The process may be accomplished in a few seconds with the aid of a stud welding gun.

Figure 2.2 shows the stress diagram for a concrete slab composite and non-composite with the steel beam.

It will be appreciated immediately that the use of shear connectors increases the ultimate strength, and so for a design resulting in the same strength as a conventional design, a smaller beam size and slab thickness, can be used. Thus, designing by composite methods produces an overall saving in steel, a reduction in the dead load, hence saving in foundations design, coupled with a reduction in storey height, making it possible on extra storeys for the same heights.

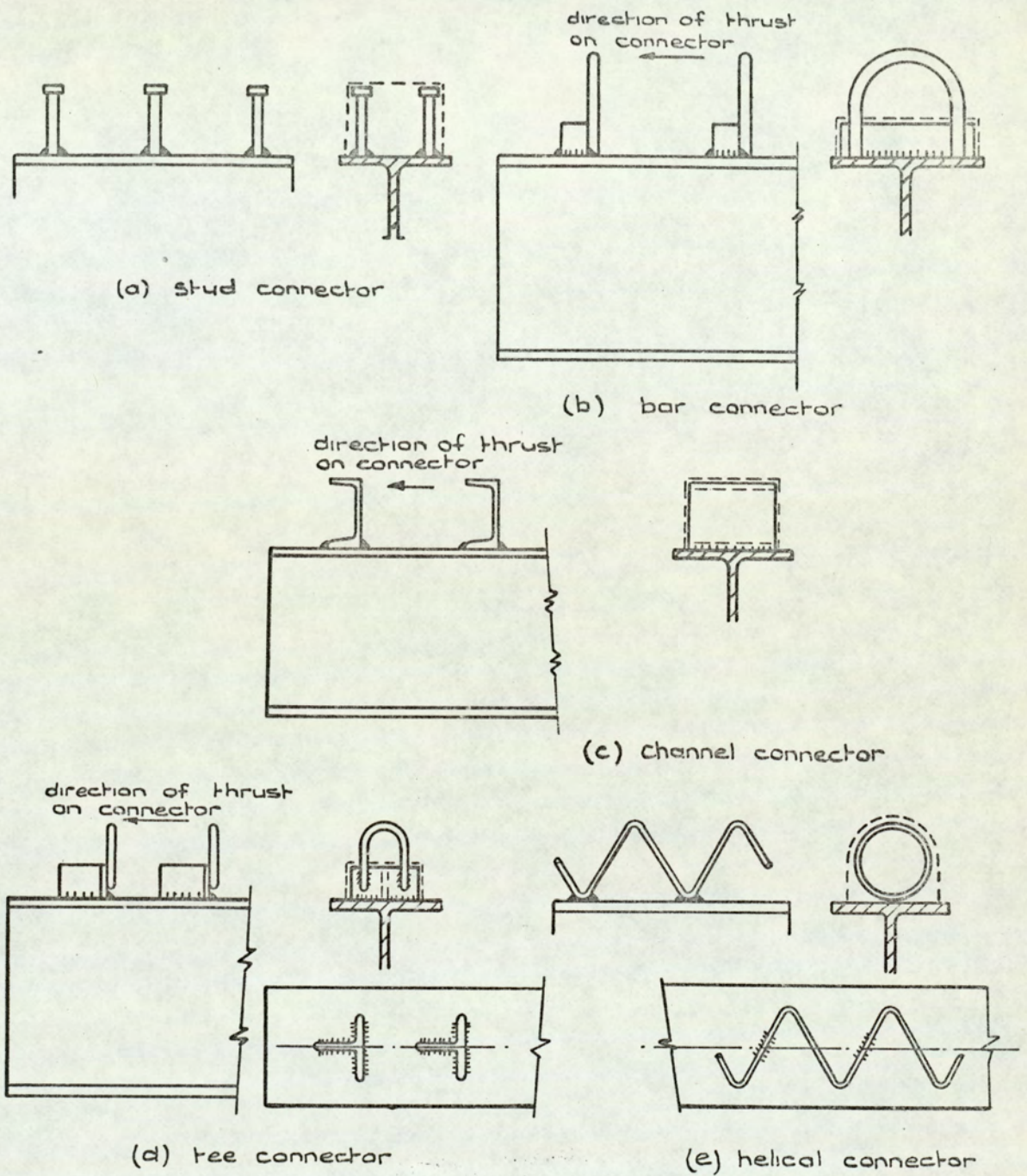


Fig. 2.1. Typical shear connectors.

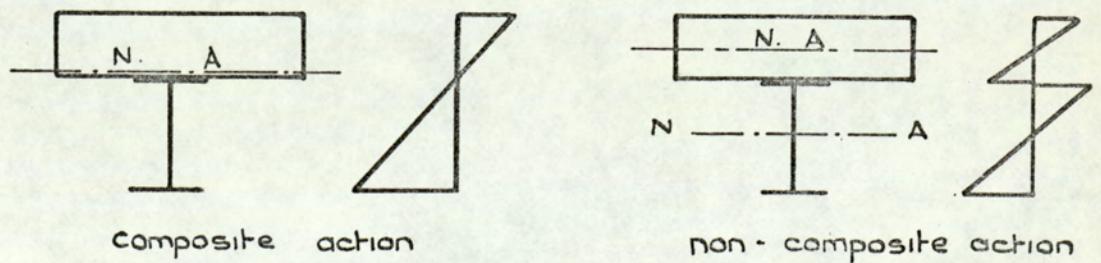


Fig. 2.2. Stress diagrams for composite and non composite action.

Investigations of composite beams were carried out as early as 1922. The Dominion Bridge Company of Canada at that time conducted tests on two floor panels, each consisting of two steel I-beams encased in concrete and a concrete slab. In reporting the results of the test, Viest⁽⁴¹⁾ quoted:

"While such beams have hitherto been designed on the assumption that the entire load is carried by the steel, it was thought that the steel and concrete might really act together so as to form a composite beam....."

Viest⁽⁴¹⁾ reviewed much of the relevant research work carried out on composite steel - concrete beams in the period 1920 - 1958. He also carried out tests⁽⁴²⁾ to determine the behaviour and load carrying capacity of stud shear connectors.

Chapman^(43 44) in 1964 carried out a series of tests on composite beams and shear connectors. He suggested that, in view of the relatively large shape factor of the composite sections, ultimate load design is particularly advantageous. Chapman⁽⁴³⁾ suggested that shear connectors should be designed on an ultimate load basis, irrespective of the method used for designing the composite section. He recommended that 80 per cent of the experimentally determined ultimate capacity of the shear connectors should be used when shear connections are designed to carry the horizontal shear force existing in the beam at ultimate load. In the case of uniformly loaded beams, he considered uniform spacing of shear connectors is satisfactory, from experiments at Lehigh University and Imperial College, as composite beams behaved as well as beams with shear connectors spaced triangularly. Chapman⁽⁴³⁾ emphasised the importance of adopting a standard testing procedure for shear connectors. All these recommendations were taken into consideration when the code of practice C.P.117 part 1⁽⁴¹⁾ came into existence in 1965.

Davies⁽⁴⁵⁾ carried out a series of tests up to collapse using a centre point loading on simply supported steel-concrete composite T-beams. Using welded studs as the means of shear connection, he examined the effect of varying the connection spacing and the amount of transverse reinforcement upon the general behaviour of the beams.

Bernard and Johnson⁽⁴⁶⁾ tested simply supported beams to predict the ultimate moment of resistance and curvature of cross-sections of composite steel-concrete beams. Bernard and Johnson⁽⁴⁷⁾ then carried out tests on plastic behaviour of continuous composite beams. They concluded that the use of simple plastic theory is justified for the design of most types of continuous beams, provided that secondary failure can be prevented. In their design of the shear connections, the stud spacing was determined by an extension of the method used for simply supported beams⁽⁴⁶⁾. The total horizontal shear force to be transmitted at collapse between adjacent sections of maximum positive and negative moments was divided by the capacity of one connector to give the number of studs required between the two sections. The studs were spaced uniformly. One of the objects of their tests⁽⁴⁷⁾ was to check this method which leads to a more uniform spacing of the studs, than that based on forces between sections of maximum moments and adjacent points of contraflexure. At the end, they concluded that because of lack of sufficient experimental evidence, it was not possible to present comprehensive recommendations for the design of continuous composite beams by ultimate strength method. Johnson, Greenwood, and van Dalen⁽⁴⁸⁾ carried out a series of push out tests on studs set in reinforced concrete slabs in tension. This followed by recommending the use of welded stud shear connectors in hogging moment regions of continuous composite beams. The design load per stud was taken as 80 per cent of the design value specified in C.P.117 part 1⁽⁴⁰⁾; that is, as 64 per cent of the ultimate capacity as found in the standard

push out test. The number of shear connectors required spaced uniformly between the hogging moment hinge and the point of contraflexure, i.e. spacing is not uniform across the length of the beam as suggested by Chapman⁽⁴³⁾ and Bernard and Johnson⁽⁴⁷⁾.

Harrop⁽⁴⁹⁾ carried out full scale tests at Leeds University on a building at all stages of its erection and found considerable increase in its strength, owing to composite action.

Thomas and Short⁽⁵⁰⁾ tested three one-third scale model beams and slab bridge-decks, two including composite action and one without. They found a considerable increase in the strength of the effective beam-section. The stiffness of the system increased, owing to the higher moment of inertia of the composite cross-section, and resulted in smaller deflections at working loads.

Johnson, Finlinson and Heyman⁽⁵¹⁾ made an interesting comparison of plastic and plastic composite methods of design, and with other older design methods in weight and cost saving on a single bay framed building at Cambridge University. Plastic composite design showed a clear advantage over the other methods, for example, 29 per cent saving in weight and 15 per cent in cost over the traditional elastic non-composite method; 15.5 per cent saving in weight and 7.5 per cent in cost over the elastic composite method, and 13 per cent saving in weight and 7 per cent in cost over the plastic non-composite method.

Composite action in columns is also significant and is related to the need for concrete casing for the columns of a frame in order to satisfy the fire-proofing requirements⁽¹³⁾. If composite action is taken into consideration in columns, then the concrete casing would be assumed to carry a proportion of the total axial load in the member, thus relieving the steel section of a certain amount of direct stress.

This is especially the case in the lower regions of a frame, where selection of suitable columns is largely controlled by the axial load in the member, considerably lighter universal columns would be found to be adequate.

The description of a modern building designed by composite action is given by Cain⁽⁵²⁾. He described the Royal Bank of Canada Building in Montreal, where the use of shear connectors resulted in a 43 per cent reduction in the weight of steel over conventional design, together with a 30 per cent saving in cost. The saving of $6\frac{1}{2}$ inches per 13 feet high storey (slab to slab), caused a reduction of 4.2 per cent in the overall height of the building, with associated reductions in the cost of the columns, curtain wall, heating and cooling.

2.6 PLASTIC COLLAPSE OF SLABS AND CONTINUOUS STRUCTURES

Some of the earliest work on plastic theory applied to slabs was carried out by Ingenslev⁽⁵³⁾, who published a paper on the strength of rectangular slabs in 1923. By studying some earlier tests on slabs, he noticed that the yielding started along the centre line and then spread into the corners, dividing the slab into four sections. Assuming that the bending moments along these lines to be maximum and constant, hence with zero shear force, then since the slab is in equilibrium, the external forces would be equated to the internal forces of the bending moment. Thus, he could calculate the collapse load and showed good agreement with the tests. By introducing a negative bending moment along the edges, expressions were evaluated for fixed or encastred slabs. Following this pioneer work of Ingenslev, Johansson⁽⁵⁴⁾ extended the work to cover much more general cases of different shaped slabs, and corner effects, together with different yield line patterns. A review of the work carried out by Ingenslev and

Johannson was published by Hognestad⁽⁵⁵⁾ in 1953. Mansfield⁽⁵⁶⁾ considered a slab with different positive and negative bending moments and extended the yield line theory to fit this case. The effective width of slabs supporting a concentrated load was studied by Ashdown⁽⁵⁷⁾ who also studied the yield line theory applied to circular and triangular slabs.

An example of a floor designed by yield line theory is given by Smyth⁽⁵⁸⁾, who describes a warehouse floor supported by columns in a hexagonal pattern. To analyse this elastically as a system of beams with a slab on top would prove very complicated and in this paper the plastic analysis giving a slab of uniform depth proves the simpler solution. Wood⁽⁵⁹⁾ carried out tests to destruction at the Building Research Station on square, simply supported and discontinuous reinforced concrete slabs supported on beams of various sizes, for various modes of collapse. His work⁽⁵⁹⁾ on upper-bound theory will be discussed in the next chapter.

On plastic collapse of continuous structures, Ockleston⁽⁶⁰⁾ in 1955 carried out a series of tests to destruction on a ten years old reinforced concrete Dental School due for demolition. He found that the plastic theories gave a reasonably satisfactory estimate of ultimate loads, where failure was due to bending in one direction, but underestimated the collapse loads of lightly reinforced slabs which failed as a result of bending in two directions by 61 per cent. At that time he agreed that this large discrepancy cannot be accounted for by strain hardening of the reinforcement or tensile membrane action, as the deflections were small. In the case where deflections become large appreciable stretching of the middle surface will occur and tensile membrane stresses will by Catenary action^(61 62) increase the carrying capacity of the slab. In his conclusion, Ockleston⁽⁶⁰⁾ did not account

satisfactorily for the unexpected strength exhibited by the slab and mentioned that the tensile strength of the concrete which was not accounted for might have influenced this discrepancy.

In 1958, Ockleston⁽⁶³⁾ came with a rational explanation of the behaviour of the two-way slabs at failure. Throughout the testing, the deflections remained small, and he attributed the unexpected strength exhibited by the slab to arching action owing to the development of compressive membrane stresses. Arching action is most likely in lightly reinforced slabs in which cracking will cause large movements of the neutral axis, and can occur only if the deflections are small, and horizontal spreading at the supports is restrained. This will greatly increase the carrying capacity of slabs. Roberts⁽⁶⁴⁾ carried out a series of tests to find the effect of compressive membrane action by investigating the load carrying capacity of slab strips restrained against longitudinal expansion. He found that the ratio of the maximum load supported to that given by Johansson's yield line theory (based on failure by bending only) is as high as 17 for slabs with high concrete strength and a low percentage of reinforcement, to 3 for slabs with a low concrete strength and a high percentage of reinforcement. The restraint provided being not less than 83 per cent of that given by an infinitely stiff surround.

The presence of compressive membrane action will be investigated in the experimental tests presented in this thesis.

Steel⁽¹⁾ carried out tests on two and three bay one-storey frame models, with composite floor slabs. The tests to destruction were carried out using point loading by hydraulic jacks through mild steel plates at the centre of each bay for the main modes of collapse of beam and slab floor systems. The tests showed a good agreement between experimental and theoretical results.

2.7 USE OF COMPUTERS

The idea of a calculating machine which would automatically follow a pre-arranged sequence of instructions is not a new one. The "Analytical Engine" which Babbage⁽⁶⁵⁾ conceived in 1833 contained most of the logical features to be found in modern computers, but he was ignored by most of his contemporaries and his machine was never built. It was not until more than 100 years later that developments in mechanical and electrical engineering stimulated the translation of his ideas into reality.

The first working computer (in the sense in which the term computer is used here) was put into service at Harvard in 1944, and the first computer to be built in this country was at Cambridge in 1949.

At first most of the problems solved on computers came from the fields of mathematical and scientific research, but gradually it came to be realised that many problems of engineering analysis and design could be solved profitably on the new machine.

The computer is obviously invaluable in structural research and much use of it then has been made at Cambridge in the work of stanchion behaviour and other development of the plastic theory. In the last fifteen years there has been a rapid development in the design, adaptability and use of computers.

In the application of computers to problems of structural analysis, Livesley⁽⁶⁶⁾ in 1956 commented:

"Within the last few years, however, the advent of the electronic digital computer has made possible a completely new approach to calculations. By carrying out standard mathematical processes automatically, the electronic computer not only cuts down the time required for a given calculation, but also provides new criteria for comparing the merits of alternative

processes." He then added: "It must be emphasised that any computer can only give answers to numerical problems. It can not consider the accuracy of the data supplied to it, nor the validity of the assumptions made during the calculations. To the structural engineer the value of a computer analysis lies in its speed and its accuracy relative to the initial data, but this mathematical accuracy does not remove the basic uncertainties of structural work, such as the value of loads, foundation restraints, and joint rigidities."

In the relation of man-machine interaction, Livesley⁽⁶⁵⁾ in 1960 commented:

"Using a standard program for his analytical work, a designer can rapidly see the effects of small changes in design constants, and relations between human and machine makes the most of efficient use of natural abilities of both. The human being has a vastly greater memory than any existing machine, together with the ability to make judgements based on intuition and previous experience. These are valuable qualities in design work. A computer, on the other hand, is far better at the numerical calculations which occur in analysis."

The computer must not be underestimated, and the real problem for the designer is to know what kind of relationship must he and his design have with the computer. A computer nowadays may do in a minute what would take a human being months.

With adequate planning and programming techniques, greater speed and hence economy of design can be obtained without any loss of the essential judgement of the designer.

INTRODUCTION TO UPPER-BOUND SOLUTIONS

3.1 INTRODUCTION

There are two methods of predicting the plastic collapse load of a structure. These are termed "upper-bound" and "lower-bound" (67) solutions; each corresponds to a theorem of plastic behaviour which is described in the early part of the chapter. This is followed by a comparison of the "two" solutions in relation to non-composite and composite structures, and a justification of the use of upper-bound solutions only in this thesis. In the latter part of the chapter an introduction to upper-bound collapse solutions as the basis for the proposed method which is to be developed in the following chapters is made.

3.2 PLASTIC THEORY

The plastic theory is based on the idealised stress-strain curve (Figure 1.1) mentioned in Chapter 1, obtained from a tension test on annealed mild steel, although the theory is also applicable to high tensile steel. In Figure 3.1, the proportion OA of the curve corresponds to the elastic range, A being the upper yield point which is neglected for an idealised stress-strain relationship. Further straining after this point has been reached results in a drop in stress to the lower yield point B. At this point the material has become fully plastic and there is no increase in stress between B and C owing to further straining. After C, strain hardening commences which is ignored in the basic assumptions of the proposed design method. The plastic theory assumes that between B and C strain can continue without any further increase in the stress, i.e. the steel has reached its yield stress and can flow plastically.

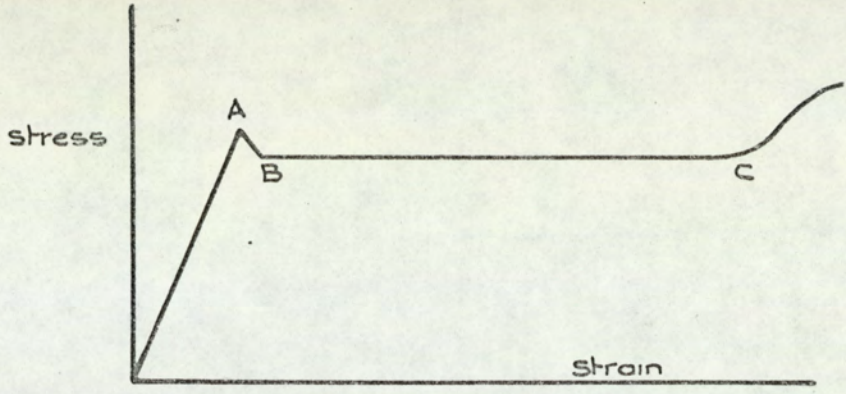


Fig. 3.1. Stress v. strain for mild steel.

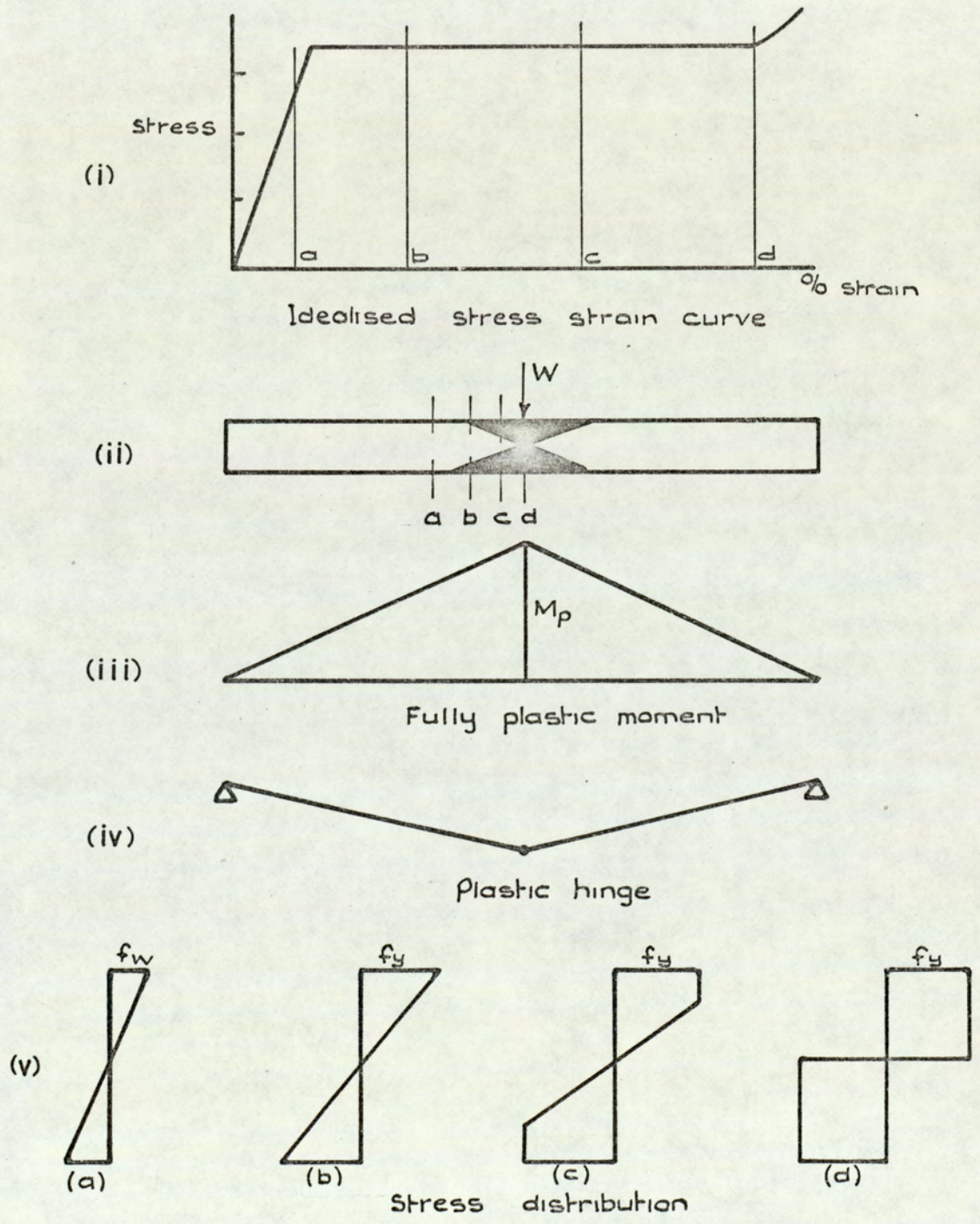


Fig. 3.2. Idealised plastic relationship.

Consequently, for the plastic theory to be applied to reinforced concrete, it is necessary for the yield point to remain constant and for the yield stress to be sustained during considerable increase in the strain. This latter fact is particularly important in all but the simplest structure. In complex structures, the first yield may take place long before the structure has deflected enough to cause further yielding at other points and, hence, collapse. Thus, an under-reinforced section would conform to the plastic theory better than an over-reinforced section, since introduction of more reinforcement increases the area of concrete in compression, and causes crushing which is rather a sudden failure lacking ductility. On the other hand, an under-reinforced section will fail in tension, the steel reinforcement following the stress-strain pattern required for this theory.

Figure 3.2 shows the change in the stress distribution for a simple rectangular beam under an increased load.

The first distribution (a) is the working stress across the section, f_w being the working stress at the outer fibres. Increase of the load results in the maximum stress (in the outer fibres) increasing to the yield stress as shown in (b). Any further increase in load now causes yield to spread towards the centre and also along the beam as shown in Figure 3.2 (ii), until eventually the beam can sustain no more load, owing to the whole section being at the yield stress (d). Any further attempt to increase the load will just cause increased deflection, the beam acting as though it were "hinged" at that point. A plastic hinge is said to have formed, and the bending moment at that point is referred to as the fully plastic moment. The formation of a plastic hinge owing to bending can be visually illustrated by coating steel specimens with a brittle resin. The properties of this resin are such that it cracks at locations where yielding of the steel has occurred. Plate 1 shows the formation of a plastic hinge at the centre of a beam, owing to pure bending.

A plastic hinge is similar to a real frictionless hinge in the sense

that both undergo continuous rotations when a structure is subjected to additional loading. While the plastic hinge is capable of withstanding a constant bending moment equal to the fully plastic hinge moment of the section, a real hinge cannot withstand any moment. In reinforced concrete slabs, these hinges can form along a line of maximum moment, when they are called fracture lines. These hinges can form in any sequence, but the structure will not collapse until the required number for a "mechanism" is present.

3.3 THEOREMS OF PLASTIC COLLAPSE

These theorems are based on the assumption that the members of a frame follow the stress-strain curve in Figure 1.1 when loaded and that the equations of statics apply equally to the deflected frame. Hence, instability and buckling effects are ignored, which are basic assumptions of the simple plastic theory.

The first theorem to be stated is based on consideration of the requirements of statical equilibrium for a structure. Hence the statical theorem which is based on bending moments in a frame at collapse may be stated thus:-

"If a distribution of bending moments exists in a frame which satisfies statical equilibrium with the external loads, and the moment nowhere exceeds the fully plastic moment, then the value of the applied loads is safe and less than or equal to the collapse load."

It is theoretically possible to have a bending moment distribution induced by external loads, which exceeds the fully plastic moment at some point, thus violating the defined conditions of the problem.

Because the set of loads corresponding to the bending moment distribution is safe, i.e. less than the collapse load, it constitutes what is termed a "lower-bound" value of the load. This statical theorem was first suggested by Kist⁽¹⁶⁾ and its proof was supplied by Horne⁽²⁴⁾

and by Greenberg and Prager⁽²⁵⁾.

The second theorem is concerned with the collapse mechanism of the frame. If a mechanism is assumed, and the internal work dissipated equated to the external work done by the applied loads, the collapse load value obtained is the true collapse load only if the assumed mechanism corresponds to the true mechanism of collapse. Hence the kinematic theorem as stated by Neal⁽¹⁴⁾ is:-

"For a given frame subjected to a set of loads W , the value of W which is found to correspond to any assumed mechanism must be either greater than or equal to the collapse load W_c ."

Thus, the definition of an "upper-bound" solution is one where the value of the applied load is greater than or equal to the collapse load. Thus, such solutions are "unsafe" in that the designer may assume a high value of the collapse load. This theorem was first established by Greenberg and Prager⁽²⁵⁾.

Finally, the uniqueness theorem remains which is a combination of the statical and kinematical theorems. Since the lower-bound solutions produces a value which is either less than or equal to the collapse load, and the upper-bound solution produces a value which is either greater than or equal to the collapse load, then it follows that when the two solutions give the same value for the collapse load, then this is the true value. Re-stating this in more general terms, Neal⁽¹⁴⁾ stated the uniqueness theorem as:-

"If for a given frame and loading at least one safe and statically admissible bending moment distribution can be found, and in this distribution the bending moment is equal to the fully plastic moment at enough cross-sections to cause failure of the frame as a mechanism, owing to rotations of plastic hinges at these sections, the corresponding load will be equal to the collapse load W_c ."

This theorem was proved by Horne⁽²⁴⁾.

3.4 UPPER AND LOWER BOUND SOLUTIONS TO NON-COMPOSITE AND COMPOSITE STRUCTURES

Applying upper-bound solutions to determine the collapse load of non-composite structures implies that a definite mode of collapse has to be considered. Virtual work methods are applied to find the collapse load corresponding to the selected pattern of yield lines. A lower-bound solution, on the other hand, does not require yield lines to form, but lines of maximum principle moment can be plotted to give a completely different "mode" to the upper-bound collapse mode for independent collapse of the slab.

Considering composite action between supporting beams and slab floor systems, upper-bound solutions can easily be modified by changing the slab moments along the centre line parallel to the main beams from $(M_b + M_s L)$ to M_c the composite moment of a beam and slab of width L . However, lower-bound solutions represent a distribution of moment (or stresses) in a slab, immediately prior to collapse, and so the problem of choosing such a distribution becomes much greater when the yield criteria vary over the slab.

In upper-bound solutions, a definite mode of collapse is chosen, automatically defining and satisfying the yield criteria. Hence composite action does not enter into independent collapse of the slab. A lower-bound solution on the other hand does not define a mode of collapse; hence the yield criteria must include composite action. Choosing a lower-bound solution requires that the bending moment function also must vary over the slab.

The problem of using lower-bound solutions involving composite action, then, consists of finding satisfactory yield criteria. This depends on an "effective width" concept for the composite slab and beam.

The moment function is then chosen to satisfy this criterion together with the equilibrium and boundary conditions. This proves to be very complicated, hence a lower-bound solution was not used for the composite beam and slab floor systems presented in this thesis.

3.5 INTRODUCTION TO UPPER-BOUND COLLAPSE SOLUTIONS

Applying upper-bound solutions to determine the collapse load of a structure implies an initial assumption of the mode of collapse. As explained earlier, if an incorrect mode is chosen, then the resulting collapse load will be high, and in fact, the true collapse load is obtained only if the actual failing mode is equal to the assumed one. This corresponds to the kinematic theorem stated earlier. Thus upper-bound solutions are unsafe, unless a sufficiently high load factor is taken over this contingency. However, Wood⁽⁵⁹⁾ and Johansen⁽⁵⁴⁾ have shown that a choice of fracture lines which depart somewhat from the correct mode of failure may nevertheless give results which are only slightly in excess of the collapse load. This error will no doubt depend on the type of structure, and since tests have shown that the use of fracture line theory, correctly applied, is still slightly conservative, it is questionable how important will be the actual error in predicting the collapse load by this intuitive approach. Reductions in collapse load owing to a deviation from the true mode of collapse are counteracted by membrane action and strain hardening of the steel. Because of the above factors, the upper-bound collapse solutions prove acceptable as a design method, and are therefore adopted as the basis for the proposed design method.

In order to obtain an upper-bound solution for the collapse load by the kinematic theorem, it is necessary to have what Prager⁽²⁾ calls a Kinematically Admissible Velocity Field, where three conditions must be satisfied:-

- (1) The system must be a proper mechanism.
- (2) The condition of incompressibility must be satisfied.
- (3) The work done by external loads must equal the internal work dissipated.

It is questionable whether the condition of incompressibility as normally understood has any meaning in the collapse mode of a reinforced concrete slab where large tension cracks develop. At all events, the second condition is ignored in fracture line theory.

The external work done on a system is the sum of the products, total load on an element times the deflection at the centre of gravity of the load. The internal work done is equal to the sum of the products, total moment times the relative rotation of the two elements. If the moment along a yield line is not parallel to a side of the slab, the projection of this moment on to a rectangular co-ordinate axis times the rotation of this axis is taken as the internal work done.

Wood⁽⁵⁹⁾ applied this upper-bound theory to the collapse of simply supported, discontinuous square, reinforced concrete slabs with isotropic reinforcement. The slab was assumed to be resting on edge beams, with no composite action between the two. Later he extended the work to cover rectangular slabs and considered⁽⁶⁸⁾ "fan" modes of collapse. The reduction of collapse load for uniformly loaded slab owing to the formation of fan modes is not great.

By applying the yield line theory stated above, Wood⁽⁵⁹⁾ showed that for independent slab collapse, Figure 3.3(a), the value of the collapse load, pL , for a load p per unit is as follows:-

The internal work dissipated in the yield lines =

$$M_s \left[(\text{projected length on 1st axis of rotation})(\text{Angular rotation about 1st axis}) + (\text{projected length on 2nd axis of rotation})(\text{Angular rotation about 2nd axis}) \right]$$

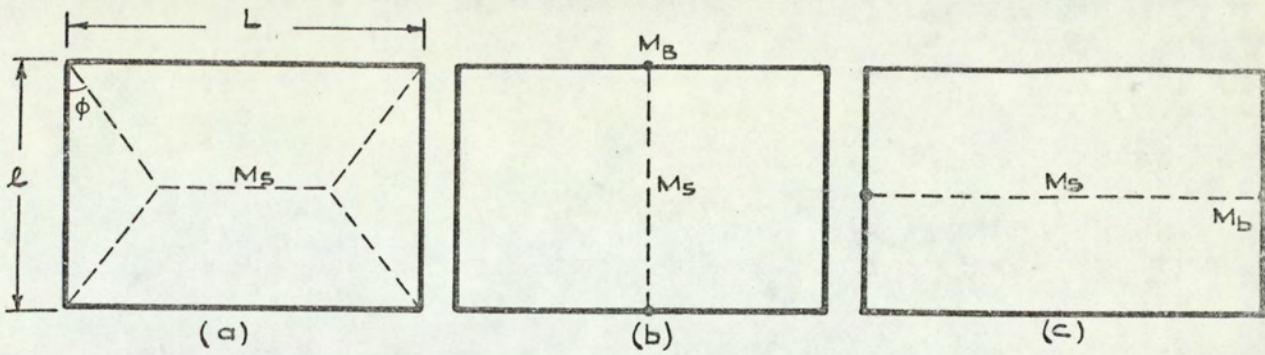


Fig. 3.3. Collapse of a simply supported rectangular slab under a U.D.L.

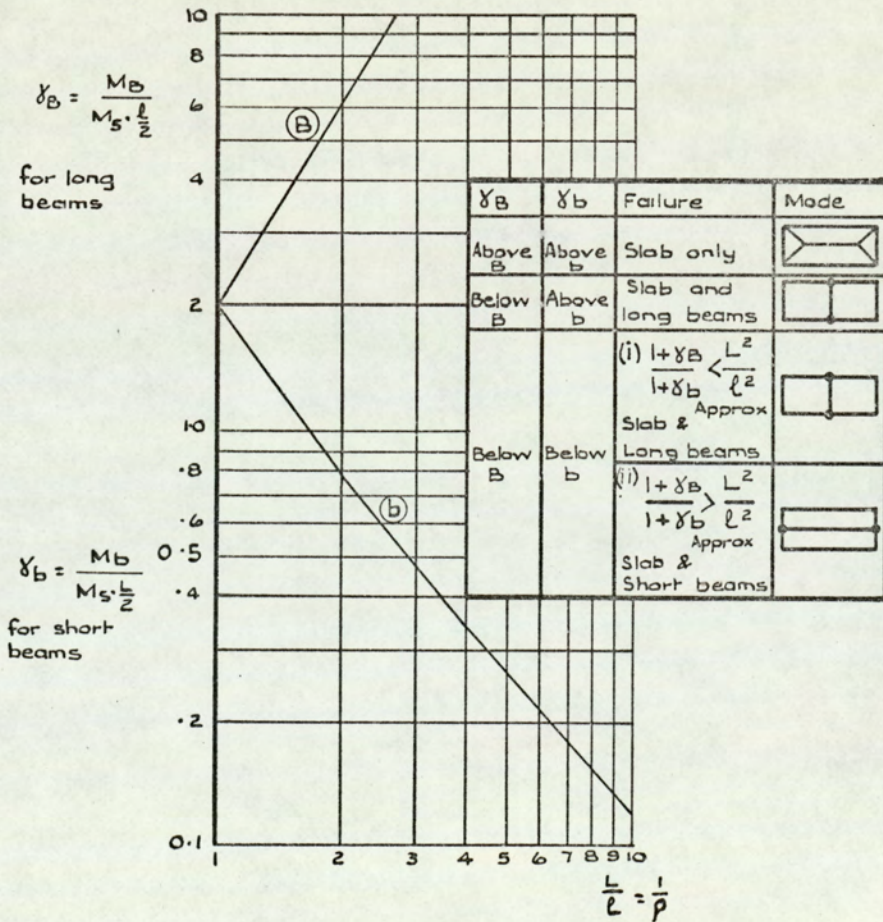


Fig. 3.4. Boundary equations for a simply supported rectangular slab. U.D.L.

$$\begin{aligned}
 &= M_s \left[\left((L - \ell \tan\phi) \times \frac{4}{\ell} + 4 \times \frac{\ell}{2} \tan\phi \times \frac{2}{\ell} \right) + \left(4 \times \frac{\ell}{2} \times \frac{2}{\ell \tan\phi} \right) \right] \\
 &= 4 M_s \left(\frac{L}{\ell} + \frac{1}{\tan\phi} \right)
 \end{aligned}$$

The external work done by applied load for a maximum deflection of a unity at the centre = p [volume of two half-pyramids + central portion]

$$= p \left[\frac{1}{3} \times 1 \times (\ell \tan\phi \times \ell) + \frac{1}{2} \times 1 \times (L - \ell \tan\phi) \times \ell \right]$$

By equating the internal work dissipated in the yield lines to the external work done by the applied load, the collapse load is found to be:-

$$p\ell L = 24 \frac{L}{\ell} \cdot \frac{1}{\tan^2\phi} \cdot M_s \quad 3.1$$

Where $\tan \phi = \sqrt{\left(\frac{\ell}{L}\right)^2 + 3} - \frac{\ell}{L}$ for a minimum value of the collapse load.

For failure of the slab and long beams Figure 3.3(b), the external work done is:-

$$\left[(p \cdot \ell \cdot \frac{L}{2} \cdot \frac{1}{2}) + (p \cdot \ell \cdot \frac{L}{2} \cdot \frac{1}{2}) \right] = p \frac{\ell L}{2} \text{ for a unit deflection of the centre}$$

yield line.

The internal work dissipated is $(M_s \cdot \ell + 2M_B)$ times the central hinge rotation $\left(\frac{1}{L/2} \cdot 2\right)$

Thus equating the external and internal work done, the collapse load is:-

$$p\ell L = 8M_s \cdot \frac{\ell}{L} + \frac{16M_B}{L} \quad 3.2$$

By similar method, the collapse load for the short beam failure, Figure 3.3(c) is given by:-

$$p\ell L = 8M_s \cdot \frac{L}{\ell} + \frac{16M_b}{\ell} \quad 3.3$$

As failure occurs at the lowest value given by equations 3.1, 3.2 and 3.3, they may be compared to give the critical "strength ratio" for change over from one mode to another. Thus comparing equations 3.1 and 3.2, collapse will be by failure of the long beams if:-

$$8 M_s \cdot \frac{l}{L} + 16 \frac{M_B}{L} < 24 \cdot M_s \cdot \frac{L}{l} \cdot \frac{1}{\tan^2 \phi}$$

Defining $\gamma_B = \frac{M_B}{M_s \cdot l/2} = \frac{\text{Plastic moment of the long beams}}{\text{Plastic moment of half short width of slab}}$

on substituting and re-arranging,

$$\gamma_B < \frac{3L^2}{l^2 \tan^2 \phi} - 1$$

i.e. if $\frac{l}{L} = \rho$ the ratio of the sides, then

$$\gamma_B < \frac{3}{\rho^2 \tan^2 \phi} - 1 \quad 3.4$$

This gives the critical "strength ratio" of the long beam to the slab for collapse to occur by failure of the long beams, and equation 3.4 may be defined as the "boundary equation" between the two modes.

Comparing the other modes of failure results in two further boundary equations being obtained. Comparing equations 3.1 and 3.3 for collapse by short beam failure,

$$\gamma_b < \frac{3}{\tan^2 \phi} - 1 \quad 3.5$$

Where $\gamma_b = \frac{M_b}{M_s \cdot l/2}$ for short beams.

Comparing equations 3.2 and 3.3 for collapse by long beam failure,

$$1 + \gamma_B < \frac{L^2}{l^2} (1 + \gamma_b)$$

or $\rho^2 < \frac{(1 + \gamma_b)}{(1 + \gamma_B)}$ 3.6

Wood⁽⁵⁹⁾ plotted these boundary equations to give the graph shown in Figure 3.4 such that the mode of failure could be determined for any given beam to slab strength ratio and hence, the collapse load calculated from the appropriate equation.

This theory will be extended in the next chapter to deal with the general cases of multi-bay continuous and non-continuous beam and slab floor systems in multi-storey buildings where composite action between the floor slabs and the supporting beams is not present.

C H A P T E R 4

DETERMINATION OF COLLAPSE LOADS BY UPPER- BOUND SOLUTIONS OF CONTINUOUS BEAM AND SLAB FLOOR SYSTEMS WITH NO COMPOSITE ACTION

4.1 INTRODUCTION

The work presented in this chapter is concerned with determining the collapse loads of structures of type (1) mentioned in Chapter 1, and hence the determination of the sizes of the supporting beams and design of the slab floors. Five different types of beam and slab floor systems, where composite action is not present, are considered, namely:-

- (1) Beam and slab floor system continuous in four directions, i.e. internal bay of multi-bay continuous frame.
- (2) Beam and slab floor system continuous in three directions, i.e. external bay of multi-bay continuous frame.
- (3) Beam and slab floor system continuous in two directions over the main beams, i.e. one bay continuous frame.
- (4) Beam and slab floor system for test M_1 , where the slab is continuous in two directions over the secondary beams.
- (5) Beam and slab floor system for test M_2 , where the slab is continuous in one direction over one secondary beam.

Internal and external bays of multi-bay continuous beam and slab floor systems are shown in Figure 4.1. It is assumed that the frame extends over many bays, where repeating internal bays are continuous in four directions, and external bays are continuous in three directions.

For the first three systems mentioned above, collapse loads corresponding to the three basic modes of collapse are found. Equations for the required fully plastic moments M_y and M_x of the secondary and main beams for collapse by modes A and B respectively are derived. Equations for the ultimate moment of the slab M_s , for independent slab collapse by

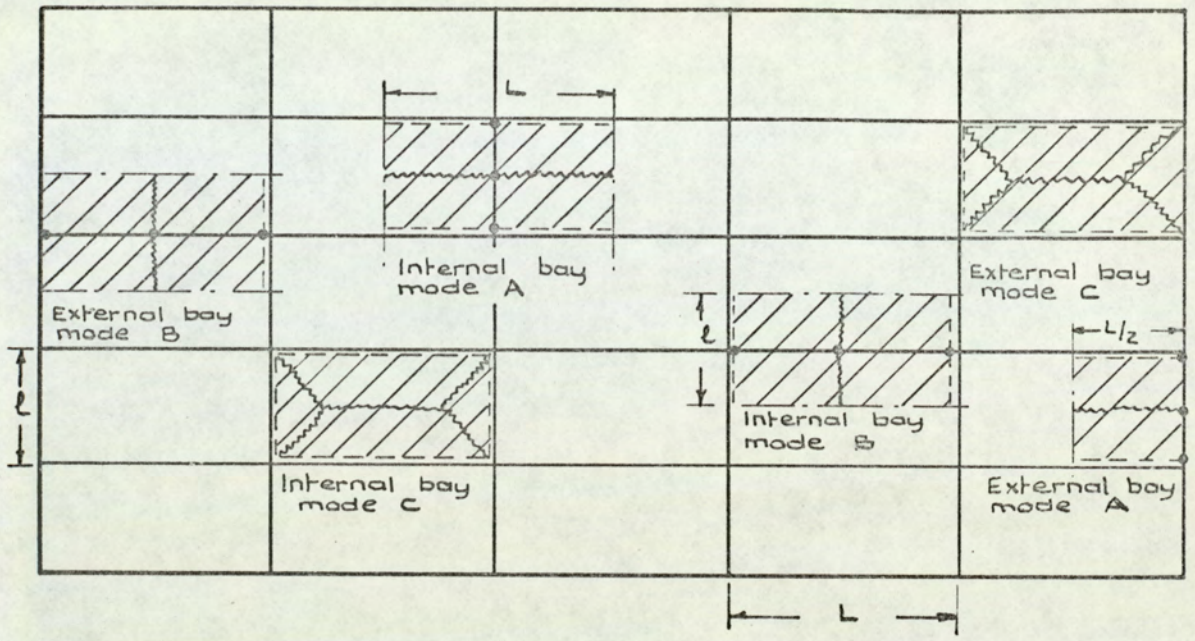


Fig. 4.1. Multi-bay continuous beam and slab floor system.

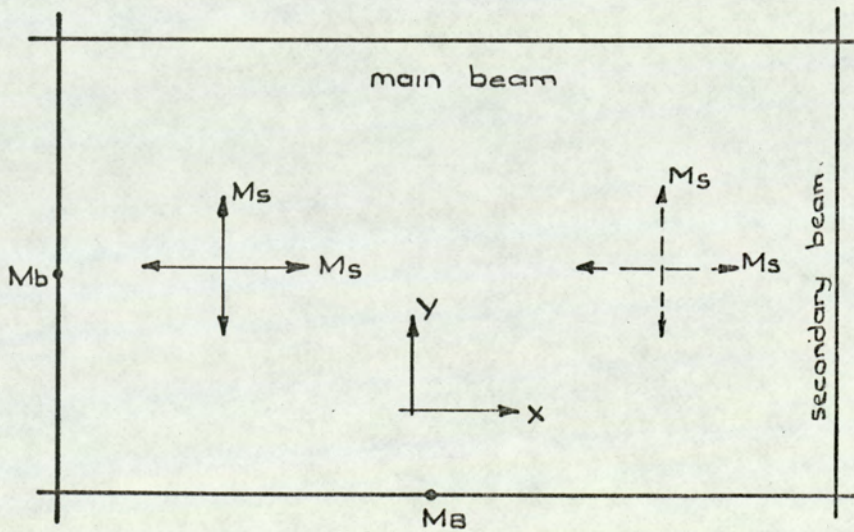


Fig. 4.2. Typical internal bay.

modes C or D are also derived. These equations are used in the computer program mentioned in Chapter 1. The program designs such systems automatically, such that collapse would occur by any of the basic mechanisms at the same applied load. Collapse loads for systems 4 and 5 above are also found.

Later in the chapter, comparisons are made of the modes of collapse for internal bay. Boundary equations between the various modes are derived and shown graphically, from which the collapse mode for any given ρ value (ratio of length of sides) may be determined. Such graphs are given as a design aid which may be used as an alternative to the computer for the more simple floor system design problem.

4.2 BEAM AND SLAB FLOOR SYSTEM CONTINUOUS IN FOUR DIRECTIONS

This corresponds to an internal bay of a multi-bay continuous frame. A typical internal bay consisting of a concrete slab on top of and continuous over four supporting beams as shown in Figure 4.2. The structure is considered under uniformly distributed loading, supported on columns at the four corners which have been designed to remain elastic up to the collapse load of the floor system. The beams spanning in the X-direction are referred to as main or edge beams, and the beams spanning in the Y-direction secondary beams. The fully plastic moments of the main and secondary beams are taken as M_B and M_b . The slab is isotropic with equal reinforcement top and bottom, thus the ultimate slab moment M_s is the same in sagging and hogging in both directions as shown in Figure 4.2.

It has been indicated in Chapter 1 that a continuous slab when loaded, can possibly collapse by any of the three basic modes. These are mode A which corresponds to collapse of the slab and secondary beams, mode B involving the collapse of the slab and main beams, and independent slab collapse by mode C or D, depending on the value of the sides ratio ρ .

The occurrence of one mode of collapse rather than the other depends on three factors, namely, the value of ρ and the two beam strengths, γ_b and γ_B . Mode A or mode B occurs with weak secondary beams or weak main beams, respectively. Modes C or D occur with strong supporting beams and relatively weak slab. Figure 4.1 shows the basic modes of collapse of internal and external bays under U.D.L. The collapse loads associated with the basic modes of failure of an internal bay are derived below.

3.2.1 Mode A

This type of failure consists of a "repeating element" of one secondary beam of length l , and a slab of width equal to the average length of the two adjacent bays. In the case of equal bays, the slab width equals the length of the bay L as shown in Figure 4.1. The failure is due to three plastic hinges forming in the secondary beam, with a sagging yield line running down the centre of the slab and two hogging yield lines running along the main beams at support as shown in Figure 4.3.

For a unit of deflection at the centre yield line, then

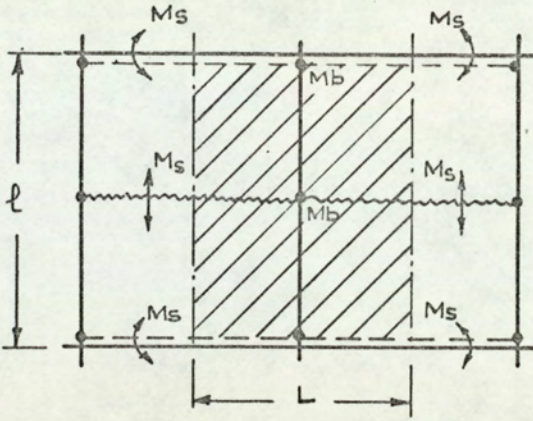
$$\theta = \frac{1}{l/2} = \frac{2}{l}$$

For a U.D.L. p /unit area of slab,

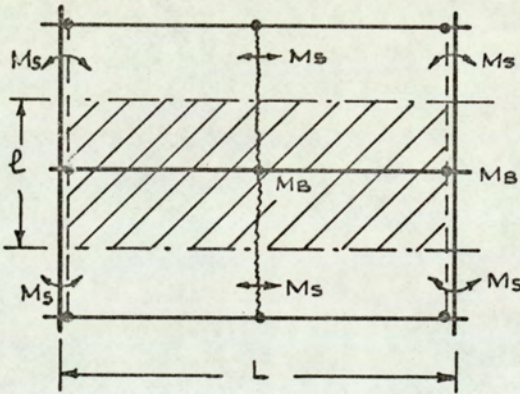
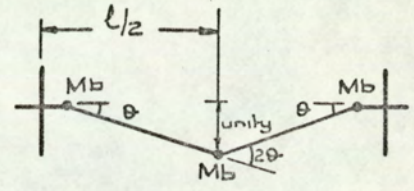
$$\begin{aligned} \text{External work (V)} &= \sum (\text{total load on an element} \times \\ &\quad \text{deflection at the centre of gravity of the load}) \\ &= pL \frac{l}{2} \times \frac{1}{2} + pL \frac{l}{2} \times \frac{1}{2} \end{aligned}$$

$$\text{thus } V = \frac{p\ell L}{2} \quad 4.1$$

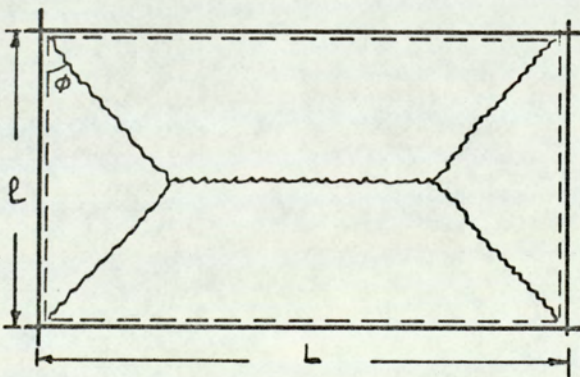
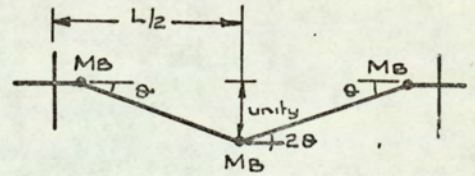
$$\text{Internal work (U)} = \sum (\text{total moment along the fracture line} \times \text{rotation about corresponding axis of rotation}) + (\text{plastic moment of the beam} \times \text{rotation of plastic hinge at that point})$$



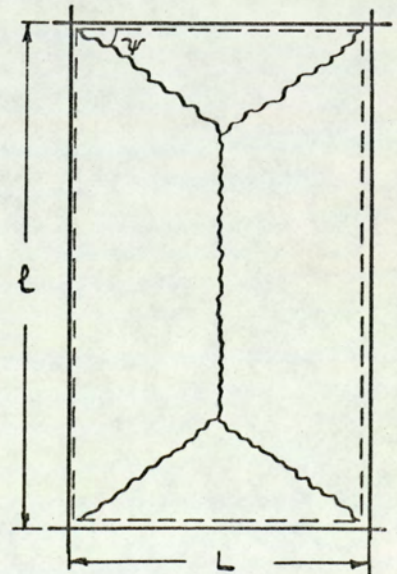
Collapse by mode A



Collapse by mode B



Collapse by mode C



Collapse by mode D

Fig. 4.3. Internal bay of multi-bay continuous frame. Basic modes of collapse for U.D.L.

$$= \sum (M_s \cdot L \cdot 2\theta + 2M_s \cdot L \cdot \theta) + (M_b \cdot \theta + M_b \cdot 2\theta + M_b \cdot \theta)$$

$$\text{thus } U = \frac{8 M_s \cdot L}{l} + \frac{8 M_b}{l} \quad 4.2$$

Equating the external and internal work done, an expression for the collapse load is obtained, namely:-

$$p \ell L = \frac{16 M_s L}{l} + \frac{16 M_b}{l} \quad 4.3$$

Re-arranging equation 4.3, the required plastic moment of the secondary beam for collapse by mode A to occur is obtained from:-

$$M_y = M_b = \frac{p \ell^2 L}{16} - M_s L \quad 4.4$$

4.2.2 Mode B

Here failure consists of a "repeating element" of one main beam and a slab of width ℓ as shown in Figure 4.1. The failure is due to three plastic hinges forming in the main beam, with three corresponding yield lines in the slab, as shown in Figure 4.3.

Following the previous method, for unit deflection at the centre yield line, $\theta = \frac{1}{l/2} = \frac{2}{l}$

$$\text{hence, } V = \left(\frac{p \ell L}{2} \times \frac{1}{2} \right) + \left(\frac{p \ell L}{2} \times \frac{1}{2} \right)$$

$$\text{thus, } V = \frac{p \ell L}{2} \quad (\text{as for mode A}) \quad 4.5$$

$$\text{and } U = (M_s \ell \cdot \theta + M_s \ell \cdot 2\theta + M_s \ell \cdot \theta) + (M_B \cdot \theta + M_B \cdot 2\theta + M_B \cdot \theta)$$

$$\therefore U = \frac{8 M_s \ell}{L} + \frac{8 M_B}{L} \quad 4.6$$

Equating equations (4.5) and (4.6), the collapse load is:-

$$p\ell L = \frac{16 M_s \ell}{L} + \frac{16 M_B}{L} \quad 4.7$$

Re-arranging equation (4.7), the required plastic moment of the main beam for collapse to occur by mode B is:-

$$M_x = M_B = \frac{p\ell L^2}{16} - M_s \ell \quad 4.8$$

4.2.3 INDEPENDENT COLLAPSE OF THE SLAB

For a uniformly distributed load, depending on the ratio of the sides, $\rho = \frac{\ell}{L}$, the two modes of collapse C or D shown in Figure 4.3 are possible.

Applying the virtual work theory, and letting the centre fracture line displace a unit distance downwards:-

$$U = \sum (\text{total moment along a fracture line} \times \text{rotation of the two elements about that line})$$

Each of these products can be resolved into the sum of two components, namely, (the projection of the moment on to each rectangular co-ordinate axis \times rotation of the elements about that axis), where the axes are parallel to the supporting sides of the rectangle.

For mode C, occurring when $\rho \leq 1.0$ (see page 55)

$$U = [4 \cdot \frac{\ell}{2} \tan\phi M_s \cdot \frac{2}{\ell} + 2 \cdot LM_s \cdot \frac{2}{\ell} + (L - \ell \tan\phi) M_s \cdot \frac{4}{\ell} + 4 \cdot \frac{\ell}{2} M_s \cdot \frac{2}{\ell \tan\phi} + 2 \cdot \ell M_s \cdot \frac{2}{\ell \tan\phi}]$$

$$\therefore U = \left[\frac{8}{\tan\phi} + \frac{8}{\rho} \right] M_s \quad 4.9$$

$V = p$ (volume of two half-pyramids + central portion)

$$V = p \left(\frac{1}{3} \ell \cdot \ell \tan\phi \cdot 1 + \frac{1}{2} \cdot \ell \cdot 1 \cdot (L - \ell \tan\phi) \right)$$

$$\therefore V = \frac{p\ell L}{6} (3 - \rho \tan\phi) \quad 4.10$$

Equating the internal and external work done, and re-arranging, the collapse load by mode C is given by:-

$$p\ell L = \frac{48}{\rho(3 - \rho \tan \phi)} \left[\frac{\rho}{\tan \phi} + 1 \right] M_s \quad 4.11$$

Where for a minimum value of p, $\tan \phi = \sqrt{\rho^2 + 3} - \rho$

The value of M_s to cause independent collapse of the slab by mode C is therefore:-

$$M_s = p\ell L \cdot \frac{\rho(3 - \rho \tan \phi)}{48 \left[\frac{\rho}{\tan \phi} + 1 \right]} \quad 4.12$$

Collapse by mode D, occurring when $\rho \geq 1.0$, can by similar means be shown to occur at a total applied load of:-

$$p\ell L = \frac{48\rho}{(3\rho - \tan \psi)} \left[\frac{1}{\tan \psi} + \rho \right] M_s \quad 4.13$$

Where for a minimum value of p, $\tan \psi = \sqrt{\frac{1}{\rho^2} + 3} - \frac{1}{\rho}$

Re-arranging equation 4.13 to find the value of M_s to cause independent slab collapse by mode D,

$$M_s = p\ell L \cdot \frac{(3\rho - \tan \psi)}{48\rho \left[\frac{1}{\tan \psi} + \rho \right]} \quad 4.14$$

4.3 BEAM AND SLAB FLOOR SYSTEM CONTINUOUS IN THREE DIRECTIONS

This corresponds to an external bay of a multi-bay continuous frame as shown in Figure 4.1. For a two-bay continuous frame, each bay is treated as an external bay, continuous in three directions as shown in Figure 4.5.

The basic modes of failure of this system are as follows:-

4.3.1 Mode A

This failure consists of one secondary beam and a slab of width equals half the length of the external bay as shown in Figure 4.1. The failure is due to three plastic hinges in the secondary beam, with three corresponding yield lines in the slab each of length $\frac{L}{2}$ as shown in Figure 4.4. The area on which the U.D.L. acts is $\frac{\ell L}{2}$.

For a unit deflection at the centre yield line, then

$$\theta = \frac{2}{\ell} \text{ and } V = p \frac{L}{2} \cdot \frac{\ell}{2} \times \frac{1}{2} + p \frac{L}{2} \cdot \frac{\ell}{2} \times \frac{1}{2}$$

$$\therefore V = \frac{p\ell L}{4} \quad 4.15$$

$$U = M_b \cdot \theta + M_b \cdot 2\theta + M_b \cdot \theta + M \frac{L}{s^2} \cdot \theta + M \frac{L}{s^2} \cdot 2\theta + M \frac{L}{s^2} \theta$$

$$\therefore U = \frac{4M_s L}{\ell} + \frac{8M_b}{\ell} \quad 4.16$$

Equating equations (4.15) and (4.16), hence the collapse load by mode A is:-

$$\frac{p\ell L}{2} = \frac{8M_s L}{\ell} + \frac{16M_b}{\ell} \quad 4.17$$

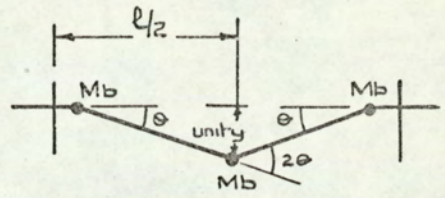
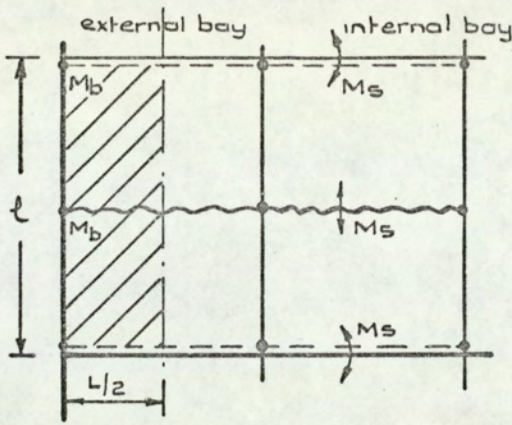
Re-arranging equation 4.17, the required M_y for collapse by mode A to occur:-

$$M_y = M_b = \frac{p\ell^2 L}{32} - \frac{M_s L}{2} \quad 4.18$$

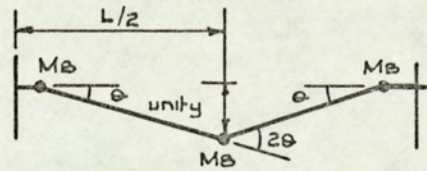
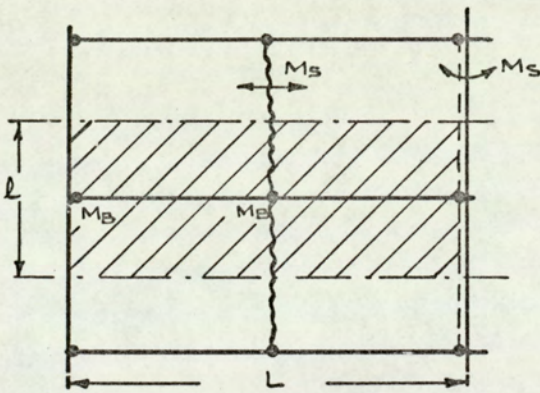
4.3.2 Mode B

Here failure consists of one main beam and a slab of width ℓ as shown in Figure 4.1. The failure is due to three plastic hinges forming in the main beam, with two corresponding yield lines in the slab as shown in Figure 4.4. For a unit deflection at the centre yield line, then

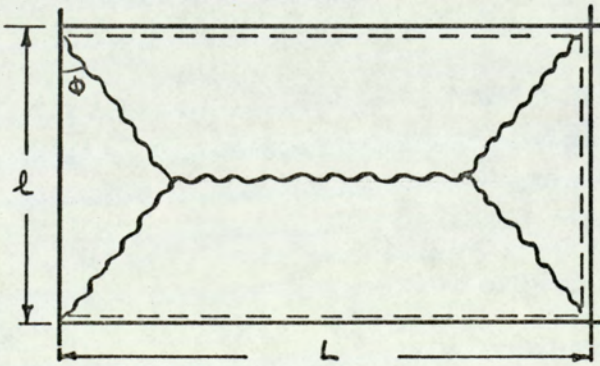
$$\theta = \frac{2}{L} \text{ and } V = \frac{p\ell L}{2} \quad (\text{As for mode B of the internal bay}) \quad 4.19$$



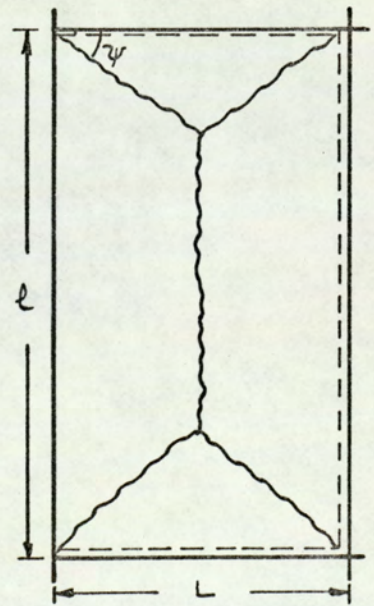
Collapse by mode A



Collapse by mode B.



Collapse by mode C



Collapse by mode D

Fig 4.4. External bay of multi-bay continuous frame. Basic modes of collapse for U.D.L.

$$U = M_s \ell \cdot 2\theta + M_s \ell \cdot \theta + M_B \cdot \theta + M_B \cdot 2\theta + M_B \cdot \theta$$

$$\therefore U = \frac{6M_s \ell}{L} + \frac{8M_B}{L} \quad 4.20$$

Equating equations (4.19) and (4.20), the collapse load by mode B is:-

$$p\ell L = \frac{12M_s \ell}{L} + \frac{16M_B}{L} \quad 4.21$$

Re-arranging equation 4.21, to obtain the value of M_x for collapse by mode B to occur:-

$$M_x = M_B = \frac{p\ell L^2}{16} - \frac{3M_s \ell}{4} \quad 4.22$$

4.3.3 INDEPENDENT COLLAPSE OF THE SLAB

For a uniformly distributed loading, depending on the sides ratio ρ , the two modes of collapse C or D shown in Figure 4.4 are possible. By a similar method to that used for an internal bay,

For mode C, occurring when $\rho \leq 1.155$, the collapse load is:-

$$p\ell L = \frac{24}{\rho(3 - \rho \tan \phi)} \left[\frac{3\rho}{2 \tan \phi} + 2 \right] M_s \quad 4.23$$

Where for a minimum value of p , $\tan \phi = \frac{3}{4} \left(\sqrt{\rho^2 + 4} - \rho \right)$

From equation 4.23, the required M_s to cause independent slab collapse is:-

$$M_s = p\ell L \cdot \frac{\rho(3 - \rho \tan \phi)}{24 \left[\frac{3\rho}{2 \tan \phi} + 2 \right]} \quad 4.24$$

For mode D, occurring when $\rho \geq 1.155$, the collapse load is:-

$$p\ell L = \frac{24\rho}{(3\rho - \tan \psi)} \left[\frac{2}{\tan \psi} + \frac{3}{2} \rho \right] \cdot M_s \quad 4.25$$

Where $\tan \psi = \frac{4}{3\rho} \left[\sqrt{1 + \frac{9}{4} \rho^2} - 1 \right]$ for minimum p

$$\text{Hence } M_s = p\ell L \cdot \frac{(3\rho - \tan \psi)}{24\rho \left[\frac{2}{\tan \psi} + \frac{3}{2} \rho \right]} \quad 4.26$$

4.4 BEAM AND SLAB FLOOR SYSTEM CONTINUOUS IN TWO DIRECTIONS

This corresponds to a one-bay continuous frame, where the slab is continuous over the main beams as shown in Figure 4.6. The equations of the basic modes of failure are derived below.

4.4.1 Mode A

This type of failure consists of two secondary beams and a slab of width equal to the length of the bay L . The failure is due to three hinges on each of the secondary beams, together with three corresponding yield lines in the slab, as shown in Figure 4.7. By similar methods to those used previously, the collapse load by mode A is:-

$$p\ell L = \frac{16 M_s L}{\ell} + \frac{32 M_b}{\ell} \quad 4.27$$

$$\text{and } M_y = M_b = \frac{p\ell^2 L}{32} - \frac{M_s L}{2} \quad 4.28$$

4.4.2 Mode B

This failure consists of one main beam and a slab of width ℓ . The failure is due to three plastic hinges in the main beam and only one sagging yield line running down the centre, as shown in Figure 4.7.

Here:-

$$p\ell L = \frac{8 M_s \ell}{L} + \frac{16 M_B}{L} \quad 4.29$$

$$\text{and } M_x = M_B = \frac{p\ell L^2}{16} - \frac{M_s \ell}{2} \quad 4.30$$

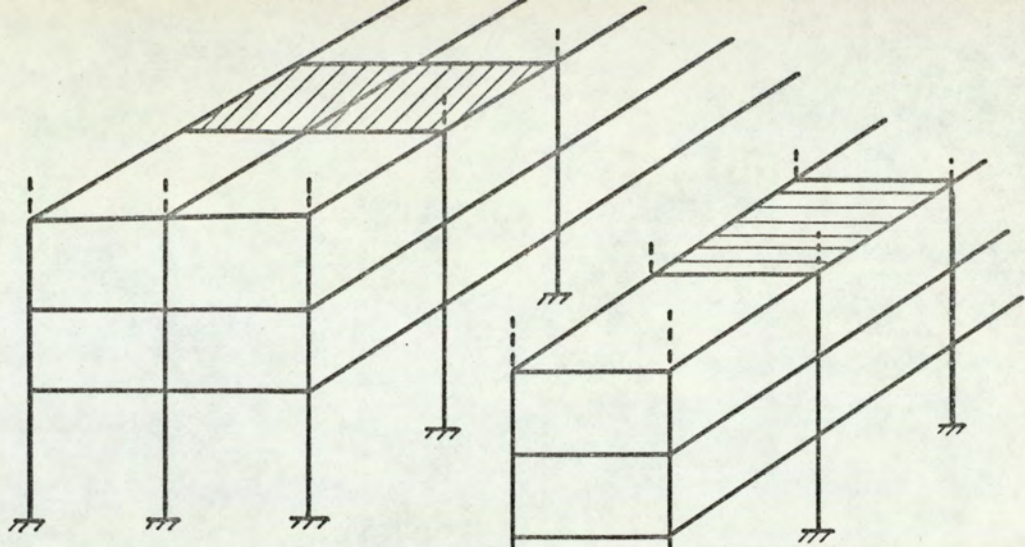


Fig. 4.5. Two-bay continuous frame.

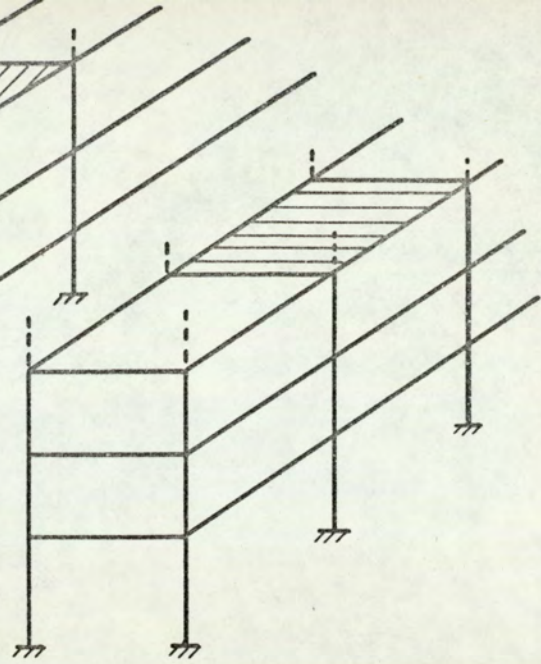
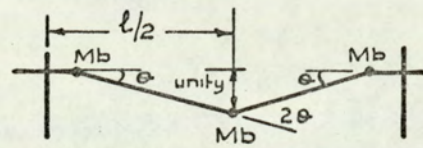
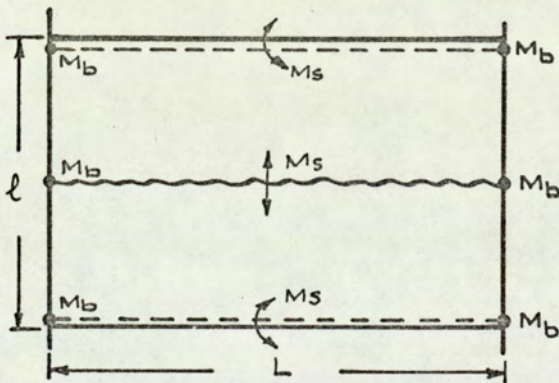
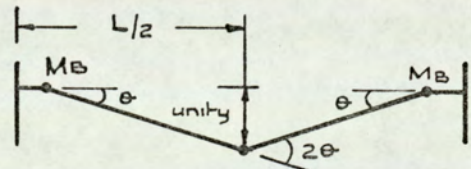
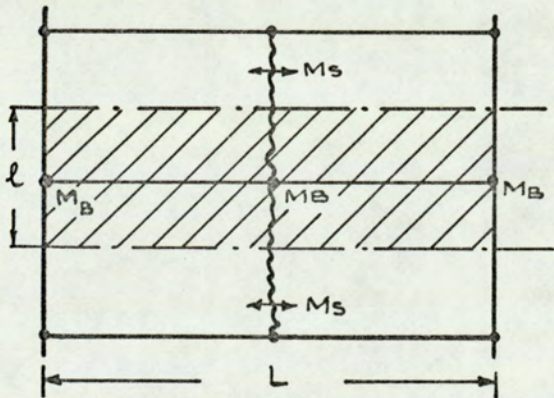


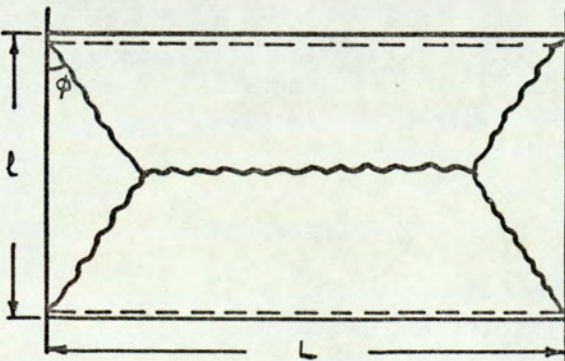
Fig 4.6. One-bay continuous frame



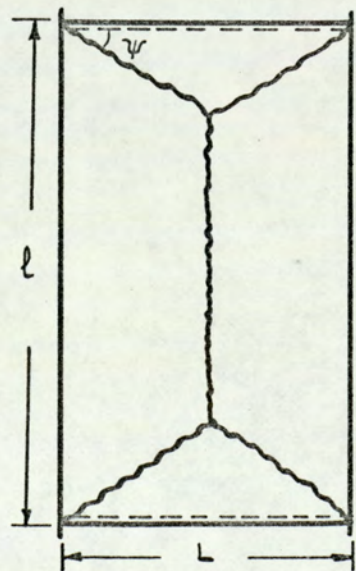
Collapse by mode A



Collapse by mode B



Collapse by mode C.



Collapse by mode D

Fig. 4.7. Basic modes of collapse for one bay continuous frame. U.D.L.

4.4.3 INDEPENDENT COLLAPSE OF SLAB

For a U.D.L., depending on ρ , the two modes of collapse C or D shown in Figure 4.7 are possible.

For mode C, occurring when $\rho \leq \sqrt{2}$ (see page 56)

$$p\ell L = \frac{24}{\rho(3 - \rho \tan\phi)} \cdot \left[\frac{\rho}{\tan\phi} + 2 \right] \cdot M_s \quad 4.31$$

Where $\tan \phi = \frac{1}{2} \left(\sqrt{\rho^2 + 6} - \rho \right)$ for minimum p

$$\text{and } M_s = p\ell L \cdot \frac{\rho(3 - \rho \tan \phi)}{24 \left[\frac{\rho}{\tan \phi} + 2 \right]} \quad 4.32$$

Mode D, occurring when $\rho \geq \sqrt{2}$

$$p\ell L = \frac{24\rho}{(3\rho - \tan\psi)} \left[\frac{2}{\tan\psi} + \rho \right] \cdot M_s \quad 4.33$$

Where $\tan \psi = \sqrt{\frac{4}{\rho^2} + 6} - \frac{2}{\rho}$ for minimum p

$$\text{and } M_s = p\ell L \cdot \frac{(3\rho - \tan \psi)}{24\rho \left[\frac{2}{\tan \psi} + \rho \right]} \quad 4.34$$

4.5 BEAM AND SLAB FLOOR SYSTEM FOR TEST M₁

This system represents a model tested to destruction in the experimental part of this work. Collapse of the system occurred by mode B. This represents failure of a multi-storey building frame owing to vertical loads only, i.e. no wind loads. In the models M₁ and M₂, the slab was composite with the supporting beams. Collapse loads in this section and the next one are found for the basic modes of failure of systems M₁ and M₂ assuming that no composite action is to be present. These will be used

in a later chapter for comparison with collapse loads of similar systems when composite action is present, to show the advantages of such construction.

The system comprises two main "edge" beams and two secondary beams with a slab at the top continuous over the secondary beams. Collapse loads by the basic modes of failure are as follows:-

4.5.1 Mode A

This failure consists of two secondary beams and a slab of width L . The failure is due to three plastic hinges on each of the secondary beams, and one corresponding sagging yield line running down the centre, as shown in Figure 4.8. By similar methods, collapse load by mode A occurs when:-

$$p\ell L = \frac{8 M_s L}{\ell} + \frac{32 M_b}{\ell} \quad 4.35$$

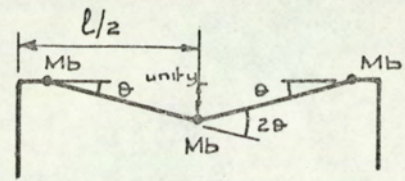
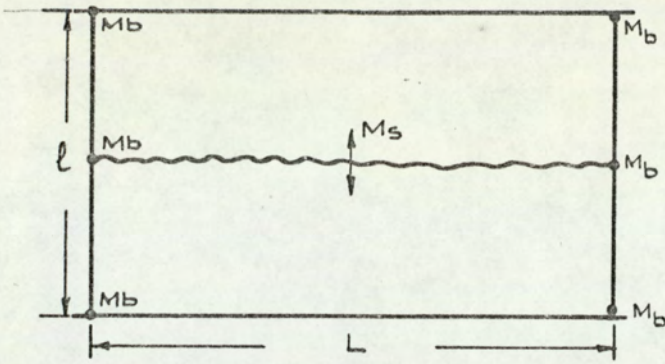
In models M_1 and M_2 , the secondary beams are considered not rigidly jointed. Thus, secondary beam plastic hinges at the supports would not develop, as shown in Figure 4.8. Failure would then be due to the formation of one plastic hinge at the centre of each beam, plus a yield line running down the centre. For collapse by mode A, equation 4.35 then becomes:-

$$p\ell L = \frac{8 M_s L}{\ell} + \frac{16 M_b}{\ell} \quad 4.36$$

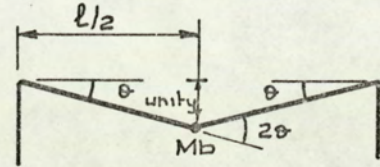
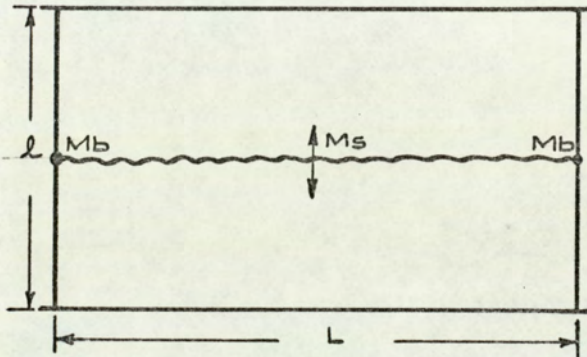
4.5.2 Mode B

Here failure consists of two main "edge" beams and a slab of width ℓ . The failure is due to three plastic hinges forming on each of the main beams and three corresponding yield lines, as shown in Figure 4.8. Thus the collapse load would be:-

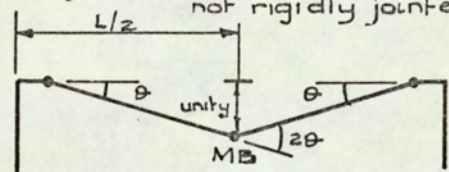
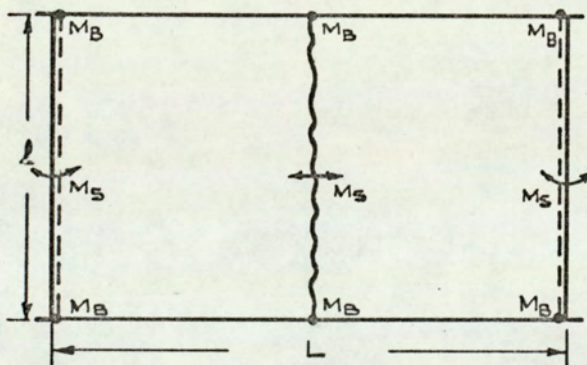
$$p\ell L = \frac{16 M_s \ell}{L} + \frac{32 M_b}{L} \quad 4.37$$



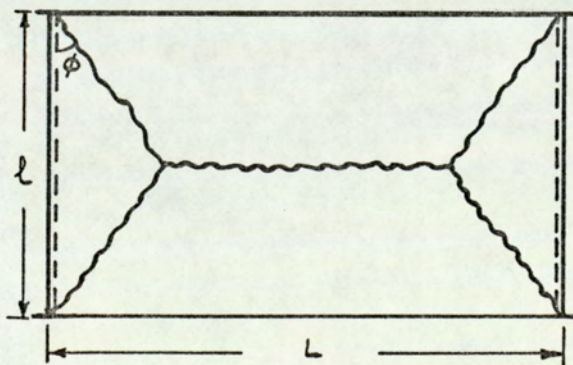
Collapse load by mode A (secondary beams at supports are rigidly jointed)



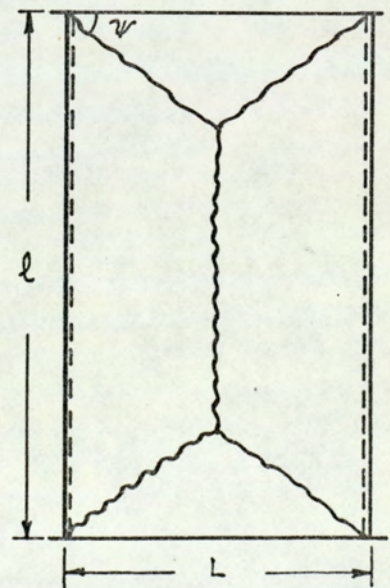
Collapse load by mode A (secondary beams at supports are not rigidly jointed).



Collapse by mode B



Collapse by mode C



Collapse by mode D.

Fig. 4.8. Basic modes of collapse for test M1. U.D.L.

4.5.3 INDEPENDENT COLLAPSE OF SLAB

For U.D.L., depending on the value of ρ , the two modes of collapse C or D, as shown in Figure 4.8, are possible.

Mode C occurs when $\rho \leq \frac{1}{\sqrt{2}}$, and the collapse load is:-

$$p\ell L = \frac{2l_t}{\rho(3 - \rho \tan\phi)} \left[\frac{2\rho}{\tan\phi} + 1 \right] \cdot M_s \quad 4.38$$

$$\text{Where } \tan\phi = \sqrt{4\rho^2 + 6} - 2\rho \quad \text{for minimum } p$$

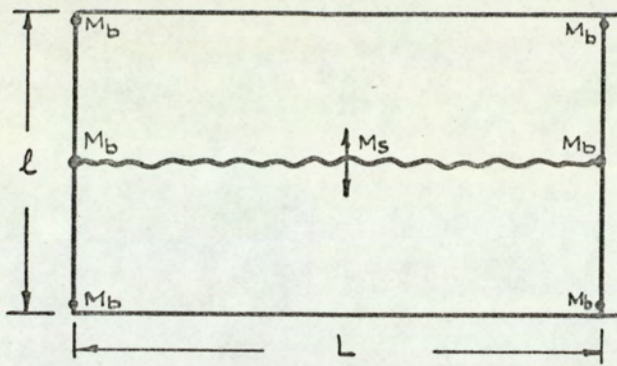
Independent slab collapse by mode D occurs when $\rho \geq \frac{1}{\sqrt{2}}$, and the collapse load is:-

$$p\ell L = \frac{2l_t\rho}{(3\rho - \tan\psi)} \left[\frac{1}{\tan\psi} + 2\rho \right] \cdot M_s \quad 4.39$$

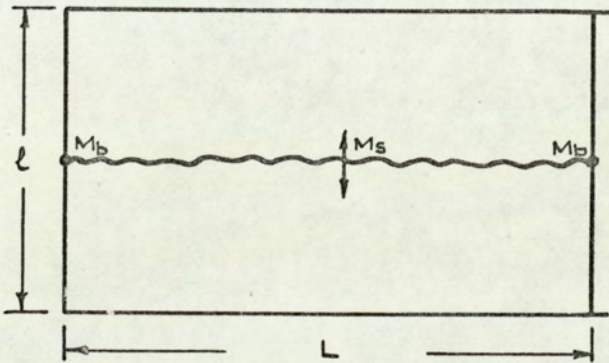
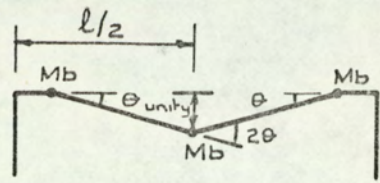
$$\text{Where } \tan\psi = \frac{1}{2} \left(\sqrt{\frac{1}{\rho^2} + 6} - \frac{1}{\rho} \right) \quad \text{for minimum } p$$

4.6 BEAM AND SLAB FLOOR SYSTEM FOR TEST M₂

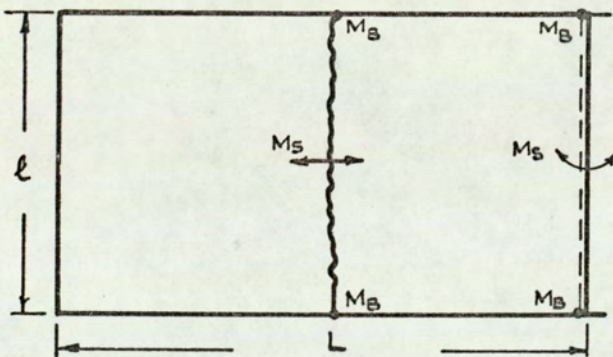
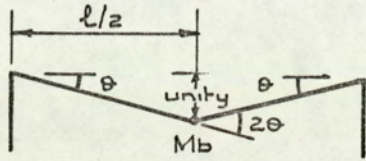
Again this system represents a model tested to destruction in the experimental part of this work. Collapse of this system occurs by mode B. This represents failure owing to a "combined mechanism" which is usually the critical design criteria for the intermediate storeys of multi-storey buildings. The system is exactly the same as that of the previous section, except that the slab and the main "edge" beams are not continuous at the windward end (L.H.S.). At that end, a hinge cancellation usually occurs in this type of failure mechanism, as shown in Figure 4.9 (mode B). Equations of collapse loads by the three basic modes of failure are given below:-



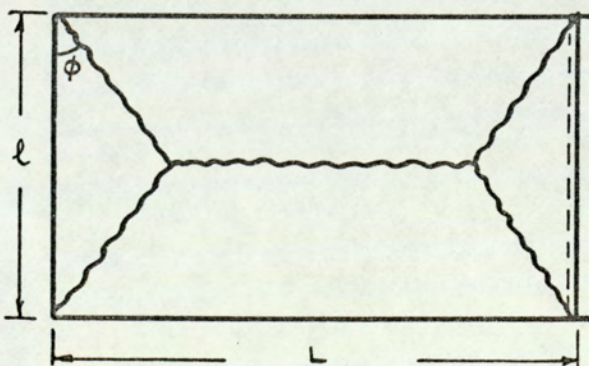
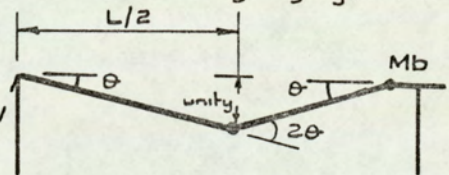
Collapse by mode A (secondary beams at supports are rigidly jointed)



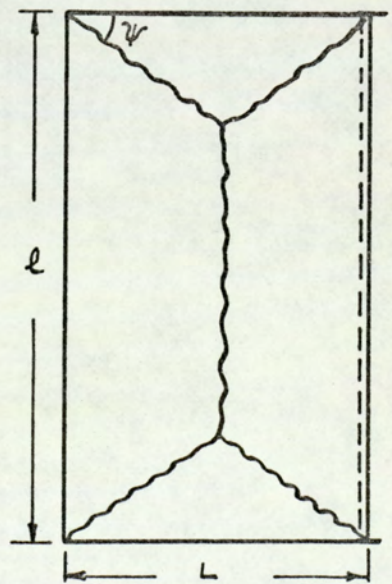
Collapse by mode A (secondary beams at supports are not rigidly jointed)



Collapse by mode B



Collapse by mode C



Collapse by mode D

Fig. 4.9 Basic modes of collapse for test M_2 U.D.L.

4.6.1 Mode A

This failure is exactly the same as that of the previous section, as shown in Figure 4.9, and equations 4.35 and 4.36 may be used to evaluate the collapse load.

4.6.2 Mode B

Here failure consists of two main "edge" beams and a slab of width l . A hinge cancellation is assumed at the windward end. Failure occurs owing to two plastic hinges only forming on each of the main beams, together with two corresponding yield lines, as shown in Figure 4.9. The collapse load is thus:-

$$p\ell L = \frac{12 M_s \ell}{L} + \frac{24 M_B}{L} \quad 4.40$$

4.6.3 INDEPENDENT COLLAPSE OF SLAB

For a U.D.L., depending on the value of ρ , the two modes of collapse C or D, as shown in Figure 4.9, are possible.

For mode C, occurring when $\rho \leq 0.82$, the collapse load is:-

$$p\ell L = \frac{24}{\rho(3 - \rho \tan\phi)} \left[\frac{3\rho}{2 \tan\phi} + 1 \right] \cdot M_s \quad 4.41$$

$$\text{Where } \tan \phi = \frac{3}{2} \left(\sqrt{\rho^2 + 2} - \rho \right) \text{ for minimum } p$$

For mode D, occurring when $\rho \geq 0.82$, the collapse load is:-

$$p\ell L = \frac{24\rho}{(3\rho - \tan\psi)} \left[\frac{1}{\tan\psi} + \frac{3}{2} \rho \right] \cdot M_s \quad 4.42$$

$$\text{Where } \tan \psi = \frac{2}{3} \left(\sqrt{\frac{1}{\rho^2} + \frac{9}{2}} - \frac{1}{\rho} \right) \text{ for minimum } p$$

4.7 COMPARISON OF COLLAPSE MODES OF THE INTERNAL BAY

The internal bay of section 4.2 was taken to illustrate the design of beam and slab floor systems by using charts similar to that of Figure 4.12.

Values of the collapse load determined in section 4.2 for the internal bay by the various modes are compared to determine which mode will occur for any given ρ value. One method of finding this is simply to calculate the collapse given by these various equations, and to select the least value as being the actual collapse load. However, by comparing the modes and combining the results on one graph, more valuable information is obtained as to the likelihood of the modes occurring. The various beam to slab strength ratios required to change from one mode to another will also be known by the use of such charts.

4.7.1 COMPARISON OF MODES A AND C

For a U.D.L., collapse will occur by mode A if the value of the collapse load $p\ell L$ given by equation 4.3 is less than that given by equation 4.11, i.e. if :-

$$\frac{16 M_s L}{\ell} + \frac{16 M_b}{\ell} < \frac{48}{\rho(3 - \rho \tan \phi)} \left[\frac{\rho}{\tan \phi} + 1 \right] \cdot M_s$$

Dividing through by M_s and introducing

$$\gamma_b = \frac{M_b}{M_s \cdot \ell / 2} = \frac{\text{Plastic moment of secondary beam}}{\text{Plastic moment of adjacent half width of slab}}$$

$$\text{then, } \frac{2}{\rho} + \frac{\gamma_b}{\rho} < \frac{6}{\rho(3 - \rho \tan \phi)} \left[\frac{\rho}{\tan \phi} + 1 \right]$$

$$\text{or } \gamma_b < \frac{6}{(3 - \rho \tan \phi)} \left[\frac{\rho}{\tan \phi} + 1 \right] - 2 \quad 4.43$$

As $\tan \phi$ is a function of ρ , γ_b can be plotted against ρ to give the graph shown in Figure 4.10 up to the value of $\rho = 1.0$. Values of $\frac{M_b}{M_s \cdot \ell / 2}$

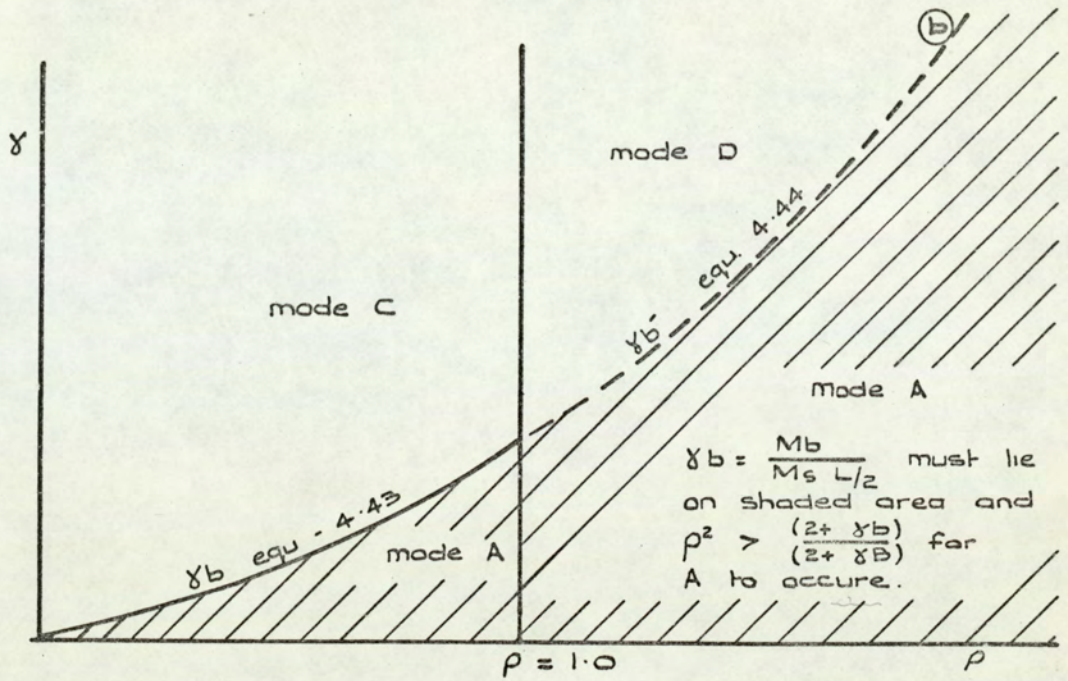


Fig. 4.10. Comparison of collapse modes for internal bay. U.D.L. for mode A to occur.

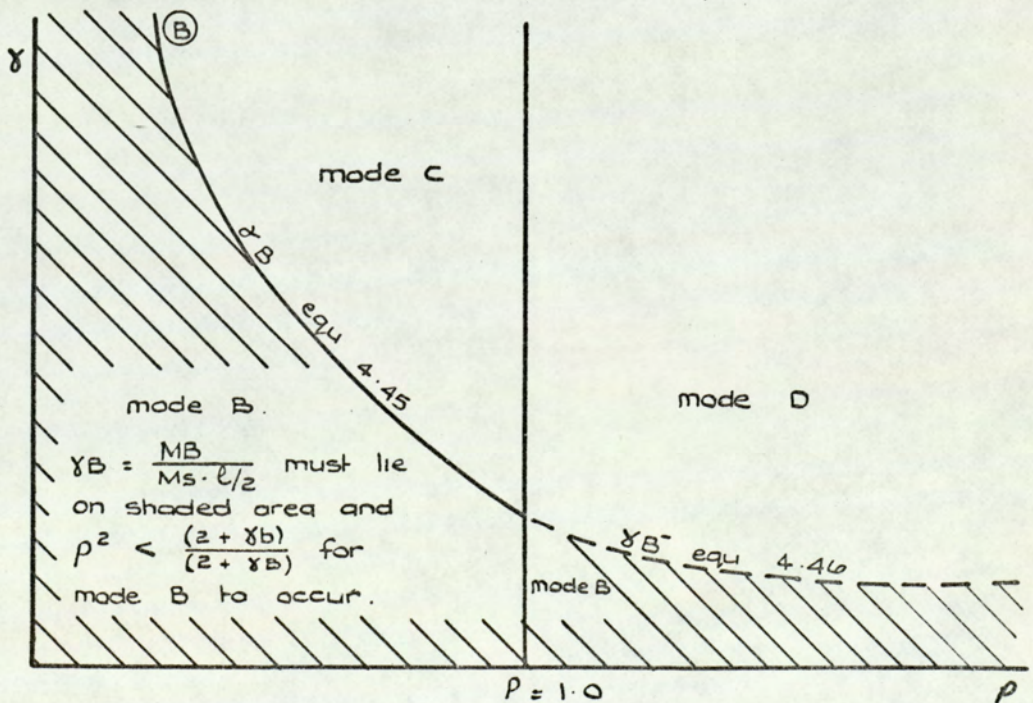


Fig. 4.11. Comparison of collapse modes for internal bay. U.D.L. for mode B to occur.

which are under the curve in the shaded area for a given ρ value corresponds to collapse by mode A and values lying above, to mode C. Hence, equation 4.43 is the "boundary equation" between these two modes.

4.7.2 COMPARISON OF MODES A AND D

Collapse will occur by mode A if $p\ell L$ given by equation 4.3 is less than that given by equation 4.13.

$$\text{or } \frac{16 M_s L}{\ell} + \frac{16 M_b}{\ell} < \frac{48p}{(3\rho - \tan \psi)} \left[\frac{1}{\tan \psi} + \rho \right] \cdot M_s$$

$$\text{Using } \gamma'_b = \frac{M_b}{M_s \cdot L/2}$$

$$\text{then } \gamma'_b < \frac{6\rho^2}{(3\rho - \tan \psi)} \left[\frac{1}{\tan \psi} + \rho \right] - 2 \quad 4.44$$

γ'_b can be plotted against ρ for values of $\rho \geq 1.0$, i.e. where change over from mode C to mode D occurs. This gives the continuation of the graph of Figure 4.10 shown as a dotted line.

4.7.3 COMPARISON OF MODES B AND C

Comparing equations 4.7 and 4.11 for collapse by mode B.

$$\frac{16 M_s \ell}{L} + \frac{16 M_B}{L} < \frac{48}{\rho(3 - \rho \tan \phi)} \left[\frac{\rho}{\tan \phi} + 1 \right] \cdot M_s$$

Introducing $\gamma_B = \frac{M_B}{M_s \cdot \ell/2}$ and re-arranging, this condition becomes:-

$$\gamma_B < \frac{6}{\rho^2(3 - \rho \tan \phi)} \left[\frac{\rho}{\tan \phi} + 1 \right] - 2 \quad 4.45$$

Similarly, values of γ_B are plotted against ρ , for values of ρ up to 1.0 as shown in Figure 4.11. Values of γ_B in the shaded area for a given ρ value correspond to collapse by mode B, and values lying above, to mode C.

4.7.4 COMPARISON OF MODES B AND D

Comparing equations 4.7 and 4.13, for collapse by mode B.

$$\frac{16 M_s \ell}{L} + \frac{16 M_B}{L} < \frac{48\rho}{(3\rho - \tan \psi)} \left[\frac{1}{\tan \psi} + \rho \right] \cdot M_s$$

Using $\gamma'_B = \frac{M}{M_s \cdot \ell/2}$

$$\gamma'_B < \frac{6}{(3\rho - \tan \psi)} \left[\frac{1}{\tan \psi} + \rho \right] - 2 \quad 4.46$$

Similarly, values of γ_B are plotted against ρ for values of $\rho \geq 1.0$, where mode D takes over from mode C. This is shown as a dotted line in Figure 4.11.

4.7.5 COMPARISON OF MODES A AND B

Comparing equations 4.3 and 4.7, collapse will be by mode B if:-

$$\frac{16 M_s \ell}{L} + \frac{16 M_B}{L} < \frac{16 M_s L}{\ell} + \frac{16 M_b}{\ell}$$

Dividing by M_s and introducing

$$\gamma_b = \frac{M_b}{M_s \cdot L/2} \quad \text{and} \quad \gamma_B = \frac{M_B}{M_s \cdot \ell/2}$$

then collapse by mode B rather than mode A occurs when

$$\rho^2 < \frac{(2 + \gamma_b)}{(2 + \gamma_B)} \quad 4.47$$

This may be compared to Wood's⁽⁵⁹⁾ value for collapse of slab and long beams as opposed to slab and short beams.

$$\rho^2 < \frac{(1 + \gamma_b)}{(1 + \gamma_B)} \quad 3.6$$

If $\gamma_b = \gamma_B$, then $\rho < 1.0$ from equation 4.47, compared with Wood's⁽⁵⁹⁾ value of $\rho < 1.0$ from equation 3.6 for collapse by mode B. This means that the

chance of mode B occurring is the same when the slab is simply supported or continuous in four directions.

Finally, the curves given in Figures 4.10 and 4.11 may be combined to give Figure 4.12, from which the collapse mode for any given ρ value may be determined. Charts for slabs with other boundary conditions can be similarly drawn.

It will be seen then that once the two beam to slab strength ratios have been determined, the mode of failure can be found and the value of collapse load calculated from the appropriate equation.

4.8 CHANGE OVER FROM MODE C TO MODE D

Change over from mode C to mode D occurs at a value of ρ depending on the boundary conditions of the slab and is independent of " γ values".

In the case of an internal bay, where the slab is continuous in four directions, the change over from equation 4.11 (mode C) to equation 4.13 (mode D) occurs at $\rho = 1$. In these two equations, for a minimum value of ρ ,

$$\tan \phi = \sqrt{\rho^2 + 3} - \rho \quad \text{and} \quad \tan \psi = \sqrt{\frac{1}{\rho^2} + 3} - \frac{1}{\rho}$$

At $\rho = 1$, $\tan \phi = \tan \psi = 1$. Hence $\phi = 45^\circ$ at the point of change over from mode C to mode D, and $\psi = 45^\circ$ at the beginning of mode D for the same corner as shown in Figure 4.3. Hence,

$$\phi + \psi = 90^\circ \tag{4.48}$$

$$\tan \phi = \tan (90 - \psi) = \cot \psi \tag{4.49}$$

Hence, at the point of change over from mode C to mode D

$$\tan \phi \cdot \tan \psi = 1 \tag{4.50}$$

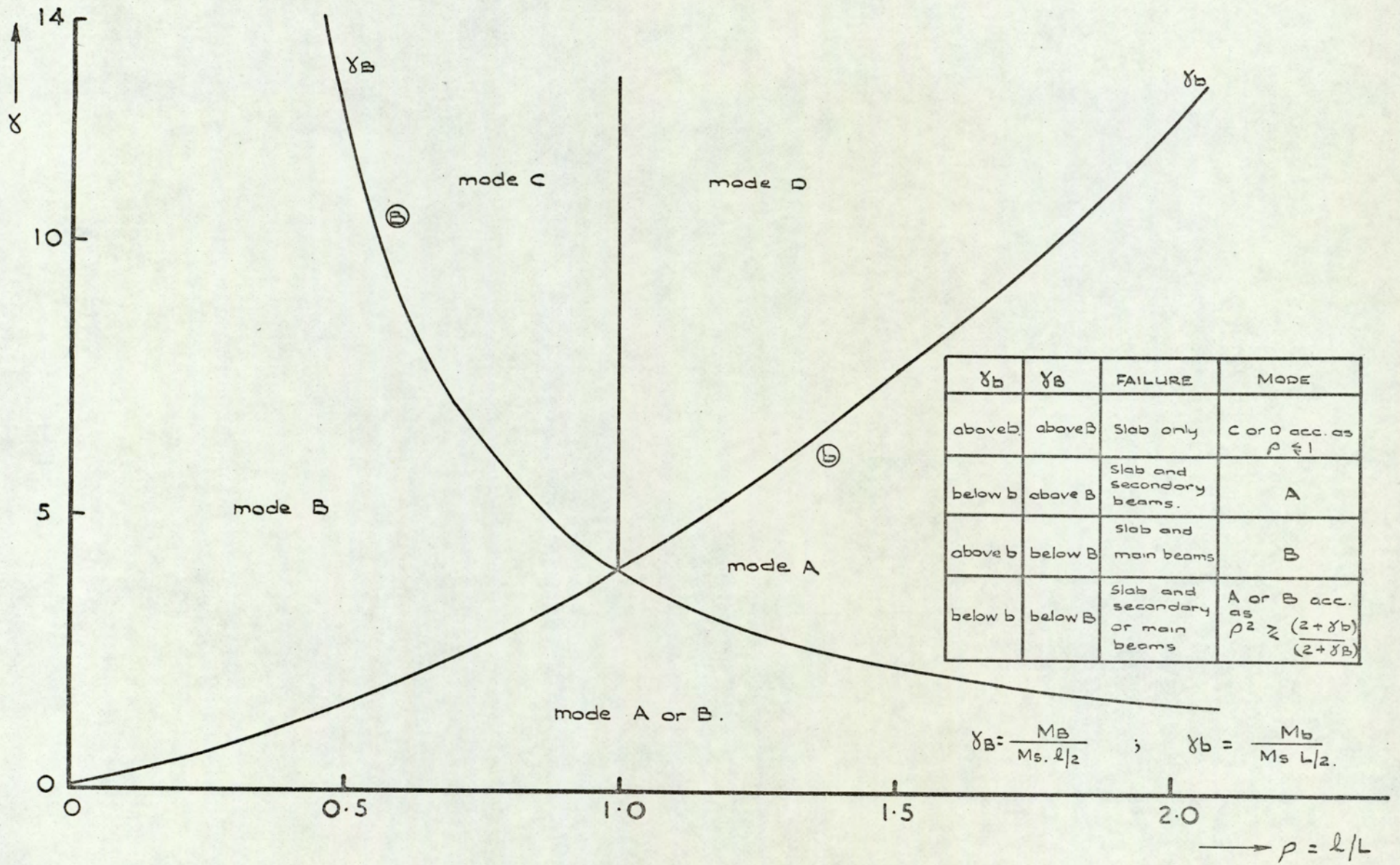


Fig. 4.12. Boundary equations. U.D.L. no composite action. slab continuous in four directions.

At the point of change over from mode C to mode D, the collapse load by the two modes should be the same. Substituting the values of $\tan \phi$ and $\tan \psi$ at $\rho = 1$ in equations 4.11 and 4.13 gives the same collapse load of $48 M_s$ for both modes. This satisfies equation 4.50 and proves that $\rho = 1$ is the point of change over from mode C to mode D.

For slabs with other boundary conditions, change over from mode C to mode D does not necessarily occur at $\rho = 1$. For example, in the case of one bay continuous frame, where the slab is continuous in two directions, change over occurs at $\rho = \sqrt{2}$. To find this value of ρ , equations 4.31 and 4.33 must give identical values of $p\ell L$ at the point of change over, i.e.

$$\frac{24}{\rho(3 - \rho \tan \phi)} \left[\frac{\rho}{\tan \phi} + 2 \right] \cdot M_s = \frac{24\rho}{(3\rho - \tan \psi)} \left[\frac{2}{\tan \psi} + \rho \right] \cdot M_s$$

$$\text{or} \quad \frac{(3\rho - \tan \psi) \left(\frac{\rho}{\tan \phi} + 2 \right)}{\rho^2 (3 - \rho \tan \phi) \left(\frac{2}{\tan \psi} + \rho \right)} = 1 \quad 4.51$$

Where for a minimum value of p

$$\tan \phi = \frac{1}{2} \left(\sqrt{\rho^2 + 6} - \rho \right) \quad \text{and} \quad \tan \psi = \sqrt{\frac{4}{\rho^2} + 6} - \frac{2}{\rho}$$

Substituting the values of $\tan \phi$ and $\tan \psi$ in equation 4.51 and solving for ρ could be very tedious. One way of solving such equations is by numerical methods. Thus, values of $\tan \phi$ and $\tan \psi$ could be found for a given value of ρ and substituted into equation 4.51. This procedure is repeated until a value of ρ satisfies equation 4.51, which will be the value when change over from mode C to mode D occurs. A better way of finding that particular value of ρ is by satisfying equation 4.50. In the case of one bay continuous frame, at $\rho = \sqrt{2}$, $\tan \phi = \frac{1}{\sqrt{2}}$ and

$\tan \psi = \sqrt{2}$. Hence, $\tan \phi \cdot \tan \psi = \frac{1}{\sqrt{2}} \times \sqrt{2} = 1$ which satisfy equation

4.50. This shows that $\rho = \sqrt{2}$ is the point of change over from mode C to mode D. To prove this again substituting the values of $\tan \phi$ and $\tan \psi$, at $\rho = \sqrt{2}$ into equations 4.31 and 4.33, collapse by modes C and D occur at the same load of $24 \sqrt{2} M_s$.

4.9 DESIGN PROCEDURE FOR THE SLAB MOMENT AND BEAM SIZES USING CHARTS

From the graph in Figure 4.12, it is possible to design a slab and obtain the sizes of the supporting beams for a given mode of collapse, knowing the loading and dimensions of one bay.

Both equations 4.12 and 4.14 are of the form $M_s = f(\rho) \cdot p \cdot l \cdot l$ and, for convenience, Figure 4.13 shows a graph of $f(\rho)$ against ρ . Knowing the value of the sides ratio ρ , the slab moment could easily be calculated with the aid of Figure 4.13. Figure 4.12 gives the critical values of the strength ratios γ_b and γ_B for collapse by any mode. Thus with M_s , l and L known, M_b and M_B can be calculated for the given mode. For independent collapse of the slab, the minimum beam sizes will be given, and for collapse involving the supporting beam, the minimum size of this beam to cause it just to fail is obtained.

4.10 EXAMPLE

For a load of 175 lb/sq.ft. (including an allowance for the dead load using a 6" thick slab) on a rectangular internal bay 30' long and 20' wide. Then with $\rho = \frac{2}{3}$, equation 4.12 or Figure 4.13 gives the minimum slab moment equal to 3,601 lb.ft./ft. run, with a load factor of 1.75.

From Figure 4.12, with $\rho = 0.67$, the critical strength ratios for independent collapse of the slab are:-

$$\frac{M_B}{M_s \cdot l/2} (\gamma_B) > 7.5 \quad \text{and} \quad \frac{M_b}{M_s \cdot L/2} (\gamma_b) > 2.25$$

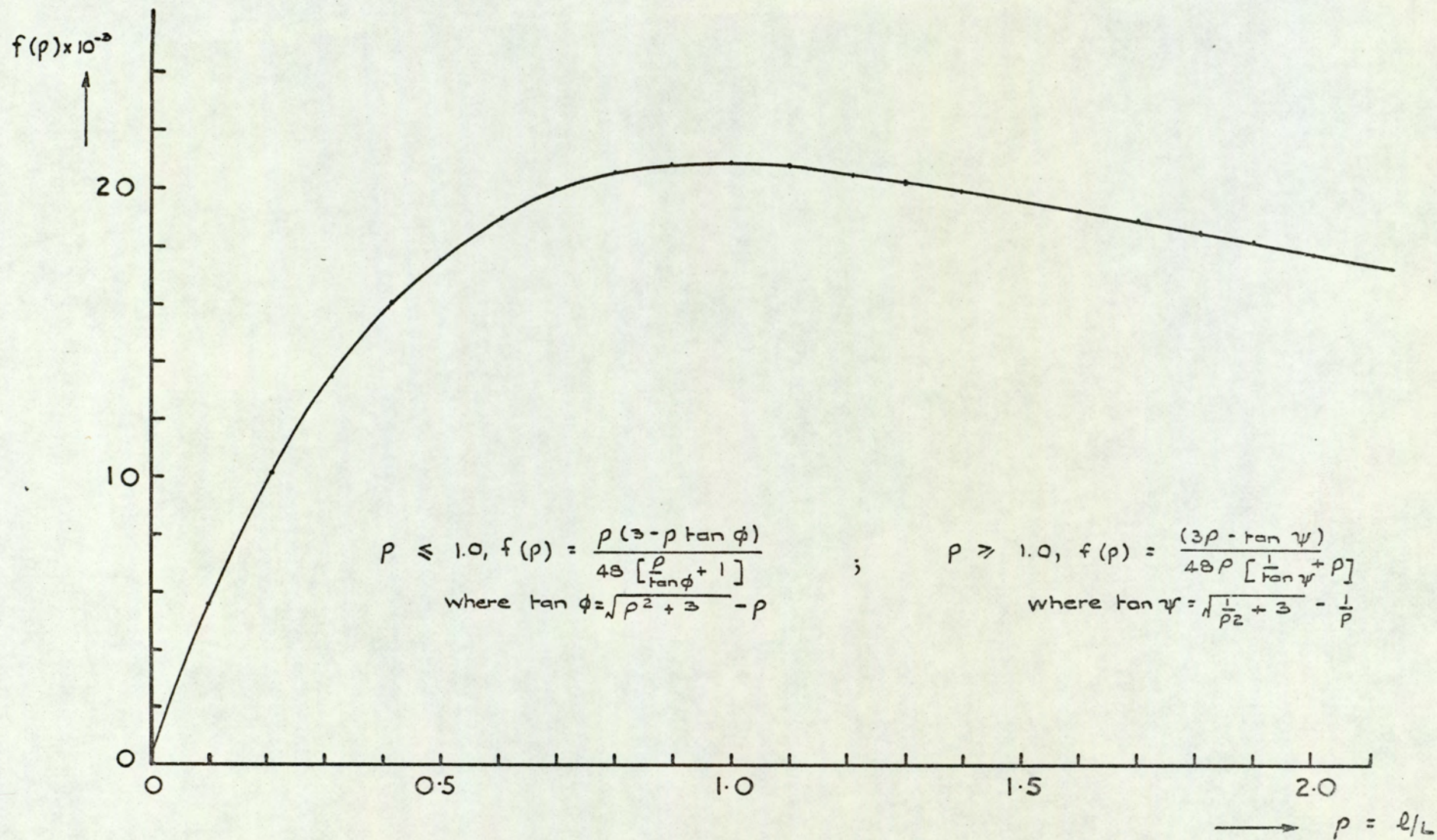


Fig. 4.13. Graph of $f(\rho)$ against ρ

Taking the yield stress of the steel beams to be 16 tons/sq.in., the required plastic moduli of the main and secondary beams are:-

$$\frac{7.5 \times 3601 \times 10 \times 12}{16 \times 2240} = 90.4 \text{ in.}^3$$

and $\frac{2.25 \times 3601 \times 15 \times 12}{16 \times 2240} = 40.7 \text{ in.}^3$

respectively. Steel tables then give the minimum sizes of these beams as a 16 x 7 x 50 Universal Beam and a 16 X 5.5 x 26 Universal Beam respectively.

In the next chapter, composite action between supporting beams and slab floors is introduced. This will deal with cases of types (2) and (3) of composite design mentioned in Chapter 1. Equations for collapse loads of the basic modes of collapse for the various systems dealt with in this chapter will be modified to include these two types of composite design. Difficulties in using charts similar to that of Figure 4.12 will also be dealt with for type(3) of composite design.

C H A P T E R 5

DETERMINATION OF COLLAPSE LOADS BY UPPER-BOUND SOLUTIONS FOR CONTINUOUS BEAM AND SLAB FLOOR SYSTEMS WHERE COMPOSITE ACTION OF TYPE (2) OR (3) IS PRESENT

5.1 INTRODUCTION

An introduction to composite action was given in Chapter 2. In this chapter, the two types of assumptions on degree of composite action (2) and (3) mentioned in Chapter 1 are considered. Composite action is present at the centre spans of secondary and main beams, and its effect at the supports is ignored.

When calculating the fully plastic composite moments M_c and M_e at the centre spans of secondary and main beams respectively, type (2) ignores the effect of slab reinforcement and type (3) considers such an effect.

Equations were derived in the previous chapter for collapse by the basic modes of failure for five different beam and slab floor systems. These equations are modified in this chapter, where necessary, to include the effect of composite action at mid-span of secondary and main beams.

Later in the chapter, comparisons are made of the basic modes of collapse for an internal bay. Boundary equations between the various modes are derived and shown graphically similar to that of Figure 4.12 of the previous chapter. Difficulties arising in the use of such graphs for type (3) of composite action are also considered.

5.2 BEAM AND SLAB FLOOR SYSTEM CONTINUOUS IN FOUR DIRECTIONS

When shear connectors are present on the secondary and main beams of an internal bay, the sagging ultimate moment at the centre line for collapse by mode A can no longer be taken as $(M_b + M_s \cdot L)$. Composite action occurs, resulting in the secondary beam and slab acting together as a T-beam, with a fully plastic moment of M_c . Similarly, the ultimate moment at the

centre line for collapse by mode B ($M_B + M_S \cdot l$) will be replaced by M_e , the fully plastic composite moment at mid-span of the main beam.

At mid-spans of the main and secondary beams at ultimate load, it is assumed⁽⁴⁰⁾ that:-

- (1) The whole of the area of steel beam below the plastic neutral axis is stressed in tension to the yield stress, f_y .
- (2) The whole of the area of steel beam above the plastic neutral axis is stressed in compression to the yield stress, f_y .
- (3) The area of concrete below the plastic neutral axis is cracked and is therefore unstressed.
- (4) The area of concrete above the plastic neutral axis is stressed to its full compressive strength U_c , which is assumed to be $4/9 U_w$, where U_w is the cube strength of concrete. For comparison with experimental results, U_c is taken as $2/3 U_w$.

To calculate the values of the fully plastic composite moments M_c and M_e , two types of assumptions on degree of composite action are considered below, i.e. type (2), ignoring slab reinforcement and type (3), including the effect of slab reinforcement.

5.2.1 TYPE (2) - IGNORING THE EFFECT OF SLAB REINFORCEMENT

When calculating the fully plastic composite moment M_c or M_e , two cases arise, namely:-

(a) Case I. Plastic neutral axis within concrete slab

$$\text{i.e. } d_n \leq t \quad (\text{Figure 5.1})$$

This occurs when

$$\alpha \cdot A_s \leq b \cdot t \quad 5.1$$

Tensile force in steel, $F_{st} = A_s f_y$

Compressive force in concrete, $F_{cc} = d_n \cdot b \cdot U_c$

For equilibrium equating total tension to total compression,

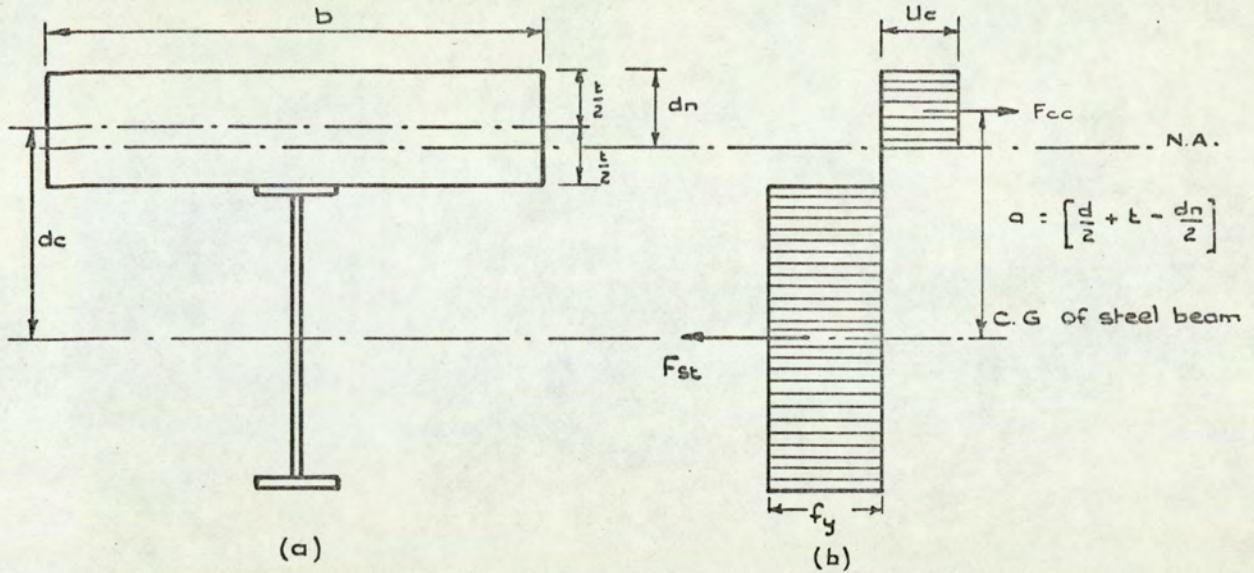


Fig. 5.1. Section and stress diagram for a composite beam with the neutral axis within the concrete slab, ignoring slab reinforcement.

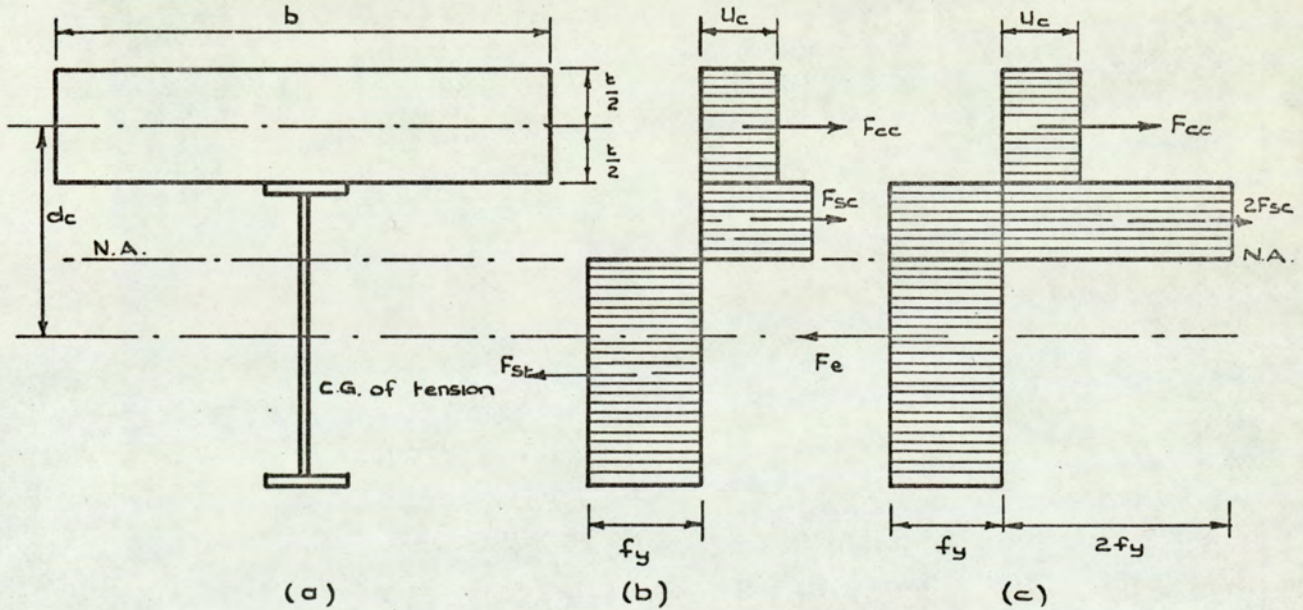


Fig. 5.2. Section and stress diagram for a composite beam with the neutral axis within the steel beam, ignoring slab reinforcement.

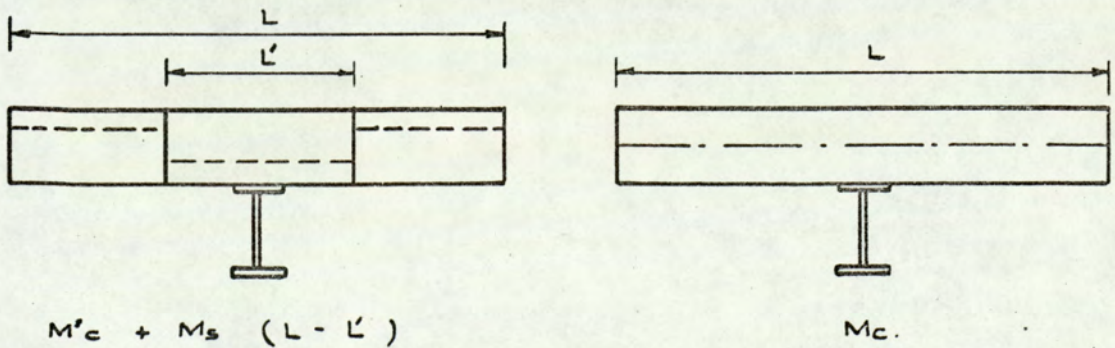


Fig. 5.3. Change in position of neutral axis by assuming the full effective width

$$\text{i.e. } F_{st} = F_{cc}$$

$$\therefore d_n = \frac{A_s f_y}{b U_c} \quad 5.2$$

To obtain the fully plastic composite moment M_c , take moments about the line of action of F_{cc} .

$$M_c = F_{st} \cdot a$$

$$a = \frac{d}{2} + t - \frac{d_n}{2} = d_c + \frac{t - d_n}{2}$$

$$\text{Hence } M_c = A_s \cdot f_y \left[\frac{d}{2} + t - \frac{d_n}{2} \right] \quad 5.3$$

Where t = slab thickness

d_n = depth of plastic neutral axis below top of slab

$$\alpha = \frac{f_y}{U_c}$$

A_s = area of steel beam

b = width of compression flange

d = depth of steel beam

$$d_c = \frac{d + t}{2}$$

(b) Case II. Plastic neutral axis within the steel beam

$$\text{i.e. } t < d_n \quad (\text{Figure 5.2})$$

This occurs when

$$b \cdot t < \alpha \cdot A_s \quad 5.4$$

In this case, the condition of equation 5.4 is not likely to arise, i.e. $A_s f_y > b \cdot t \cdot U_c$, since the value of $b \cdot t \cdot U_c$ is necessarily large, owing to large "b" values, thus requiring either a very thin slab or a very deep steel beam to fall outside the limits of equation 5.1.

The stress distribution at ultimate load is shown in Figure 5.2.b.

The derivation of the formulae is simplified by adding equal but opposite forces to the steel beam above the neutral axis, giving the equivalent stress distribution shown in Figure 5.2.c.

Thus the steel beam is assumed to be stressed in tension to yield throughout its full depth, the total equivalent tensile force F_e being balanced by the compressive force F_{cc} in the concrete, plus twice the compressive force F_{sc} in the steel section above the neutral axis.

$$F_e = A_s f_y$$

$$F_{cc} = \frac{b \cdot t}{\alpha} \cdot f_y$$

$$2F_{sc} = 2 (\text{area of steel in compression}) \cdot f_y$$

$$\therefore \text{Area of steel in compression } F_{sc} = \frac{1}{2} \left[A_s - \frac{b \cdot t}{\alpha} \right] \quad 5.5$$

d_n may be determined from the dimensions of the steel section. In the case of rolled steel section or welded plate girder with rectangular top flange of an area $A_f = b_f \times t_f$, where b_f and t_f are the breadth and thickness of the top flange respectively, and a constant web thickness t_w , Case II may be subdivided as follows:-

(i) Plastic neutral axis within top flange of steel beam

$$\text{i.e. } t < d_n < (t + t_f)$$

This occurs when

$$b \cdot t < \alpha \cdot A_s < (b \cdot t + 2\alpha \cdot A_f) \quad 5.6$$

$$d_n = t + \frac{\alpha \cdot A_s - b \cdot t}{2b_f \cdot \alpha} \quad 5.7$$

$$M_c = f_y [A_s \cdot d_c - b_f \cdot d_n (d_n - t)] \quad 5.8$$

(ii) Plastic neutral axis within web of steel beam

$$\text{i.e. } d_n > t + t_f$$

This occurs when

$$\alpha (A_s - 2 A_f) > b \cdot t \quad 5.9$$

$$d_n = t + t_f + \frac{\alpha (A_s - 2 A_f) - b \cdot t}{2 \alpha \cdot t_w} \quad 5.10$$

$$M_c = f_y [A_s \cdot d_c - A_f (t + t_f) - t_w (d_n + t_f)(d_n - t - t_f)] \quad 5.11$$

5.2.2 TYPE (3) - INCLUDING THE EFFECT OF SLAB REINFORCEMENT

In the experimental part of this work, beam and slab floor systems were tested to destruction. It was found that the actual collapse loads were greater than the theoretical collapse loads. Evidently that was partly due to the effect of slab reinforcement. When the reinforcement yielded in tension, it did increase the ultimate moment of the composite section as the plastic neutral axis was always high in the slab (Figure 5.4). It can also be shown from Table 5(i) that the plastic neutral axis is usually high in the slab for various Universal Beams and slab widths.

In this section, the slab reinforcement is introduced when calculating the fully plastic composite moments M_c and M_e . Equations 5.1 - 5.11 are modified to include this effect. It is assumed that when the plastic neutral axis is within the concrete slab, which is usually the case, the slab reinforcement is stressed in tension to the yield stress t_y . In the case of the plastic neutral axis within the steel beam, the slab reinforcement is assumed stressed in compression to the yield stress t_y . It is also assumed that the slab reinforcement in the whole width of the section is included when the plastic composite moment of type (3) of composite design is calculated.

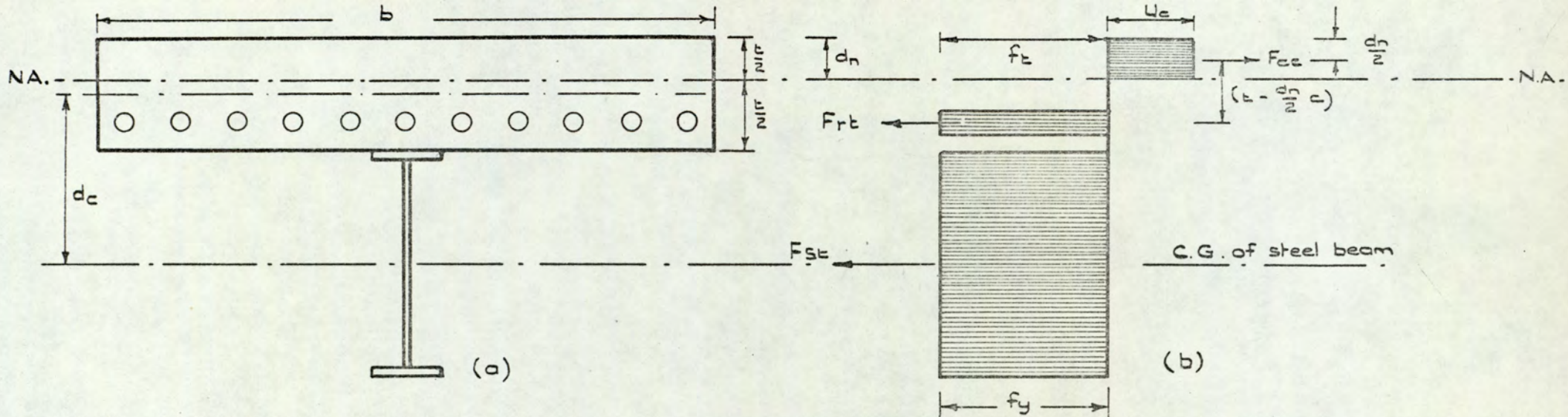


Fig. 5.4. Section & stress diagram for a sagging composite beam with the neutral axis within the concrete slab. Slab reinforcement are included.

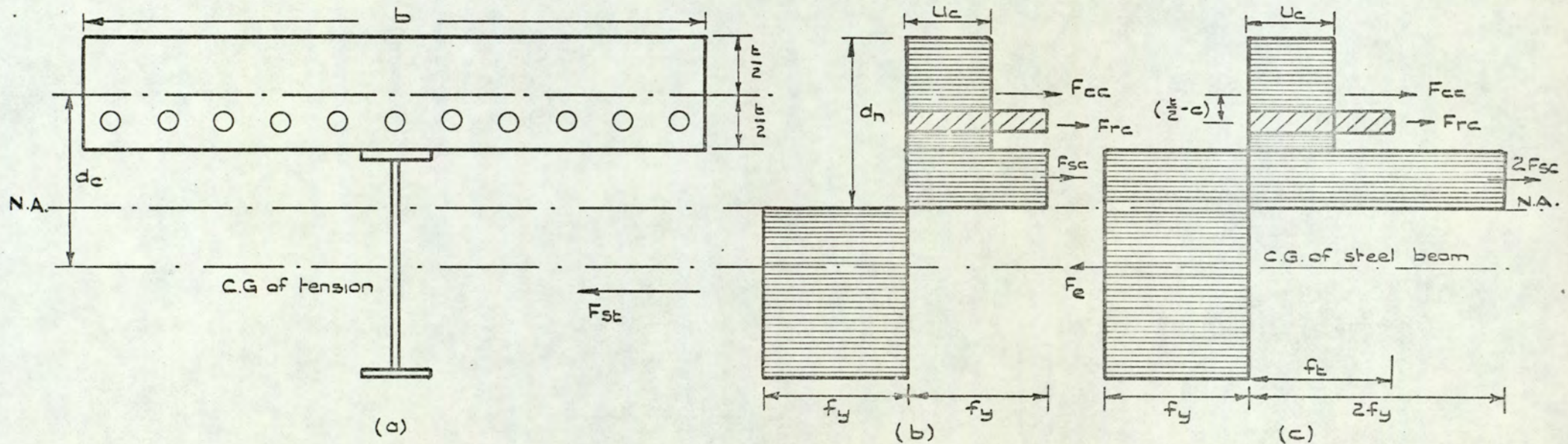


Fig. 5.5. Section & stress diagram for a sagging composite beam with the neutral axis within the steel beam. Slab reinforcement are included.

Cube strength = 6000 lbs./in.²

Beam size	slab width (ft.)	plastic N.A. (in.)	(M _c + M _b) kips - ft. slab thickness (in.)				
			4	5	6	7	8
12 × 5 × 25 U.B. M _b = 98.3	15	0.5	311.3	333.3	355.2	377.2	399.1
	20	0.4	312.8	334.8	356.7	378.7	400.6
	25	0.3	313.7	335.7	357.6	379.6	401.5
	30	0.2	314.3	336.3	358.2	380.2	402.1
15 × 6 × 35 U.B. M _b = 174.7	15	0.8	516.3	547.1	577.8	608.5	639.3
	20	0.6	519.3	550.0	580.8	611.5	642.2
	25	0.5	521.1	551.8	582.5	613.3	644.0
	30	0.4	522.2	553.0	583.7	614.4	645.2
16 × 7 × 36 U.B. M _b = 190.5	15	0.8	555.2	586.8	618.5	650.1	681.7
	20	0.6	558.3	590.0	621.6	653.2	684.9
	25	0.5	560.2	591.8	623.5	655.1	686.7
	30	0.4	561.5	593.1	624.7	656.4	688.0
14 × 6 ³ / ₄ × 38 U.B. M _b = 183.7	15	0.8	538.7	572.1	605.5	638.8	672.2
	20	0.6	542.2	575.6	608.9	642.3	675.7
	25	0.5	544.3	577.7	611.0	644.4	677.8
	30	0.4	545.7	579.1	612.4	645.8	679.1
15 × 6 × 40 U.B. M _b = 201.6	15	0.9	593.1	628.2	663.4	698.5	733.7
	20	0.7	596.9	632.1	667.2	702.4	737.5
	25	0.5	599.2	634.4	669.5	704.7	739.8
	30	0.4	600.8	635.9	671.1	706.2	741.4

Table 5(i). Values of the sum of Composite and Beam Moment (M_c + M_b).

Similarly, when calculating M_c or M_e , two cases arise, namely:-

(a) Case I. Plastic neutral axis within concrete slab

$$\text{i.e. } d_n \leq t \quad (\text{Figure 5.4})$$

This occurs when

$$\alpha \cdot A_s + b \cdot A_t \cdot \frac{t_y}{U_c} \leq b \cdot t \quad 5.12$$

$$d_n = \frac{A_s f_y + b \cdot A_t \cdot t_y}{b \cdot U_c} \quad 5.13$$

Similarly, taking moments about the line of action of F_{cc}

$$\therefore M_c = A_s f_y \left[\frac{d}{2} + t - \frac{d_n}{2} \right] + b \cdot A_t \cdot t_y \left[t - \frac{d_n}{2} - c \right] \quad 5.14$$

Where A_t = area of slab reinforcement/unit run

t_y = yield stress of slab reinforcement

c = concrete cover for slab reinforcement + $\frac{1}{2}$ diameter of reinforcing bar

(b) Case II. Plastic neutral axis within the steel beam

$$\text{i.e. } t < d_n$$

This occurs when

$$b \cdot t + b \cdot A_t \cdot \frac{t_y}{U_c} < \alpha \cdot A_s \quad 5.15$$

Again the stress distribution at ultimate load is shown in Figure

5.5.b. The equivalent stress distribution is shown in Figure

5.5.c.

Similarly, the area of steel in compression

$$= \frac{1}{2} \left[A_s - \frac{b \cdot t}{\alpha} - b \cdot A_t \cdot \frac{t_y}{f_y} \right] \quad 5.16$$

d_n may be determined from the dimensions of the steel section.

Case II may be subdivided into two sections as follows:-

(i) Plastic neutral axis within top flange of steel beam

$$\text{i.e. } t < d_n < t + t_f$$

This occurs when

$$(b \cdot t + b \cdot A_t \cdot \frac{t y}{\bar{U}_c}) < \alpha \cdot A_s < (b \cdot t + 2\alpha \cdot A_f + b \cdot A_t \cdot \frac{t y}{\bar{U}_c}) \quad 5.17$$

$$d_n = t + \frac{(\alpha \cdot A_s - b \cdot t - b \cdot A_t \cdot \frac{t y}{\bar{U}_c})}{2 b_f \cdot \alpha} \quad 5.18$$

$$M_c = f_y [A_s \cdot d_c - b_f \cdot d_n (d_n - t) - b \cdot A_t \cdot \frac{t y}{\bar{f}_y} (\frac{t}{2} - c)] \quad 5.19$$

(ii) Plastic neutral axis within web of steel beam

$$\text{i.e. } d_n > t + t_f$$

This occurs when

$$\alpha (A_s - 2A_f) > (b \cdot t + b \cdot A_t \cdot \frac{t y}{\bar{U}_c}) \quad 5.20$$

$$d_n = t + t_f + \frac{[\alpha (A_s - 2A_f) - b \cdot t - b \cdot A_t \cdot \frac{t y}{\bar{U}_c}]}{2 \alpha \cdot t_w} \quad 5.21$$

$$M_c = f_y [A_s \cdot d_c - A_f (t + t_f) - t_w (d_n + t_f) (d_n - t - t_f) - b \cdot A_t \cdot \frac{t y}{\bar{f}_y} (\frac{t}{2} - c)] \quad 5.22$$

5.2.3 EFFECTIVE WIDTH OF SLAB COMPRESSION FLANGE

For elastic design according to C.P.117⁽⁴⁰⁾, three conditions are put forward⁽⁶⁹⁾ for the effective width of the compression flange, namely:-

- the least of:
- (1) 1/3 of the effective span of the T-beam;
 - (2) distance between centres of the ribs of T-beams;
 - (3) 12 x thickness of the slab + breadth of the rib, when the steel member is encased.

Applying the above equations to calculate M_e along the centre line of the main beam gives the concrete flange width $b = \ell$, the frame width.

Similarly, when calculating M_c of the secondary beam, b is replaced by L , the length of the bay for equal bays frame. If the bays are not equal then b is replaced by the average length of two adjacent bays to calculate M_c .

Figure 5.3 shows that if the ultimate composite moment is taken for only a part of the slab, then the ultimate slab moment must be taken for the remainder. The position of the neutral axis is only changed slightly by taking the whole width as the compression flange. This is because it can be shown that the effect of the extra compression concrete and the extra tensile reinforcement multiplied by their respective lever arms is negligible for an increase of the effective width above the minimum of the three elastic conditions, compared with the tension in the steel beam multiplied by its lever arm. The difference between M_c and $[M_c' + M_s (L - L')]$ is negligible, when M_c is calculated for the whole width of the compression flange.

5.2.4 DETERMINATION OF NUMBER OF SHEAR CONNECTORS REQUIRED

Sufficient shear connectors should be provided in the zone between the sections of zero and maximum moment to transfer the total horizontal force between the concrete slab and the steel beam at ultimate load. Break down of shear connection can occur by failure of the shear connectors or by crushing of the concrete or both. In the later case, the necessary number of shear connectors are used to transfer the horizontal force between the concrete slab and the steel beam at ultimate load.

To determine the number of shear connectors required, two cases arise, namely:-

Case I. Plastic neutral axis within the concrete slab

This case may be subdivided into (i) and (ii) below.

(i) Type (2) - slab reinforcement is ignored

i.e. the condition of equation 5.1 must be satisfied.

From Figure 5.1, the total horizontal shear force is equal to the total compressive force in the concrete, and equal to F_{st} , the tensile force in the steel beam.

$$\text{No. of shear connectors required} = \frac{F_{cc}}{P_c} = \frac{F_{st}}{P_c}$$

$$\therefore \text{No. required} = \frac{Asf_y}{P_c} \quad 5.23$$

Where P_c = design value of one shear connector

(ii) Type (3) - slab reinforcement is included

i.e. the condition of equation 5.12 must be satisfied.

From Figure 5.4, equating the total compressive force to the total tensile force, hence,

$$F_{cc} = F_{st} + F_{rt} \quad 5.24$$

from equation 5.24, the number of shear connectors can be taken as $\frac{F_{cc}}{P_c}$, but this number is more than necessary. Since the shear connectors are welded to the steel beam, then the maximum shear force the steel beam can take is its own tensile force F_{st} . This indicates that the total horizontal shear force between the concrete slab and the steel beam cannot exceed F_{st} . Hence the number of shear connectors required remains that given by equation 5.23.

Case II. Plastic neutral axis within the steel beam

Again this case is subdivided into (i) and (ii) below.

(i) Type (2)

From Figure 5.2, the total horizontal shear force is equal to the total compressive force in the concrete F_{cc} , hence,

$$\text{No. required} = \frac{F_{cc}}{P_c} = \frac{U_c \cdot b \cdot t}{P_c} \quad 5.25$$

(ii) Type (3)

From Figure 5.5, the total horizontal shear force is equal to the total compressive force in the concrete F_{cc} plus the total compressive force in the slab reinforcement F_{rc} , hence,

$$\text{No. required} = \frac{F_{cc} + F_{rc}}{P_c}$$

$$\therefore \text{No. required} = \frac{U_c \cdot b \cdot t + b \cdot A_t \cdot t_v}{P_c} \quad 5.26$$

The number of shear connectors determined from the equations above may normally be uniformly spaced (⁴⁰) between each end of the beam and the section of maximum moment, for U.D.L.

$$\text{i.e. spacing of shear connectors} = \frac{1/2 \text{ span of composite beam}}{\text{No. required}}$$

5.2.5 BASIC MODES OF FAILURE FOR INTERNAL BAY

The value of collapse load by mode A, given by equation 4.3, can now be modified for composite design of type (2) or (3). At the ends of the span of the secondary beam, the slab forms the tension flange of the composite beam and in this chapter, this type of composite action is ignored; hence the end moments remain as M_b . At the mid-span where the slab forms the compression flange, the moment ($M_b + M_s L$) is replaced by M_c . On substitution, collapse by mode A becomes:-

$$p\ell L = \frac{8(M_c + M_b)}{\ell} + \frac{8 M_s L}{\ell} \quad 5.27$$

When composite design of type (2) or (3) is considered, M_y becomes the sum of the plastic composite moment at mid-span M_c and the beam plastic moment at the support M_b . Re-arranging equation 5.27, the required sum of

plastic moments M_y for collapse by mode A to occur is obtained from:-

$$M_y = (M_c + M_b) = \frac{p\ell^2 L}{8} - M_s L \quad 5.28$$

Similarly for collapse by mode B, the end moments at supports remain M_B each, but the mid-span moment ($M_B + M_s \ell$) is replaced by M_e . Hence equation 4.7 can now be modified for composite design by type (2) or (3) and becomes:-

$$p\ell L = \frac{8(M_e + M_B)}{L} + \frac{8 M_s \ell}{L} \quad 5.29$$

Similarly for type (2) or (3) of composite design,

$$M_x = M_e + M_B$$

Re-arranging equation 5.29, the required M_x for collapse by mode B to occur is obtained from:-

$$M_x = (M_e + M_B) = \frac{p\ell L^2}{8} - M_s \ell \quad 5.30$$

For square slabs $\ell = L$, and if the supporting beam sizes are equal then $M_e = M_c$ and hence the value of the collapse load is identical from equations 5.27 or 5.29. This would then correspond to what Wood⁽⁵⁹⁾ calls a "junction mode".

The values of collapse load for modes C and D remain as given by equations 4.11 and 4.13 respectively.

$$\text{i.e. } p\ell L = \frac{48}{\rho(3 - \rho \tan\phi)} \left[\frac{\rho}{\tan\phi} + 1 \right] \cdot M_s \quad 4.11$$

$$\text{and } p\ell L = \frac{48\rho}{(3\rho - \tan\psi)} \left[\frac{1}{\tan\psi} + \rho \right] \cdot M_s \quad 4.13$$

Where for minimum p , $\tan\phi = \sqrt{\rho^2 + 3} - \rho$ and $\tan\psi = \sqrt{\frac{1}{\rho^2} + 3} - \frac{1}{\rho}$

The value of M_s can then be found from equation 4.12 or 4.14 depending on the value of the sides ratio ρ . By knowing the value of M_s and deciding on the slab thickness and cube strength to be used, then the amount of slab reinforcement in the longitudinal direction (X - direction) A_{t1} in²/ft. run to produce the necessary value of M_s in that direction can be found from the equation below.

$$\frac{M_s}{12 d_1^2 t_y} = \rho_1 \left(1 - \frac{1}{2} \rho_1 \frac{t_y}{U_c} \right) \quad 5.31$$

$$\rho_1 = \frac{A_{t1}}{12d_1} \quad 5.32$$

For an under-reinforced section $\rho_1 < \frac{2U_w}{9t_y}$ 5.33

Where d_1 = effective depth of the section in X - direction.

Re-arranging equation 5.31, the value of ρ_1 can be found as shown: -

$$\rho_1 = \frac{d_1 \cdot U_c - \sqrt{d_1^2 \cdot U_c^2 - U_c \cdot M_s / 6}}{d_1 \cdot t_y} \quad 5.34$$

Once the value of ρ_1 is found, the area of reinforcement A_{t1} can be found from equation 5.32, remembering that the condition of equation 5.33 must always be satisfied.

Similarly, the area of reinforcement in the transverse direction (Y - direction) A_{t2} in²/ft. run can be calculated from the above equations by substituting d_2 of the effective depth of the transverse reinforcement instead of d_1 . The values of A_{t1} and A_{t2} can similarly be found for beam and slab floor systems with other boundary conditions.

When type (3) of composite design is used, the values of A_{t1} and A_{t2} are required immediately to calculate M_c and M_e from equations 5.12 - 5.22.

5.3 BEAM AND SLAB FLOOR SYSTEM CONTINUOUS IN THREE DIRECTIONS

The value of collapse load by mode A given by equation 4.17 is now modified for composite design of type (2) or (3). As before, the end moments remain M_b . The mid-span moment $(M_b + M_s \cdot \frac{L}{2})$ is replaced by M_c , where the width of the concrete flange is taken for half of the external bay span. On substitution, equation 4.17 becomes:-

$$\frac{plL}{2} = \frac{8(M_c + M_b)}{l} + \frac{4M_s L}{l} \quad 5.35$$

Re-arranging equation 5.35, the required M_y for collapse by mode A is:-

$$M_y = (M_c + M_b) = \frac{pl^2 L}{16} - \frac{M_s L}{2} \quad 5.36$$

For collapse by mode B, the end moments remain M_B , and the mid-span moment $(M_B + M_s l)$ is replaced by M_e . Hence equation 4.21 becomes:-

$$plL = \frac{8(M_e + M_B)}{L} + \frac{4M_s l}{L} \quad 5.37$$

Re-arranging equation 5.37, the required M_x for collapse by mode B is:-

$$M_x = (M_e + M_B) = \frac{plL^2}{8} - \frac{M_s l}{2} \quad 5.38$$

The values of collapse load for modes C and D remain as given by equations 4.23 and 4.25.

5.4 BEAM AND SLAB FLOOR SYSTEM CONTINUOUS IN TWO DIRECTIONS

For one-bay continuous frame, the value of collapse load given by equation 4.27 for collapse by mode A is now modified for composite design of type (2) or (3). Once again, the end moments remain M_b . The mid-span moment $(2 M_b + M_s L)$ is replaced by $2 M_c$, where M_c is the composite mid-span moment of width $(L/2)$ of slab and one secondary beam. On substitution:-

$$p\ell L = \frac{16(M_c + M_b)}{\ell} + \frac{8 M_s L}{\ell} \quad 5.39$$

$$\text{and } M_y = (M_c + M_b) = \frac{p\ell^2 L}{16} - \frac{M_s L}{2} \quad 5.40$$

For collapse by mode B, the mid-span moment ($M_B + M_s \ell$) is replaced by M_e , end moments remain M_B . Equation 4.29 is modified as shown:-

$$p\ell L = \frac{8(M_e + M_B)}{L} \quad 5.41$$

$$\text{and } M_x = (M_e + M_B) = \frac{p\ell L^2}{8} \quad 5.42$$

For modes C and D, equations 4.31 and 4.33 still hold.

5.5 BEAM AND SLAB FLOOR SYSTEM FOR TEST M₁

Here, for collapse by mode A, equation 4.35 is modified to include composite design of type (2) or (3). On substitution, the mid-span moment ($2M_b + M_s L$) is replaced by $2 M_c$. Where M_c is of width $L/2$ of slab and one secondary beam, the end moments remain M_b . Thus the collapse load would be:-

$$p\ell L = \frac{16(M_c + M_b)}{\ell} \quad 5.43$$

Similarly, when the secondary beams are not considered rigidly jointed, thus plastic hinges would not develop at the ends of the beams, then equation 5.43 becomes:-

$$p\ell L = \frac{16M_c}{\ell} \quad 5.44$$

For collapse by mode B, the end moments remain M_B . The mid-span moment ($2 M_B + M_s \ell$) is replaced by $2 M_e$, where M_e is for width $\ell/2$ of slab and one edge beam. Thus equation 4.37 becomes:-

$$p\ell L = \frac{16(M_e + M_B)}{L} + \frac{8M_s \ell}{L} \quad 5.45$$

The values of collapse load for modes C and D remain as given by equations 4.38 and 4.39.

5.6 BEAM AND SLAB FLOOR SYSTEM FOR TEST M₂

For collapse by mode A, this failure is exactly the same as in 5.5 and equations 5.43 and 5.44 may be used to evaluate the collapse load.

For collapse by mode B, the right hand side end moments remain M_B and the mid-span moment ($2M_B + M_s \ell$) is replaced by $2M_e$ (Figure 4.9). Hence, for type (2) or (3) of composite design, equation 4.40 becomes:-

$$p\ell L = \frac{8(2M_e + M_B)}{L} + \frac{4M_s \ell}{L} \quad 5.46$$

For modes C and D, equations 4.41 and 4.42 still hold.

5.7 COMPARISON OF COLLAPSE MODES OF THE INTERNAL BAY

Equations of collapse load by modes A, B, C and D, where composite action is present at mid-span of the supporting beams, can be compared to produce boundary equations. These boundary equations can be graphically plotted, by a similar procedure to that used in the previous chapter, to enable the mode of collapse to be determined.

Comparing equations 5.27 and 4.11 of modes A and C, collapse will be by mode A if:-

$$\frac{8(M_c + M_b)}{\ell} + \frac{8M_s L}{\ell} < \frac{48}{\rho(3 - \rho \tan \phi)} \left[\frac{\rho}{\tan \phi} + 1 \right] \cdot M_s$$

Introducing a new strength ratio, $\gamma_c = \frac{M_c + M_b}{M_s \cdot L/2}$ then

$$\gamma_c < \frac{12}{(3 - \rho \tan \phi)} \left[\frac{\rho}{\tan \phi} + 1 \right] - 2 \quad 5.47$$

Comparing equations 5.27 and 4.13 of modes A and D, collapse will be by mode A if:-

$$\frac{8(M_c + M_b)}{l} + \frac{8 M_s l}{l} < \frac{48\rho}{(3\rho - \tan\psi)} \left[\frac{1}{\tan\psi} + \rho \right] \cdot M_s$$

Using $\gamma'_c = \frac{M_c + M_b}{M_s \cdot l/2}$ then,

$$\gamma'_c < \frac{12\rho^2}{(3\rho - \tan\psi)} \left[\frac{1}{\tan\psi} + \rho \right] - 2 \quad 5.48$$

Comparing equations 5.29 and 4.11 of modes B and C, collapse will be by mode B if:-

$$\frac{8(M_e + M_B)}{L} + \frac{8M_s l}{L} < \frac{48}{\rho(3 - \rho \tan\phi)} \left[\frac{\rho}{\tan\phi} + 1 \right] \cdot M_s$$

Introducing a new strength ratio, $\gamma_e = \frac{M_e + M_B}{M_s \cdot l/2}$ then,

$$\gamma_e < \frac{12}{\rho^2(3 - \rho \tan\phi)} \left[\frac{\rho}{\tan\phi} + 1 \right] - 2 \quad 5.49$$

Comparing equations 5.29 and 4.13 of modes B and D, collapse will be by mode B if:-

$$\frac{8(M_e + M_B)}{L} + \frac{8M_s l}{L} < \frac{48\rho}{(3\rho - \tan\psi)} \left[\frac{1}{\tan\psi} + \rho \right] \cdot M_s$$

Using $\gamma'_e = \frac{M_e + M_B}{M_s \cdot l/2}$ then,

$$\gamma'_e < \frac{12}{(3\rho - \tan\psi)} \left[\frac{1}{\tan\psi} + \rho \right] - 2 \quad 5.50$$

Finally, comparing equations 5.27 and 5.29 of modes A and B, collapse will be by mode B if:-

$$\frac{8(M_e + M_B)}{L} + \frac{8M_s l}{L} < \frac{8(M_c + M_b)}{l} + \frac{8M_s L}{l}$$

Dividing by M_s and introducing $\gamma_c = \frac{M_c + M_b}{M_s \cdot l/2}$ and $\gamma_e = \frac{M_e + M_B}{M_s \cdot l/2}$ then,

$$\rho^2 < \left(\frac{2 + \gamma_c}{2 + \gamma_e} \right) \quad 5.51$$

Plotting these inequalities gives the graph of Figure 5.6 from which the mode of collapse can be determined, hence the collapse load. Knowing the sides ratio, the limits of the strength ratios γ_c and γ_e can be determined for any of the basic modes of collapse. Charts for slabs with other boundary conditions can be similarly drawn.

5.8 DESIGN PROCEDURE FOR THE SLAB MOMENT AND BEAM SIZES USING CHARTS

Figure 5.6 can also be used for design purposes of type (2) of composite design, following the same procedure as for the design in the previous chapter. The difficulties of using such graphs for designs of type (3) of composite design will be discussed later in the section.

M_s is first determined from equation 4.11 or 4.13, depending on whether $\rho \geq 1.0$, or from Figure 4.13. The critical values of γ_e and γ_c can then be found for a given value of the sides ratio ρ , and hence the limits of the required values of $(M_e + M_B)$ and $(M_c + M_b)$ are found for collapse by a given mode, knowing the loading and the slab size. The sizes of the supporting beams and slab thickness can be chosen from Table 5(i), such that $(M_e + M_B)$ and $(M_c + M_b)$ have the required values.

A computer program was written in Atlas Autocode^(70 71) for the Atlas Computer to calculate the fully plastic moment M_b , the fully plastic composite moment M_c , the depth of the plastic neutral axis d_n and the sum of $(M_c + M_b)$ using equations 5.1 - 5.11. This was done for all the

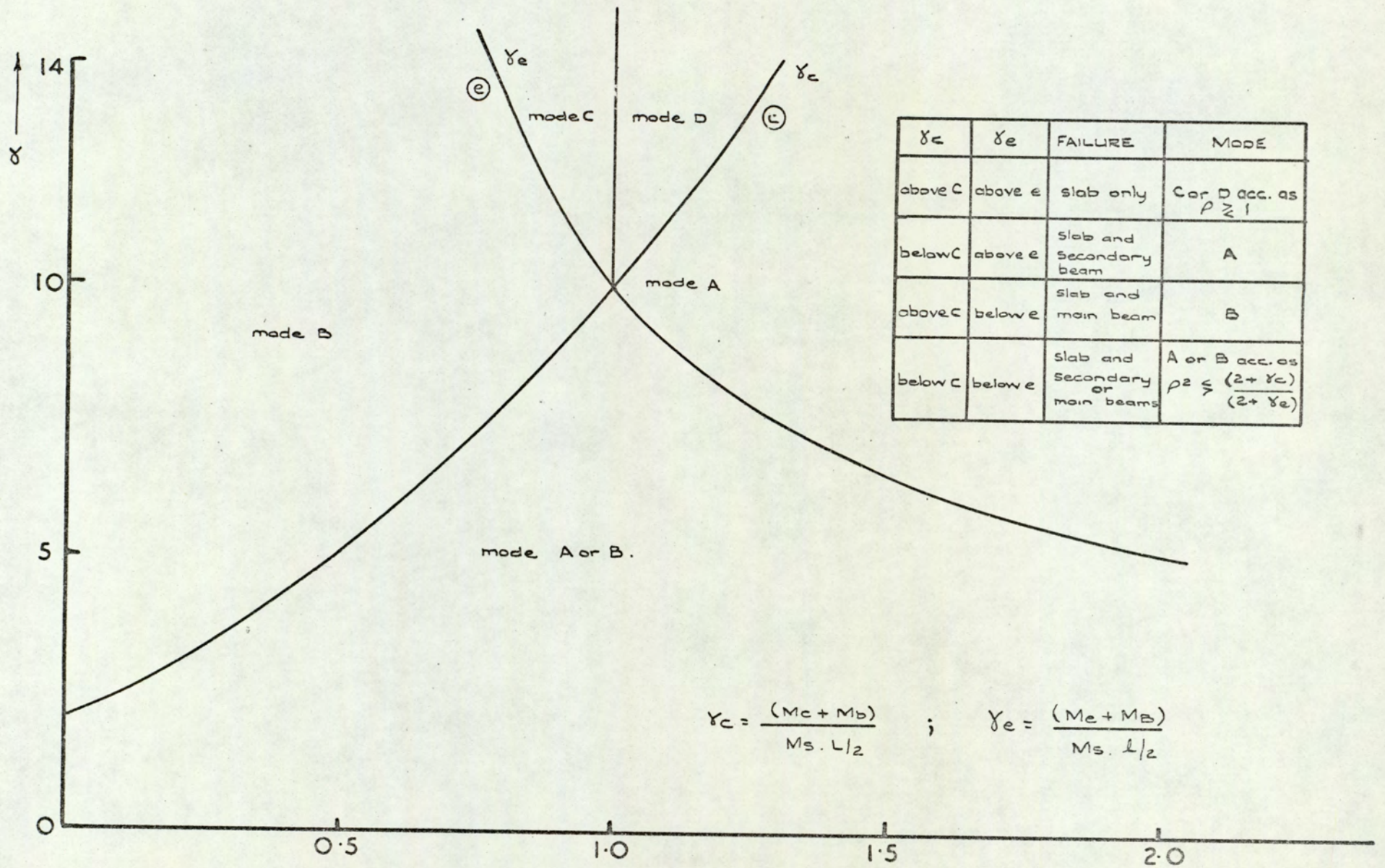


Fig. 5.6. Boundary equations UDL. composite action at middle span of secondary and main beams. Slab continuous in four directions. $\rho = l/L$

existing steel beams⁽⁷²⁾ for different cube strengths, slab thicknesses and slab widths. Table 5(i) shows some of the typical print out from this program for a limited number of Universal Beams. The flow diagram for this program is shown in Figure 5.7 and the program itself is shown in Appendix 1.

5.9 EXAMPLE

Using the same loading of 175 lb./sq.ft. and the same 30' x 20' slab, composite with and continuous over the main and secondary beams, then $M_s = 3601$ lbs.ft./ft. run as in the previous example of Chapter 4.

From Figure 5.6, for independent collapse of the slab, then $\gamma_e > 17.0$ and $\gamma_c > 6.5$.

$$\text{Hence, } \frac{M_e + M_B}{M_s \cdot l/2} > 17.0 \text{ and } \frac{M_c + M_b}{M_s \cdot l/2} > 6.5,$$

$$\begin{aligned} \text{or } (M_e + M_B) &> 17.0 \times 3601 \times 10 \text{ lbs. ft.} \\ &> 612.2 \text{ kips - ft.} \end{aligned}$$

$$\begin{aligned} \text{and } (M_c + M_b) &> 6.5 \times 3601 \times 15 \text{ lbs. ft.} \\ &> 351.1 \text{ kips - ft.} \end{aligned}$$

For the main beam with a slab width of 20', for 6000 lbs./sq.in. cube strength and using the same 6" slab thickness as in the previous example, Table 5(i) gives the minimum size of this beam as a 16 x 7 x 36 U.B. + 6" thick slab. The value of $(M_e + M_B)$ of the chosen composite beam is 621.6 kips - ft., which is more than the required value of 612.2 kips - ft. Other allowable combinations of various main beam sizes and slab thicknesses to satisfy the required $(M_e + M_B)$ value are chosen from Table 5(i) as follows:-

15 x 6 x 40 U.B. + 5" thick slab

14 x 6 $\frac{3}{4}$ x 38 U.B. + 7" thick slab

15 x 6 x 35 U.B. + 8" thick slab

Similarly for the secondary beam with a slab width of 30', for 6000 lbs./sq.in. cube strength using the same 6" thick slab, Table 5(i) gives the minimum size of this beam as a 12 x 5 x 25 U.B. + 6" thick slab. The value of $(M_c + M_b)$ of the chosen composite beam is 356.7 kips - ft., which is greater than the required value of 351.1 kips - ft. Allowable combinations of various beam sizes and slab thicknesses for the secondary beam similar to those of the main beam can be made, using the original printed tables produced by the above mentioned program.

For type (3) of composite design, tables similar to Table 5(i) are essential for the hand computation method of selecting the appropriate sizes of the supporting beams. Here the slab reinforcement is included when the plastic composite moment M_c or M_e is calculated. The area and size of slab reinforcement are in addition to the other variables of type (2) of composite design when M_c or M_e is calculated from equations 5.12 - 5.22. The area of longitudinal or transverse reinforcement A_{t1} or A_{t2} from equations 5.32 and 5.34 depends on the value of M_s , which in turn depends on the loading applied and the dimensions of the slab as shown by equation 4.12 or 4.14, depending on the sides ratio ρ . Hence, to produce tables for type (3) of composite design similar to Table 5(i) involves so many variables such as the area of slab reinforcement, which in turn depends on the loading and dimensions of the slab, cube strength, slab thickness, slab width, and the size of slab reinforcement used. Such tables could be done with the aid of computer, but prove to be very complicated to use. For this reason, type (3) of composite design could not be easily employed without the use of the computer directly.

Using the automatic computer program mentioned in Chapter 1 for type (3) of composite design to solve the above example again with 6" thick slab and 6000 lbs./sq.in. cube strength, the computer selects and prints the minimum available sizes of the main and secondary beams as a

15 × 6 × 35 U.B. and a 12 × 4 × 19 U.B. respectively. The chosen $(M_e + M_B)$ and $(M_c + M_b)$ for the main and secondary beams are 645.5 kips - ft. and 379.5 kips - ft. respectively.

In the next chapter, composite design of types (4) and (5) will be introduced, where composite behaviour is considered to be present at both mid-span and supports of main and secondary beams. Equations for collapse load by basic modes of collapse for the various beam and slab floor systems, dealt with in this chapter, will be modified to include these two new types of composite design.

DETERMINATION OF COLLAPSE LOADS BY UPPER-BOUND SOLUTIONS
FOR CONTINUOUS BEAM AND SLAB FLOOR SYSTEMS WHERE
COMPOSITE ACTION OF TYPES (4) OR (5) IS PRESENT

6.1 INTRODUCTION

In Chapter 1, five types of assumptions on degree of composite action were described. In this chapter, the last two types, namely (4) and (5), are considered. Here the effect of composite action is considered at mid-spans and supports of secondary and main beams (i.e. both regions of sagging and hogging bending). For both types of composite design, the hogging plastic composite moments at supports of secondary and main beams are taken as M_n and M_N respectively and their values are calculated from equations 6.1 - 6.11, derived in the next section. Type (4) of composite design ignores the effect of slab reinforcement when the mid-span sagging plastic composite moments M_c and M_e are calculated from equations 5.1 - 5.11 of Chapter 5. Type (5) of composite design takes the effect of slab reinforcement into consideration when M_c and M_e are calculated from equations 5.12 - 5.22 of Chapter 5.

Equations were derived in the previous chapter for five different beam and slab floor systems for collapse load by the basic modes of failure, where composite action of type (2) or (3) is present. These equations are modified in this chapter to include the effect of composite action at the supports of secondary and main beams to make the two new assumptions on degree of composite action (4) and (5) mentioned above.

Later in the chapter, comparisons are made of the basic modes of collapse for an internal bay. Boundary equations between the various modes are also derived and shown graphically in a similar manner to that of Figure 5.6. Difficulties arising in the use of tables (similar to

Table 5(i)) and graphs for type (4) or (5) of composite design are also considered. These difficulties are such that computers offer the only acceptable way of design for types (4) and (5) of composite design. This is illustrated at the end of the chapter by reference to the example of Chapter 5.

6.2 BEAM AND SLAB FLOOR SYSTEM CONTINUOUS IN FOUR DIRECTIONS

When an adequate number of shear connectors are provided to ensure full composite action at the supports, as well as mid-spans of secondary and main beams, resulting in the beams and slab acting together as T-beams along the whole length of the supporting beams, then at the supports the concrete flange will be in tension and the hogging ultimate moment for collapse by mode A ($M_b + M_s L$) will be replaced by M_n , the fully plastic hogging composite moment at support of the secondary beam. At mid-span the concrete flange will be in compression and the sagging ultimate moment ($M_b + M_s L$) for collapse by mode A will be replaced by M_c the fully plastic composite moment already dealt with in the previous chapter. Similarly, for collapse by mode B, the hogging ultimate moment at the support ($M_B + M_s \ell$) will be replaced by M_N the fully plastic composite moment at the support of the main beam. At mid-span of the main beam, the sagging ultimate moment ($M_B + M_s \ell$) for collapse by mode B will be replaced by M_e the fully plastic composite moment at mid-span of the main beam.

At the supports of the main and secondary beams at ultimate load, it is assumed that:-

- (1) The whole of the area of the steel beam below the plastic neutral axis is stressed in compression to the yield stress, f_y .
- (2) The whole of the area of steel beam above the plastic neutral axis is stressed in tension to the yield stress, f_y .
- (3) The area of concrete above the plastic neutral axis is cracked

and is therefore unstressed.

- (4) The area of concrete below the plastic neutral axis is stressed to its full compressive strength U_c , which is assumed to be $4/9 U_w$. For comparison with experimental results U_c is taken as $2/3 U_w$.
- (5) The slab is isotropic with equal ultimate slab moment M_s in sagging and hogging in both directions (Figure 4.2), thus the top and bottom slab reinforcement at the supports and mid-spans of the main and secondary beams are equal.
- (6) The hogging slab reinforcement in the whole width of the section is included and stressed in tension to the yield stress, t_y .

Assumptions were considered in the previous chapter to calculate M_c and M_e at mid-spans of main and secondary beams for type (2) or (3) of composite design. These assumptions are used again in this chapter to calculate M_c and M_e for type (4) or (5) of composite design.

When calculating the fully plastic hogging composite moment M_N or M_n two cases arise, namely:-

(a) Case I. Plastic neutral axis within concrete slab

$$\text{i.e. } d_n \leq t \quad (\text{Figure 6.1})$$

This occurs when

$$A_s \cdot f_y \leq b \cdot A_t \cdot t_y \quad 6.1$$

Tensile force in hogging reinforcement, $F_{rt} = b \cdot A_t \cdot t_y$

Compressive force in concrete, $F_{cc} = (t - d'_n) b \cdot U_c$

Compressive force in steel beam, $F_{sc} = A_s \cdot f_y$

For equilibrium equating total tension to total compression,

$$\text{i.e. } F_{rt} = F_{cc} + F_{sc}$$

$$\therefore d'_n = \frac{b \cdot t \cdot U_c + A_s \cdot f_y - b \cdot A_t \cdot t_y}{b \cdot U_c} \quad 6.2$$

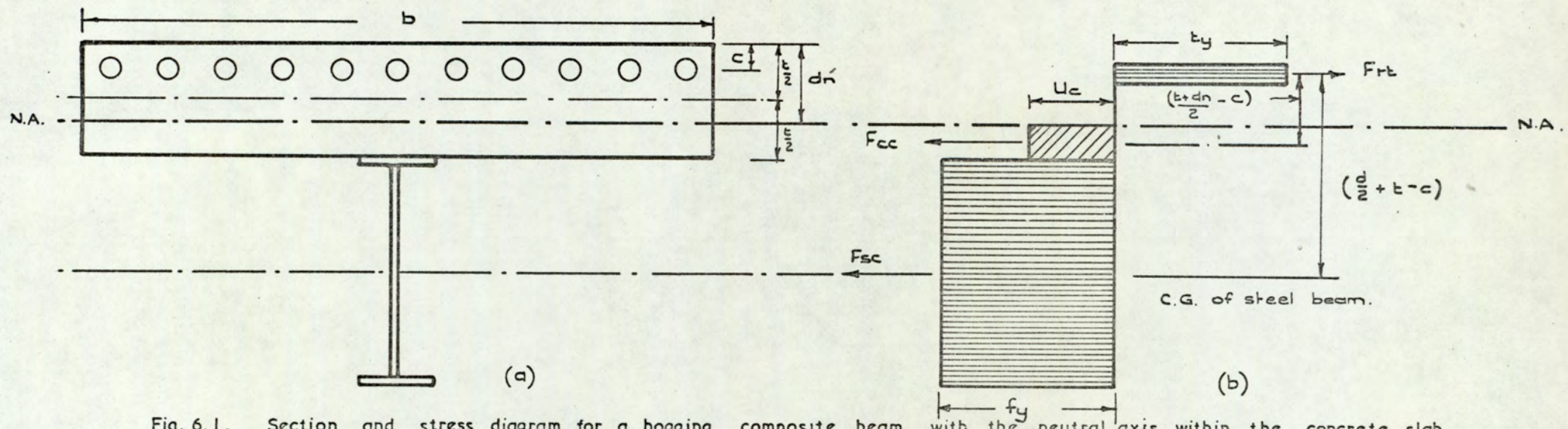


Fig. 6.1. Section and stress diagram for a hogging composite beam with the neutral axis within the concrete slab

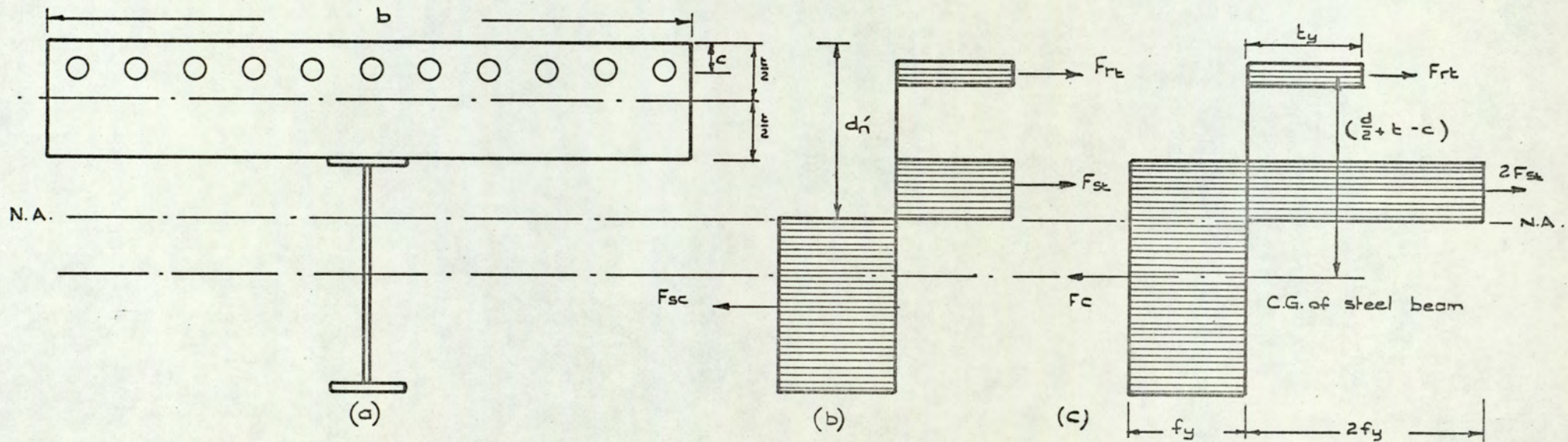


Fig 6.2 Section and stress diagram for a hogging composite beam with the neutral axis within the steel beam.

To obtain the fully plastic hogging composite moment M_n , take moments about the line of action of F_{rt} , hence:-

$$M_n = A_s \cdot f_y \left(\frac{d}{2} + t - c \right) + b(t - d'_n) U_c \left(\frac{t + d'_n}{2} - c \right) \quad 6.3$$

Where d'_n = depth of plastic neutral axis at support below top of slab

(b) Case II. Plastic neutral axis within the steel beam

$$\text{i.e. } t < d'_n \quad (\text{Figure 6.2})$$

This occurs when

$$b \cdot A_t \cdot t_y < A_s \cdot f_y \quad 6.4$$

The stress distribution at ultimate load is shown in Figure 6.2.b.

A similar procedure to that of the previous chapter is adopted for calculating M_n when the plastic neutral axis is within the steel beam. The derivation of the formulae is simplified by adding equal but opposite forces to the steel beam above the neutral axis, giving the equivalent stress distribution shown in Figure 6.2.c.

Thus the steel beam is assumed to be stressed in compression throughout its full depth, the total equivalent compressive force F_e being balanced by the tensile force F_{rt} in the hogging reinforcement, plus twice the tensile force F_{st} in the steel section above the neutral axis.

$$F_e = A_s \cdot f_y$$

$$F_{rt} = b \cdot A_t \cdot t_y$$

$$2 F_{st} = 2 (\text{area of steel beam in tension}) \cdot f_y$$

$$\therefore \text{Area of steel beam in tension} = \frac{1}{2} \left[A_s - b \cdot A_t \cdot \frac{t_y}{f_y} \right] \quad 6.5$$

d'_n may be determined from the dimensions of the steel section. In the case of rolled steel sections or plate girders with a rectangular top flange, Case II may be treated in a similar manner to that of the previous chapter and subdivided as follows:-

(i) Plastic neutral axis within top flange of steel beam

$$\text{i.e. } t < d'_n < (t + t_f)$$

This occurs when

$$b \cdot A_t \cdot t_y < A_s \cdot f_y < (b \cdot A_t \cdot t_y + 2 A_f \cdot f_y) \quad 6.6$$

$$d'_n = t + \frac{A_s - b \cdot A_t \cdot t_y / f_y}{2 b_f} \quad 6.7$$

$$M_n = f_y \left[A_s \left(\frac{d}{2} + t - c \right) - b_f (d'_n - t)(d'_n + t - 2c) \right] \quad 6.8$$

(ii) Plastic neutral axis within web of steel beam

$$\text{i.e. } d'_n > t + t_f$$

This occurs when

$$A_s \cdot f_y - 2 A_f \cdot f_y > b \cdot A_t \cdot t_y \quad 6.9$$

$$d'_n = t + t_f + \frac{(A_s - 2 A_f) - b \cdot A_t \cdot t_y / f_y}{2 t_w} \quad 6.10$$

$$M_n = f_y \left[A_s \left(\frac{d}{2} + t - c \right) - A_f (2t + t_f - 2c) - t_w (d'_n - t - t_f)(d'_n + t_f + t - 2c) \right] \quad 6.11$$

6.2.1 EFFECTIVE WIDTH OF HOGGING CONCRETE FLANGE AT SUPPORTS

In the previous chapter, it was shown that, to satisfy the three conditions put forward for elastic design⁽⁶⁹⁾, or to take the whole width of the section when the plastic composite moment M_c is calculated, the difference between M_c and $[M'_c + M_s (L - L')]$ is small (Figure 5.3).

Similarly, when M_n is calculated, if the plastic hogging composite moment M_n' is taken for only a part of the slab, the ultimate slab moment $M_s(L - L')$ must be taken for the remainder. The difference between M_n and $[M_n' + M_s(L - L')]$ is not great when M_n is calculated for the whole width of the tension concrete flange.

The above equation may be modified to calculate the plastic hogging composite moment of the main beam by substituting l for b . This applies for the hogging tensile reinforcement and to the concrete compression flange width if d_n' within slab. Similarly, when M_n of the secondary beam is calculated, b is replaced by L , the length of the bay for equal bays frame. When M_n is calculated for unequal bays frame, then b is replaced by the average of two adjacent bays.

6.2.2 DETERMINATION OF NUMBER OF SHEAR CONNECTORS REQUIRED

A sufficient number of shear connectors should be provided along the supporting beams for composite action at supports and mid-spans to occur. To determine the number of shear connectors to provide composite action at the supports, two cases arise, namely:-

Case I. Plastic neutral axis within the concrete slab

Here the condition of equation 6.1 must be satisfied. From Figure 6.1, the total horizontal shear force cannot exceed the compressive force in the steel beam.

$$\therefore \text{No. of shear connectors required} = \frac{A_s \cdot f_y}{P_c'} \quad 6.12$$

Where $P_c' = 80$ per cent of design value⁽⁴⁸⁾ of one shear connector

Case II. Plastic neutral axis within the steel beam

Here the condition of equation 6.4 must be satisfied. From Figure

6.2, the total horizontal shear force is equal to the tensile force in the hogging reinforcement F_{rt} , hence:-

$$\text{No. of shear connectors required} = \frac{F_{rt}}{P'_c} = \frac{b \cdot A_t \cdot t_v}{P'_c} \quad 6.13$$

For type (4) of composite design, the number of shear connectors found from equation 6.12 or 6.13, depending on the position of the neutral axis, may be added to the number required for mid-span composite action found from equation 5.23 or 5.25, again depending on the position of neutral axis. The total number of shear connectors required for type (4) of composite design may be spaced uniformly along the main and the secondary beams.

For type (5) of composite design, the number of shear connectors required for composite action at the supports may be found again from equation 6.12 or 6.13, depending on the position of the neutral axis. The number of shear connectors required to provide mid-span composite action may be found from equation 5.23 or 5.26, again depending on the position of the neutral axis. The number of shear connectors required to provide composite action at supports and mid-spans found from the appropriate equations above may be added together and spaced uniformly for type (5) of composite design. Such spacing was found satisfactory in the experimental part of the research.

6.2.3 BASIC MODES OF FAILURE FOR INTERNAL BAY

The value of collapse load by mode A, given by equation 5.27, can now be modified for composite action of type (4) or (5). It was shown earlier that each of the end moments ($M_b + M_s L$) is replaced by M_n and the mid-span composite moment remains as M_c of Chapter 5. On substitution, collapse by mode A becomes:-

$$p\ell L = \frac{8(M_c + M_n)}{\ell} \quad 6.14$$

When composite design of type (4) or (5) is considered, M_y becomes the sum of plastic sagging and hogging composite moments M_c and M_n at mid-span and support of the secondary beam. Re-arranging equation 6.14, the required sum of composite moments M_y for collapse by mode A to occur is obtained from:-

$$M_y = (M_c + M_n) = \frac{p\ell^2 L}{8} \quad 6.15$$

Similarly, for collapse by mode B, each of the end moments ($M_B + M_{s\ell}$) is replaced by M_N and the mid-span moment remains as M_e of the previous chapter. Hence, equation 5.29 can now be modified for composite design by type (4) or (5) and becomes:-

$$p\ell L = \frac{8(M_e + M_N)}{L} \quad 6.16$$

Similarly, for type (4) or (5) of composite design,

$$M_x = M_e + M_N$$

Re-arranging equation 6.16, the required M_x for collapse by mode B to occur is obtained from:-

$$M_x = (M_e + M_N) = \frac{p\ell L^2}{8} \quad 6.17$$

Again, similar to composite design of type (2) or (3), for square slabs $\ell = L$, and equal main and secondary beam sizes, then $M_e = M_c$ and $M_N = M_n$ and hence the value of collapse load for type (4) or (5) of composite design is identical from either equation 6.14 or 6.16. This would again correspond to what Wood⁽⁵⁹⁾ calls a "junction mode".

The value of collapse load for modes C and D remain as given by equations 4.11 and 4.13 respectively.

6.3 BEAM AND SLAB FLOOR SYSTEM CONTINUOUS IN THREE DIRECTIONS

For an external bay, the value of collapse load by mode A, given by equation 5.35, is now modified for composite design of type (4) or (5). Each of the end moments ($M_b + M_s \frac{L}{2}$) is replaced by M_n and the mid-span moment remains as M_c of the previous chapter, where M_c and M_n are considered for a width of the concrete flange equal to half of the external bay span and one secondary beam. On substitution, equation 5.35 becomes:-

$$\frac{p\ell L}{2} = \frac{8(M_c + M_n)}{\ell} \quad 6.18$$

Re-arranging equation 6.18, the required M_y for collapse by mode A is:-

$$M_y = (M_c + M_n) = \frac{p\ell^2 L}{16} \quad 6.19$$

For collapse by mode B (Figures 4.1 and 4.4), the main beam at the left hand support is not continuous and therefore yield lines along the external side could not develop, owing to the rotation of the secondary beam and hogging reinforcement could be placed in that position. Hence the end moment at the left hand support remains as M_B . At the right hand support, continuity exists and therefore the end moment there ($M_B + M_s \ell$) is replaced by M_N . The mid-span composite moment M_e replaces ($M_B + M_s \ell$) as in the previous chapter. Hence equation 5.37 becomes:-

$$p\ell L = \frac{8(M_e + 0.5 M_N + 0.5 M_B)}{L} \quad 6.20$$

Now putting $M_x = (M_e + 0.5 M_N + 0.5 M_B)$ and re-arranging equation 6.20, the required M_x for collapse by mode B is:-

$$M_x = (M_e + 0.5 M_N + 0.5 M_B) = \frac{p\ell L^2}{8} \quad 6.21$$

The values of collapse load for modes C and D remain as given by equation 4.23 and 4.25.

6.4 BEAM AND SLAB FLOOR SYSTEM CONTINUOUS IN TWO DIRECTIONS

For one-bay continuous frame (Figure 4.7), the value of collapse load given by equation 5.39 for collapse by mode A is now modified for composite design for type (4) or (5). The end moment $(M_b + M_s \frac{L}{2})$ is replaced by M_n . In the previous chapter, the mid-span moment $(2 M_b + M_s L)$ was replaced by $2 M_c$, where M_c and M_n are the composite mid-span and support moments of width $L/2$ of slab and one secondary beam. On substitution:-

$$p\ell L = \frac{16 (M_c + M_n)}{\ell} \quad 6.22$$

$$\text{and } M_y = (M_c + M_n) = \frac{p\ell^2 L}{16} \quad 6.23$$

For collapse by mode B, again the mid-span moment $(M_B + M_s \ell)$ was replaced by M_e in the previous chapter. The end moments still remain M_B as the frame is not continuous in this direction at either support (Figures 4.5 and 4.7). Hence, equation 5.41 still holds for collapse by mode B for type (4) or (5) of composite design.

$$\text{i.e. } p\ell L = \frac{8 (M_e + M_B)}{L} \quad 6.24$$

$$\text{and } M_x = (M_e + M_B) = \frac{p\ell L^2}{8} \quad 6.25$$

Hence, for one-bay continuous frame over the main beams (Figure 4.5) for collapse by mode B, types (2) and (4) and also types (3) and (5) of composite design give the same results. This is due to the discontinuity at the supports of the main beam which prevents plastic hogging composite moments from forming there. This shows that for this type of beam and slab floor system, for collapse by mode B, there is no advantage in

changing the composite design from type (2) to (4) or from type (3) to (5). For modes C and D, equations 4.31 and 4.33 still hold.

6.5 BEAM AND SLAB FLOOR SYSTEM FOR TEST M₁

Here for collapse by mode A (Figure 4.8), the mid-span composite moment ($2 M_b + M_s L$) was replaced by $2 M_c$ in the previous chapter, but the end moments still remain as M_b . Thus equation 5.43 may still be used to evaluate the collapse load for type (4) or (5) of composite design,

$$\text{i.e. } p\ell L = \frac{16 (M_c + M_b)}{\ell} \quad 6.26$$

Similarly, when the secondary beams are not considered rigidly jointed and plastic hinges do not develop at the ends of secondary beams, equation 5.43 becomes:-

$$\text{i.e. } p\ell L = \frac{16 M_c}{\ell} \quad 6.27$$

Here again there is no advantage in changing the composite design from type (2) to (4) or from type (3) to (5) for collapse by mode A.

For collapse by mode B, each of the end moments ($2 M_B + M_s \ell$) is replaced by $2 M_N$ and the mid-span moment ($2 M_B + M_s \ell$) is replaced by $2 M_e$ as in the previous chapter, where M_e and M_N are for width $\ell/2$ of slab and one edge beam. Hence, for type (4) or (5) of composite design, equation 5.45 becomes:-

$$p\ell L = \frac{16 (M_e + M_N)}{L} \quad 6.28$$

The value of collapse load for modes C and D remain as given by equations 4.38 and 4.39.

6.6. BEAM AND SLAB FLOOR SYSTEM FOR TEST M₂

For collapse by mode A (Figure 4.9), this failure is exactly the same

as that of test M_1 and equations 5.43 and 5.44 may be used to evaluate the collapse load. It was shown in the previous section that there is no advantage in using type (4) of composite design rather than type (2) or type (5) instead of type (3) for collapse by mode A.

For collapse by mode B (Figure 4.9), the right hand side end moment ($2 M_E + M_S \ell$) is replaced by $2 M_N$. The mid-span moment ($2 M_B + M_S \ell$) was replaced by $2 M_e$ in Chapter 5, where M_e and M_N are of width $\ell/2$ of slab and one edge beam. Hence, for type (4) or (5) of composite design, equation 5.46 becomes:-

$$p\ell L = \frac{8 (2 M_e + M_N)}{L} \quad 6.29$$

For modes C and D, the value of collapse load remain as given by equations 4.41 and 4.42.

6.7 COMPARISON OF COLLAPSE MODES OF THE INTERNAL BAY

Equations of collapse load by modes A, B, C and D, where composite action is present at the supports and mid-spans of the supporting beams, can be compared to produce boundary equations. These boundary equations can be plotted graphically by a similar procedure to that used in the previous two chapters.

Comparing equations 6.14 and 4.11 for modes A and C, collapse will be by mode A if:-

$$\frac{8 (M_c + M_n)}{\ell} < \frac{48}{\rho(3 - \rho \tan\phi)} \left[\frac{\rho}{\tan\phi} + 1 \right] \cdot M_s$$

Introducing a new strength ratio, $\gamma_n = \frac{M_c + M_n}{M_s \cdot \ell/2}$ then,

$$\gamma_n < \frac{12}{(3 - \rho \tan\phi)} \left[\frac{\rho}{\tan\phi} + 1 \right] \quad 6.30$$

Comparing equations 6.14 and 4.13 of modes A and D, collapse will be by mode A if:-

$$\frac{8 (M_c + M_n)}{l} < \frac{48\rho}{(3\rho - \tan\psi)} \left[\frac{1}{\tan\psi} + \rho \right] \cdot M_s$$

Using $\gamma'_n = \frac{M_c + M_n}{M_s \cdot l/2}$ then,

$$\gamma'_n < \frac{12\rho^2}{(3\rho - \tan\psi)} \left[\frac{1}{\tan\psi} + \rho \right] \quad 6.31$$

Comparing equations 6.16 and 4.11 of modes B and C, collapse will be by mode B if:-

$$\frac{8 (M_e + M_n)}{L} < \frac{48}{\rho(3 - \rho\tan\phi)} \left[\frac{\rho}{\tan\phi} + 1 \right] \cdot M_s$$

Introducing a new strength ratio, $\gamma_N = \frac{M_e + M_n}{M_s \cdot l/2}$ then,

$$\gamma_N = \frac{12}{\rho^2(3 - \rho\tan\phi)} \left[\frac{\rho}{\tan\phi} + 1 \right] \quad 6.32$$

Comparing equations 6.16 and 4.13 of modes B and D, collapse will be by mode B if:-

$$\frac{8 (M_e + M_n)}{L} < \frac{48\rho}{(3\rho - \tan\psi)} \left[\frac{1}{\tan\psi} + \rho \right] \cdot M_s$$

Using $\gamma'_N = \frac{M_e + M_n}{M_s \cdot l/2}$ then,

$$\gamma'_N < \frac{12}{(3\rho - \tan\psi)} \left[\frac{1}{\tan\psi} + \rho \right] \quad 6.33$$

Finally, comparing equations 6.14 and 6.16 of modes A and B, collapse will be by mode B if:-

$$\frac{8 (M_e + M_n)}{L} < \frac{8 (M_c + M_n)}{l}$$

Introducing $\gamma_n = \frac{M_c + M_n}{M_s \cdot l/2}$ and $\gamma_N = \frac{M_e + M_N}{M_s \cdot l/2}$, and dividing by M_s then,

$$\rho^2 < \frac{(2 + \gamma_n)}{(2 + \gamma_N)} \quad 6.34$$

Plotting these inequalities gives the graph of Figure 6.3. Charts for slabs with other boundary conditions can be similarly drawn. Knowing the sides ratio ρ , the limits of the strength ratios γ_n and γ_N can be determined from Figure 6.3 for any of the basic modes of collapse. Although the limits of the strength ratios for any mode of collapse can be found easily from Figure 6.3, difficulties in finding the minimum sizes of the supporting beams with the aid of a table similar to Table 5(i) for type (4) or (5) of composite design will arise. Such difficulties and the need for the use of computer for type (4) and (5) of composite design will be discussed in the following section.

6.8 DESIGN PROCEDURE FOR SLAB MOMENT AND BEAM SIZES

To use Figure 6.3, together with tables similar to Table 5(i) of Chapter 5 for type (4) or (5) of composite design is very complicated.

M_s is first determined from equation 4.11 or 4.13, depending on whether the sides ratio $\rho \lesseqgtr 1.0$ or from Figure 4.13. The critical values of γ_n and γ_N can then be found for a given value of the sides ratio ρ from Figure 6.3, and hence the limits of the required values of $(M_e + M_N)$ and $(M_c + M_n)$ are found for collapse by a given mode, knowing the loading and slab size.

For type (4) or (5) of composite design tables similar to Table 5(i) are essential for the hand computation method of selecting the appropriate sizes of the supporting beams in a reasonable time. To produce such tables involves the calculation of M_n , and M_c if slab reinforcement is included, for many variables such as the area of slab reinforcement which in turn depends on the loading and dimensions of the slab, cube strength,

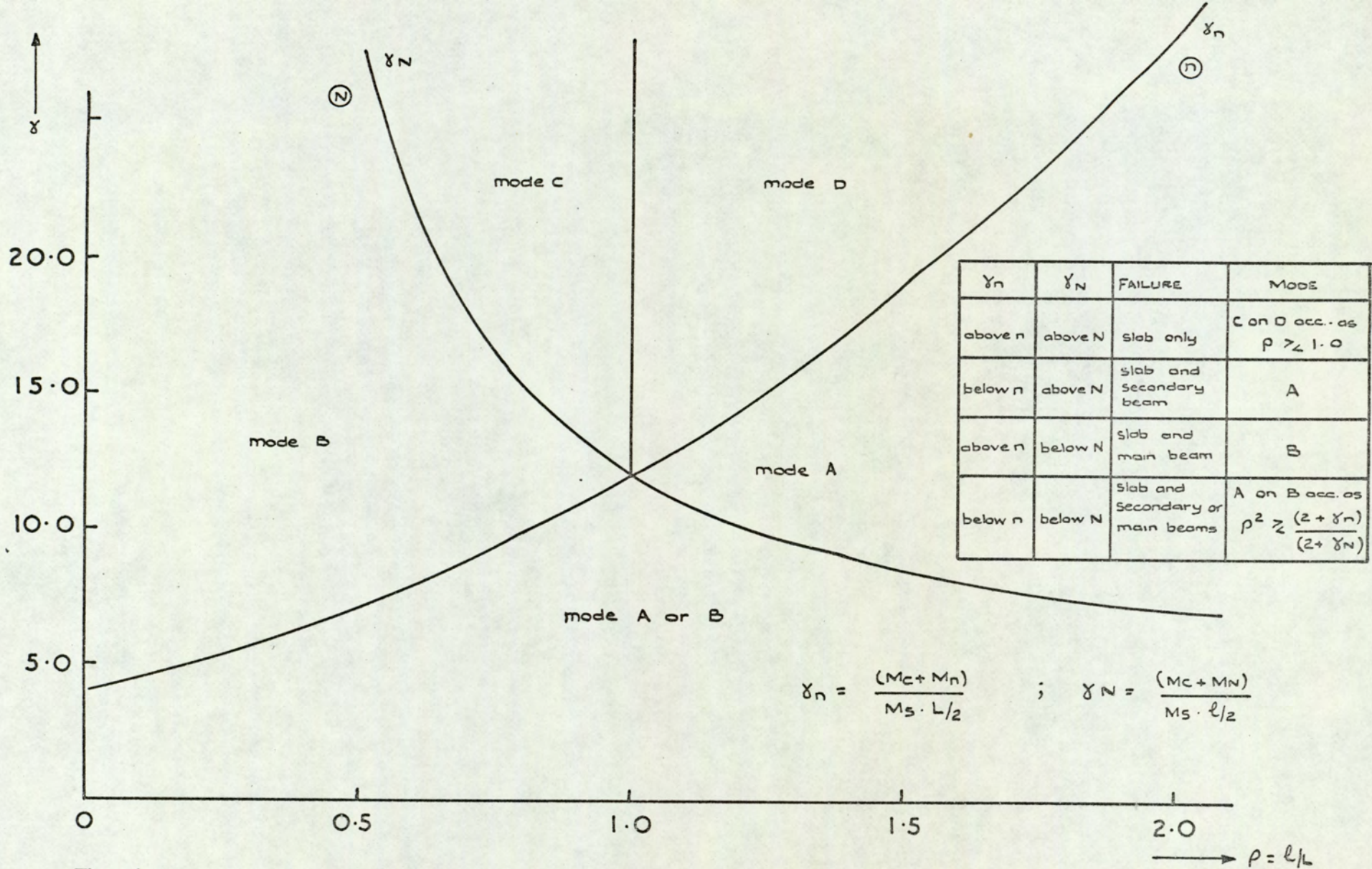


Fig. 6.3. Boundary equations U.D.L. composite action at middle spans and supports of secondary and main beams. slab continuous in four directions.

slab thickness, slab width and size of slab reinforcement used. Such tables could be drawn up with the aid of computer but prove to be very complicated to use. Hence, it could be concluded that type (4) or (5) of composite design could not be employed without the use of computers directly.

The computer program mentioned in Chapter 1 can design automatically beam and slab floor systems with different boundary conditions by type (4) or (5) of composite design as well as types (1), (2) and (3) discussed earlier. One facet of the computer program is to select and print minimum adequate sizes of the supporting beams.

6.9 EXAMPLE

Solving the same example of the previous two chapters by type (4) and type (5) of composite design, where a loading of 175 lbs./sq.ft. (including an allowance for dead load) on a 30' by 20' slab composite at mid-span and supports and continuous over the main and secondary beams, then $M_s = 3601$ lbs. ft./ft. run as in the previous examples of Chapters 4 and 5. The same 6" slab thickness and 6000 lbs./sq.in. cube strength are assumed.

From Figure 6.3, for independent collapse of the slab, then $\Upsilon_N > 19.0$ and $\Upsilon_n > 8.5$.

$$\text{Hence, } \frac{M_e + M_N}{M_s \cdot \ell/2} > 19.0 \text{ and } \frac{M_c + M_n}{M_s \cdot L/2} > 8.5,$$

$$\begin{aligned} \text{or } (M_e + M_N) &> 19.0 \times 3601 \times 10 \text{ lbs.ft.} \\ &> 684.2 \text{ kips - ft.} \end{aligned}$$

$$\begin{aligned} \text{and } (M_c + M_n) &> 8.5 \times 3601 \times 15 \text{ lbs. ft.} \\ &> 459.1 \text{ kips - ft.} \end{aligned}$$

Now to select the minimum sizes of the supporting beams for type (4) or type (5) of composite design to satisfy the above limits of the chart of Figure 6.3 for independent collapse of the slab requires a table

similar to Table 5(i) which is rather complicated to use as explained earlier.

This example is solved by the use of the computer directly for type (4) and type (5) of composite design as shown below. For maximum economy the structural sections are chosen to give a collapse load by the basic mechanisms which are identical. Hence the values of the required $(M_e + M_N)$ and $(M_c + M_n)$ should be equal to, instead of greater than 684.2 kips - ft. and 459.1 kips - ft. respectively for the basic mechanisms to be identical.

For type (4) of composite design the computer automatically calculates and prints the value of M_s as 3601 lbs. ft./ft. run and the areas of slab reinforcement in longitudinal and transverse directions A_{t1} and A_{t2} as 0.2386 in²/ft. run and 0.2653 in²/ft. run. For the main beam with a slab width of 20' the computer selects and prints the minimum size of this beam as a 15 x 6 x 35 U.B. + 6" thick slab. The following values are also obtained from the computer; $M_e = 406.0$ kips - ft., $M_N = 299.0$ kips - ft., $M_B = 174.72$ kips - ft. and $(M_e + M_N) = 705.0$ kips - ft. for the selected main beam. The value of $(M_e + M_N) = 705.0$ kips - ft. is greater than the required value of 684.2 kips - ft. as the selected main beam is the most economical section available to give the nearest value of $(M_e + M_N)$ to the required one. Similarly, for the secondary beam with a slab width of 30' the computer selects the minimum size of this beam as a 12 x 4 x 22 U.B. + 6" thick slab with $(M_c + M_n) = 464.3$ kips - ft. which is greater than the required value of 459.1 kips - ft.

For type (5) of composite design, where slab reinforcement is included in calculating M_e and M_c , more economical sections for the main and secondary beams are expected to be selected by the computer. For the main beam, the computer selects this beam as a 16 x 5 $\frac{1}{2}$ x 31 U.B. + 6" thick slab with $M_e = 437.8$ kips - ft., $M_N = 285.4$ kips - ft.,

$M_B = 161.6$ kips - ft. and $(M_e + M_N) = 723.2$ kips - ft., which is greater than the required value of 684.2 kips - ft. Similarly, for the secondary beam, the computer selects the minimum size of this beam as a $12 \times 4 \times 16\frac{1}{2}$ U.B. + 6" thick slab with $(M_c + M_n) = 477.4$ kips - ft. which is greater than the required value of 459.1 kips - ft.

In the next chapter, a detailed account of the general computer program embodying the design of beam and slab floor systems by the various assumptions on degree of composite action, discussed already, will be given. Comparisons between the various assumptions on degree of composite action will be made from the point of view of weight saving and deflection on a series of design examples of beam and slab floor systems of multi-storey buildings. The effect of different slab thicknesses and cube strengths on weight saving and deflection of composite and non-composite constructions will also be investigated.

THE DESIGN OF BEAM AND SLAB FLOOR SYSTEMS BY
COMPUTER AND THE COMPARISON AND EVALUATION OF
RELATIVE ECONOMY OF THE VARIOUS DESIGN SOLUTIONS

7.1 INTRODUCTION

A detailed account of a general computer program embodying the various assumptions on degree of composite action will be given in this chapter.

The data input consists of sectional properties, values refer to the assumption on degree of composite action to be adopted, loading, yield stresses of beams and slab reinforcement, size of reinforcing bars to be used in both directions and frame properties and geometry. The machine output gives the ultimate slab moment M_s , the areas of slab reinforcement A_{t1} and A_{t2} required in both directions and the size of the sections to be used for all the members of the system, together with their plastic composite moment and the depth of neutral axis at supports and mid-spans. Other useful information is also printed, such as the total horizontal shear force between the concrete slab and the supporting beams, this helps in finding the number of shear connectors required on each beam. The limits of the mid-span deflection of the supporting beams and the total weight of beams, slab reinforcement, concrete and of the whole system for a given cube strength and slab thickness is also printed.

The program was written in Atlas Autocode (70 71) for use on the Atlas Computer.

Designs were prepared on a series of examples of beam and slab floor systems of multi-storey buildings shown in Figure 7.1 for various assumptions on degree of composite action. These designs were compared with each other and with the plastic collapse approach with no composite action from the point of view of weight saving and deflection. In these examples

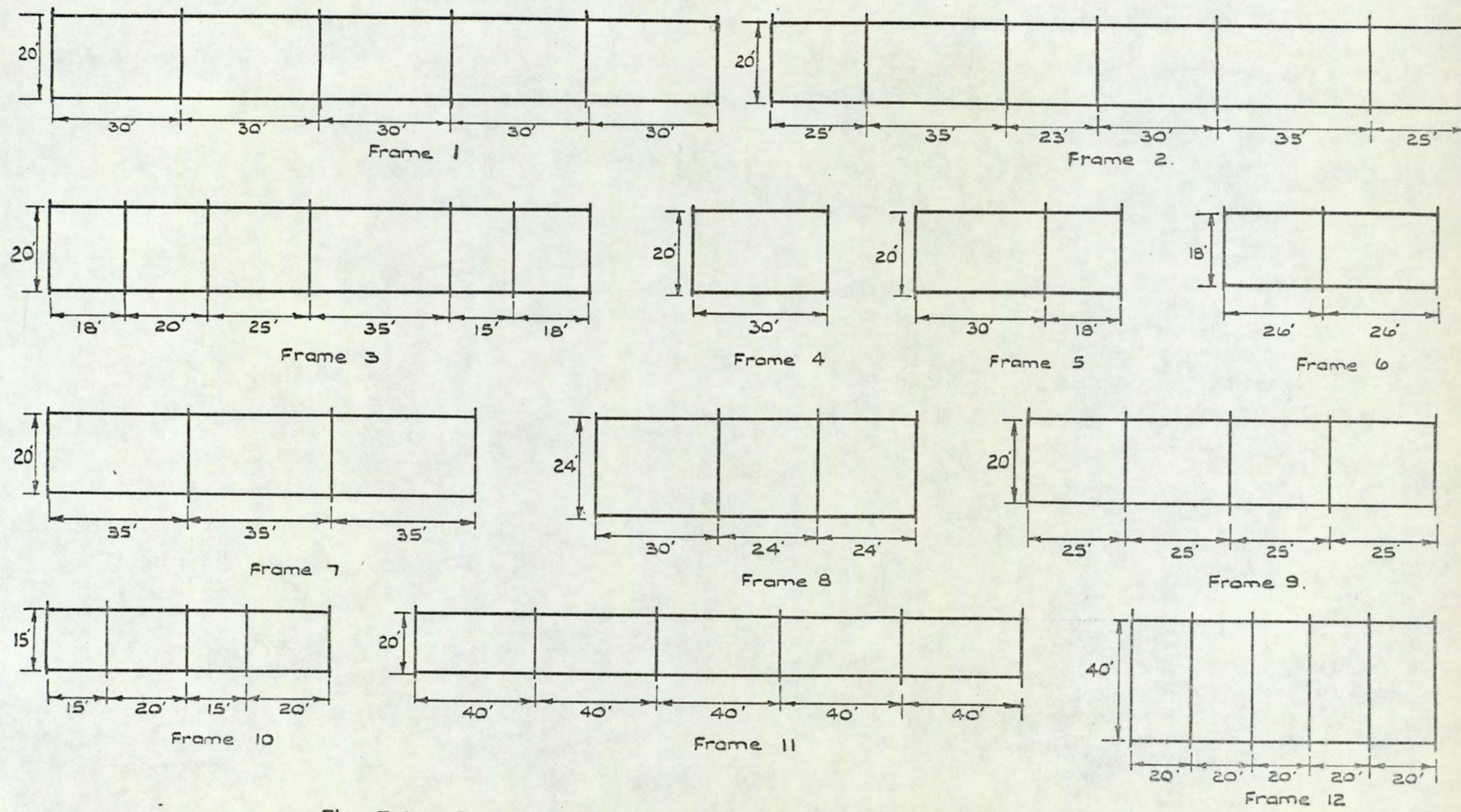


Fig. 7.1. Design examples of beam and slab floor systems.

the effect of slab thicknesses, cube strengths, sides ratios (ρ) and magnitude of live loads were investigated and their influence on the weight of the beam and slab floor systems was determined.

7.2 DESIGN PROCEDURE

The complete design approach by the various assumptions on degree of composite action has been described in Chapters 4, 5 and 6. The design of multi-bay beam and slab floor systems may be summarised as follows:-

- (1) The sections and frame data are read in.
- (2) The first cube strength is selected.
- (3) The first slab thickness is selected.
- (4) The first internal bay is selected.
- (5) The total load (dead load + live load) is calculated and multiplied by the chosen load factor. This factor is taken as 1.75 for all the design examples.
- (6) From the limit of the sides ratio (ρ), the appropriate equation is used to calculate the ultimate slab moment M_s . The areas of slab reinforcement per ft. run in both directions are also calculated.
- (7) Knowing from the data read in which assumption on the degree of composite action is to be considered, the appropriate equations are used to calculate the required M_x and M_y for the main and secondary beams.
- (8) From the list of standard sections read in, suitable section sizes are selected automatically for the main and secondary beams with their M_x and M_y values equal to or greater than the required values. The composite moments at supports and mid-spans of the selected beams are calculated together with the depth of their plastic neutral axes.

- (9) The weight of the main and secondary beams, slab reinforcement and concrete are calculated.
- (10) The maximum allowable deflections and the limits of deflection at mid-span of the selected main beam and secondary beam are calculated.
- (11) Steps 5 - 10 are repeated for the next internal bay until all the internal bays are designed. In the case of equal bay frames, where the internal bays are identical, only the first internal bay is designed, and the weights of its selected beams, slab reinforcement and concrete are multiplied by the number of internal bays.
- (12) The first external bay is selected and steps 5 - 10 are repeated using the appropriate equations of an external bay.
- (13) The last external bay is selected and steps 5 - 10 are repeated. In the case of equal bay frames, where the two external bays are identical, only the first external bay is designed and the weights of its selected beams, slab reinforcement and concrete are multiplied by two.
- (14) The total weight of the selected beams, slab reinforcement, concrete and of the whole system is calculated.
- (15) Steps 4 - 14 are repeated for the next slab thickness up to the final slab thickness.
- (16) Steps 3 - 14 are repeated for the next cube strength up to the final cube strength. In the case of a one-bay frame, steps 1 - 10 and step 14 are used for the various cube strengths and slab thicknesses, employing the appropriate equations for beam and slab floor system continuous in two directions.

In the case of two-bay frames, the two bays are treated as two external bays with a fictitious internal bay in between. Hence the system will be

treated as a three-bay frame. When the system is designed, the weight of the beams, slab reinforcement and concrete of the internal fictitious bay will be ignored.

A flow diagram of the general program which designs beam and slab floor systems with any number of bays for any of the five assumptions on degree of composite action is shown in Figure 7.2. The program itself is shown in Appendix 2.

7.3 ARRANGEMENT OF THE DATA TAPE

This refers to the general computer program shown in Appendix 2. One complete design of a frame for any of the five assumptions on degree of composite action is denoted as one case. Cases may follow one another in sequence on the data tape.

The following data must be presented in the correct sequence, using consistent units.

1. Section Data

- (a) The total number of sections presented.
- (b) For each section, in ascending numerical order:-
 - (i) Area (in.^2),
 - (ii) Depth of the section (in.),
 - (iii) Plastic modulus about the major axis (in.^3),
 - (iv) Flange width (in.),
 - (v) Flange thickness (in.),
 - (vi) Web thickness (in.),
 - (vii) Second moment of area about the major axis of bending (in.^4),
 - (viii), (ix) and (x) Figures presented in the steel tables⁽⁷²⁾ to indicate the section size,
i.e. $\underline{18} \times \underline{6} \times \underline{45}$ U.B.

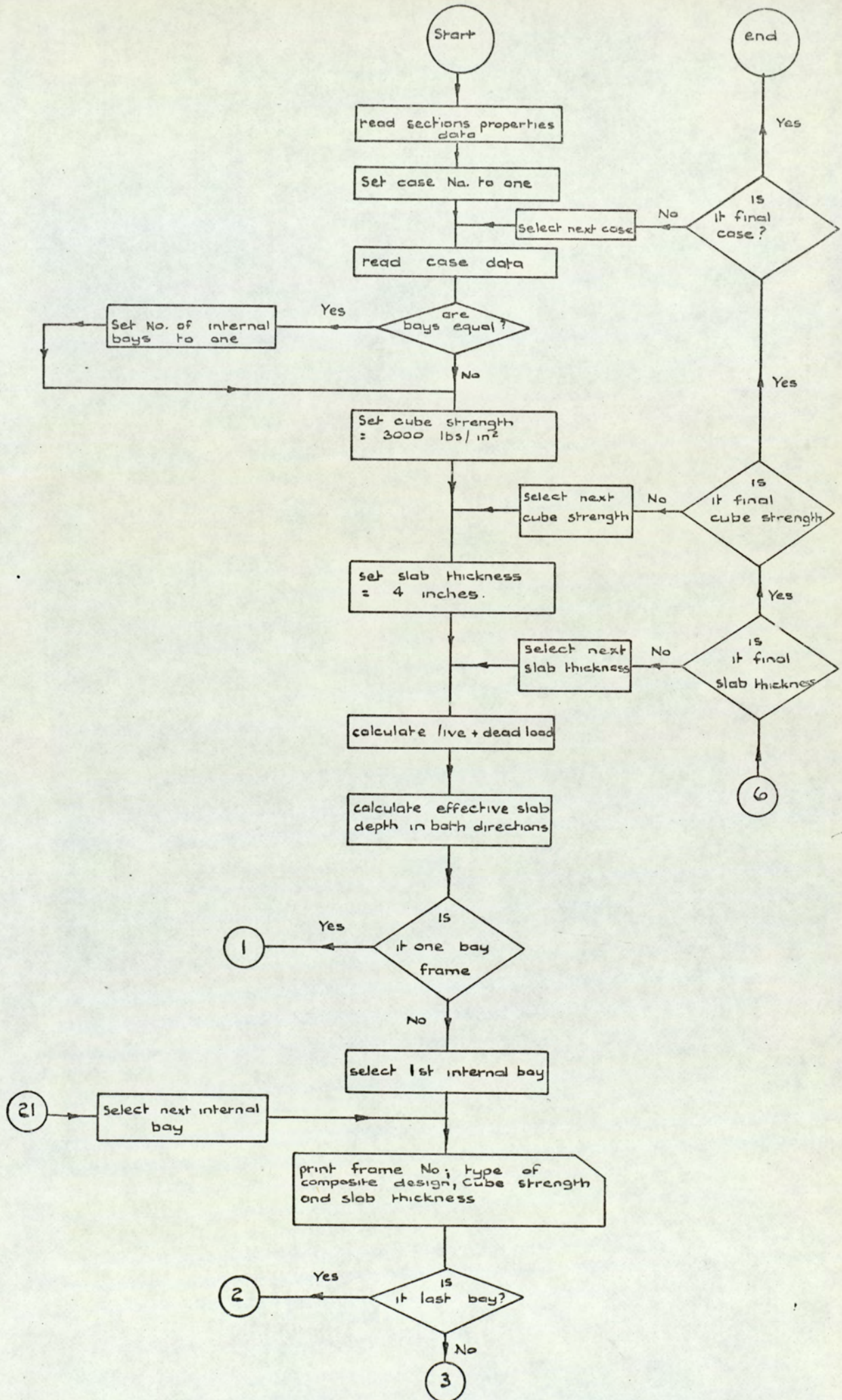
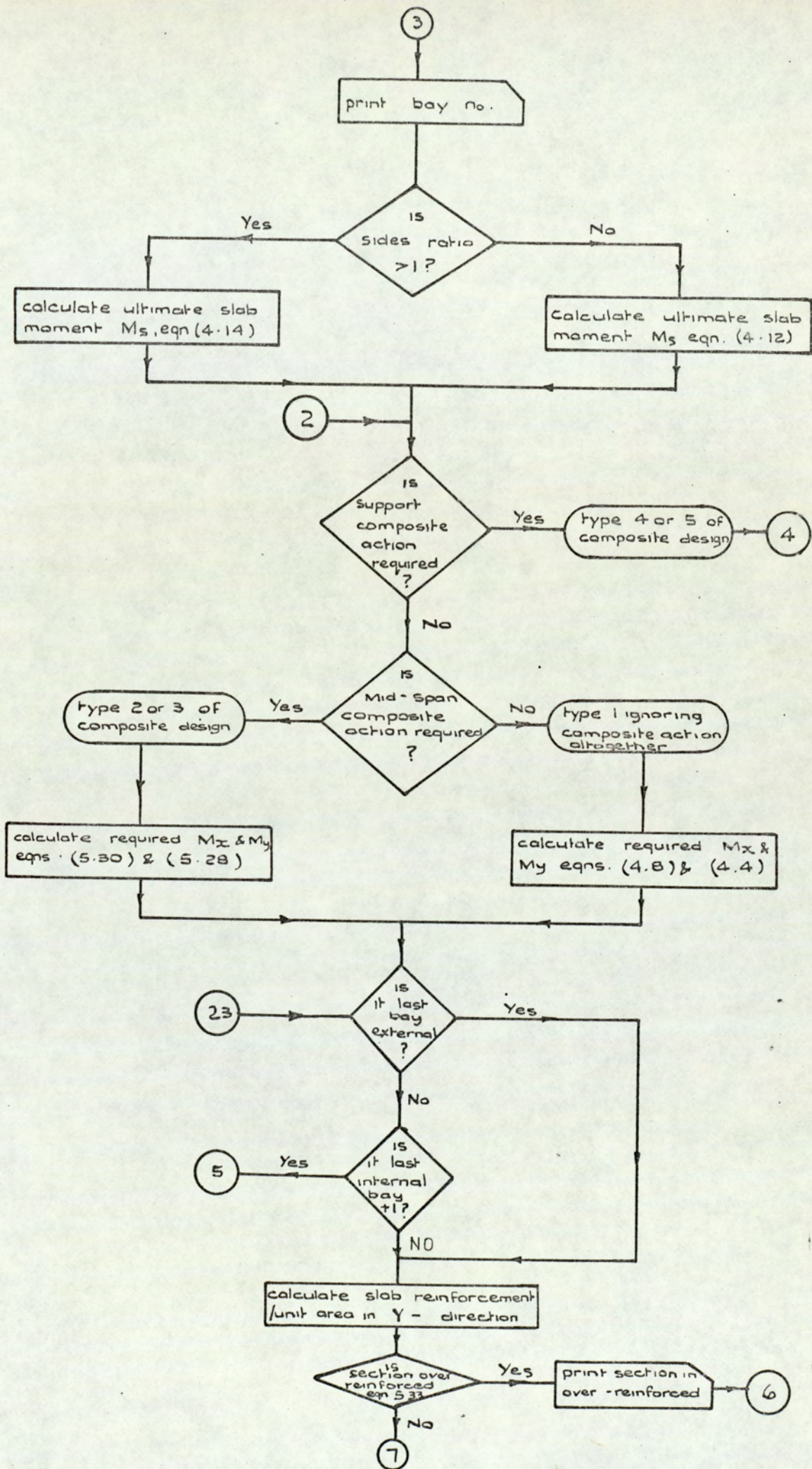
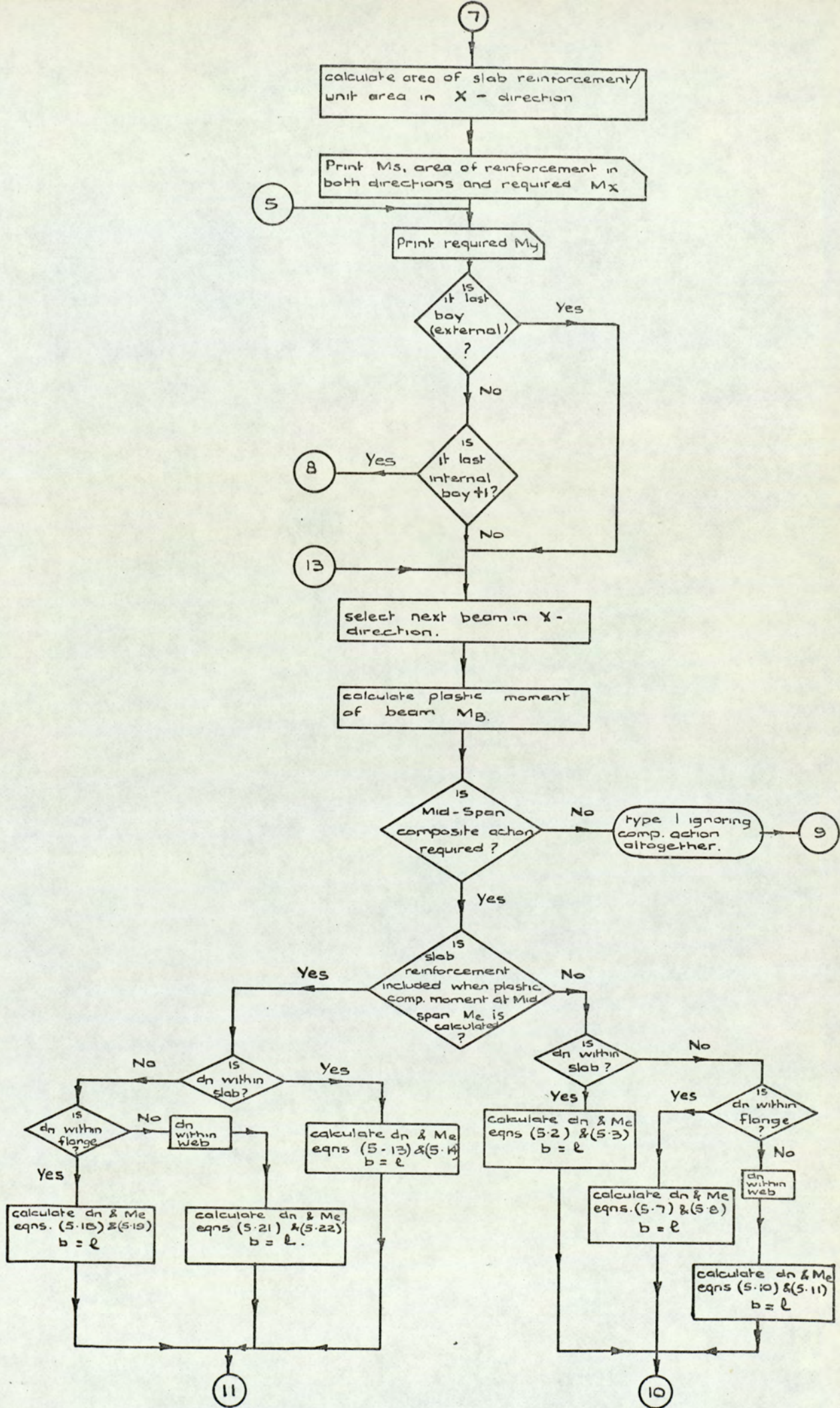
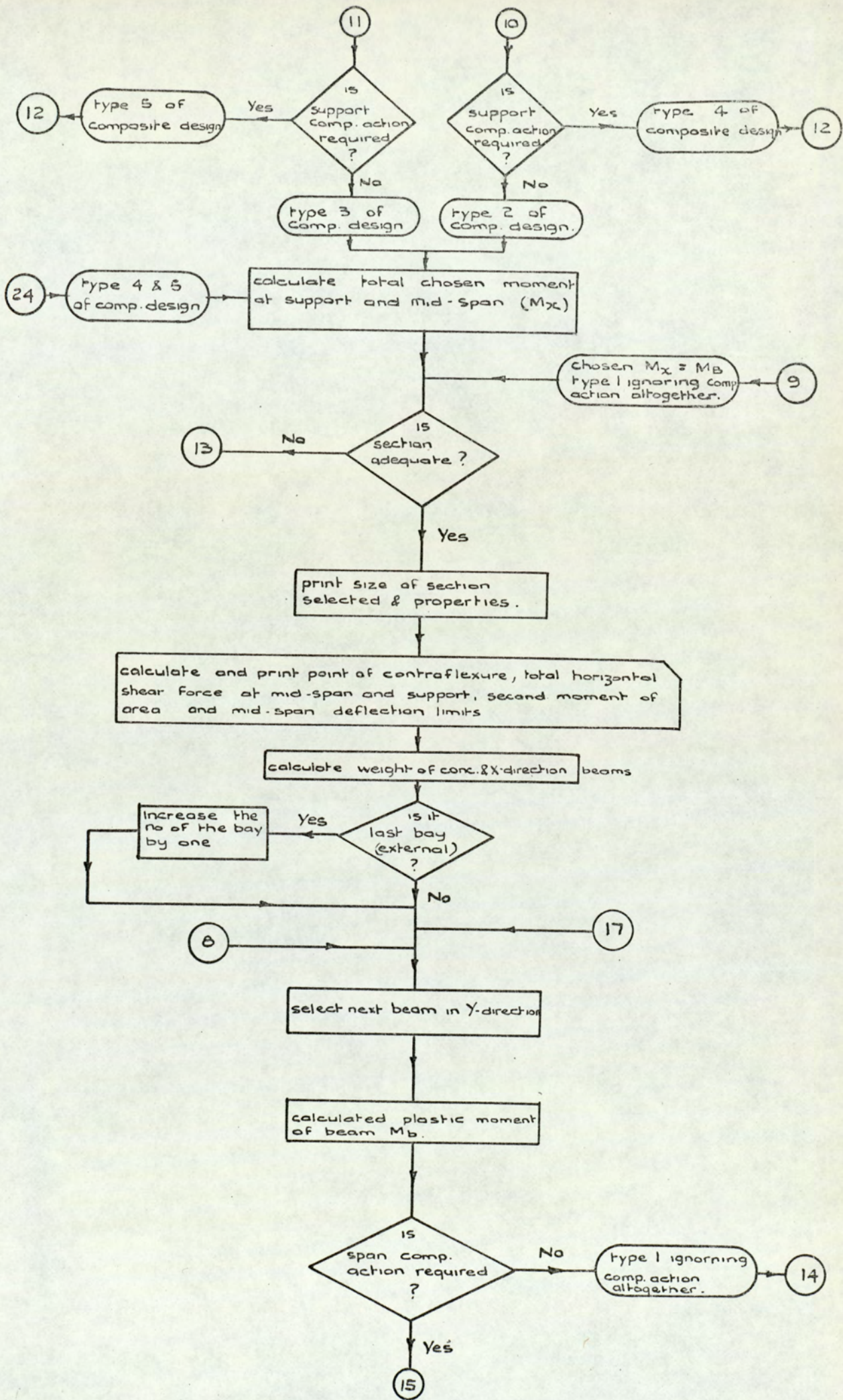
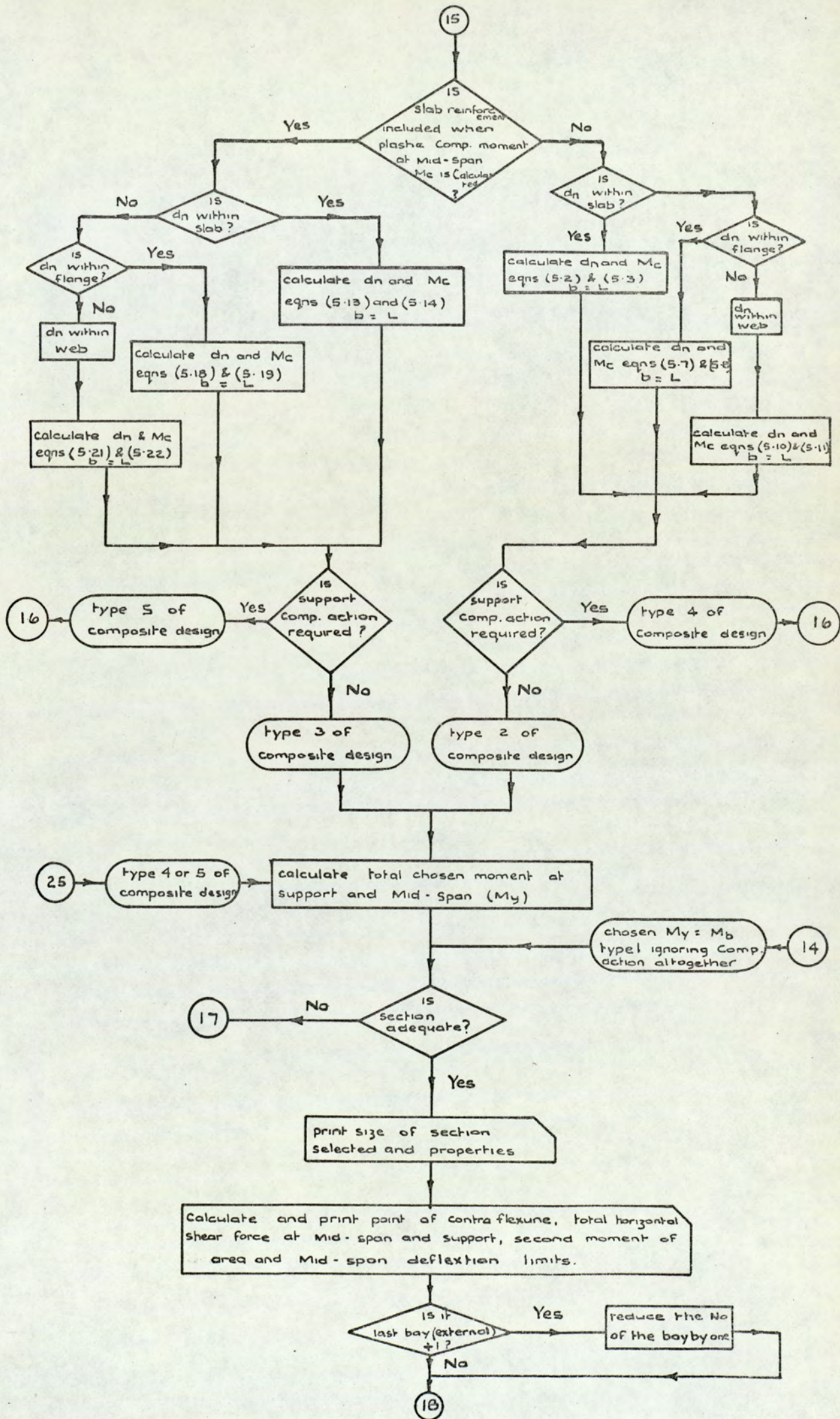


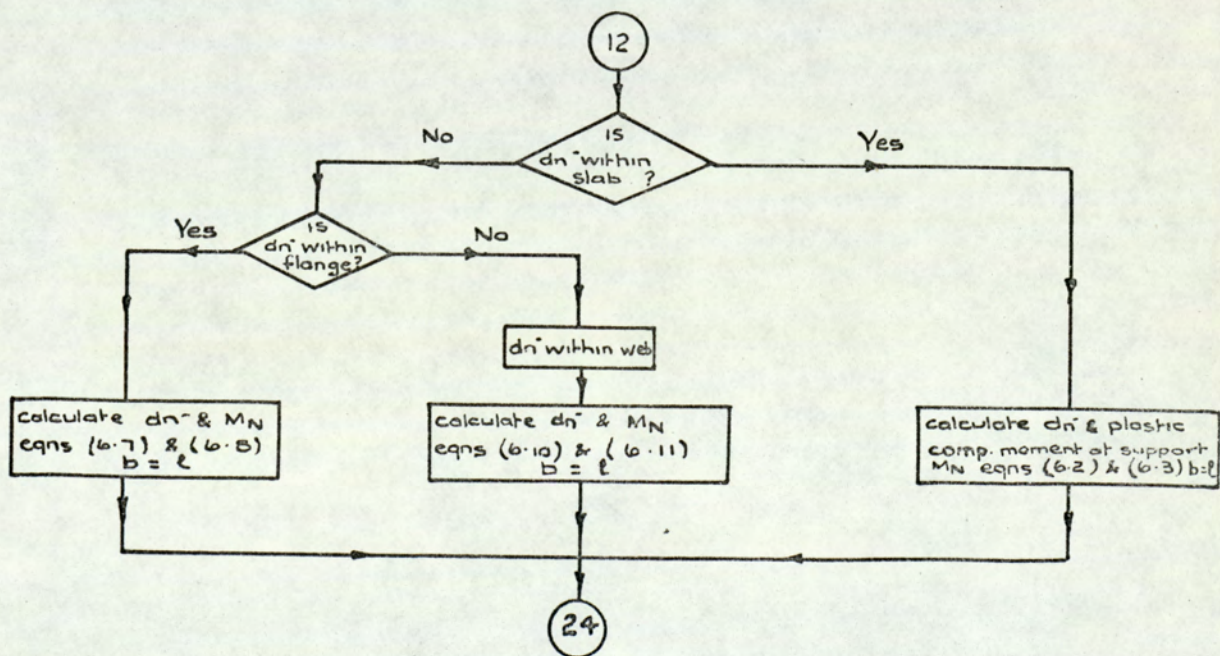
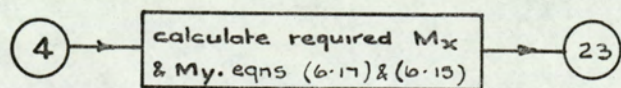
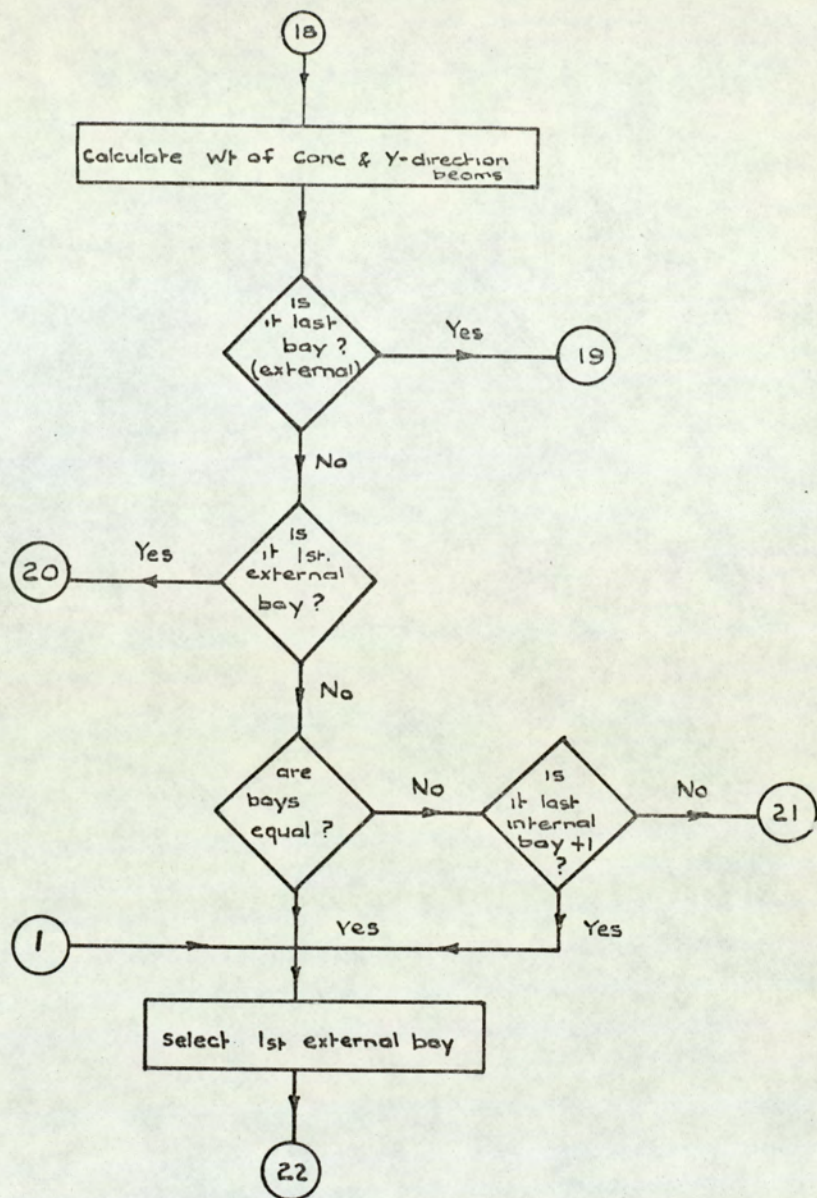
Fig. 7. 2 . Flow diagram of the general computer program for the design of beam and slab floor systems.

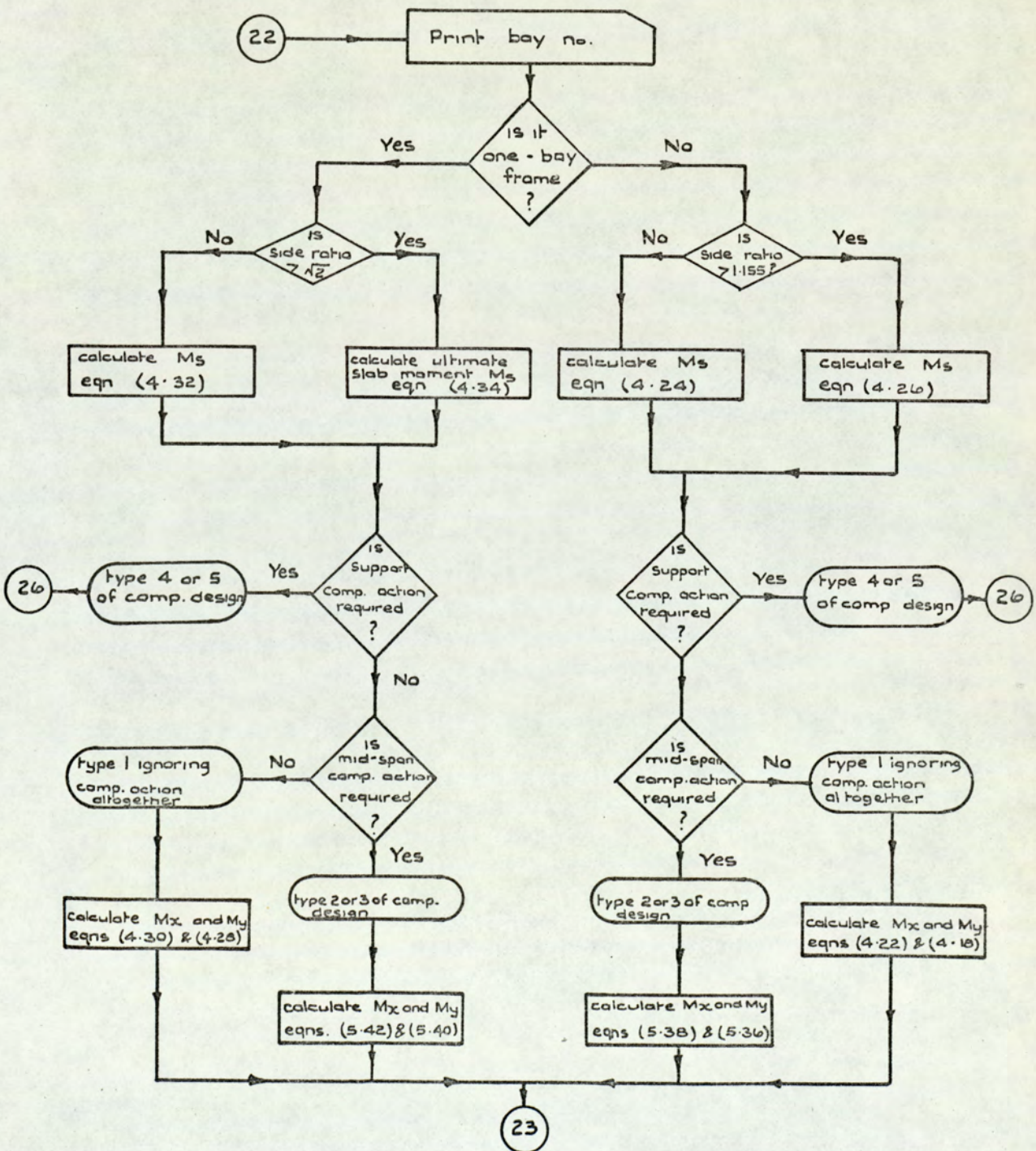
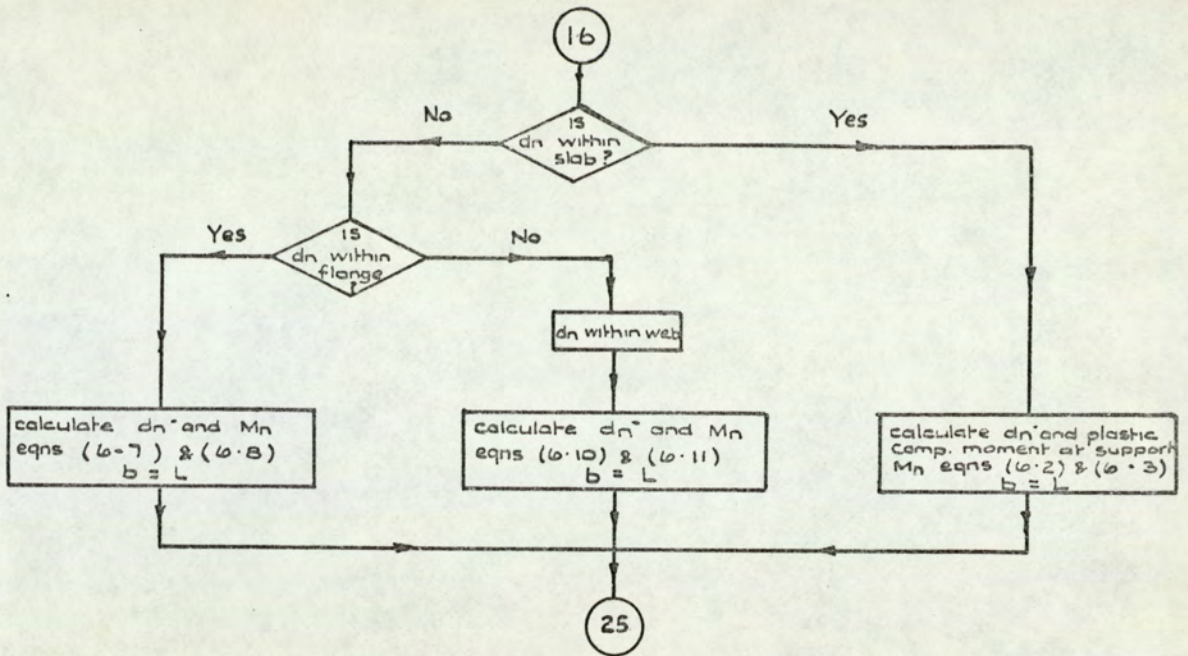


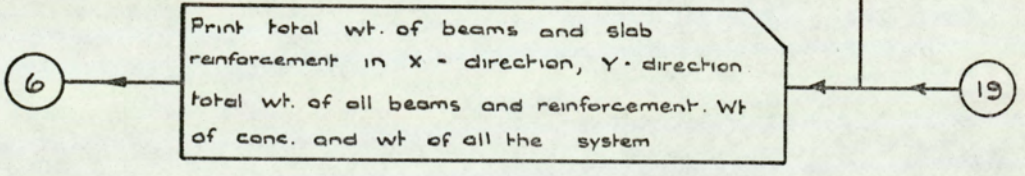
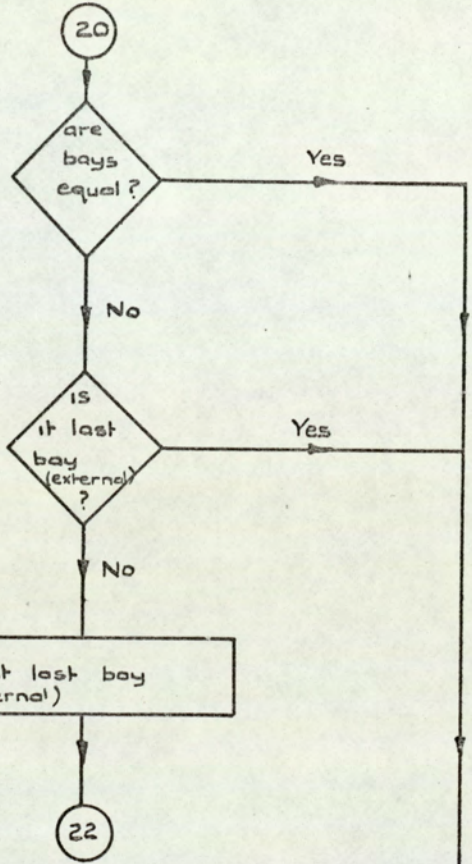
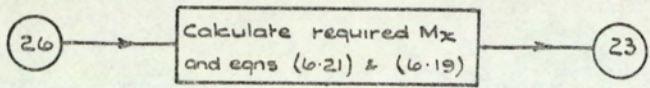












2. Number of Cases

3. Live Load (lbs./sq.ft.)

4. Data Representing Which Assumption On Degree
Of Composite Action Is Being Considered

- (a) A zero value to indicate that composite action at the supports of the main and secondary beams is ignored, i.e. type (1), (2) or (3) assumption on degree of composite action. This value will be 1.0 if composite action at the supports is taken into consideration, i.e. type (4) or (5) of composite design.
- (b) A value of 1.0 indicates no composite action at all, i.e. type (1). A zero value indicates types (2), (3), (4) and (5).
- (c) A value of zero indicates that slab reinforcement effects are ignored when the plastic composite moments at mid-spans of the supporting beams M_c and M_e are calculated, i.e. type (1) of non-composite design or types (2) and (4) of composite design. A value of unity indicates types (3) and (5) of composite design, where slab reinforcement effects are included when M_c and M_e are calculated.

5. Yield Stresses and Sizes of Slab Reinforcement Data

- (a) Yield stress of sections (lbs./in.²)
- (b) Yield stress of slab reinforcement (lbs./in.²)
- (c) Concrete cover for the reinforcing bars + $\frac{1}{2}$ the diameter of the X - direction slab reinforcement.
- (d) Concrete cover for the reinforcing bars + the diameter of the X - direction slab reinforcement + $\frac{1}{2}$ the diameter of the Y - direction slab reinforcement.

6. Frame Data

- (a) Frame number
- (b) Total number of bays

- (c) Type of assumption on degree of composite action
- (d) A value always put in as zero except in the case of two-bay frames when 1.0 is used
- (e) A value of zero indicates that the bays are of equal length. This value will be unity for unequal bay frames.
- (f) Width of the frame (ft.)
- (g) A zero value for the length of the fictitious bay before the first (external) bay length
- (h) The length of each bay (ft.). In the case of equal two-bay frames, the length of the internal fictitious bay is the same as that of the external bays. For unequal two-bay frames, the length of the internal fictitious bay must always be equal to that of the left hand side external bay.
- (i) A zero value for the length of the fictitious bay after the last (external) bay length

This completes the data for any one case. Further cases (i.e. any of the other assumptions on degree of composite action, or another frame altogether for any of the five types of assumptions on degree of composite action) may be designed by repeating sections (3) to (6) for each case.

The data tape is terminated with

*** Z

7.4 EXPLANATION

This refers to the preparation of the data tape in the previous section.

7.4.1 SECTION DATA

The properties of all the sections presented are stored in an array form, row by row for each section, (two dimensional array). This data could be stored permanently on a magnetic tape so that it can be used as required.

In the design examples attempted seventy four Universal Beam sections were used, i.e. all the Universal Beam sections available in the steel tables⁽⁷²⁾. Owing to the lack of availability of a complete range of sections, from the point of view of weight per unit length, and for more accurate comparison between the various assumptions on degree of composite action in weight saving, the six joists available in the steel tables⁽⁷²⁾ were also used.

The data for the lightest beam is input in the first row followed by that of the next heaviest in the second row and so on. Where more than one beam section has the same weight per unit length, then the data of the section with the smallest plastic modulus, which is usually the shallowest, is input first. It was found for beam sections having the same weight per unit length that the plastic modulus was directly proportional to both their plastic moment and the sum of their plastic moment at support and mid-span (i.e. M_x or M_y) for the various assumptions on degree of composite action. Hence the beams selected by the computer, according to the section's input data sequence, are the most economical sections available.

There are several limitations imposed upon the standard sections which could lead to the rejection of several of them:-

- (a) Plastic hinge action is not permitted in a section (whether it is to be used as a beam or a column) if the flange width to thickness ratio exceeds 15 in the case of high yield steel or 18 in the case of mild steel to B.S.15⁽⁷³⁾. Exceeding these limits will lead to premature local buckling in the plastic range. For mild steel (used in all the design examples) all the standard sections are satisfactory in this respect. If high tensile steel is to be used, then several sections are unsuitable. (These may be found in the steel tables⁽⁷²⁾).
- (b) Premature web buckling may occur⁽⁷⁴⁾ if the mean axial stress

exceeds a value related to the size of the section, and if the web depth to thickness ratio exceeds 44 in the case of high tensile steel or 53 in the case of mild steel. No Universal Beam sections are liable to such buckling if used as beams.

- (c) Where beams are not laterally restrained by the floors, a limit is set to the slenderness ($\frac{L}{r}$) ratio. The limit is $13.5 \sqrt{T}$ ⁽⁷⁵⁾ with a maximum value of 150, where T is a measure of the torsional stiffness of the beam. In all the designs attempted for type (1) assumptions on degree of composite action (where composite action is assumed not to exist between floors and the supporting beams) lateral restraint is assumed to exist. For the other four assumptions on degree of composite action, composite action is present and hence lateral restraint is also present.

As mentioned earlier, there are seventy-four Universal Beams given in the steel tables ⁽⁷²⁾. However, if there is no restriction on the depth of the sections selected, then the most economical design from the point of view of weight and deflection for any of the assumptions on degree of composite action may be obtained by using a limited range of thirty-one of these. Each of the remaining forty-three sections has a plastic modulus which is less than that of one of the other thirty-one, with a weight per unit length which is at least as great. Thus, in this case, none of these forty-three beams needs to be considered, since, when selecting a beam, there is always another section which is stronger (whether composite or non-composite), yet no heavier. For reference purposes, the sectional properties of this limited range of Universal Beams is given in Table 7(i). If only these thirty-one beams are used instead of the above mentioned seventy-four beams, then a considerable amount of computer storage and time will be saved.

7.4.2 YIELD STRESSES AND SIZES OF SLAB REINFORCEMENT DATA

- (a) Mild steel to B.S.15 ⁽⁷³⁾ is assumed for all the beam sections,

Ref. No.	Area of Section (in. ²)	Depth of Section (in.)	Fully Plastic Modulus (in. ³)	Width of Section (in.)	Thickness		Second Moment of Area (in. ⁴)	Serial Size
					Flange (in.)	Web (in.)		
1	4.40	10.00	16.0	4.0	0.269	0.230	68.8	10 × 4 × 15
2	4.86	12.00	20.6	4.0	0.269	0.230	105.3	12 × 4 × 16 $\frac{1}{2}$
3	5.62	12.16	24.8	4.01	0.349	0.240	130.1	12 × 4 × 19
4	6.47	13.72	32.8	4.936	0.335	0.233	196.2	14 × 5 × 22
5	7.35	11.96	32.9	4.864	0.421	0.284	171.6	12 × 5 × 25
6	7.64	15.64	43.9	5.582	0.340	0.249	298.1	16 × 5 $\frac{1}{2}$ × 26
7	8.81	13.86	47.1	6.733	0.383	0.270	289.6	14 × 6 $\frac{3}{4}$ × 30
8	9.12	15.84	54.1	5.605	0.440	0.272	374.9	16 × 5 $\frac{1}{2}$ × 31
9	10.00	14.00	54.5	6.750	0.453	0.287	339.2	14 × 6 $\frac{3}{4}$ × 34
10	10.29	15.00	58.5	6.000	0.490	0.306	385.5	15 × 6 × 35
11	10.59	15.85	63.8	6.992	0.428	0.229	446.3	16 × 7 × 36
12	11.77	16.00	72.7	7.0	0.503	0.307	515.5	16 × 7 × 40
13	13.23	17.86	89.6	7.476	0.500	0.334	704.8	18 × 7 $\frac{1}{2}$ × 45
14	14.71	18.00	100.9	7.500	0.570	0.358	800.6	18 × 7 $\frac{1}{2}$ × 50
15	16.17	20.80	125.2	8.216	0.520	0.376	1137.6	21 × 8 $\frac{1}{4}$ × 55
16	18.23	20.99	144.1	8.24	0.615	0.400	1326.8	21 × 8 $\frac{1}{4}$ × 62
17	20.00	23.71	175.6	8.961	0.582	0.416	1815.1	24 × 9 × 68
18	22.37	23.91	200.3	8.985	0.682	0.440	2096.4	24 × 9 × 76
19	24.71	26.69	243.3	9.962	0.637	0.462	2827.7	27 × 10 × 84
20	27.65	26.91	277.8	9.990	0.747	0.490	3266.8	27 × 10 × 94
21	29.11	29.68	315.1	10.444	0.690	0.580	4049.1	30 × 10 $\frac{1}{2}$ × 99
22	33.53	27.28	342.7	10.070	0.932	0.570	4080.5	27 × 10 × 114
23	34.13	30.00	377.5	10.50	0.850	0.564	4919.1	30 × 10 $\frac{1}{2}$ × 116
24	34.69	32.87	414.7	11.482	0.740	0.552	5896.0	33 × 11 $\frac{1}{2}$ × 118
25	38.26	33.10	465.9	11.510	0.855	0.580	6699.0	33 × 11 $\frac{1}{2}$ × 130
26	39.69	35.55	509.2	11.944	0.795	0.597	7801.3	36 × 12 × 135
27	44.16	35.84	580.0	11.972	0.940	0.625	9012.1	36 × 12 × 150
28	49.98	36.16	667.0	12.027	1.100	0.680	10470.0	36 × 12 × 170
29	57.11	36.48	766.8	12.117	1.260	0.770	12103.0	36 × 12 × 194
30	67.73	35.88	942.5	16.475	1.260	0.765	14988.0	36 × 16 $\frac{1}{2}$ × 230
31	76.56	36.24	1076.0	16.555	1.440	0.845	17234.0	36 × 16 $\frac{1}{2}$ × 260

Table 7(i). Sectional properties of 31 Universal Beams

giving a yield stress of 16.0 tons/sq.in.

- (b) Mild steel is assumed for the slab reinforcement in all the design examples, giving a yield stress of 36,000 lbs./sq.in. in accordance with Table II of C.P. 114⁽⁶⁹⁾.
- (c) According to C.P. 114⁽⁶⁹⁾ a minimum concrete cover not less than $\frac{1}{2}$ inch nor less than the diameter of the reinforcement must be used. Assuming $\frac{1}{2}$ inch diameter bars for the slab reinforcement in both directions for all the design examples. The concrete cover + half the diameter of reinforcement is therefore taken as 0.75 inch. This value is input in the data to determine the effective slab depth in the (longitudinal) X - direction ($t - 0.75$), where t is the slab thickness.
- (d) Similarly, the value of the concrete cover + one and a half times the diameter of reinforcement, as slab reinforcement is equal in both directions, is taken as 1.25 inches. This is the value input in the data to determine the effective slab depth in the (transverse) Y - direction.

7.4.3 FRAME DATA

Failure by mode A of an internal bay (Figure 4.1) consists of one secondary beam and a slab width equal to the average length of the two adjacent bays. This slab width equals the length of the bay for equal bay frames. For an external bay failure by mode A (Figure 4.1) consists of one secondary beam and a slab width equal to half the length of the external bay. The average of the two adjacent bays is always taken automatically by the computers for each bay. For this reason, a zero value for a fictitious bay length is always input in the data tape before the first (external) bay length and the average of the two adjacent bays, in this case, is the same as half the length of the external bay. For the same

reason, a zero value is input after the last (external) bay length.

In the case of two-bay frames, the reason for having a fictitious bay inbetween the two bays is to enable the secondary beam between them ($L_y(2)a$, Figure 7.3.a) to be designed. The width of the slab on the top of this beam for failure by mode A is the average length of the two adjacent bays as shown in the shaded area Figure 7.3.a. The width of the slab on the top of the same beam for the frame with the fictitious internal bay inbetween, shown shaded in Figure 7.3.b., must always be the same as that of Figure 7.3.a. For this reason the length of the fictitious internal bay for unequal two-bay frames must always be the same as that of the left hand side external bay. In the case of equal two-bay frames (e.g. Frame No. 6 Figure 7.4.a) the length of the fictitious internal bay is the same as that of the external bays as shown in Figure 7.4.b. In the case of two-bay frames, a value of 1 is input in the data tape in position 7.3.6.(d). Hence the weight of the internal fictitious bay beams $L_x(2)b$ and $L_y(2)b$, slab reinforcement and concrete shown in Figure 7.3.b, will be ignored and the complete design will be that of a two-bay frame, Figure 7.3.a.

The frame data for the unequal two-bay frame 5, Figure 7.3.a, shown with the fictitious bay inbetween in Figure 7.3.b, for type (2) assumption on degree of composite action are shown below:-

(a) -> (f) 5 3 2 1 1 20.0

(g) -> (i) 0 30.0 30.0 18.0 0

The (g) -> (i) frame data values for the two equal bay frame 6, Figure 7.4.a, are:-

0 26.0 26.0 26.0 0

The frame data for the one-bay frame 4 for type (3) assumption on degree of composite action are shown below:-

(a) -> (f) 4 1 3 0 0 20.0

(g) -> (i) 0 30.0 0

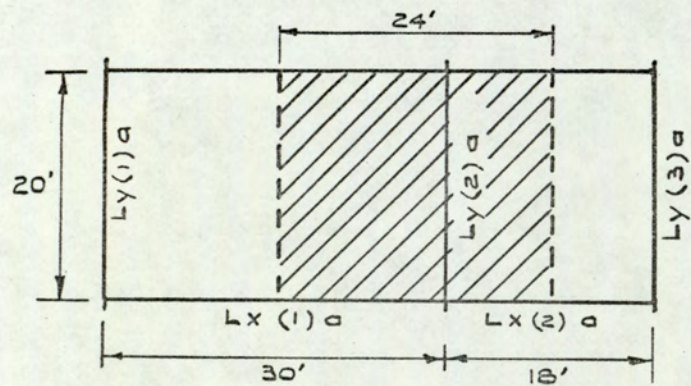


Fig. 7.3.a. Unequal two-bay frame 5.

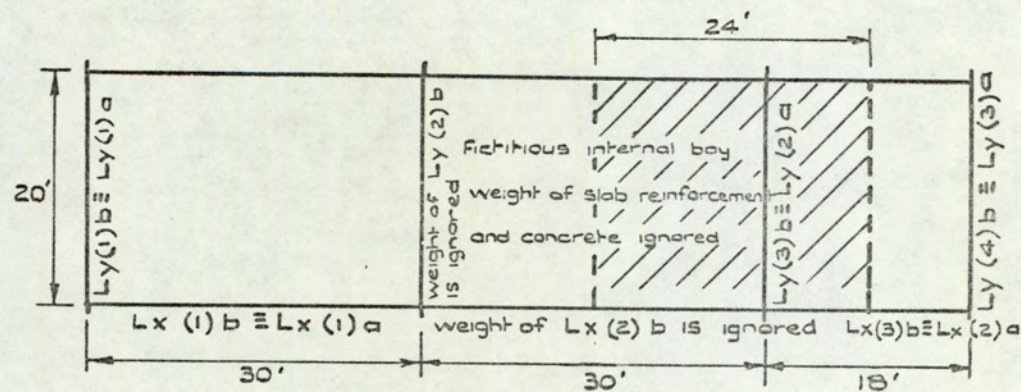


Fig. 7.3. b. Unequal two-bay frame 5 with a fictitious bay inbetween.

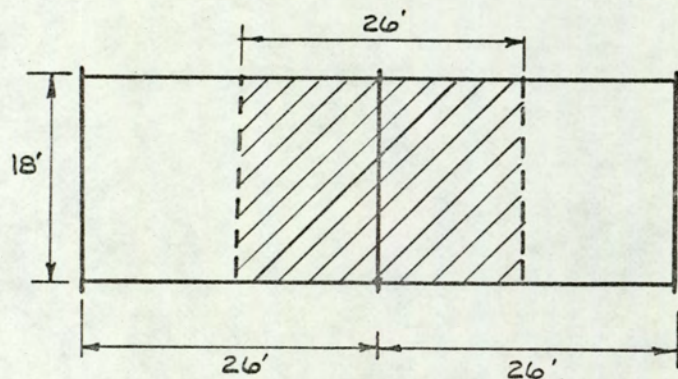


Fig. 7.4. a. Equal two-bay frame 6.

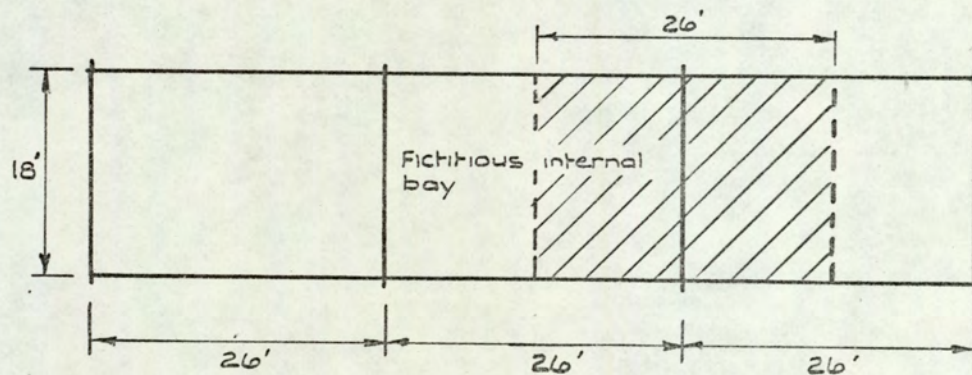


Fig. 7.4. b. Equal two-bay frame 6 with a fictitious bay inbetween.

In the next section, a typical output of the computer program for the complete design of frame 1 (Figure 7.1) for type (5) assumption on degree of composite action will be shown. The complete data for this design is as follows:-

80								Number of beams
1.32	3.0	1.539	2.0	0.224				Properties of
0.15	2.0	3.0	2.0	4.5				3 × 2 × 4 $\frac{1}{2}$ Joist
Section properties for the other five joists								
4.40	10.0	16.0	4.0	0.269				Properties of
0.230	68.8	10.0	4.0	15.0				10 × 4 × 15 U.B.
Section properties for the other seventy-three Universal Beams								
1								Total number of cases
100								Live load
1.0	0	1						(a) -> (c) Data for type
								(5) of composite design
35840	36000	0.75	1.25					(a) -> (d) Data for yield
								stresses and slab rein-
								forcement
1	5	5	0	0	20.0			(a) -> (f) Frame data
0	30.0	30.0	30.0	30.0	30.0	0		(g) -> (i) Frame data
***Z								

7.5 TYPICAL OUTPUT OF THE COMPUTER PROGRAM

Frame 1 (Figure 7.1) is used to demonstrate a typical output of the computer program for the complete design of a frame. Frame 1 consists of five equal bays of length 30 feet. The width of the frame is 20 feet. Hence the sides ratio (ρ) is 0.67, which implies mode C independent slab collapse for the internal and external bays. A live load of 100 lbs./sq.ft. is applied, with an assumed cube strength of 4,000 lbs./sq.in. and a slab

thickness of 5 inches. Consideration is given to type (5) assumption on degree of composite action.

The computer selects the first internal bay (bay no. 2) and calculates its ultimate slab moment per unit run M_s , hence the area of reinforcement in both directions A_{t1} and A_{t2} . The main beam $L_x(2)$ (i.e. beam spanning in the X - direction (bay no. 2)) and the secondary beam $L_y(2)$ (i.e. beam spanning in the Y - direction (bay no. 2)) are then designed and their composite properties are calculated. Since all the internal bays are identical, the computer designs only the first internal bay. The first external bay is then selected and similarly designed. Since the two external bays are identical, the design of the whole frame is complete. Finally, the weight of the beams, slab reinforcement, concrete and of the whole frame are printed. The complete output design of Frame 1 for type (5) assumption on degree of composite action is shown below:-

Frame 1 type (5)

Cube strength = 4000 lbs./sq.in.

Slab thickness = 5 inches

Bay No. 2

$M_s(2) = 3.38$ kips - ft./ft.run (equation 4.12)

$A_{t1} = 0.28$ in.²/ft.run (equation 5.32)

$A_{t2} = 0.33$ in.²/ft.run

Required $M_x(2) = 639.84$ kips - ft. (equation 6.17)

Required $M_y(2) = 430.83$ kips - ft. (equation 6.15)

CHOSEN BEAM SIZE IN $L_x(2)$ DIRECTION = $16 \times 5\frac{1}{2} \times 31$ U.B.

$M_B = 161.58$ kips - ft. $M_N = 283.14$ kips - ft. $M_e = 396.26$ kips - ft.

Chosen $M_x(2) = 679.4$ kips - ft.

d_n (at mid-span) = 1.24 inches d'_n (at support) = 5.31 inches

Distance of point of contraflexure from support = 3.54 feet

Horizontal shear force in $L_x(2)$ direction due to mid-span composite action
= 145.92 tons

Horizontal shear force in Lx(2) direction due to support composite action
= 90.39 tons

Second moment of area of Lx(2) composite section = 1410.56 in.⁴

Maximum allowable deflection at mid-span = 1.0 inch

Limits of mid-span deflection = 0.89" → 0.17" (i.e. limits of mid-span deflection at working load of the composite section if considered simply supported or encastré depending on the stiffness of the supporting columns)

CHOSEN BEAM SIZE IN Ly(2) DIRECTION = 12 × 4 × 16 $\frac{1}{2}$ U.B.

M_b = 61.53 kips - ft. M_n = 194.62 kips - ft. M_c = 251.3 kips - ft.

d_n = 0.82 inches d_n' = 4.72 inches

Distance of point of contraflexure frame support = 2.49 feet

Horizontal shear force in Lx(2) direction due to mid-span composite action
= 77.76 tons

Horizontal shear force in Ly(2) direction due to support composite action
= 77.76 tons

Second moment of area of Ly(2) composite section = 562.6 in.⁴

Maximum allowable deflection at mid-span = 0.67 inches

Limits of mid-span deflection = 0.659" → 0.132"

Bay No. 1

M_s(1) = 3.73 kips - ft./ft.run (equation 4.24)

A_{t1} = 0.31 in.²/ft. run A_{t2} = 0.36 in.²/ft.run

Required M_x(1) = 639.84 kips - ft. (equation 6.21)

Required M_y(1) = 215.41 kips - ft. (equation 6.19)

CHOSEN BEAM SIZE IN Lx(1) DIRECTION = 15 × 6 × 35 U.B.

M_B = 174.72 kips - ft. M_N = 305.44 kips - ft. M_e = 429.3 kips - ft.

Chosen M_x(1) = 669.39 kips - ft.

d_n = 1.39 inches d_n' = 5.34 inches

Distance of point of contraflexure from support = 5.53 feet

Horizontal shear force in Lx(1) direction due to mid-span composite action
= 164.64 tons

Horizontal shear force in $L_x(1)$ direction due to support composite action
= 100.25 tons

Second moment of area of $L_x(1)$ composite section = 1447.22 in.⁴

Maximum allowable deflection at mid-span = 1.0 inch

Limits of mid-span deflection = 0.87" → 0.17"

CHOSEN BEAM SIZE IN $L_y(1)$ DIRECTION = 6 × 3 $\frac{1}{2}$ × 11 $\frac{1}{2}$ JOIST

$M_b = 23.92$ kips - ft. $M_n = 90.47$ kips - ft. $M_c = 128.65$ kips - ft.

Chosen $M_y(1) = 219.13$ kips - ft.

$d_n = 0.99$ inches $d'_n = 4.77$ inches

Distance of point of contraflexure from support = 2.34 feet

Horizontal shear force in $L_y(1)$ direction due to mid-span composite action
= 54.08 tons

Horizontal shear force in $L_y(1)$ direction due to support composite action
= 54.08 tons

Second moment of area of $L_y(1)$ composite section = 174.38 in.⁴

Maximum allowable deflection at mid-span = 0.67 inches

Limits of mid-span deflection = 1.06" → 0.21"

Total weight of beams in L_x direction = 2.183 tons

Total weight of beams in L_y direction = 0.795 tons

Total weight of all the supporting beams in the frame = 2.978 tons

Total weight of slab reinforcement in L_x direction (longitudinal) = 1.593 tons

Total weight of slab reinforcement in L_y direction (transverse) = 1.929 tons

Total weight of all slab reinforcement in the frame = 3.522 tons

Total weight of all the concrete in the frame = 80.357 tons

Total weight of the whole frame = 86.857 tons

The time taken to design this frame for four different cube strengths and four slab thicknesses on the Atlas Computer is 30 seconds. Hence the computer time taken to design the complete output above (i.e. one cube strength and one slab thickness) is approximately two seconds.

The results of the complete design of frame 1 by type (5) composite design, together with the designs by the other four assumptions on degree of composite action are shown in Figure 7.5. All these designs are considered for a live load of 100 lbs./sq.ft., a cube strength of 4000 lbs./sq.in. and a slab thickness of 5 inches. Figure 7.6 also shows the results of the complete design of frame 1 by the five types of assumptions on degree of composite action for the same applied live load and cube strength, but for a slab thickness of 7 inches.

7.6 DESIGN EXAMPLES

In order to test the capability of the program to design single-bay and multi-bay beam and slab floor systems, twelve frames were deliberately devised. These frames were used to investigate the effects of various parameters on their weights. These frames were also used to compare the various assumptions on degree of composite action from the point of view of weight and deflection savings. The geometry of every frame is shown in Figure 7.1. A brief discussion on each frame is given below.

Frame 1:-

This is a five equal bay frame. The sides ratio (ρ) is 0.67, hence independent slab collapse occurs by mode C for both internal and external bays. The designs of this frame, together with that of frame 2 below for various types of composite action are investigated in detail to study the effects of varying the slab thickness and cube strength on the weight of beam and slab floor systems. Comparisons between the beams selected by the various types of assumptions on degree of composite action from the point of view of deflection, overall structural efficiency and failure load are made using this frame.

Frames 2 and 3:-

Frame 2 is an unequal six-bay frame, where the two external bays and the first and last internal bays are identical. This was devised to check

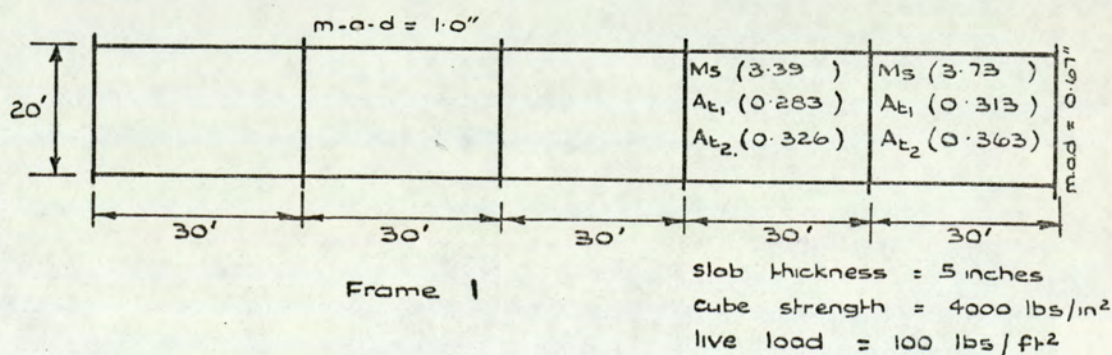
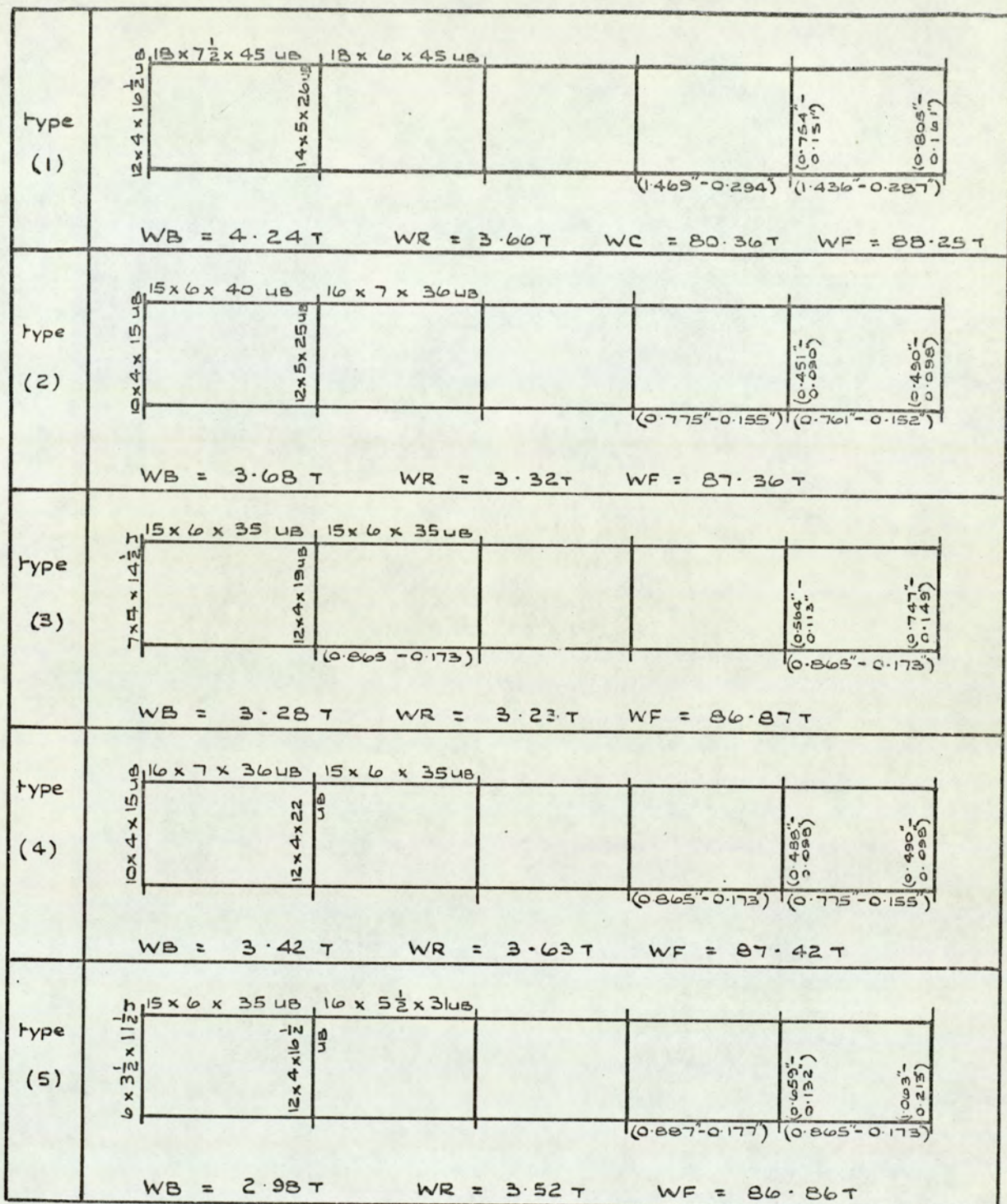
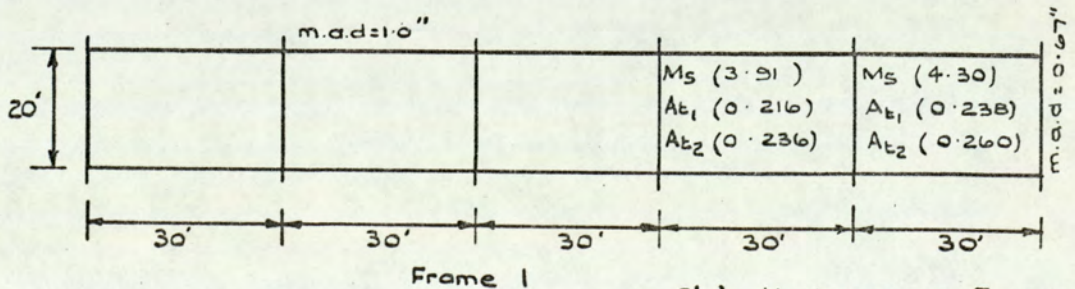


Fig. 7. 5. The complete design of frame I for each of the five types of assumptions on degree of composite action.

type (1)		$WB = 4.85 T$ $WR = 2.71 T$ $WC = 112.5 T$ $WF = 120.05 T$
type (2)		$WB = 3.88 T$ $WR = 2.43 T$ $WF = 118.80 T$
type (3)		$WB = 3.31 T$ $WR = 2.36 T$ $WF = 118.17 T$
type (4)		$WB = 3.57 T$ $WR = 2.64 T$ $WF = 118.71 T$
type (5)		



Slab thickness = 7 inches
 cube strength = 4000 lbs/in²
 live load = 100 lbs/ft²

Fig. 7. 6. The complete design of frame 1 for each of the five types of assumptions on degree of composite action.

the accuracy of the program. Independent slab failure of both internal and external bays of this frame occurs by mode C. Figures 7.7 and 7.8 show the results of the complete design of frame 2 by the five types of assumptions on degree of composite action for two slab thicknesses 5 inches and 7 inches and the same cube strength of 4000 lbs./sq.in. and live load of 100 lbs./sq.ft. The time taken on the Atlas Computer to design frame 2 by any of the five types of assumptions shown in Figure 7.7 or 7.8 for one cube strength and one slab thickness is approximately four seconds.

Frame 3 is another six unequal bay frame with different sides ratio (ρ) for each bay. The sides ratio (ρ) of the internal bays vary between 0.57 and 1.33, hence independent slab collapse occurs by mode C or D depending on whether the sides ratio (ρ) \geq 1.0.

Frame 4:-

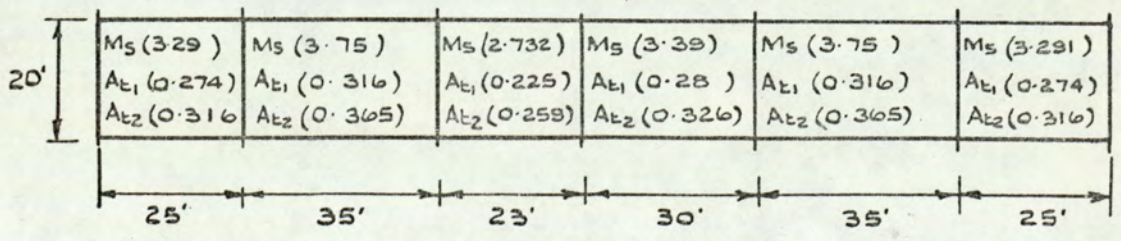
This is a one-bay frame devised to test the capability of the program for the design of single-bay frames. Figure 7.9 shows the results of the complete design of this frame by the five types of assumption on degree of composite action for a slab thickness of 5 inches, cube strength of 4000 lbs./sq.in. and live load of 100 lbs./sq.ft.

Frames 5 and 6:-

Both of these frames are two-bay frames, where a fictitious bay has to be inserted inbetween the two bays for the frame to be designed by the computer program. Hence each frame is treated as a three-bay frame with the weight of the internal fictitious bay ignored.

Frame 5 has two unequal bays, the frame data preparation for it is shown in section 7.4.3 (Figures 7.3.a and 7.3.b). Figure 7.10 shows the results of the complete design of this frame for the five types of assumptions on degree of composite action for slab thickness of 5 inches, cube strength of 4000 lbs./sq.in. and live load of 100 lbs./sq.ft.

type (1)		$WR = 4.13$ $WB = 4.87T$ $WC = 92.68T$ $WF = 101.67T$
type (2)		$WR = 3.74T$ $WB = 4.01T$ $WF = 100.43T$
type (3)		$WR = 3.60T$ $WB = 3.75T$ $WF = 100.06T$
type (4)		$WR = 4.09T$ $WB = 3.90T$ $WF = 100.66T$
type (5)		$WR = 3.96T$ $WB = 3.56T$ $WF = 100.20T$



Frame 2.

slab thickness = 5 inches.
 cube strength = 4000 lbs/in².
 live load = 100 lbs/ft².

Fig. 7.7. The complete design of frame 2 for each of the five types of assumptions on degree of composite action.

Type (1)		$WR = 3.05T$	$WB = 5.32T$	$WC = 129.75T$	$WF = 138.12T$
Type (2)		$WR = 2.72T$	$WB = 4.39T$	$WF = 136.86T$	
Type (3)		$WR = 2.64T$	$WB = 3.70T$	$WF = 136.09T$	
Type (4)		$WR = 2.97T$	$WB = 3.94T$	$WF = 136.66T$	
Type (5)		$WR = 2.89T$	$WB = 3.56T$	$WF = 136.20T$	

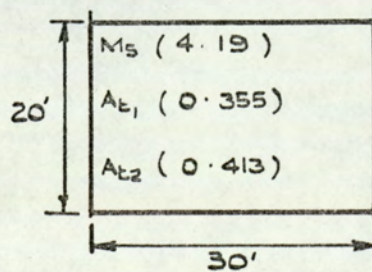
20'	M _s (3.80)	M _s (4.33)	M _s (3.15)	M _s (3.91)	M _s (4.33)	M _s (3.80)
	A _{t1} (0.209)	A _{t1} (0.240)	A _{t1} (0.173)	A _{t1} (0.216)	A _{t1} (0.240)	A _{t1} (0.209)
	A _{t2} (0.229)	A _{t2} (0.262)	A _{t2} (0.262)	A _{t2} (0.236)	A _{t2} (0.229)	A _{t2} (0.229)
	25'	35'	23'	30'	35'	25'

Frame 2.

slab thickness = 7 inches.
 cube strength = 4000 lbs/in².
 live load = 100 lbs/ft².

Fig. 7. 8. The complete design of frame 2 for each of the five types of assumptions on degree of composite action.

type (1)		$WB = 0.94T$ $WR = 0.81T$ $WC = 16.07T$ $WF = 17.82T$
type (2)		$WB = 0.80T$ $WR = 0.76T$ $WF = 17.63T$
type (3)		$WB = 0.69T$ $WR = 0.73T$ $WF = 17.49T$
type (4)		$WB = 0.80T$ $WR = 0.82T$ $WF = 17.68T$
type (5)		$WB = 0.69T$ $WR = 0.79T$ $WF = 17.56T$

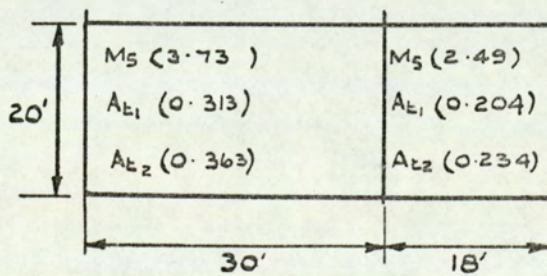


slab thickness = 5 inches.
cube strength = 4000 lbs/in²
live load = 100 lbs/ft²

Frame 4.

Fig. 7.9. The complete design of frame 4 for each of the five types of assumptions on degree of composite action.

type (1)		$WB = 1.26T$ $WR = 1.05T$ $WC = 25.71T$ $WF = 28.02T$
type (2)		$WB = 1.13T$ $WR = 0.96T$ $WF = 27.80T$
type (3)		$WB = 0.97T$ $WR = 0.93T$ $WF = 27.61T$
type (4)		$WB = 1.02T$ $WR = 1.03T$ $WF = 27.76T$
type (5)		$WB = 0.92T$ $WR = 1.00T$ $WF = 27.64T$



Slab thickness = 5 inches
 cube strength = 4000 lbs/ft²
 live load = 100 lbs/ft².

Frame 5

Fig. 7.10. The complete design of frame 5 for each of the five types of assumptions on degree of composite action.

Frame 6 has two equal bays. This frame was devised to test the capability of the computer program for the design of equal two-bay frames. As the two bays are identical and treated as two external bays with fictitious internal bay inbetween, the computer designs only one of them. The data arrangement for the lengths of the bays is shown in Section 7.4.3.

Frames 7 and 8:-

These two frames are both three-bay frames; where frame 7 has equal bays and frame 8 has unequal bays. Figure 7.11 shows the results for the complete design of frame 8 by the five types of assumptions on degree of composite action for slab thickness of 5 inches, cube strength of 4,000 lbs./sq.in. and live load of 100 lbs./sq.ft. It can be shown from Figure 7.11 of frame 8 that the main beam $L_x(2)$ and the secondary beam $L_y(3)$ selected are always the same, as the conditions for modes A and B on the secondary and main beams $L_y(3)$ and $L_x(2)$ respectively are always identical (i.e. width of slab, span and ultimate slab moment are identical in both directions).

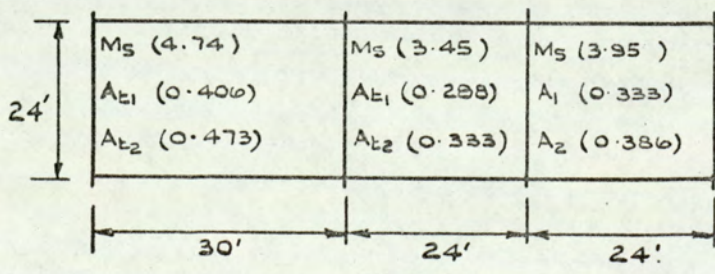
Frames 9 and 10:-

These two frames are both four-bay frames; where frame 9 has equal bays and frame 10 has unequal bays. Frame 10 is chosen, together with frames 1 and 3, to investigate the effects of extreme loading conditions on the weight of beam and slab floor systems.

Frames 11 and 12:-

These two frames are both five-bay frames with equal bays. Frame 11 has sides ratio (ρ) of 0.5, whereas frame 12 has sides ratio (ρ) of 2.0. Both frames have equal total areas and equal individual bay areas. These two frames were chosen to investigate the effect of extreme values of sides ratios on the weight of beam and slab floor systems having the same slab

type (1)		$WB = 2.65T$ $WR = 2.65T$ $WC = 50.14T$ $WR = 55.45T$
type (2)		$WB = 2.19T$ $WR = 2.43T$ $WF = 54.76T$
type (3)		$WB = 1.99T$ $WR = 2.36T$ $WF = 54.50T$
type (4)		$WB = 2.07T$ $WR = 2.64T$ $WF = 54.85T$
type (5)		$WB = 1.83T$ $WR = 2.56T$ $WF = 54.54T$



slab thickness = 5 inches
cube strength = 4000 lbs/in²
live load = 100 lbs/ft²

Frame 8

Fig. 7.11. The complete design of frame 8 for each of the five types of assumptions on degree of composite action.

thickness, cube strength and loading. Figures 7.12 and 7.13 show the results of the complete design of frames 11 and 12 respectively by each of the five types of assumption on degree of composite action.

7.7 EFFECT OF VARIATION OF SLAB THICKNESS ON THE WEIGHT OF BEAM AND SLAB FLOOR SYSTEMS

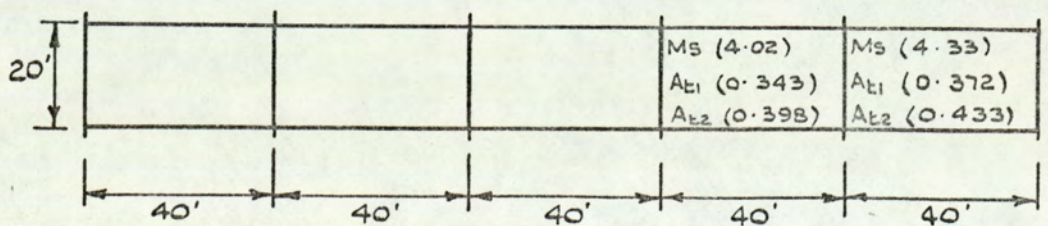
Four slab thicknesses 4 inches, 5 inches, 6 inches and 7 inches were used to investigate the effect of increasing slab thicknesses on the whole beam and slab floor system (i.e. supporting beams, slab reinforcement and concrete).

Figures 7.5 and 7.6 of frame 1 show that the weight of the supporting beams designed by types (1), (2), (3) and (4) assumptions on degree of composite action increases, and those designed by type (5) keep constant when the slab thickness increases from 5 inches to 7 inches. Similar observations are made from Figures 7.7 and 7.8 of frame 2, except that in this case, there is a slight reduction in the weight of the supporting beams designed by type (3) assumption for the same increase in slab thickness.

Figures 7.14 - 7.17 show for frames 1, 2, 5 and 8 the weights of the selected supporting beams of these frames for each of the five types of composite action for the four slab thicknesses used. It can be seen from these figures that in the majority of cases the weight of the supporting beams either increases or keeps constant with increasing slab thickness.

Figures 7.5 and 7.6 of frame 1 show an increase in the weight of the internal bay beam Lx(2) (i.e. main beam spanning in the X - direction, bay no. 2), designed by type (2) assumption, owing to an increase in slab thickness from 5 inches to 7 inches. Table 7(ii) shows the size of this section, together with the required M_x moment, the selected section M_x moment and the excess in the strength (chosen M_x moment) of the selected section compared to the required section for each of the four slab thicknesses used. It can be seen from Table 7(ii) that at $t = 4"$, the selected section is a

type (1)		$WB = 7.30 T$	$WR = 5.83 T$	$WC = 107.14 T$	$WF = 120.33 T$
type (2)		$WB = 6.38 T$	$WR = 5.34 T$	$WF = 118.92 T$	
type (3)		$WB = 5.96$	$WR = 5.15 T$	$WF = 118.30 T$	
type (4)		$WB = 6.11 T$	$WR = 5.86 T$	$WF = 119.18 T$	
type (5)		$WB = 5.85 T$	$WR = 5.64 T$	$WF = 118.69 T$	

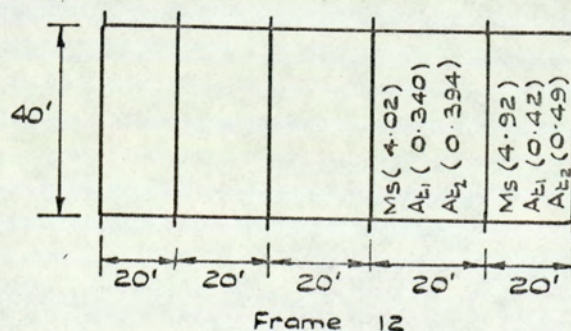


Frame 11

Slab thickness = 5 inches.
 cube strength = 4000 lbs/ins².
 live load = 100 lbs/ft².

Fig. 7.12. The complete design of frame 11 for each of the five types of assumptions on degree of composite action.

type (1)	$14 \times 6 \frac{3}{4} \times 30$ $16 \times 5 \frac{1}{2} \times 26$ UB $16 \times 6 \times 45$ UB $14 \times 9 \times 68$ UB	WB = 7.70 T WR = 6.19 T WC = 107.14 T WF = 121.10 T
type (2)	$16 \times 5 \frac{1}{2} \times 31$ $16 \times 5 \frac{1}{2} \times 26$ UB $15 \times 6 \times 35$ UB $21 \times 6 \frac{1}{4} \times 55$ UB	WB = 6.43 T WR = 5.70 T WF = 119.33 T
type (3)	$12 \times 4 \times 22$ $12 \times 4 \times 19$ UB $14 \times 6 \frac{3}{4} \times 34$ UB $21 \times 6 \frac{1}{4} \times 55$ UB	WB = 6.05 T WR = 5.54 T WF = 118.82 T
type (4)	$14 \times 6 \frac{3}{4} \times 30$ $14 \times 5 \times 26$ UB $16 \times 5 \frac{1}{2} \times 31$ UB $18 \times 6 \times 55$ UB	WB = 6.27 T WR = 6.16 T WF = 119.64 T
type (5)	$12 \times 4 \times 22$ $10 \times 4 \times 19$ UB $16 \times 5 \frac{1}{2} \times 31$ UB $18 \times 6 \times 55$ UB	WB = 5.94 T WR = 5.49 T WF = 119.08 T



slab thickness = 5 ins.
 cube strength = 4000 lbs/in²
 live load = 100 lbs/ft².

Fig. 7.13. Complete design of frame 12 for each of the five types of assumptions on degree of composite action.

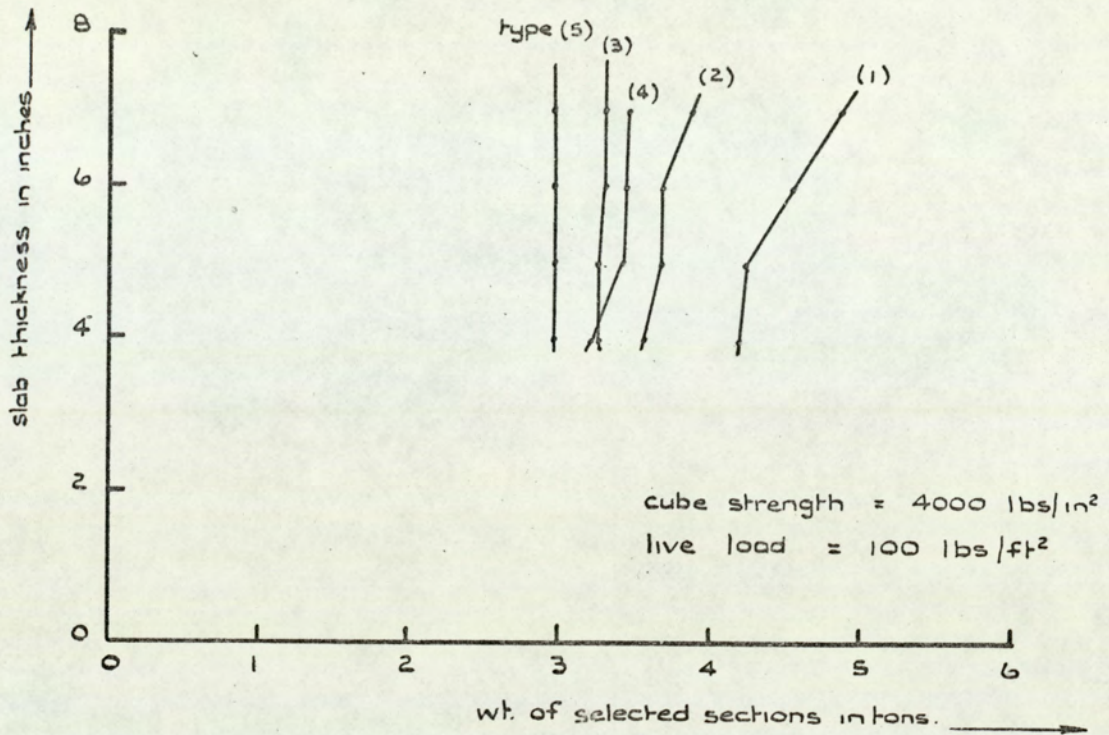


Fig. 7.14. Weight of the selected supporting beams of frame 1 for the five types of assumptions on degree of composite action, for different slab thicknesses.

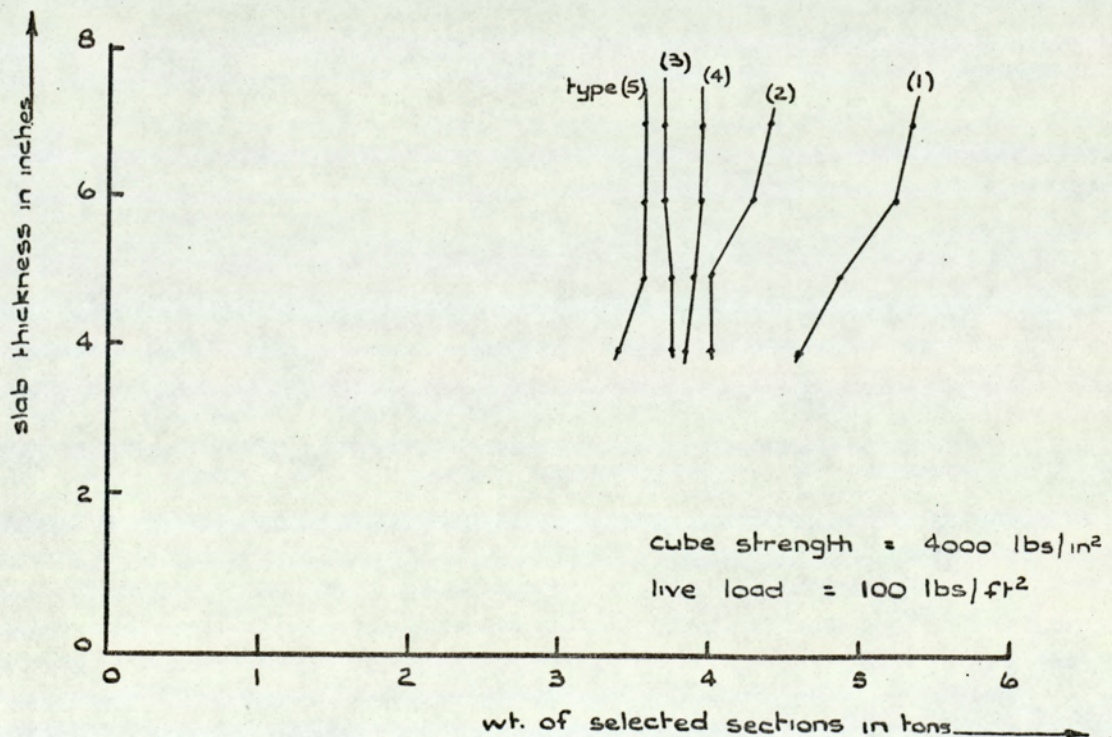


Fig. 7.15. Weight of the selected supporting beams of frame 2 for the five types of assumptions on degree of composite action, for different slab thicknesses.

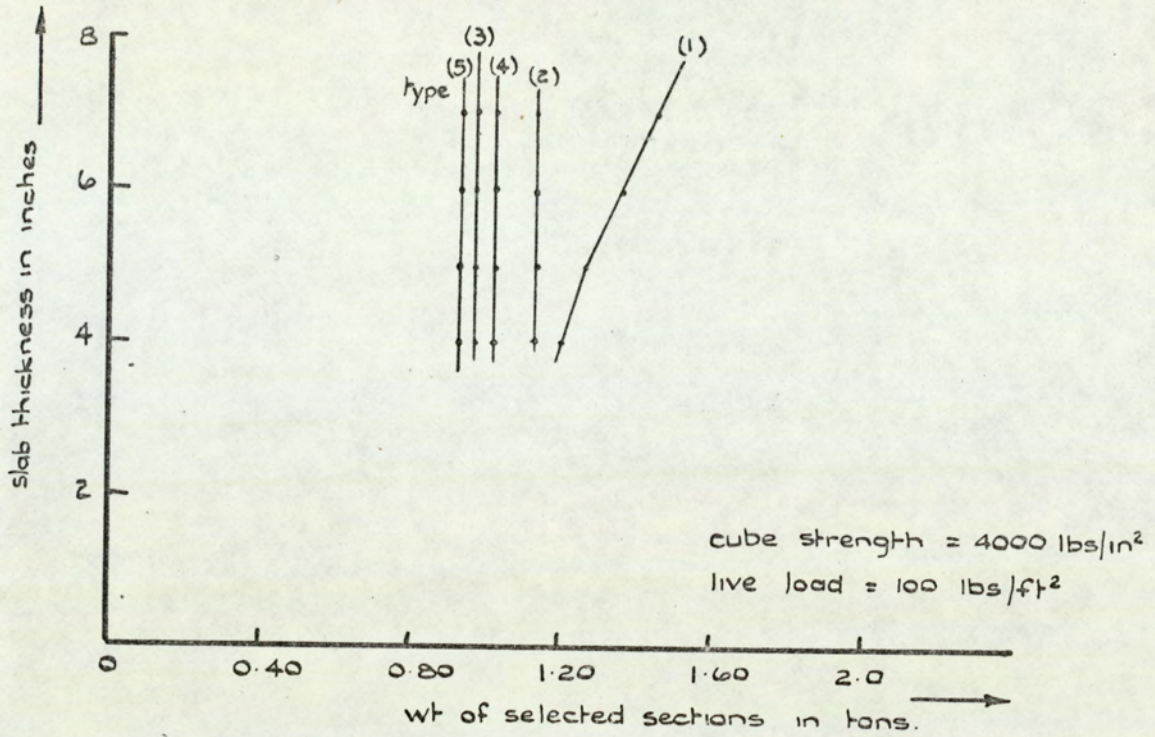


Fig. 7.16. Weight of the selected supporting beams of frame 5 for the five types of assumptions on degree of composite action, for different slab thicknesses.

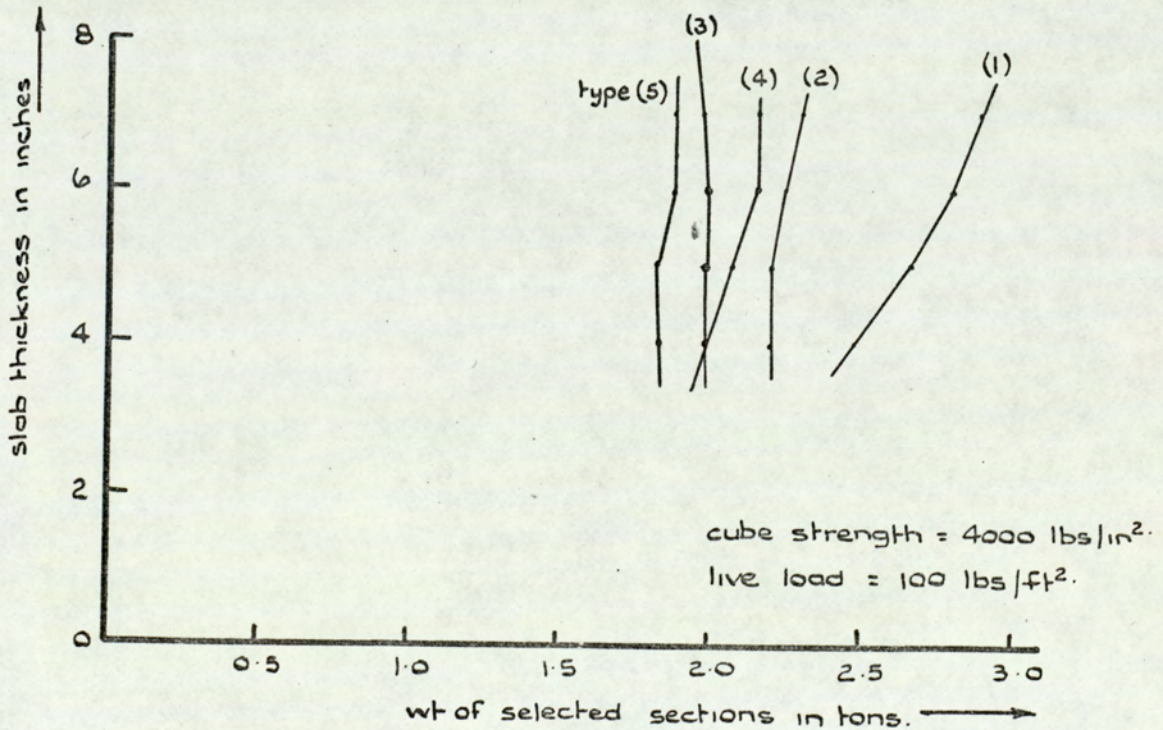


Fig. 7.17. Weight of the selected supporting beams of frame 8 for the five types of assumptions on degree of composite action, for different slab thicknesses.

Slab Thickness Inches	Selected Beam Size U.B.	Required M_x Moment kips - ft.	Chosen M_x Moment kips - ft.	Excess in the Chosen M_x Moment than the Required kips - ft.
4	16 x 7 x 36	528.13	553.65	25.52
5	16 x 7 x 36	572.14	585.28	13.14
6	16 x 7 x 36	616.15	616.91	0.76
7	15 x 6 x 40	660.16	696.58	36.42

Table 7(ii). Excess in the strength (chosen M_x moment) of $L_x(2)$ beam than the required for various slab thicknesses. Frame 1 Type (2) of composite design.

Slab Thickness inches	Selected Beam Size U.B.	Required M_x Moment kips - ft.	Chosen M_x Moment kips - ft.	Excess in the Chosen M_x Moment than the required kips - ft.
4	15 x 6 x 35	590.62	627.90	37.28
5	15 x 6 x 35	639.84	669.38	29.54
6	15 x 6 x 35	689.06	709.92	20.86
7	15 x 6 x 35	738.55	750.03	11.52

Table 7(iii). Excess in the strength (chosen M_x moment) of $L_x(1)$ beam than the required for various slab thicknesses. Frame 1 Type (5) of composite design.

Slab Thickness inches	Selected Beam Size Joist	Required M_y Moment kips - ft.	Chosen M_y Moment kips - ft.	Excess in the Chosen M_y Moment than the required kips - ft.
4	7 x 4 x $14\frac{1}{2}$	127.72	155.91	28.19
5	7 x 4 x $14\frac{1}{2}$	138.37	174.13	35.76
6	6 x $3\frac{1}{2}$ x $11\frac{1}{2}$	149.01	152.34	3.33
7	6 x $3\frac{1}{2}$ x $11\frac{1}{2}$	159.65	166.16	6.51

Table 7(iv). Excess in the strength (chosen M_y moment) of $L_y(1)$ beam than the required for various slab thicknesses. Frame 2 Type (3) of composite design.

16 x 7 x 36 U.B. with an excess in its strength of 25.52 kips - ft. relative to the required section. At $t = 6$ ", the same section is selected but the excess in strength in this case is only 0.76 kips - ft. At $t = 7$ ", a bigger section was selected, viz. 15 x 6 x 40 U.B., as the previous section was not adequate. Similar observations can be made from Table 7(iii) for the external bay beam Lx(1) of frame 1 (Figures 7.5 and 7.6), designed by type (5) assumption, where for higher slab thicknesses the excess in the strength selected to that required decreases when the same section is selected. Hence, for sections which have not a large excess in strength of selected over required, then heavier sections have to be selected at greater slab thicknesses as in the case of the beam Lx(2) of frame 1 (Table 7(ii)). This is due to the fact that when a greater slab thickness is used, then the increase in the required M_x or M_y moment resulting from the extra dead load is greater than the increase in the strength of the same section resulting from an increase in the lever arm of the composite section. This is true for all the composite T-beams of beam and slab floor systems. However, in the case of composite L-beams (i.e. the secondary beams of the external bays), the increase in the composite section strength (chosen M_y moment), owing to the increase in the lever arm of the composite section, is increasing at a greater rate than that of the required M_y moment. This occurs because of the extra dead load which results from the increased slab thickness, as shown in Table 7(iv). Owing to this phenomenon, in certain cases a slight reduction in the weight of the secondary beams of the external bays results when the slab thickness increases. This can be seen from Figures 7.7 and 7.8 and Table 7(iv) of frame 2 type (3) assumption. When the slab thickness increases from 5 inches to 7 inches, a lighter section, viz. 6 x 3 $\frac{1}{2}$ x 11 $\frac{1}{2}$ Joist is selected for the L-composite beams Ly(1) and Ly(6) (i.e. the secondary beams of the first and the last external bays of frame 2) instead of the previous section, viz. 7 x 4 x 14 $\frac{1}{2}$ Joist.

For type (1) design, where composite action is assumed not to be present, Figures 7.14 - 7.17 of frames 1, 2, 5 and 8 show that when the slab thickness increases, the weight of the supporting beams selected by this method of design also increases in all cases. This is brought about by the fact that, as the slab thickness increases, with no composite action assumed to be present, then the increase in the required M_x or M_y moment, resulting from an increase in the dead load, is not counteracted by an increase in the strength (chosen M_x or M_y moment) of the section, as this is constant for type (1) design.

The weight of the hogging reinforcement is assumed to extend to the point of contraflexure of the supporting beams. For this reason, the total weight of slab reinforcement for the whole system will vary slightly from one type of design to another, as shown in Figures 7.5 - 7.13.

A considerable reduction in the slab reinforcement weight results from an increase in the slab thickness for the same ultimate slab moment M_s , as shown in Figure 7.18(a). Figure 7.19 shows the percentage reduction in slab reinforcement of frame 1 to produce the same ultimate slab moment when the slab thickness increases from 4 inches to 7 inches for various cube strengths.

When the slab thickness increases from 5 inches to 7 inches for frame 1 (Figures 7.5 and 7.6), then there is 40% increase in the weight of concrete, together with 14.4%, 5.32%, 0.8%, 1.1% and zero% increases in the weight of the supporting beams designed by types (1) - (5) respectively. Also, owing to this increase in slab thickness, heavier supporting columns and more substantial foundations would be required. Against all this, there is only a 27% reduction in the weight of slab reinforcement for the same ultimate slab moment for the same increase in slab thickness. This indicates very clearly the disadvantages in increasing the slab thickness on the whole economy of non-composite and composite constructions.

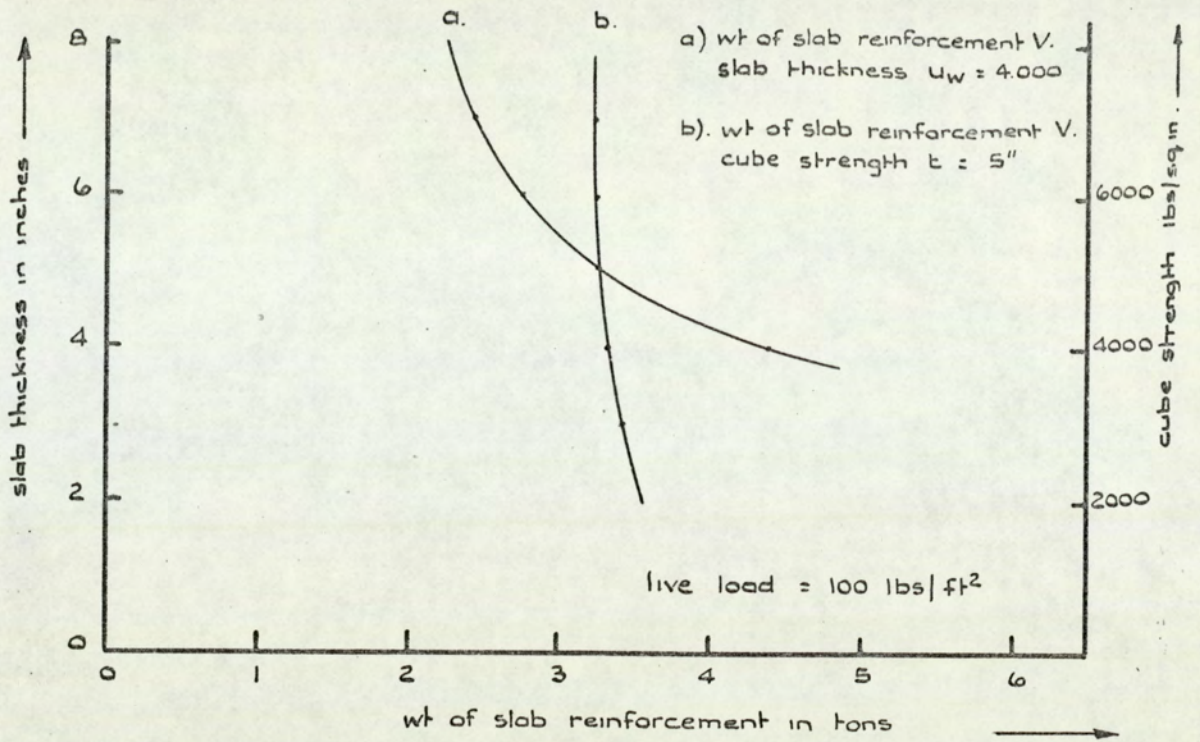


Fig. 7. 18. Decrease in the wt. of slab reinforcement of frame I owing to an increase in slab thickness or cube strength, to produce the same ultimate slab moment M_s .

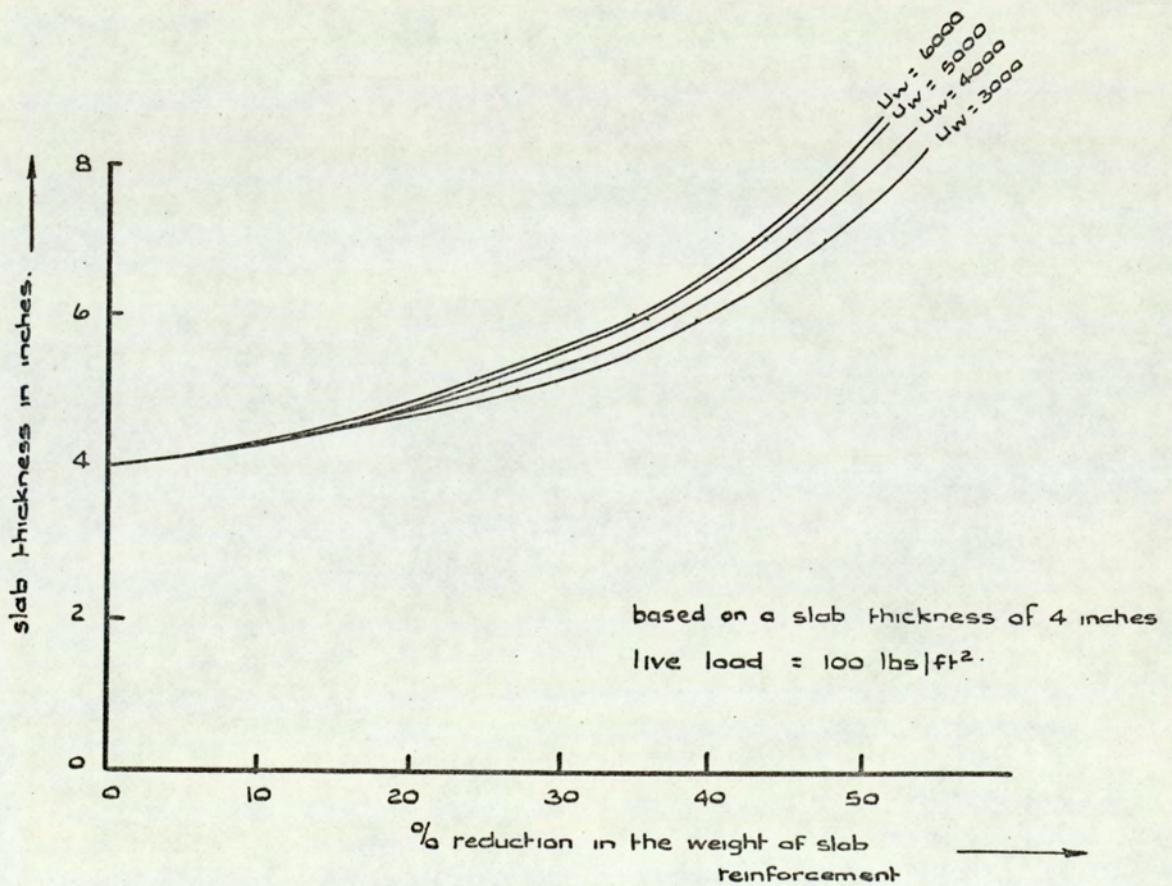


Fig. 7. 19. Percentage reduction in the wt. of the slab reinforcement of frame I at higher slab thicknesses than four inches, to produce the same ultimate slab moment M_s , for different cube strengths.

Figure 7.20 of frame 2 shows the total weight of the system designed by each of the five types of degree of composite action for various slab thicknesses. A fairly linear relationship is seen from this figure between the increase in the total weight of the system and the increase in slab thickness. This can be attributed to the great weight of the concrete, which is directly proportional to the increase in slab thickness, compared to the weight of the slab reinforcement and the supporting beams. For the same reason, the total weight of the system designed by each of the five types mentioned above are very close to each other.

7.8 EFFECT OF VARIATION OF CUBE STRENGTH ON THE WEIGHT OF BEAM AND SLAB FLOOR SYSTEMS

Four cubestrengths, 3000, 4000, 5000 and 6000 lbs./sq.in. were used to investigate the effect of increasing the cube strength on the weight of the supporting beams and slab reinforcement of beam and slab floor systems. A constant slab thickness of 5 inches was used for all these frames.

Figures 7.21 and 7.22 of frames 1 and 2 show that the weight of the supporting beams is usually constant when the cube strength increases. In some cases, a slight reduction in the weight of the supporting beams occurs when the cube strength increases, e.g. frame 1 designed by type (3) degree of composite action (Figure 7.21) when the cube strength increased from 3,000 to 4,000 lbs./sq.in.

When the cube strength increases, the plastic composite moment of the section increases, owing to the rise in the depth of the plastic neutral axis in the slab. At a cube strength of 3,000 lbs./sq.in., the main beam of the external bay Lx(1) of frame 1 for type (3) degree of composite action is a 16 x 7 x 36 U.B. with a strength (chosen M_T moment) of 632,43 kips - ft., where the required M_T moment is only 602.54 kips - ft. At the same cube strength, a lighter section (15 x 6 x 35 U.B.) is available, but this has an

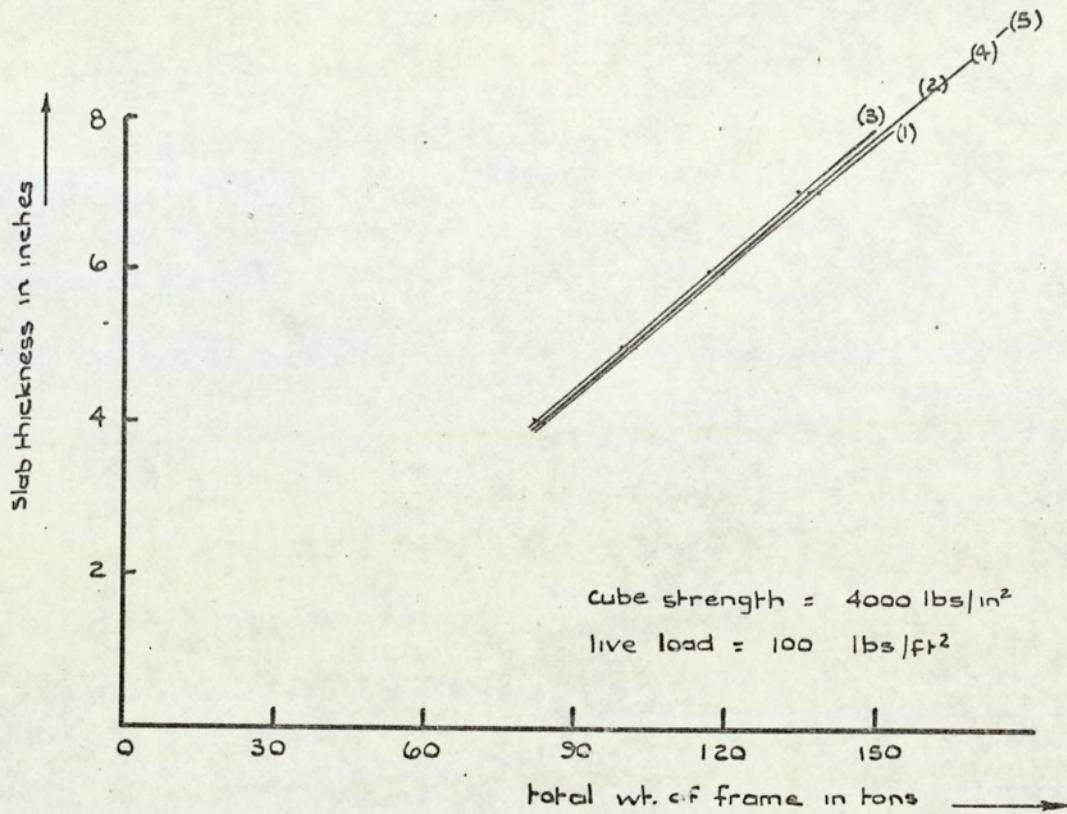


Fig. 7.20. Total weight of frame 2 for the five types of assumptions on degree of composite action, for different slab thicknesses.

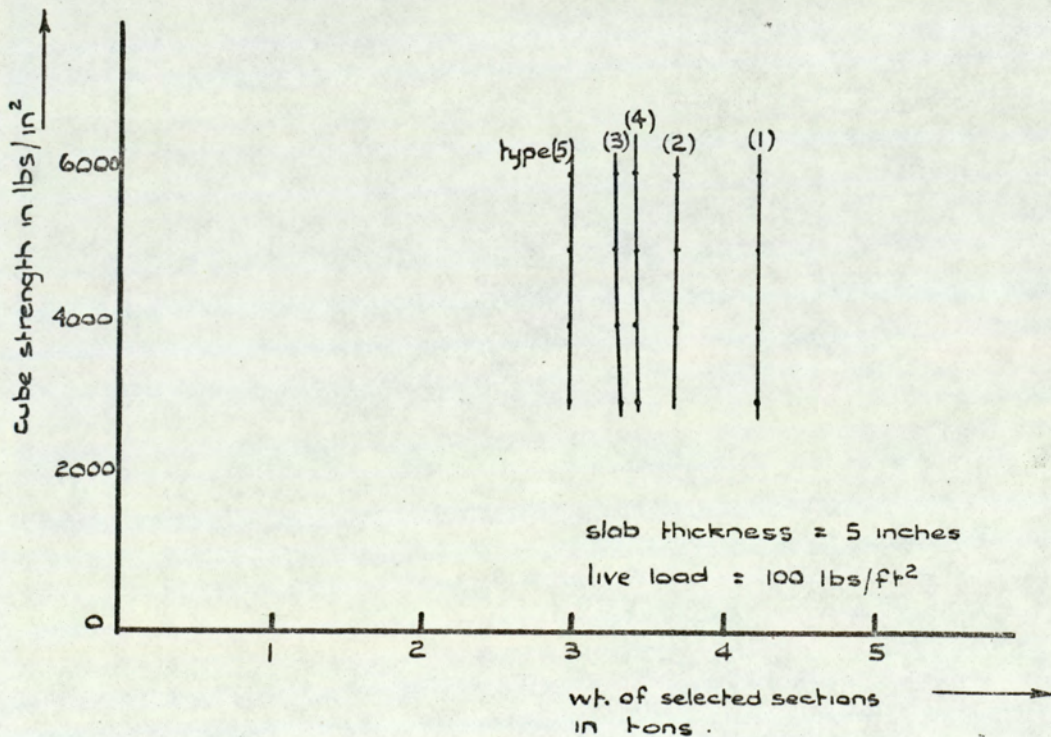


Fig. 7.21. Weight of the selected supporting beams of frame 1 for five types of assumptions on degree of composite action, for different cube strengths.

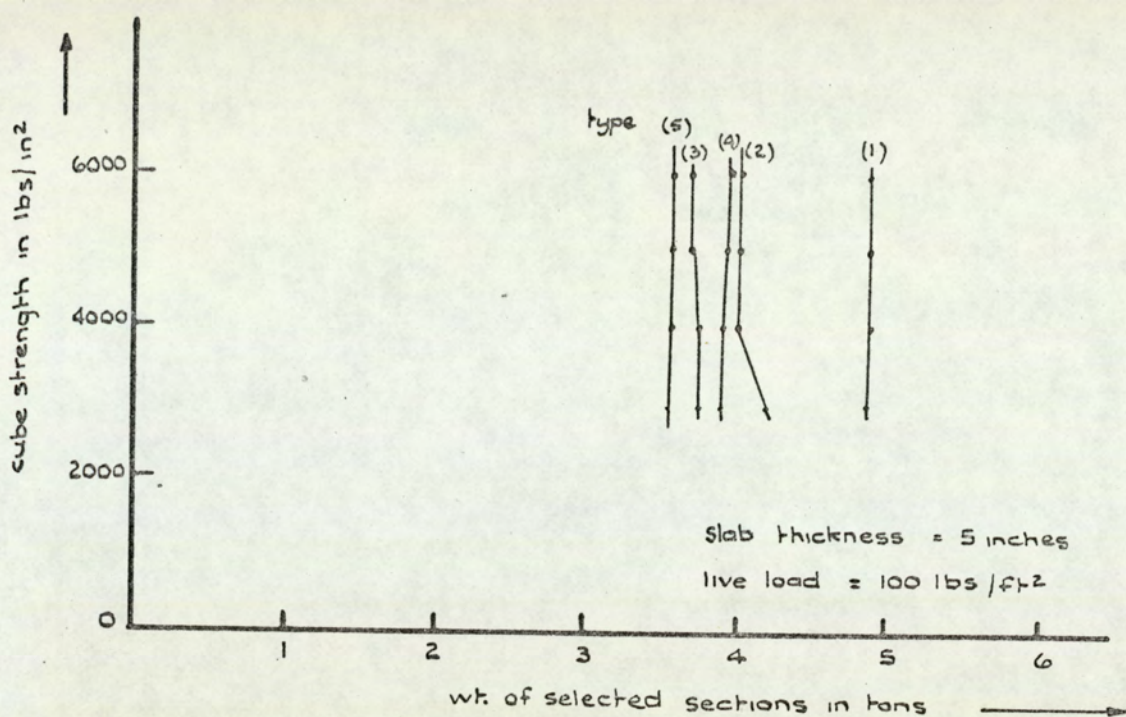


Fig. 7.22. Weight of the selected supporting beams of frame 2 for the five types of assumptions on degree of composite action for different cube strengths.

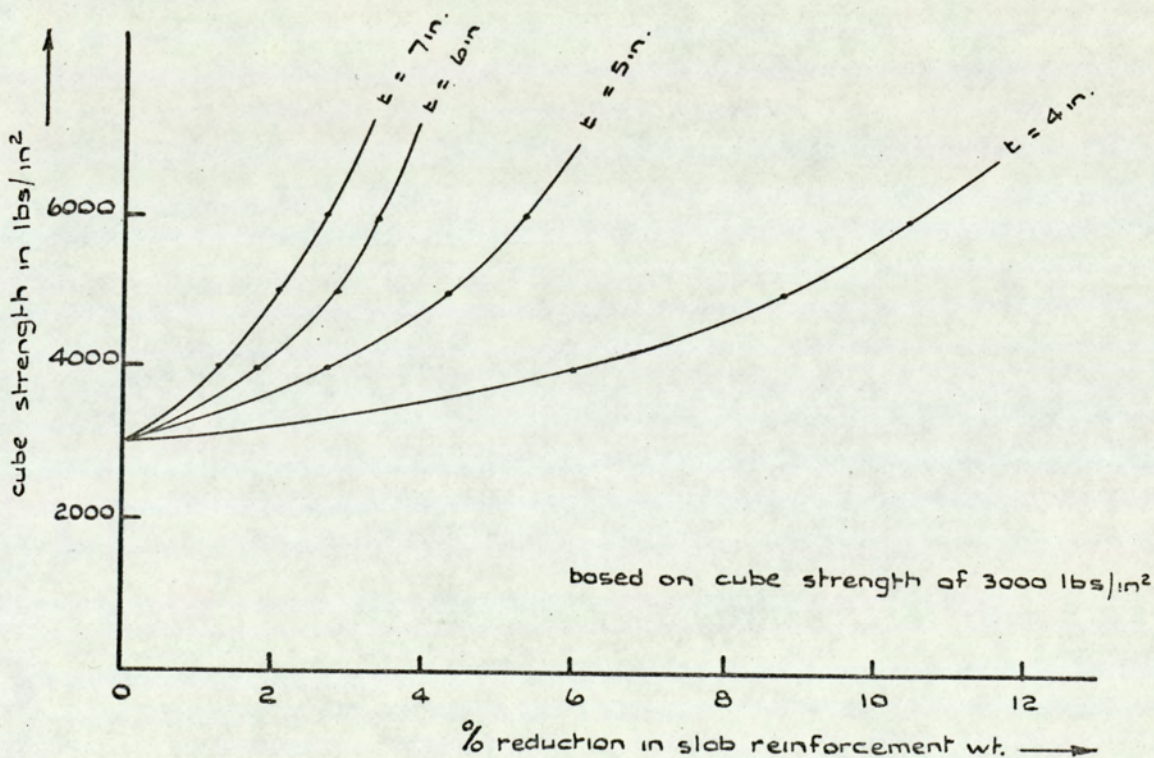


Fig. 7.23. Percentage reduction in the weight of the slab reinforcement of frame 1 at higher cube strengths than 3000 lbs/in^2 to produce the same ultimate slab moment M_s , for different slab thicknesses.

M_x moment of 593.2 kips - ft., which is slightly less than the required. At a cube strength of 4,000 lbs./sq.in., the 15 x 6 x 35 U.B. gained slightly less than a 2% increase in its M_x moment and became 604.02 kips - ft., which is slightly greater than the required of 602.54 kips - ft. Hence, this lighter section (15 x 6 x 35 U.B.) is selected when the cube strength increases to 4,000 lbs./sq.in. This is how the slight saving in the weight of the supporting beams of frame 1 type (3) design shown in Figure 7.21 occurred when the cube strength increased from 3,000 lbs./sq.in. to 4,000 lbs./sq.in. For similar reasons, a reduction in the weight of the supporting beams of frame 2 occurred in some cases, owing to the increase in the cube strength, as shown in Figure 7.22. 1 - 4% reduction in the weight of the supporting beams, owing to the increase in cube strength, is made in the cases of Figures 7.21 and 7.22 of frames 1 and 2. This slight reduction in the weight of the supporting beams only occurs in rare cases where there is a lighter section which could not be chosen at certain cube strength because its M_x moment is slightly less than the required, but at a higher cube strength, it will be adequate. Hence, it may be concluded that there is no advantage in increasing the cube strength on weight saving in the supporting beams. In the case of type (1) design, where composite action is assumed not to be present between supporting beams and slab floors, higher cube strengths have no effect whatsoever on the weight of the supporting beams.

The weight of the slab reinforcement of frame 1 at a slab thickness of 5 inches for various cube strengths is shown in Figure 7.18(b). A slight reduction in the weight of slab reinforcement results from using higher cube strengths. Figure 7.23 shows the percentage reduction in the slab reinforcement of frame 1 for higher cube strengths than 3,000 lbs./sq.in. For example, an increase in the cube strength from 3,000 to 6,000 lbs./sq.in. for frame 1, only results in a 5.3% reduction in the weight of the slab reinforcement. This figure reduces to 2.7% when a slab thickness of 7

inches is used to produce the same ultimate slab moment M_s . The percentage reduction in the weight of slab reinforcement of frame 1, when greater slab thicknesses than 4 inches are used to produce the same ultimate slab moment M_s , is shown in Figure 7.19 for several values of cube strength.

7.9 DEFLECTION OF NON-COMPOSITE AND COMPOSITE BEAM AND SLAB FLOOR SYSTEMS

According to C.P.117⁽⁴⁰⁾, the maximum allowable deflection of composite sections, owing to working loads other than the weight of the structural floors or roof, steel work casing, if any, is the same as that of non-composite sections and shall not exceed $1/360$ of the span⁽¹³⁾.

In beam and slab floor systems, the real deflection of the supporting beams, whether non-composite as in type (1), or composite as in types (2) - (5), must lie between the limits for simply supported and encastré spans, depending on the stiffness and type of connection of the supporting columns.

For simply supported non-composite and composite sections, the central deflection is $\frac{5 W L^3}{384 E I_c}$ where W is the applied working live load, L is the span of the section, E is the elastic modulus of steel and I_c is the sum of the second moment of area of the beam section and that of the slab for non-composite construction (type (1)) or the second moment of area of the composite section for composite construction (types (2) - (5)), for both cases in steel units. The central deflection of the composite section when considered encastré will be approximately $1/5$ th of the simply supported deflection. Figures 7.5 and 7.6 show in parenthesis the limits of the central deflection of the selected supporting beams of frame 1 designed by the various types of degree of composite action for slab thickness of 5 inches and 7 inches, together with their maximum allowable deflection.

The external bay main beam $L_x(1)$ of frame 1 designed by type (1), where composite action is assumed not to be present, is an $18 \times 7\frac{1}{2} \times 45$ U.B. for a slab thickness of 5 inches (Figure 7.5) and have the limits of central

deflection lie between 1.44 inches and 0.29 inches, whilst the maximum allowable deflection is 1.0 inch. The real deflection of this beam is nearer to 0.29 inches (encasté) than to 1.44 inches (simply supported) and it is reasonable to assume that this beam satisfies the deflection criterion. For the case of full composite action of type (5), where the lightest sections are selected, a 15 x 6 x 35 U.B. is selected for the same span with limits of central deflection between 0.86 and 0.17 inches. Even if this composite section is assumed simply supported, which it is not, it will satisfy the deflection criterion. In this particular case, there is a 39.7% reduction in deflection on top of the 22.2% saving in weight when composite, rather than non-composite construction is used. This shows very clearly the great advantages of composite over non-composite construction in reducing the deflection of the supporting beams as well as in saving of weight.

At a slab thickness of 7 inches for the same frame, none of the sections selected by any of the five assumptions on degree of composite action violates the deflection criterion, even if the beams are assumed simply supported, as shown in Figure 7.6.

A reduction in the deflection of composite sections occurs when the same section is selected at higher slab thicknesses. In the case of the external bay beam Lx(1) of frame 1 selected by type (2) of composite design, when the slab thickness increased from 5 inches to 7 inches, the same section, a 15 x 6 x 40 U.B. is selected with 28.4% reduction in deflection (Figures 7.5 and 7.6).

7.10 EFFECT OF THE SIDES RATIO (ρ) ON THE WEIGHT OF BEAM AND SLAB FLOOR SYSTEMS

Frames 11 and 12 are both five equal bay frames and have equal floor areas, but their sides ratios (ρ) are 0.5 and 2.0 respectively. In these two frames, the extreme values of the sides ratios are used to investigate

the effect of sides ratio on the weight of the supporting beams and slab reinforcement. Figures 7.12 and 7.13 show the results of the complete designs of these frames by the various assumptions on degree of composite action for a slab thickness of 5 inches, a cube strength of 4,000 lbs./sq.in. and a live load of 100 lbs./sq.ft.

At the internal bays, as the slab is continuous in four directions, change over from mode C to mode D occurs at $\rho = 1.0$ for independent slab collapse, and the end conditions of the main and secondary beams are similar, symmetry will exist. For this reason, the ultimate slab moment M_s and hence the areas and the weight of slab reinforcement are equal for frames 11 and 12. Also, the sizes and hence the weights of the selected supporting beams by the various types of degree of composite action are the same for both frames. However, the selected beam sizes will be in different directions, as shown in Figures 7.12 and 7.13.

At the external bays, since the slab is only continuous in three directions, symmetry there does not exist. For this reason, the ultimate slab moment M_s is different for each frame. The discontinuous side of the external bay at $\rho = 2.0$ has a longer side (40 feet) than at $\rho = 0.5$ (20 feet). Hence the ultimate slab moment M_s required to produce the same collapse load by mode c for the external bays of both frames, is higher for frame 12 at $\rho = 2.0$ than that for frame 11 at $\rho = 0.5$, viz. 4.92 kips - ft./ft.run and 4.33 kips - ft./ft.run at slab thickness of 5 inches for frames 12 and 11 respectively. Because of this, a greater area and hence weight of slab reinforcement is required at $\rho = 2.0$ of frame 12 than at $\rho = 0.5$ of frame 11 as shown in Figures 7.12 and 7.13.

In addition to the variation in the ultimate slab moment of the external bays for both frames, the end conditions of the main and the secondary beams are also different. For the secondary beam (spanning in the Y - direction) continuity is assumed to exist at both supports, whereas for the main beam (spanning in the X - direction) continuity only exists at the R.H.S. as at

the L.H.S. the beam is not continuous (modes A and B of the external bay Figure 4.1). Also, the main beam at $\rho = 0.5$ (frame 11) carried the whole external bay area for collapse by mode B, and when it becomes a secondary beam at $\rho = 2.0$ (frame 12), it will only carry half the external bay floor area for collapse by mode A (Figure 4.1). For all these reasons, as well as the availability of sections, the weight of the supporting beams of the external bays vary when the sides ratio (ρ) changes from 0.5 to 2.0 for the same floor area.

Slab Thickness (inches)	Frame No.	Sides Ratio (ρ)	WB (type 1) tons	WB (type 2) tons	WB (type 3) tons	WB (type 4) tons	WB (type 5) tons	WR tons
5	11	0.5	7.30	6.38	5.96	6.12	5.85	5.34
	12	2.0	7.70	6.43	6.05	6.29	5.94	5.70
7	11	0.5	8.23	6.90	6.21	6.38	5.80	3.86
	12	2.0	8.60	7.07	6.16	6.43	5.94	4.11

Table 7(v). Weight of the selected supporting beams and slab reinforcement of frames 11 and 12.

The weights of the supporting beams designed by the five types of degree of composite action, together with weight of slab reinforcement for slab thickness of 5 inches and 7 inches and cube strength of 4,000 lbs./sq.in. are shown in Table 7(v). In all cases, except that of type (3) of composite design at $t = 7"$, the weight of the supporting beams is greater at sides ratio (ρ) = 2.0 (frame 12) than at sides ratio (ρ) = 0.5 (frame 11). The weight of slab reinforcement is greater at $\rho = 2.0$ than at $\rho = 0.5$ for both slab thicknesses. Hence, for the same floor area, in this case, it is slightly more economical to use the frame 11 arrangement which has smaller sides ratio (ρ) = 0.5 than the frame 12 arrangement which has sides ratio (ρ) = 2.0.

7.11 EFFECT OF INCREASING THE APPLIED LIVE LOAD
ON THE WEIGHT OF BEAM AND SLAB FLOOR SYSTEMS

Three live loads, 50, 100 and 200 lbs./sq.ft. were applied on frames 1, 3 and 10 to study their effect on the weight of the supporting beams and slab reinforcement. Two slab thicknesses, 5 inches and 7 inches, were used for each case and a cube strength of 4,000 lbs./sq.in. was used in all the design examples.

The three frames used have a different number of bays and different sides ratios, hence different beams will be selected for each frame for each of the five assumptions on degree of composite action. This will give a fairly accurate averaging effect on the weight of the supporting beams, when the applied live load increases.

Figure 7.24 shows the weights of the selected supporting beams of frame 1 for the five types of degree of composite action and the weight of the slab reinforcement for the three applied live loads. A steady increase in the weight of the selected supporting beams and the slab reinforcement is seen from this figure and the relationship is approximately linear for all the cases considered.

Table 7(vi) shows the percentage increase in the weight of the selected supporting beams of the three frames for each of the five types of degree of composite action, owing to an increase in the applied live load at a slab thickness of 5 inches and a cube strength of 4,000 lbs./sq.in. The percentage increases in the weight of the selected supporting beams for the five types of design for the three frames are fairly close for increases in the applied load from 50 -> 100 lbs./sq.ft. and 50 -> 200 lbs./sq.ft. The small difference is due to the lack of availability of a complete range of sections. It is interesting to note from Table 7(vi) that the percentage increases in the slab reinforcement for the three frames are very close for both increases in the applied live load.

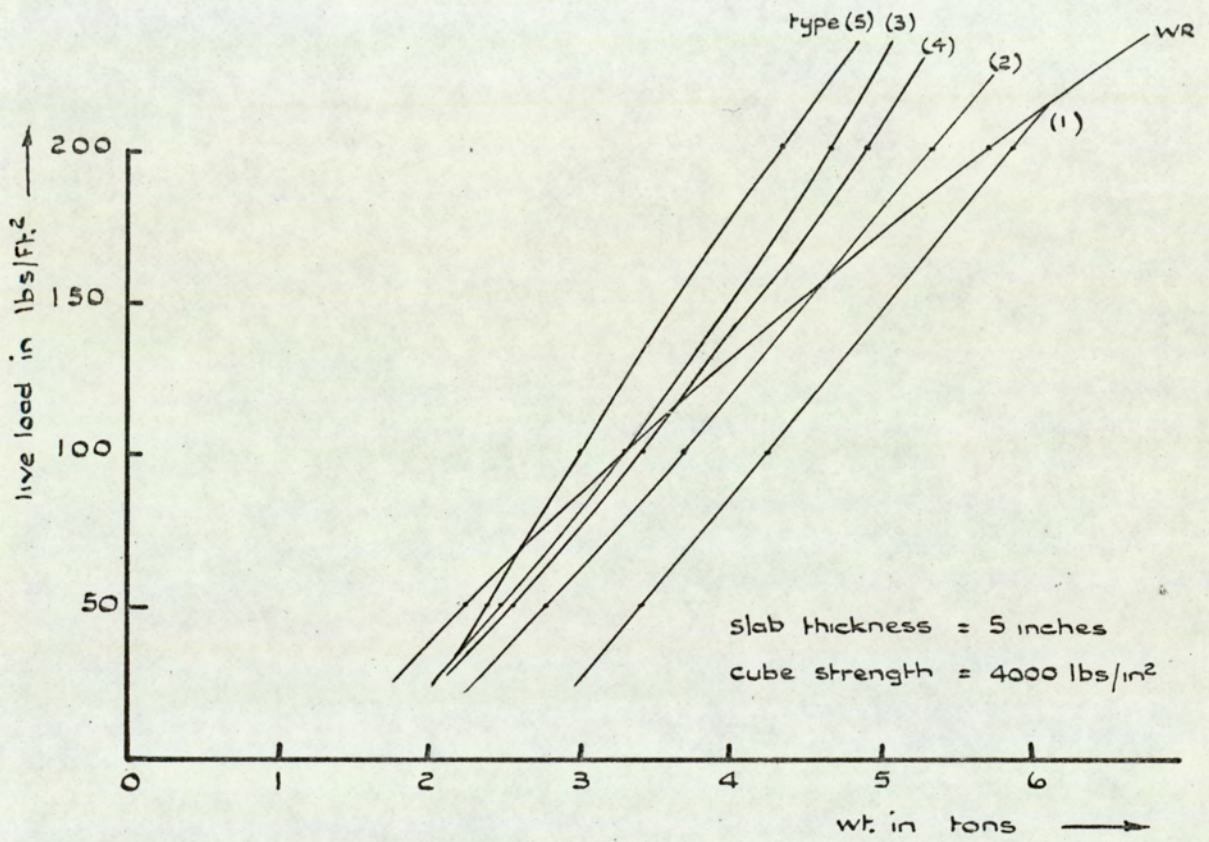


Fig. 7.24. Weight of the selected supporting beams of frame I for the five types of assumptions on degree of composite action and the weight of slab reinforcement, for different applied live loads.

slab thickness = 5 inches

cube strength = 4,000 lbs./sq.in.

Increase in Applied Live Load From... (lbs./sq.ft.)	Frame No.	% Increase In WB (type 1)	% Increase In WB (type 2)	% Increase In WB (type 3)	% Increase In WB (type 4)	% Increase In WB (type 5)	% Increase In WR
50 -> 100	1	23.7	32.1	32.2	35.0	24.2	48.9
	3	22.5	22.4	21.8	28.7	22.1	48.4
	10	32.4	23.3	36.7	23.5	28.1	48.5
50 -> 200	1	70.3	91.2	89.6	94.4	81.2	155.9
	3	65.3	74.4	69.7	77.6	61.8	152.6
	10	78.9	88.3	82.2	72.1	75.3	153.4

Table 7(vi). Percentage increase in the weight of the supporting beams and slab reinforcement of frames 1, 3 and 10, owing to an increase in the applied live load.

Increase in Applied Live Load From... (lbs./sq.ft.)	Slab Thickness (ins.)	% Increase In WB (type 1)	% Increase In WB (type 2)	% Increase In WB (type 3)	% Increase In WB (type 4)	% Increase In WB (type 5)	% Increase In WR
50 -> 100	5	26.2	25.9	30.2	29.1	24.8	48.6
	7	20.8	27.6	27.0	24.6	20.8	38.5
50 -> 200	5	71.5	84.2	80.4	81.4	72.8	153.9
	7	62.4	76.3	72.9	69.7	66.9	118.1

Table 7(vii). Average percentage increase in the weight of the supporting beams and slab reinforcement of frames 1, 3 and 10, owing to an increase in the applied live load.

It can be seen from Table 7(vii) that, in general, the average increase in the weight of the supporting beams for the five types of design is greater for a slab thickness of 5 inches than for a slab thickness of 7 inches. This again is due to the availability of the sections.

It is interesting to note from Table 7(vii) that the percentage increase in the weight of the supporting beams and slab reinforcement for an increase in live load of 50 → 200 is $2\frac{1}{2}$ to 3 times as much as for an increase in live load of 50 → 100 for each of the five types of design at both slab thicknesses of 5 and 7 inches. For the slab reinforcement, this increase will be nearly three times as much for both slab thicknesses.

7.12 COMPARISON BETWEEN THE VARIOUS ASSUMPTIONS ON DEGREE OF COMPOSITE ACTION

The twelve beam and slab floor systems shown in Figure 7.1 were designed for each of the five assumptions on degree of composite action with the aid of the general computer program of Appendix 2. Comparisons in weight saving between these five types of assumption were made for each of the twelve frames. An applied live load of 100 lbs./sq.ft. and a cube strength of 4,000 lbs./sq.in. were assumed, and four slab thicknesses 4 inches, 5 inches, 6 inches and 7 inches were used for each frame.

Type (1) assumption ignores composite action altogether. This leads to heavier selected sections for the supporting beams than those selected by the other four types, where composite action is present. Comparisons between each of the four assumptions ((2) - (5)), where composite action is present, and that of type (1) in weight saving are made for each of the twelve frames. Tables 7(viii) and 7(ix) show the percentage saving in the weight of the selected supporting beams by each of the four composite types ((2) - (5)) relative to the non-composite type (1) for slab thicknesses of 4, 5, 6 and 7 inches.

cube strength = 4000 lbs./sq.in.

live load = 100 lbs./sq.ft.

Slab Thickness (inches)	Frame No.	Comparison with type (1) in weight saving				Comparison with type (2) in weight saving		
		% saving by type (5)	% saving by type (3)	% saving by type (4)	% saving by type (2)	% saving by type (5)	% saving by type (3)	% saving by type (4)
4	1	29.3	22.1	22.5	15.2	16.6	8.1	8.6
	2	26.0	18.6	16.5	12.9	15.0	6.5	4.1
	3	27.4	20.8	17.1	13.9	15.7	8.0	3.7
	4	21.1	21.1	8.7	7.7	14.6	14.6	1.1
	5	23.9	20.6	16.3	7.5	17.6	14.1	9.5
	6	25.6	25.6	20.7	19.1	8.1	8.1	2.0
	7	22.5	18.8	17.0	9.3	14.5	10.5	8.4
	8	26.1	19.8	19.8	11.5	16.5	9.4	9.4
	9	23.3	13.9	13.9	9.9	14.8	4.4	4.4
	10	29.5	29.4	17.3	16.0	16.0	16.0	1.6
	11	23.5	18.4	16.3	15.9	9.0	2.9	0.4
	12	27.7	20.3	17.8	15.7	14.2	5.4	2.5
5	1	29.7	22.6	19.2	13.2	19.1	10.8	6.9
	2	26.8	23.0	19.9	17.7	11.1	6.5	2.8
	3	28.6	24.8	21.3	17.4	13.6	8.9	4.6
	4	26.8	26.8	15.2	14.3	14.6	14.6	1.1
	5	26.1	22.9	18.8	10.3	17.6	14.1	9.5
	6	30.7	27.5	22.7	21.1	12.1	8.1	2.0
	7	25.1	23.8	20.6	14.9	12.0	10.5	6.6
	8	30.9	25.0	23.9	17.3	16.5	9.4	5.6
	9	32.7	24.5	24.5	21.3	14.4	4.0	4.0
	10	29.5	29.5	19.0	16.0	16.0	16.0	3.5
	11	19.8	18.4	16.3	12.5	8.4	6.7	4.3
	12	23.7	21.0	18.6	16.5	8.7	5.4	2.5

Table 7(viii). Comparison between the five types of assumptions on degree of composite action in weight saving of the selected supporting beams of frames 1 to 12 for slab thicknesses 4 inches and 5 inches.

cube strength = 4000 lbs./sq.in.

live load = 100 lbs./sq.ft.

slab thickness (inches)	Frame No.	Comparison with type (1) in weight saving				Comparison with type (2) in weight saving		
		% saving by type (5)	% saving by type (3)	% saving by type (4)	% saving by type (2)	% saving by type (5)	% saving by type (3)	% saving by type (4)
6	1	34.9	27.6	22.8	19.5	19.1	10.1	4.0
	2	31.8	29.2	24.9	17.9	16.9	13.7	8.4
	3	33.0	29.4	26.1	20.2	16.0	11.5	7.4
	4	28.7	28.7	17.5	16.6	14.6	14.6	1.1
	5	31.2	27.3	20.4	16.5	17.7	12.9	4.7
	6	30.7	27.5	22.7	21.1	12.1	8.0	2.0
	7	27.6	26.1	18.2	15.3	14.5	12.7	3.4
	8	32.5	28.8	22.8	19.6	16.1	11.5	4.0
	9	33.8	27.8	22.7	19.2	18.1	10.6	4.2
	10	30.8	30.8	22.3	19.2	14.4	14.4	3.9
	11	28.3	27.0	24.8	15.3	15.3	13.7	11.1
	12	29.3	27.6	25.1	17.0	14.7	12.7	9.7
7	1	38.6	31.8	26.3	20.1	23.1	14.6	7.8
	2	37.9	30.5	26.0	17.4	18.9	15.9	10.4
	3	33.3	31.3	27.4	20.9	15.7	13.2	8.3
	4	28.1	28.1	16.4	15.5	14.9	14.9	1.0
	5	35.5	31.8	25.3	21.7	17.6	12.9	4.7
	6	35.4	35.4	28.0	19.6	19.7	19.7	10.4
	7	33.1	27.8	24.5	21.8	14.5	12.8	3.4
	8	34.5	25.1	31.5	20.5	17.6	13.9	5.8
	9	36.0	30.2	25.3	21.9	18.1	10.6	4.2
	10	32.7	32.7	26.3	21.4	14.4	14.4	6.3
	11	29.0	24.6	22.4	16.2	15.3	10.1	7.5
	12	30.7	29.1	25.0	17.5	16.0	14.1	9.1

Table 7(ix). Comparison between the five types of assumptions on degree of composite action in weight saving of the selected supporting beams of frames 1 to 12 for slab thicknesses 6 inches and 7 inches.

Type (2) assumption embodies the simplest form of composite action⁽¹⁾. In this type, composite action is assumed only at mid-spans of the supporting beams and the effect of slab reinforcement at mid-span is ignored when M_e or M_c are calculated. In the other three types (3), (4) and (5), the effect of slab reinforcement at mid-spans or the effect of composite action at supports or both are included. This leads to more economical sections being selected for the supporting beams. Comparisons between the three types (3), (4) and (5) and type (2) in weight saving were also made for each of the twelve frames, and these results are also shown in Tables 7(viii) and 7(ix) for various slab thicknesses.

For any of the five types of assumption, when a section is selected, there is always an excess in its strength (M_x or M_y moment) over that required. The reason for this excess is due to the lack of a complete range of sections⁽⁷²⁾ and the amount of the excess depends on the section selected. In the twelve frames designed, many different sections were selected for the same type of assumption, all with different levels of excess between required and selected sections. Hence, the average of the percentages in weight saving of all the twelve frames was determined to give a more accurate picture of the relative economy of the various types of assumption; this is shown in Table 7(x).

Table 7(x) shows that type (5) assumption, where full composite action is present at supports and mid-spans and the effect of slab reinforcement at mid-span is included, produces the highest average percentage saving in the weight of the selected supporting beams for the four slab thicknesses. For example, at a slab thickness of 5 inches, the average percentage savings in the weight of the selected beams by type (5) relative to types (1) and (2) are 27.5% and 13.7% respectively. Type (3) assumption, where composite action is present at mid-span only and the effect of slab reinforcement is included when M_c and M_e are calculated, proves to give the second highest

cube strength = 4000 lbs./sq.in.

live load = 100 lbs./sq.in.

Slab Thickness (inches)	Average Comparison with type (1) in weight saving				Average Comparison with type (2) in weight saving		
	Average % Saving by Type (5)	Average % Saving by Type (3)	Average % Saving by Type (4)	Average % Saving by Type (2)	Average % Saving by Type (5)	Average % Saving by Type (3)	Average % Saving by Type (4)
4	25.5	20.8	16.8	12.7	14.6	9.3	4.6
5	27.5	24.1	20.0	15.7	13.7	9.6	4.4
6	31.0	28.1	22.2	18.0	15.9	12.3	5.1
7	33.9	30.1	25.3	19.7	16.9	13.9	6.2

Table 7(x). Average comparison between the five types of assumptions on degree of composite action in weight saving of the selected supporting beams of the twelve frames for various slab thicknesses.

average percentage of saving in the weight of the selected supporting beam for all the slab thicknesses. For the same slab thickness of 5 inches, the average percentage of weight saving by type (3) relative to type (1) and type (2) are 24.1% and 9.6% compared with 20.0% and 4.4% for type (4). This shows that type (3) assumption is more economical than type (4) assumption, where composite action is present at the supports and mid-spans, but the effect of slab reinforcement is ignored when M_c and M_e are calculated.

The percentage in weight saving by types (2), (3), (4) and (5), where composite action is present, relative to type (1), where composite action is ignored, increases when the slab thickness increases as shown in Table 7(x). As explained earlier, this is due to the fact that when the slab thickness increases, then heavier sections are required for type (1) assumption which ignores composite action, whereas for the other types, as composite action is present, the same sections or only slightly heavier ones will be selected at higher slab thicknesses.

Figure 7.12 of frame 11 shows that the secondary beam Ly(2) selected for both types (1) and (2) is the same, i.e. a $16 \times 5\frac{1}{2} \times 26$ U.B. For type (1), where composite action is ignored, the total mid-span plastic moment of the beam and the yield line ($M_b + M_{sl}$) for collapse by mode A is 293.3 kips - ft. For type (2), where the simplest form of composite action is present, the plastic mid-span composite moment of the same section for the same mode is 288.9 kips - ft., which in fact is less than that of type (1), where composite action is ignored. This is because the width of the compression slab at mid-span is very large (40 ft.). For this reason, the same section is selected by both methods. Hence, in cases like this, where the compression flange is very wide, there is no advantage in using composite action of type (2) rather than the non-composite action case of type (1). For types (3), (4) and (5) with a higher degree of composite action, lighter beams are selected. These are:-

$12 \times 4 \times 22$ U.B., $14 \times 5 \times 26$ U.B. and $10 \times 4 \times 19$ U.B. respectively.

Table 7(xi) shows a clear picture of the overall saving in extra strength, weight, deflection and depth between the various assumptions on degree of composite action, where different sections are selected by each of the five types of design for the main beam of the external bay Lx(1) of frame 1. For example, the overall savings by type (5), where a $15 \times 6 \times 35$ U.B. is selected, over type (1), where an $18 \times 7\frac{1}{2} \times 45$ U.B. is selected are:- 23.3 kips - ft. extra strength (chosen M_x moment), 22.2% saving in weight, 39.7% saving in deflection and 2.9 inches saving in depth.

Similarly, the saving by the same section $15 \times 6 \times 35$ U.B. selected by type (5) over type (2), where a $15 \times 6 \times 40$ U.B. is selected, are:- 6.8 kips - ft. extra strength, 12.5% saving in weight, 13.7% increase in deflection and a very slight saving in depth. The section selected by type (3) is the same as that selected by type (5), where that selected by type (4) is heavier section a $16 \times 7 \times 36$ U.B.

Finally, comparisons between the various assumptions on degree of composite action are made from the point of view of failure load for the same weight of the supporting beams. When the same section selected by type (1) assumption, where composite action is not present, is used in conjunction with the other four assumptions, where composite action is present, for the same span, higher failure loads are expected for the same mode of collapse. For the internal bay main beam Lx(2) of frame 1 (Figure 7.5), the computer selects this beam for type (1) as an $18 \times 6 \times 45$ U.B. for a collapse load of 78.6 tons for collapse by mode B. If the same section is used for collapse by the same mode for types (2), (3), (4) and (5), the collapse loads will be 102.5 tons, 108.3 tons, 105.8 tons and 111.7 tons respectively. This shows that type (5) assumption gives the highest collapse load for a constant section. The next highest collapse load is that of type (3), as in weight saving this type of composite design comes next to type (5) in efficiency as well as in weight saving.

Frame 1. Bay No. 1. Main beam Lx(1)

slab thickness = 5 inches

cube strength = 4000 lbs./sq.in.

live load = 100 lbs./sq.ft.

Type of assumption on degree of composite action	Selected beam size	Required M_x moment kips-ft.	Chosen M_x moment kips-ft.	Excess in M_x moment than required kips-ft.	Comparison with the beam selected for type (1)				Comparison with the beam selected for type (2)			
					Extra excess in M_x moment kips-ft.	% saving in weight	% reduction in deflection	Saving in depth (inches)	Extra excess in M_x moment	% saving in weight	% Increase in deflection	Saving in depth (inches)
Type (1)	18x7 $\frac{1}{2}$ x45	264.0	267.6	3.6 x 2	-	-	-	-	-	-	-	-
Type (2)	15x6 x40	602.5	626.3	23.7	16.5	11.1	47.0	2.7	-	-	-	-
Type (3)	15x6 x35	602.5	604.0	1.5	-5.8	22.2	39.7	2.9	-22.2	12.5	13.7	0.2
Type (4)	16x7 x36	639.8	652.7	12.9	5.6	20.0	46.1	2.0	-10.9	10.0	2.0	-0.7
Type (5)	15x6 x35	639.8	669.4	30.6	23.3	22.2	39.7	2.9	6.8	12.5	13.7	0.2

Table 7(xi). Overall comparison between the five types of assumptions on degree of composite action.

(The negative sign indicates that type (1) or type (2) has greater excess in M_x moment than the other types).

Table 7(xii) shows a comparison between the collapse loads of frame 1 for the five types of assumptions on degree of composite action for collapse by mode B, using the same sections selected by type (1) shown in Figure 7.5. The same table also shows weight saving of the selected supporting beams for the same collapse load.

	Comparison with type (1)			
	type (2)	type (3)	type (4)	type (5)
% Increase in the collapse load	29.8	37.5	34.9	42.7
% Saving in weight	16.4	22.2	21.3	27.5

Table 7(xii). Comparison between the five types of non-composite and composite design in collapse load and weight saving. Frame 1.

Higher percentage increases in collapse load than in weight saving are seen in Table 7(xii) for each of the four types of composite design, when compared with that of type (1) of non-composite design. For example, 42.7% higher collapse load by type (5) than type (1) compared with 27.5% saving in weight. This is expected as, when comparisons are made for collapse loads for the five types of assumptions on degree on composite action, the same set of sections is used for each type and hence a true comparison is made between these assumptions. For the case of weight saving comparisons, these are not really true comparisons as they depend to some extent on the availability of the section from the range of sections available in the existing tables⁽⁷²⁾. Other than saving in weight, in the latter case, there will be saving in depth, deflection and extra strength than required.

From the various design examples of beam and slab floor systems dealt with in this chapter, the following may be concluded:-

- (1) Increasing the slab thickness results in a heavier or the same section being selected for the supporting beams, and also heavier

columns and more substantial foundations. Against this, there is only some saving in the weight of slab reinforcement to produce the same ultimate moment M_s . This indicates very clearly the disadvantage of increasing the slab thickness on the whole economy of non-composite and composite construction. A minimum slab thickness to provide the required M_s value with the under-reinforced condition is recommended in the design of beam and slab floor systems.

- (2) There is no advantage in increasing the cube strength in terms of saving in weight of the supporting beams. Only a slight reduction in the weight of the slab reinforcement occurs when the cube strength increases, to produce the same ultimate moment M_s . A minimum cube strength is recommended for the design of beam and slab floor systems.
- (3) A considerable reduction in the deflection of the selected supported beams, as well as saving in weight, results by using composite rather than non-composite construction.
- (4) For beam and slab floor systems having the same floor area, a slight reduction in the weight of the supporting beams and slab reinforcement can be obtained by using the system with the smaller sides ratio (ρ).
- (5) The relationship between live load and the weight of the selected supported beams and slab reinforcement is approximately a directly proportional one. For an increase in the live load from 50 \rightarrow 100 lbs./ft.² there is 25-30% increase in the weight of the selected beams and 48.6% increase in the weight of the slab reinforcement at a slab thickness of 5 inches. When the live load increased from 50 \rightarrow 200 lbs./ft.² (three times as much as the previous increase), the percentage increases in the weight of the selected beams and slab reinforcement increases by three times as much as

the previous percentages. At a higher slab thickness of 7 inches these percentage increases reduce for the same increase in the live load.

- (6) Type (5) assumption on degree of composite action gives the most economical sections for the supporting beams compared with the other assumptions, after type (5), type (3) is the most economical assumption (Figures 7.14 - 7.17). This is also true for overall structural efficiency.

In the experimental part of this research work, type (5) assumption, which has the greatest degree of composite action and gives the most economical design, was used in the design of the beam and slab floor systems M_1 and M_2 which were tested to collapse. Recommendations as to which of the various assumptions regarding the degree of composite action most accurately describes the observed experimental behaviour will be made in Chapters 10 and 11.

In the next chapter, the effect of composite action between the slab system and the supporting beams will be introduced into the plastic design method originally proposed by Gandhi⁽⁴⁾ for the design of multi-storey buildings. Also the effect of composite floors on the stiffness of the beams will be considered.

C H A P T E R 8

THE SIGNIFICANCE OF COMPOSITE ACTION BETWEEN BEAMS AND FLOOR SLABS IN THE DESIGN OF MULTI-STOREY BUILDING FRAMES

8.1 INTRODUCTION

In the previous chapters, the effect of composite behaviour with its various assumptions on the degree of composite action, is considered between beams and floor slabs representing bays of multi-storey buildings for collapse owing to vertical loading alone. In this chapter, the effect of composite action between the slab system and the supporting beams of type (2) or (3), where composite action is assumed present at the mid-spans of the supporting beams only, will be introduced into the plastic design method originally proposed by Gandhi⁽⁴⁾ for the design of multi-storey buildings. The design approach of this method is based on the simple plastic theory with the effects of instability introduced at the outset by introducing only one extra factor (magnification factor A). The effect of the composite floors on the stiffness of the supporting beams and hence on the magnification factors will also be considered.

8.2 PLASTIC DESIGN OF MULTI-STOREY BUILDINGS

Simple plastic theory has been used in the past as a convenient tool for the design of rigid jointed frameworks, including building frames of low height. It was mentioned in Chapter 1 that simple plastic theory cannot be safely applied to the design of multi-storey frames because of the limitations imposed by the assumptions on which the plastic theory is based. Two of these assumptions are of particular importance here:-

- (a) The equilibrium equations can be based on the undeformed structure, i.e. deflections are small;
- (b) Instability of an individual member or of the frame as a whole does not occur.

Both these assumptions are quite valid when dealing with comparatively small structures. However, for multi-storey frameworks, neither of them may

be assumed to be true, particularly if the members of the frame carry large axial forces or if the frame itself is subjected to heavy applied wind loading.

A plastic design method originally proposed by Gandhi⁽⁴⁾ takes due account of instability and sway deflection under wind load. The design procedure consists of two stages; in the first stage the beams and columns are designed and sections selected, by the simple plastic theory in a way somewhat similar to that suggested by Calladine⁽⁶⁾. In the second stage these sections are checked and increased, if necessary, to allow for instability and sway deflection effects; this is done by using the m , n and o instability functions⁽⁵⁾.

This design method starts with given geometry, loading and required load factors. Member sizes are then selected in such a way that:-

- (a) The framework shall be capable of withstanding dead load plus vertical live load at some load factor λ_1 of 1.75.
- (b) The framework shall be capable of withstanding a combination of dead load plus live load plus wind load at some load factor λ_2 of 1.4. The reduced value of λ_2 corresponds to the 25% increase in the allowable stresses in the presence of wind loading, as permitted in B.S.449⁽¹³⁾.
- (c) The frame shall be fully elastic at working load.
- (d) Plastic hinges shall not occur in the columns below the design load factor under either system of loading; so for the purpose of analysis at any intermediate stage of loading, the columns are elastic.

The selection of section sizes in accordance with the above design criteria limits the number of possible plastic collapse failure mechanisms to three. These are indicated in Figure 8.1 for typical internal bays and storeys. The type of mechanism which will occur in any given instance is governed by the magnitude of wind shear to vertical load ratio; where this

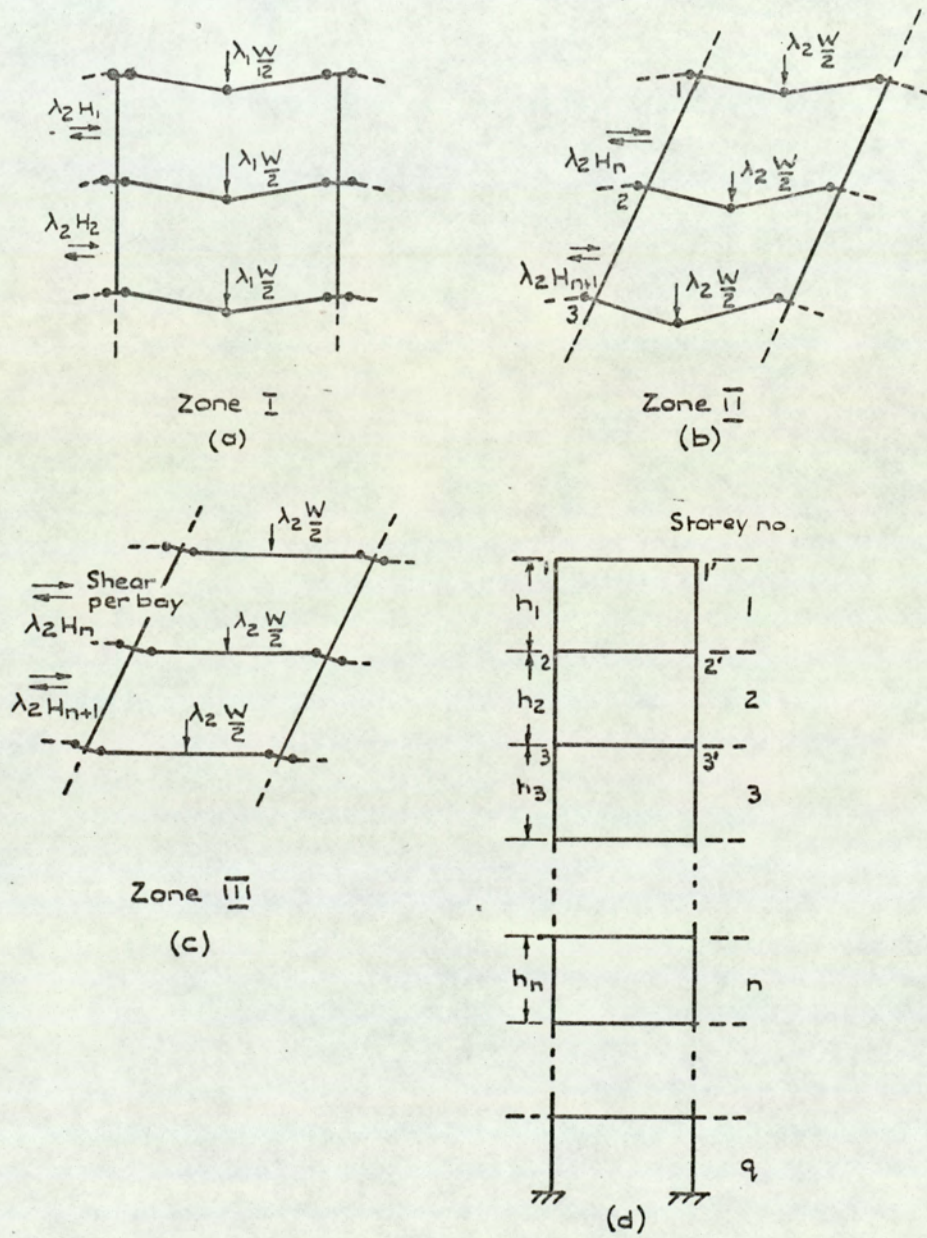


Fig. 8.1. Plastic design of multi-storey sway frames.

is small, see Figure 8.1(a), a beam mechanism will occur; for intermediate values, Figure 8.1(b), a combined mechanism will occur; and for larger values, Figure 8.1(c), a sway mechanism will occur. Thus, in multi-storey frames, the selection of member sections may be such that the upper storeys fail by Zone I mechanism, the middle storeys by Zone II mechanism and the lower storeys by Zone III mechanism.

It was found possible ⁽⁴⁾ to group the corrections to the simple plastic theory owing to instability into one factor. This has been termed the magnification factor (viz., A) which is a function of the m , n and o stability functions, Euler ratio (axial load/Euler load) and relative stiffnesses of members. Hence, the magnification factor can be defined as the degree by which the bending moments are modified, owing to the instability effects. Thus the beam and column sections finally designed are the simple plastic theory sections increased, where necessary, to allow for instability effects by introducing the magnification factor into the simple plastic theory equations.

This method is developed further by Sinclair-Jones ⁽³⁷⁾ which includes an improved and more accurate method of dealing with the boundary regions (i.e. upper storey, lower storey and external bays of a frame). Also this improved method predicts values for the magnification factor which generally reduces the number of iterations or eliminates the need for iterations entirely.

8.3 SIMPLE PLASTIC DESIGN

The theory will be developed for a general rigid jointed sway frame having r bays, each of span L , and q storeys, each of height h . The assumptions concerning the structure and its loading are as follows:-

- (1) The number of bays and number of storeys are large, hence the effect of the unsymmetrical loading conditions of the end bays on a typical internal bay is negligible.
- (2) The span loading is uniformly distributed and of magnitude W per

bay at working load (considered as a central point load equal to half the applied uniform load).

- (3) No bending moment and therefore no shear forces are induced in the internal columns by the vertical loading, as implied by (1).
- (4) The wind shear is resisted entirely by frame action and no wind bracing is provided in the form of cladding etc. An equal shear force, H , is induced in each internal column in a storey by the application of wind loading. H is defined as the sum of all the applied wind forces above the storey in question, divided by the number of bays.
- (5) Owing to wind loading, the columns bend in double curvature in such a way that points of contraflexure exist at their mid-heights.
- (6) The axial forces developed in the beams are small and may be neglected.
- (7) The axial force in an internal column is equal to the force in a column above, plus half the loads on the adjoining beams.

The derivation of the simple plastic design equations is as follows:-

8.3.1 FAILURE UNDER VERTICAL LOADING

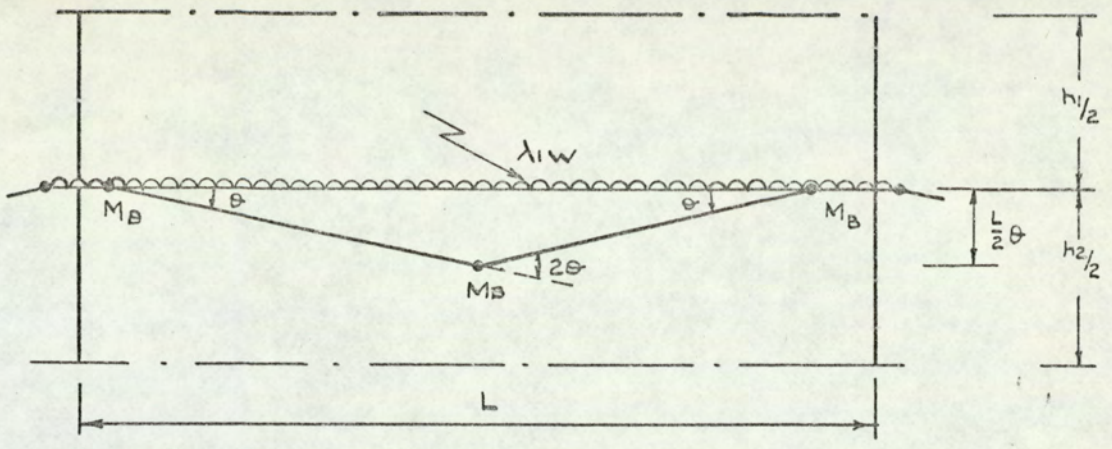
The only possible mode of failure under this type of loading involves the independent collapse of each beam as shown in Figure 8.2(a). M_B is the fully plastic moment required for this simple beam mechanism to occur at a load factor λ_1 and may be obtained by equating the work done by the loads to the work absorbed by the plastic hinges. Thus, referring to Figure 8.2(a) for any beam:-

$$M_B (2\theta + \theta + \theta) = \frac{\lambda_1 W}{2} \cdot \frac{L}{2} \cdot \theta$$

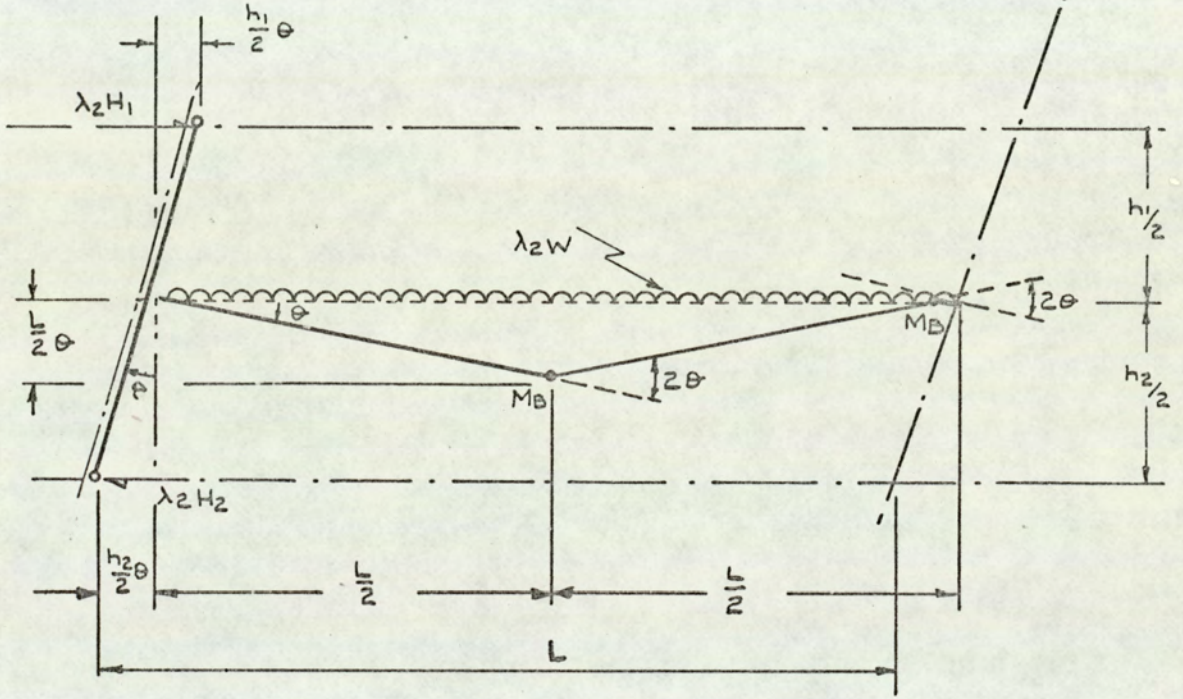
$$\therefore M_B = \lambda_1 \frac{WL}{16} \qquad 8.1$$

Theoretically, since the internal columns carry only axial load, their required value of plastic moment C_I may be taken as zero.

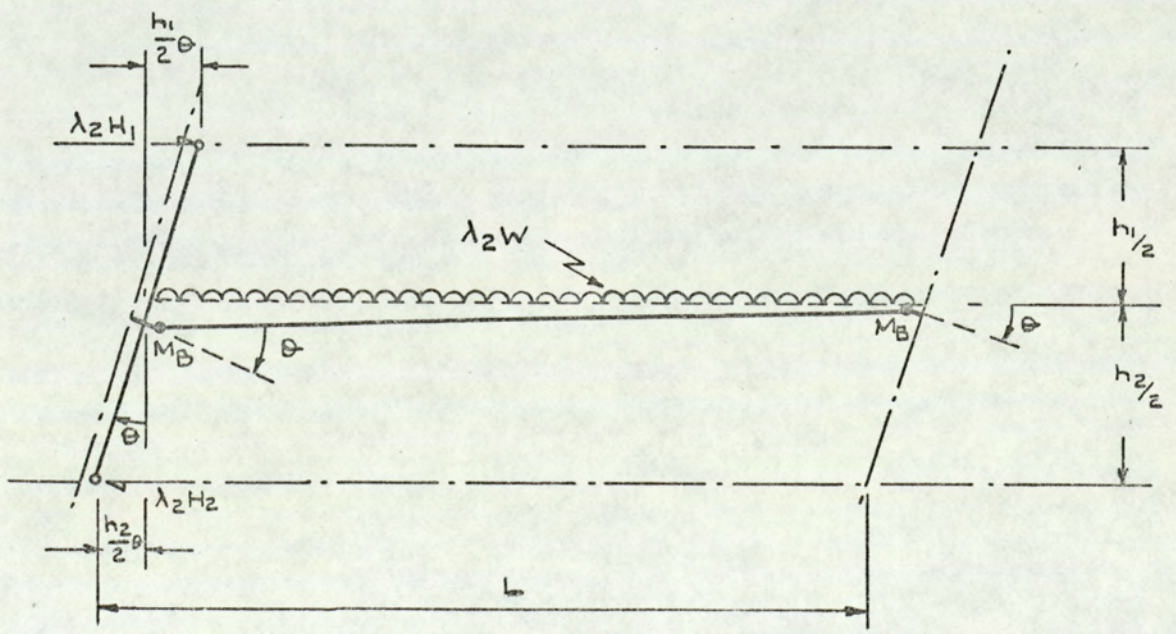
This type of failure is demonstrated by test M_1 in the experimental part



a. Zone I - Collapse mechanism under vertical load alone.



b. Zone II - Combined mechanism.



c. Zone III - Sway mechanism.

Fig. 8.2. Failure mechanisms of multi-storey frames. Isolated bay.

of this research, with the effect of composite action between the floor system and the supporting beams included.

8.3.2 FAILURE UNDER COMBINED MECHANISM

Under a combination of vertical and horizontal loading the subassemblage may be reduced to a mechanism in one of two ways, both of which are accompanied by sway deformation. Only two plastic hinges are required in each beam to create these mechanisms. In both cases, a hinge is bound to form at the leeward end of the beam, since at this location the bending moments induced by the vertical and horizontal loadings act in the same sense, and are therefore cumulative. The position of the second plastic hinge that is required to cause failure depends on the relative magnitudes of the moments induced by the two types of loading. In general, this second hinge forms in the span of the beam, producing the "combined mechanism" shown in Figure 8.2(b). It has been assumed ⁽³⁷⁾ that this second hinge forms exactly in the centre of the beam. This assumption is sufficiently accurate for design purposes. However, in cases of very heavy wind loading, the second hinge may form at the windward end of the beam, producing the "sway mechanism" shown in Figure 8.2(c).

Considering first the combined mechanism in Figure 8.2(b), if the column sways through a small angle θ , each plastic hinge rotates by 2θ , and work is done by both vertical and horizontal loads. The corresponding work equation is:-

$$4 M_B \cdot \theta = \frac{\lambda_2 W}{2} \cdot \frac{L}{2} \cdot \theta + \lambda_2 H_1 \cdot \frac{h_1}{2} \cdot \theta + \lambda_2 H_2 \cdot \frac{h_2}{2} \cdot \theta$$

$$\therefore M_B = \lambda_2 \frac{WL}{4} \left[\frac{1}{4} + \frac{(Hh)_{av}}{WL} \right] \quad 8.2$$

$$\text{Whence } (Hh)_{av} = \frac{H_1 \cdot h_1 + H_2 \cdot h_2}{2}$$

The quantity $\frac{(Hh)_{av}}{WL}$ is hereafter referred to as the "wind ratio" representing the relative intensities of wind loading and vertical loading.

Consider now the sway mechanism of Figure 8.2(c). In this case, if

the column sways through an angle θ , the plastic hinges both rotate by θ , and the vertical loading does no work. The resulting work equation is:-

$$2 M_B \theta = \lambda_2 H_1 \cdot \frac{h_1}{2} \cdot \theta + \lambda_2 H_2 \cdot \frac{h_2}{2} \cdot \theta$$

$$\therefore M_B = \lambda_2 \frac{(Hh)_{av}}{2} \quad 8.3$$

For either the combined or sway mechanism, the maximum column moments occur at the level of the beam and are simply equal to the shear in the column multiplied by the distance from the joint to the assumed point of contraflexure at its mid-height. Therefore, for both types of mechanism, a plastic hinge will not form in the column if:-

$$C_I > \lambda_2 \frac{Hh}{2} \quad 8.4$$

Where C_I represents the reduced plastic moment of the column in the presence of axial load.

8.3.3 SELECTION OF THE CRITICAL EQUATIONS

The point at which change over from beam mechanism to combined mechanism occurs is given by the intersection of equations 8.1 and 8.2,

$$\text{i.e. when } \lambda_1 \frac{WL}{16} = \lambda_2 \frac{WL}{4} \left[\frac{1}{4} + \frac{(Hh)_{av}}{WL} \right]$$

Since $\lambda_1 = 1.75$ and $\lambda_2 = 1.4$, hence $\lambda_1 = \frac{5}{4} \lambda_2$

$$\therefore \frac{5}{4} \lambda_2 \frac{WL}{16} = \lambda_2 \frac{WL}{4} \left[\frac{1}{4} + \frac{(Hh)_{av}}{WL} \right]$$

$$\text{i.e. when } \frac{1}{16} = \frac{(Hh)_{av}}{WL}$$

When the wind ratio is greater than this value, failure will be by combined mechanism.

Similarly, the point at which the wind loading becomes predominant is given by the intersection of equations 8.2 and 8.3,

$$\text{i.e. when } \lambda_2 \frac{(Hh)_{av}}{2} = \lambda_2 \frac{WL}{4} \left[\frac{1}{4} + \frac{(Hh)_{av}}{WL} \right]$$

i.e. when $\frac{(Hh)_{av}}{WL} = \frac{1}{4}$

When the wind ratio is greater than this value, failure will be by side sway mechanism.

Hence the design of structure can be split into three zones, as described in the previous section. The simple plastic design equations are summarised below,

ZONE I when $0 \leq \frac{(Hh)_{av}}{WL} \leq \frac{1}{16}$

$$M_B = \lambda_1 \frac{WL}{16} \quad 8.1$$

ZONE II when $\frac{1}{16} \leq \frac{(Hh)_{av}}{WL} \leq \frac{1}{4}$

$$M_B = \lambda_2 \frac{WL}{4} \left[\frac{1}{4} + \frac{(Hh)_{av}}{WL} \right] \quad 8.2$$

ZONE III when $\frac{1}{4} \leq \frac{(Hh)_{av}}{WL}$

$$M_B = \lambda_2 \frac{(Hh)_{av}}{2} \quad 8.3$$

In all zones,

$$C_I > \lambda_2 \frac{Hh}{2} \quad 8.4$$

It is quite possible, depending upon the design wind ratio, for a building to have varying numbers of storeys designed in all three zones or to be designed as falling entirely in one zone.

For design in all zones, the column size is selected using equation 8.4. This equation, which is based on the shear force in the column, is independent of the wind ratio. Under vertical load alone, the column carries only axial forces, and so equation 8.4 always dictates the required plastic moment, and automatically satisfies the final design criterion given in section 8.2.

8.4. MODIFICATIONS TO THE SIMPLE PLASTIC DESIGN PROCEDURE

The simple plastic design approach used so far is adequate for frames in which there are small axial loads in the columns and also small sidesway deflections. This is not usually the case for tall structures where premature

instability failure can occur and therefore a certain number of modifications must be made to the simple plastic design method.

8.4.1 P δ EFFECT (WITHOUT JOINT ROTATION)

Figure 8.3 shows a column subjected to an axial load P and a horizontal shear H. If the horizontal deflection of the column is neglected as in Figure 8.3(a), then taking moments about A gives:-

$$M_1 + M_2 = Hh$$

In fact some horizontal deflection must occur, as shown in Figure 8.3(b), so that in reality:-

$$M_1 + M_2 = Hh + P\delta$$

Merchant⁽³²⁾ has shown that the additional moment P δ , owing to axial load and sway deflection, can be allowed for by using a factor m such that:-

$$M_1 + M_2 = Hh + P\delta = mHh$$

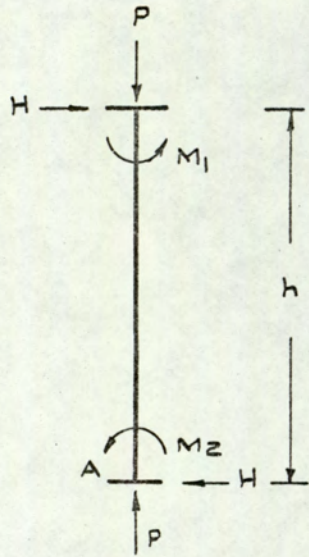
The variable m is a function of the ratio of the axial load in the column to its Euler load ($\rho = \frac{P}{P_e}$). Values of this factor have been tabulated by Livesley and Chandler⁽⁵⁾. Thus, if Hh is replaced by mHh in equations 8.1 to 8.4, these equations will take account of the P δ effect (neglecting joint rotation).

8.4.2 OTHER EFFECTS

The further modifications to the simple plastic design discussed here involves consideration of the following factors:-

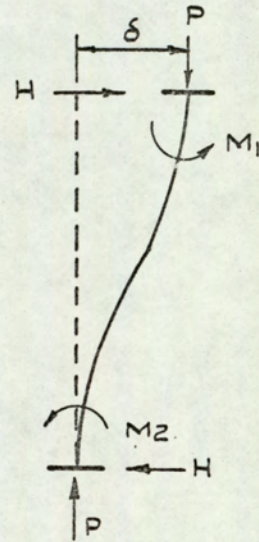
- (i) Reduction in column stiffness, owing to axial load;
- (ii) Sidesway deflection, owing to joint rotation and hence additional moment;
- (iii) Reduction of effective beam stiffness, owing to the formation of a plastic hinge.

The combined results of the above effects can be allowed for by taken factors A for beams and A_c for columns. These factors are known as the magnification factors and their values depend upon which zone is under consideration. The detailed determination of the factors A and A_c is given in section 8.7.



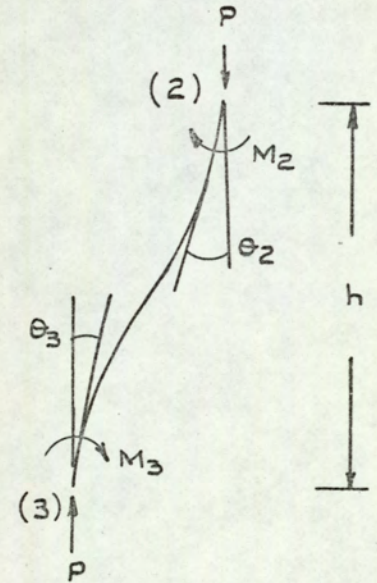
(a) No sway.

Fig. 8.3. (a).



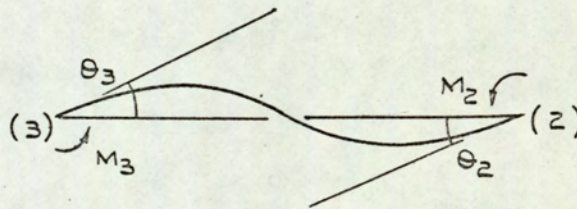
(b) Sway without joint rotation.

Fig. 8.3. (b)



Typical column member
sway with zero shear.

Fig. 8.4.



Typical beam member no sway
and zero axial force.

Fig. 8.5.

Thus, the effects considered in sections 8.4.1 and 8.4.2 above will introduce factors m_A and m_{A_c} into equations 8.1 to 8.4. Hence the modified design equations, which are assumed to allow automatically for the instability effects, may therefore be summarised as follows:-

$$\underline{\text{ZONE I}} \quad \text{when} \quad 0 \leq \frac{A(m_H h)av}{WL} \leq \frac{1}{16}$$

$$M_B = \lambda_1 \frac{WL}{16} \quad 8.5$$

$$\underline{\text{ZONE II}} \quad \text{when} \quad \frac{1}{16} \leq \frac{A(m_H h)av}{WL} \leq \frac{1}{4}$$

$$M_B = \lambda_2 \frac{WL}{4} \left[\frac{1}{4} + \frac{A(m_H h)av}{WL} \right] \quad 8.6$$

$$\underline{\text{ZONE III}} \quad \text{when} \quad \frac{1}{4} \leq \frac{A(m_H h)av}{WL}$$

$$M_B = \lambda_2 \frac{A(m_H h)av}{2} \quad 8.7$$

In all zones,

$$C_I > \lambda_2 \frac{A_c m_H h}{2} \quad 8.8$$

The above equations relate to the case of a typical inner bay of a frame and therefore the design of the external columns does not occur. Most frames however, have only a small number of bays and the design of columns then becomes of importance. In all three zones, a plastic hinge will not form in the external column if:-

$$C_E > \frac{M_B}{2} \quad 8.9$$

For the top storey, where there is only one column, then:-

$$C_E > M_B \quad 8.10$$

Where C_E represents the reduced plastic moment of the external column in the presence of axial load.

The above two equations are assumed adequate for the design of the external columns. More accurate methods of dealing with the external columns, upper storey and lower storey, are found elsewhere⁽³⁷⁾

8.5 INTRODUCTION OF COMPOSITE ACTION INTO THE DESIGN OF MULTI-STOUREY FRAMES

The effects of types (2) and (3) assumptions on degree of composite action, where composite action is assumed present at the mid-spans of the supporting beams only, will be introduced into the plastic design equations 8.5 to 8.10.

For both types of assumptions (2) and (3), the mid-span plastic moment M_B will be replaced by M_e , the plastic composite moment at mid-span. At the supports, the plastic moment will remain as M_B and the hogging or sagging ultimate slab moment M_{sl} (Figure 4.1, mode B) will be ignored here for simplicity, although there is no reason of principle preventing its inclusion if desired.

For vertical load failure (Figure 8.2(a)), when type (2) or (3) of composite action is introduced, equation 8.5 becomes:-

$$0.5 (M_e + M_B) = \frac{\lambda_1 WL}{16} \quad 8.11$$

For combined mechanism (Figure 8.2(b)), when type (2) or (3) of composite action is introduced, equation 8.6 becomes:-

$$0.5 (M_e + M_B) = \lambda_2 \frac{WL}{4} \left[\frac{1}{4} + \frac{A(m.H.h)av}{WL} \right] \quad 8.12$$

For sway mechanism (Figure 8.2(c)), a plastic hinge will not form at mid-span, and type (2) or (3) of composite action has no effect on the beam design. Hence, equation 8.7 remains as:-

$$M_B = \lambda_2 \frac{A(m.H.h)av}{2} \quad 8.13$$

The design equations for the internal and external columns remain as given by equations 8.8, 8.9 and 8.10.

The critical equations for the change over from one zone to another will now be different from that of the bare steel frame, as shown below.

As the composite plastic moment M_e is present in both equations 8.11 and 8.12, the change over from Zone I to Zone II will be the same as that

of the bare steel frame,

$$\text{i.e. when } \frac{1}{16} = \frac{A(mHh)_{av}}{WL}$$

Change over from the combined mechanism to the sway mechanism will be different from that of the bare steel frame and is given by the intersection of equations 8.12 and 8.13,

$$\text{i.e. when } \lambda_2 \frac{A(mHh)_{av}}{2} = \frac{\lambda_2 WL}{8} + \lambda_2 \frac{A(mHh)_{av}}{2} - M_e$$

$$\text{i.e. when } \frac{M_e}{\lambda_2 WL} = \frac{1}{8}$$

Hence the modified design equations, including the effect of composite action of types (2) or (3) (ignoring the effect of the hogging or sagging ultimate slab moment M_{sl} at supports), may be summarised as follows:-

$$\underline{\text{ZONE I}} \quad \text{when } 0 \leq \frac{A(mHh)_{av}}{WL} \leq \frac{1}{16}$$

$$0.5 (M_e + M_B) = \lambda_1 \frac{WL}{16} \quad 8.11$$

$$\underline{\text{ZONE II}} \quad \text{when } \frac{1}{16} \leq \frac{A(mHh)_{av}}{WL} \quad \text{and} \quad \frac{M_e}{\lambda_2 WL} \leq \frac{1}{8}$$

$$0.5 (M_e + M_B) = \lambda_2 \frac{WL}{4} \left[\frac{1}{4} + \frac{A(mHh)_{av}}{WL} \right] \quad 8.12$$

$$\underline{\text{ZONE III}} \quad \text{when } \frac{M_e}{\lambda_2 WL} \geq \frac{1}{8}$$

$$M_B = \lambda_2 \frac{A(mHh)_{av}}{2} \quad 8.13$$

In all zones,

$$C_I > \lambda_2 \frac{A_c m' H h}{2} \quad 8.14$$

$$C_E > \frac{M_B}{2} \quad 8.15$$

$$\text{For top storey, } C_E > M_B \quad 8.16$$

The detailed determination of the above magnification factors A and A_c is given in section 8.7, and the magnification factors will be compared with those for the bare steel frame.

The design equations 8.11 to 8.16 apply for composite action of both

types (2) and (3). If type (2) of composite design is to be adopted, the plastic composite moment M_e is calculated using equations 5.1 to 5.11, where the effect of slab reinforcement is ignored. For type (3) of composite design, M_e is calculated using equations 5.12 to 5.22 to include the effect of slab reinforcement.

The ultimate slab moment M_s is normally designed for vertical load failure at a load factor $\lambda_1 = 1.75$. If the reduced value of λ_2 of 1.4 is used to design the ultimate slab moment M_s for Zones II and III and if the yield line rotation at the support is assumed to be the same as that of the joint under consideration, then the ultimate slab moment along the yield lines at the supports $M_s \ell$ (Figure 4.1, mode B) can be taken into consideration into equations 8.11 to 8.13.

Using the same assumption of Chapter 4, Figure 4.2, that the slab is isotropic, then the sagging and hogging ultimate slab moments are equal. Therefore, by including the effect of the ultimate slab moment $M_s \ell$ at the supports, equations 8.11 to 8.13 become:-

$$0.5 (M_e + M_B + M_s \ell) = \lambda_1 \frac{WL}{16} \quad 8.11'$$

$$0.5 (M_e + M_B + M_s \ell) = \lambda_2 \frac{WL}{4} \left[\frac{1}{4} + \frac{A(mHh)_{av}}{WL} \right] \quad 8.12'$$

$$(M_B + M_s \ell) = \lambda_2 \frac{A(mHh)_{av}}{2} \quad 8.13'$$

The critical equations for Zones I, II and III will be the same as that when the $M_s \ell$ values at the support are ignored.

The effect of types (4) and (5) of composite action, where full composite action is assumed at mid-spans and supports, on the plastic design equations 8.5 to 8.7 can be included in a similar manner to that of types (2) and (3). In this case, the mid-span plastic moment M_B will be replaced by M_e as for types (2) and (3), and the support plastic moment M_B will be replaced by M_N , the plastic composite moment at supports.

8.6 DIRECT MOMENT DISTRIBUTION

The traditional moment distribution method uses stiffnesses which are related to arbitrarily assumed conditions at the far end of a member. For example, the stiffness at one end of a member with the far end fixed is $\frac{4EI}{L}$. If the far end is pinned, the effective stiffness becomes $\frac{3EI}{L}$. If, however, stiffnesses are related to the real rotations which occur at the ends of a member when it forms part of a structure, the moment distribution process can be reduced to one cycle only. Thus, it is only necessary to write down the fixed end moments and then balance at the joints, no carry over of moment from one end of a member to the other is involved. The joints are balanced using "real distribution factors" which are calculated from the real stiffnesses. Hence the real stiffness of a member of a structure can be defined as the moment to produce unit rotation at one end of the member, whilst the far end of the member rotates through an angle equal to the actual angle of rotation which occurs in the structure under consideration for the given loading. Figure 8.4 shows a column (23) subjected to axial load and end moments (but no horizontal shear) giving rise to end rotations θ_2 and θ_3 . It has been shown by Holmes and Gandhi⁽⁷⁶⁾ that the stiffness of such a member related to the real end rotations, i.e. the "real stiffnesses" are given by:-

At end (3)

$$\frac{M_3}{\theta_3} = S_{32}^r = \left(n - \frac{o}{R_3}\right) \frac{EI}{h} \quad 8.17$$

At end (2)

$$\frac{M_2}{\theta_2} = S_{23}^r = (n - R_3 o) \frac{EI}{h} \quad 8.18$$

Where R_3 is the ratio of end rotations, i.e. $\frac{\theta_3}{\theta_2}$, and n and o are stability functions as tabulated by Livesley and Chandler⁽⁵⁾.

For the beams of a multi-storey frame, the axial load and lateral displacement of the beam ends are negligible. Hence, referring to Figure 8.5 of a typical fully elastic beam bending in double curvature, the real stiff-

nesses for this beam can be written down (7e) as:-

$$\frac{M_3}{\theta_3} = S_{32}^r = \left(4 + \frac{2}{R_3}\right) \frac{EI}{L} \quad 8.19$$

and
$$\frac{M_2}{\theta_2} = S_{23}^r = (4 + 2 R_3) \frac{EI}{L} \quad 8.20$$

The real stiffnesses of all the members of a multi-storey frame may be obtained by substituting suitable values of R in equations 8.17 to 8.20.

It has already been assumed in 8.3 (5) that the columns bend in double curvature under the action of wind loading, with points of contraflexure existing at their mid-heights. This implies that the end rotations of any column must be equal, so that $R = 1$. Therefore, from equations 8.17 and 8.18, approximate expressions for the no-shear stiffnesses of any column are given by:-

$$S_{32}^r = S_{23}^r = (n - o) \frac{EI}{h} \quad 8.21$$

For the purpose of developing the general theory for a typical internal bay, it was also stated in 8.3 (1) that the total number of internal bays r is considered to be large. Therefore, since the same sections are used for each internal column, each bay behaves in an identical manner, and every beam will bend in exact double curvature under the action of horizontal loading. The end rotations of the beam will be equal, so that R is again equal to unity. Therefore, substituting in equations 8.19 and 8.20, the approximate values for the real stiffness of the beams are:-

$$S_{32}^r = S_{23}^r = 6 \frac{EI}{L} \quad 8.22$$

The use of these approximate values of real stiffness results in a considerable saving in design time, without introducing any large degree of error. The precise way in which they are applied to develop expressions for the magnification factors for composite and bare steel frames, using the direct moment distribution technique, is shown in the following section.

8.7 DERIVATION OF THE MAGNIFICATION FACTORS

The values of the magnification factors A and A_c will vary depending

upon whether the particular storey being considered falls into Zones I, II or III. These factors are derived for each zone in turn for the case where composite action of type (2) or (3) is introduced into the plastic design of steel frames, i.e. equations 8.11 to 8.14. The derived equations of these factors will be compared with those of the bare steel frame, i.e. equations 8.5 to 8.8.

8.7.1 ZONE I

$$0 \leq \frac{A(mHh)_{av}}{WL} \leq \frac{1}{16}$$

In this zone, the beam and column sizes are selected using equations 8.5 and 8.8 respectively for the bare steel frame, or equations 8.11 and 8.14 respectively for the composite frame. Although the condition of vertical load alone is critical in selecting the beam size, the combined loading condition dictates the column size. The beam is independent of the magnitude of wind loading and of the magnification factor, which must be obtained therefore by considering the combined loading case. This is identical to the treatment for Zone II.

8.7.2 ZONE II

$$\frac{1}{16} \leq \frac{A(mHh)_{av}}{WL} \text{ and } \frac{M_e}{\lambda_2 WL} \leq \frac{1}{8}$$

The loading sequence adopted in deriving the values of A and A_c is that the wind loading increases from zero to its maximum intensity, irrespective of the vertical loading. That is, initially the factored vertical load is applied to the sub assemblage, and this is followed by the horizontal loading.

In this zone, under the vertical load alone, the beam may remain elastic or may develop plastic hinges, and it is necessary to differentiate between these two types of behaviour.

Consider the beam in Figure 8.6(a) under the action of vertical load at a load factor λ_2 , the bending moment diagram is as shown in Figure 8.6(b). The required fully plastic moment of a beam falling in this zone is given by equation 8.12,

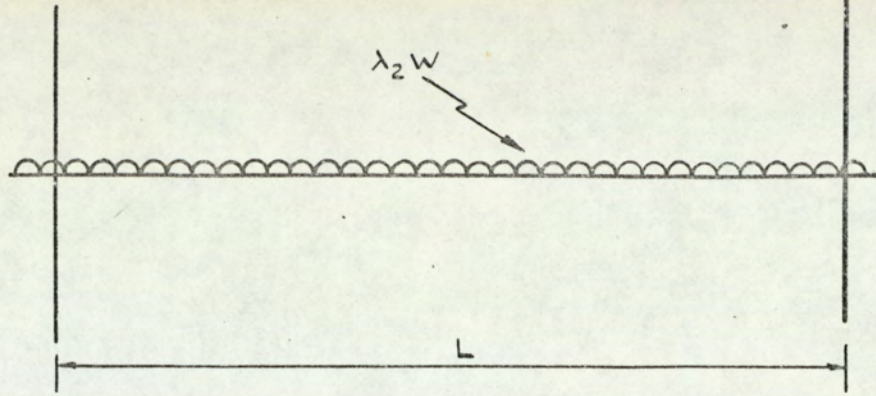


Fig. 8.6.(a) Fully elastic beam - vertical load alone; $\lambda = \lambda_2$

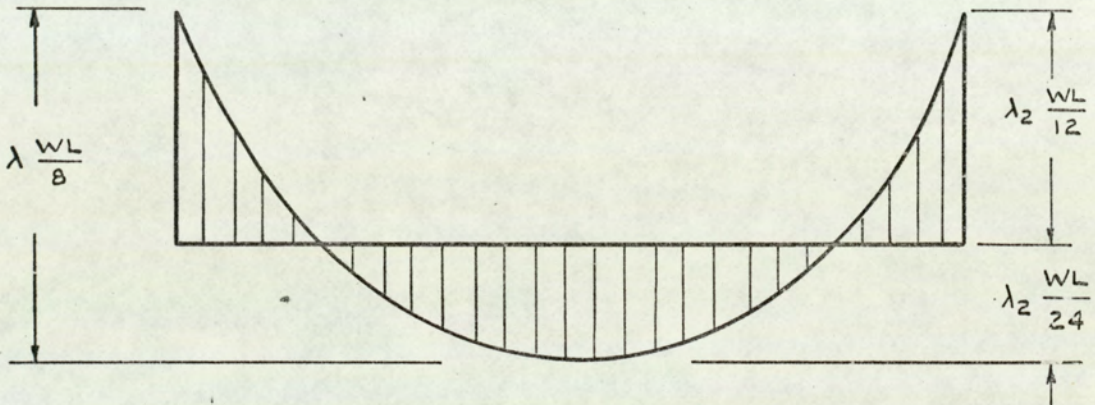


Fig. 8.6. (b) Bending moment diagram.

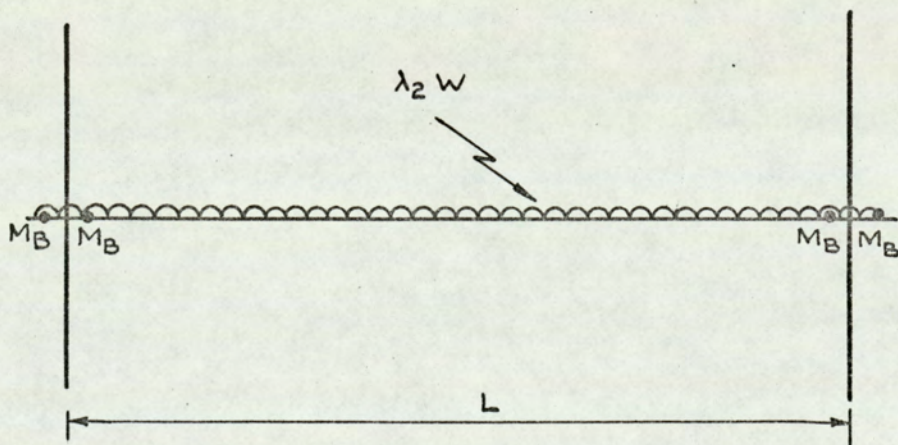


Fig. 8.7.(a) Partially plastic beam - vertical load alone; $\lambda = \lambda_2$

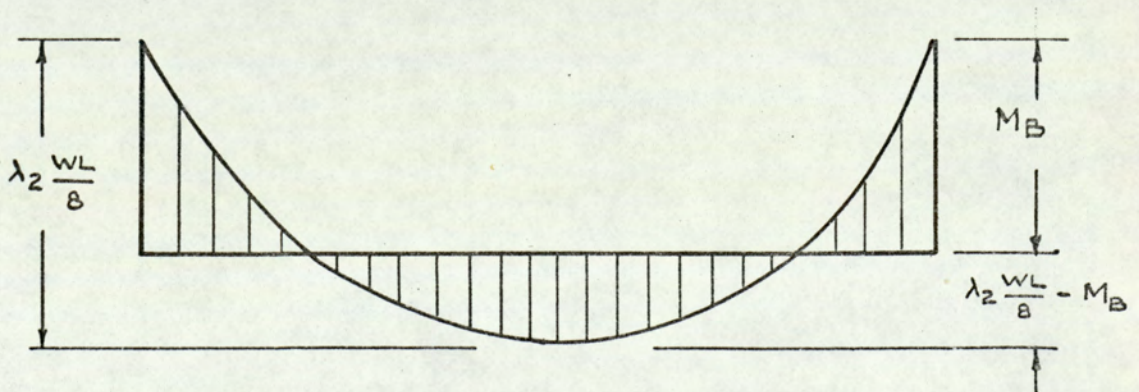


Fig. 8.7. (b) Bending moment diagram.

$$\text{i.e. } MB = 2 \cdot \lambda_2 \frac{WL}{4} \left[\frac{1}{4} + \frac{A(mHh)_{av}}{WL} \right] - M_e$$

Therefore, under this load, plastic hinges will have formed at the ends of the beam if,

$$\lambda_2 \frac{WL}{12} \geq 2 \cdot \lambda_2 \frac{WL}{4} \left[\frac{1}{4} + \frac{A(mHh)_{av}}{WL} \right] - M_e$$

which reduces to the condition:-

$$\frac{A(mHh)_{av}}{WL} \leq \frac{2 M_e}{\lambda_2 WL} - \frac{1}{12}$$

In the case of bare steel frames (equation 8.6), the above condition becomes:-

$$\frac{A(mHh)_{av}}{WL} \leq \frac{1}{12}$$

This zone may therefore be subdivided into two separate zones, which are considered in turn below.

8.7.2(a) ZONE II (i)

$$\frac{1}{16} \leq \frac{A(mHh)_{av}}{WL} \leq \left(\frac{2 M_e}{\lambda_2 WL} - \frac{1}{12} \right)$$

Plastic hinges form at the ends of each beam before the full vertical load has been applied. At load factor λ_2 , the frame is as shown in Figure 8.7(a) and the corresponding bending moment diagram is given in Figure 8.7(b).

On application of the wind loading, the plastic hinge at the leeward end of the beam continues to rotate as before. However, the hinge at the windward end tends to rotate in the opposite direction and therefore immediately disappears. The presence of a plastic hinge at the end of each beam effectively isolates one bay from the next. In the typical bay in Figure 8.8, the real stiffnesses of the columns at joint 2 may be obtained from equation 8.21. Thus,

$$S_{21}^r = (n_1 - o_1) K_{c1}$$

and
$$S_{23}^r = (n_2 - o_2) K_{c2}$$

Where K_{c1} and K_{c2} are the flexural rigidities of the upper and lower columns at joint 2.

Also, since the plastic hinge at 2' may be considered to behave in an

identical manner to a real hinge, the real stiffness of the composite beam at joint 2 is given by:-

$$S_{22}^r = 3 K_{b2}^e$$

Where K_{b2}^e is the flexural rigidity of an equivalent uniform composite beam. In the case of bare steel frames, K_{b2}^e is equal to K_{b2} the flexural rigidity of the steel section.

Therefore, the total stiffness at joint 2 is:-

$$\Sigma S_2^r = (n_1 - o_1) K_{c1} + (n_2 - o_2) K_{c2} + 3 K_{b2}^e$$

Let α^Δ represent the real distribution factors at 2 in the presence of a plastic hinge at 2', then:-

$$\alpha_{21}^\Delta = \frac{S_{21}^r}{\Sigma S_2^r} = \frac{(n_1 - o_1) K_{c1}}{\Sigma S_2^r}$$

$$\alpha_{23}^\Delta = \frac{S_{23}^r}{\Sigma S_2^r} = \frac{(n_2 - o_2) K_{c2}}{\Sigma S_2^r}$$

$$\alpha_{22'}^\Delta = \frac{S_{22'}^r}{\Sigma S_2^r} = \frac{3 K_{b2}^e}{\Sigma S_2^r}$$

These may be written in the following form:-

$$\alpha_{21}^\Delta = \frac{(n_1 - o_1) \bar{K} K_2}{K_2 V + 3} \quad 8.23$$

$$\alpha_{23}^\Delta = \frac{(n_2 - o_2) K_2}{K_2 V + 3} \quad 8.24$$

$$\alpha_{22'}^\Delta = \frac{3}{K_2 V + 3} \quad 8.25$$

Where, $K_2 = \frac{K_{c2}}{K_{b2}^e}, \quad \bar{K} = \frac{K_{c1}}{K_{c2}}$

and $V = \bar{K} (n_1 - o_1) + (n_2 - o_2)$

The total out of balance moment at joint 2 is:-

$$F.E.M._2 = -\lambda_2 \frac{m_1 H_1 h_1}{2} - \lambda_2 \frac{m_2 H_2 h_2}{2} = -\lambda_2 (m H h)_{av}$$

Therefore, the total moment to be distributed at joint 2, in order to satisfy joint equilibrium, is $+\lambda_2 (mHh)av$. The final moments at the joint, owing to wind loading alone, are shown in Figure 8.8(a), whilst the moment owing to combined vertical and horizontal loading at load factor λ_2 are given in Figure 8.8(b).

In this zone, failure occurs owing to the formation of a combined mechanism, and the span hinge is assumed to form exactly in the centre of the beam. The bending moment at this location must therefore be equal to the fully plastic composite moment of the beam M_e . Thus, referring to Figure 8.8(b):-

$$\left(\lambda_2 \frac{WL}{8} - M_B\right) + \frac{1}{2} \cdot a_{22}' \cdot \lambda_2 (mHh)av = M_e$$

This reduces to,

$$0.5 (M_e + M_B) = \lambda_2 \frac{WL}{4} \left[\frac{1}{4} + a_{22}' \cdot \frac{(mHh)av}{WL} \right]$$

However, in this zone,

$$0.5 (M_e + M_B) = \lambda_2 \frac{WL}{4} \left[\frac{1}{4} + A \cdot \frac{(mHh)av}{WL} \right] \quad 8.12$$

$$\therefore A = a_{22}' \quad 8.26$$

The above equation is also true for the case of bare steel frames, where $M_e = M_B$. In this case, equation 8.12 reduces to equation 8.6. Referring again to Figure 8.8(b), the moment in the lower column is:-

$$\begin{aligned} M_{23} &= -\lambda_2 \frac{m_2 H_2 h_2}{2} + a_{23}' \cdot \lambda_2 (mHh)av \\ &= -\lambda_2 \left(1 - 2 a_{23}' \cdot p_2\right) \cdot \frac{m_2 H_2 h_2}{2} \end{aligned}$$

$$\text{Where } p_2 = \frac{(mHh)av}{m_2 H_2 h_2}$$

$$\text{However } C_I > |M_{23}| = \lambda_2 \cdot A_c \cdot \frac{m_2 H_2 h_2}{2}$$

$$\therefore A_c = 1 - 2 a_{23}' \cdot p_2 \quad 8.27$$

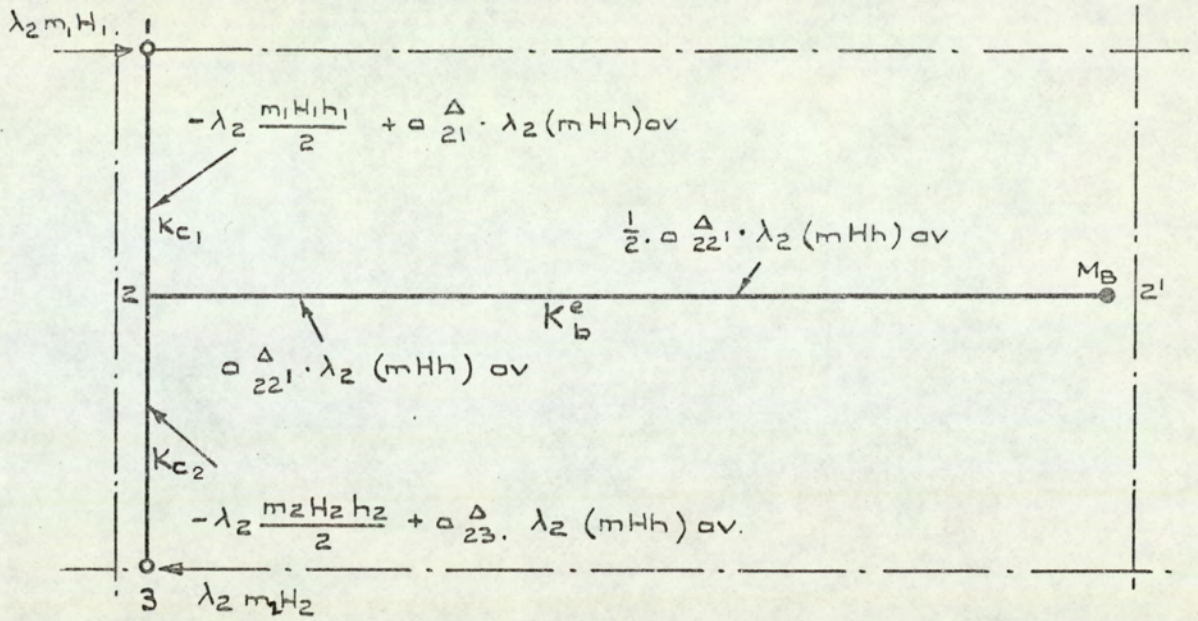


Fig 8.8.(a). Bending moments due to wind load alone
- Zone 2.(i).

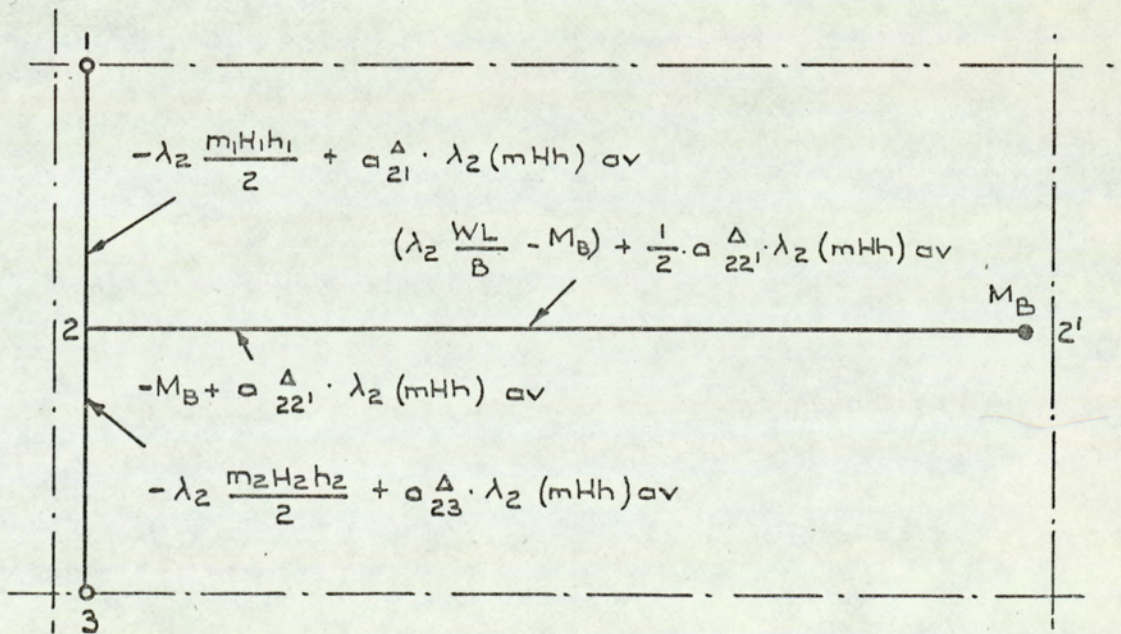


Fig. 8.8.(b) Bending moments at ultimate combined load
- Zone 2(i).

8.7.2(b) ZONE II (ii)

$$\left(\frac{2 M_e}{\lambda_2 WL} - \frac{1}{12} \right) \leq \frac{A(mHh)av}{WL} \quad \text{and} \quad \frac{M_e}{\lambda_2 WL} \leq \frac{1}{8}$$

In this zone, the beams remain completely elastic under the factored vertical load alone, and the bending moment diagram is as shown previously in Figure 8.6(b). On application of the horizontal loading, the moment at the windward end reduces, and that at the leeward end increases. The real stiffness of each beam connected to a joint is therefore given by equation 8.22, i.e.

$$S_{22}^r = 6K_{b2}$$

Since there are two beams connected to each joint, the total joint stiffness in this case is given by:-

$$\Sigma S_2^r = (n_1 - o_1) K_{c1} + (n_2 - o_2) K_{c2} + 12K_{b2}^e$$

Let α^∞ denote the real distribution factors for the case when the beam is fully elastic, using the same notation as before,

$$\alpha_{21}^\infty = \frac{S_{21}^r}{\Sigma S_2^r} = \frac{(n_1 - o_1) \bar{K} K_2}{K_2 V + 12} \quad 8.28$$

$$\alpha_{23}^\infty = \frac{S_{23}^r}{\Sigma S_2^r} = \frac{(n_2 - o_2) K_2}{K_2 V + 12} \quad 8.29$$

$$\alpha_{22}^\infty = \frac{S_{22}^r}{\Sigma S_2^r} = \frac{12}{K_2 V + 12} \quad 8.30$$

It may be seen that the real distribution factor for each beam is equal to

$$\frac{\alpha_{22}^\infty}{2}$$

As the wind load increases, eventually a plastic hinge forms at the leeward end of the beam, at some load factor α , where α is less than λ_2 . For this intensity of wind loading, the initial out of balance moment at joint 2 is given by:-

$$F.E.M._2 = -\alpha (mHh)av$$

The bending moments obtained after distribution of the balancing moment are given in Figure 8.9(a).

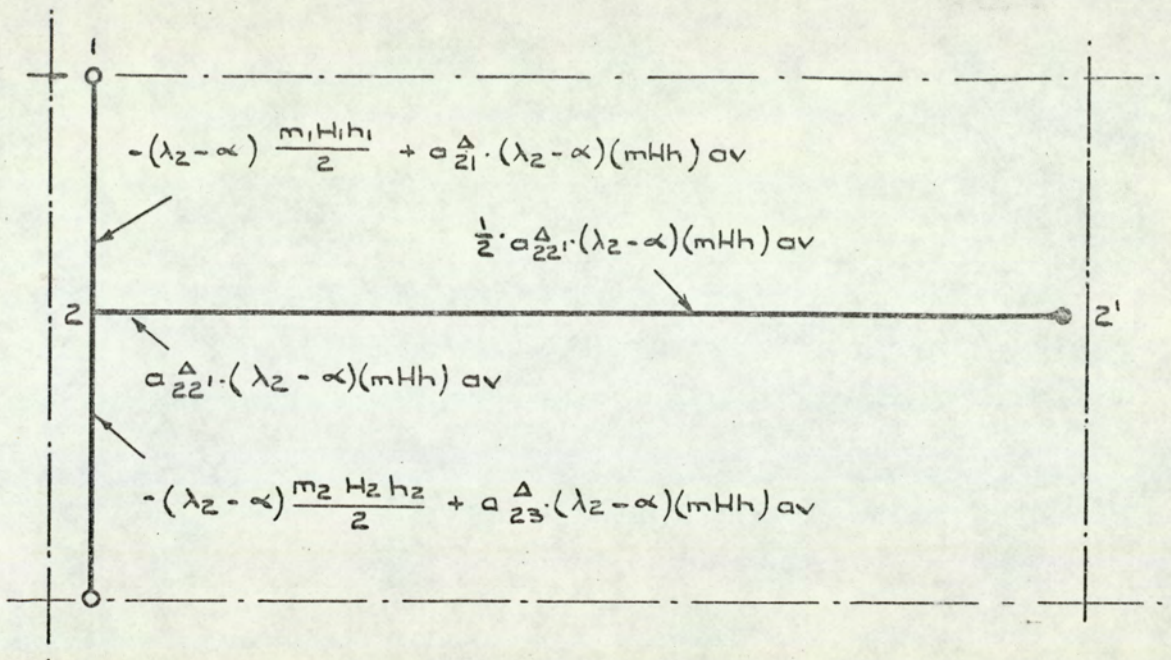


Fig. 8·10.(a) Bending moments due to wind load in the range α to λ_2 - Zone 2 (ii).

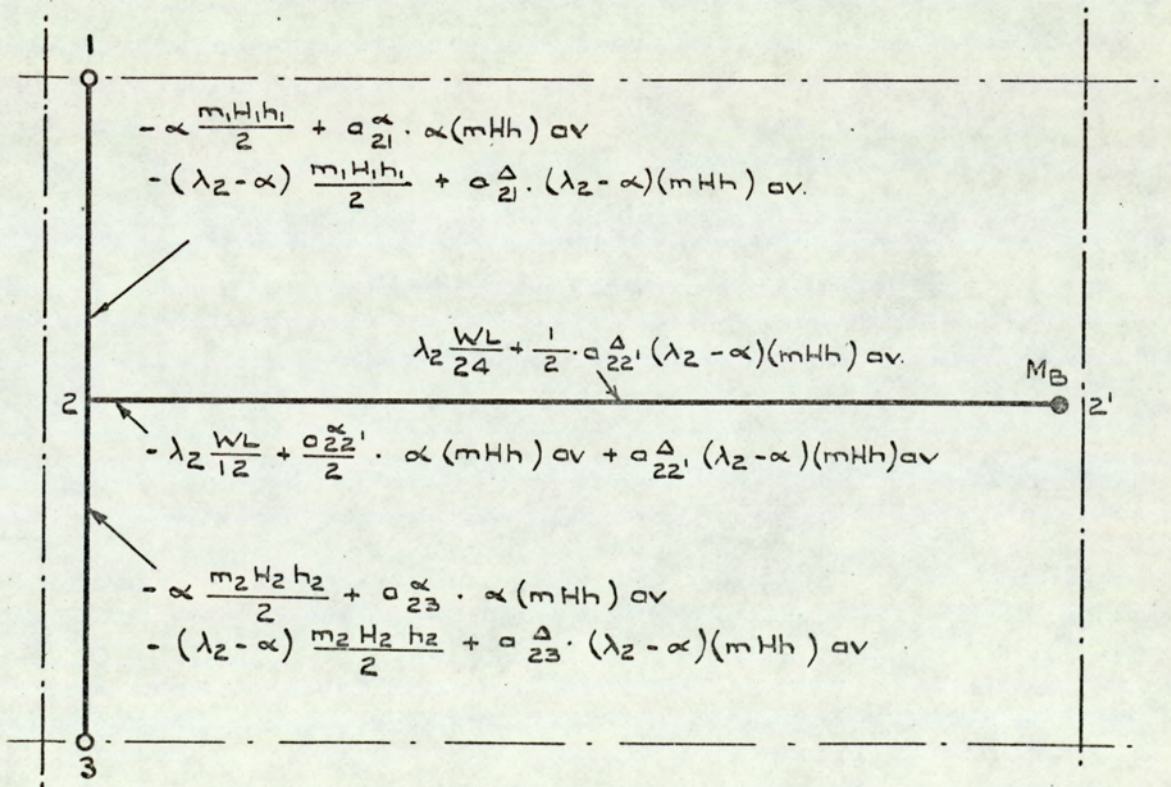


Fig. 8·10.(b) Bending moment at ultimate combined load - Zone 2 (ii).

Figure 8.9(b) shows the bending moments due to the combination of vertical load at load factor λ_2 plus wind load at load factor α . For a plastic hinge to occur at 2' under these loads:-

$$\lambda_2 \frac{WL}{12} + \frac{\alpha_{22}'}{2} \cdot \alpha (mHh)_{av} = M_B \quad 8.31$$

However, from equation 8.12, for Zone II,

$$\lambda_2 \frac{WL}{8} + \lambda_2 \frac{A(mHh)_{av}}{2} - M_e = M_B$$

From equations 8.31 and 8.12, the value of α is given by:-

$$\frac{\alpha}{\lambda_2} = \frac{2A}{\alpha_{22}'} \left[\frac{WL}{24A(mHh)_{av}} + \frac{1}{2} - \frac{M_e}{\lambda_2 A(mHh)_{av}} \right] \quad 8.32$$

In the case of bare steel frames, the above equation reduces to:-

$$\frac{\alpha}{\lambda_2} = \frac{A}{\alpha_{22}'} \left[\frac{1}{2} - \frac{WL}{24 A(mHh)_{av}} \right] \quad 8.33$$

At load factor α , a plastic hinge forms at 2', and the stiffness of the beam at 2 is reduced to $3K_{b2}^e$. Therefore, in the subsequent wind loading, in the range α to λ_2 , the real distribution factors are identical to those used in Zone II(i), namely, α_{21}^Δ , α_{23}^Δ and $\alpha_{22}'^\Delta$. Owing to the additional horizontal loading, the initial sway moment at the joint is given by:-

$$F.E.M._2 = -(\lambda_2 - \alpha) (mHh)_{av}$$

The bending moments produced at the critical locations owing to this loading are given in Figure 8.10(a). Figure 8.10(b) is obtained by superimposing Figures 8.9(b) and 8.10(a), and shows the resulting moments under combined load at λ_2 . Again, in this zone, failure occurs when a plastic hinge forms at the centre of the span. Therefore:-

$$\lambda_2 \frac{WL}{24} + \frac{1}{2} \cdot \alpha_{22}'^\Delta (\lambda_2 - \alpha) (mHh)_{av} = M_e$$

Adding equation 8.31 to the above equation results in:-

$$0.5 (M_e + M_B) = \lambda_2 \frac{WL}{4} \left\{ \frac{1}{4} + \left[\frac{\alpha}{\lambda_2} \cdot \alpha_{22}^{\alpha'} + \left(1 - \frac{\alpha}{\lambda_2}\right) \cdot \alpha_{22}'^\Delta \right] \frac{(mHh)_{av}}{WL} \right\}$$

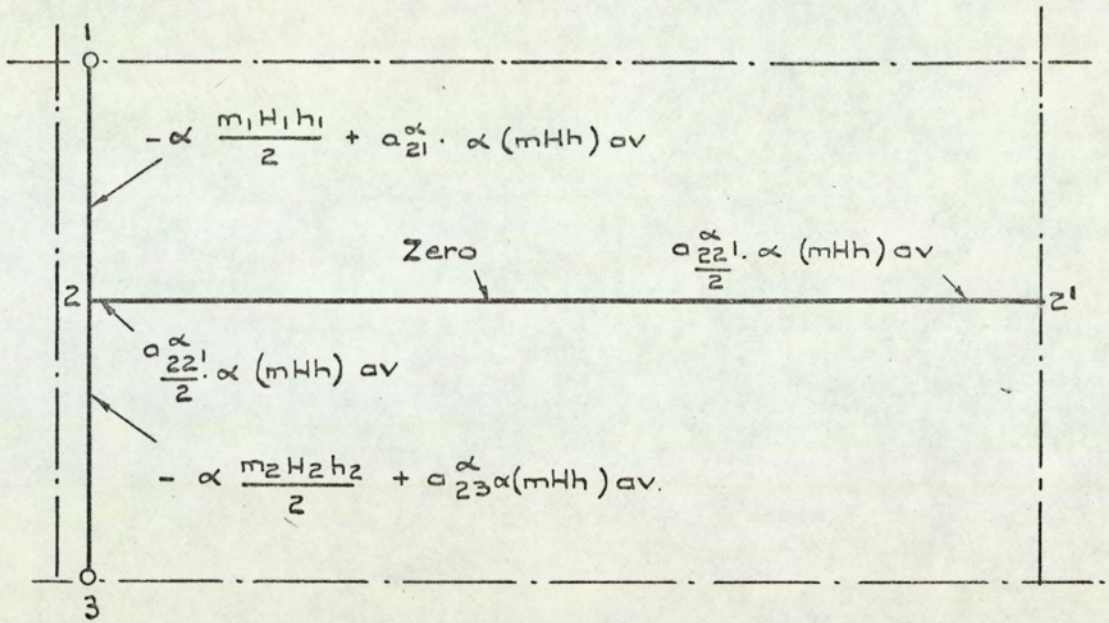


Fig. 8.9. (a) Bending moments due to wind load at load factor α - Zone 2 (ii).

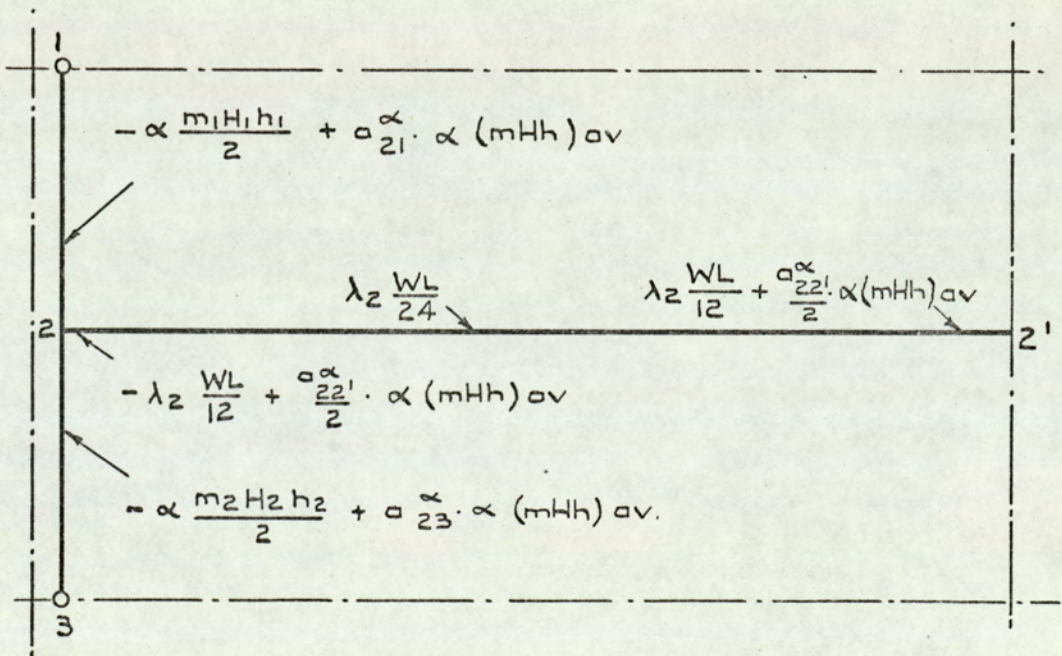


Fig. 8.9. (b) Bending moments due to vertical load at λ_2 plus wind load at α - Zone 2(ii).

$$\text{But } 0.5 (M_e + M_B) = \lambda_2 \frac{WL}{4} \left[\frac{1}{4} + A \cdot \frac{(mHh)_{av}}{WL} \right] \quad 8.12$$

Therefore, composite beam magnification factor for this zone is given by:-

$$A = \frac{\alpha}{\lambda_2} \cdot \alpha_{22}^{\alpha} + \left(1 - \frac{\alpha}{\lambda_2}\right) \cdot \alpha_{22}^{\Delta} \quad 8.34$$

The value of α can be determined using equation 8.32.

For bare steel frames, the beam magnification factor for this zone can be obtained by using the same equation 8.34, but the value of α must be determined using equation 8.33.

Similarly, the resulting moment in the lower column may be written as:-

$$\begin{aligned} M_{23} &= -\frac{m_2 H_2 h_2}{2} \left[\alpha (1 - 2\alpha_{23}^{\alpha} \cdot p_2) + (\lambda_2 - \alpha) (1 - 2\alpha_{23}^{\Delta} \cdot p_2) \right] \\ &= -\lambda_2 \left[\frac{\alpha}{\lambda_2} \cdot (1 - 2\alpha_{23}^{\alpha} \cdot p_2) + \left(1 - \frac{\alpha}{\lambda_2}\right) \cdot (1 - 2\alpha_{23}^{\Delta} \cdot p_2) \right] \cdot \frac{m_2 H_2 h_2}{2} \end{aligned}$$

$$\text{As before } C_I > |M_{23}| = \lambda_2 \cdot A_c \cdot \frac{m_2 H_2 h_2}{2}$$

$$\therefore A_c = \frac{\alpha}{\lambda_2} \cdot (1 - 2\alpha_{23}^{\alpha} \cdot p_2) + \left(1 - \frac{\alpha}{\lambda_2}\right) \cdot (1 - 2\alpha_{23}^{\Delta} \cdot p_2) \quad 8.35$$

8.7.3 ZONE III

$$\frac{M_e}{\lambda_2 WL} \geq \frac{1}{8}$$

In Zone III, the beam is fully elastic under vertical load alone. The expressions for A and A_c are identical to those derived for Zone II(ii), but the value of α , the load factor for horizontal loading at which the first plastic hinge forms, is different.

The bending moments under full vertical load, plus wind load at load factor α , are identical to those shown in Figure 8.9(b), and the condition for the first hinge to form in the beams is again given by equation 8.31,

$$\text{i.e. } \lambda_2 \frac{WL}{12} + \frac{\alpha_{22}^{\alpha}}{2} \cdot \alpha (mHh)_{av} = M_B$$

In this case, however,

$$M_B = \lambda_2 \frac{A(mHh)_{av}}{2}$$

$$\therefore \frac{\alpha}{\lambda_2} = \frac{A}{a_{22}^{\alpha}} \left[1 - \frac{WL}{6A(mHh)_{av}} \right] \quad 8.36$$

This value of α in this zone is the same for composite and bare steel frames.

8.7.4 SUMMARY OF THE MAGNIFICATION FACTORS

A summary of the basic design equations of multi-storey frames with the effect of composite action of types (2) and (3) taken into consideration was given in Section 8.5. It can be seen that these are easily solved if values of the magnification factors A and A_c are known. These factors are summarised below:-

$$\underline{\text{ZONE I}} \quad 0 \leq \frac{A(mHh)_{av}}{WL} \leq \frac{1}{16}$$

$$A = a_{22}^{\Delta} \quad 8.26$$

$$A_c = 1 - 2 a_{23}^{\Delta} \cdot p_2 \quad 8.27$$

$$\underline{\text{ZONE II(i)}} \quad \frac{1}{16} \leq \frac{A(mHh)_{av}}{WL} \leq \left(\frac{2 M_e}{\lambda_2 WL} - \frac{1}{12} \right)$$

The expression for A and A_c are identical to those for Zone I, i.e. equations 8.26 and 8.27.

$$\underline{\text{ZONE II(ii)}} \quad \left(\frac{2 M_e}{\lambda_2 WL} - \frac{1}{12} \right) \leq \frac{A(mHh)_{av}}{WL} \text{ and } \frac{M_e}{\lambda_2 WL} \leq \frac{1}{8}$$

$$A = \frac{\alpha}{\lambda_2} \cdot a_{22}^{\alpha} + \left(1 - \frac{\alpha}{\lambda_2} \right) \cdot a_{22}^{\Delta} \quad 8.34$$

$$A_c = \frac{\alpha}{\lambda_2} \cdot (1 - 2 a_{23}^{\alpha} \cdot p_2) + \left(1 - \frac{\alpha}{\lambda_2} \right) \cdot (1 - 2 a_{23}^{\Delta} \cdot p_2) \quad 8.35$$

$$\frac{\alpha}{\lambda_2} = \frac{2A}{a_{22}^{\alpha}} \left[\frac{WL}{24A(mHh)_{av}} + \frac{1}{2} - \frac{M_e}{\lambda_2 A(mHh)_{av}} \right] \quad 8.32$$

$$\underline{\text{ZONE III}} \quad \frac{M_e}{\lambda_2 WL} \geq \frac{1}{8}$$

The expressions for A and A_c are identical to those for Zone II(ii), i.e. equations 8.34 and 8.35.

$$\frac{\alpha}{\lambda_2} = \frac{A}{a_{22}^{\alpha}} \left[1 - \frac{WL}{6A(mHh)_{av}} \right] \quad 8.36$$

In all three zones,

$$p_2 = \frac{(mHh)_{av}}{m_2 H_2 h_2}$$

$$\alpha_{22'}^{\Delta} = \frac{12}{K_2 V + 12} ; \quad \alpha_{23}^{\alpha} = \frac{(n_2 - o_2) K_2}{K_2 V + 12} ;$$

Also,
$$V = (n_1 - o_1) \bar{K} + (n_2 - o_2)$$

$$\bar{K} = \frac{K_{c1}}{K_{c2}} ; \quad K_2 = \frac{K_{c2}}{K_{b2}^e}$$

Under the simple plastic conditions (i.e. with zero axial forces in the columns), A and A_c are both equal to unity in all zones. This is so since, when $\rho' = 0$, $(n - o) = 0$ and therefore $V = 0$. Thus, $\alpha_{22'}^{\Delta} = \alpha_{22'}^{\alpha} = 1$, and $\alpha_{23}^{\Delta} = \alpha_{23}^{\alpha} = 0$, and all the magnification factors become unity.

As ρ' increases, A and A_c increases in all zones, since $(n - o)$, and therefore V , become negative. This leads to values of $\alpha_{22'}^{\Delta}$ and $\alpha_{22'}^{\alpha}$ greater than unity, and to negative values of α_{23}^{Δ} and α_{23}^{α} .

In addition, it may be seen that the ratio of beam stiffness to column stiffness, K_2 , controls the values of the magnification factors to a large extent. This important observation will be discussed in the following sections, where composite action effects the flexural rigidity of the beam and hence the K_2 value considerably.

8.8 THE EFFECT OF COMPOSITE ACTION ON THE STIFFNESS OF THE BEAMS

When the effect of composite action of type (2) or (3) is introduced into the plastic design of multi-storey frames, its presence between the floor system and the supporting beam over the whole beam span is assumed as shown in Figure 8.11. That is the middle half of the beam, where it is assumed to be in compression, will be composite with the floor system and the second moment of area of the composite section is I_c . The end quarters of the beam are assumed to be in tension, hence no composite action present between the floor system and the beam and the second moment of area of these two quarter spans are of the steel section I_b .

In Zone I, where failure occurs owing to beam mechanism, the bending moment at collapse is as shown in Figure 8.12. Since the plastic composite moment at mid-span M_e is much bigger than the beam plastic moment at supports,

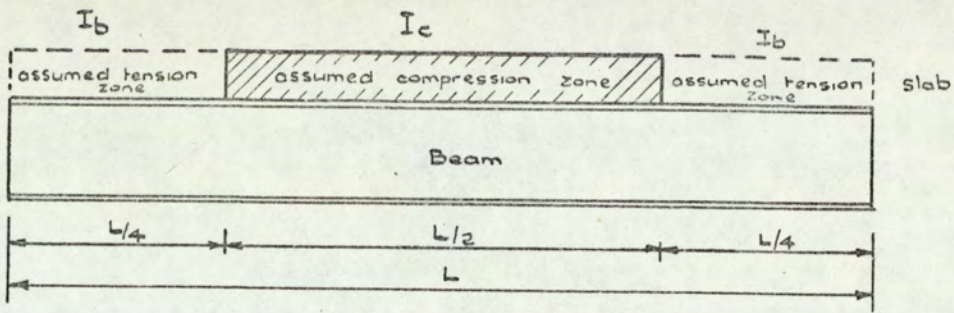


Fig. 8.11. Assumed effect of composite action on the beam span.

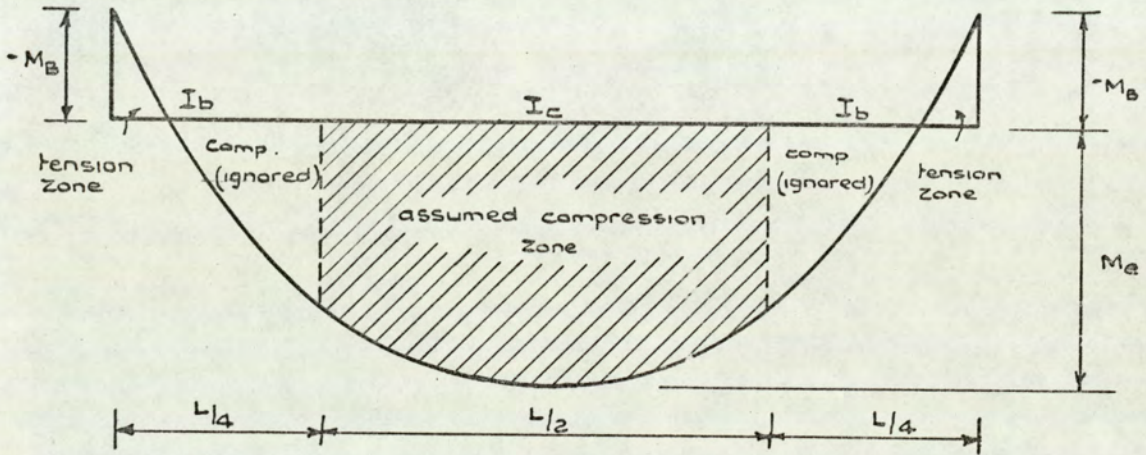


Fig. 8.12. Bending moment diagram. Zone I.

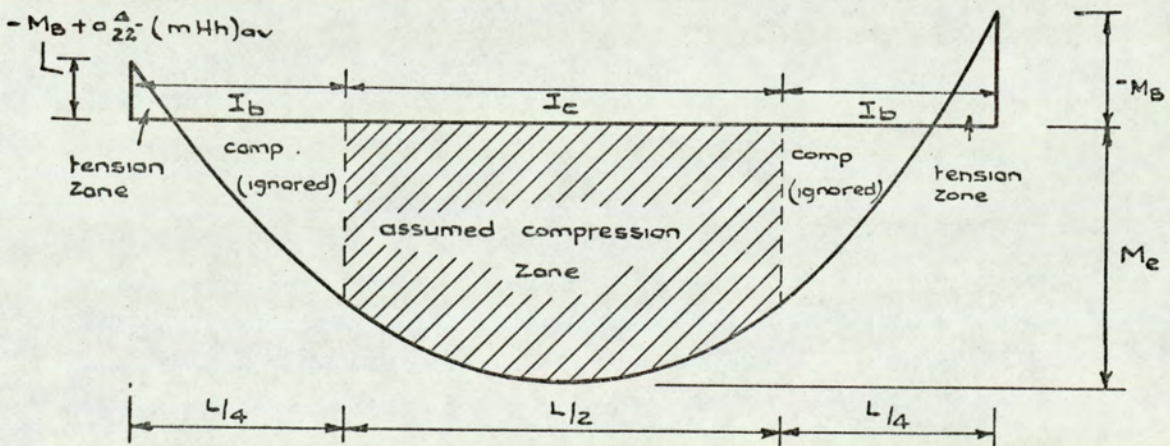


Fig. 8.13. Bending moment diagram Zone II

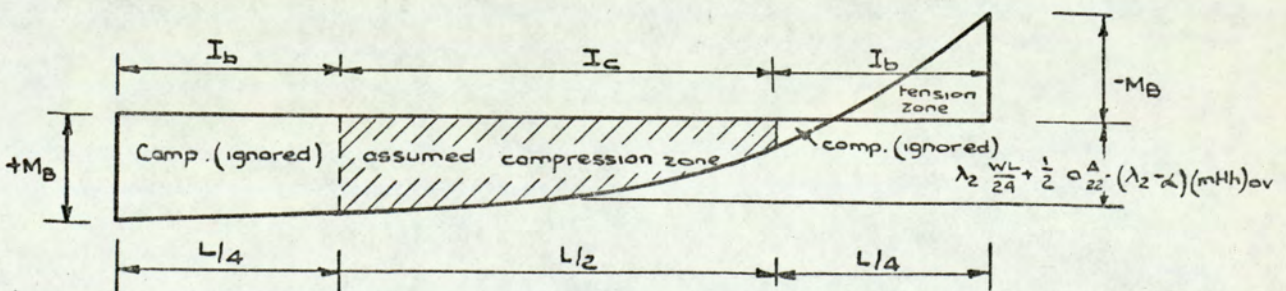


Fig. 8.14. Bending moment diagram. Zone III.

the distance of the point of contraflexure is much less than quarter of the span from the support, as shown in Figure 8.12. Hence, in this zone, the length of the compression part of the beam is more than the half middle span.

In Zone II, where the beam fails owing to combined mechanism, the windward end beam moment is less than M_B (i.e. $-M_P + \alpha_{22} \Delta \cdot (mHh)av$) and that of the mid-span and the leeward end are M_e and M_B respectively. Figure 8.13 shows the bending moment diagram for this zone and from this figure, it can be seen that the length of the composite section in compression is also more than the middle half span.

In Zone III, failure occurs owing to the formation of two plastic hinges at the supports (sway mechanism) with the windward end hinge in compression and the leeward end hinge in tension. The mid-span moment is less than M_e (i.e. $\lambda_2 \frac{WL}{2L} + \frac{1}{2} \alpha_{22} \Delta (\lambda_2 - \alpha)(mHh)av$). Figure 8.14 shows the bending moment diagram for this zone and from this figure, it can be seen that the length of the composite section in compression is more than the middle half span. Hence, it can be concluded that for the three zones, the assumption of Figure 8.11 is reasonable and on the safe side.

For the composite beam of Figure 8.11, representing beams in multi-storey frames under the effect of type (2) or (3) of composite action, where the axial load and the lateral displacement of the beam ends are negligible. Referring to Figure 8.5, the real stiffnesses are:-

$$\frac{M_3}{\theta_3} = S_{32}^r = (F_1 + \frac{F_2}{R_3}) \frac{EI'}{L} \quad 8.37$$

$$\frac{M_2}{\theta_2} = S_{23}^r = (F_1 + F_2 R_3) \frac{EI'}{L} \quad 8.38$$

$$\text{Where } F_1 = \frac{(19\beta + 13)}{(7\beta + 1)} ; F_2 = \frac{(5\beta + 11)}{(7\beta + 1)}$$

$$\beta = \frac{I_c}{I_b} ; I' = \frac{2\beta I_b}{(1 + \beta)} \text{ and } R_3 = \frac{\theta_3}{\theta_2}$$

When composite action is not present (i.e. bare steel frame), then $I_c = I_b$. Therefore,

$$\beta = 1 ; F_1 = 4 ; F_2 = 2 \text{ and } I' = I_b$$

Substituting the above values in equation 8.37,

$$\frac{M_3}{\theta_3} = S_{32}^r = \left(4 + \frac{2}{R_3}\right) \frac{EI_b}{L}$$

which is again equation 8.19 for the real stiffness of typical fully elastic beam.

When composite action of type (2) or (3) is present (Figure 8.11), the stiffness of the beam is greater than that of a beam alone, as will be shown in the following section.

8.8.1 EQUIVALENT UNIFORM BEAM

When the floor system becomes composite with the supporting beams, the second moment of area of the composite section will be much greater than that of the steel section. For example, in section 7.5 for frame 1 at a slab thickness of 5 inches, the beam section selected for the internal bay was a $16 \times 5\frac{1}{2} \times 31$ U.B. The second moment of area of the composite section was 1410.6 in.^4 compared with 374.9 in.^4 of the steel section. This composite beam will be used as an example to calculate the equivalent stiffness of a uniform beam rather than the partial composite section of Figure 8.11 for various end conditions.

8.8.1(a) THE FAR END PINNED

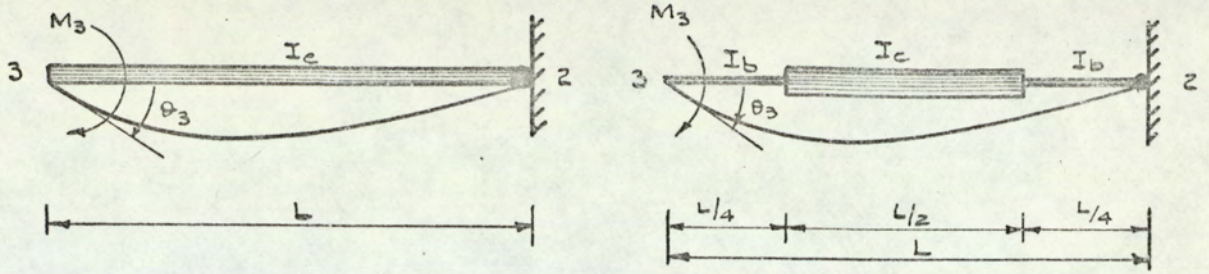
This corresponds to the case when a plastic hinge forms at the leeward end. From equations 8.37 and 8.38, the real stiffness of the partially composite section with the far end pinned, shown in Figure 8.15(a) is given by:-

$$\frac{M_3}{\theta_3} = S_{32}^r = \frac{EI'}{L F_1} (F_1^2 - F_2^2) \quad 8.39$$

Using the second moment of area values of the $16 \times 5\frac{1}{2} \times 31$ U.B. to show the effect of this partially composite beam on the stiffness of the beam when a plastic hinge forms at the leeward end,

$$I_c = 1410.6 \text{ in.}^4 \text{ and } I_b = 374.9 \text{ in.}^4. \text{ Therefore,}$$

$$\beta = 3.76 ; F_1 = 3.09 ; F_2 = 1.09 \text{ and } I' = 1.58 I_b$$



(b) equivalent uniform composite section with the far end pinned. (a) partially composite section with the far end pinned.

Fig. 8.15.

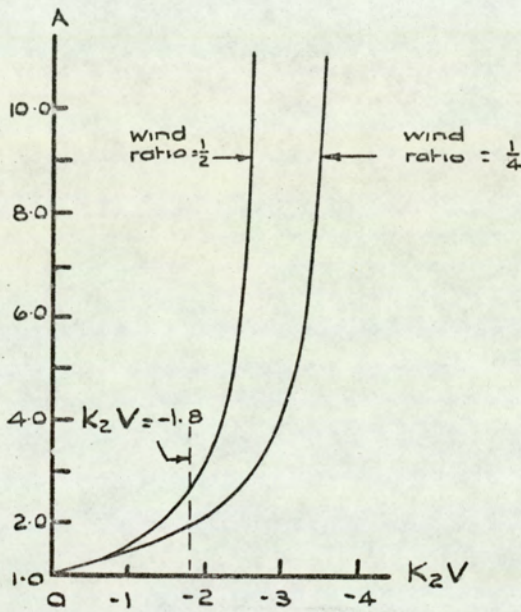


Fig 8.16. Variation of A with $K_2 V$ in Zone II(ii).

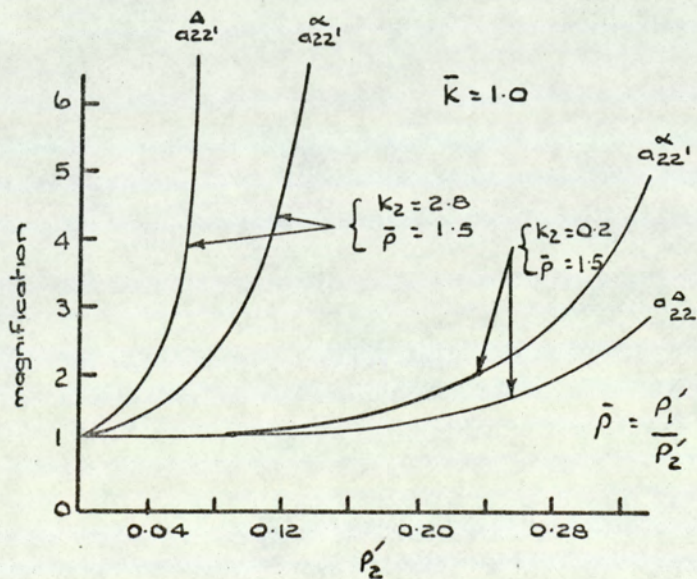


Fig. 8.17. Variation of the magnification with K_2 .

Substituting the above values in equation 8.39, the stiffness of the beam

$$S_{32}^r = 4.28 \frac{E I_b}{L}$$

If the composite beam is uniform, then the stiffness becomes $\frac{3 E I_c}{L}$. The stiffness of the partially composite beam will be equivalent to that of a uniform section (Figure 8.15(b)) if:-

$$4.28 \frac{E I_b}{L} = \frac{3 E I_e}{L}$$

$$\therefore I_e = 1.43 I_b$$

where I_e is the equivalent second moment of the area of uniform section.

Hence, the flexural rigidity of the partially composite section, treated as an equivalent uniform section, K_b^e is 43% greater than that of the steel section K_b .

The increase in the flexural rigidity of the steel section owing to the presence of type (2) or (3) of composite action will effect the values of the real plastic distribution factors α_{21}^Δ , α_{23}^Δ and α_{22}^Δ of equations 8.23, 8.24 and 8.25. As the values of \bar{K} and V are independent of the beam flexural rigidity, it is only the value of K_2 that will be effected, $K_2 = \frac{K_{c2}}{K_{b2}^e}$, and this in turn effects the values of the plastic distribution factors. The value of K_{b2}^e will be replaced by $1.43 K_{b2}$. This value will vary from one section to another. Also it is dependent upon the value of the slab thickness.

8.8.1(b) THE BEAM IS FULLY ELASTIC UNDER THE FACTORED VERTICAL LOAD λ_2

Using the assumptions of section 8.6, that for a typical internal bay the beam will bend in exact double curvature under the action of horizontal loading. The end rotations of the beam will be equal, so R is equal to unity. Substituting this value of R into equation 8.37, the stiffness of the $16 \times 5\frac{1}{2} \times 31$ U.B. plus 5" slab thickness, elastic composite section $S_{32}^r = 6.61 \frac{E I_b}{L}$. If the composite section is uniform, this stiffness becomes $\frac{6 E I_c}{L}$. The stiffness of the partially composite beam will be

equivalent to that of a uniform section if:-

$$6.61 \frac{E I_b}{L} = \frac{6 E I_e}{L}$$

$$\therefore I_e = 1.1 I_b$$

Hence, the flexural rigidity of the partially composite section, which is completely elastic under the factored vertical load λ_2 and treated as an equivalent uniform section, K_b^e is 10% greater than that of the steel section K_b . Again, the value of $K_2 = \frac{K_{c2}}{K_{b2}^e}$ will be replaced by $K_2 = \frac{K_{c2}}{1.1 K_{b2}}$ which in turn effects the values of the real distribution factors for the case when the beam is fully elastic α_{21}^∞ , α_{23}^∞ and $\alpha_{22}'^\infty$ of equations 8.28, 8.29 and 8.30.

8.9 THE EFFECT OF THE BEAM STIFFNESS ON THE MAGNIFICATION FACTOR

The magnification factors are basically functions of the same variables and themselves vary in a similar manner. For example, Figure 8.16 shows the variation of the magnification factor A with K_2V for two values of wind ratio where K_2V is a function of relative beam and column stiffness and column axial load. The figure indicates that at zero axial load A is unity, i.e. that there is no magnification of simple plastic theory moments, as A is defined originally as the degree by which the bending moments are magnified owing to the instability effects. A increases as K_2V reduces, i.e. becomes negative when $\rho' > 0$, so that as the axial load increases, A increases. The bending moments are therefore greater than those assumed in the simple plastic design. Any frame which is designed assuming $A = 1$, whilst carrying these axial loads, is unlikely to attain the required load factor. Under very heavy axial loads, $A \rightarrow \infty$ at some limiting value of K_2V , as shown in Figure 8.16. This infinite value of A occurs when the total joint stiffness is zero.

The design method contains many approximations, and although all of these are considered to be justifiable, it is clearly inadvisable to permit high values of the magnification factors. Any such value indicates that

the frame is very close to the point of instability.

In order to control the instability effects, for design purposes, an arbitrarily fixed limit of - 1.80 has been imposed ⁽³⁷⁾ on the value of K_2V . If, during the design of a particular storey of a bare steel frame, K_2V is found to be less than - 1.80, its value must be increased by suitable alteration to the selected sections. This is considered below:-

For bare steel frames, $K_b^e = K_b$. Expanding K_2V

$$\begin{aligned} K_2V &= \frac{K_{c2}}{K_{b2}} [(n_1 - o_1) \bar{K} + (n_2 - o_2)] \\ &= \frac{I_{c2}}{I_{b2}} \cdot \frac{L}{h_2} [(n_1 - o_1) \frac{I_{c1}}{I_{c2}} \cdot \frac{h_2}{h_1} + (n_2 - o_2)] \end{aligned}$$

Now, by inspection of the stability functions, $(n - o)$ is approximately proportional to ρ' , the Euler ratio. Also, ρ' is inversely proportional to the second moment of area of the column. Therefore, approximately,

$$(n_1 - o_1) \propto \rho'_1 \propto \frac{1}{I_{c1}}$$

and, $(n_2 - o_2) \propto \rho'_2 \propto \frac{1}{I_{c2}}$

Alternatively, $(n_1 - o_1) = \frac{a_1}{I_{c1}}$ and $(n_2 - o_2) = \frac{a_2}{I_{c2}}$

where a_1 and a_2 are constants. Therefore K_2V may be written as follows:-

$$\begin{aligned} K_2V &= \frac{I_{c2}}{I_{b2}} \cdot \frac{L}{h_2} \left[\frac{a_1}{I_{c1}} \cdot \frac{I_{c1}}{I_{c2}} \cdot \frac{h_2}{h_1} + \frac{a_2}{I_{c2}} \right] \\ &= \frac{1}{I_{b2}} \cdot \frac{L}{h_2} [a_1 \cdot \frac{h_2}{h_1} + a_2] \end{aligned}$$

All the terms, apart from I_{b2} , are constants, so that:-

$$K_2V \propto \frac{1}{I_{b2}}$$

Thus, any alteration in the column size has a negligible effect on the magnitude of K_2V , which is basically a function of I_{b2} . Figure 8.17 shows that with high K_2 (relatively weak beam), the magnification increases rapidly with ρ'_2 giving instability, whereas for low values of K_2 (relatively strong beam), stability is greatly improved. Hence, it is the beam size, and not

the column size, that controls the instability effects. Therefore, for the case of bare steel frames, in order to increase K_2V above the limiting value of -1.80 , it is simply necessary to select a new beam with a larger second moment of area.

When composite action of type (2) or (3) is introduced into the plastic design of bare steel frames, then $K_2V \propto \frac{1}{I_{e2}}$, where I_{e2} is the equivalent second moment of area of a uniform composite section. It has been shown in the previous section that when the composite section $16 \times 5\frac{1}{2} \times 31$ U.B., plus 5" slab thickness is considered, its equivalent second moment of area I_{e2} is increased by 43% relative to that of the steel section when a plastic hinge is assumed to form at the leeward end, and by 10% when the beam is fully elastic. Hence, with the introduction of these greater values of the equivalent second moments of area, a larger section might not necessarily be required to reduce the K_2V term to its limiting value of -1.80 . The K_2V value effects the values of the distribution factors of the beams and the columns considerably. Hence, with the introduction of composite action, the stability of the frame as a whole will improve considerably.

Tabulated values of the magnification factor were produced by Gandhi⁽⁴⁾ for the design of multi-storey frames by hand computation. With the introduction of composite action into his design method, it is still possible to use hand computation by using tables similar to Table 5(i) to find steel sections with adequate $(M_e + M_B)$ plastic composite moment. For type (3) of composite action, the use of a computer becomes a necessity in the design of multi-storey frames for the reasons given in section 5.9.

It had already been shown in the previous chapter that considerable saving in the weight of the beams occurs by using type (2) or (3) of composite action rather than type (1), which ignores composite action altogether. Now with the introduction of either of these two types of composite action into the design of bare steel frames, even more saving in the weight of the

frame will be made. Hence, it can be concluded that composite action of the simplest form of type (2) or (3), when introduced to the plastic design of multi-storey frames, even with the conservative assumption of its effectiveness on the beam span, improves the stability of the frame greatly. It also results in considerable saving in the weight of the frame as a whole.

In the next chapter, a detailed account of the testing program for the experimental part of this work will be given.

DESCRIPTION OF EXPERIMENTAL WORK9.1 INTRODUCTION

It is essential to test the validity of design methods and assumptions as extensively as possible. Assumptions (3), (4) and (5) on degree of composite action compare favourably with type (2), as was shown in Chapter 7, which corresponds to the design method proposed by Steel⁽¹⁾. There is, however, the need to test the method by taking practical designs in order to check which of the assumptions on degree of composite action is more valid. The ideal situation would be to design several full size composite multi-storey frames and test them under experimental conditions until failure occurs. This, of course, was impossible because of the sheer size of the problem. It was therefore necessary to reduce the size and consider the design of model structures. Since it is considered that the behaviour of models can safely be used to predict the behaviour of full-scale tests.

To investigate the experimental behaviour and to evaluate the validity of the assumptions made in developing the theory of composite beam and slab floor systems, described in Chapters 4, 5 and 6, three large scale models, together with two slab strips, were built and tested to destruction.

The first test referred to as test M_1 , for collapse of the slab and the main "edge" beams, represents failure of a typical bay, owing to vertical loading. This corresponds to zone I failure in the design of multi-storey frames. The second test referred to as test M_2 , also for collapse of the slab and the main "edge" beams, represents failure, owing to combined mechanism, which corresponds to zone II in the design of multi-storey frames. Test M_3 is a control test to find the experimental values of the plastic composite moments at mid-span and supports which would occur in tests M_1 and M_2 . Tests of two slab strips, referred to as S_1 and S_2 , was another control test to find the value of the ultimate slab moment applicable to tests M_1 and M_2 . To simulate uniform load, it proved possible to use a

system of interconnected hydraulic jacks for the tests on models M_1 and M_2 .

Details of the gauging of each test are given, including the type of gauge used and the positioning of the gauges.

9.2 MATERIALS FOR MODELS

All the various materials required for the models were ordered in one delivery, in order to minimise the fluctuations in properties of these materials.

9.2.1 CEMENT

Ordinary Portland cement produced by the Blue Circle Group was used in all test specimens.

9.2.2 AGGREGATES

Zone III sand and $3/8$ in. crushed gravel supplied by the Midland Gravel Co. Ltd. from pits in the Birmingham Area was used in all the specimens. Sieve Analyses of both the sand and the crushed gravel are presented in Tables 9(i) and 9(ii) respectively.

9.2.3 CONCRETE MIXES

Trial mixes were used to produce a concrete mix with a 14 day cube strength of about 6,000 lbs./sq.in. The aggregates were completely dried before weighing. The dry weight proportions of cement, sand and crushed gravel and the water/cement ratio used in all tests were 1 : 2 : 4 and 0.5 respectively.

9.2.4 CONCRETE CONTROL SPECIMENS

With each mixing a set of concrete control specimens was cast. This set of control specimens consisted of:-

- (a) six 6 in. cubes
- (b) two 12 in. x 6 in. cylinders

Compressive strengths were determined by testing the 6 in. cubes and averaging the six results.

The elastic modulus of the concrete (E_c) was determined by testing the

Sieve Size or No.	%
Retained 3/16 in.	7.37
Retained 7	18.19
Retained 14	11.15
Retained 25	10.99
Retained 52	33.72
Retained 100	14.69
Passing 100	3.85

Table 9(i). Sieve analysis of Zone III sand

Sieve Size	%
Retained 1/2 in.	0
Retained 3/8 in.	7.59
Retained 1/4 in.	74.61
Retained 3/16 in.	12.17
Retained 1/8 in.	4.16
Passing 1/8 in.	1.44

Table 9(ii). Sieve analysis of 3/8 in. crushed gravel

Young's Modulus lbs/in ²	yield stress f_t lbs/in ²	yield strain (Micro strains)
31.6×10^6	52740	1670

Table 9(iii). Steel properties - 3/8 in. diameter mild steel

Young's Modulus lbs/in ²	yield stress f_y lbs/in ²	yield strain (Micro strains)
35.4×10^6	42470	1200

Table 9(iv). Steel properties - 3" x 1 1/2" x 4 lbs./ft. R.S.J.

12 in. x 6 in. cylinders. The cylinders were capped with a cement paste after casting. Strains were measured by two diametrically opposed Tinsley electrical resistance wire gauges type 7A. Readings from these gauges were recorded on a Peekel B103U strain recorder. E_c values were found to be almost constant in all tests at a value of 4.2×10^6 lbs./sq.in. A typical stress-strain curve for the concrete is shown in Figure 9.1.

The control tests were carried out in compliance with the instructions set out in B.S. 1881 (77) for the testing of concrete. Loading was applied by means of a 120 ton capacity Denison compression testing machine.

9.2.5 SLAB REINFORCEMENT

Slab reinforcement mesh was made up of $3/8$ in. mild steel reinforcing bars supplied by G.K.N. Tensile test results on specimens supplied by the manufacturers indicated that elastic and plastic characteristics were favourable to the requirements of the investigation. A fairly sharp yield point and little strain hardening during yield were the principle properties influencing its choice. All the $3/8$ in. mild steel reinforcing bars were supplied in twenty foot lengths cut from the same reel. Twenty tensile tests were carried out on random samples of the steel in a Denison Universal Testing Machine. Stress-strain plots were obtained using a Baldwin automatic strain recorder. The relative mechanical properties such as Youngs Modulus, yield stress and yield strain were found to be consistent enough to enable an averaging of results to be carried out. These are summarised in Table 9(iii). A typical stress-strain curve for the $3/8$ in. mild steel bars is shown in Figure 9.2.

9.2.6 SUPPORTING BEAMS

To keep the size and the collapse load of the model frames within acceptable limits, the main "edge" and secondary beams were chosen as the smallest rolled steel joist section available, namely, a 3 in. x $1\frac{1}{2}$ in. x 4 lbs./ft. run R.S.J.

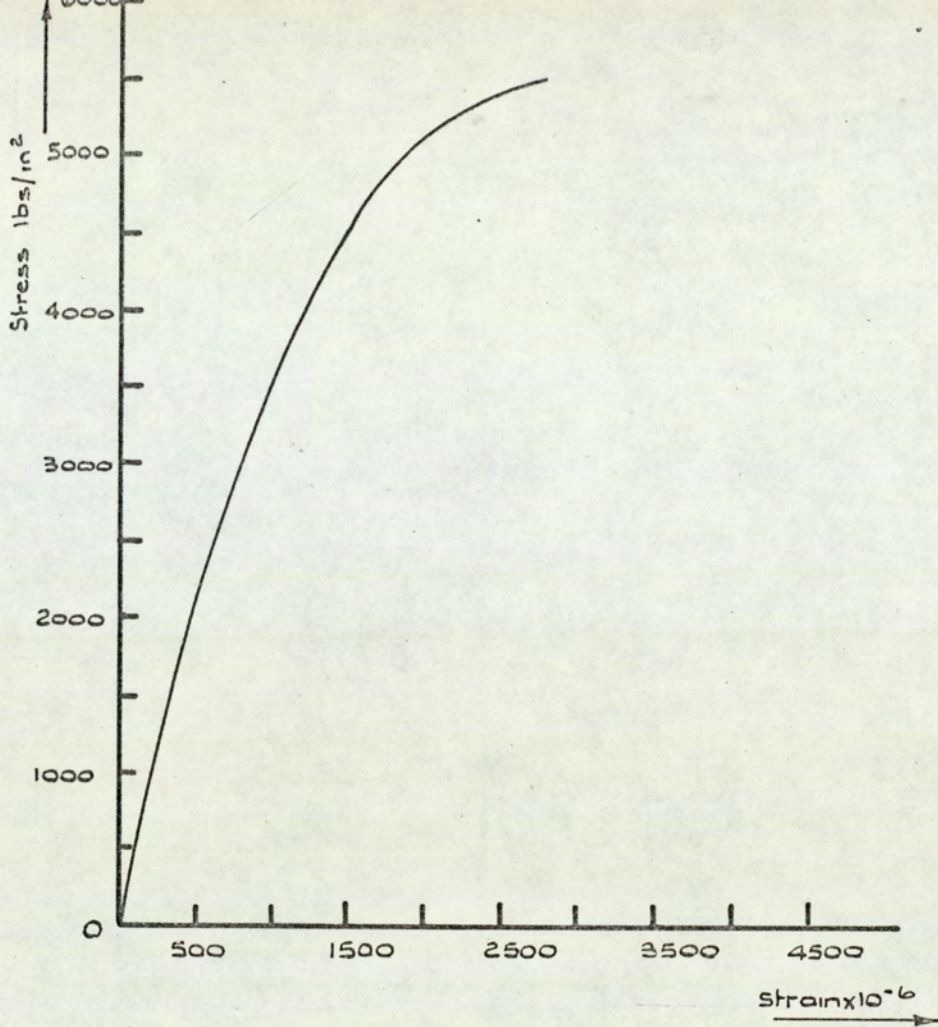


Fig. 9.1 Typical stress/strain curve for the concrete used in the testing program.

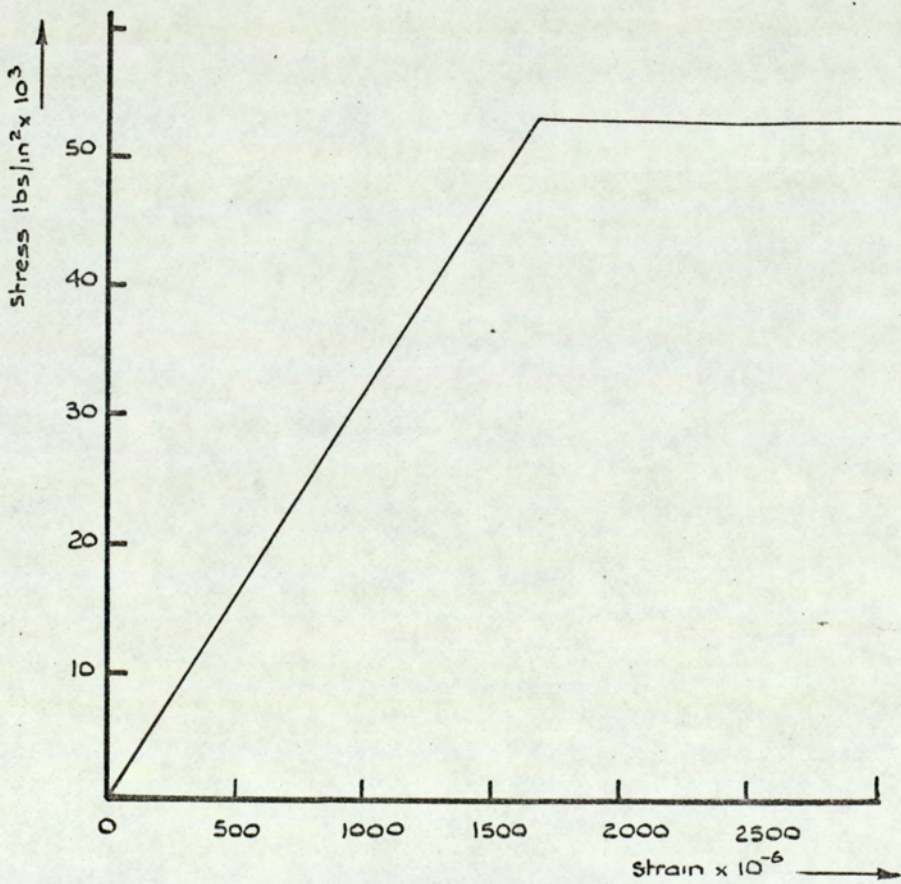


Fig. 9.2. $\frac{3}{8}$ in. mild steel reinforcement stress-strain curve.

Seven bending tests were carried out on random samples of the 3 in. x 1½ in. x 4 lbs./ft. R.S.J. These were loaded through two points 24 in. apart to provide a region of constant bending moment over which strains and deflections could be measured. On each sample two electrical strain gauges were fixed to the upper and lower flanges of the R.S.J. at mid-span. The type of gauge and the strain measurement technique used are identical to those described in section 9.9.1(i). The central deflection of the samples was measured by means of a 2 in. travel Mercer dial gauge reading to an accuracy of 0.001 in. per division. The test set up is shown in detail in Plate 2. The various mechanical properties such as Youngs Modulus, yield stress and yield strain were found consistent enough to enable an averaging of the results to be carried out. These are summarised in Table 9(iv). A typical load-deflection and load-strain graph for the 3 in. x 1½ in. x 4 lbs./ft. R.S.J. tested in bending under two point loading is given in Figure 9.3.

Tensile tests on random samples of the flange of the 3 in. x 1½ in. x 4 lbs./ft. R.S.J., machined in compliance with the instructions set out in B.S. 18⁽⁷⁸⁾ for tensile testing of metals, were carried out in the Denison Universal Testing Machine. From these tests it was found that this joist exhibited some strain hardening properties.

9.3 TEST M₁

This test of a model taken to destruction for collapse by mode B (Figure 4.8) represents failure of a typical bay, owing to vertical loading alone, which corresponds to zone I failure in the design of multi-storey frames.

In order to keep the size of the model and failure load within acceptable limits, several slab sizes were investigated and finally a 9'-0" by 5'-0" slab was decided upon with a slab thickness of 2½ inches. The supporting beams were set out to form a rectangle of 7'-0" by 4'-0" (L x l). The model, thus comprised of two main "edge" beams 7' long and two secondary beams 4' long with a 9' x 5' and 2½" thick slab cast over the top of the

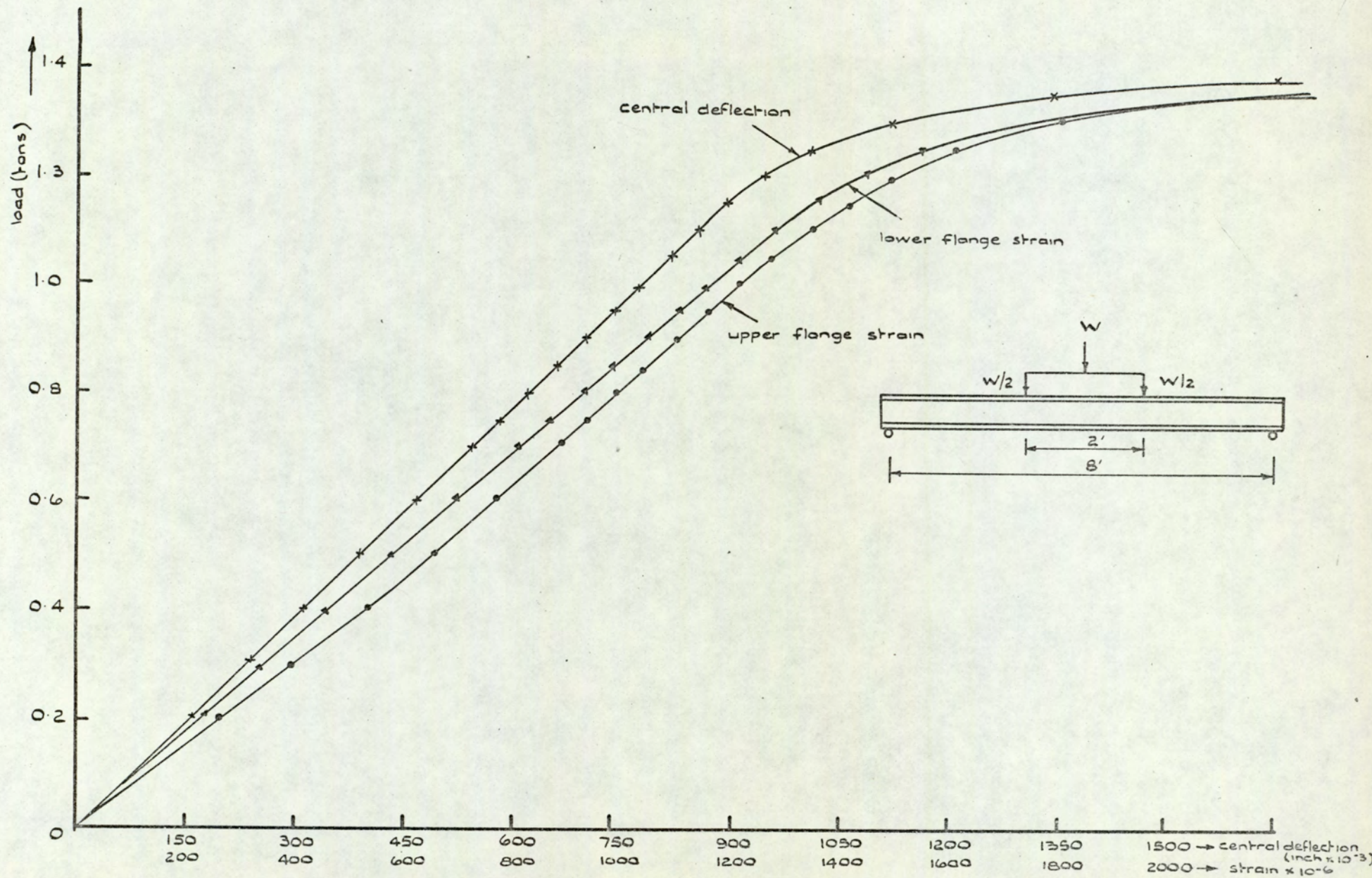


Fig. 9.3. Load against deflection and load against strain graph for $3'' \times 1\frac{1}{2}'' \times 4$ lbs/ft R.S.J.

beams which was continuous over the secondary beams as shown in Figures 9.4 and 9.5. Continuity of the slab over the secondary beams was produced by means of four lever arms connected to each of the secondary beams and fixed at their ends through proving rings to the test rig. This prevented the secondary beams from rotating by applying vertical loads to the lever arms, as shown in Figures 9.4 and 9.5. A detailed description of these lever arms will be given in section 9.7.

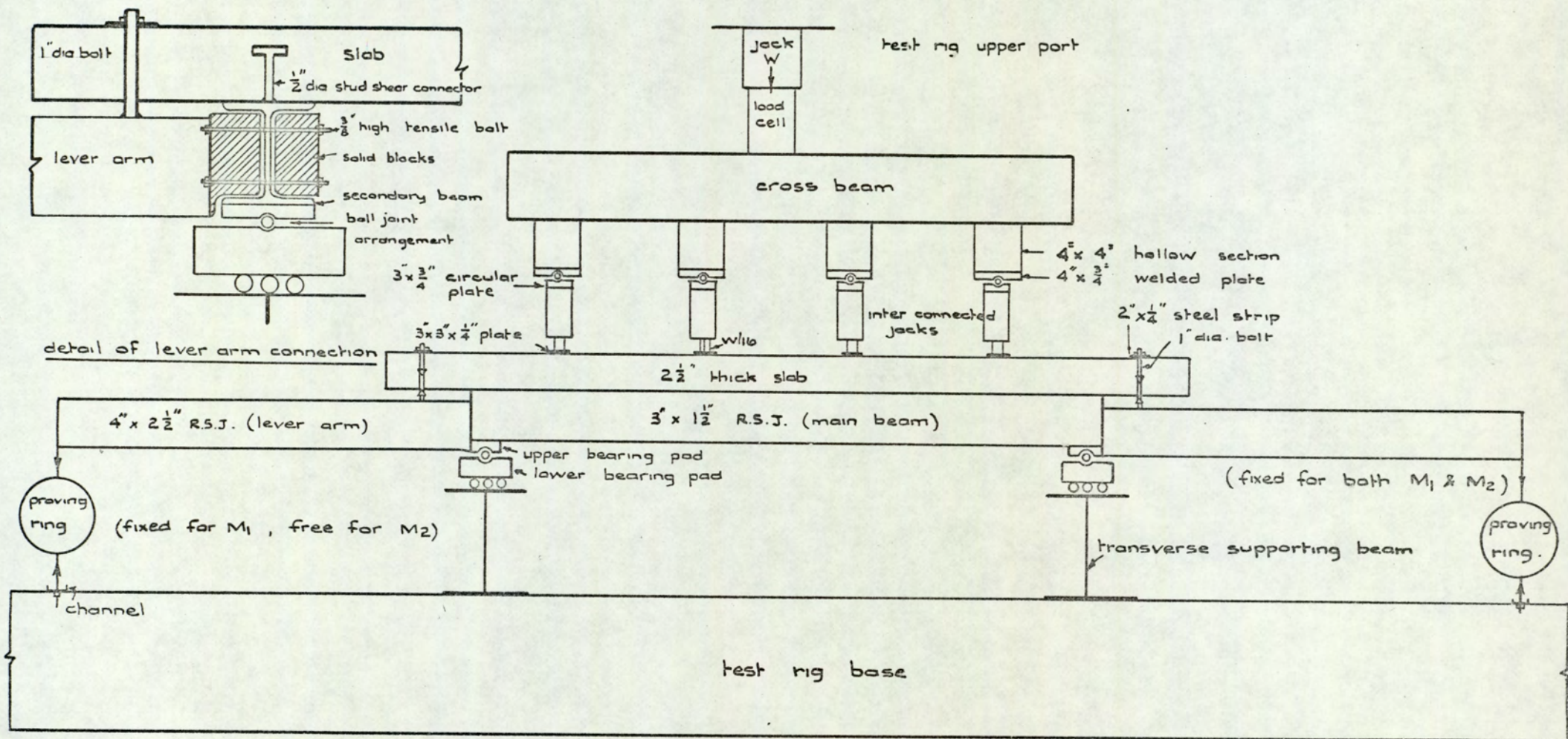
The load applied to the model simulated a uniformly distributed load and was produced by a system of interconnected hydraulic jacks, details of which are given in section 9.7.

Composite action between the slab and the supporting beams was made by means of 2 in. long and 1/2 in. diameter stud shear connectors. The design of these connectors for the M_1 model are shown in section 9.5.

The model was designed for type (5) assumption on degree of composite action, which assumes full composite at mid-spans and supports of the main "edge" beams. Although the model was designed for this assumption, theoretical values of its collapse load for the other four assumptions on degree of composite action were carried out as well as that for type (5). These theoretical collapse loads were compared with the actual collapse load to see which of the five assumptions on degree of composite action most closely represents the observed experimental behaviour of the model.

For collapse of the main "edge" beams and the slab (mode B, Figure 4.8) to occur, the other two possible modes of collapse of the secondary beams and the slab (mode A, Figure 4.8) and independent slab collapse (mode C, Figure 4.8) must be prevented for the various assumptions on degree of composite action. This was achieved by suitable selection of values for the sides ratio $\rho \left(\frac{b}{l}\right)$ and the bending strength of the slab.

Limits of the critical strength ratios of this system for collapse by mode B can be found by using charts similar to Figures 4.12, 5.6 and 6.3,



section 1-1 of figure 9.4

Fig. 9.5. Tests M_1 and M_2 set up.

for an internal bay, for the various assumptions on degree of composite action. Several ultimate slab moments and hence areas of slab reinforcement were tried and finally a mesh of $3/8$ in. diameter mild steel bars was used at 4 in. centres for the bottom layer in the longitudinal direction. Using this area of slab reinforcement, the condition of equation 5.33 for an under reinforced section was still satisfied (i.e. $0.331 \text{ in.}^2/\text{ft. run}$). The slab was considered isotropic, i.e. the hogging and sagging ultimate moments were the same. The hogging slab reinforcement at the supports of the main "edge" beams was provided by hooking up the bottom slab reinforcement at the end of the slab, as shown in Figure 9.10. The 12 in. overhang of the slab from the main "edge" beams supports shown in Figures 9.4 and 9.5 was provided to ensure adequate bond for the hogging slab reinforcement as well as to strengthen the model against collapse by mode A. The top layer of mesh also consisted of $3/8$ in. mild steel bars in the transverse direction. Because of the lower effective depth of the top layer of steel, which lay directly on top of the bottom layer, and to keep the slab isotropic, it was necessary to reduce the spacing of the bars from 4 in. to 3 in. centres (i.e. $0.442 \text{ in.}^2/\text{ft. run}$). Under laboratory conditions, it was possible to use a $3/8$ in. concrete cover for both the bottom layer and the hogging slab reinforcement.

The ultimate moment/ft. run M_s can be determined from:-

$$M_s = A_t \cdot t_y \left[d_1 - \frac{A_t \cdot t_y}{24 \cdot U_c} \right] \quad 9.1$$

The actual cube strength obtained by test (U_w) was equal to 6820 lbs./sq.in.

To find the theoretical ultimate slab moment M_s , the following values are substituted into equation 9.1,

$$A_t = 0.331 \text{ sq.in.}; \quad t_y = 52740 \text{ lbs./sq.in.}; \quad d_1 = 1.94 \text{ in.}$$

$$U_c = 2/3 \times 6820 = 4540 \text{ lbs./sq.in. (for experimental work}$$

$$U_c = 2/3 U_w)$$

Therefore, $M_s = \underline{31,000 \text{ lbs.in./ft.run}}$ or $\underline{2.586 \text{ kips - ft./ft. run}}$

In the following sections, the theoretical collapse load of model M_1 by mode B under U.D.L. will be calculated for each of the five assumptions on degree of composite action.

9.3.1 COLLAPSE LOAD FOR TYPE (1) ASSUMPTION

From section 4.5.2, the collapse load of model M_1 by mode B can be obtained from equation 4.37,

$$\text{i.e.} \quad p\ell L = \frac{16 M_s \ell}{L} + \frac{32 M_B}{L} \quad 9.2$$

From the bending tests on the 3 in. \times 1 $\frac{1}{2}$ in. \times 4 lbs./ft. run R.S.J., the average plastic moment value of the joist equals 55,690 lbs.in. or 4.64 kips - ft.

$$\text{Therefore,} \quad p\ell L = \frac{16 \times 2.586 \times 4}{7} + \frac{32 \times 4.64}{7} \text{ kips}$$

or collapse load by mode B for type (1) assumption = 20.02 tons

9.3.2 COLLAPSE LOAD FOR TYPE (2) ASSUMPTION

From section 5.5, the collapse load of model M_1 by mode B for type (2) assumption on degree of composite action can be obtained from equation 5.45,

$$\text{i.e.} \quad p\ell L = \frac{16 (M_e + M_B)}{L} + \frac{8 M_s \ell}{L} \quad 9.3$$

The plastic composite moment at mid-span M_e for type (2) assumption can be calculated from equations 5.2 and 5.3, assuming the plastic neutral axis lies within the slab,

$$\text{i.e.} \quad d_n = \frac{A_s \cdot f_y}{b \cdot U_c} \quad 9.4$$

$$\text{and} \quad M_e = A_s \cdot f_y \left[\frac{d}{2} + t - \frac{d_n}{2} \right] \quad 9.5$$

Substituting into equations 9.4 and 9.5 the following values,

$A_s = 1.18 \text{ sq.in.}; f_y = 42,470 \text{ lbs./sq.in.}; b = 30 \text{ in. (half the slab width)}$

$U_c = 4540 \text{ lbs./sq.in.}; d = 3 \text{ in.}; t = 2\frac{1}{2} \text{ in.}$

\therefore $M_e = 191,250 \text{ lbs.in.}$ or 15.94 kips - ft.

Substituting the values 15.94 kips - ft. , 4.64 kips - ft. and 2.586 kips -

ft./ft. run for M_e , M_B and M_s respectively into equation 9.3, then:-

the collapse by mode B for type (2) assumption = 26.27 tons

9.3.3 COLLAPSE LOAD FOR TYPE (3) ASSUMPTION

The equation for the collapse load of model M_1 by mode B for type (3) assumption on degree of composite action is the same as that for type (2) assumption, i.e. equation 9.3. It is only the value of M_e which will be different from that of type (2) assumption, as in this case the effect of the slab reinforcement will be included.

To calculate the value of M_e , assuming the plastic neutral axis within the slab, equations 5.13 and 5.14 are used,

$$\text{i.e.} \quad d_n = \frac{A_s \cdot f_y + b \cdot A_t \cdot t_y}{b \cdot U_c} \quad 9.6$$

$$\text{and} \quad M_e = A_s \cdot f_y \left[\frac{d}{2} + t - \frac{d_n}{2} \right] + b \cdot A_t \cdot t_y \left[t - \frac{d_n}{2} - c \right] \quad 9.7$$

Substituting into equations 9.6 and 9.7 the following values,

$$A_s = 1.18 \text{ sq.in.}; \quad f_y = 42,470 \text{ lbs./sq.in.}; \quad b = 30 \text{ in.}$$

$$U_c = 4540 \text{ lbs./sq.in.}; \quad d = 3 \text{ in.}; \quad t = 2\frac{1}{2} \text{ in.}$$

$$A_t = 0.331 \text{ in.}^2/\text{ft.run}; \quad t_y = 52,740 \text{ lbs./sq.in.}; \quad c = 0.56 \text{ in.}$$

Therefore, $M_e = 252,560 \text{ lbs.in.}$ or 21.06 kips - ft.

On substitution into equation 9.3,

$$p\ell L = \frac{16(21.06 + 4.64)}{7} + \frac{8 \times 2.586 \times 4}{7} \text{ kips}$$

or collapse load by mode B for type (3) assumption = 31.50 tons

9.3.4 COLLAPSE LOAD FOR TYPE (4) ASSUMPTION

The collapse load of model M_1 by mode B for type (4) assumption on degree of composite action can be obtained from equation 6.28,

$$\text{i.e.} \quad p\ell L = \frac{16 (M_e + M_N)}{L} \quad 9.8$$

The hogging plastic composite moment at the supports of the main "edge" beam M_N can be calculated from equations 6.7 and 6.8, assuming the plastic neutral axis lies within the flange of the joist,

$$\text{i.e.} \quad d_n' = t + \frac{A_s - b \cdot A_t \cdot t_y / f_y}{2 b_f} \quad 9.9$$

$$\text{and} \quad M_N = f_y [A_s \left(\frac{d}{2} + t - c\right) - b_f (d_n' - t)(d_n' + t - 2c)] \quad 9.10$$

M_N is obtained from equations 9.9 and 9.10, where:-

$$t = 2\frac{1}{2} \text{ in.}; \quad A_s = 1.18 \text{ sq.in.}; \quad b = 2.5 \text{ ft.}; \quad A_t = 0.331 \text{ in.}^2/\text{ft.run}$$

$$t_y = 52,470 \text{ lbs./sq.in.}; \quad f_y = 42,470 \text{ lbs./sq.in.}; \quad b_f = 0.249 \text{ in.};$$

$$d = 3 \text{ in.}$$

$$\therefore \quad \underline{M_N = 158,750 \text{ lbs.in.} \quad \text{or} \quad 13.23 \text{ kips - ft.}}$$

The value of M_e for type (4) assumption on degree of composite action is the same as that for type (2) assumption obtained from equation 9.5, i.e. the value of M_e for type (4) assumption equals 15.94 kips - ft. Substituting the values 15.94 kips - ft. and 13.23 kips - ft. of M_e and M_N into equation 9.8, gives:-

$$\underline{\text{collapse load by mode B for type (4) assumption} = 29.76 \text{ tons}}$$

9.3.5 COLLAPSE FOR TYPE (5) ASSUMPTION

The equation for collapse load of model M_1 by mode B for type (5) assumption on degree of composite action is the same as that for type (4) assumption, i.e. equation 9.8.

The value of M_N for this assumption is the same as that for type (4) assumption = 13.23 kips - ft. The value of M_e will be the same as that for type (3) assumption, i.e. 21.06 kips - ft. Substituting these values of M_N and M_e into equation 9.8, gives:-

$$\underline{\text{collapse load by mode B for type (5) assumption} = 35.01 \text{ tons}}$$

To ensure that the least load required to produce failure of the system will be by mode B for each of the five assumptions on degree of composite action, the theoretical collapse load by the other two possible modes of collapse A and C were calculated.

Independent collapse of the slab will occur by mode C if the sides ratio ρ of the model $(0.57) < \frac{1}{\sqrt{2}}$ (see section 4.5.3). For collapse of

the system by mode C, equation 4.38 must be used for any of the five assumptions on degree of composite action,

$$\text{i.e. } p\ell L = \frac{24}{\rho(3 - \rho \tan\phi)} \left[\frac{2\rho}{\tan\phi} + 1 \right] M_s \quad 9.11$$

$$\text{Where } \tan\phi = \sqrt{4\rho^2 + 6 - 2\rho} \quad \text{for minimum } p$$

$$\text{where } \rho = 0.57, \tan\phi = 1.56$$

Substituting the above values of ρ and $\tan\phi$ together with the value of $M_s = 2.586$ kips - ft./ft. run into equation 9.11, gives:-

$$\underline{\text{collapse load by mode C for any of the five assumptions} = 38.84 \text{ tons}}$$

This value of collapse load by mode C is higher than that by mode B for any of the five assumptions on degree of composite action, which proves that mode B always occurs before mode C for this system.

The collapse load of the secondary beams and the slab by mode A was calculated for the five assumptions using equations 4.36, 5.44 and 6.27. In all cases, it was found that a lower load was required for collapse by mode B than by mode A. A summary of the collapse load of model M_1 by modes A, B and C is shown in Table 9(v) for each of the five assumptions. From this table, it can be seen that the least load required to produce collapse of the model will be that given by mode B.

9.3.6 TOTAL MOMENT AT THE SUPPORTS OF MODEL M_1

By ignoring the effect of composite action at the supports of model M_1 , the theoretical total moment there when plastic hinges form in the beams and a hogging yield line forms in the slab (Figure 4.8, mode B)

$$= 2 M_B + M_s \ell = 2 \times 4.64 + 2.586 \times 5 \text{ kips-ft.} = 22.21 \text{ kips-ft.}$$

Taking the effect of composite moment at the supports into consideration, the total theoretical plastic composite moment there

$$= 2 M_N = 2 \times 13.23 \text{ kips-ft.}$$

$$= \underline{26.46 \text{ kips-ft.}}$$

The above two theoretical values will be compared in Chapters 10 and 11

Test No.	Type of assumption on degree of composite action	Collapse load by mode B (tons)	Collapse load by mode A (tons)	Collapse load by mode C (tons)
M ₁	(1)	20.02	24.45	39.84
	(2)	26.27	30.05	39.84
	(3)	31.51	39.27	39.84
	(4)	29.76	30.05	39.84
	(5)	35.01	39.27	39.84
M ₂	(1)	15.04	24.45	35.61
	(2)	21.30	30.12	35.61
	(3)	26.58	39.42	35.61
	(4)	23.04	30.12	35.61
	(5)	28.32	39.42	35.61

Table 9(v). Summary of the theoretical collapse loads by modes A, B and C for Tests M₁ and M₂.

with the maximum experimental moments measured at the supports by means of the lever arms attached to the secondary beams, to investigate whether composite action at the supports of the model was present or not.

9.4 TEST M₂

The size of model M₂ was exactly the same as that of model M₁, i.e. 9' by 5' and 2 $\frac{1}{2}$ " thick slab composite and on top of a 7' by 4' steel frame of 3 in. \times 1 $\frac{1}{2}$ in. \times 4 lbs./ft. R.S.J. The slab was considered isotropic, using the same area of reinforcement as for model M₁, i.e. 3/8 in. mild steel bars at 4 in. and 3 in. centres for the longitudinal and transverse slab reinforcement respectively. Uniformly distributed loading was applied to model M₂ by the same interconnected hydraulic jacks system used in test M₁. The only difference in this test, compared to test M₁, was that the lever arms were omitted from one end. Thus, the main "edge" beams of this end were simply supported and hence no plastic hinge could develop. The model thus represented a hinge cancellation at the windward end of a typical bay of a multi-storey frame, owing to horizontal loading. Failure of the model was thus due to the formation of plastic hinges and yield lines at mid-span and one support for collapse by mode B (Figure 4.9). This represents failure of a typical bay of multi-storey frames, owing to combined mechanism, which corresponds to Zone II failure in the design of multi-storey frames.

Model M₂ was also designed for type (5) assumption on degree of composite action which assumes full composite action at mid-span and one support. In the following sections, the theoretical collapse load of model M₂ by mode B under U.D.L. is calculated for each of the five assumptions on degree of composite action to see which of these assumptions most closely corresponds to the observed experimental behaviour.

9.4.1 COLLAPSE LOAD FOR TYPE (1) ASSUMPTION

From section 4.6.2, the collapse load of model M₂ by mode B can be obtained from equation 4.40,

$$\text{i.e.} \quad p\ell L = \frac{12 M_s \ell}{L} + \frac{24 M_B}{L} \quad 9.12$$

The actual cube strength (U_w) for this test was 7010 lbs./sq.in., which was slightly higher than that for test M_1 (6820 lbs./sq.in.). Therefore the theoretical value of M_s will increase slightly.

$$U_c = 2/3 \times 7010 = 4670 \text{ lbs./sq.in.}$$

Substituting this value of U_c into equation 9.1, gives the theoretical value of M_s for test $M_2 = \underline{31,100 \text{ lbs./ft.run}}$ or 2.592 kips-ft./ft.run

Substituting this value of $M_s = 2.592 \text{ kips-ft./ft.run}$ and the value of

$M_B = 4.64 \text{ kips-ft.}$ into equation 9.12, gives:-

$$p\ell L = \frac{12 \times 2.592 \times 4}{7} + \frac{24 \times 4.64}{7} \quad \text{kips}$$

or collapse load by mode B for type (1) assumption = 15.04 tons

9.4.2 COLLAPSE LOAD FOR TYPE (2) ASSUMPTION

From section 5.6, the collapse load of model M_1 by mode B for type (2) assumption on degree of composite action can be obtained from equation 5.46,

$$\text{i.e.} \quad p\ell L = \frac{8 (2 M_e + M_B)}{L} + \frac{4 M_s \ell}{L} \quad 9.13$$

The theoretical value of M_e for this test will increase slightly compared to that for test M_1 , owing to the slight increase in the cube strength. Substituting the new value of $U_c = 4670 \text{ lbs./sq.in.}$ into equation 9.4, gives from equation 9.5, the theoretical value of M_e of this test for type (2) assumption = 191,520 lbs./in. or 15.96 kips-ft.

Substituting the values 15.96 kips-ft., 4.64 kips-ft. and 2.592 kips-ft./ft.run of M_e , M_B , and M_s respectively into equation 9.13, gives:-

$$\underline{\text{the collapse load by mode B for type (2) assumption} = 21.30 \text{ tons}}$$

9.4.3 COLLAPSE LOAD FOR TYPE (3) ASSUMPTION

The equation for collapse load of model M_2 by mode B for type (3) assumption is the same as that for type (2), i.e. equation 9.13. Substituting the value of $U_c = 4670 \text{ lbs./sq.in.}$ into equation 9.6, and using equation 9.7, the theoretical value of M_e , for this test, for type (3)

assumption = 253,680 lbs.in. or 21.14 kips-ft.

On substitution into equation 9.13,

$$p\ell L = \frac{8(2 \times 21.14 + 4.64)}{7} + \frac{4 \times 2.592 \times 4}{7} \quad \text{kips}$$

or collapse load by mode B for type (3) assumption = 26.58 tons

9.4.4 COLLAPSE LOAD FOR TYPE (4) ASSUMPTION

From section 6.6, the collapse load of this system by mode B for type (4) assumption on degree of composite action can be obtained by using equation 6.29,

$$\text{i.e.} \quad p\ell L = \frac{8 (2 M_e + M_N)}{L} \quad 9.14$$

The hogging plastic composite moment at the fixed support (M_N) will have the same value as that for test M_1 , irrespective of the difference in cube strength between the two tests, i.e. 13.23 kips-ft. This is due to the fact that the plastic neutral axis lies within the flange of the joist (equations 9.9 and 9.10). The value of M_e will be that of type (2) assumption, i.e. 15.96 kips-ft. On substituting the values 15.96 kips-ft. and 13.23 kips-ft. for M_e and M_N respectively into equation 9.14,

The collapse load by mode B for type (4) assumption = 23.04 tons

9.4.5 COLLAPSE LOAD FOR TYPE (5) ASSUMPTION

The collapse load equation for this assumption by mode B is the same as that for type (4) assumption, i.e. equation 9.14. The value of M_e will be that for type (3) assumption, i.e. 21.14 kips-ft. Substituting the values 21.14 kips-ft. and 13.23 kips-ft. for M_e and M_N into equation 9.14,

The collapse load by mode B for type (5) assumption = 28.32 tons

To ensure that the least load required to produce failure of model M_2 will be by mode B for each of the five assumptions on degree of composite action, the theoretical collapse load by the other two possible modes of collapse, namely A and C, were calculated.

Independent collapse of the slab will occur by mode C, as the sides

ratio of the model ρ (0.57) < 0.82 (see section 4.6.3). For collapse of model M_2 by mode C, equation 4.41 can be used,

$$\text{i.e.} \quad p\ell L = \frac{24}{\rho(3 - \rho \tan\phi)} \left[\frac{3\rho}{2\tan\phi} + 1 \right] \cdot M_s \quad 9.15$$

Where $\tan\phi = \frac{3}{2} \left(\sqrt{\rho^2 + 2} - \rho \right)$ for minimum p

where $\rho = 0.57$, $\tan\phi = 1.4307$

Substituting the above values of ρ and $\tan\phi$ together with the value of M_s of 2.592 kips-ft./ft. run into equation 9.15,

The collapse load by mode C for any of the five assumptions = 35.61 tons

The collapse load of the secondary beams and slab by mode A was calculated for the five assumptions using the same equations (4.36, 5.44 and 6.27) as for test M_1 . In all cases, it was found that collapse occurs by mode B rather than by mode A. A summary of the collapse load of model M_2 by modes A, B and C is shown in Table 9(v) for each of the five assumptions on degree of composite action. From this table, it can be seen that the least load required to produce collapse of the system will always be by mode B.

The total theoretical moment at the fixed supports of model M_2 when plastic hinges and yield line forms is 22.24 kips-ft. or 26.46 kips-ft., depending upon whether composite action at the supports is present or not. These two values are compared in Chapters 10 and 11 with the corresponding experimental values, to determine whether or not composite action was present at the fixed end.

9.5 DESIGN OF THE SHEAR CONNECTORS

Composite action between the slab and the supporting beams of the models was achieved by means of 2 in. long and 1/2 in. diameter stud shear connectors. Three push-out specimens were made to determine the ultimate capacity and the load/slip characteristics of these studs. The lowest collapse load of these tests, viz. 3.55 tons, was taken as the ultimate capacity of the studs⁽⁴⁰⁾. Figure 9.6 shows the load/slip characteristics of these studs.

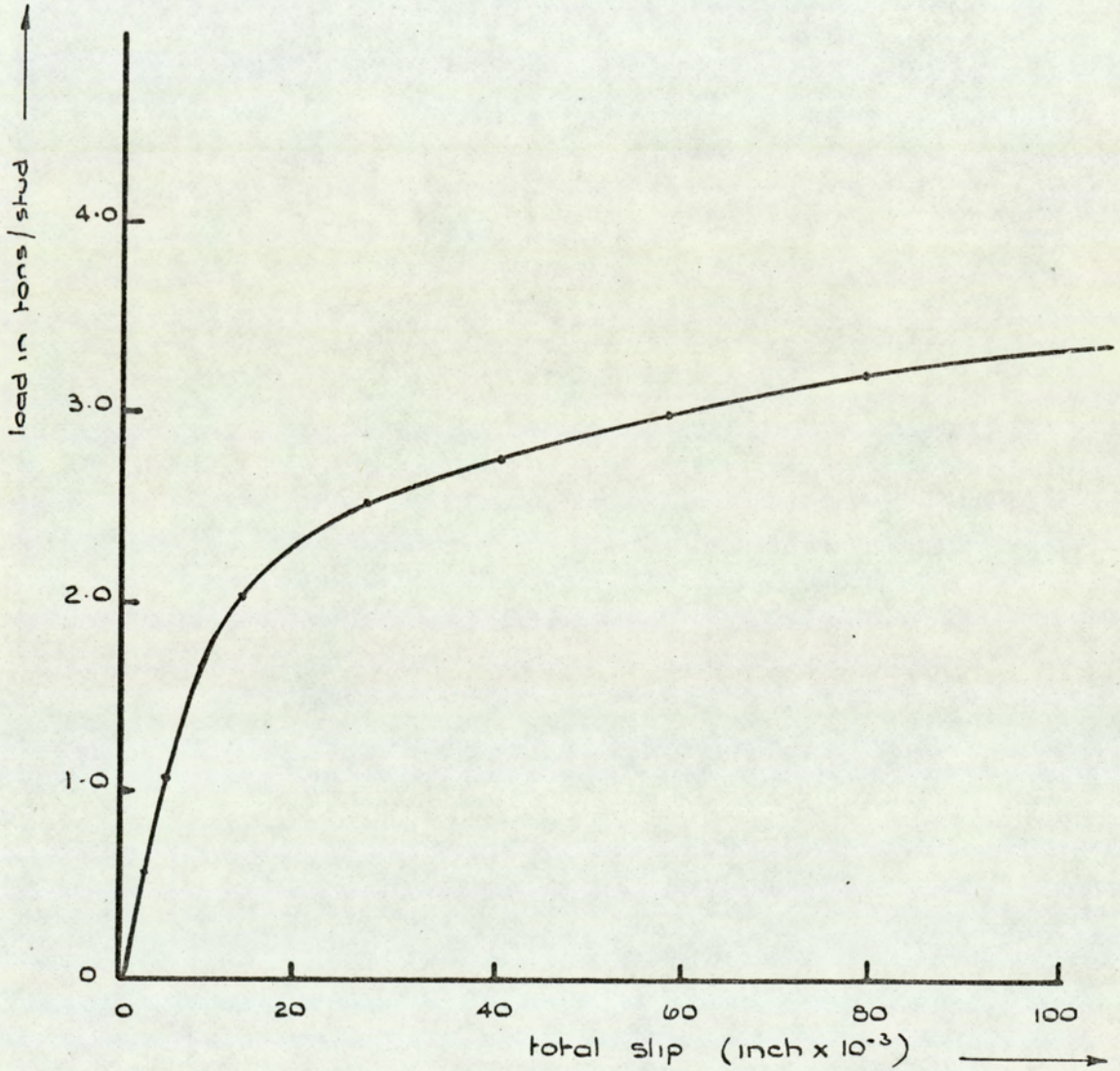


Fig 9. 6. Load v. slip characteristics of $\frac{1}{2}$ in. diameter
2 in. high mid steel stud shear connector.

The total slip of the stud at ultimate load was measured as 80×10^{-3} inch.

To provide composite action at the supports and mid-span of the main "edge" beams of models M_1 and M_2 for type (5) assumption, the following procedure was adopted to find the number of shear connectors required.

(i) Mid-span composite action

The plastic neutral axis at mid-span of the main "edge" beams was within the slab. The effect of slab reinforcement was included for type (5) assumption. Therefore, from section 5.2.4, the number of shear connectors to provide mid-span composite action was given by equation 5.23,

$$\text{i.e.} \quad \text{Number required} = \frac{A_s \cdot f_y}{P_c} \quad 9.16$$

Substituting into equation 9.16 the following values,

$$A_s = 1.18 \text{ sq.in.}; \quad f_y = 18.96 \text{ tons/sq.in.}$$

$$P_c = 0.80 \times 3.55 \quad (P_c = 80\% \text{ of ultimate capacity of} \\ = 2.84 \text{ tons} \quad \text{one stud shear connector})$$

$$\text{Number required} = 7.87 \quad \text{or} \quad \underline{8 \text{ studs per half span}}$$

(ii) Composite action at supports

The plastic neutral axis at the supports of the main "edge" beams was within the joist flange. Therefore, from section 6.2.2, the number of shear connectors to provide composite action at the supports was given by equation 6.13,

$$\text{i.e.} \quad \text{Number required} = \frac{b \cdot A_t \cdot t_y}{P'_c} \quad 9.17$$

Substituting into equation 9.17 the following values,

$$b = 2.5 \text{ ft.}; \quad A_t = 0.331 \text{ in.}^2/\text{ft.run}; \quad t_y = 23.54 \text{ tons/sq.in.}$$

$$P'_c = 0.64 \times 3.55 \quad (P'_c = 64\% \text{ of ultimate capacity} \\ = 2.27 \text{ tons} \quad \text{of one stud shear connector})$$

$$\therefore \text{Number required} = 8.57 \quad \text{or} \quad \underline{9 \text{ studs per half span}}$$

Therefore, from (i) and (ii) above, the total number of shear connectors required to provide mid-span and support composite action of the main "edge" beams is 17 studs per half span or 34 studs for the whole length of the beam.

For the secondary beams, composite action was assumed at mid-span only. The plastic neutral axis at mid-span lies within the slab and since the same joist was used for secondary and main beams, then from (i) the number of studs required was 8 studs per half the span or 16 studs for the whole span. 30 studs were in fact used on the secondary beams, instead of the required 16 studs. The extra 14 studs were placed to assist the development of continuity of the slab along the secondary beam, since the rotation of these beams, owing to vertical loading, was prevented by the lever arms attached to them.

The studs were automatically welded to the upper flange of the joist and uniformly spaced along the spans of the secondary and main "edge" beams in a single line, as shown in Plate 3. The same number of studs on the secondary and main beams respectively were used in all model tests.

9.6 CONSTRUCTION OF THE MODELS

The secondary and main beams were welded together to form the steel frame shown in Plates 3 and 4. For ease of constructing the formwork, the models were cast in an inverted position, as shown in Plate 4.

Casting was carried out on two variable speed vibrating tables, shown in Plate 4, after the concrete had been mixed in a mixer of the non-tilting drum type. The longitudinal reinforcement was bent up at the ends in such a way as to give cover of $\frac{3}{8}$ in. to the sagging and hogging reinforcement within the $2\frac{1}{2}$ in. thick slab, as shown in Figure 9.10. This cover was maintained by placing mortar blocks between the reinforcement and the formwork.

Curing of the models, however, could not be carried out in the constant humidity room, owing to size restrictions. Consequently, the models were covered with a polythene covered wooden framework immediately after casting. Wet hessian was laid over the slab surface after the initial set of the concrete was complete. The sides were stripped after two days, the sacking being soaked twice a day and the polythene covers being kept in position over the models to prevent excess evaporation. The upper surface shown in

Plate 4, which was in fact the lower slab surface, was carefully trowelled after casting, so that a smooth finish ensued.

As the models were tested after 14 days, the slab elements were allowed to dry four days before testing. The last three days before testing were devoted to fixing and connecting gauges, and setting up the model for testing.

9.7 SETTING UP OF THE APPARATUS FOR TESTS M₁ AND M₂

Tests were carried out within a large permanent portable testing rig. This rig was constructed from I-sections in such a way that a 6 in. space existed between the two I-sections making up the base. The total width of the base was 18 in. and it was therefore necessary to support the corners of the models, which were 4 ft. apart, on two suitably stiffened 12 in. x 5 in. I-sections 5'-6" long placed transversely to the length of the main rig. Mechanical jacks were placed at the ends of the transverse beams in order to prevent deflection of the supports of the model during testing, as shown in Plate 5. The lateral restraints, owing to bending, were eliminated by using bearing pads placed at all four corners of the model, as shown in Figure 9.5. The upper pads were 2 in. x 1½ in. x ¾ in. solid metal blocks welded to the frame before casting with a ball recess placed on its surface centrally to each corner. This is shown in Plate 4. The lower bearing pads were 4 in. x 4 in. x 3 in. solid metal blocks with a similar ball recess. A 1 in. hardened steel ball was placed between the two recessed blocks. The ball joint arrangement ensured that the reactive forces acted vertically throughout the test, while eliminating any torsional restraints. Half-inch diameter rollers were placed underneath the bearing pads to prevent membrane forces building up in the models during testing. The rollers in turn rested directly on the upper face of the transverse I-sections. Plate 6 shows a close view of the ball joint arrangement with the 1/2 in. diameter rollers underneath one of the corners of the model.

Point loads were applied to the model to simulate uniformly distributed loading. This was achieved using interconnected hydraulic jacks positioned

in four rows. Within the boundaries of the supporting beams, each longitudinal row of jacks covered one foot width of the slab. Altogether there were 16 jacks arranged in four jacks per row, with the area covered by each jack being equal. Thus, when the load applied to the model was W , each jack received $W/16$ of that load. The position of the jacks is shown in Figure 9.4. It can be seen from Figure 9.7 (a) and (b) that in the case of simply supported beams, this loading system does simulate uniformly distributed loading very accurately, as the central moment for both cases is the same. On the other hand, for an encastré beam (Figure 9.7 (c) and (d)), the adopted loading system results in an error of -6% and $+3\%$ in the central and ends moments respectively, compared to a U.D.L.

Each jack had a capacity of 6 tons with a ram diameter of $1\frac{1}{4}$ in. and a travel of $2\frac{1}{2}$ in. The jacks pressure was maintained at a constant level manually. To safeguard against punching shear failure of the slab, a 3 in. \times 3 in. \times $1/4$ in. plate was placed under each jack. To ensure vertical loading, care was taken that each jack maintained an upright position during the setting up of the system. A plate 3 in. diameter and $3/4$ in. thick was placed on top of each jack, with a ball recess at the centre of the upper surface of each plate, into which a $3/4$ in. diameter hardened steel ball was placed. This was to ensure that the load acting on each jack was axial.

The applied loads imposed by each transverse row of jacks was distributed by means of a beam of 4 in. \times 4 in. \times $1/4$ in. hollow section. To the lower surface of this beam four plates 4 in. \times 4 in. \times $3/4$ in. were welded with a recess to accommodate the steel balls. Care was taken that when the hollow beam rested on the jacks, the distance between the centres of the steel balls was 12 inches. Details of the ball joint arrangement between the hollow section and the jacks are shown in Plate 5 and also in Figure 9.5. In Plate 5, the interconnected jacks are shown in position, where it is noticed that each row of jacks were backed by one hollow beam.

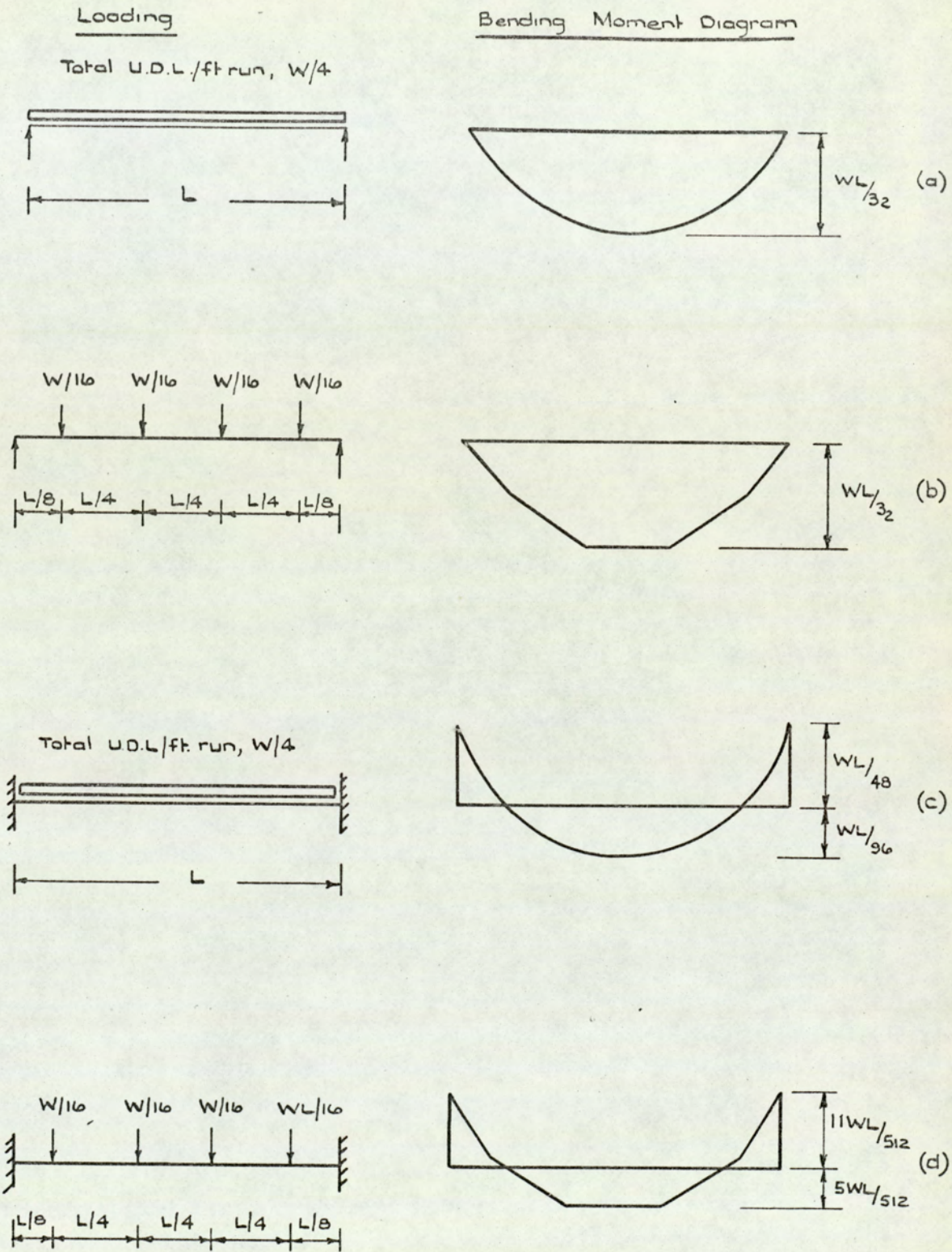


Fig. 9.7. Limits of end conditions of slab and main "edge" beams.
Tests M_1 and M_2 .

The four hollow beams were in turn backed by means of a 12 in. x 5 in. cross beam placed centrally on top of the hollow section beams.

The cross beam was loaded centrally through a load cell with a 200 ton capacity. The lower part of this cell consisted of two cylindrical solid blocks with a central recess for a 3 in. diameter hardened steel ball, thus ensuring the application of the load vertically. On top of the cell a 50 ton capacity, long travel, jack was placed to react against the loading rig, operated by a hand pump system.

Continuity at the supports of the main "edge" beams and of the slab along the secondary beams was achieved by means of four stiffened lever arms. These were connected to the secondary beam at 12 in. centres and prevented the rotation of the latter during the loading procedure. Each lever arm was a 4 in. x $2\frac{1}{2}$ in. joist connected to the secondary beam by means of two solid blocks at either side of the secondary beam. Both blocks were machined to fit the inside of the secondary beams with the machined surfaces coming in contact with the web and the flanges of the secondary beam. One of the blocks was welded to the lever arm, while the secondary beam was secured in position between the blocks by means of four $\frac{3}{8}$ in. high tensile bolts through drilled holes in the web of the secondary beam, as shown in Plate 3. Details of the connection of the two machined blocks to the secondary beam are shown in Figure 9.5, and also in Plate 7.

To ensure continuity at the supports along the secondary beam, each lever arm was bolted to the slab by means of 1 in. diameter bolt welded to the top flange. These bolts were positioned 6 in. away from the web of the secondary beam and passed through pre-set holes in the slab. A transverse plate $1\frac{1}{2}$ in. x $\frac{1}{4}$ in. and 5 ft. long was placed on the top slab surface before fastening the nuts, thus ensuring that the four lever arms acted as an integral system. Details of the connection of the slab to the lever arm are shown in Plate 7 and in Figure 9.5, where it is also noticed that the slab was separated from the lever arms by a $\frac{1}{2}$ in. gap. In this

manner, contact was not allowed between the lever arms and the slab except through the bolts.

At their far ends, each pair of lever arms was connected by means of a beam of T-section. To the centre of this beam, between the lever arms, a 5 ton capacity proving ring was connected. In this manner, any load exerted on the proving ring was equally shared by a pair of the lever arms. Altogether, two proving rings were used to be shared by four lever arms. These proving rings were connected by bolts to a channel section fixed to the testing rig. Details of the connection of the proving ring to the T-section and to the channel are shown in Plate 8.

Any load applied to the model tended to rotate the secondary beams. In turn, this led to a tendency to rotate the lever arms and cause their far ends to rise. This uplift was prevented by the proving rings which recorded the force required to prevent this uplift. This gave rise to a moment equal to the product of the recorded force and the 64 in. distance between the proving ring and the centre line of the secondary beam. The total moment produced by the lever arm system gave the fixing hogging moment acting at the support. The uplift force at the end of the lever arms also produced a force in the bolts on top of the lever arms, which were connected to the slab, thus producing continuity of the slab along the secondary beam.

Two types of boundary conditions were imposed. In test M_1 , all the lever arms were connected to their proving rings, thus producing fixing moments at both ends of the model to simulate collapse, owing to vertical loading. In test M_2 , only one end of the model was restrained, thus simulating the case of failure by combined mechanism.

During test M_1 , it was noticed that the rectangular hollow beams backing the hydraulic jacks developed excessive deflections. In test M_2 , this defect was rectified by filling these sections with concrete. It was also noticed that loading of the model gave rise to slight lateral movement

of the cross beam, thus tending to give a sideways movement to the whole model. This was also rectified by inserting rollers between the cross beam and the hollow sections. An improved ball joint arrangement, complete with 1/4 in. rollers underneath, was used at the supports of the model M_2 . Details of these improvements, together with the complete set up of test M_2 , are shown in Plate 9. A fourth improvement was achieved by moving the two pairs of lever arms as far apart as possible, so that the outer lever arms came as near as possible to the main beams of the model. This reduced twisting of the main beams.

9.8 EXPERIMENTAL VALUES OF BEAM AND SLAB STRENGTHS

To find the theoretical collapse load for the frames in tests M_1 and M_2 , values of the composite slab and beam ultimate moment at mid-span and supports (M_e and M_N) and the slab ultimate moment (M_s) need to be known. These have been evaluated theoretically, using the actual cube strength of the concrete, for the various assumptions on degree of composite action. A more accurate estimate of the collapse load could be obtained if the experimental values of M_e , M_N and M_s were substituted, these values being obtained from control tests on single elements. According to this, units identical to those in models M_1 and M_2 were constructed and tested to destruction. These control tests are described below.

9.8.1 TEST M_3

The composite beams and slab model for this test was an exact replica of models M_1 and M_2 . Test M_3 was divided into three control tests. The first test was to find the experimental value of M_e at mid-span and the other two were to find the experimental value of M_N at both supports. These three control tests are denoted C_1 , C_2 and C_3 respectively and are described below.

(i) Test C_1

This was a simple bending test to find the experimental value of M_e . The cube strength for this test was 6780 lbs./sq.in. Because of the time

taken to complete a main test, it was not feasible to carry out the related control tests on the same day. This explains why the main tests and the control tests have concrete of slightly differing cube strengths. Consequently, the theoretical values of M_e for the various assumptions on degree of composite action were recalculated using the actual cube strength of this test. The theoretical value of M_e for type (2) or (4) assumption equals 15.93 kips-ft. and that for type (3) or (5) assumption equals 21.06 kips-ft. These two values will be compared with the experimental value of M_e , obtained from this test, in Chapter 11.

The bending test was carried out using a central line load 5 ft. long applied through three 3 in. \times 1 $\frac{1}{2}$ in. \times 4 lbs./ft. run R.S.J. welded together. At the lower face of this line load, blocks were welded to give clearance for electrical strain gauges placed on the concrete along and perpendicular to the transverse central line of the model. Loading for the test was by the same 50 ton capacity, long travel, jack and 200 ton load cell used in tests M_1 and M_2 .

The model was supported on bearing pads similar to those of models M_1 and M_2 . Only this time, the upper bearing pads were welded to the lower flange surface of the joist 12 in. away from the corners of the steel frame making the span of the main beams 5 ft., compared with 7 ft. in tests M_1 and M_2 . This alteration was made to investigate the possibility of compressive membrane action between the concrete slab and supporting beam. Details of the experimental arrangements are shown in Plate 10.

(ii) Tests C_2 and C_3

Control tests C_2 and C_3 were carried out to find the experimental total moment at both ends of model M_3 .

After the collapse of model M_3 at mid-span, owing to the bending test C_1 , the model was resealed on the corner supports of the steel frame, as shown in Figure 9.8. A bearing pads system similar to that of tests M_1 and

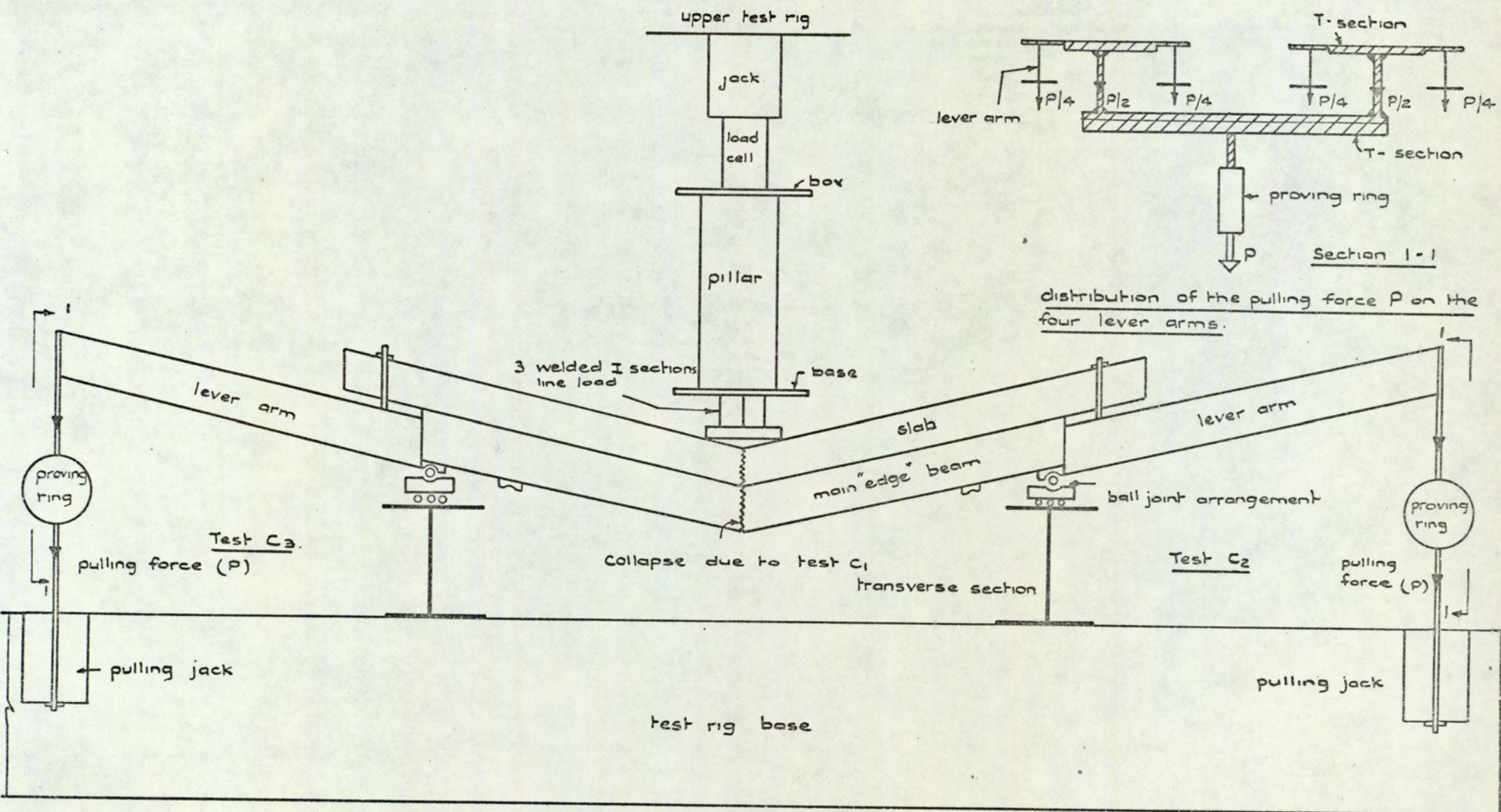


Fig. 9.8. Control tests C₂ and C₃ set up.

M_2 was used at the supports, with the upper bearing pads, seen in Plate 10, welded to the corners of the steel frame before casting. The secondary and main beams of the model at the corner supports were not affected by the bending test C_1 .

The lever arms used in tests M_1 and M_2 were connected to the secondary beams of the model on both ends. The slab was connected to the lever arms using the welded bolts on top of the lever arms, in a manner similar to that used for tests M_1 and M_2 .

Load was first applied to the lever arms at one end of the model (test C_2) until the ultimate moment condition was reached at the support to which the lever arms were connected. Subsequently, the lever arms at the other end were loaded (test C_3) and the ultimate support moment again recorded.

The experimental values of the total moment at both ends of the model, owing to tests C_2 and C_3 , are compared in Chapter 11 with the total theoretical moments at the supports.

9.8.2 SLAB STRIPS S_1 AND S_2

To find the value of the ultimate slab moment M_s experimentally, two slab strips 2'-0" by 4'-10" and 2 $\frac{1}{2}$ " thick were constructed and reinforced with the same area of reinforcement/ft. run as that in tests M_1 and M_2 using the same $\frac{3}{8}$ in. mild steel bars. These strips were loaded through two line loads 16 in. apart to provide a region of constant bending moment, over which strains could be measured. Details of the experimental arrangements of this test can be seen in Plate 11.

The actual cube strength of the two slab strips was 6920 lbs./sq.in., therefore $U_c = 4610$ lbs./sq.in. Substituting this value of U_c into equation 9.1, the theoretical value of M_s for the two slab strips = 31,068 lbs. in./ft. run or 2.589 kips-ft./ft. run, which is very nearly the same as that of tests M_1 and M_2 . This theoretical value of M_s is compared in Chapter 11 with the experimental values of M_s obtained from testing slab strips S_1 and S_2 .

9.9 INSTRUMENTATION

9.9.1 STRAIN MEASUREMENT

Strain gauges were attached to the models to determine the variation of strain both along and perpendicular to the centre lines, including the upper and lower surface of the slab. Strains were also measured parallel to the main "edge" beam and parallel and perpendicular to the secondary beam on the upper and lower surface of the slab. At some possible "hinge" positions, strain gauges were fixed to the steel beams, reinforcement and concrete slab, to observe the onset of yield and to provide a picture of the distribution of strain through the composite section. The gauges used to measure the strain on the steel beams, reinforcement and concrete slab are described in the following sections.

(i) Supporting beams strain

Steel strains of the supporting beams of the models were measured by placing electrical strain gauges at possible hinge positions, as shown in Plate 4. The gauges used were Tinsley foil strain gauges type LSG9A/2/CN/E which had a nominal gauge length of 1/4 in. Budd GA-2 two component epoxy adhesive was used for bonding the gauge to the joist. The manufacturer's specifications were followed closely, special care being taken to sand the metal bright with wet and dry paper and to degrease and neutralise the surface with Trichlorethylene and 10% dilute Ammonia solution. The gauges had been fixed to the joist with the aid of Sellotape strips, the cement was cured under infra-red radiation for about eight hours, after which time the Sellotape strips were peeled off, leaving the gauges exposed. Electrical wires from a wire core, manufactured by Radiospares Limited, was soldered to the exposed tabs of the gauges. It was found easier to fix the strain gauges in position on the supporting beams before casting the model, and because of curing of the slab, the gauges were waterproofed before casting, using a synthetic rubber coating compound "Gagekote # 2" made of two parts.

(ii) Reinforcement Strains

These were measured by placing electrical resistance strain gauges on the reinforcing bars at possible hinge positions of the model. The gauges used were also Tinsley foil gauges type SGD1C/2/CN/E of a nominal gauge length of $1/8$ in. The cement used for fixing the gauges to the bars, surface preparations and curing were similar to those used on the supporting beams. The gauge was set up in the direction of the reinforcement and to follow the high transverse curvature of the bar, after fixing the gauge with the aid of a Sellotape strip to the cement at the position required, a second Sellotape strip was applied around the bar and the gauge in such a way that adequate pressure was exerted on the gauge. After curing the cement, the Sellotape strips were peeled off, leaving the gauges exposed. Electrical wires similar to those used on the beams were soldered to the exposed taps of the gauges. The gauges were then waterproofed using the "Gagekote # 2" compound. Plate 12 shows a close-up view of a gauge fixed to the reinforcement in one of the models.

(iii) Concrete Strains

Two types of gauge were used to measure the strain on the concrete slab. These are:-

(a) Electrical strain gauges

These were Tinsley electrical resistance wire gauges type 7A with a nominal gauge length of $2\frac{1}{2}$ in. and a width of 0.4 in. The positions of these gauges were sanded to remove any bad slab surface characteristics and thoroughly cleansed with acetone and carefully marked. F.88 dental cement manufactured by Tridox Products, Philadelphia, U.S.A., was used to fix the gauges to the concrete surface. This quick drying cement had been found to be particularly successful when used in conjunction with the Tinsley felt-backed wire gauges which were used throughout this investigation. The same type of wire used with the strain gauges on the steel beam and reinforcement was soldered to the tabs of these strain gauges.

(b) Demec gauges

These were used on model M₃ and slab strips S₁ and S₂. At mid-span, at a possible hinge position, strains through the depth of the slab were measured with a Demec gauge over an eight inch length to prevent the recording of too high local strains, owing to cracks. In tests C₂ and C₃ on model M₃, the hogging strains on the top slab surface perpendicular to the secondary beams were measured with a Demec gauge over a four inch length.

Electrical gauge positions and respective colour wires were numbered and then connected to a similar number on the extension box for ease of strain recording. The extension boxes used were of the type 48U in conjunction with a Peekel 103U strain recorder which automatically converts resistance changes into micro strains. A dummy block was constructed with the electrical strain gauges fixed to it of the same type and batch as those used for live gauges. This block acted as a central dummy for the three different sets of readings with a dummy gauge for every 24 active gauges employed. The dummy block was placed close to the model during testing so that temperature compensation was adequate. The leads joining the dummy gauges to the extension boxes were of the same length as those connecting the active gauges, so that no inaccuracies developed through electrical imbalance.

9.9.2 DEFLECTION MEASUREMENT

Mercer 2 in. travel dial gauges reading to an accuracy of 0.001 in. per one division were used to measure the deflections of selected points on the bottom surface of the models. These points were normally the centre of the slab and the mid-spans of the secondary and main beams. The gauges were supported on adjustable stands so that they could be re-set when the deflections exceeded 2 in.

9.9.3 SLIP MEASUREMENT

Slip between the concrete slab and the supporting beams, through the stud shear connectors, during the loading procedure, was measured using

Mercer 1/2 in. travel dial gauges. In tests M_1 and M_2 , these gauges were placed at mid-spans and supports of the secondary and main beams, as shown in Plates 6 and 9. In model M_3 , these gauges were placed along the whole length of the main beam as shown in Plate 10. These gauges were magnetically fixed to the web of the joist with their plunger bearing against a piece of perspex material, as shown in Plate 10.

9.9.4 LOAD MEASUREMENT

Loads on models M_1 , M_2 and M_3 were measured by means of the 200 ton capacity load cell set up as described in section 9.7. The cell was calibrated by the Industrial Research Laboratories of the Public Works Department in Birmingham and re-calibrated twice in the Denison machine during the testing period. At collapse of the models, it was not feasible to read the failure load from the load cell dial gauge. The collapse load was therefore taken from the pressure reading of the 50 ton jack used for load application. This pressure reading was converted to load by calibration against the Denison machine.

9.9.5 MOMENT MEASUREMENT

The total moment at the supports of the model along the secondary beam was the product of the tensile forces in the proving rings and the distance between the proving rings and the supports as described in section 9.7. The proving rings used were of 5 ton capacity in tension, manufactured by Clockhouse Engineering and Instrument Company. Certificates of calibration of these proving rings were provided by the manufacturers. However, these calibration charts were checked for each proving ring against the Denison Universal testing machine.

9.9.6 GAUGE POSITIONS

Details of the gauge positioning for each test are shown in Figures 9.9 to 9.21. It can be seen from these Figures that the electrical strain gauges on the beams, reinforcement and concrete slab were denoted by the

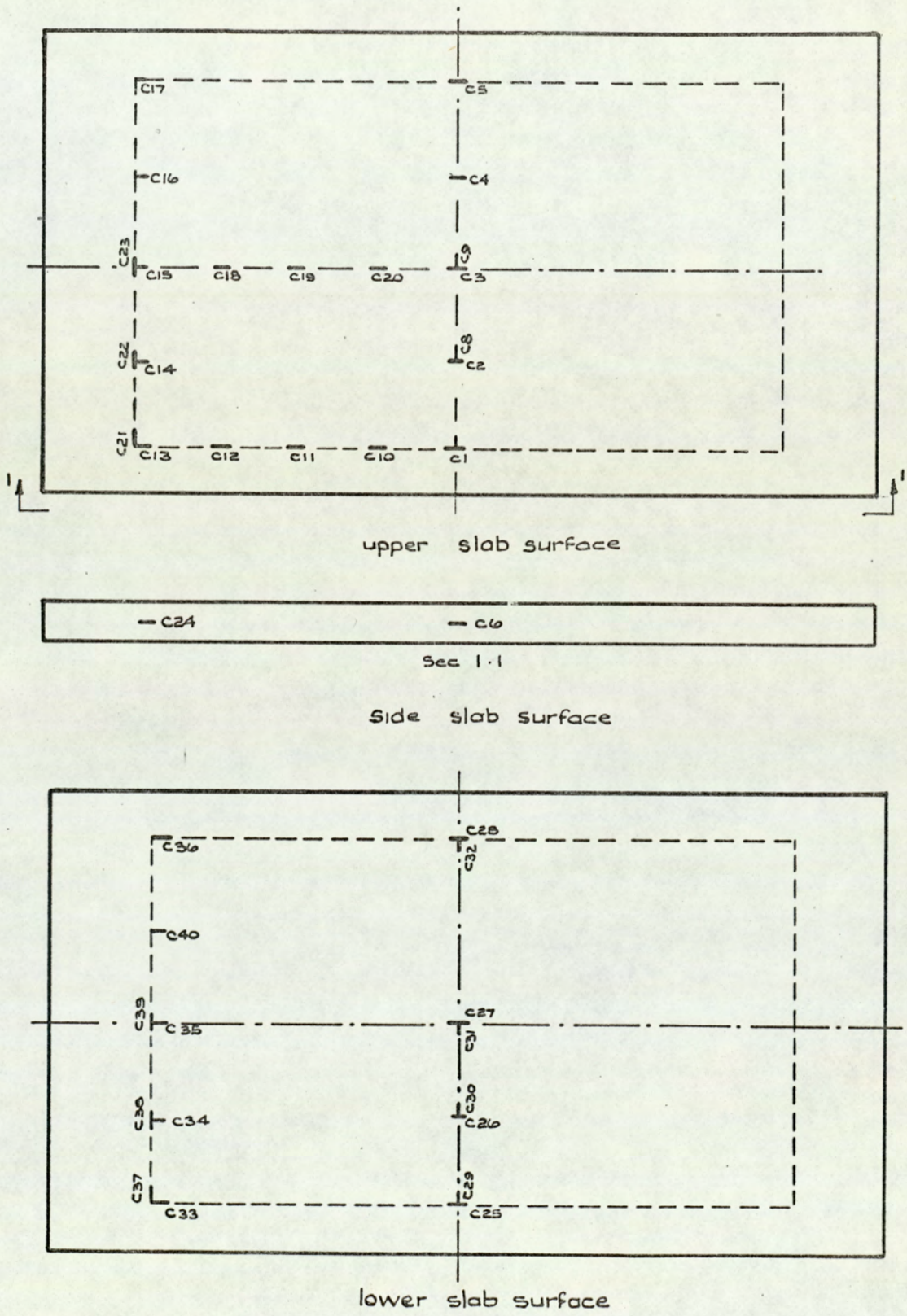


Fig. 9.9. Location of concrete strain gauges
test M_1

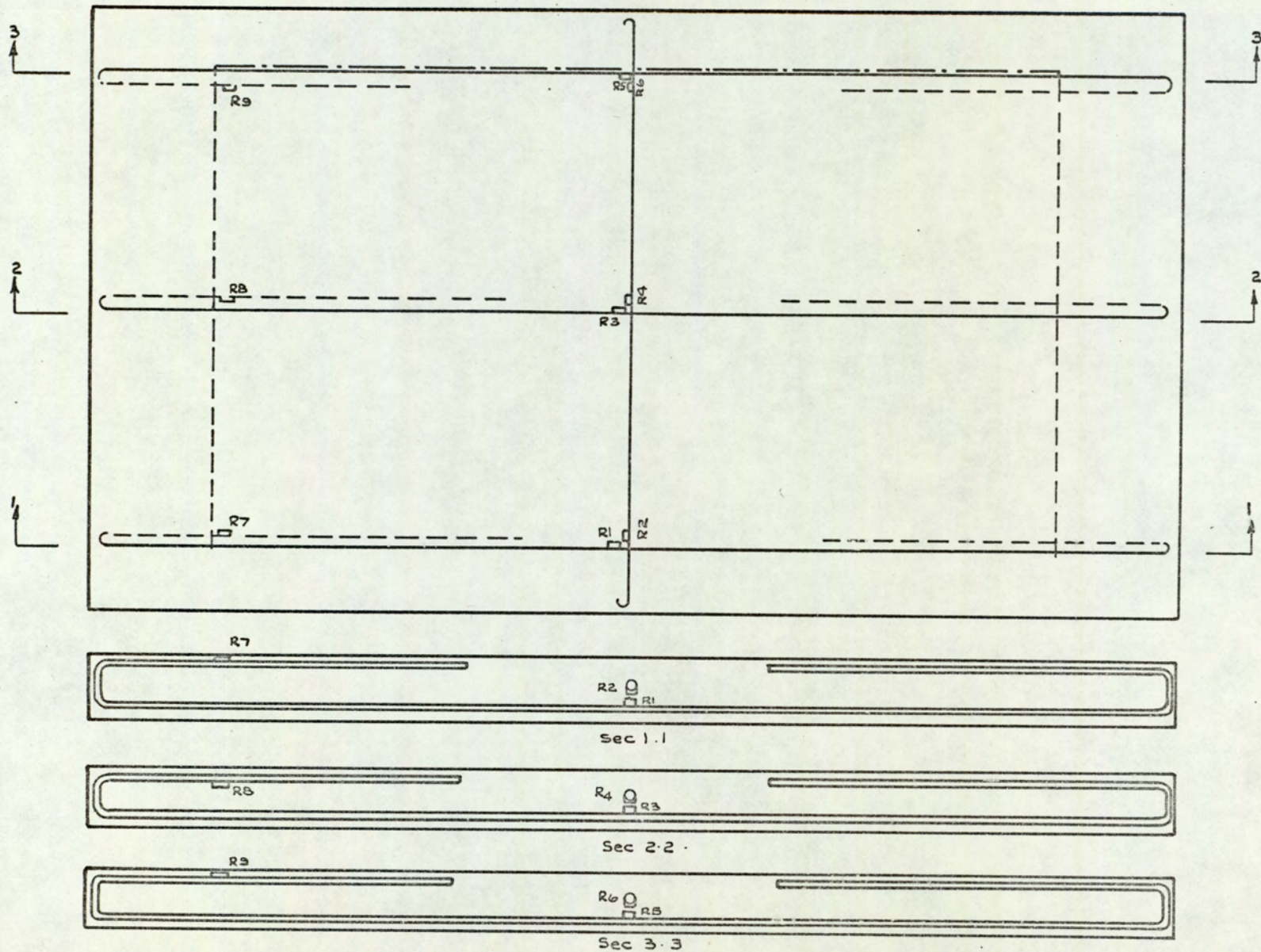


Fig. 9.10. Location of strain gauges on reinforcement bars test Mi.

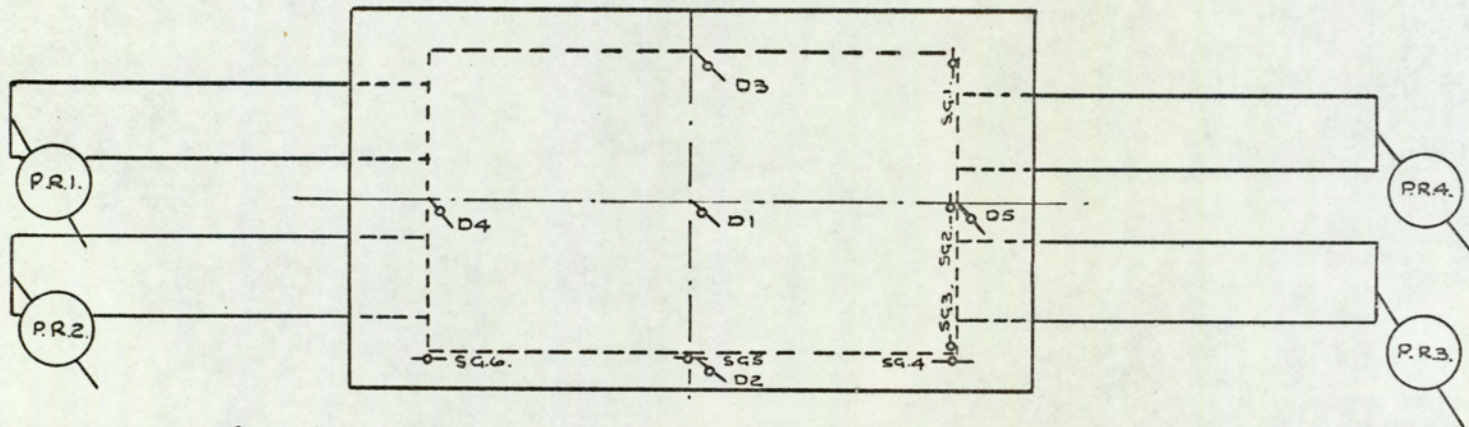


Fig. 9.11. Location of deflection, slip and proving ring gauges. Test. MI.

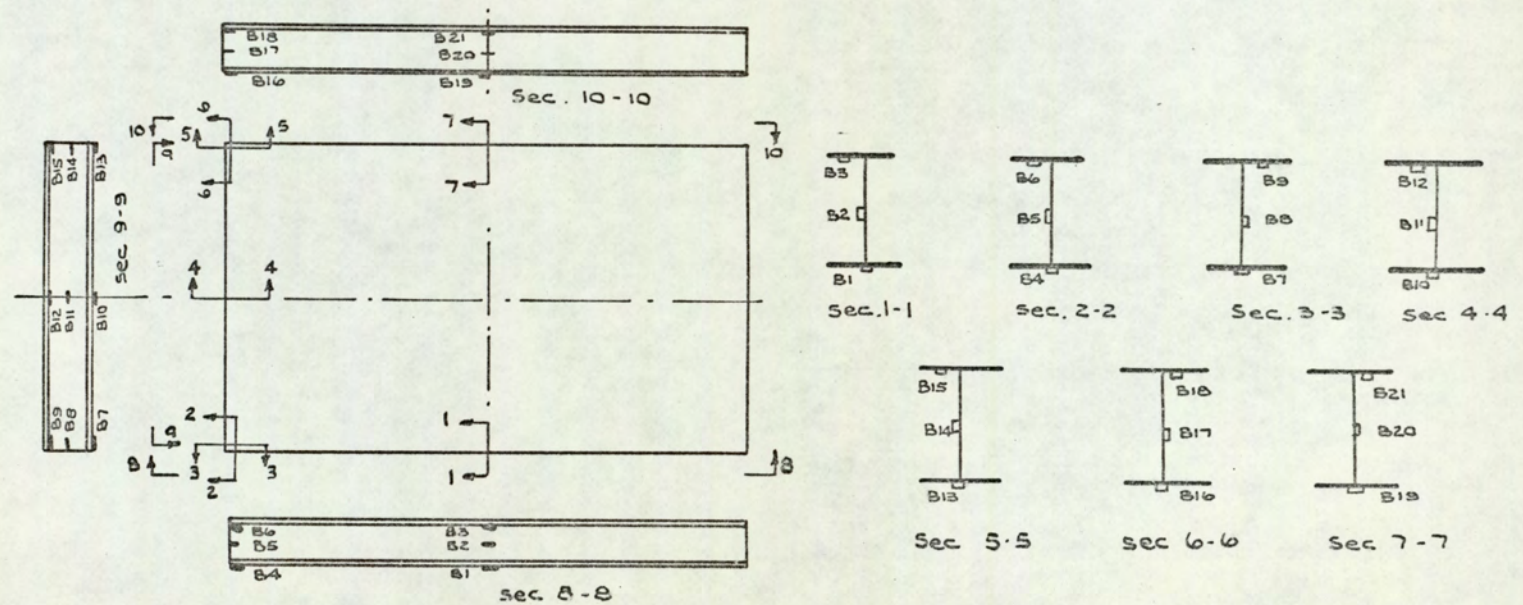
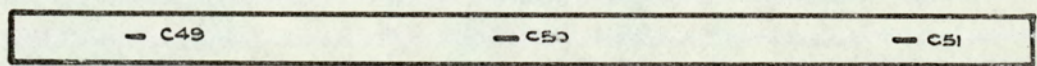
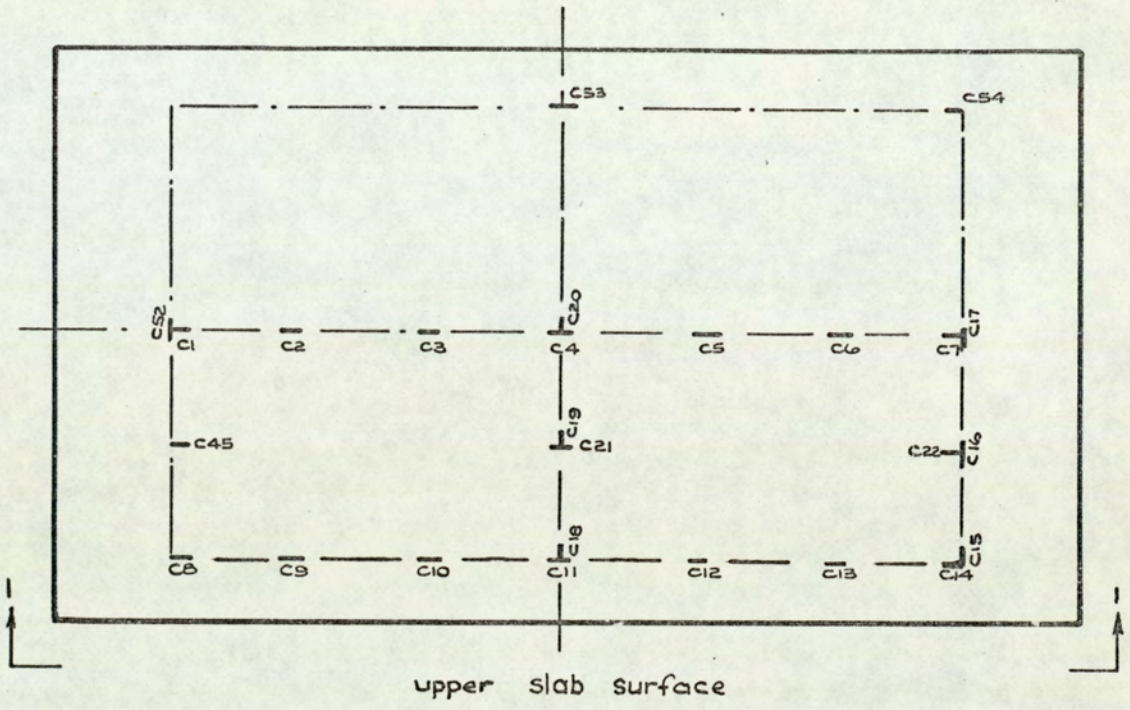


Fig. 9.12. Location of strain gauges on the steel frame. Test. MI.



Sec 1-1
side slab surface

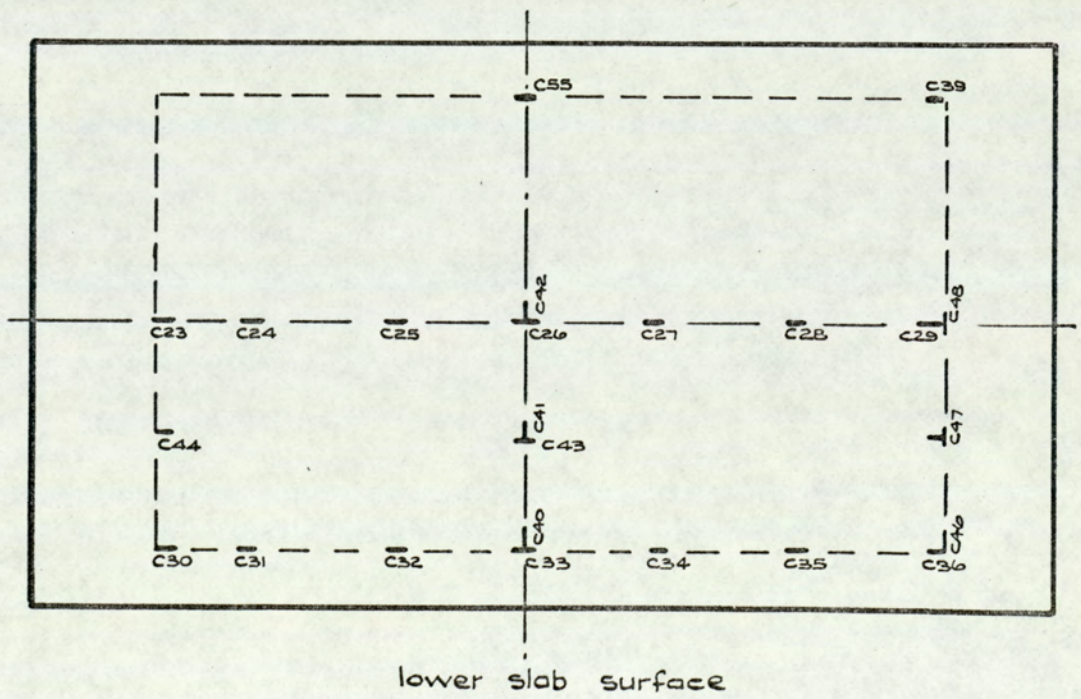


Fig. 9.13. Location of concrete strain gauges test M_2 .

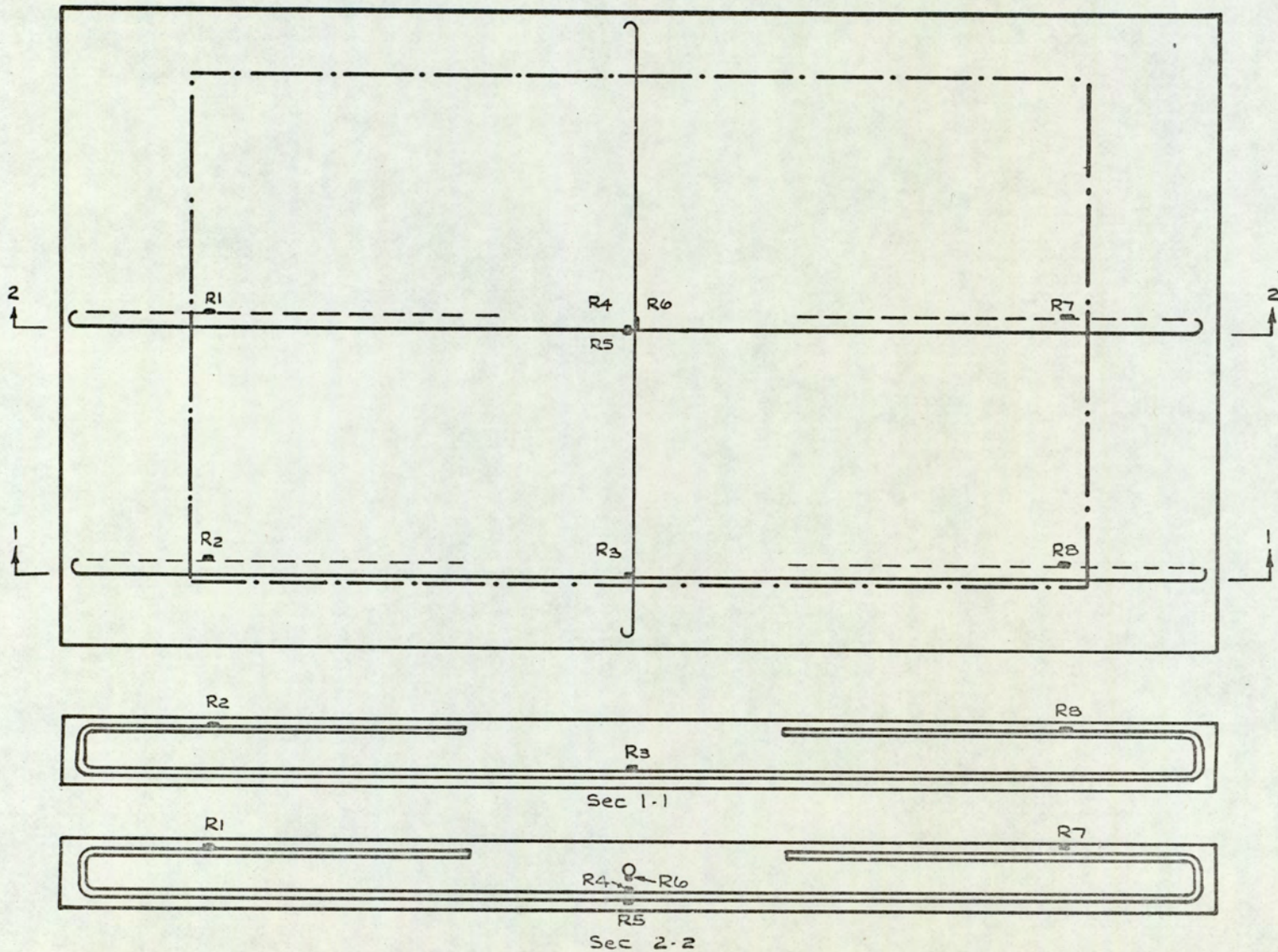


Fig. 9.14. Location of strain gauges on reinforcement bars. test M₂.

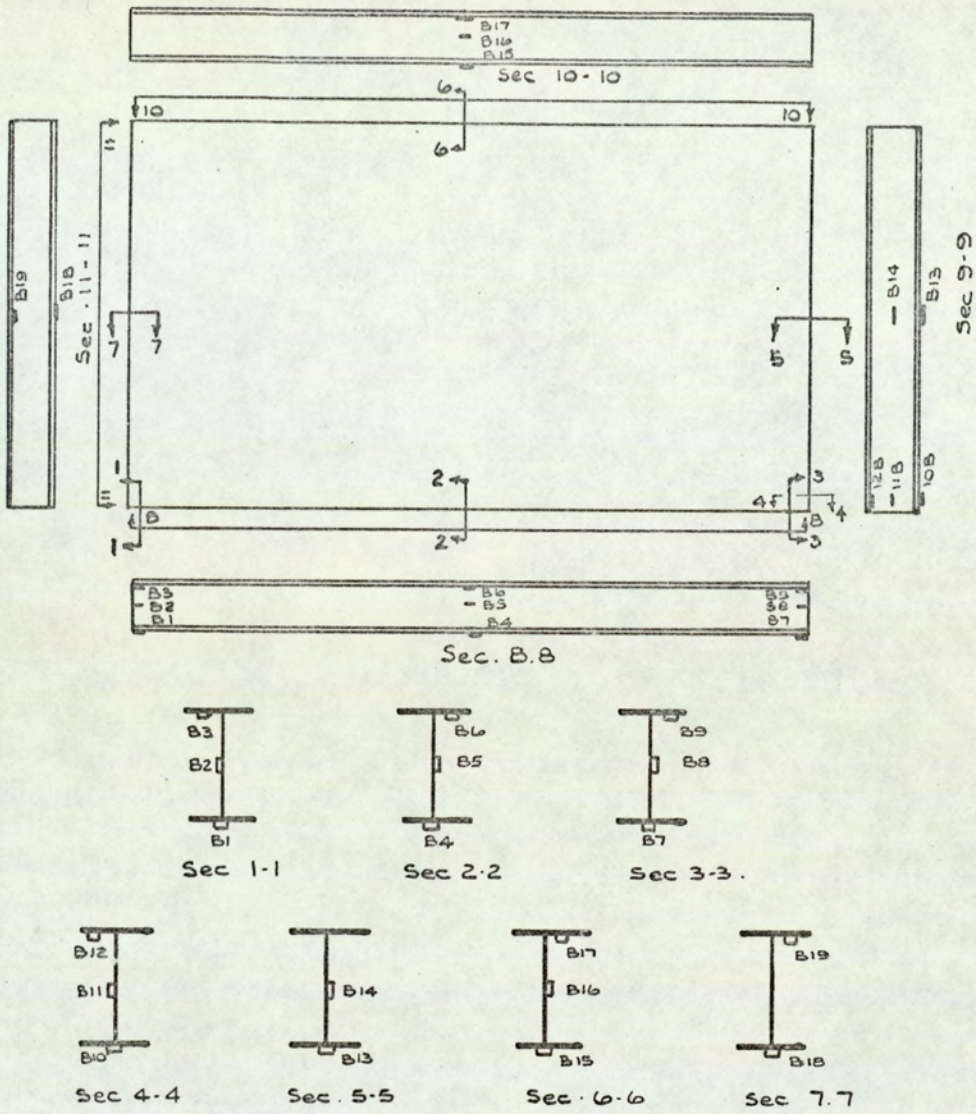


Fig. 9. 15. Location of strain gauges on the steel frame.
Test M2.

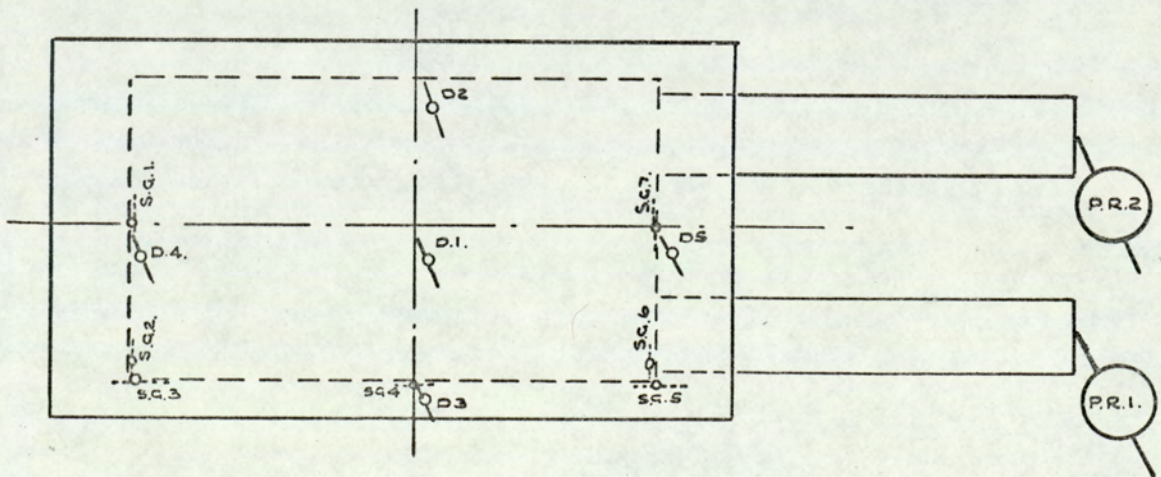


Fig. 9. 16. Location of deflection, slip and proving ring gauges.
Test M2.

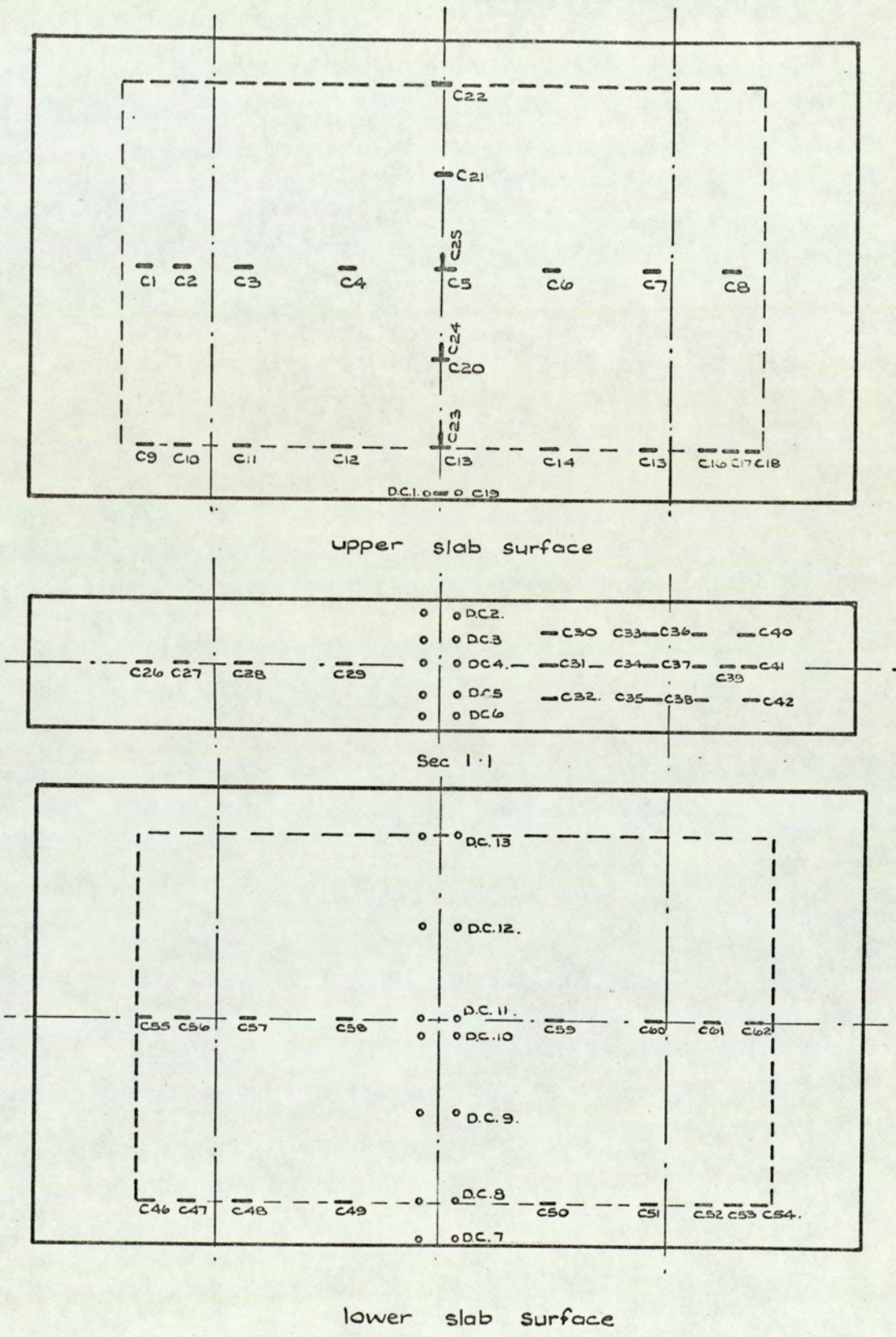


Fig. 9.17. Location of concrete electrical and demec strain gauges, test M₃.

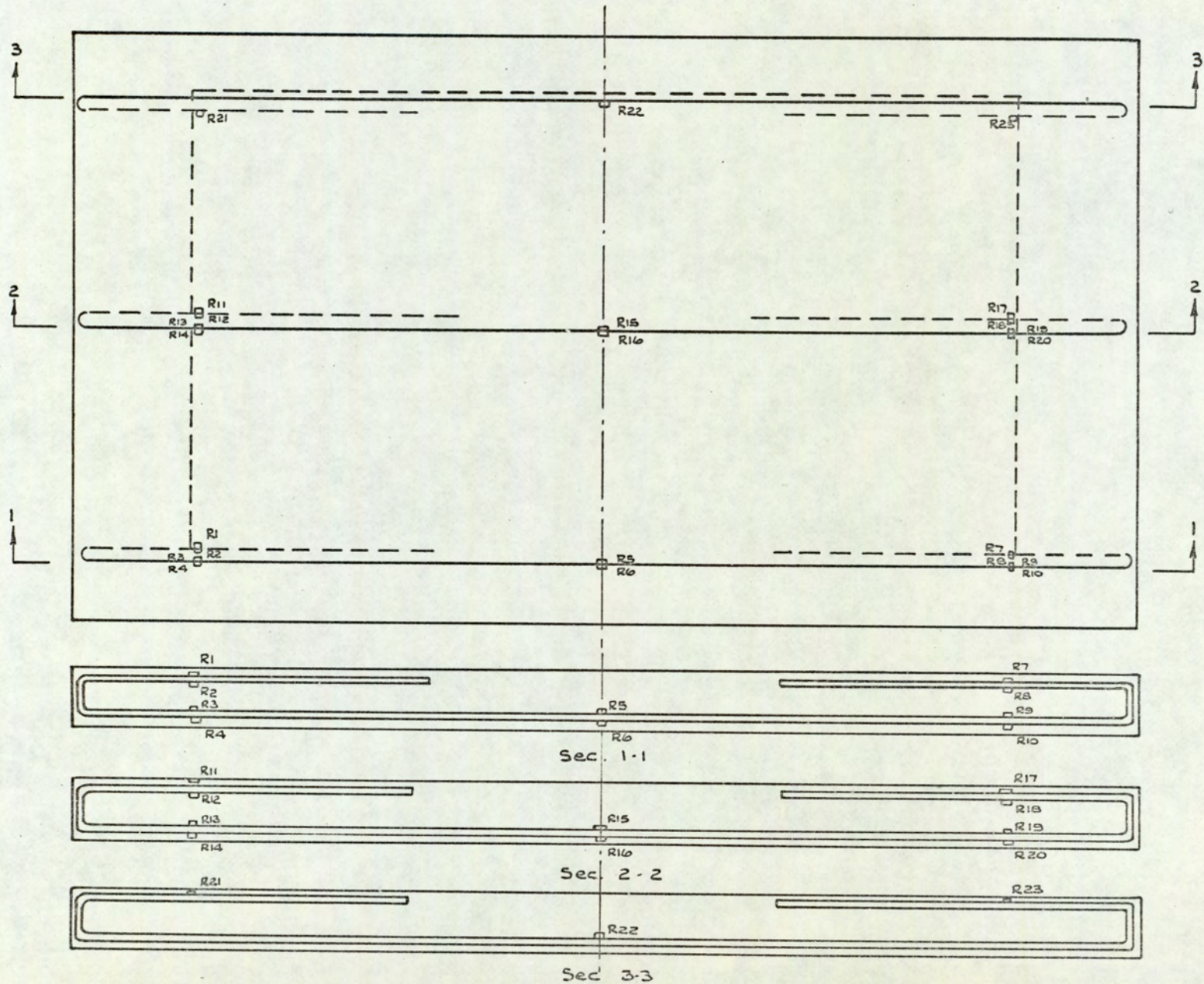
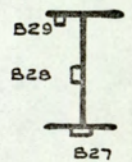
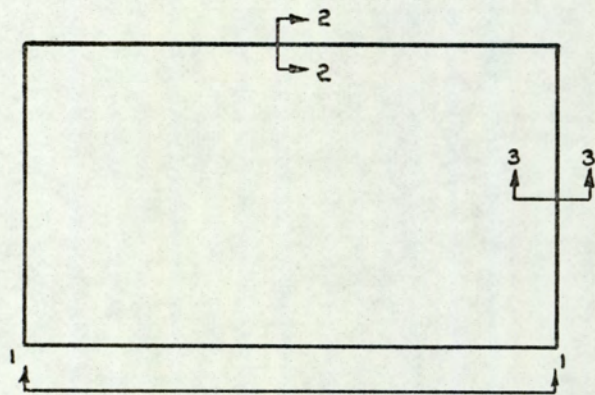
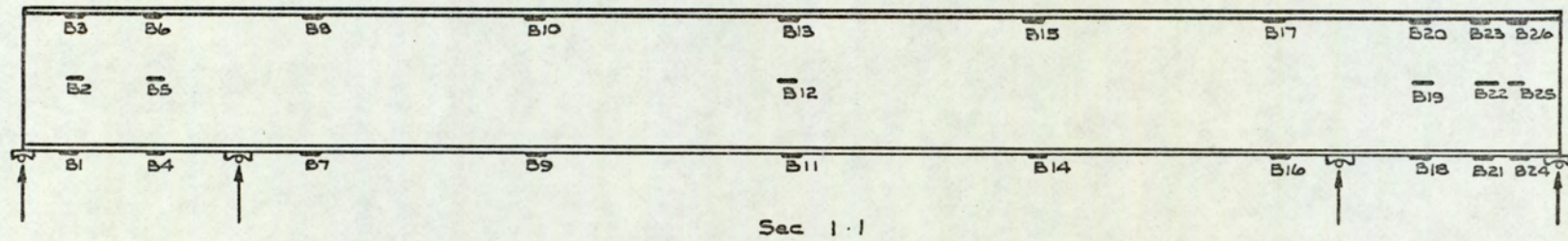
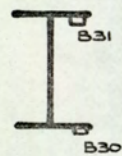


Fig. 9.18. Location of strain gauges on reinforcement bars test M-



Sec 2-2



Sec 3-3

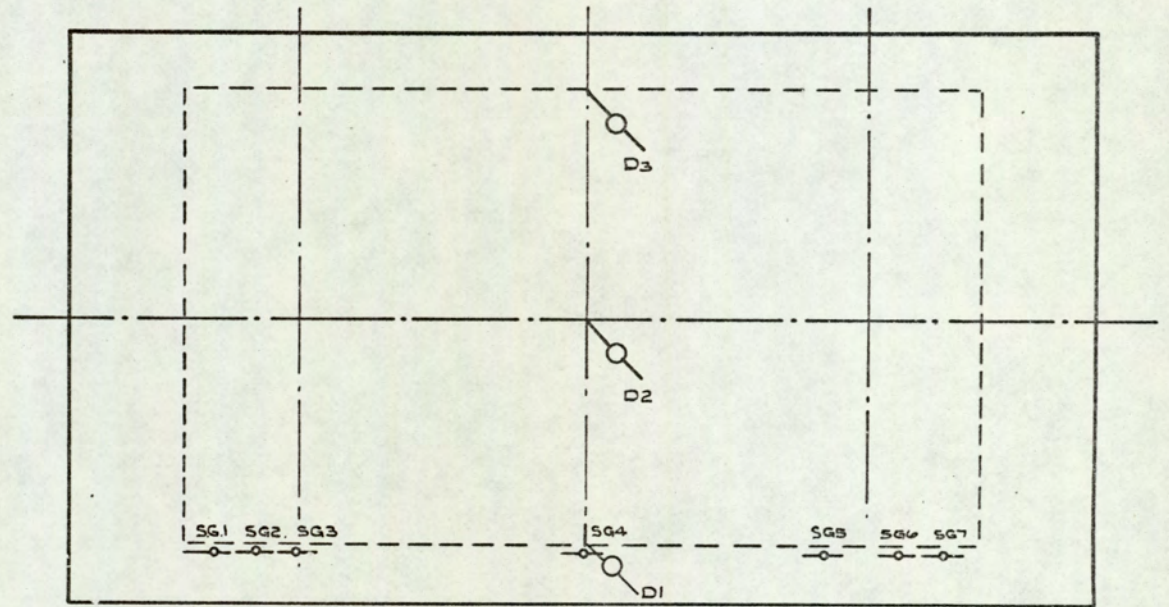
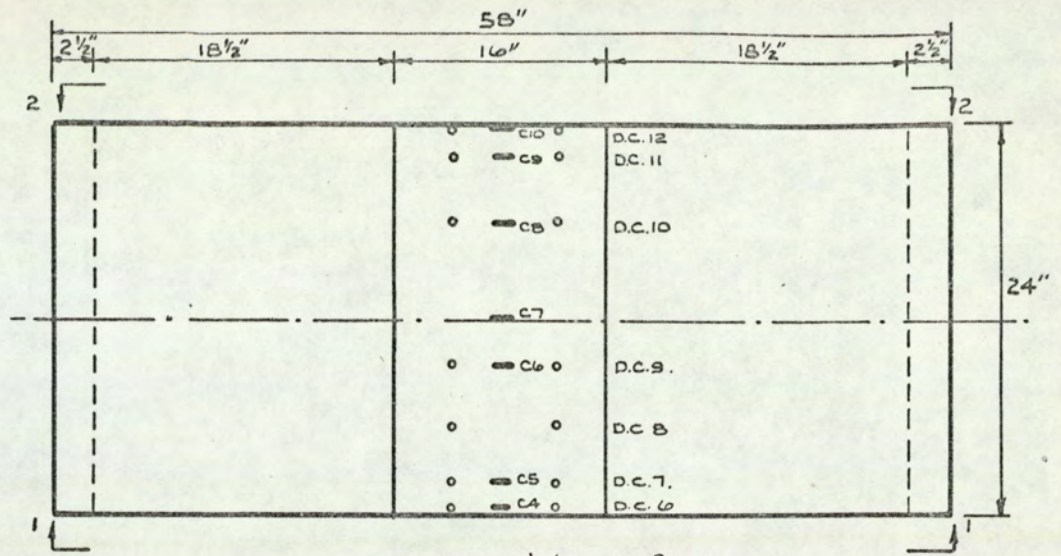
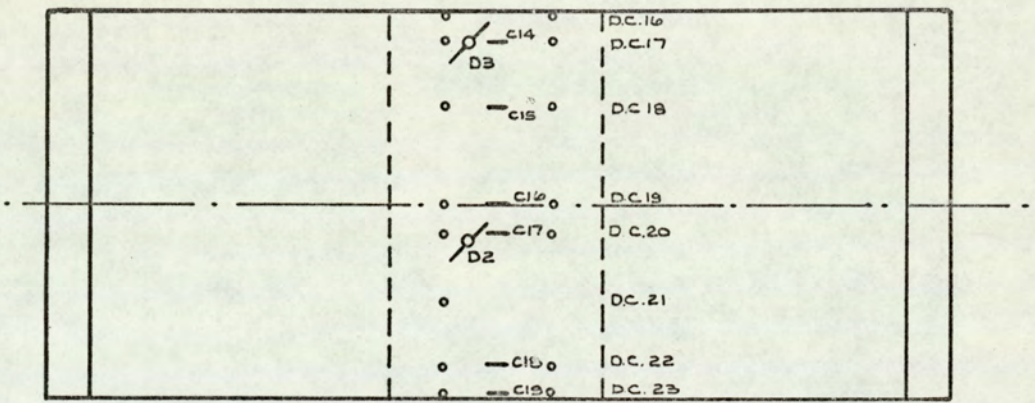


Fig. 9.19. Location of deflection & slip gauges. test $M_3 (C_1)$.

Fig.9. 20. Location of strain gauges on steel frame. test M_3 .



upper slab surface
location of electrical and demec strain gauges



lower slab surface

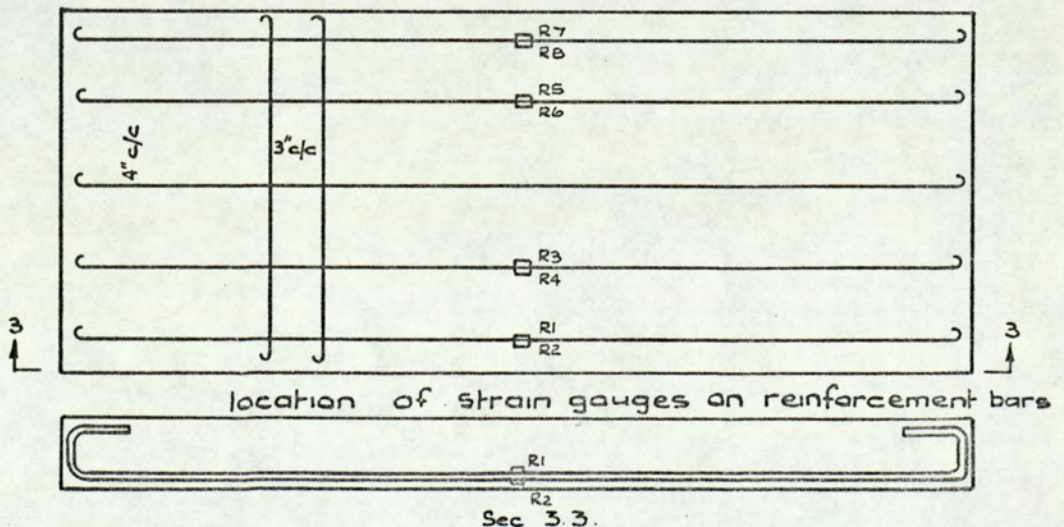
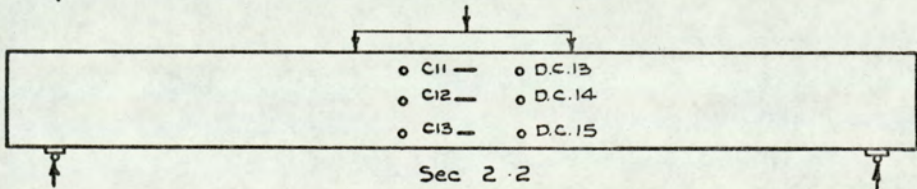
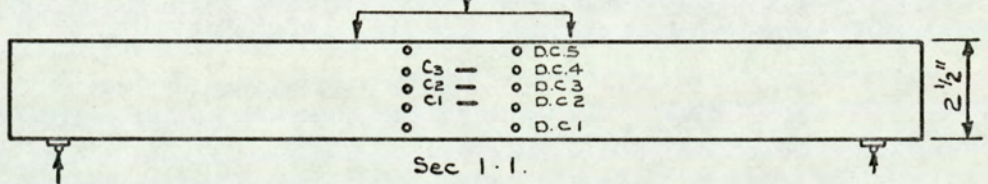


Fig. 9. 21. Dimensions and gauging of slab strips S₁ & S₂.

letters B, R and c respectively, followed by the number of each gauge. Similarly, for the deflection, slip, Demec and proving ring gauges, these were denoted by the letters D, S.G., D.C. and P.R. respectively, followed by the number of each gauge.

The experimental behaviour of the composite beam and slab floor models will be discussed in the next chapter.

C H A P T E R 1 0

THE EXPERIMENTAL BEHAVIOUR OF COMPOSITE BEAM AND SLAB FLOOR SYSTEMS

10.1 INTRODUCTION

After completion of the tests described in the previous chapter, graphs of deflection and strain were plotted to illustrate the experimental behaviour of the composite beam and slab floor models. This chapter contains a discussion of this behaviour for each individual test, and where relevant, comparisons are made between the tests.

10.2 TEST M₁

An overall picture of the behaviour of this model is provided by Figure 10.1, which shows the load deflection graphs for the centre of the slab and the mid-spans of the supporting beams. The central deflection of the slab increased linearly until a load of 14.0 tons, after which there were cracks in the lower slab surface parallel to the transverse central line. The mid-span deflection of the two main beams followed that of the slab centre closely up to collapse. This was due to the effect of composite action between the supporting beams and the slab, as the slab and the two main beams behaved as T-beams. As expected, the longer main beams deflected more than the secondary beams. Failure of the model occurred at a deflection of the slab centre equal to 1.1 in. and of the mid-spans of the main beams equal to 1.0 in. and 0.8 in.

Tension cracks at the supports on the top surface of the slab along the secondary beams started at a load of 18.0 tons. By the end of the test, these cracks were running along the full width of the slab and were 1/16 in. to 1/8 in. wide and 2 in. deep into the slab. Plates 13 and 14 show these cracks at both ends of the model.

The last recorded readings were taken at a load of 35.64 tons. An attempt to increase the applied load above this value resulted in continuous deflection of the slab centre and mid-spans of the main "edge" beams, after

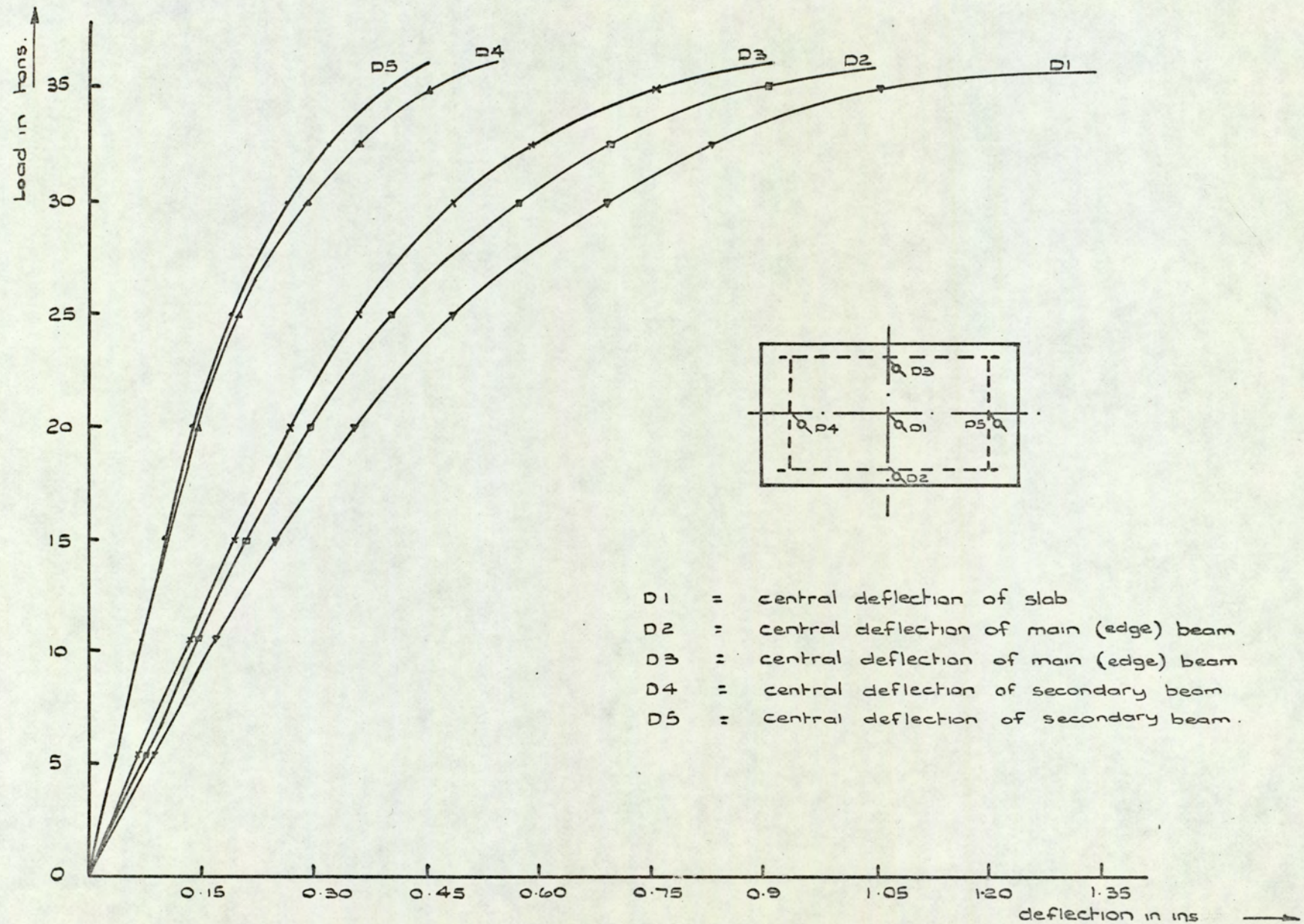


Fig. 10.1. Load against deflection graph for test M_1 .

which collapse of the model occurred. Thus the collapse load of model M₁ was considered to be 35.64 tons.

The picture may be enlarged upon by referring to Figures 10.2 to 10.8, showing the distribution of strain along the main beam and along and perpendicular to the slab centre line and the secondary beam on both slab surfaces. The first of these figures (Figure 10.2) shows that along the top of the main beam the concrete was predominantly in compression along most of the span, with tension at the supports. This is to be expected, the pattern following that of an encastré beam. At a load of 18 tons, no more readings were obtained from gauge c₁₃ (Figures 9.9 and 10.2), owing to a tension crack developed under the gauge at the support, seen in Plate 13. All tensile strains have been plotted as positive and compressive strains as negative.

Figure 10.3 shows the distribution of strain perpendicular to the transverse centre line of the top slab surface, where the whole width of the slab was in compression. The compression strain across the whole width of the slab was almost constant up to a load of 29 tons, after which a maximum strain of 1250×10^{-6} was recorded on the upper surface of the main beams at collapse. Figure 10.4 shows the strain distribution along the transverse centre line of the slab upper surface. As a two-way slab, a maximum compressive strain of 1000×10^{-6} was recorded at the centre, where maximum curvature in this direction occurred, and very little strain was recorded near the main beam where the slab was supported. Figure 10.5 shows the strain distribution along the secondary beam at the level of the upper slab surface. Again, as the slab was two-way, a maximum strain of 1600×10^{-6} occurred at mid-span. The strain distribution is similar to that of Figure 10.4, except that the strains recorded along the composite section upper surface were higher than those recorded along the transverse centre line of the slab.

At the lower slab surface, Figure 10.6 shows the distribution of the

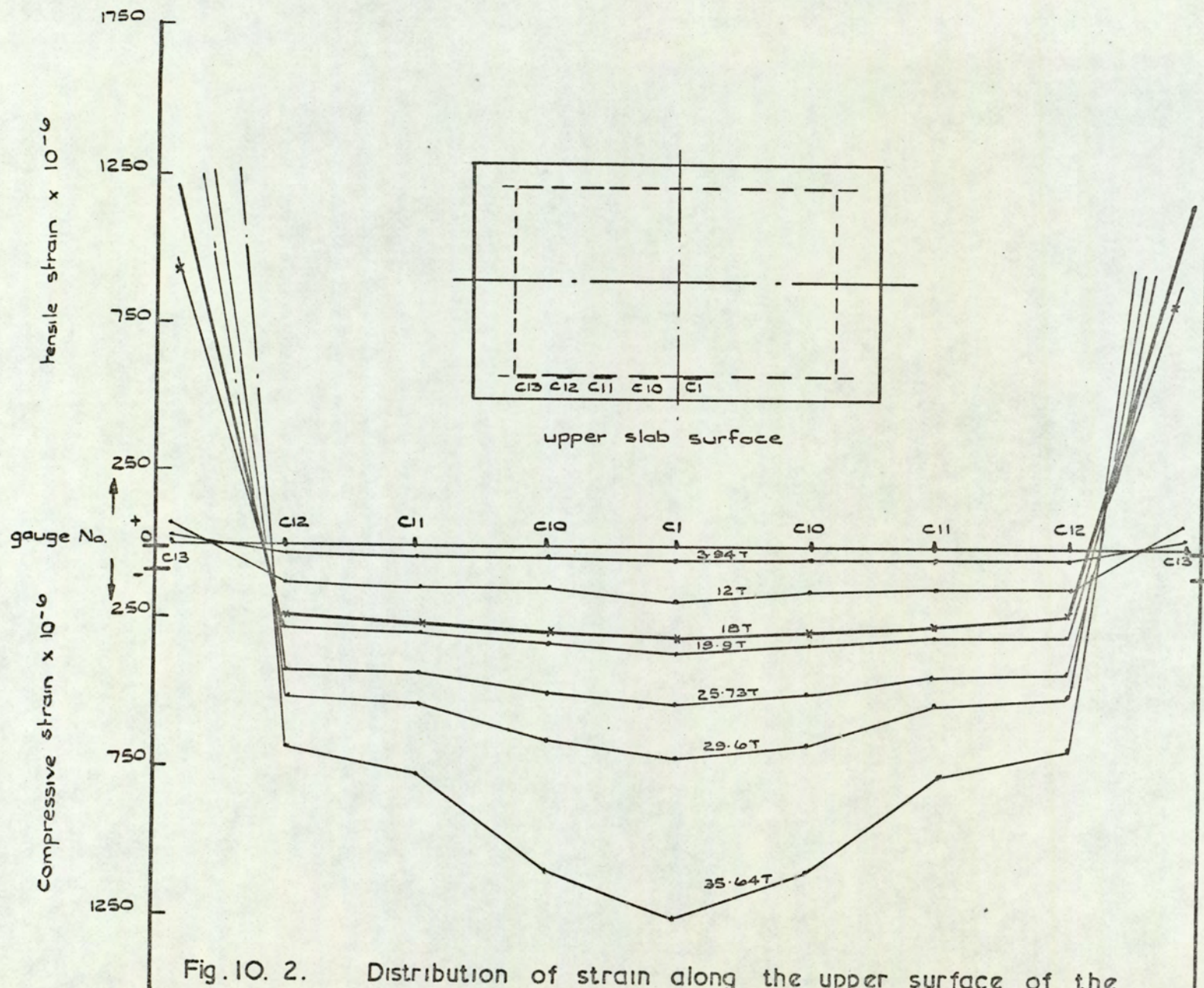


Fig. 10. 2. Distribution of strain along the upper surface of the main composite beam. Test M₁.

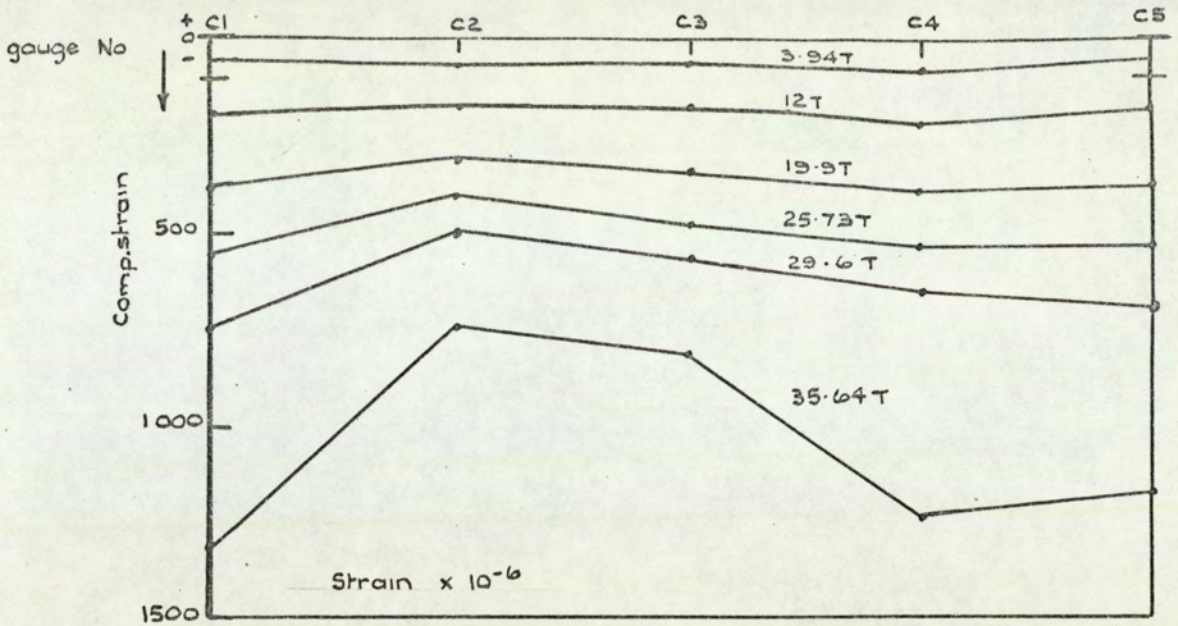


Fig. 10.3. Distribution of strain \perp to the transverse ℓ of the slab upper surface. Test M_1 .

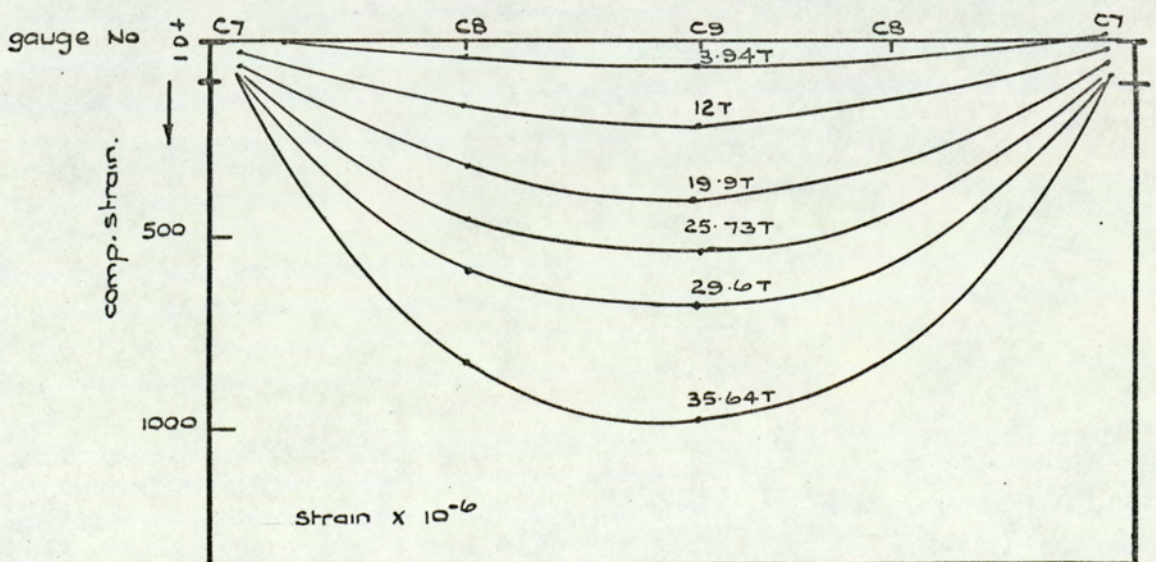
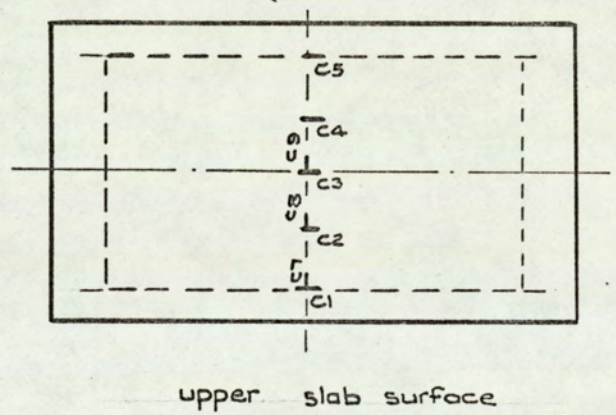


Fig. 10.4. Distribution of strain along the transverse ℓ of the slab upper surface. Test M_1 .

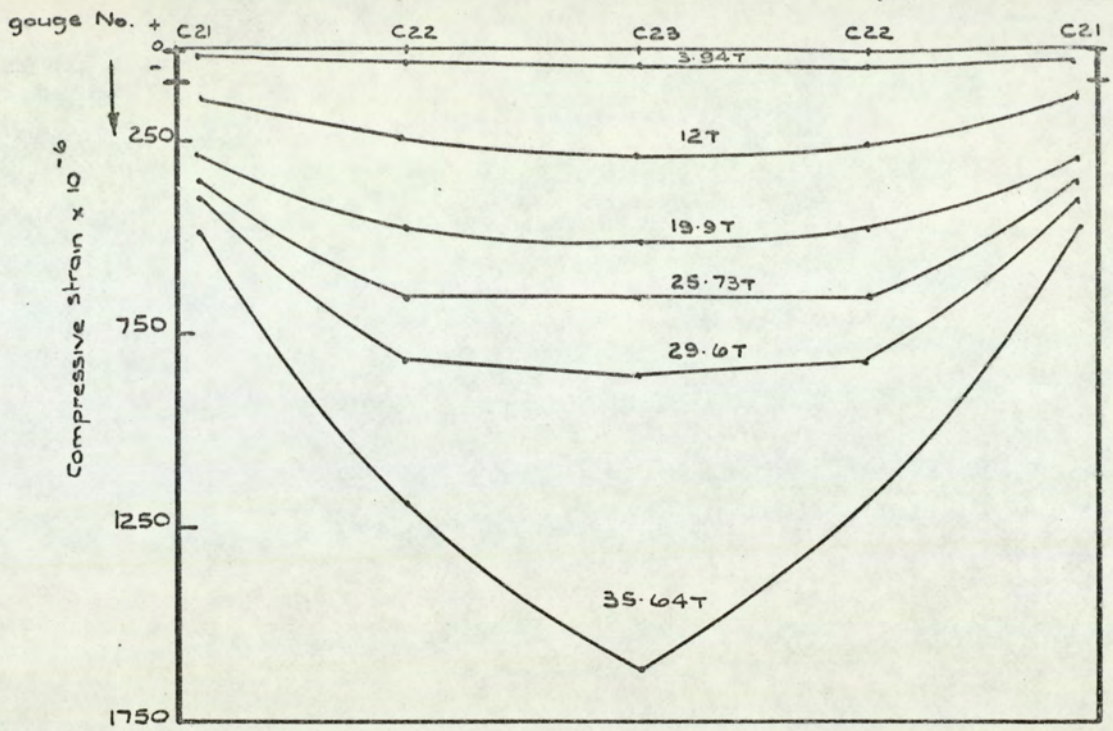


Fig.10.5. Distribution of strain along the secondary beam. upper slab surface. Test M1.

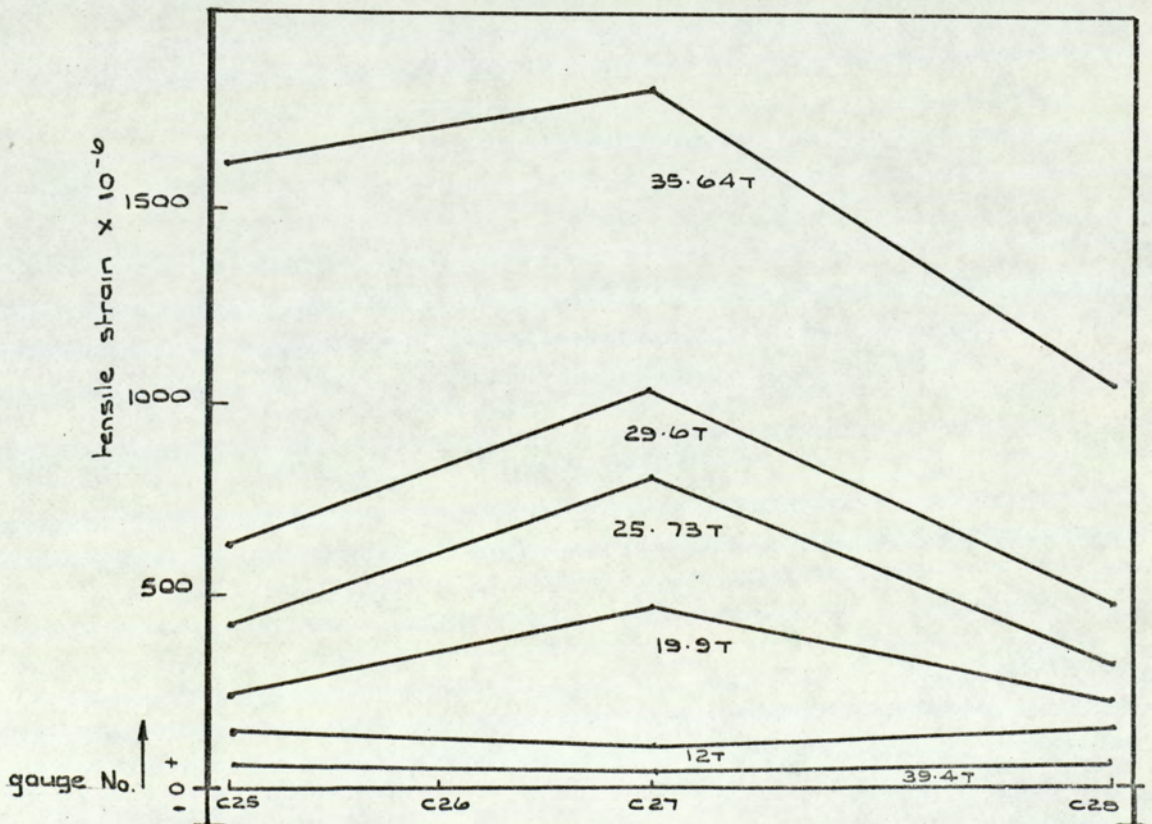
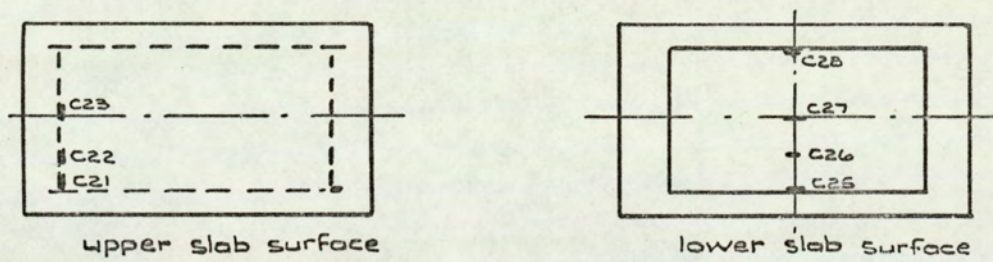


Fig.10.6. Distribution of strain \perp to the transverse E of the lower slab surface, Test M1.

strain perpendicular to the transverse centre line of the slab. Considerable tensile strains were recorded across the whole width of the slab with a maximum of 1750×10^{-6} recorded at mid-span before collapse. This indicates that along the whole width of the composite main beams and slab, the neutral axis was within the concrete composite slab, as expected. This also indicates that considerable tensile forces were present in the slab reinforcement, which contributed considerably to the ultimate strength of the composite sections. The strains recorded by Gauges c_{29} , c_{30} , c_{31} and c_{32} (Figure 9.9) along the transverse centre line of the lower slab surface were very small, in the region of 100×10^{-6} , compared with those of Figure 10.4 for the upper slab surface.

At the supports, considerable tensile strains, in the region of 700×10^{-6} , were recorded on the upper slab surface at a load of 16 tons by gauges c_{13} to c_{17} (Figure 9.9), which were perpendicular to the secondary beam. At a load of 18 tons, no more strain readings were obtained from these gauges, owing to cracks forming underneath them, which ran along the secondary beam across the full width of the slab, as can be seen from Plate 13. At the lower slab surface perpendicular to the secondary beam, the strain distribution across the whole width is shown in Figure 10.7, where considerable compressive strains were recorded with a maximum of 2250×10^{-6} . This figure indicates that the continuity produced by the lever arms during the loading procedure was not uniform across the full width of the slab. The distribution of strain along the secondary beam at the lower slab surface is shown in Figure 10.8, where the whole width was in tension with a maximum tensile strain of 2000×10^{-6} recorded at mid-span. This was due to the sagging of the composite secondary beam, and indicates that the neutral axis in this direction was also within the composite concrete slab and that the tensile forces in the transverse reinforcement contributed a considerable amount to the strength of the composite section in preventing collapse by mode A.

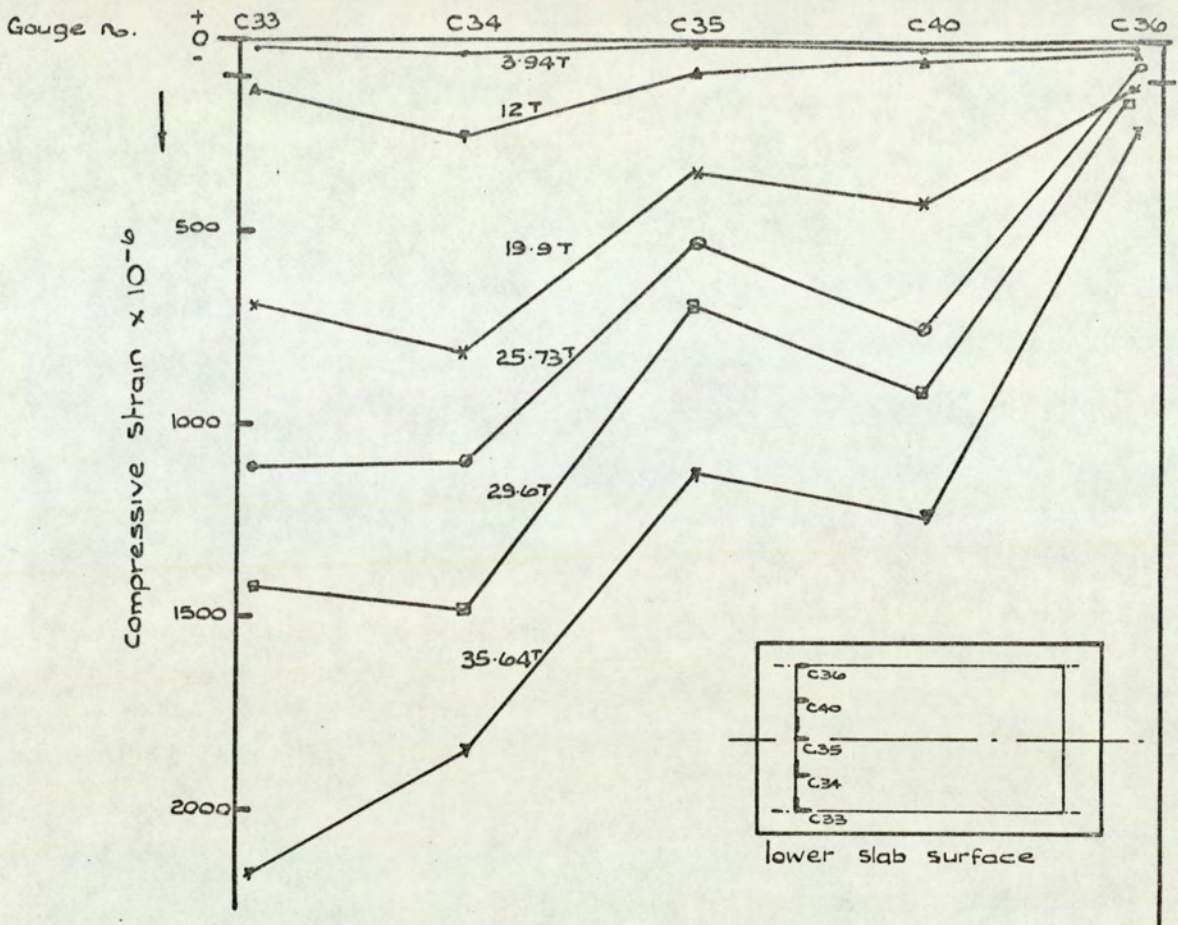


Fig. 10.7. Distribution of strain \perp to secondary beam. Lower slab surface. test M₁.

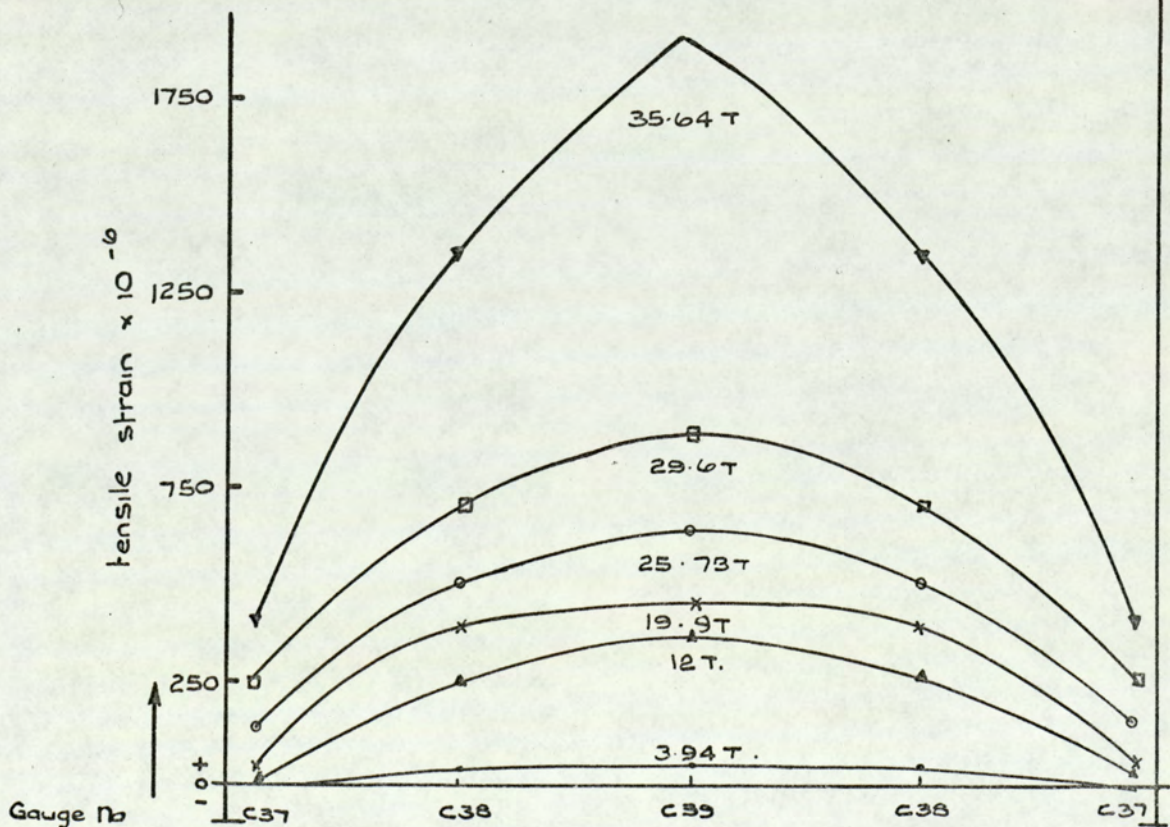


Fig. 10.8. Distribution of strain along the secondary beam. Lower slab surface test M₁.

The load against strain graph of Figure 10.9 for mid-span of the main composite beam gives some idea of the load at which a plastic hinge formed there. The shape of the load-strain relationship was similar to that of the load-deflection graph of Figure 10.1. The recorded tensile strain in the lower flange of the composite beam (Gauge B₁) was 1200×10^{-6} at a load of 28 tons. This may be compared with the strain in the lower flange at onset of yield of the 3 in. \times 1 $\frac{1}{2}$ in. \times 4 lbs./ft. R.S.J. of 1200×10^{-6} (Figure 9.3). At a load of 32 tons, the middle of the web of the composite beam (Gauge B₂) yielded, at a recorded tensile strain of 1250×10^{-6} . At the collapse load of 35.64 tons, the recorded tensile strain in the upper flange of the beam (Gauge B₃) was 1000×10^{-6} . Attempts to increase the applied load above 35.64 tons resulted in a continuous deflection of the composite beam at mid-span, which indicates that the whole composite section at mid-span went plastic forming a plastic hinge there, after which collapse occurred.

A set of two strain gauges were fixed to the upper and lower surfaces of the longitudinal reinforcement at mid-spans of the main beams and the centre of the slab (Figure 9.10). Unfortunately, the gauges fixed to the lower surfaces of the reinforcing bars were broken. However, Gauge R₁, which was under a combination of bending compressive strain and direct tensile strain, at the upper surface of the reinforcing bar, recorded a tensile strain of 500×10^{-6} before collapse. Similar readings were recorded from Gauges R₃ and R₅ (Figure 9.10). These indicate that the lower surfaces of these bars, which were both under a combination of tensile bending strain and direct tensile strain, had much higher tensile strains which contributed considerably to the ultimate strength of the composite sections. Gauges R₂, R₄ and R₆ of Figure 9.10 recorded tensile strains of 100×10^{-6} , 540×10^{-6} and 250×10^{-6} respectively before collapse for the transverse reinforcing bars at the same level and position as those of the longitudinal reinforcement. These strains were less than the strains

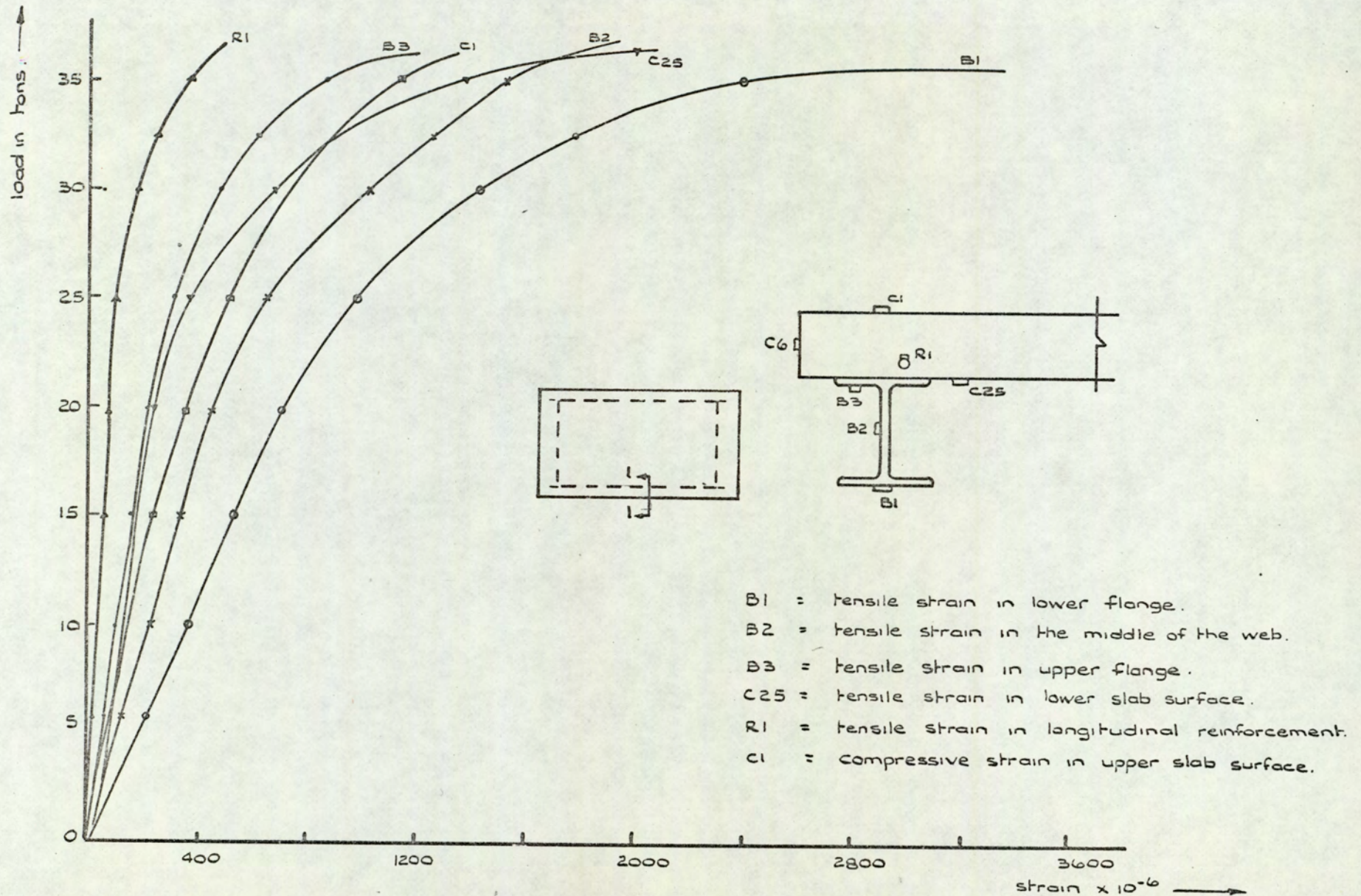


Fig. 10. 9. Load against strain graph for composite beam and slab at mid-span. Test M₁.

recorded on the longitudinal bars at the same level. The load-strain behaviour at mid-span of the other composite main beam (Section 7-7, Figure 9.12) was similar to that of Figure 10.9 (Section 1-1, Figure 9.9).

The strains recorded at the supports of the main beams were not as expected. Although the rotation of the secondary beams during the loading procedure was prevented by the lever arms attached to them, there was a small space between the flanges of the outer lever arms and the centre lines of the main beams in which the secondary beams were able to rotate. Since the secondary and main beams were welded together, the secondary beam rotation resulted in a tensile force being exerted on the lower flange of the main beam at the supports and causing it to be in tension rather than compression. Figure 10.10 shows load against strain at the support of the main beam (Section 2-2, Figure 9.12). The lower flange of the beam (Gauge B₄) yielded in tension instead of compression at a load of 30 tons. The middle of the web of the beam (Gauge B₅) yielded in compression at the collapse load of 35.64 tons and the upper flange (Gauge B₆) recorded about 500 micro strains in compression at collapse. Gauge R₇ on the upper surface of the hogging reinforcing bar (Figure 9.10) recorded a tensile strain of 600×10^{-6} at a load of 23.5 tons, after which no more readings were obtained. Gauge R₉ (Figure 9.10) at the opposite support recorded a tensile strain of 14.00×10^{-6} at collapse, whilst Gauge R₈ at the lower surface of hogging reinforcing bar at mid-span recorded a tensile strain of 3350×10^{-6} at collapse. This indicates that all the hogging reinforcement yielded when collapse occurred. The local deformation of the main beam at the support, as shown in Plate 7, affected the whole set of strain readings there and probably a plastic hinge would have formed there at a lower load. Similarly, local deformation occurred at the support of the other main beam (Section 6-6, Figure 9.12), and similar local deformation occurred in the lower flange of the secondary beam at both supports (Sections 3-3 and 5-5, Figure 9.12), owing to the rotation of the main beams during the loading

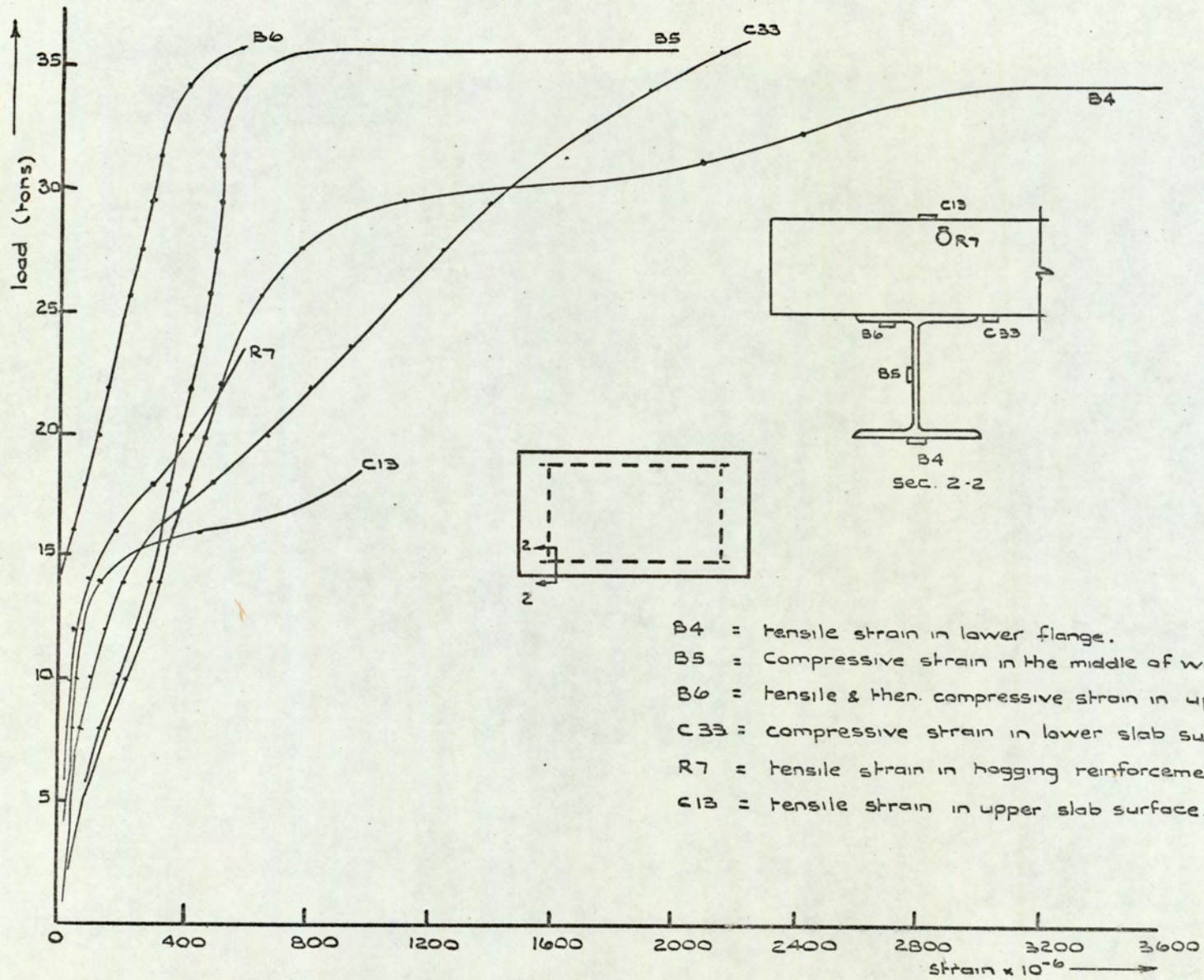


Fig. 10. 10. Load v. strain for main composite beam at support. Test M1.

procedure.

Figure 10.11 shows the distribution of strain through the composite main beam at mid-span (Section 1-1, Figure 10.9). The strain distribution through the section shows a high degree of composite action between the slab and the supporting beam, although Figure 10.11 shows evidence of a certain amount of slip, especially at higher loads. The maximum recorded slip between the slab and the main beam at this section (Gauge S.G.5, Figure 9.11) was 20×10^{-3} inch. This may be compared with the 80×10^{-3} inch slip for the ultimate capacity of the stud shear connectors obtained from the push out tests (Figure 9.6). Figure 10.11 also shows the tendency of the neutral axis to rise at higher loads, and indicates that the slab reinforcement had high tensile strains before collapse. This would contribute considerably to the ultimate strength of the composite section. The strain distribution through the mid-span of the other composite main beam (i.e. Section 7-7, Figure 9.12) is similar to that of Figure 10.11, owing to symmetry.

Figure 10.12 shows the strain distribution through the composite main beam at the support (Section 2-2, Figure 10.10). A reversal in stress to tension occurred at the lower flange of the beam, owing to local effects caused by the rotation of the secondary beam at the support. The lower half of the beam had a cross-sectional distortion about the X-axis, thus a different degree of composite action resulted at the support when compared with that at mid-span (Figure 10.11). Similarly, strain distribution through the other composite main beam at the support (Section 6-6, Figure 9.12) was found to have similar local deformation. The maximum recorded slip between the slab and the main beam at the support (Gauge S.G.6) before collapse was 26×10^{-3} inch. The Slip Gauges on the secondary beam recorded a maximum slip of 7×10^{-3} inch at the support (Gauge S.G.1). This demonstrates very lucidly that the stud shear connectors on the secondary and main beams were functioning adequately up to collapse of the model.

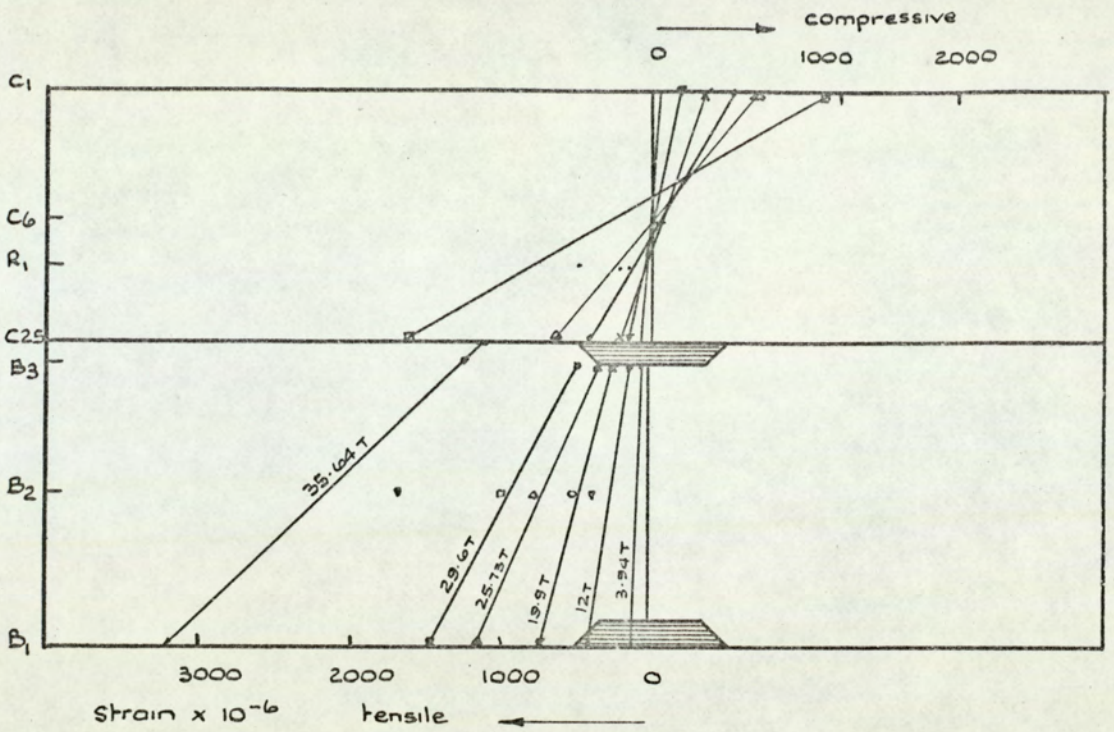


Fig. 10.11. Distribution of strain through main composite beam at mid-span. Test M1.

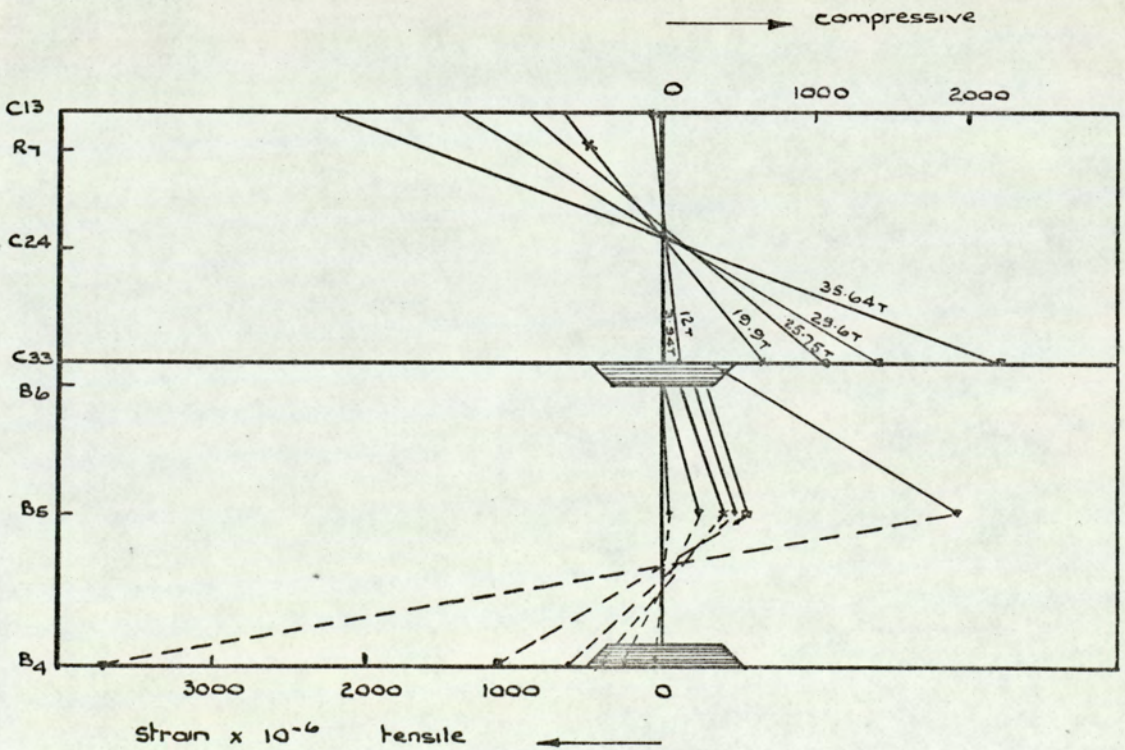


Fig. 10.12. Distribution of strain through main composite beam at support. Test M1.

Figure 10.13 shows the applied load against both end moments recorded by each of the two proving rings which were attached to the "moment" lever arms; the total for the two proving rings is also shown. The total moment recorded at each support were 13.1 kips-ft. and 12.8 kips-ft. These values were much lower than the theoretical values of 26.46 kips-ft. or 22.21 kips-ft., depending on whether or not composite action is assumed at the supports (Section 9.3.6). Obviously the tensile force readings obtained from these proving rings were affected by the local deformation at the supports and probably an external moment formed at the end of the lever arms affected these readings.

The collapse of the model occurred by mode B involving the two main "edge" beams and the slab as predicted. The final shape of the system after collapse is shown in Plate 15, where a maximum deflection occurred at the centre of the main beams and the slab at the supports was horizontal, owing to the restraint effects of the lever arms. After collapse, the shape of the cracks in the lower slab surface indicated a tendency for the yield lines associated with collapse by mode C to form, as shown in Plate 16. From this plate, it can be seen that several hogging yield lines formed across the whole width of the slab for about 12 inches on each side of the centre line, with the cracks running through more than half the slab depth from the underside, as shown in Plate 15. This is due to the bending moment in this region being constant as the loading was a four point loading system (Figure 9.7(d)).

10.3 TEST M₂

As explained in the previous chapter, the model was an exact replica of model M₁, except that the lever arms at one support were not fixed to the test rig, so that collapse by combined mechanism could be simulated. Improvements in the setting up of model M₂ were made to increase the stability of the jacks and to minimise local deformations at the supports by moving the lever arms as far apart as possible, so that the outer lever arms

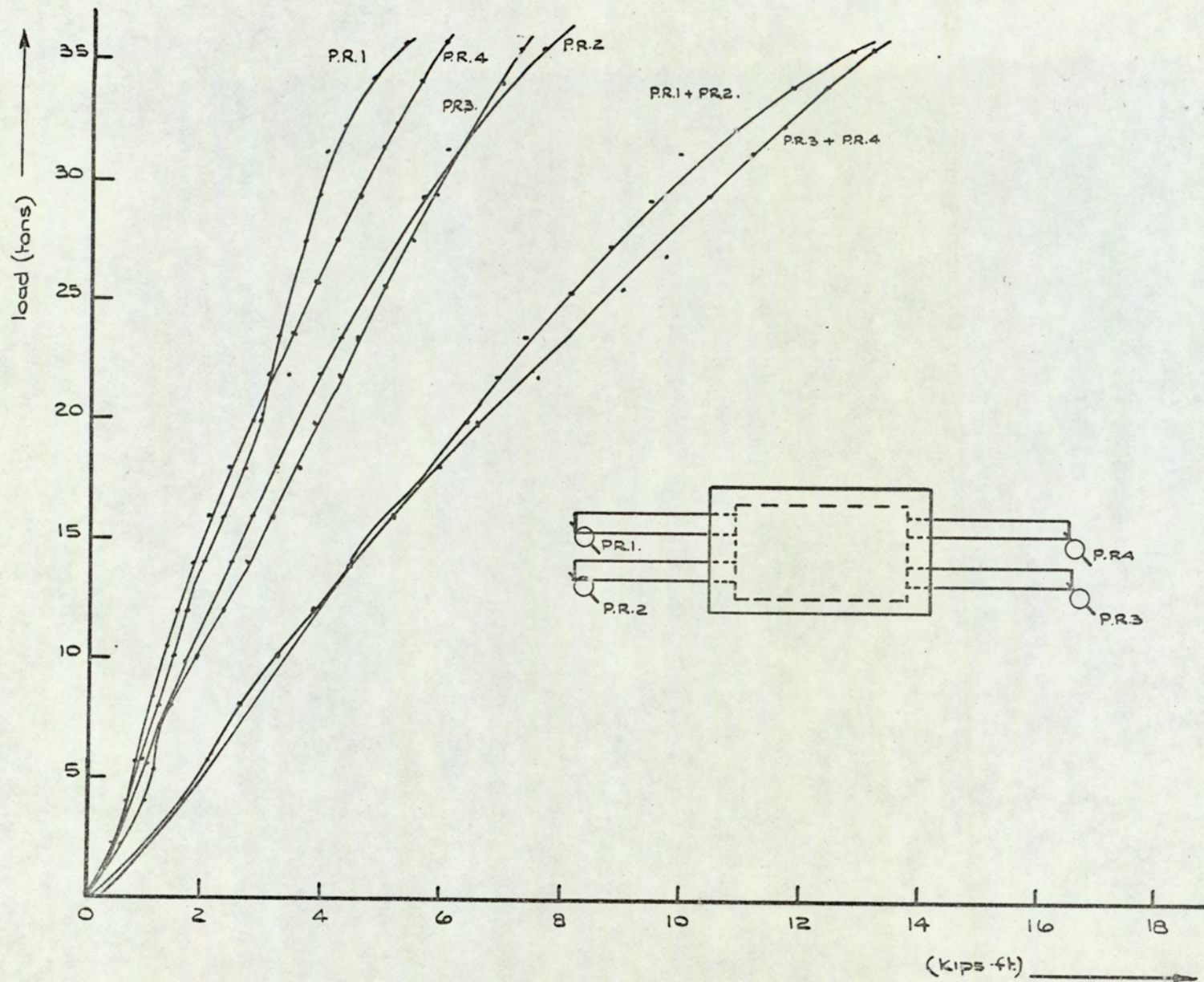


Fig. 10. 13. Load against end moment. Test M₁

came as near as possible to the main beams.

The load-deflection graph in Figure 10.14 shows very clearly the behaviour of the composite system in this test. The central deflection of the slab increased linearly until a load of 9 tons, after which cracks in the lower slab surface appeared. As in test M_1 , the central deflection of the slab was greater than that at mid-span of the composite main beams, which followed each other very closely up to collapse. The last recorded deflections at the centre of the slab and mid-span of the main beams (Figure 10.14) were 2.40 in., 2.05 in. and 1.95 in. respectively. These deflections were twice as much as those obtained from test M_1 at the same locations (Figure 10.1). As expected, the longer main beams deflected more than the secondary beams. The last recorded readings were obtained at a load of 37.92 tons. An attempt to increase the load above this value resulted in continuous deflection of Gauges D_1 , D_2 and D_3 at the centre of the slab and mid-span of the main beams (Figure 10.14), after which collapse of the model occurred.

The system tested was unsymmetrical, owing to the fact that one support of the model was fixed, whereas the other was simply supported. The strains, therefore, were measured along the whole length of the longitudinal slab centre line and the main beam at both slab surfaces. These strain distributions are representative of the bending moments in the slab and the composite beam respectively. Figure 10.15 shows the distribution of strain along the longitudinal centre line of the slab upper surface. Most of the slab span in this direction was in compression, reaching a maximum of 2200×10^{-6} (Gauge c_2). High tensile strains were recorded by Gauge c_1 at the simply supported end, owing to the restraint effects of composite action between the slab and the secondary beam. At the restrained end of the model, a strain of 1500×10^{-6} was recorded by Gauge c_7 at a load of 12 tons, after which the gauge was damaged, owing to cracks formed underneath it along the secondary beam. Figure 10.16 shows the distribution of the

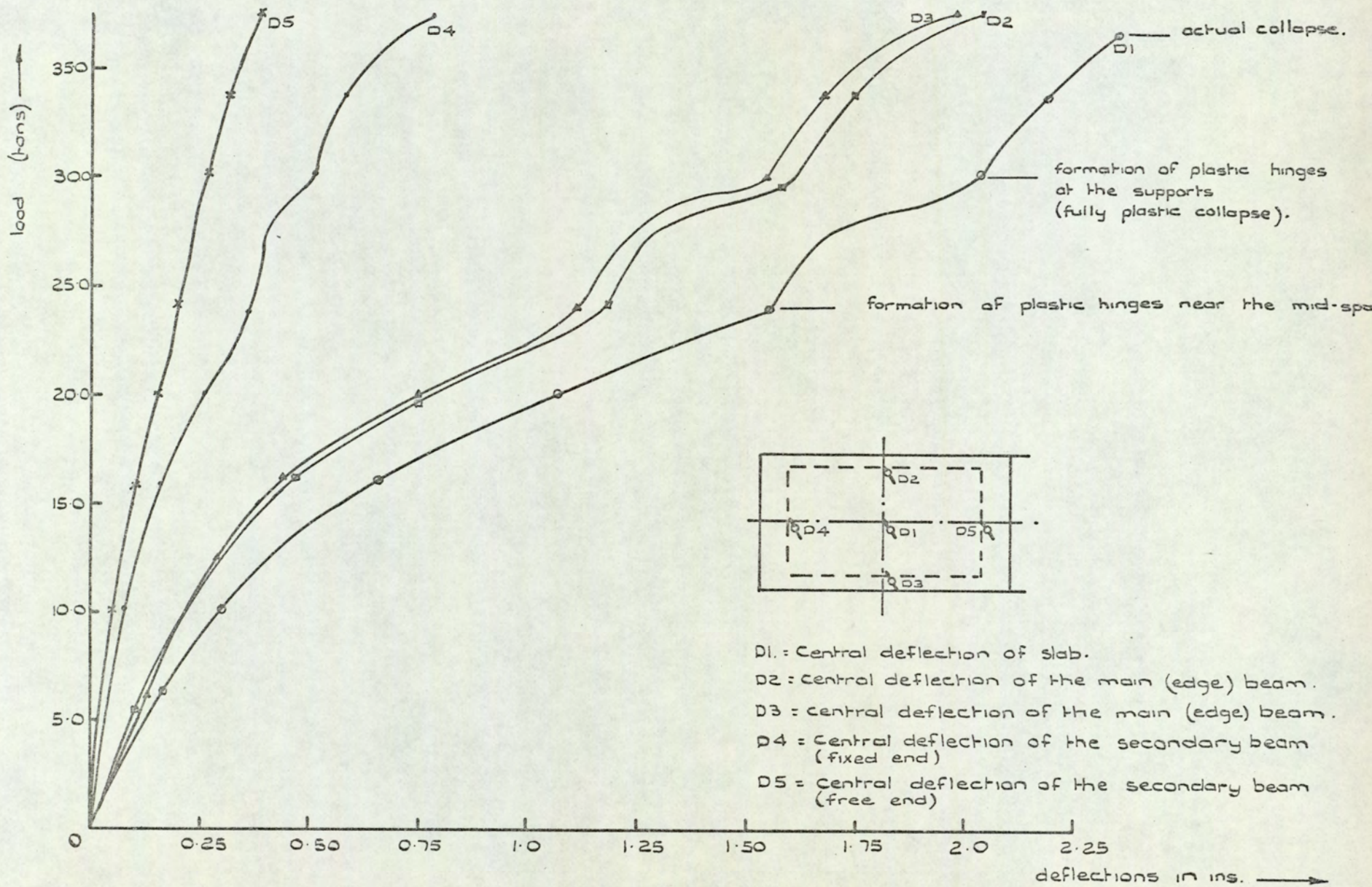


Fig. 10.14. Load against deflection graph for test M2.

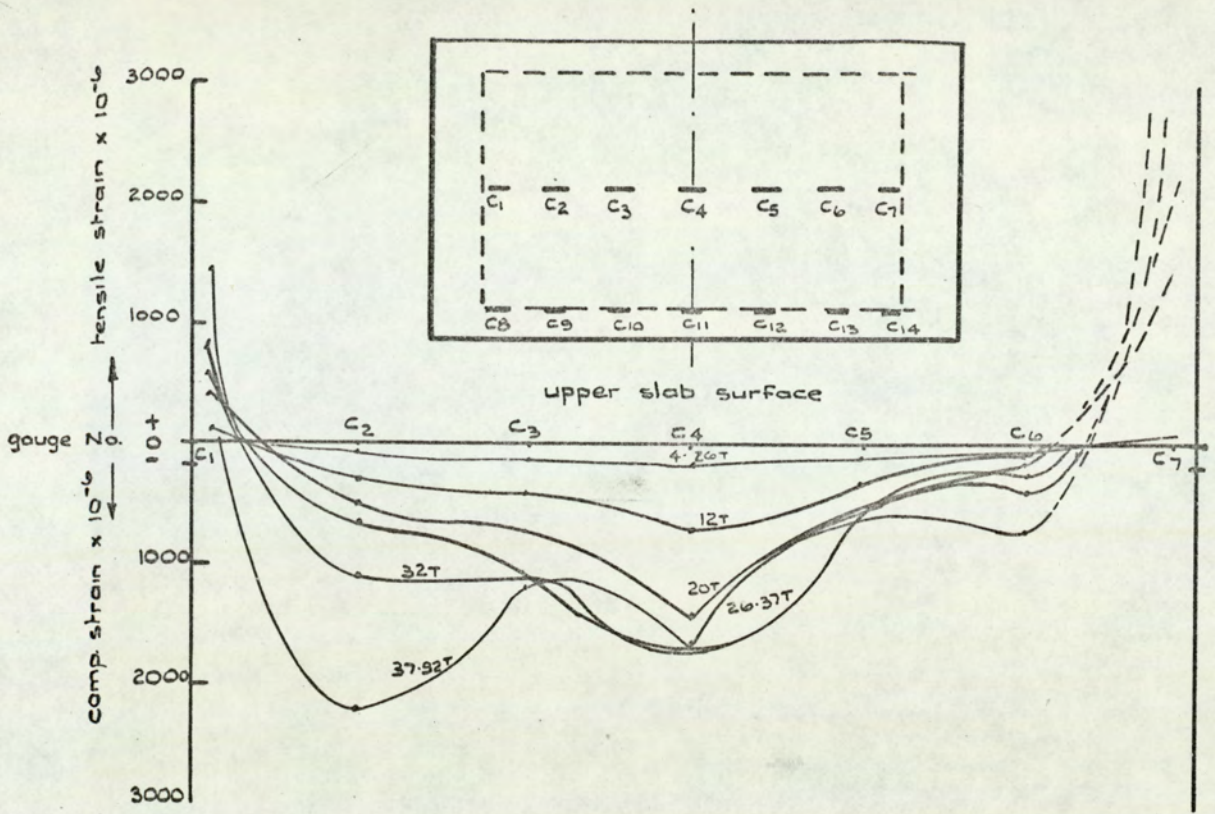


Fig 10.15. Distribution of strain along the longitudinal ξ of the upper surface of the slab. Test M₂.

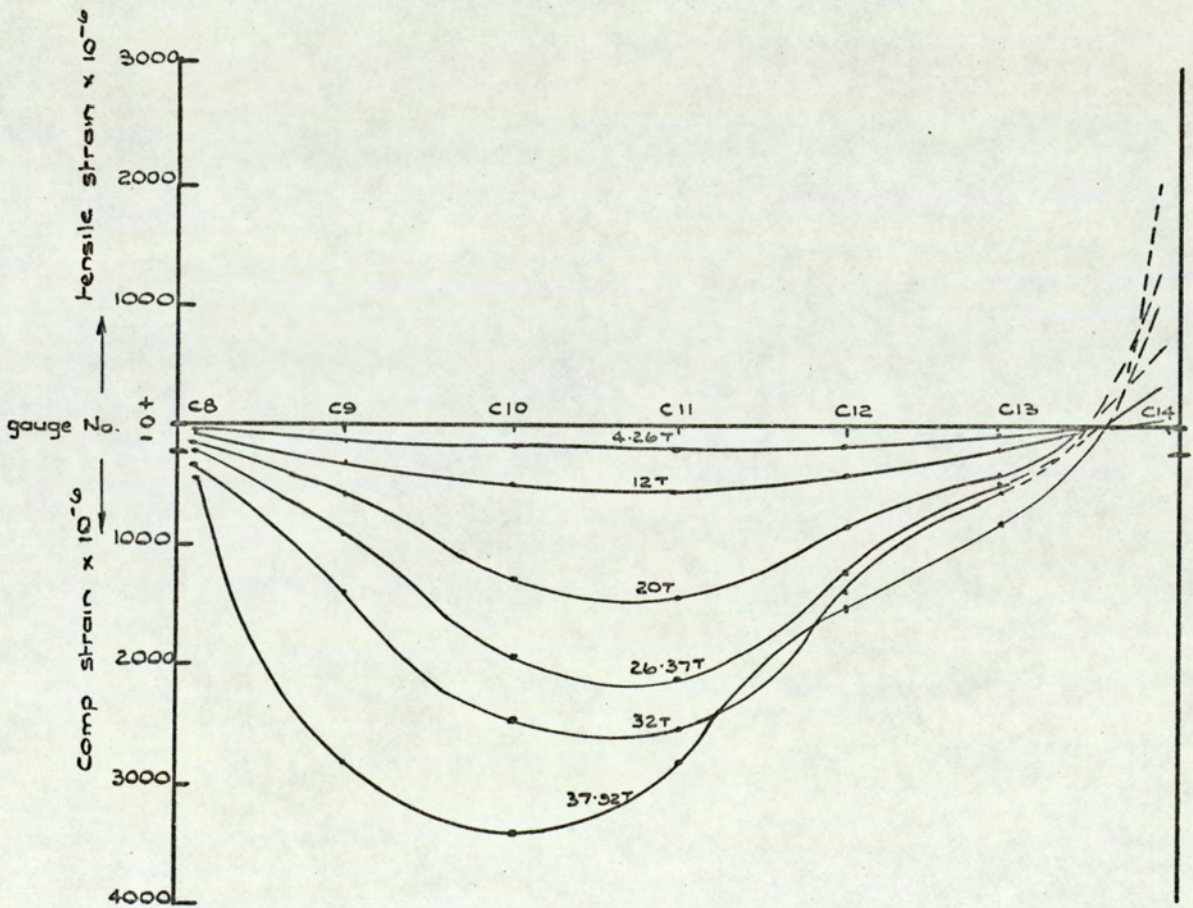


Fig. 10.16. Distribution of strain along the upper surface of the main composite beam. Test M₂.

strain along the composite main beam upper surface. This strain distribution represents the bending moment of the main composite beam. Over 90% of the span of the composite beam upper surface was in compression with a maximum of 3500×10^{-6} recorded by Gauge c_{10} before collapse. This figure indicates very clearly that the maximum bending moment did not occur at mid-span of the composite beam, as assumed, but about 10 in. off the centre towards the simply supported end. This is also confirmed by Plate 17, which shows the hogging yield lines at the lower slab surface across the full width formed off the centre line. Plate 18 shows the same hogging yield lines as those seen in Plate 17. Theoretically, yield lines forming off the centre line would be predicted for the combined mechanism case in multi-storey frames, when a plastic hinge assumed to form exactly at mid-span of the beam is only an approximation (see Section 8.3.2). Considerable strains were recorded along the main composite beam lower slab surface where a maximum tensile strain of 1800×10^{-6} developed between Gauges c_{32} and c_{33} (Figure 9.13) at a load of 22 tons, this became 3000×10^{-6} at collapse. Large tensile strains were also recorded along the longitudinal centre line of the lower surface of the slab (Figure 9.13), where most of the slab span was in tension.

Figure 10.17 shows the strain distribution perpendicular to the transverse centre line of the slab upper surface. The compressive strain distribution across the full width of the slab was almost constant at lower loads. Subsequently, it became a maximum (2800×10^{-6}) at the upper surface of the composite beam before collapse. At the centre of the slab, the maximum recorded compressive strain was 1700×10^{-6} at a load of 26 tons, after which slightly lower strains were recorded for increasing loads. These strain readings were twice as large as those recorded at similar locations during test M_1 (Figure 10.3). As the slab was two-way spanning, the strain distribution along the transverse centre line of the upper slab surface is shown in Figure 10.18. This strain distribution was similar to

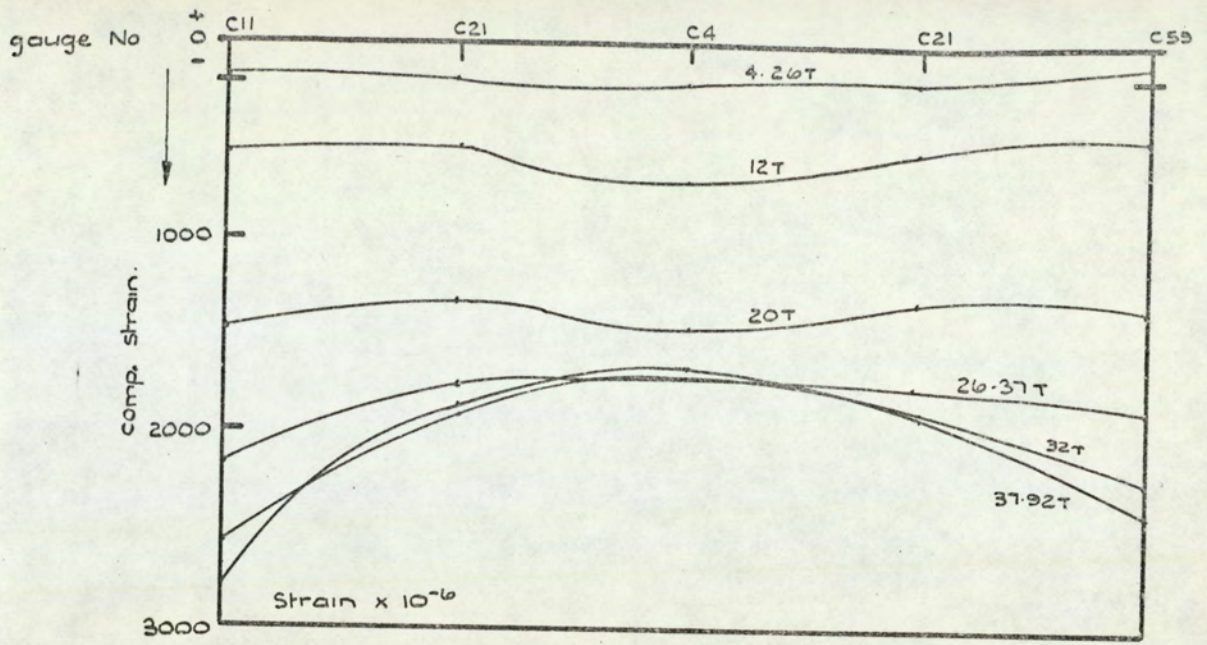
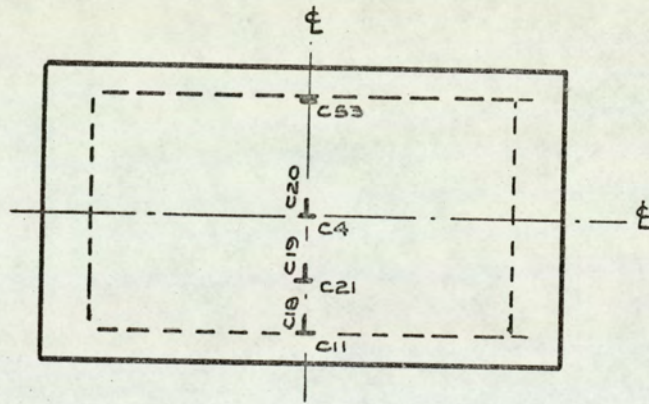


Fig. 10.17. Distribution of strain \perp to the transverse E of the slab upper surface. Test M₂



upper slab surface

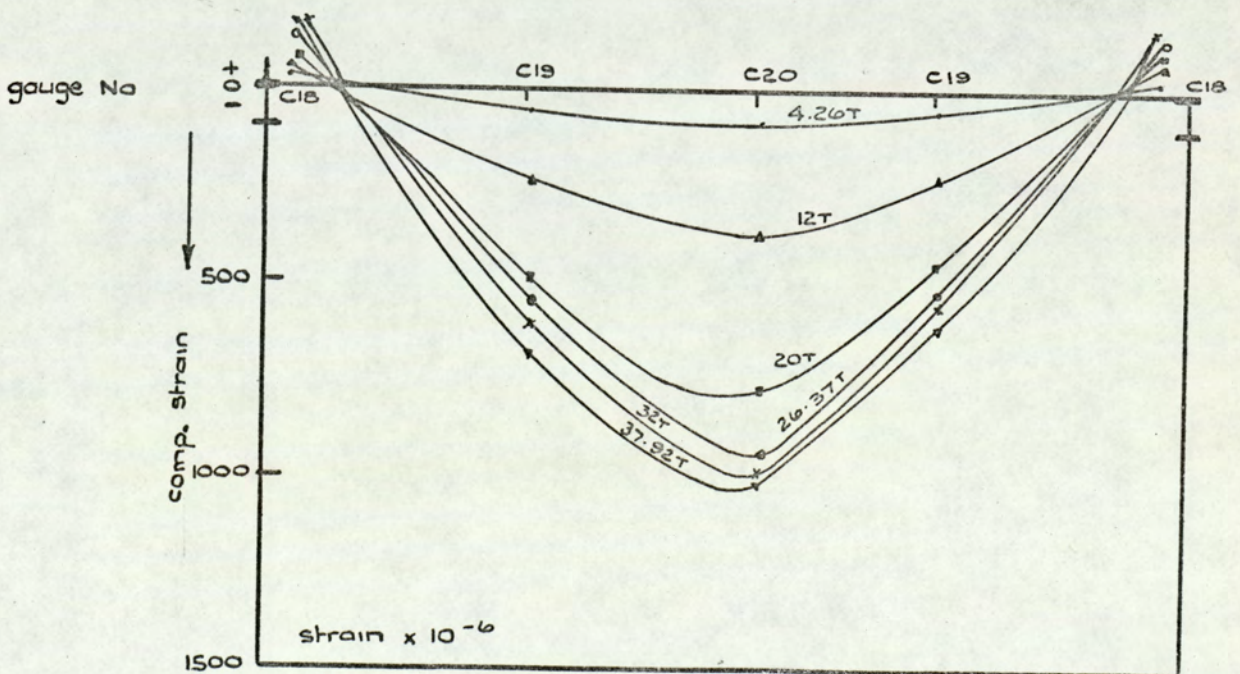


Fig. 10.18. Distribution of strain along the transverse E of the slab upper surface. Test M₂.

that of test M_1 (Figure 10.4) with approximately the same strain values, except that little tensile strain was recorded at the support by Gauge c_{18} .

Gauges c_{33} , c_{43} and c_{55} perpendicular to the transverse centre line of the lower slab surface (Figure 9.13) recorded very high tensile strains across the full width of the slab with a maximum of 2000×10^{-6} (Gauge c_{43}) at a load of 20 tons. Higher applied loads resulted in damage to these gauges, owing to cracks formed underneath them. As in test M_1 , this indicates that along the full width of the "two main beams and slab composite" the neutral axis was within the concrete slab as expected. It also indicates that considerable tensile forces were present in the slab reinforcement, especially 10 in. off the centre towards the free end where the bending moment was maximum (Figure 10.16), which contributed significantly to the ultimate strength of the composite sections.

At the fixed end, strain distribution perpendicular to the secondary beam on the upper slab surface was observed up to a load of 12 tons where a maximum tensile strain of 1500×10^{-6} occurred at the centre, as shown in Figure 10.19. Loads higher than 12 tons produced a hogging yield line along the secondary beam, which ran underneath the concrete gauges and damaged them, as can be seen from Plate 18. Figure 10.20 shows the distribution of strain along the secondary composite beam upper surface. As a two-way slab, the strain distribution was similar to that at mid-span of Figure 10.18, except that higher strains were recorded along the secondary beam. The strain values were similar to those recorded during test M_1 (Figure 10.5) at similar positions, except that of Gauge c_{15} , where tensile instead of compression strains were recorded. Figure 10.21 shows the strain distribution perpendicular to the secondary beam lower slab surface. The strain distribution in this direction was almost uniform across the full slab width up to a load of 12 tons, after which it became non-uniform. At collapse, the compression strains across the slab width varied between 2500×10^{-6} and 4000×10^{-6} . These compressive strains were twice as large

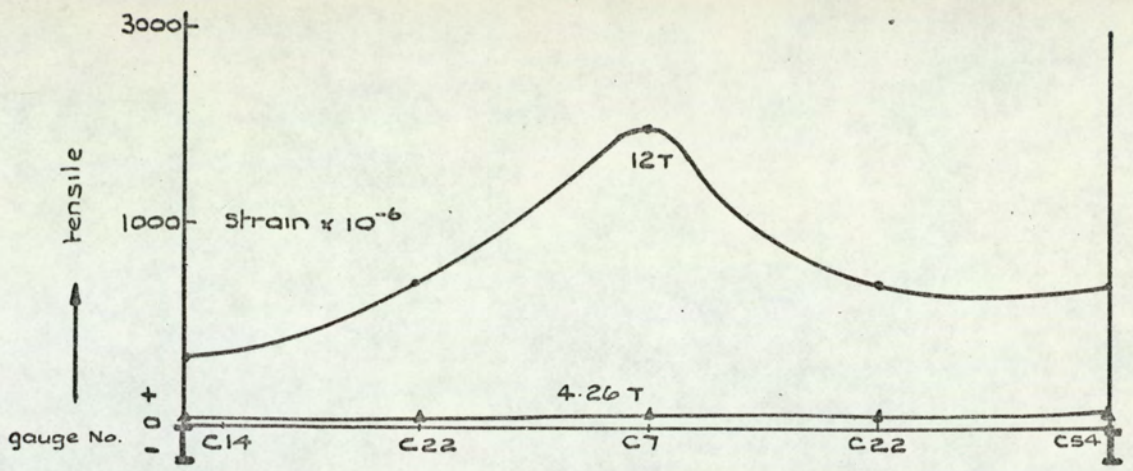


Fig. 10.19. Distribution of strain \perp to the secondary beam where the slab is continuous. Top slab surface. test M_2 .

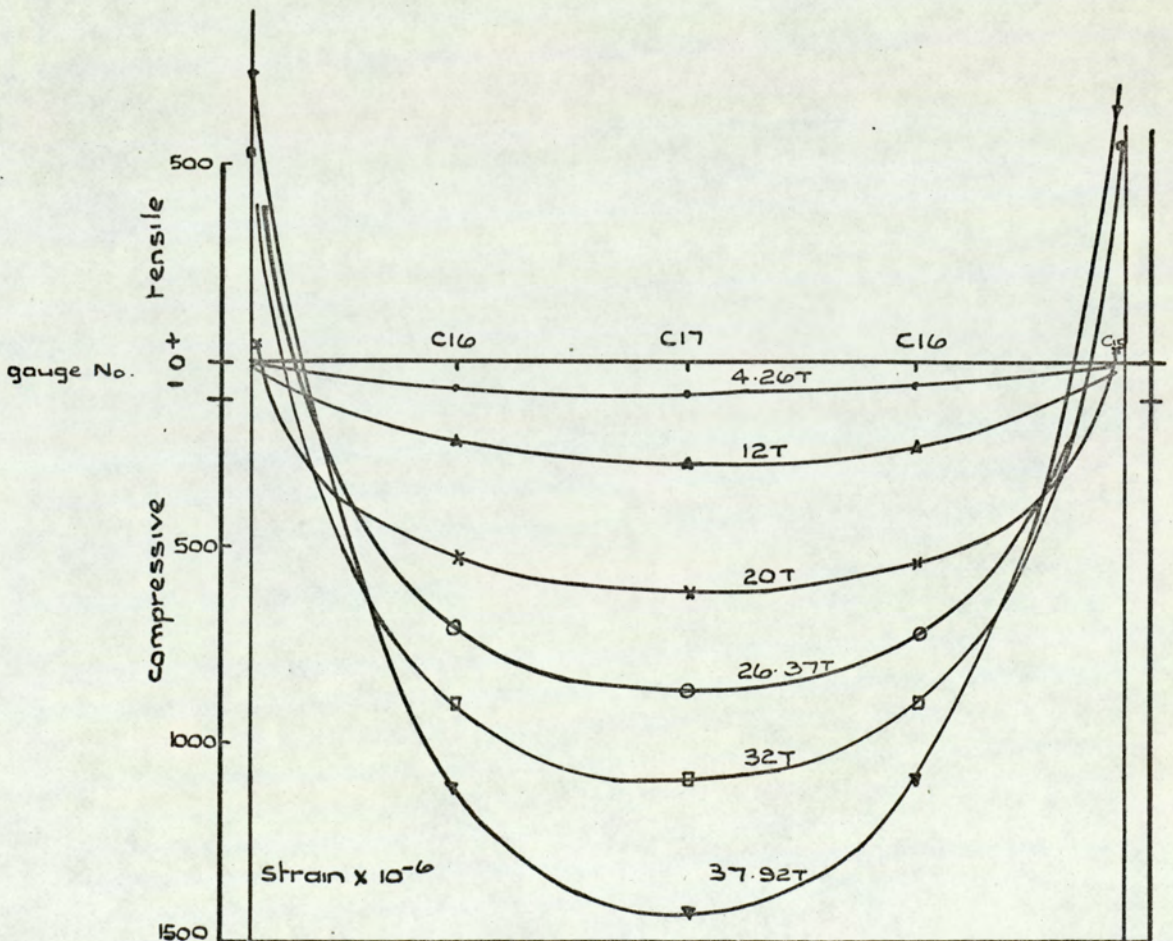
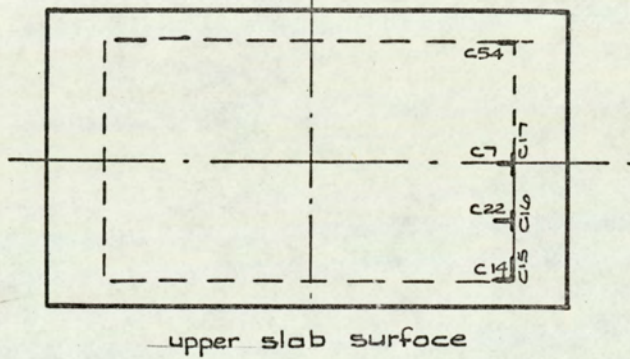


Fig. 10.20. Distribution of strain along the secondary beam where the slab is continuous. Top slab surface. test M_2 .

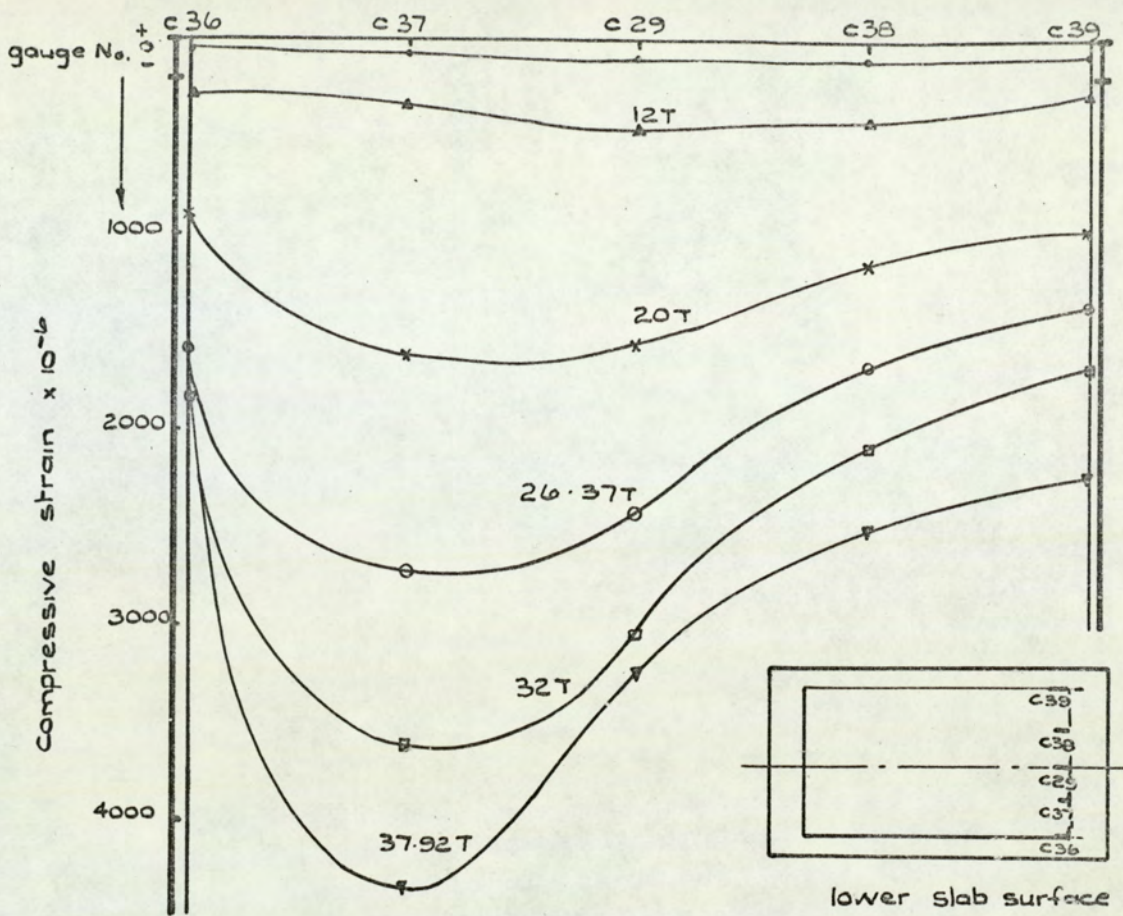


Fig. 10. 21. Distribution of strain \perp to the secondary beam where the slab is continuous. Lower slab surface. test M_2 .

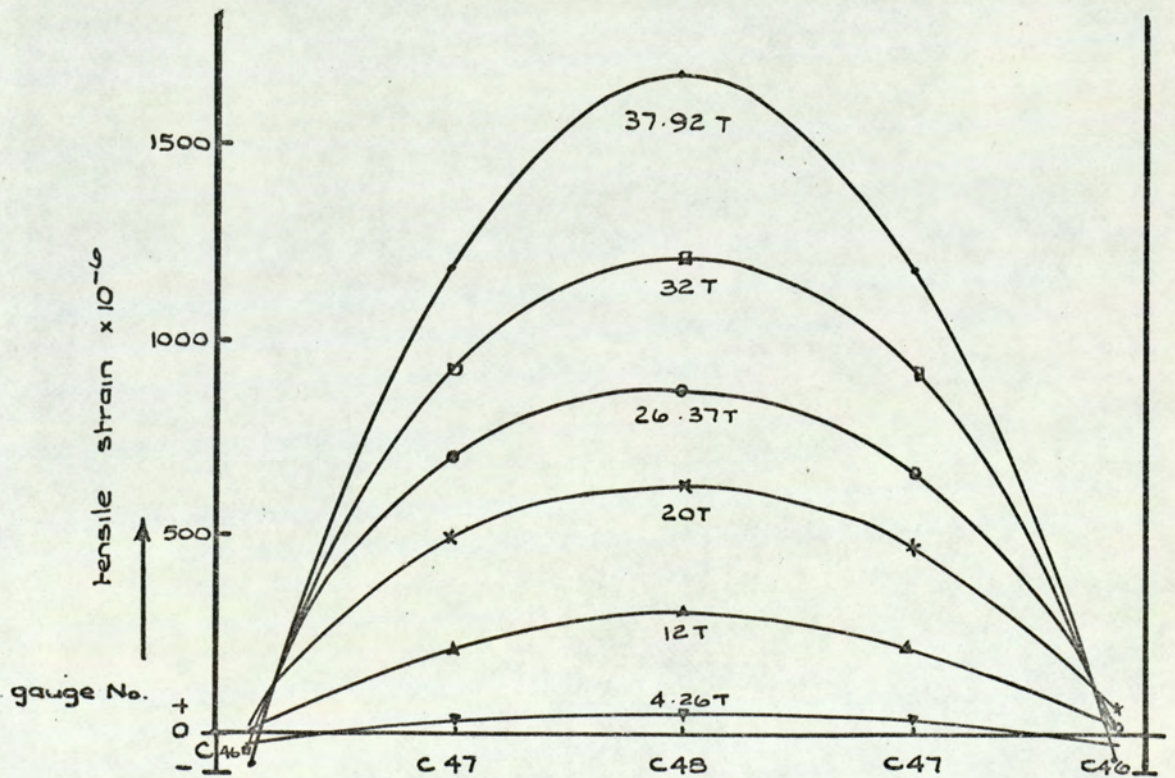


Fig. 10. 22. Distribution of strain along the secondary beam where the slab is continuous. Lower slab surface. test M_2 .

as those recorded during test M_1 at similar positions (Figure 10.7). Figure 10.22 shows the distribution of strain along the secondary beam lower slab surface where almost the whole slab span was in tension, owing to two-way spanning.

The load-strain graph in Figure 10.23 of the composite main beam at mid-span (Section 6-6, Figure 9.15) gives some idea of the load at which a plastic hinge formed near the centre, where the bending moment was maximum as seen from Figure 10.16. The shape of the load-strain relationship of the composite section was similar to that for load-deflection (Figure 10.14). From this graph, it can be seen that the lower flange of the beam yielded at a load of 16 tons (Gauge B_{15}). At a load of 20 tons, the middle of the web yielded (Gauge B_{16}) and almost the whole section yielded at a load of 24 tons. As the bending moment 10 in. off the centre towards the free end was higher than that at the centre of the main beam, hence it can be deduced that a plastic hinge formed there at this load. This is confirmed from the direct tensile strain reading obtained from Gauges R_4 and R_5 (Figure 9.14) at the centre of the longitudinal reinforcement recording a maximum of 550×10^{-6} at a load of 24 tons, as higher loads did not affect this reading. Similarly, a maximum tensile strain reading was recorded from Gauge R_3 at the same load. In addition, a plastic hinge occurred near the middle span of the other main beam (Section 2-2, Figure 9.15) at the same load of 24 tons, as can be seen from Figure 10.24. The formation of plastic hinges near the mid-span of the main beams at a load of 24 tons accounts for the strain hardening effects which occurred after this load in the system and observed in Figures 10.14, 10.23 and 10.24.

The strain gauges attached to the main beam at the fixed end were unfortunately damaged during the setting up of the test. However, Gauges R_7 and R_8 (Figure 9.14) on the hogging reinforcement recorded high tensile strains of 3000×10^{-6} and 2000×10^{-6} respectively at a load of 29.74 tons and the hogging yield line which formed along the secondary beam developed

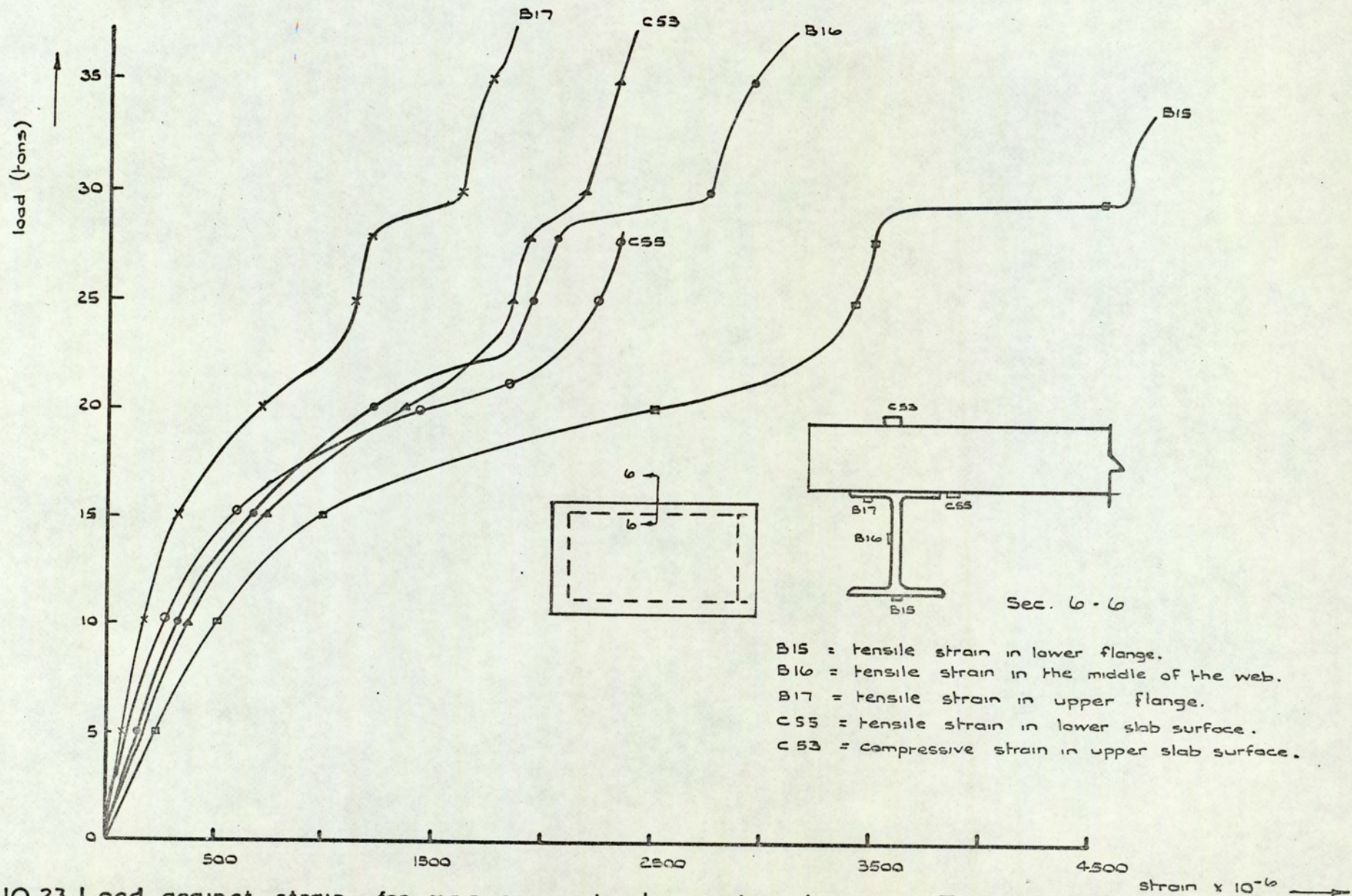


Fig. 10.23. Load against strain for main composite beam at mid-span. Test M₂.

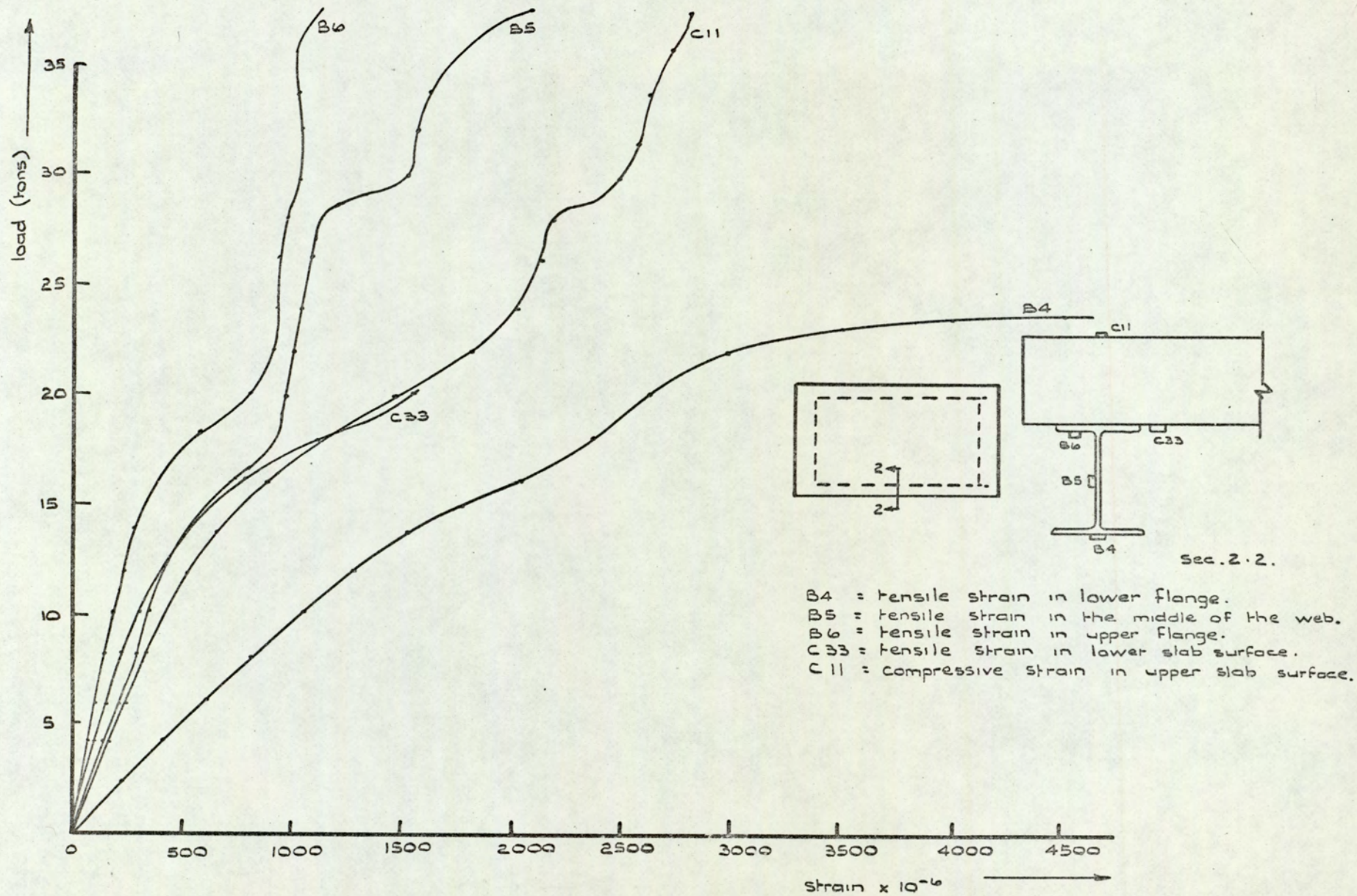


Fig. 10. 24. Load against strain for main composite beam at mid-span. Test M2.

a crack about $1/8$ in. wide. The total moment produced at the fixed end by the lever arms reached a maximum value of 18.0 kips-ft. at a load of 29.74 tons and higher applied loads hardly affected this value, as shown in Figure 10.25. This indicates very clearly that at a load of 29.74 tons plastic hinges formed at the supports of the fixed end, after which strain hardening effects commenced again, as shown in Figures 10.14, 10.23 and 10.24, until collapse of the system occurred at a load of 37.92 tons. Hence, the collapse load of the model may be taken as 29.74 tons and it is this value which will be compared with the theoretical collapse load in the next chapter, for the various assumptions on degree of composite action. The total moment produced at the support of 18.0 kips-ft. at a load of 29.74 tons is still lower than the theoretical values of 26.46 kips-ft. or 22.24 kips-ft., depending on whether or not composite action of the support is assumed to be present. However, this value is higher than that obtained in test M_1 of 13.1 kips-ft. at even a higher load of 35.64 tons. This relatively higher moment, at a lower load, occurred owing to the improvement made in reducing the local deformation at the support by moving the outer lever arms towards the centre line of the main beams. This indicates that the local deformation at the support did effect the proving ring readings.

Figure 10.26 shows the strain distribution through the composite main beam at mid-span (Section 6-6, Figure 10.23). This distribution indicates a high degree of composite action between the slab and the supporting beam, although more slip was in evidence between the slab and the beam than in test M_1 (Figure 10.11). The maximum recorded slip at mid-span before collapse was 42×10^{-3} (Gauge S.G.4, Figure 9.16). A similar amount of slip before collapse was recorded at the fixed end (Gauge S.G.5). Little slip (13×10^{-3} inch) was recorded at the free end (Gauge S.G.3). These slip measurements indicate that the shear connectors on the main beam were functioning adequately up to collapse. Figure 10.26 also shows that the neutral axis tends to rise in the slab at higher loads and that high tensile

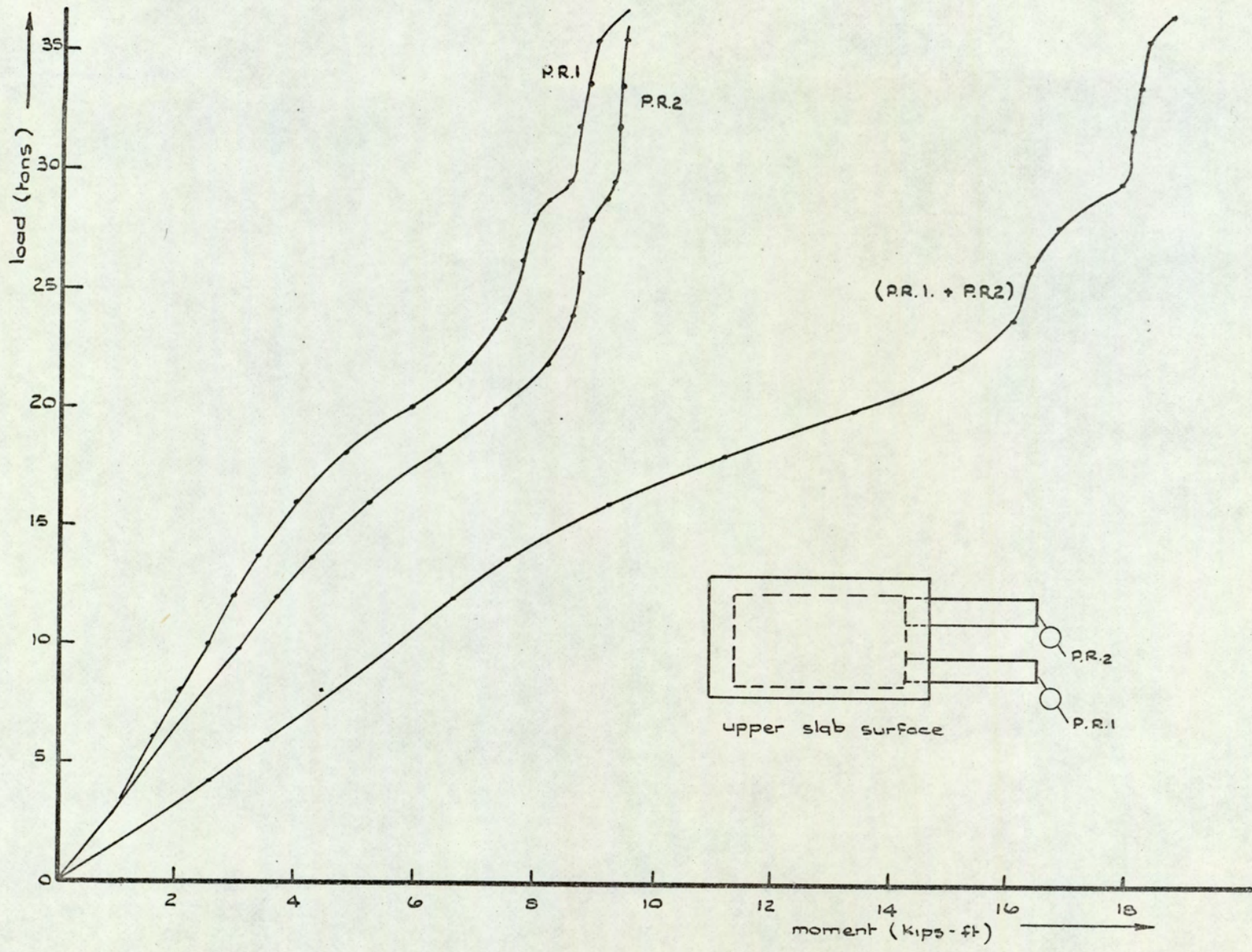


Fig. 10.25. Load against end moment. Test M₂.

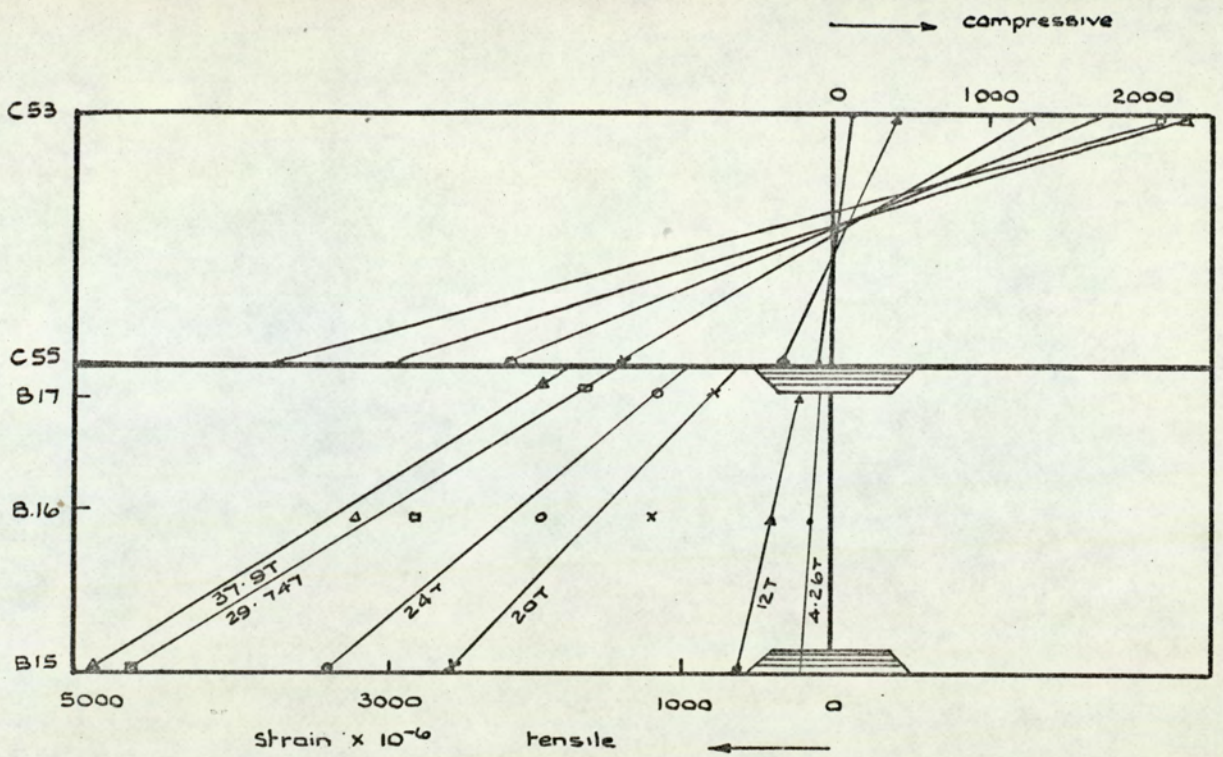


Fig. 10.26. Distribution of strain through main composite beam at mid-span. Test M2.

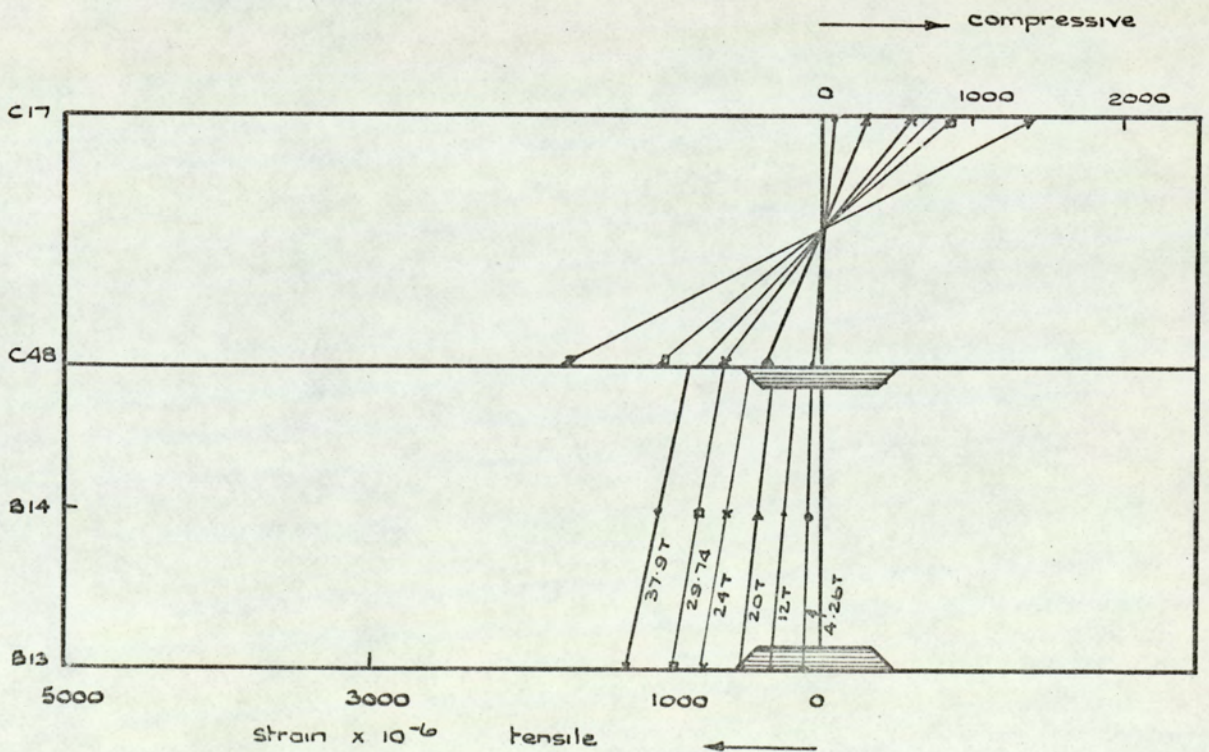


Fig. 10. 27. Distribution of strain through secondary composite beam at mid-span. (fixed end). Test M2.

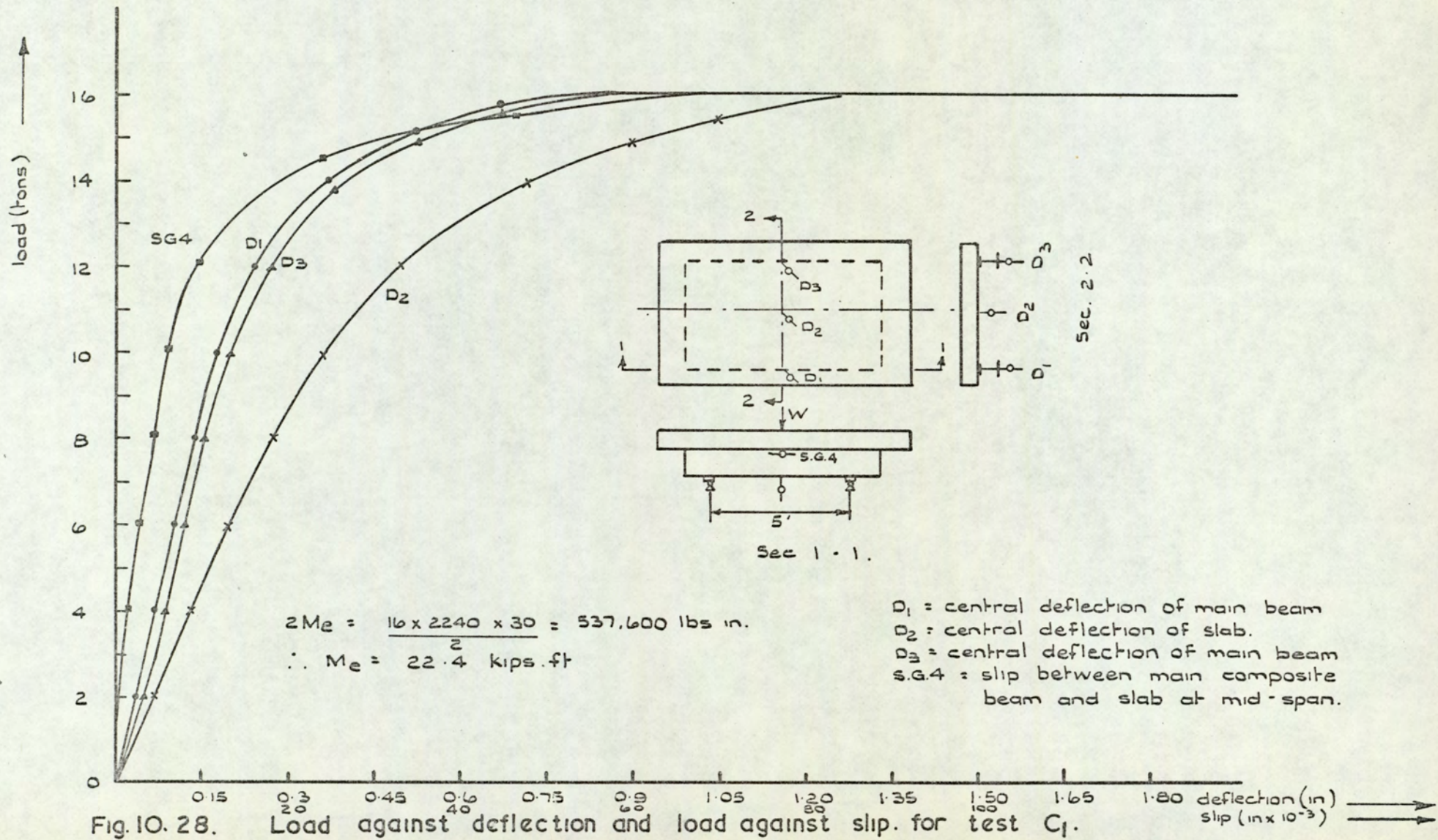
forces were present in the reinforcement, which contributed considerably to the ultimate strength of the composite section. Similar strain distribution to that of Figure 10.26 were obtained for the other composite main beam. Figure 10.27 shows the strain distribution through the mid-span of the secondary composite beam at the fixed end (Section 5-5, Figure 9.15), where a high degree of composite action between the slab and the beam was in evidence, as very little slip was recorded. The neutral axis was almost constant at the same position during the loading sequence.

The collapse of the model occurred by mode B as predicted, involving the two main "edge" beams and the slab. The final shape of the system after collapse is shown in Plate 18 with the maximum deflection of the main beams off the centre towards the free end. After collapse, the shape of the cracks in the lower slab surface indicated a tendency to form the yield lines associated with collapse by mode C, as shown in Plate 17.

10.4 CONTROL TESTS

10.4.1 TEST C₁

An overall picture of the behaviour of model M₃ during the simple bending control test C₁ is shown in Figure 10.28. The central deflection of the slab was greater than that of the mid-span of the main composite beams which followed each other very closely up to collapse. The central deflection of the slab and the main beams at collapse were 1.3 in., 0.8 in. and 0.75 in. respectively. Collapse of the model at mid-span occurred at a load of 16 tons. Hence, the experimental plastic composite moment of one main beam and half the slab width was 22.4 kips-ft. The shear connectors on the main beams were functioning adequately up to collapse. The maximum slip between the slab and the main beam along its whole length was found to occur at mid-span, reaching a value of 68×10^{-3} inch at collapse (S.G.4, Figure 9.19). Load against slip graph for slip between the slab and the main beam at mid-span is also shown in Figure 10.28. Little slip was recorded at the support or at other locations by Slip Gauges S.G.1,



S.G.2 and S.G.3, a maximum of 4×10^{-3} inch at the support (Gauge S.G.3) was recorded before collapse. Similarly, little slip was recorded by Slip Gauges at the other end of the main beam.

Figure 10.29 shows the distribution of strain perpendicular to the transverse centre line of the upper slab surface. Very high compressive strains were recorded across the full slab width with a maximum of 6400×10^{-6} at the centre, where deflection was maximum, before collapse. At collapse, a crushing yield line formed along the full width of the slab upper surface at mid-span, as shown in Plate 19. Very high tensile strains were recorded by Demec gauges at the lower slab surface perpendicular to the transverse centre line, reaching a maximum of 13000×10^{-6} and 9000×10^{-6} at the centre and the main beams respectively before collapse. This indicates very clearly that all the longitudinal slab reinforcement at mid-span yielded at collapse. However, low strain readings, if any, were obtained from the gauges on the reinforcing bars at this position, except that of Gauge R₂₂ (Figure 9.18), which recorded a tensile strain of 4030×10^{-6} before collapse (i.e. well above yield). The reason for the other electrical strain gauges not functioning properly could be due to a leakage in the waterproofing material or the material itself was not satisfactory. At collapse, the tension crack which formed along the transverse centre line at the lower slab surface was between $5/16$ in. to $3/8$ in. wide, shown in Plate 20. This plate, together with Plate 19, shows the collapse of model M₃ at mid-span, owing to the formation of plastic composite hinges there, which involves the composite formed by two main beams and the whole width of the slab. This indicates that the slab acted compositely with the main beams across its full width up to collapse.

The possibility of the presence of compressive membrane action in the system during the testing procedure was investigated thoroughly. The model was supported on bearing pads, as explained in Chapter 9, thus eliminating membrane forces, owing to friction, building up in the model.

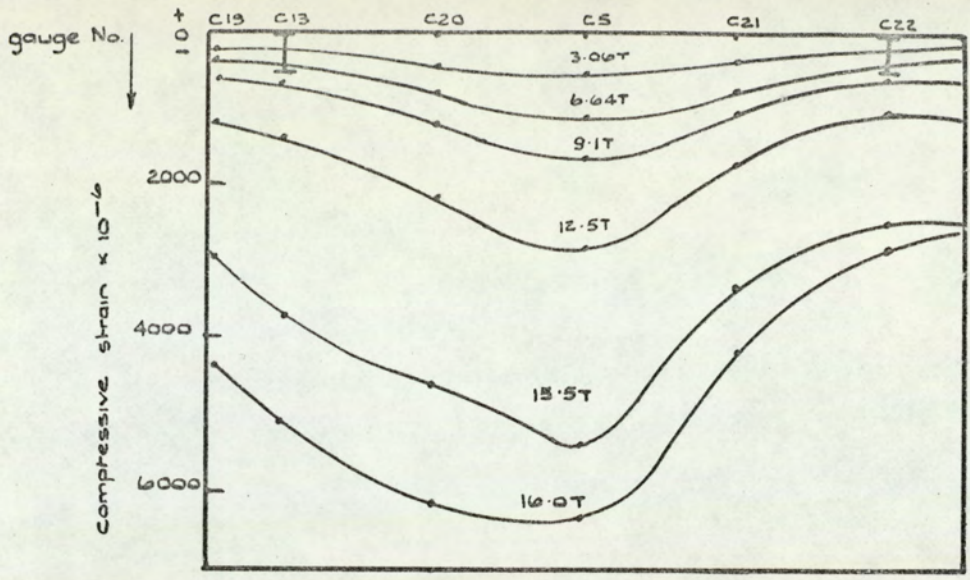


Fig. 10.29. Distribution of strain ϵ_r to the transverse ϵ_t of the slab upper surface. Test C1.

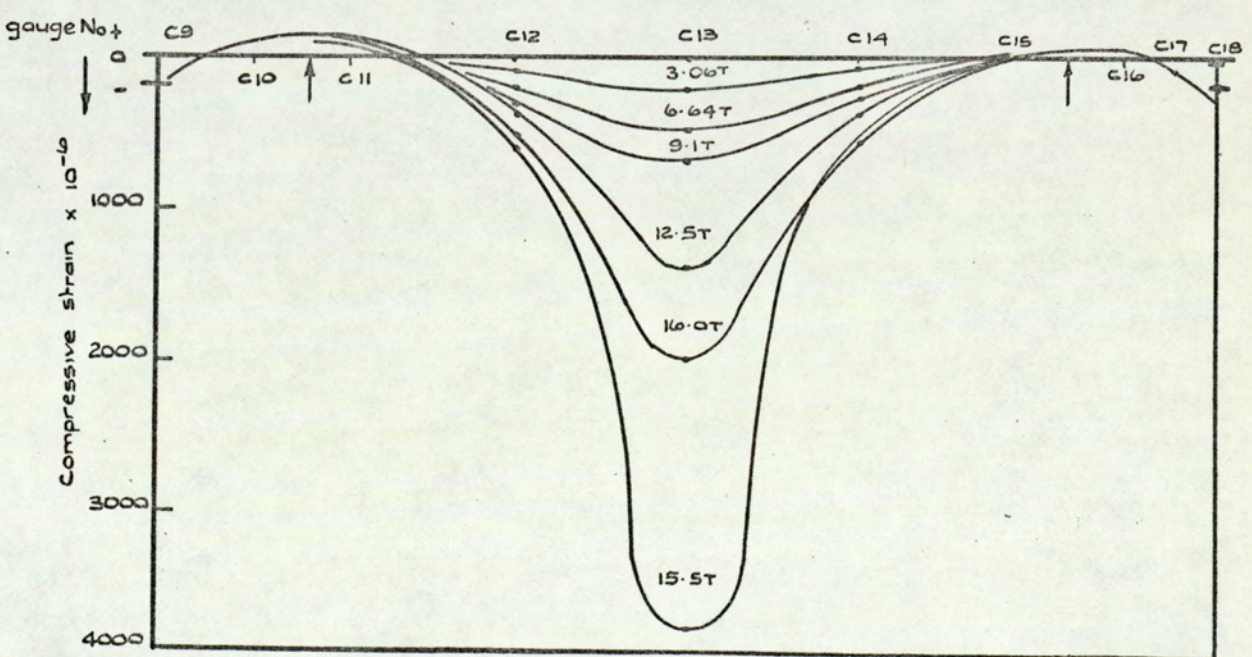
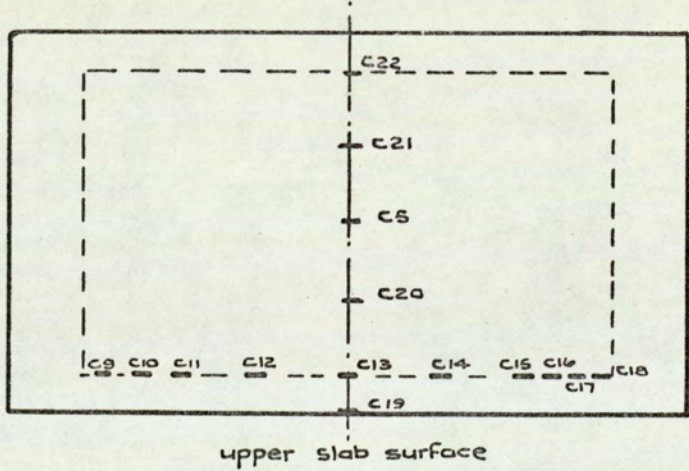


Fig. 10.30. Distribution of strain along the upper surface of the main composite beam. Test C1.

However, the supporting beams with the stud shear connectors welded to their upper flanges (Plate 3) might have behaved as a compression member holding the composite slab against horizontal movement. This would produce compressive membrane forces in the slab, which in turn would have resulted in higher collapse loads. This possibility was investigated by placing electrical strain gauges on the composite main beam through its entire depth and outside the span by up to 12 in. from both supports. Figure 10.30 shows the distribution of strain along the main composite beam upper surface, where compression was maximum at the centre and reduced to very small strains at the supports and outside of the span. The strain distribution along the longitudinal centre line of the slab upper surface was similar to that of Figure 10.30. Figures 10.31 and 10.32 show the strain distribution along the slab and the composite steel beam respectively at their interface. These strain distributions are similar to that of Figure 10.30, where, as expected, very high strains were recorded at the centre, which reduce to very small strains at the supports and outside the span. The maximum tensile strains recorded in the slab and the beam at their interface outside the span before collapse (Figures 10.31 and 10.32) were 800×10^{-6} at gauge position c_{53} (Figure 9.17) and 250×10^{-6} at the same location (Gauge B_{23} , Figure 9.20). This indicates that compressive membrane forces in the slab caused by the supporting beams through the stud shear connectors were not present during the loading procedure. The small strains recorded outside the span were probably due to the shear force effect between the slab and the composite beam, or to the effect of high local stresses at the supports, or both.

Figures 10.33 and 10.34 show the load against strain graphs at mid-span for both composite main beams. From these graphs, it can be seen that the steel beams became wholly plastic at a load of 15 tons. Further loading up to collapse at a load of 16 tons was obviously taken by the slab reinforcement. The shape of the load-strain relationship was similar to that

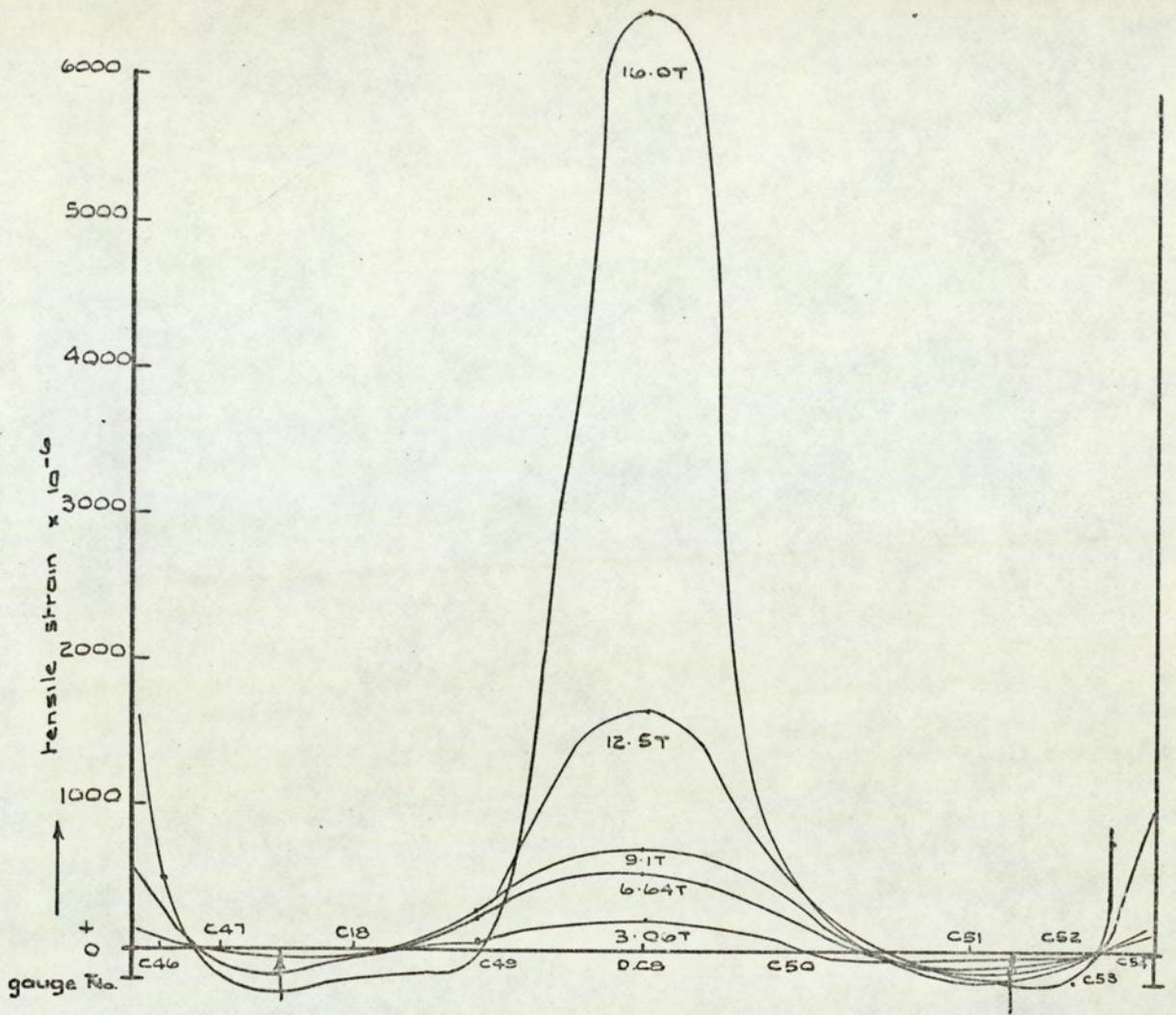


Fig. 10. 31. Distribution of strain along lower surface of slab, on the line of the main composite beam. Test.C1.

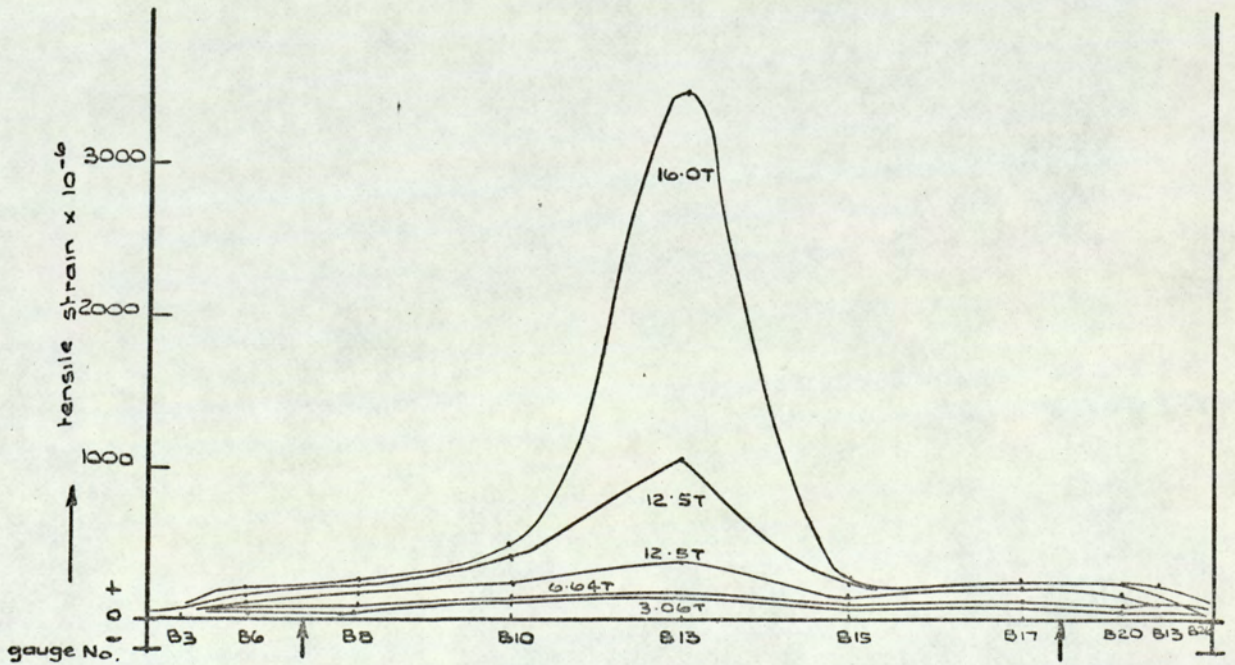


Fig.10. 32. Distribution of strain along the lower surface of the top flange of the main composite beam. Test C1.

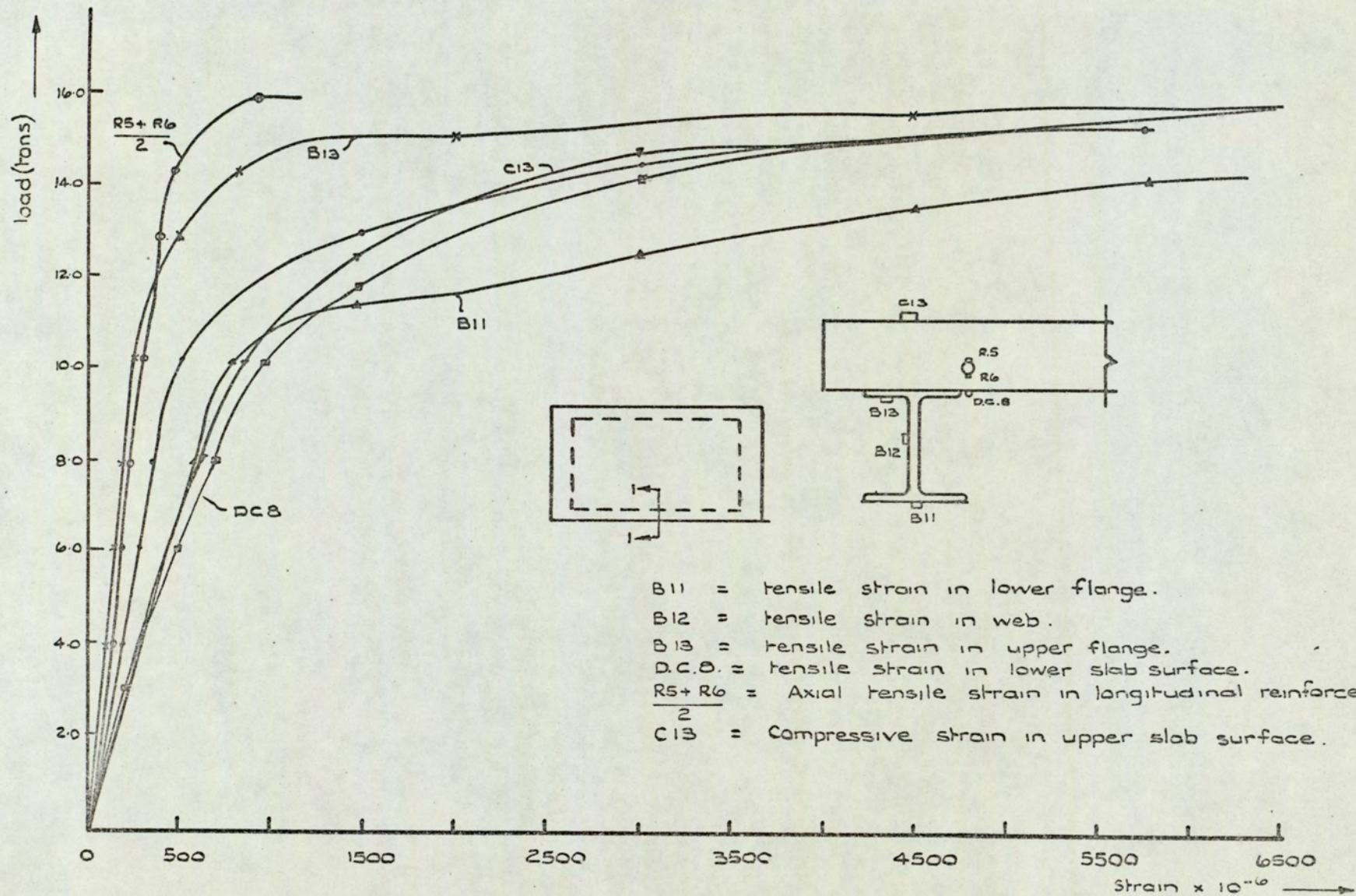


Fig. 10.33. Load against strain graph at the centre of the main beam. Test C₁.

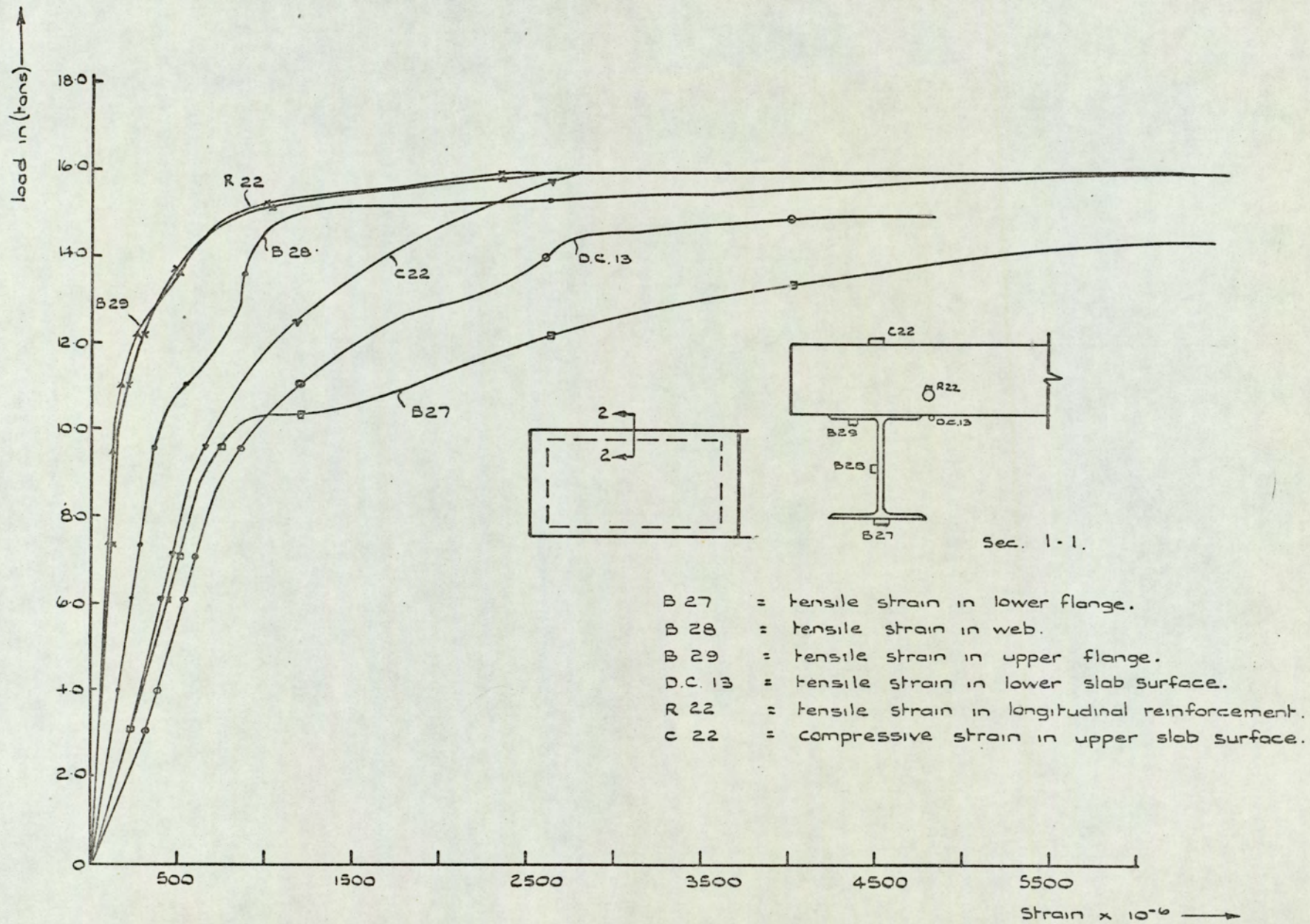


Fig. 10.34. Load against strain graph at the centre of the main beam. Test C₁.

of the load-deflection shown in Figure 10.28. Figure 10.35 shows the distribution of strain through the composite main beam at mid-span (Section 1-1, Figure 10.33). The strain distribution indicated a high degree of composite action between the slab and the supporting beam. The direct tensile strain readings on the reinforcing bar (Gauges R_5 and R_6 , Figure 9.18) were very low (even at high loads), compared with the apparent strains measured on the cracked concrete at steel reinforcement level shown in Figure 10.35. This indicates that the strain readings obtained from gauges on the slab reinforcement were not reliable. This is probably true for all the strain readings on reinforcement obtained during this test series. This could be due to a leakage in the waterproofing material or the material itself was not adequate, as mentioned earlier. Loss of bond between the reinforcing bar and the concrete at the position of the gauges, owing to the waterproofing material (see Plate 12) is another factor which tends to make such gauges unreliable.

A comparison can be made between Figures 10.11, 10.26 and 10.35 which show the strain distributions through the composite main beams at mid-span in tests M_1 and M_2 and control test C_1 respectively. Such a comparison shows that the neutral axis tends to rise in the slab at higher loads and that its position was almost the same at collapse in all three tests.

10.4.2 TESTS C_2 AND C_3

After the collapse of model M_3 at mid-span in the bending test C_1 , the model was reseated at the outer supports, as explained in the previous chapter. An external moment was applied at the supports by a 20 ton capacity jack through a proving ring at the end of the lever arms in such a way that the load was distributed equally between the lever arms, as shown in Figure 9.8.

For test C_2 , Figure 10.36 shows the strain distribution along the lower flange level of the composite main beam for different external moments up to collapse. At a moment of 27.1 kips-ft., Gauges B_{24} , B_{25} and B_{26} (Figure

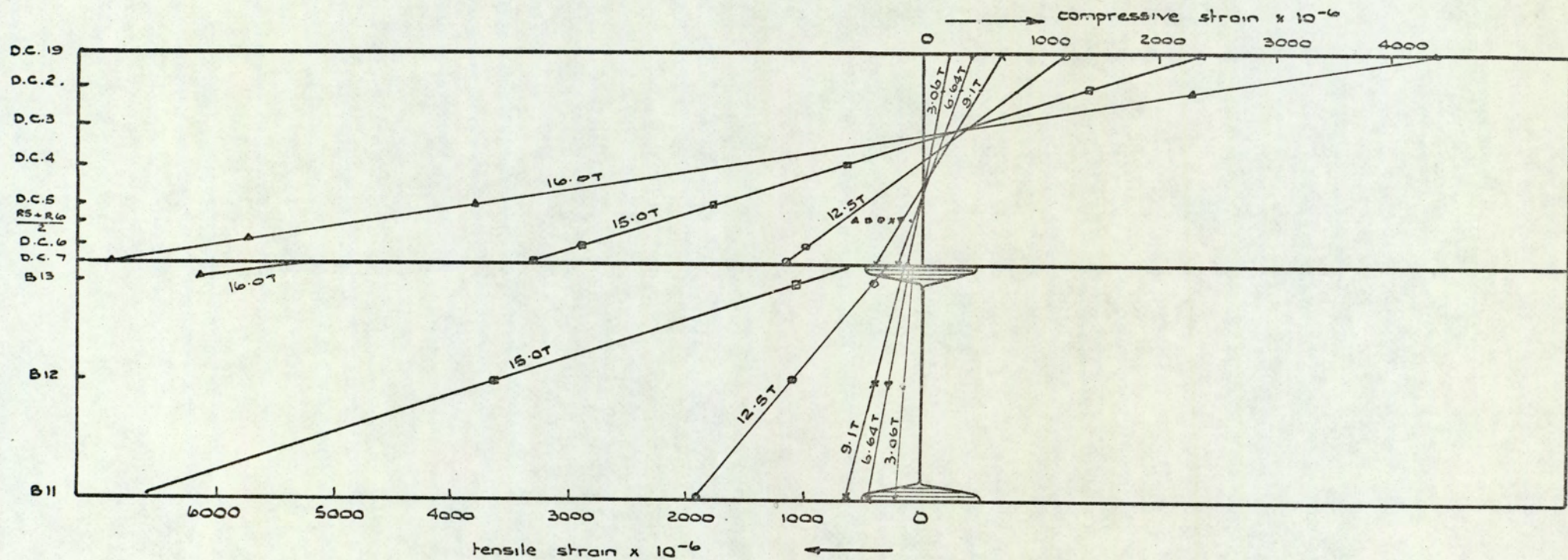


Fig. 10. 35. Distribution of strain through main composite beam at mid-span. Test C1.

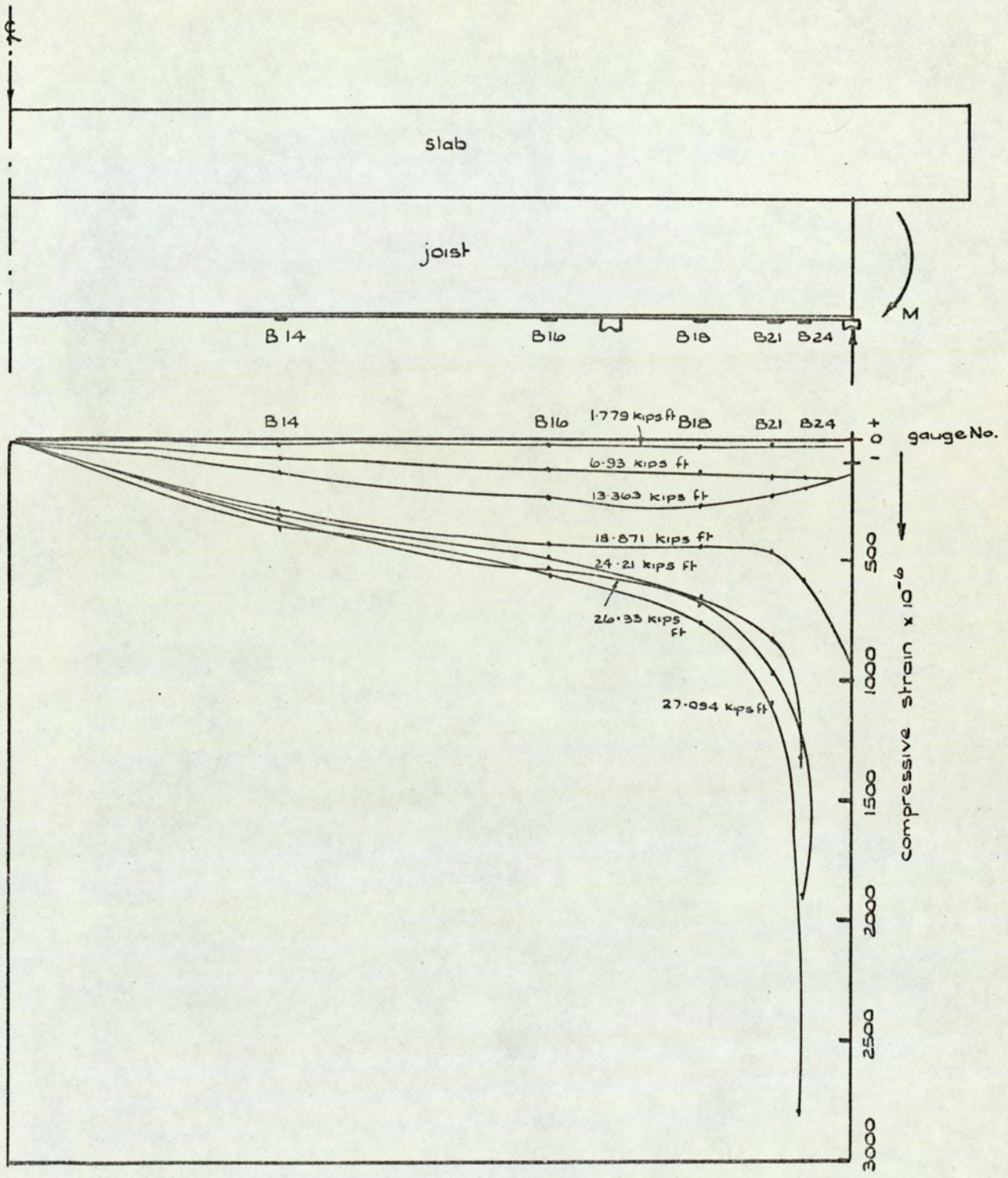


Fig. 10. 36. Distribution of strain along the main composite beam at lower flange level. Test C₂.

9.20) became plastic and the supports could not take any extra moment, which indicates that the whole section became plastic. Thus, the experimental, plastic, hogging, composite moment of the two main beams and the composite slab at the support was 27.1 kips-ft. The maximum slip between the slab and the beam was 36×10^{-3} inch recorded by Slip Gauge S.G.7 (Figure 9.19) 4 in. away from the support. Unfortunately, no readings were obtained from the gauges on the hogging reinforcement, but obviously they did yield at collapse, as the tension crack which formed at the supports along the secondary beam was 1/8 in. to 3/8 in. wide and about 2 in. deep into the slab. A compression crushing failure also developed along the secondary beam at the lower slab surface.

Test C₃ was a repeat of test C₂ carried out at the other end of the specimen. Here the maximum external moment applied before collapse at the supports was 26.75 kips-ft. Thus the plastic hogging composite moment of the two main beams and the slab at the supports of the other end of model M₃ was 26.75 kips-ft. The maximum slip between the slab and the beam was 40×10^{-3} inch recorded by Slip Gauge S.G.1 at the support. A tension crack, similar to that in test C₂, developed along the secondary beam upper slab surface. A compression crushing failure at the lower slab surface along the secondary beam also developed at collapse.

The general shape of model M₃ after the three "control" bending tests C₁, C₂ and C₃ is shown in Plate 21.

10.4.3 SLAB STRIPS S₁ AND S₂

The load against deflection and load against strain graphs of slab strips S₁ and S₂ are shown in Figures 10.37 and 10.38 respectively. The load-strain curves followed that of the load-deflection closely until cracks started to appear at the lower slab surfaces at a load of 0.5 ton. Collapse of slab strips S₁ and S₂ occurred at loads of 3.1 tons and 3.05 tons, producing experimental values of the ultimate slab moment of 2.676 kips-ft./ft.run and 2.633 kips-ft./ft.run respectively. Figures 10.37

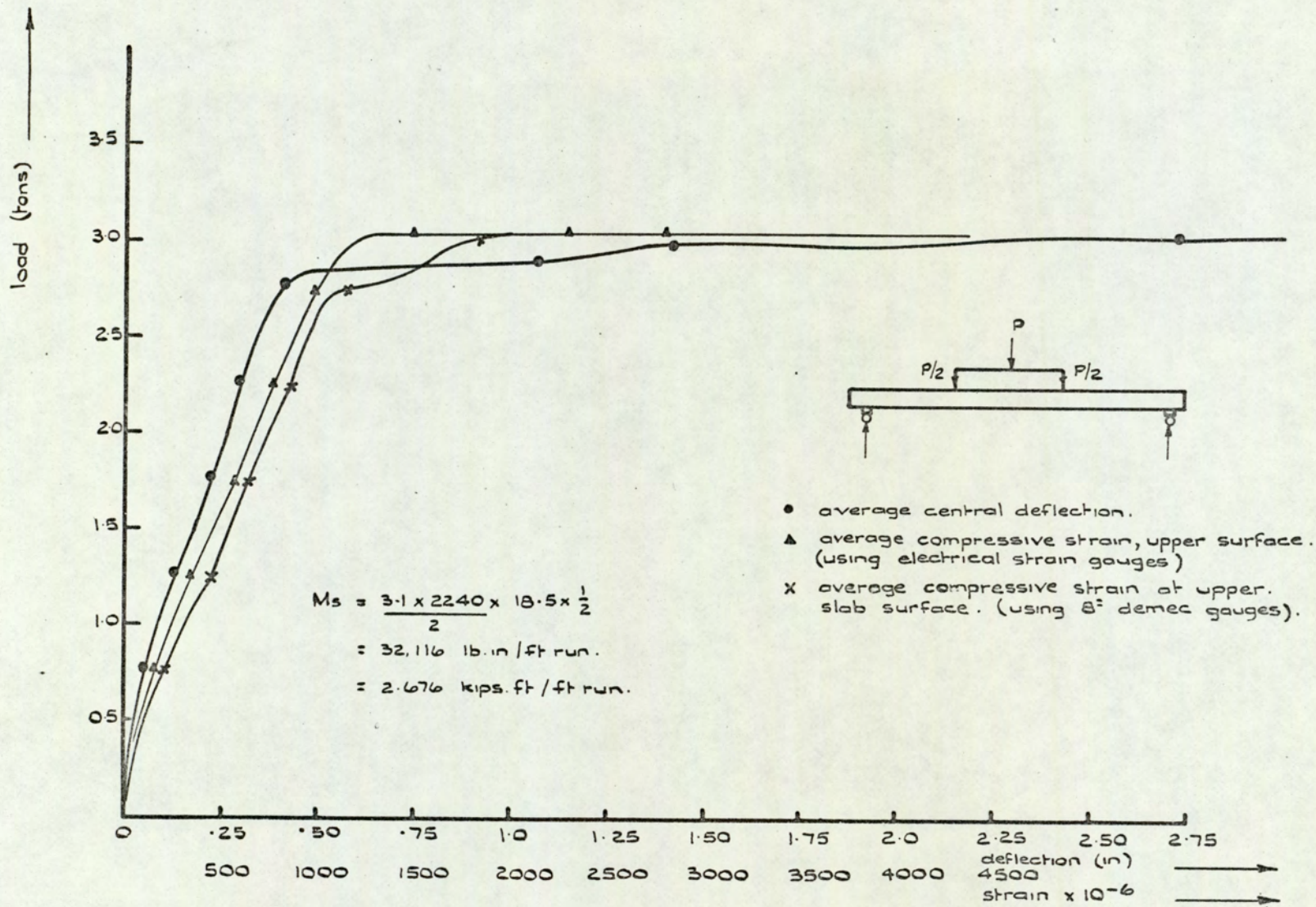


Fig.10.37. Load against deflection and load against strain for slab strip S1.

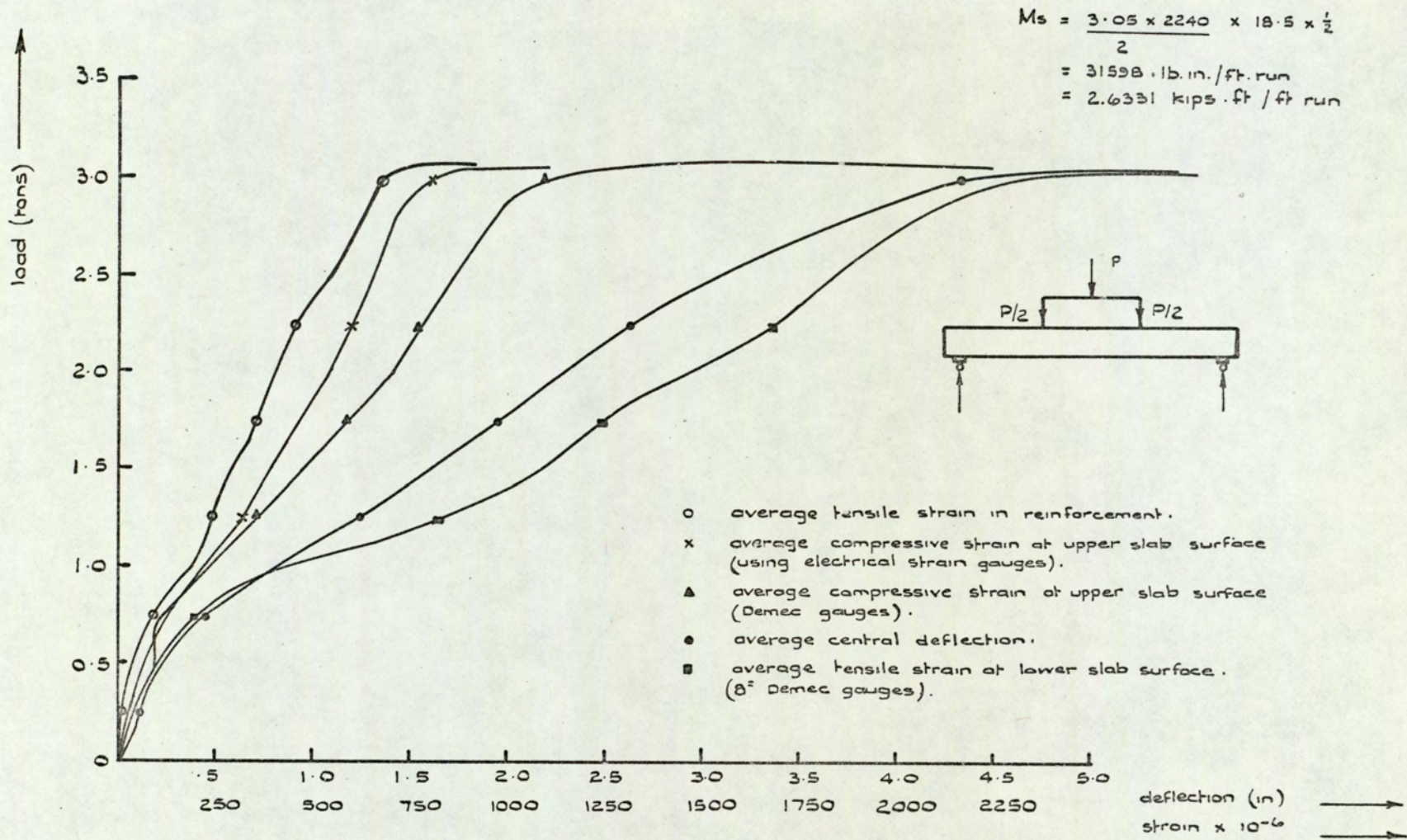


Fig. 10.38. Load against deflection and load against strain for slab strip S2.

and 10.38 also show the difference between the average of the compressive strain readings perpendicular to the transverse centre lines of slab strips S_1 and S_2 upper surfaces, which were obtained using Demec gauges and electrical strain gauges.

The distribution of strain through slab strips S_1 and S_2 , shown in Figure 10.39, indicate that the neutral axis, in both tests, remained almost constant at a depth of $3/4$ in., which is one quarter of the slab depth, whereas in composite sections, it tends to rise at higher loads. Plate 22 shows slab strip S_1 at collapse. Plates 23 and 24 show the yield lines which formed at the lower surfaces of slab strips S_1 and S_2 in the constant region of maximum bending moment, where they were similar in both bending tests.

Shear failure between the slab and the supporting beams did not occur in any of tests M_1 , M_2 or M_3 , as the shear stresses between the slab and the beams during the loading procedure were passing through the stud shear connectors, which were adequate, up to collapse. This can be seen from the strain distributions through the composite sections of these models.

In the next chapter, comparisons between the experimental and theoretical results of these tests will be made to see which of the five assumptions on degree of composite action most closely represents the observed experimental behaviour of the models.

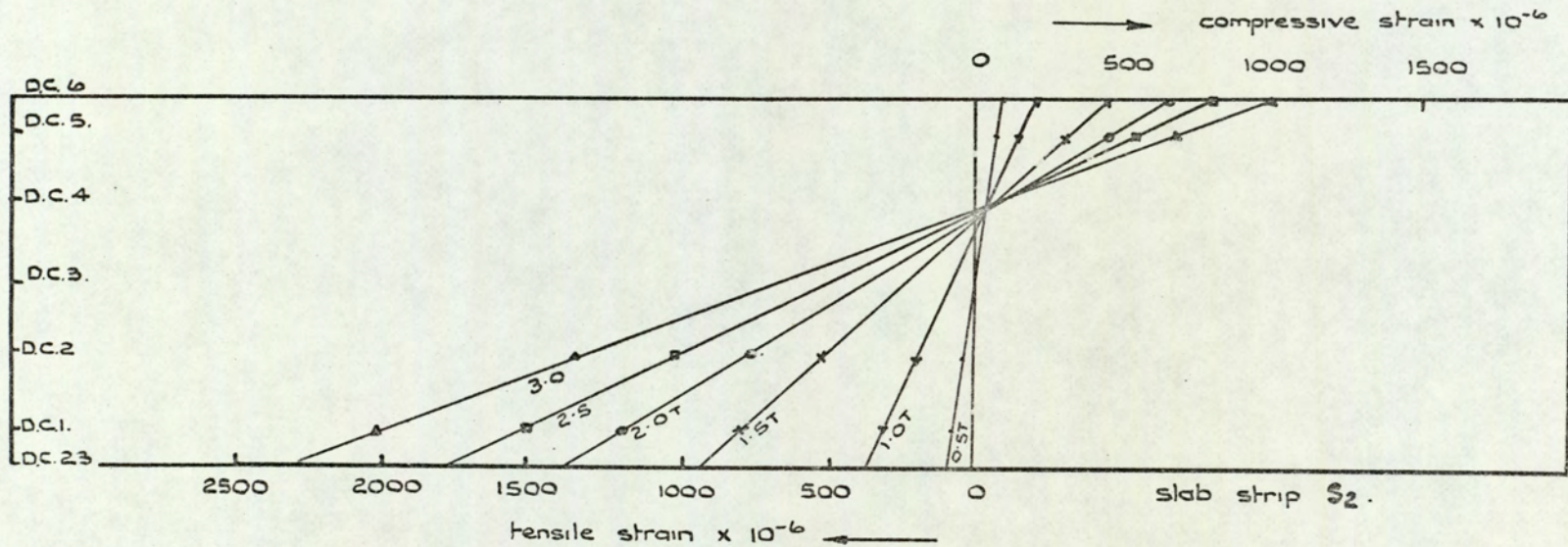
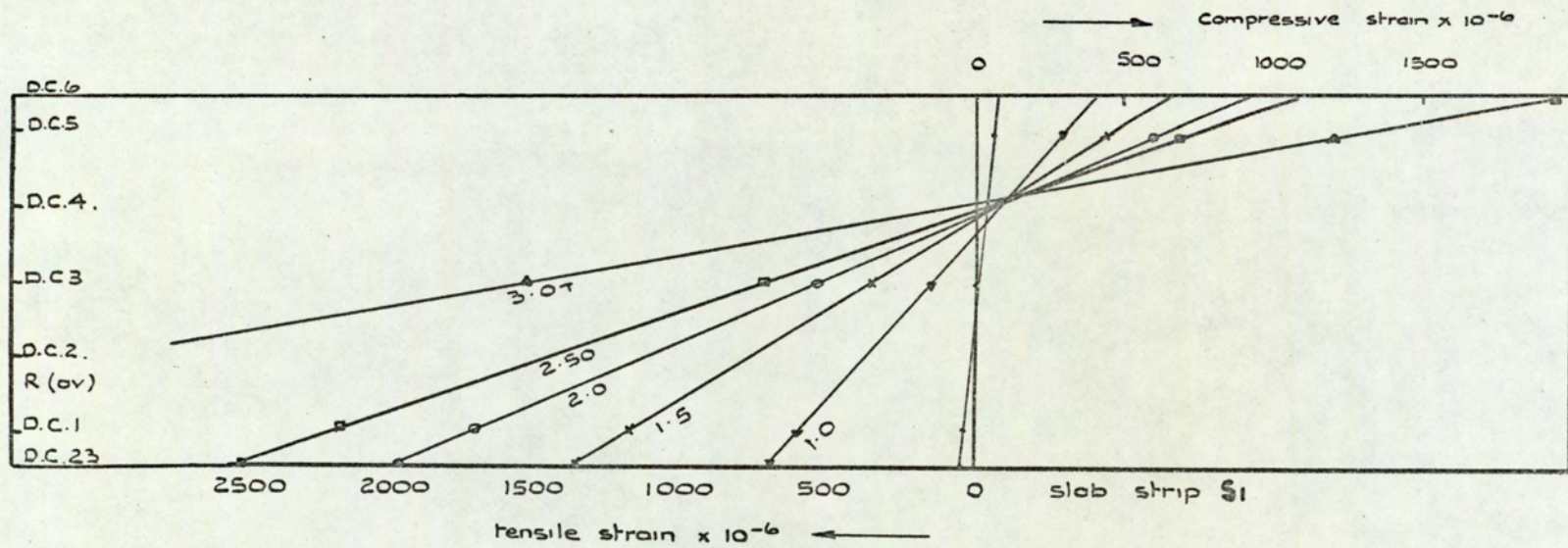


Fig. 10.39. Distribution of strain through slab strips S_1 and S_2 at mid-span.

C H A P T E R 1 1

COMPARISON OF EXPERIMENTAL AND THEORETICAL RESULTS

11.1 INTRODUCTION

The values of the fully plastic moments of the slab strips (M_s) and the composite beam and slab model M_3 at mid-span (M_e) and supports (M_N) obtained from the control tests are compared with the theoretical values, and any discrepancy commented upon. These comparisons will determine the degree of composite action between the slab and the supporting beams at mid-span and supports of composite beam and slab floor systems. The experimental collapse loads of models M_1 and M_2 , obtained in Chapter 10, are compared with the theoretical collapse loads, determined in Chapter 9, to see which of the assumptions on degree of composite action most closely represents the experimental behaviour of the models. Finally, the experimental moments M_e and M_N are used to provide the values of the calculated collapse loads of models M_1 and M_2 , which are compared with the experimental and the theoretical collapse loads. Finally, all the results are summarised in Table 11(i).

11.2 CONTROL TESTS

From the load-deflection graphs in Figures 10.37 and 10.38, the average experimental value of the ultimate slab moment M_s from tests S_1 and S_2 is 2.655 kips-ft./ft.run. This represents an increase of 2.5% on the theoretical value of M_s which equals 2.589 kips-ft./ft.run, as shown in Chapter 9. The agreement, therefore, is very good. Experimentally, it is not possible to know within a quarter of an inch the exact position of the reinforcement after the concrete has been placed. Thus, this small discrepancy between the theoretical and experimental values of M_s is partly due to small displacements of the reinforcement and partly due to strain hardening in the reinforcement.

From the load-deflection graph in Figure 10.28, the value of M_e from

Test No.	Type of assumption	Theoretical collapse load (mode B) (tons)	Experimental collapse load (tons)	% increase in expt. over theo. collapse load
M ₁	(1)	20.02	35.64	43.8
	(2)	26.27		26.3
	(3)	31.51		11.6
	(4)	29.76		16.5
	(5)	35.01		1.8
M ₂	(1)	15.04	29.74	49.2
	(2)	21.30		28.4
	(3)	26.58		10.6
	(4)	23.04		22.5
	(5)	28.32		4.8

(a) Comparison between experimental and theoretical collapse loads for each of the five assumptions on degree of composite action

Test No.	Theoretical collapse load (tons)	Calculated collapse load (tons)	Experimental collapse load (tons)	$\frac{p\ell L(\text{expt})}{p\ell L(\text{theo})}$	$\frac{p\ell L(\text{expt})}{p\ell L(\text{calc})}$
M ₁	35.01	36.59	35.64	1.018	0.974
M ₂	28.32	29.77	29.74	1.050	0.999

(b) Comparisons of theoretical, calculated and experimental collapse loads. Type (5) assumption.

Table 11(i) Summary of Test Results

Theoretical M_e (ignoring slab reinf.) kips-ft.	Theoretical M_e (including slab reinf.) kips-ft.	Experimental M_e kips-ft.	% increase in expt. over theo. M_e (ignoring slab reinf.)	% increase in expt. over theo. M_e (including slab reinf.)
15.93	21.06	22.4	40.6	6.3

- (c). Comparison between experimental and theoretical values of the plastic composite moment at mid-span of model M_3 (test C_1) with and without the effect of slab reinforcement.

Theoretical $(2M_B + M_{Sl})$ kips-ft.	Theoretical $2M_N$ kips-ft.	Average experimental total moment at supports kips-ft.	% increase in expt. moment over $(2M_B + M_{Sl})$ moment	% increase in expt. moment over $2M_N$ moment
22.21	26.46	26.93	21.2	1.8

- (d). Comparison between experimental and theoretical values of the fully plastic moment at supports of model M_3 (tests C_2 and C_3) with and without the effect of composite action.

Theoretical M_s kips-ft.	Experimental M_s kips-ft.	% increase in expt. over theo. M_s
2.589	2.655	2.5

- (e). Comparison between theoretical and experimental values of M_s (tests S_1 and S_2)

Table 11(i) continued. Summary of test results

test C₁ is 22.4 kips-ft. This experimental value of M_e represents an increase of 40.6% on the theoretical value of 15.93 kips-ft., calculated in Chapter 9 for type (2) or (4) assumption on degree of composite action which ignores the effect of slab reinforcement. However, the experimental value of M_e only represents an increase of 6.3% on the theoretical value of 21.06 kips-ft., calculated in Chapter 9 for type (3) or (5) assumption, which takes the effect of slab reinforcement into consideration. From the experimental behaviour observed in this test and in tests M₁ and M₂, it is apparent that the slab reinforcement plays a significant part in contributing towards the ultimate strength of the composite section. Also, comparisons of the above experimental and theoretical results indicate very clearly that, when the effect of slab reinforcement is taken into consideration, i.e. type (3) or (5) assumption, the results are very much closer than when this effect is excluded, i.e. type (2) or (4) assumption. The 6.3% increase in the experimental value of M_e over the theoretical value for type (3) or (5) assumption is probably due to strain hardening in the steel beam or the slab reinforcement or both.

It is interesting to compare the experimental fully plastic moment values at mid-span for model M₃ with and without the effect of composite action, to show the great advantage of introducing such an effect. The total fully plastic moment at mid-span of model M₃ if composite action were not present, i.e. type (1) assumption, equals $(2M_B + M_S \cdot \ell)$. Substituting the experimental values of 4.64 kips-ft. and 2.655 kips-ft./ft.run for M_B and M_S and of 5 ft. for ℓ , results in a total calculated moment of 22.56 kips-ft. This value compares favourably with the theoretical non-composite value of $(2M_B + M_S \ell)$ of 22.23 kips-ft. When the experimental value of $(2M_B + M_S \ell)$ is compared with the total experimental composite moment (2M_e) of 44.8 kips-ft. obtained from test C₁, it is seen that composite action results in an increase of approximately 100% in the total moment. This confirms the theoretical comparisons made in Chapter 7

between composite and non-composite action at mid-span of the supporting beams, which resulted in considerable savings in weight of the supporting beams when composite action was introduced.

The average experimental fully plastic moment at the supports from tests C₂ and C₃ was 26.93 kips-ft. This represents an increase of 21.2% on the total theoretical moment value ($2M_B + M_{sl}$) of 22.21 kips-ft. which assumes non-composite action at the supports. However, the experimental moment of 26.93 kips-ft. represents an increase of only 1.8% over the total theoretical fully plastic composite moment at the supports ($2M_N$) of 26.46 kips-ft. Therefore, the experimental total moment at the support compares favourably with the theoretical plastic moment, including the effect of composite action.

Test C₁ proved that when the fully plastic composite moment at mid-span is calculated, the effect of slab reinforcement should be taken into consideration. Tests C₂ and C₃ proved that the effect of composite action at the supports can safely be taken into consideration. Therefore, these tests support the adoption of type (5) assumption on degree of composite action, which assumes full composite action at both mid-span and support and the inclusion of the effect of slab reinforcement at mid-span. However, the theoretical collapse loads of models M₁ and M₂ for the five assumptions on degree of composite action are compared with the experimental collapse loads in the next two sections, to see whether or not type (5) assumption does indeed represent most closely the experimental behaviour of the models.

11.3 TEST M₁

From Table 11(i), it can be seen very clearly that the theoretical collapse load of model M₁ calculated for type (5) assumption (35.01 tons) most closely represents the actual collapse load of 35.64 tons, and that the other four assumptions do not give such good agreement. This represents an increase of only 1.7% of the experimental collapse load on the

theoretical collapse load calculated for type (5) assumption.

A further comparison can be made by recalculating the theoretical value, using the experimental values of M_e and M_N obtained from the control tests in equation 9.8.

$$\begin{aligned} \text{i.e. } p\ell L \text{ (calc.)} &= \frac{16 (22.4 + 13.465)}{7} \text{ kips} \\ &= 36.59 \text{ tons} \end{aligned}$$

This also compares favourably with the experimental collapse load (35.64 tons), giving an experimental value only 2.6% less than the calculated value based on type (5) assumption. The slight difference between the actual collapse load of model M_1 and the theoretical or calculated collapse load for type (5) assumption is probably due to the fact that uniformly distributed load was simulated by four point load jacks which results in an error of -6% and +3% in the central and end moments respectively, compared with a U.D.L., as shown in Figure 9.7 ((c) and (d)).

11.4 TEST M_2

It was mentioned in the previous chapter that model M_2 underwent two stages of strain hardening during the loading procedure. This was concluded from a study of Figure 10.14, showing load against deflection which gave an overall picture of the behaviour of model M_2 . The first stage of strain hardening began at a load of 24 tons. Figures 10.23 and 10.24 for load against strain at mid-span of the composite main beams indicated that these sections went almost wholly plastic at a load of 24 tons. However, it was shown in Figure 10.16 that the maximum bending moment of the composite beam occurred some 10 in. off the centre line towards the free end. Therefore, it was concluded that plastic composite hinges formed at this load about 10 in. off the mid-span. For a unit displacement 10 in. off the centre line towards the free end, the total load required for plastic composite hinges to form is given by:-

$$\frac{p\ell L}{2} = 2 M_e \cdot (\theta_1 + \theta_2)$$

$$\text{or } p\ell L = 4M_e \cdot \left(\frac{1}{2.67} + \frac{1}{4.33} \right) \quad 11.1$$

On substituting the experimental moment value of M_e of 22.4 kips-ft. into the above equation, the calculated collapse load is 24.2 tons. This value compares favourably with the load of 24 tons shown in Figure 10.14, at which the first stage of strain hardening in the system began after the formation of plastic hinges near the centre line.

The second stage of strain hardening began at a load of 29.7 tons after the formation of plastic hinges at the fixed end. This was confirmed from Figure 10.25, which showed that the maximum recorded moment produced by the lever arms occurred at a load of 29.74 tons, as higher loads hardly effected its value. The collapse load of model M_2 was, therefore, assumed to be 29.74 tons, at which load the second stage of strain hardening commenced, as shown in Figures 10.14, 10.23, 10.24 and 10.25. For a unit displacement 10 in. off the centre line towards the free end, the total calculated load required for plastic hinges to form at this position and at the fixed end supports is given by:-

$$\frac{p\ell L}{2} = 2 M_e (\theta_1 + \theta_2) + 2 M_N \cdot \theta_1$$

$$\text{or } p\ell L = 4 M_e \left(\frac{1}{2.67} + \frac{1}{4.33} \right) + 4 M_N \cdot \frac{1}{4.33} \quad 11.2$$

On substituting the experimental values of M_e of 22.4 kips-ft. and M_N of 13.47 kips-ft., which were obtained from the control tests, into the above equation, the calculated collapse load is found to be 29.78 tons. This value compares very favourably with the assumed experimental value of 29.74 tons. This calculated collapse load of 29.78 tons represents type (5) assumption on degree of composite action, as the experimental values of M_e and M_N which were substituted into equation 11.2 were for full composite action at mid-span and support and included the effect of slab reinforcement. These conditions are the basis of type (5) assumption, as shown in Section 11.2. Table 11(i) also indicates that the theoretical collapse load of

28.32 tons for type (5) assumption most closely represents the actual collapse load of 29.74 tons. The other four assumptions do not give such good agreement. This represents an increase of 4.7% in the actual collapse load over the theoretical collapse load. If the theoretical values of M_e and M_N of 21.14 kips-ft. and 13.23 kips-ft. are substituted into equation 11.2 for plastic hinges 10 in. off the mid-span towards the free end, the resulting theoretical collapse load for type (5) assumption will be the same as that obtained if the plastic hinges are assumed to form exactly at mid-span, i.e. 28.32 tons.

The total maximum recorded end moment of 18.0 kips-ft. at an applied load of 29.74 tons was lower than the theoretical fully plastic moments of either 26.46 kips-ft. or 22.24 kips-ft., depending on assuming composite or non-composite action. This recorded moment is also less than the experimental average total plastic moment of 26.93 kips-ft. obtained from control tests C_1 and C_2 . Since the theoretical and calculated collapse loads are very close to the experimental collapse load, the recorded total moment readings must have been affected by local deformation at the support or by formation of a moment at the end of the lever arms. However, this recorded total moment is higher than that obtained during test M_1 . This is due to the improvements made by increasing the spacing of the lever arms, so that the outer lever arms came in line with the main beams, thus reducing the local deformation at the supports.

Figures 10.14, 10.23 and 10.24 all indicate very clearly that at a load of 29.74 the model underwent the second stage of strain hardening, after the formation of the plastic hinges at the fixed end. An additional load of 8.18 tons was applied, until collapse occurred at a load of 37.92 tons. This extra load before collapse could be due to strain hardening effects in the supporting beams, or in the slab reinforcement, or both. Pieces of the flange of the 3 in. \times 1 $\frac{1}{2}$ in. \times 4 lbs./ft. R.S.J. of the supporting beams exhibited some strain hardening properties during the

tensile tests described in Chapter 9. It was also mentioned in Chapter 9 that stiffeners were welded at the corners of the supporting beams. These were introduced to strengthen the main beams against local deformation. As plastic hinges form at the supports of the fixed end, these stiffeners might increase the fully plastic moment of the beams there, and hence an extra load would be required to cause collapse. A further point to be taken into consideration is the possibility of a local deformation in the upper flange of the main beam at the support, owing to rotation of the secondary beam producing a tensile force in this flange. This was indicated by the low readings in the proving rings at the end of the lever arms. The tensile force in the upper flange could have the effect of reducing the compression in the lower flange, thus delaying the formation of the plastic hinge at the support. This too can cause an increase in the collapse load. Also, there could be some compression membrane action in the system, owing to some accidental friction during the loading procedure which would result in a higher collapse load. Finally, as mentioned earlier, there is some error in simulating the uniformly distributed loading by four equi-distant, equal point loads. Therefore, the high ultimate failure load of model M_2 of 37.92 tons must be due to one or more of the above effects and the experimental fully plastic collapse load of 29.74 tons obtained from Figures 10.14, 10.23 and 10.24 is quite justified.

It is interesting to note from Table 11(i) that for both tests M_1 and M_2 , type (5) assumption produces the highest theoretical collapse load and the closest agreement with the actual collapse load. After type (5), type (3) gives the highest collapse load. This compares favourably with the conclusion obtained in Chapter 7 from comparisons between the various assumptions on degree of composite action that type (5) assumption produces the highest collapse load. Therefore, the highest saving in weight, compared with type (1) or (2)⁽⁴⁾ assumption and next to it is type (3) assumption. This is also true from the point of view of structural efficiency.

Finally, from the comparisons and studies of the experimental behaviour of the composite beam and slab floor systems, the following may be concluded:-

- (1) Control test C_1 and tests M_1 and M_2 indicated that the slab reinforcement contributed considerably to the ultimate capacity of the composite section at mid-span. The experimental value of M_e was 40.6% higher than the theoretical value when the effect of slab reinforcement was ignored. This difference became only 6.3% when this effect was included.
- (2) Control tests C_2 and C_3 showed that the experimental fully plastic moments at the ends of model M_3 were very close to the theoretical moment assuming full composite action with a difference of only 1.8%. This difference was 21.2% when the experimental moment was compared with the theoretical moment assuming no composite at the supports.
- (3) (1) and (2) above lead to the adoption of type (5) assumption which considers full composite action at the mid-span and the supports and includes the effect of slab reinforcement at the mid-span.
- (4) Comparisons between the theoretical and actual collapse loads of models M_1 and M_2 in Table 11(i) showed that type (5) assumption gives theoretical loads which most closely represent the actual collapse loads with a difference of 1.7% and 4.8% between the two values for models M_1 and M_2 respectively. On substituting the experimental values of M_e and M_N obtained from (1) and (2) above into the theoretical equations for collapse of models M_1 and M_2 for type (5) assumption, these differences became 2.6% and 0.1% respectively.
- (5) Collapse of models M_1 and M_2 occurred by mode B, as predicted.
- (6) During the testing of models M_1 , M_2 and M_3 , the stud shear

connectors welded on the top of the supporting beams, which were designed for type (5) assumption, behaved adequately up to collapse.

- (7) From the above, it can be concluded that type (5) assumption, which gives the highest savings in weight, etc. compared with the other four assumptions, can safely be used in the design of composite beam and slab floor systems.
- (8) However, if type (3) assumption is to be used, considerable savings in weight, etc. will be made compared with types (1), (2)⁽¹⁾ or (4), as the difference in weight saving and structural efficiency between types (3) and (5) is small.

All the results from this chapter are summarised in Table 11(i).

In the following chapter, specific conclusions on individual items in this thesis, together with a general conclusion on this research work, will be made. Finally, the thesis is concluded by one or two suggestions as to fields of related research work, which might be investigated in the future.

CONCLUSIONS12.1 INTRODUCTION

This chapter contains specific conclusions on individual items in this thesis, together with a general conclusion on the use of the most suitable assumption on degree of composite action in the design of beam and slab floor systems, using upper-bound solutions.

Five assumptions on degree of composite action have been developed in Chapters 4, 5 and 6. Throughout this research work, considerable attention has been paid to the validity and economy of each of the five assumptions of the proposed design method, which has been found to possess distinct advantages over many other methods. Comparisons are made between these assumptions, from the point of view of weight-saving, deflection and structural efficiency, using twelve design examples. These comparisons were carried out with the aid of a general computer program developed in the course of the present work.

The effect of composite action was introduced into the plastic design method proposed by Gandhi⁽⁴⁾ for the design of multi-storey frames, taking the effect of instability into consideration. The effect of composite action on the stiffness of the supporting beams, and hence on the magnification factors and the instability of the frame as a whole, was also considered.

The agreement between experiment and theory for each of the five assumptions on degree of composite action is discussed.

Finally, one or two suggestions are made for additional research work which would help to develop the full potentials of this design approach.

12.2 CONCLUSIONS

In the design of both non-composite and composite beam and slab floor systems, only the upper-bound solutions were considered. This is because this type of solution can be easily modified to include composite action.

It is a fact that a lower-bound solution gives a "safe value" for the collapse load of a structure and thus should be preferred to an upper-bound solution. However, the use of a lower-bound solution in the case of composite structures invariably complicates the problem. Nevertheless, in using an upper-bound solution, it should be remembered that there are many factors that can play a part to improve the safety of the solution. These are tensile or compressive membrane action which counteracts the reduction in collapse load from the true mode of collapse, strain hardening in the steel and other factors which result in the fracture line theory, even applied correctly, being generally conservative.

Three basic modes of collapse of beam and slab floor systems were considered in this thesis. These are:-

- (i) The collapse of the slab and the secondary beams which was termed mode A in this thesis.
- (ii) The collapse of the slab and main beam by mode B.
- (iii) The independent collapse of the slab by mode C or D, depending on the value of the sides ratio (ρ). "Fan modes" were not considered since, for uniformly loaded slabs, the reduction in the collapse load is not large.

Expressions were derived for the collapse load of five non-composite floor systems with different boundary conditions, that is type (1) assumption, for the three basic modes of collapse. From these, the required M_x , M_y and M_s were obtained. A design chart was produced in Chapter 4 for a typical internal bay. From this chart, knowing the loading and the dimensions of the frame, it was possible to determine the beam sizes, as well as the slab moment. A typical example, using the design chart of Chapter 4, was given. Chapter 5 contained the modified design equations of Chapter 4 for the case when the slab is composite with the supporting beams for types (2) and (3) assumptions. The slab was assumed composite at mid-span of the supporting beams only. Type (2) ignores the effect of

slab reinforcement. When M_c and M_e are calculated, type (3) considers such an effect. A modified design chart of the typical internal bay was prepared for types (2) and (3) assumptions. Using a frame of the same size and loading as that given in the example in Chapter 4, new beam sizes were obtained for type (2) assumption. This was done by using Table 5(i) to select the appropriate composite sections. It was not convenient to prepare similar tables for type (3) assumption because of the greater number of parameters involved. For this reason, type (3) assumption could only be employed with the direct use of a computer. The same example, solved for types (1) and (2) assumptions by the use of charts, was solved using the computer directly and the beam sizes and slab moment were obtained.

In Chapter 6, the design equations of Chapter 5 for types (2) and (3) assumptions were modified to include composite action for types (4) and (5) assumptions. Both these assume full composite action at mid-span and the supports of the beam. However, type (4), like type (2), ignores the effect of slab reinforcement when M_c and M_e are calculated. On the other hand, type (5), like type (3), considers such an effect. Once again, it was found difficult to use tables or charts and the use of computers, in the design of types (4) and (5), was shown to be unavoidable. This is illustrated by referring to the example used in Chapters 4 and 5 when new beam sizes are selected for both assumptions with the aid of the computer.

From comparisons on the same design example shown in Chapters 4, 5 and 6 between the various assumptions on degree of composite action, it was found that type (5) assumption gives the most economical beam sections. Although type (3) assumption is not as economical, it seems to give reasonably good results. With a 6 in. slab, the saving in weight of the steel main beam per foot run for type (5) assumption was 38% over type (1) which ignores composite action altogether and 14% over type (2), the simplest form of composite action which was proposed by Steel⁽¹⁾. This apparent saving in cost, together with the associated saving in depth of composite

beam giving reduced height of a building, less cladding, heating, etc., must be balanced against the cost of welding the shear connectors to the beams. However, composite structures are being built in this country and abroad (cf. example in Chapter 2) with considerable saving of overall cost.

A general computer program was developed in the course of the present work in Atlas Autocode. This program embodied the design of beam and slab floor systems with various boundary conditions for each of the five assumptions on degree of composite action. The three basic modes of failure A, B and C or D were considered in this program in such a way that collapse would occur by any of these basic mechanisms at the same applied load, thus producing an economic design. The program was written in such a manner as to require a minimum of input information and therefore the data preparation is easy. A change from one assumption to another for the same problem requires a variation of only one or two values in the input data. The machine output consists of the ultimate slab moment M_s , area of slab reinforcement in both directions and the size of the supporting beams with their plastic composite and non-composite moments at mid-span and supports. Other useful information, also given, was the total horizontal shear force between the slab and the supporting beams. This helps in finding the number of the shear connectors required on each beam. The computer output also gave the limits of the mid-span deflections, together with the weight of the beams, reinforcement, concrete and of the whole system.

In order to test the capability of the program to design single-bay and multi-bay floor systems, twelve frames with various boundary conditions, number of bays, equal and unequal bays and sides ratios (ρ) were deliberately devised in Chapter 7. From these design examples, it is concluded that:-

- (1) Increasing the slab thickness results in selecting a heavier or the same section for the supporting beams. This also gives heavier columns and more substantial foundations. Against this,

there is only some saving in the weight of slab reinforcement to produce the same ultimate moment M_s . This indicates very clearly the disadvantage of increasing the slab thickness on the whole economy of non-composite and composite structures. A minimum slab thickness to provide the required M_s value with the under-reinforced condition is recommended in the design of beam and slab floor systems.

- (2) There is no advantage in increasing the cube strength in terms of saving in weight of the supporting beams of the non-composite and composite structures. Only a slight reduction in the weight of the slab reinforcement occurs when the cube strength increases to provide the same ultimate slab moment M_s . A minimum cube strength is recommended for the design of beam and slab floor systems.
- (3) A considerable reduction in the deflection of the selected supporting beams, as well as saving in weight, results by using composite rather than non-composite construction.
- (4) For the same floor area, a slight reduction in the weight of the supporting beams and slab reinforcement can be obtained by using the system with the smaller sides ratio (ρ).
- (5) The relationship between live load and the weight of the selected supporting beams and slab reinforcement is approximately linear. In the case of a 5 in. thick slab, it was noticed that an increase in the live load from 50 \rightarrow 100 lbs./ft.². There was 25-30% increase in the weight of the selected beams and 48.6% increase in the slab reinforcement.
- (6) Type (5) assumption gives the most economical sections for the supporting beams compared with the other four assumptions. This is followed by type (3). This is also true for overall structural efficiency.

In Chapter 8, the effect of composite action of types (2) and (3) was introduced into the plastic design method originally proposed by Gandhi⁽⁴⁾ for the design of multi-storey frames with the effect of instability taken into consideration. It was found possible to modify the design equations for the three zones of failure of multi-storey frames to include the effect of composite action at mid-span of the supporting beams for types (2) and (3) assumptions. In beam and slab floor systems, considerable saving in the weight of the beams occurs by using type (2) or (3) of composite design rather than type (1), which ignores composite action altogether. Now with the introduction of either of these two types of composite action into the design of bare steel frames, even more saving in the weight of the frame will be made. In this chapter, it was shown that the beam size was more effective than the column size in controlling the instability effects. Therefore, the introduction of composite action of types (2) or (3), even with the conservative assumption of its effectiveness as to act within the middle half span of the supporting beams, improves the stability of the frame greatly. An example was given of a $16 \times 5\frac{1}{2} \times 31$ U.B. plus 5 in. thick slab. This showed that the stiffness of the section increases by 43% relative to that of a bare steel section when a plastic hinge is assumed to form at the leeward end, and 10% when the beam is fully elastic.

Therefore, with the introduction of the greater values of the second moment of area in the elastic and plastic stages, a larger section might not be required to reduce the K_2V to its limiting value of -1.8. The K_2V value affects the distribution factors of the beams and the columns considerably. Hence, with the introduction of composite action, the stability of the frame as a whole improves considerably.

With the introduction of composite action of type (2), it is still possible to use the proposed design method manually, by making use of tabulated values of the magnification factors⁽⁴⁾, together with tables similar to Table 5(i) to find the composite sections with adequate $(M_e + M_B)$.

However, at this stage, the use of a computer becomes more advantageous and at any rate, using the more economical method of composite design type (3) would make the use of a computer a necessity.

The series of control tests carried out on one-storey composite beams and slab floor model M_3 show good agreement between experimental and theoretical results for type (5). This is for full composite action at mid-span and supports of the beam and the inclusion of the slab reinforcement effect at mid-span. Comparisons of experimental and theoretical results of models M_1 and M_2 show that type (5) assumption represents the actual collapse load most closely, compared with the other four assumptions, with good agreement between experimental and theoretical results. This is in spite of the fact that model M_2 failed at a higher load, owing to strain hardening and other effects which were ignored in the analysis.

It was found possible to use a system of interconnected hydraulic jacks to simulate uniformly distributed loading. Collapse of models M_1 and M_2 occurred by mode B, as expected. Slab strips S_1 and S_2 control specimens gave results very close to the theoretical values.

The shear connectors were designed to simulate type (5) composite design. Careful observations, with the aid of slip gauges, were made on models M_1 , M_2 and M_3 . These observations showed that the behaviour of these shear connectors were adequate throughout the testing process.

It could be generally concluded that the test series confirmed that type (5) assumption, which gives the greatest saving in weight and structural efficiency, can be safely applied in the design of composite beam and slab floor systems. However, type (3) assumption also gave results which were in good agreement with experimental values, and would make the best alternative to the use of type (5) assumption.

12.3 SUGGESTIONS FOR FUTURE RESEARCH:-

- (1) This thesis shows that there are many design advantages in using composite action between slabs and beams. The interaction

between these two elements is by no means the only one in a structure. Whenever any continuity exists between two components, there is bound to be a certain degree of structural interaction, and the basic philosophy of composite design is that this interaction should be both recognised and allowed for during the design process. It is usual for specifications to allow no provision to be made for the effect of cladding and to stipulate that all wind forces should be carried on the bare steelwork. While it may be true that certain types of cladding add very little strength to a framework, almost all cladding will increase the stiffness of the structure. The effect of the walls on the bare steel frame of the Empire State Building has been found to increase the stiffness by a factor of about 4.5. The effect of stiffness owing to cladding should, therefore, be made use of in design. It would be extremely useful to utilise the effects of cladding in the design of tall structures. This is one suggestion for future investigators.

- (2) The development is also suggested of an automatic computer program for the plastic design of multi-storey frames, taking into consideration the effects of instability and that of composite action (cf. Chapter 8). Once this is achieved, comparisons can be made between these designs, which include the effect of composite action, and the traditional design of bare steel frames. Only such a comparison can reveal the relative importance of such effects as stability and economy achieved by using composite action.
- (3) Should it be required to use reinforced concrete casing for the columns of a steel frame in order to satisfy the fire proofing requirements⁽¹³⁾, then it would be possible to modify the computer program suggested above, in order to take full advantage of the

extra strength available. In the proposed design method shown in Chapter 8, it has been shown that the column ends are not required to undergo any rotation owing to the formation of a fully plastic hinge. Therefore, the concrete casing would be assumed to carry a proportion of the total axial load in the member, thus relieving the steel section of a certain amount of direct stress. In the lower regions of the frame, where the selection of suitable columns is largely controlled by the axial load in the member, considerably lighter Universal Columns would be found to be adequate.

APPENDIX 1

A PROGRAM TO CALCULATE THE SUM OF COMPOSITE AND BEAM MOMENT(M_c+M_b)

```
begin
integer i,j,n,Uw,b,t,l
real z,dn,Mc,Mb,My,Uc,fy,a,dc,x,h,h',h'',e,e',g,g'
read(fy,n)
begin
array A(1:n,1:10)
read array(A)
newline
j=0
cycle Uw=3000,1000,6000
Uc=4*Uw/9
cycle i=1,1,n
newlines(3)
print(A(i,8),2,1)
space
caption $ X
space
print(A(i,9),2,2)
space
caption $ X
space
print(A(i,10),3,1)
spaces(2)
caption LBS. $ U. $ B.
spaces(19)
caption PLASTIC $ COMPOSITE $ MOMENT $ Mc $ (KIPS-FT.) $ FOR $ U $ = $
print(Uw,4,0)
newline
Mb=(fy*A(i,3))/12000
caption Mb $ =
print(Mb,4,1)
spaces(2)
caption KIPS-FT.
newline
caption SLAB
spaces(4)
caption SLAB
space
caption THICKNESS
spaces(6)
caption SLAB
```

```

space
caption THICKNESS
newline
caption WIDTH
spaces(6)
caption 4 ½ INCHES
spaces(12)
caption 5 ½ INCHES
spaces(12)
caption 6 ½ INCHES
spaces(12)
caption 7 ½ INCHES
spaces(12)
caption 8 ½ INCHES
newline
caption (FT.)
spaces(3)
caption (Mc)
spaces(4)
caption (Mc+Mb)
spaces(6)
caption (Mc)
spaces(4)
caption (Mc+Mb)
newline
cycle b=10,5,40
l=b*12
newline
print(b,2,0)
spaces(4)
cycle t=4,1,8
a=A(i,1)*fy
-> 1 if a > (Uc*t*1)
dn=a/(Uc*1)
h'=(A(i,2)+2*t-dn)
Mc=(0.5*a*h')/12000
My=Mc+Mb
print(Mc,4,1)
spaces(2)
print(My,4,1)
spaces(4)
-> 2
1: h'=A(i,4)*A(i,5)*fy
-> 3 if (t*Uc*1+2*h') < a
h''=A(i,4)*fy
z=0.5*(a-Uc*t*1)/h''
dn=t+z
dc=0.5*(A(i,2)+t)
e=dn-t

```

```

Mc=(a*dc-h'*dn*e)/12000
My=Mc+Mb
print(Mc,4,1)
spaces(2)
print(My,4,1)
spaces(4)
-> 2
3: e=A(i,4)*A(i,5)*fy
e'=A(i,6)*fy
z=0.5*(a-2*e-1*Uc*t)/e'
dn=t+A(i,5)+z
dc=0.5*(A(i,2)+t)
g=t+A(i,5)
g'=dn+A(i,5)
Mc=(a*dc-e*g-e'*g'*z)/12000
My=Mc+Mb
print(Mc,4,1)
spaces(2)
print(My,4,1)
spaces(4)
2: repeat
repeat
j=j+1
x=j/3
if fracpt(x) > 0.00001 then -> 5
newlines(2)
spaces(55)
print(x,3,0)
newpage
5: repeat
repeat
end
end of program

```

DATA

1. Yield stress of beams in lbs./sq.in.
2. Number of beams used.
3. Properties of each beam,
 - (i) area
 - (ii) depth
 - (iii) plastic modulus
 - (iv) width of flange
 - (v) thickness of flange
 - (vi) thickness of web
 - (vii) → (ix) beam size.

***Z

APPENDIX 2

A GENERAL PROGRAM FOR THE DESIGN OF BEAM AND SLAB FLOOR SYSTEMS

```

begin
integer n
select input (1)
read(n)
begin
array A(1:n,1:10)
read array (A)
begin
integer N,N',B,D,i,j,F,Uw,t,y,s,H1,H2,T,case
real fi,rw,rw',rw'',l,p,c,c',fy,ft,z,dn,dc,Uc,d,At1,At2,y',E,d1,d2,
MB,Mb,MB',Mb',Me,Mc,Mx,My,Ms,a,a',a'',h',h'',h,dn',e,e',e'',g,g',g'',
k',r,r',q,k,x',fc,x,k'',WBX,WBY,WB,WC,WRX,WRY,WR,WF,R,x'',m,p',m',W,
ds,df,dn,IG,IC,AC
read(N')
cycle case=1,1,N'
read(p',E,R,s,fy,ft,c,c',H1,N,H2,T,D,1)
comment N IS THE TOTAL NO. OF BAYS
array L(0:N+1)
read array (L)
B=N+1
if D= 0 then B= 3
newline
k= 0
Me=0
Mc=0
dn=0
dn'=0
cycle Uw=3000,1000,6000
Uc=4*Uw/9
cycle t=40,10,70
d=0.1*t
p=p'+0.001*(12.5*d*1.75)
d1=d-c
d2=d-c'
k''=0
WBX=0
WBY=0
WRX=0
WRY=0
WC=0
g=0
-> 500 if N=1
comment INTERNAL BAYS
cycle i= 2,1,B-1
newline
caption FRAME ‡ NO. ‡ (
print(H1,2,0)
caption )
spaces(3)
caption TYPE ‡ (
print(H2,1,0)
caption )
newline

```

```

caption CUBE § STRENGTH § =
print(Uw,4,0)
spaces(2)
caption LBS. § / § SQ. § INCH
newline
caption SLAB § THICKNESS § =
print(d,2,1)
spaces(2)
caption INCHES
newline
-> 83 if i=B-1 and D=1
caption BAY § NO. § (
print(i,2,0)
caption )
spaces(10)
rw = 1/L(i)
-> 1 if rw > 1
fi = sqrt(rw*rw+3)-rw
Ms=(p*1*L(i)*rw*(3-rw*fi))/(48*(rw/fi+1))
-> 83
1: fi=sqrt(1/(rw*rw)+3)-1/rw
Ms=(p*1*L(i)*(3*rw-fi))/(48*rw*(1/fi+rw))
83: -> 8 if E > 0.5
if R > 0.5 then Mx=1*(0.0625*p*L(i)^-Ms)
if R > 0.5 then My=0.5*(L(i)+L(i-1))*(0.0625*p*1^-Ms)
-> 82 if R > 0.5
Mx=1*(0.125*p*L(i)*L(i)-Ms)
My=0.5*(L(i-1)+L(i))*(0.125*p*1*1-Ms)
82: if i=N and k'=1 then -> 109
-> 180 if i=B-1 and D=1
-> 999 if (4500*Ms) > (d2^*Uw)
109: rw''=(4*d2*Uw-sqrt(16*d2^*Uw^-6*Uw*Ms*12000))/(9*ft*d2)
if rw'' > ((2*Uw)/(9*ft)) then caption At2 § IS § OVER § REINFORCED
spaces(10)
rw'=(4*d1*Uw-sqrt(16*d1^*Uw^-6*Uw*Ms*12000))/(9*ft*d1)
if rw' > ((2*Uw)/(9*ft)) then caption At1 § IS § OVER § REINFORCED
At1=rw'*12*d1
At2=rw''*12*d2
newlines(2)
caption Ms § (
print(i,2,0)
caption ) § =
print(Ms,2,4)
spaces(2)
caption KIPS § FT. § / § FT. § RUN
spaces(5)
caption At § 1 § =
print(At1,2,4)
spaces(2)
caption IN. § SQ. § / § FT. § RUN
spaces(5)
caption At § 2 § =
print(At2,2,4)
spaces(2)
caption IN. § SQ. § / § FT. § RUN
newline
caption REQUIRED § Mx § (
print(i,2,0)
caption ) § =
print(Mx,5,5)

```

```

spaces(2)
caption KIPS  $\frac{1}{2}$  -  $\frac{1}{2}$  FT.
180; newline
caption REQUIRED  $\frac{1}{2}$  My  $\frac{1}{2}$  (
print(i,2,0)
caption )  $\frac{1}{2}$  =
print(My,5,5)
spaces(2)
caption KIPS  $\frac{1}{2}$  -  $\frac{1}{2}$  FT.
-> 182 if i=N and k'=1
-> 181 if i=B-1 and D=1
182; newline
a'=At1*ft*s
a''=12*Uc
y=0
cycle j=1,1,n
MB'=(A(j,3)*fy)/12000
MB=MB'
-> 3 if R > 0.5
a=A(j,1)*fy
-> 2 if a > (a'*1+a''*d*1)
dn=(a+a'*1)/(a''*1)
h'=(A(j,2)+2*d-dn)
h''=(d-0.5*dn-c)
Me=(0.5*a*h'+a'*1*h'')/12000
-> 3
2: h'=A(j,4)*A(j,5)*fy
-> 4 if (d*a''*1+2*h'+a'*1) < a
h''=A(j,4)*fy
z=0.5*(a-a''*d*1-a'*1)/h''
dn=d+z
dc=0.5*(A(j,2)+d)
e=A(j,4)*fy
g'=0.5*d-c
Me=(a*dc-e*dn*z-a'*1*g')/12000
-> 3
4: e=A(j,6)*fy
g'=A(j,4)*A(j,5)*fy
z=0.5*(a-2*g'-a''*1*d-a'*1)/e
dn=d+A(j,5)+z
dc=0.5*(A(j,2)+d)
r'=d+A(j,5)
e'=dn+A(j,5)
h''=0.5*d-c
Me=(a*dc-g'*r'-e*e'*z-a'*1*h'')/12000
dn'=0
3: -> 85 if g > 0.5
92: if g > 0.5 and i=1 then y'=Me+0.5*MB+0.5*MB'
if g > 0.5 and N=1 and i=1 then y'=Me+MB'
if g > 0.5 and N=1 and i=1 then MB=MB'
-> 95 if g>0.5 and i=1
if g > 0.5 and i= N and k''=1 then y'= Me +0.5*MB+0.5*MB'
-> 95 if g > 0.5 and i= N and k''=1
y' = MB + Me
95: if y' > Mx then y= 1
-> 6 if y > 0.5
repeat
6; newline
caption CHOSEN  $\frac{1}{2}$  BEAM  $\frac{1}{2}$  SIZE  $\frac{1}{2}$  IN  $\frac{1}{2}$  Lx(
print(i,2,0)

```

```

caption ) § DIRECTION § = §
print(A(j,8),2,1)
spaces(2)
caption § X §
print(A(j,9),2,2)
spaces(2)
caption X §
print(A(j,10),3,1)
spaces(2)
caption LBS. § U. § B.
newlines(2)
caption COMPOSITE § MN § (
print(i,2,0)
caption ) § AT § SUPPORT § =
print(MB,4,4)
spaces(2)
caption KIPS § - § FT.
newline
caption MB § (
print(i,2,0)
caption ) § =
print(MB',4,4)
spaces(2)
caption KIPS § - § FT.
newline
caption Me § (
print(i,2,0)
caption ) § =
print(Me,4,4)
spaces(2)
caption KIPS § - § FT.
newline
caption CHOSEN § Mx § (
print(i,2,0)
caption ) § =
print(y',4,4)
spaces(2)
caption KIPS § - § FT.
newlines(2)
caption DEPTH § OF § PLASTIC § NEUTRAL § AXIS § dn § AT § CENTRE § IN § Lx § (
print(i,2,0)
caption ) § DIRECTION § =
print(dn,2,2)
spaces(2)
caption INCHES
newline
caption DEPTH § OF § PLASTIC § NEUTRAL § AXIS § dn' § AT § SUPPORT § IN § Lx §
print(i,2,0)
caption ) § DIRECTION § =
print(dn',2,2)
spaces(2)
caption INCHES
newline
caption DISTANCES § OF § POINT § OF § CONTRAFLEXURE § FROM § SUPPORT § =
x' = 0.5*L(i)*(1-sqrt(Me/(Me+MB)))
if R > 0.5 then x' = 0.14645*L(i)
print(x',2,2)
spaces(2)
caption FT.
newline

```

```

caption TOTAL § HORIZONTAL § SHEAR § FORCE § Fcc § AT § CENTRE § IN § Lx § (
print(i,2,0)
caption ) § DIRECTION § =
if R > 0.5 then fc=0
-> 99 if R > 0.5
if dn < d then fc= A(j,1)*fy/2240
if dn > d then fc = (Uc*d*1*12+At1*1*ft*s)/2240
99: print(fc,3,3)
spaces(2)
caption TONS
newline
fc = 0
caption TOTAL § HORIZONTAL § SHEAR § FORCE § Fcc § AT § SUPPORT § IN § Lx § (
print(i,2,0)
caption ) § DIRECTION § =
if dn' < d and E > 0.5 then fc= A(j,1)*fy/2240
if dn' > d and E > 0.5 then fc = At1*1*ft/2240
if N=1 then fc=0
print(fc,3,3)
spaces(2)
caption TONS
IC=(1*d^3)/15
AC=d*1*0.8
-> 601 if R > 0.5
h=0.5*A(j,2)+d
dn=(1.25*A(j,1)/1)*(sqrt(1+(1.6*h*1)/A(j,1))-1)
-> 600 if dn > d
IG=A(j,7)+A(j,1)*(h-dn)^(1*12*dn^3)/45
-> 602
600: dn=(AC*0.5*d+A(j,1)*h)/(AC+A(j,1))
IG=IC+AC*(dn-0.5*d)^(1*12*dn^3)/45
601: if R > 0.5 then IG=IC+A(j,7)
602: W=(p'*1000*1*L(i))/1.75
ds=(5*W*L(i)^3*1728)/(384*13000*2240*IG)
df=0.20*ds
dm=L(i)/30
newline
caption MOMENT § OF § INERTIA § OF § Lx § (
print(i,2,0)
caption ) § SECTION § =
print(IG,5,2)
spaces(2)
caption IN.4
newline
caption MAX. § ALLOWABLE § DEFLECTION § AT § CENTRE § OF § Lx § (
print(i,2,0)
caption ) § =
print(dm,2,3)
spaces(2)
caption IN.
newline
caption DEFLECTION § AT § CENTRE § OF § Lx § (
print(i,2,0)
caption ) § IF § CONSIDERED § SIMPLY § SUPPORTED § =
print(ds,2,3)
spaces(2)
caption IN.
newline
caption DEFLECTION § AT § CENTRE § OF § Lx § (
print(i,2,0)
caption ) § IF § CONSIDERED § FIXED § ENDED § =

```

```

print(df,2,3)
spaces(2)
caption IN.
-> 275 if N=1
m=1
if T=1 and N=3 and i=2 then m=0
-> 251 if D=0
WBX=WBX+(A(j,10)*L(i)*m)/2240
WC=WC+(12*1*L(i)*d*m)/2240
251: if D=0 and i=2 then WBX=((N-2)*A(j,10)*L(i)*m)/2240
if D=0 and i=2 then WC=((N-2)*12*1*L(i)*d*m)/2240
if D=0 and i=1 then WBX=WBX+(2*A(j,10)*L(i))/2240
if D=0 and i=1 then WC=WC+(2*12*1*L(i)*d)/2240
275: if N=1 then WBX=(A(j,10)*L(i))/2240
if N=1 then WC=(12*1*L(i)*d)/2240
newline
if i=N and k'=1 then i=N+1
181: y = 0
a'=At2*ft*s
cycle j=1,1,n
Mb'=(A(j,3)*fy)/12000
Mb=Mb'
-> 9 if R > 0.5
a=A(j,1)*fy
-> 7 if a > (a'*0.5*(L(i-1)+L(i))+a'*d*0.5*(L(i-1)+L(i)))
dn=(a+a'*0.5*(L(i-1)+L(i)))/(a'*0.5*(L(i-1)+L(i)))
h'=(A(j,2)+2*d-dn)
h'=(d-0.5*dn-c')
Mc=(0.5*a*h'+a'*0.5*(L(i-1)+L(i))*h')/12000
-> 9
7: h'=A(j,4)*A(j,5)*fy
-> 10 if (d*a'*0.5*(L(i-1)+L(i))+2*h'+a'*0.5*(L(i-1)+L(i))) < a
h'=(A(j,4)*fy)
z=0.5*(a-a'*d*0.5*(L(i-1)+L(i))-a'*0.5*(L(i-1)+L(i)))/h'
dn=d+z
dc=0.5*(A(j,2)+d)
e=A(j,4)*fy
g'=0.5*d-c'
k'=0.5*(L(i-1)+L(i))
Mc=(a*dc-e*dn*z-a'*k'*g')/12000
-> 9
10: e=A(j,6)*fy
g'=A(j,4)*A(j,5)*fy
k'=0.5*(L(i-1)+L(i))
z=0.5*(a-2*g'-a'*k'*d-a'*k')/e
dn=d+A(j,5)+z
dc=0.5*(A(j,2)+d)
r'=d+A(j,5)
e'=dn+A(j,5)
h'=0.5*d-c'
Mc=(a*dc-g'*r'-e*e'*z-a'*k'*h')/12000
9: -> 57 if g > 0.5
73: y'=Mb+Mc
if y' > My then y=1
-> 11 if y > 0.5
repeat
11: newline
caption CHOSEN § BEAM § SIZE § IN § Ly § (
print(i,2,0)
caption ) § DIRECTION § = §

```

```

print(A(j,8),2,1)
spaces(2)
caption X ‡
print(A(j,9),2,2)
spaces(2)
caption X ‡
print(A(j,10),3,1)
spaces(2)
caption LBS. ‡ U. ‡ B.
newlines(2)
caption COMPOSITE ‡ Mn' ‡ (
print(i,2,0)
caption ) ‡ AT ‡ SUPPORT ‡ =
print(Mb,4,4)
spaces(2)
caption KIPS ‡ - ‡ FT.
newline
caption Mb' ‡ (
print(i,2,0)
caption ) ‡ =
print(Mb',4,4)
spaces(2)
caption KIPS ‡ - ‡ FT.
newline
caption Mc ‡ (
print(i,2,0)
caption ) ‡ =
print(Mc,4,4)
spaces(2)
caption KIPS ‡ - ‡ FT.
newline
caption CHOSEN ‡ My ‡ (
print(i,2,0)
caption ) ‡ =
print(y',4,4)
spaces(2)
caption KIPS ‡ - ‡ FT.
newlines(2)
caption DEPTH ‡ OF ‡ PLASTIC ‡ NEUTRAL ‡ AXIS ‡ dn ‡ AT ‡ CENTRE ‡ IN ‡ Ly ‡ (
print(i,2,0)
caption ) ‡ DIRECTION ‡ =
print(dn,2,2)
spaces(2)
caption INCHES
newline
caption DEPTH ‡ OF ‡ PLASTIC ‡ NEUTRAL ‡ AXIS ‡ dn' ‡ AT ‡ SUPPORT ‡ IN ‡ Ly ‡ (
print(i,2,0)
caption ) ‡ DIRECTION ‡ =
print(dn',2,2)
spaces(2)
caption INCHES
newline
caption DISTANCE ‡ OF ‡ POINT ‡ OF ‡ CONTRAFLEXURE ‡ FROM ‡ SUPPORT ‡ =
 $x''=0.5*1*(1-\text{sqrt}(Mc/(Mc+Mb)))$ 
if R > 0.5 then  $x''=0.14645*1$ 
print(x'',2,2)
spaces(2)
caption FT.
newline
caption TOTAL ‡ HORIZONTAL ‡ SHEAR ‡ FORCE ‡ Fcc ‡ AT ‡ CENTRE ‡ IN ‡ Ly ‡ (

```

```

print(i,2,0)
caption ) $ DIRECTION $ =
if R > 0.5 then fc=0
-> 121 if R > 0.5
if dn < d then fc=A(j,1)*fy/2240
m'=0.5*(L(i)+L(i-1))
if dn > d then fr=(Uc*d*m'*12+At2*m'*ft*s)/2240
121: print(fc,3,3)
spaces(2)
caption TONS
newline
fc=0
caption TOTAL $ HORIZONTAL $ SHEAR $ FORCE $ Fcc $ AT $ SUPPORT $ IN $ Ly $ (
print(i,2,0)
caption ) $ DIRECTION $ =
if dn' < d and E > 0.5 then fc=A(j,1)*fy/2240
if dn' > d and E > 0.5 then fc=At2 *m'*ft/2240
print(fc,3,3)
spaces(2)
caption TONS
m'=0.5*(L(i)+L(i-1))
IC=(m'*d^3)/15
AC=d*m'*0.8
-> 701 if R > 0.5
h=0.5*A(j,2)+d
dn=(1.25*A(j,1)/m')*(sqrt(1+(1.6*h*m')/A(j,1))-1)
-> 700 if dn > d
IG=A(j,7)+A(j,1)*(h-dn)^+(m'*12*dn^3)/45
-> 702
700: dn=(AC*0.5*d+A(j,1)*h)/(AC+A(j,1))
IG=IC+AC*(dn-0.5*d)^+A(j,7)+A(j,1)*(h-dn)^
701: if R > 0.5 then IG=IC+A(j,7)
702: W=(p'*1000*1*m')/1.75
ds=(5*W*1^3*1728)/(384*13000*2240*IG)
df=0.20*ds
dm=1/30
newline
caption MOMENT $ OF $ INERTIA $ OF $ Ly $ (
print(i,2,0)
caption ) $ SECTION $ =
print(IG,5,2)
spaces(2)
caption IN.4
newline
caption MAX. $ ALLOWABLE $ DEFLECTION $ AT $ CENTRE $ OF $ Ly $ (
print(i,2,0)
caption ) $ =
print(dm,2,3)
spaces(2)
caption IN.
newline
caption DEFLECTION $ AT $ CENTRE $ OF $ Ly $ (
print(i,2,0)
caption ) $ IF $ CONSIDERED $ SIMPLY $ SUPPORTED $ =
print(ds,2,3)
spaces(2)
caption IN.
newline
caption DEFLECTION $ AT $ CENTRE $ OF $ Ly $ (
print(i,2,0)

```

```

caption ) § IF § CONSIDERED § FIXED § ENDED § =
print(df,2,3)
spaces(2)
caption IN.
if i=N+1 and k''=1 then i=N
if N=1 then WRX=(At1*L(i)*490)/(144*2240)
if N=1 then WRY=((At2*L(i)*1+At2*L(i)*2*x'')*490)/(144*2240)
-> 280 if N=1
m=1
if T=1 and N=3 and i=2 then m=0
-> 260 if i=B-1 and D=1 and k''=0
-> 254 if D=0
-> 265 if i=1 and D=1
-> 266 if i=N and k''=1 and D=1
WRX=WRX+((At1*L(i)*m+At1*L(i)*2*x'*m)*490)/(144*2240)
265: if i=1 then WRX=WRX+((At1*L(i)*m+At1*L(i)*x'*m)*490)/(144*2240)
266: if i=N and k''=1 then WRX=WRX+((At1*L(i)*m+At1*L(i)*x'*m)*490)/(144*2240)
WRY=WRY+((At2*L(i)*1*m+At2*L(i)*2*x'*m)*490)/(144*2240)
-> 260 if D=1
254: if D=0 and i=2 then WRX=(((N-2)*At1*L(i)*m+(N-2)*At1*L(i)*2*x'*m)*490) / (144*2240)
if D=0 and i=1 then WRX=WRX+((2*At1*L(i)*m+2*At1*L(i)*x'*m)*490)/(144*2240)
if D=0 and i=2 then WRY=(((N-2)*At2*L(i)*1*m+(N-2)*At2*L(i)*2*x'*m)*490) / (144*2240)
if D=0 and i=1 then WRY=WRY+((2*At2*L(i)*1*m+2*At2*L(i)*2*x'*m)*490) / (144*2240)
260: -> 250 if D=0
WBY=WBY+(A(j,10)*1*m)/2240
250: if D=0 and i=2 then WBY=((N-1)*A(j,10)*1)/2240
if D=0 and i=2 and T=1 and N=3 then WBY=(A(j,10)*1)/2240
if D=0 and i=1 then WBY=WBY+(2*A(j,10)*1)/2240
280: if D=0 and N=1 then WBY=(2*A(j,10)*1)/2240
newline
k=k+1
x=k
-> 55 if i=N and k''=1
-> 340 if i=1 and D=0
newlines(2)
spaces(55)
print(x,3,0)
newpage
340: -> 55 if i=1
12: repeat
500: i=1
if N=1 and E>0.5 then g=1
-> 44
8: Mx=p*L(i)^1*0.125
My=0.125*p*0.5*(L(i)+L(i-1))*1^
g=1
-> 82
85: q=At1*ft
-> 14 if (1*q) < a
dn'=(a+a'*1*d-q*1)/(a'*1)
e=0.5*A(j,2)+d-c
e'=d-dn'
e''=0.5*(d+dn'-2*c)
MB=(p*e+1*e'*a'*e'')/12000
-> 92
14: h'=A(j,4)*A(j,5)*fy
-> 16 if (q*1+2*h') < a

```

```

h' = A(j, 4) * fy
z = 0.5 * (a - q * 1) / h'
dn' = d + z
e = 0.5 * A(j, 2) + d - c
e' = dn' + d - 2 * c
MB = (a * e - h' * z * e') / 12000
-> 92
16: e = A(j, 4) * A(j, 5) * fy
e' = A(j, 6) * fy
e'' = 0.5 * A(j, 2) + d - c
g' = 2 * d + A(j, 5) - 2 * c
z = 0.5 * (a - 2 * e - 1 * q) / e'
dn' = d + A(j, 5) + z
k' = dn' + A(j, 5) + d - 2 * c
MB = (a * e'' - e * g' - e' * z * k') / 12000
-> 92
57: q = At2 * ft
-> 20 if ((L(i-1) + L(i)) * 0.5 * q) < a
k' = 0.5 * (L(i-1) + L(i))
dn' = (a + e'' * k' * d - q * k') / (a'' * k')
e = 0.5 * A(j, 2) + d - c'
e' = d - dn'
e'' = 0.5 * (d + dn' - 2 * c')
Mb = (a * e + k' * e'' * a'' * e'') / 12000
-> 73
20: h' = A(j, 4) * A(j, 5) * fy
k' = 0.5 * (L(i-1) + L(i))
-> 21 if (q * k' + 2 * h') < a
h'' = A(j, 4) * fy
z = 0.5 * (a - q * k') / h''
dn' = d + z
e = 0.5 * A(j, 2) + d - c'
e' = dn' + d - 2 * c'
Mb = (a * e - h'' * z * e') / 12000
-> 73
21: e = A(j, 4) * A(j, 5) * fy
e' = A(j, 6) * fy
e'' = 0.5 * A(j, 2) + d - c'
r' = 0.5 * (L(i-1) + L(i))
z = 0.5 * (a - 2 * e - r' * q) / e'
dn' = d + A(j, 5) + z
g' = 2 * d + A(j, 5) - 2 * c'
k' = dn' + A(j, 5) + d - 2 * c'
Mb = (a * e'' - e * g' - e' * z * k') / 12000
-> 73
comment OUTSIDE BAYS
44: F=D
35: caption FRAME $ NO. $ (
print(H1, 2, 0)
caption )
spaces(3)
caption TYPE $ (
print(H2, 1, 0)
caption )
newline
caption CUBE $ STRENGTH $ =
print(Uw, 4, 0)
spaces(2)
caption LBS. $ / $ SQ. $ INCH

```

```

newline
caption SLAB § THICKNESS § =
print(d,2,1)
spaces(2)
caption INCHES
newline
caption BAY § NO. § (
print(i,2,0)
caption )
spaces(10)
rw=1/L(i)
-> 28 if rw > 1
fi = 0.75*sqrt(rw*rw+4)-0.75*rw
Ms=(p*L(i)*1*rw*(3-rw*fi))/(24*(1.5*rw/fi+2))
if N=1 then fi=0.5*(sqrt(rw^+6)-rw)
if N=1 then Ms=(p*L(i)*1*rw*(3-rw*fi))/(24*(rw/fi+2))
-> 29
28; fi=(4*(sqrt(1+9*rw*rw/4)-1))/(3*rw)
Ms=(p*L(i)*1*(3*rw-fi))/(24*rw*(2/fi+1.5*rw))
if N=1 then fi=sqrt(4/(rw^+6)-1/rw)
if N=1 then Ms=(p*1*L(i)*(3*rw-fi))/(24*rw*(2/fi+rw))
29; -> 31 if E > 0.5
if R > 0.5 then Mx=1*(p*L(i)^*0.0625-0.75*Ms)
if R > 0.5 and N=1 then Mx=1*(p*L(i)^*0.0625-0.5*Ms)
if R > 0.5 then My=L(i)*(0.03125*p*1^-0.5*Ms)
-> 82 if R > 0.5
Mx=0.125*1*(p*L(i)*L(i)-4*Ms)
if N=1 then Mx=0.125*p*1*L(i)^
My=L(i)*(p*1*1/16-0.5*Ms)
-> 82
31; Mx=0.125*p*1*L(i)^
My=p*L(i)*1^ /16
-> 82
55; if F=0 then -> 100
i=N
F=0
k''=1
-> 35
100; newline
caption TOTAL § WEIGHT § OF § BEAMS § IN § Lx § DIRECTION § =
print(WBX,4,3)
spaces(2)
caption TONS
newline
caption TOTAL § WEIGHT § OF § BEAMS § IN § Ly § DIRECTION § =
print(WBY,4,3)
spaces(2)
caption TONS
newline
caption TOTAL § WEIGHT § OF § ALL § THE § BEAMS § IN § THE § FRAME § c
FOR § U § =
print(Uw,4,0)
caption § AND § SLAB § THICKNESS § =
print(d,2,1)
caption § =
WB=WBX+WBY
print(WB,4,3)
spaces(2)
caption TONS
newline
caption TOTAL § WEIGHT § OF § REINFORCEMENT § At1 § =

```

```

print(WRX,2,2)
space
caption TONS
spaces(2)
caption TOTAL § WEIGHT § OF § REINFORCEMENT § At2 § =
print(WRY,2,2)
space
caption TONS
newline
caption TOTAL § WEIGHT § OF § ALL § THE § REINFORCEMENT § IN § THE § FRAME § =
WR=WRX+WRY
print(WR,4,3)
spaces(2)
caption TONS
newline
caption TOTAL § WEIGHT § OF § ALL § THE § CONCRETE § IN § THE § FRAME § =
print(WC,4,3)
spaces(2)
caption TONS
newline
WE=WC+WR+WB
caption TOTAL § WEIGHT § OF § THE § WHOLE § FRAME § =
print(WF,4,3)
spaces(2)
caption TONS
newline
spaces(55)
print(x,3,0)
newpage
999: repeat
repeat
repeat
end
end
end of program

```

R E F E R E N C E S

1. Steel, K.A.
"Plastic collapse of composite structures".
Ph.D. Thesis University of Leeds 1964.
2. Prager, W.; Hodge, P.
"Theory of perfectly plastic solids".
Chapman and Hall Limited London 1951.
3. Wood, R.H.
"The stability of tall buildings".
Proceedings of the Institution of Civil Engineers.
September 1958.
4. Gandhi, S.N.
"Collapse load for multi-storey steel frames".
Ph.D. Thesis University of Leeds 1964.
5. Livesley, E.K.; Chandler, D.B.
"Stability functions for structural frameworks".
Manchester University Press 1956.
6. Calladine, C.R.
Discussion on paper by Heyman⁽³¹⁾.
Proceedings of the Institution of Civil Engineers.
April 1962.
7. Clough, C.J.
"An investigation into the design of a tall building".
Ph.D. Thesis University of Leeds 1966.
8. Steel Structures Research Committee.
Final Report.
H.M.S.O. 1936.
9. Baker, Sir J.F.; Williams, E.L.
"The effect of wind on frames with semi-rigid connections".
Final Report S.S.R.C.
H.M.S.O. London.
10. Wood, R.H.
"An economical design of rigid steel frames
for multi-storey buildings".
National Building Studies, Research Paper No. 10.
H.M.S.O. London 1951.

11. Lightfoot, E.
"Moment distribution".
E. and F.N. Span London 1961.
12. Naylor, N.
"Sidesway in symmetrical building frames".
The Structural Engineer.
April 1950.
13. British Standards Institution.
"The use of structural steel in building".
B.S.449 : 1965.
14. Neal, B.G.
"The plastic methods of structural analysis".
Chapmand and Hall 1959.
15. Kazincy, G.
"Kiserletek befalazott tartokkal".
Beton szemle, Volume 2, No. 68, 1914.
16. Kist, N.C.
"Leidt een Sterkteberekening, die Uitgaat van de
Evenredigheid van kracht en Vormverandering, tot
een goede Constructie van Ijzeren Bruggen en gebouwen".
Inaugural Dissertation - Polytechnic Institute, Delft.
December 1917.
17. Gruning, M.
"Die Tragfähigkeit statisch unbestimmten Tragwerke
aus stahl bei beliebig häufig wiederholter Belastung".
Julius Springer Berlin 1926.
18. Maier-Leibnitz, H.
"Beitrag zur Frage der tatsächlichen Tragfähigkeit
einfacher und durchlaufender Balkenträger aus
Baustahl St. 37 und aus Holz".
Bautechnik Vol. 6 1928.
19. Maier-Leibnitz, H.
"Versuche, Ausdeutung und Anwendung der Ergebnisse".
Preliminary Publication - 2nd Congress of the
International Association for Bridge and Structural
Engineering.
Berlin 1936.
20. van den Broek, J.A.
"Theory of limit design".
Transactions of the American Society of Civil Engineers.
Vol. 105 1940.

21. van den Broek, J.A.
"Theory of limit design".
John Wiley (New York) 1948.
22. Baker, Sir J.F.; Roderick, J.W.
"An experimental investigation of the
strength of seven portal frames".
Transactions of the Institute of Welding.
Vol. 1 1938.
23. British Standards Institution.
B.S. 449 : 1948.
24. Horne, M.R.
"Fundamental propositions in the plastic
theory of structures".
Journal of the Institution of Civil Engineers.
Vol. 34 1950.
25. Greenberg, H.J.; Prager, W.
"On limit design of beams and frames".
Transactions of the American Society of Civil Engineers.
Vol. 77 1951.
26. Neal, B.G.; Symonds, P.S.
"The rapid calculation of the plastic
collapse load for a framed structure".
Proceedings of the Institution of Civil Engineers.
Vol. 1, Part III 1952.
27. Neal, B.G.; Symonds, P.S.
"The calculation of plastic collapse loads for plane frames".
Preliminary Publication - 4th Congress of the International
Association for Bridge and Structural Engineering.
Cambridge and London 1952.
28. Neal, B.G.; Symonds, P.S.
"The calculation of collapse loads for framed structures".
Journal of the Institution of Civil Engineers.
Vol. 35 1950-1.
29. Horne, M.R.
"A moment distribution method for the analysis and
design of structures by the plastic theory".
Proceedings of the Institution of Civil Engineers.
Vol. 3, Part III 1954.
30. Baker, Sir J.F.; Horne, M.R.; Heyman, J.
"The steel skeleton - Vol. II".
Cambridge University Press 1956.

31. Heyman, J.
"An approach to the design of tall steel buildings".
Proceedings of the Institution of Civil Engineers.
December 1960.
32. Merchant, W.
"Critical loads of tall building frames".
Structural Engineer
Part I March 1955
Part II August 1956
Part III September 1956
Part IV June 1958
33. Merchant, W.
"Frame instability in plastic range".
Journal of British Welding.
Vol. 3 1956.
34. Merchant, W.
"The failure load of rigidly jointed frameworks
as influenced by stability".
Structural Engineer.
July 1954.
35. Low, M.W.
"Some model tests on multi-storey rigid steel frames".
Proceedings of the Institution of Civil Engineers.
July 1959.
36. Holmes, M.; Gandhi, S.N.
"Ultimate load design of tall steel buildings
allowing for instability".
Proceedings of the Institution of Civil Engineers.
January 1965.
37. Sinclair-Jones, H.W.
"Plastic design of multi-storey sway frames".
Ph.D. Thesis University of Aston in Birmingham 1969.
38. Holmes, M.; Sinclair-Jones, H.W.
"Plastic design of multi-storey sway frames".
Proceedings of the Institution of Civil Engineers.
September 1969.
39. Majid, K.I.; Anderson, D.
"Elastic-plastic design of sway frames by computer".
Proceedings of the Institution of Civil Engineers.
December 1968.

40. The Council for Codes of Practice British Standards Institution.
"Composite construction in structural steel and concrete".
C.P.117 : Part I : 1965.
41. Viest, I.M.
"Review of research on composite steel-concrete beams".
Journal of the Structural Division.
Proceedings of the American Society of Civil Engineers.
June 1960.
42. Viest, I.M.
"Investigation of stud shear connectors for
composite concrete and steel T-beams".
Journal of the American Concrete Institute.
April 1956.
43. Chapman, J.C.
"Composite construction in steel and concrete -
The behaviour of composite beams".
The Structural Engineer.
April 1964.
44. Chapman, J.C.; Balakrishnan, S.
"Experiments on composite beams".
The Structural Engineer.
November 1964.
45. Davis, C.
"Tests on half-scale steel-concrete composite
beams with welded stud connectors".
The Structural Engineer.
January 1969.
46. Barnard, P.R.; Johnson, R.P.J.
"Ultimate strength of composite beams".
Proceedings of the Institution of Civil Engineers.
October 1965.
47. Barnard, P.R.; Johnson, R.P.J.
"Plastic behaviour of continuous composite beams".
Proceedings of the Institution of Civil Engineers.
October 1965.
48. Johnson, R.P.; Greenwood, R.D.; van Dalen, K.
"Stud shear connectors in hogging moment regions
of composite beams".
The Structural Engineer.
September 1969.

49. Harrop, J.
"Analysis of stresses in steel framed and reinforced concrete structures".
Ph.D. Thesis University of Leeds 1956.
50. Short, A.; Thomas, F.G.
"Studies on bridge-deck systems, Part III : Tests on model slab and girder bridge-deck systems".
National Building Studies.
Research Paper 37 1963 H.M.S.O.
51. Johnson, R.P.; Finlinson, J.C.; Heyman, J.
"A plastic composite design".
Proceedings of the Institution of Civil Engineers.
October 1965.
52. Cain, G.B.
"Composite building construction comes of age".
Civil Engineering.
Vol. 32, No. 6 June 1962.
53. Ingerslev, A.
"Strength of rectangular slabs".
Journal of the Institution of Structural Engineers.
Vol. 1, No. 1 January 1923.
54. Johansen, K.W.
"Bruchmomente der kreuzweise bewehrten Platten".
(Fracture moments of cross-reinforced slabs)
International Association for Bridge and Structural Engineering.
1932.
55. Hognestad, E.
"Yield line theory for the ultimate flexural strength of reinforced concrete slabs".
Proceedings of the American Concrete Institute.
Vol. 49 March 1953.
56. Mansfield, E.H.
"An analysis of slabs supported along all edges".
Concrete and Construction Engineering.
Vol. 55 September 1960.
57. Ashdown, A.J.
"Design of slabs by yield line method".
Concrete and Construction Engineering.
Vol. 55 June-July 1960.

58. Smyth, W.J.R.
"Designing a slab using fracture line theory".
Civil Engineering and Public Works Review.
Vol. 53, No. 620 February 1958.
59. Wood, R.H.
"Studies in composite construction, Part II : The
interaction of floors and beams in multi-storey buildings".
National Building Studies.
Research Paper No. 22 H.M.S.O.
60. Ockleston, A.J.
"Load tests on a three storey reinforced
concrete building in Johannesburg".
The Structural Engineer.
October 1955.
61. Onat, E.T.; Haythornthwaite, R.M.
"The load carrying capacity of circular
plates at large deflection".
Journal of Applied Mechanics.
March 1956.
62. Lawton, W.T.
"Discussion on Reference 61 above".
The Structural Engineer.
October 1956.
63. Ockleston, A.J.
"Arching action in reinforced concrete slabs".
The Structural Engineer.
June 1958.
64. Roberts, E.H.
"Load carrying capacity of slab strips
restrained against longitudinal expansion".
Concrete Vol. 3, No. 9 September 1969.
65. Livesley, R.K.
"The place of digital computer in Civil Engineering".
Proceedings of the Institution of Civil Engineers.
January 1960.
66. Livesley, R.K.
"The application of an electronic digital computer
to some problems of structural analysis".
The Structural Engineer.
January 1960.

67. Kemp, K.O.
"A lower-bound solution to the collapse of an orthotropically reinforced concrete slab on simple supports".
Magazine of Concrete Research.
Vol. 14, No. 41 July 1962.
68. Wood, R.H.
"Plastic and elastic design of slabs and plates".
Thomas and Hudson 1961.
69. The Council for Codes of Practice British Standards Institution.
"The structural use of reinforced concrete in buildings".
C.P.114 : 1965.
70. Mitchell, G.P.; Willmott, A.J.
"Programming a computer in Atlas Autocode".
Manchester University Press 1965.
71. Brooker, R.A.; Rohl, J.S.
"Atlas Autocode reference manual".
University of Manchester Computer Science Department 1965.
72. British Constructional Steelwork Association.
"Handbook on structural steelwork".
1964.
73. British Standards Institution.
"Specification for mild steel for general structural purposes".
B.S.15 : 1961.
74. Horne, M.R.
"The plastic design of columns".
British Constructional Steelwork Association.
Publication No. 23 1964.
75. Institute of Structural Engineers and the Institute of Welding.
"Joint Committee Report on fully rigid multi-storey welded steel frames".
December 1964.
76. Holmes, M.; Gandhi, S.N.
"Direct moment distribution" - Parts I, II and III.
Civil Engineering and Public Works Review.
June, July and August 1963.
77. British Standards Institution.
"Methods of testing concrete".
B.S. 1881 : 1952.
78. British Standards Institution.
"Methods for tensile testing of metals".
B.S. 18 : 1962.



BENDING

Plate 1. Formation of a plastic hinge at the centre of a beam due to pure bending.

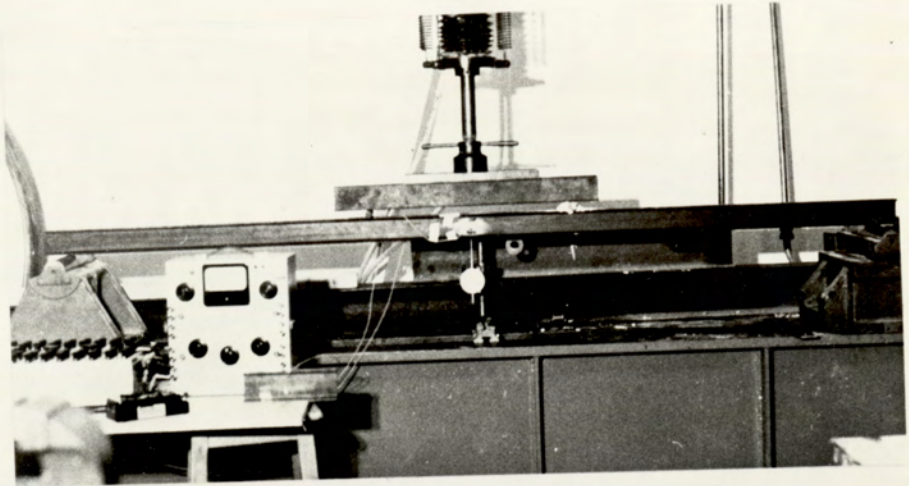


Plate 2. Simple bending test - $3" \times 1\frac{1}{2}" \times 4 \text{ lbs./ft. R.S.J.}$

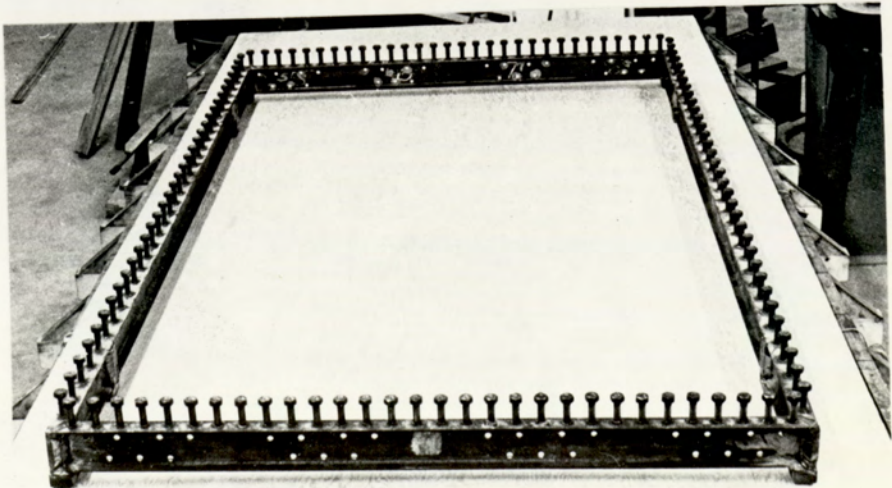


Plate 3. Stud shear connectors welded on top of the steel frame of the models.



Plate 4. Model before casting.

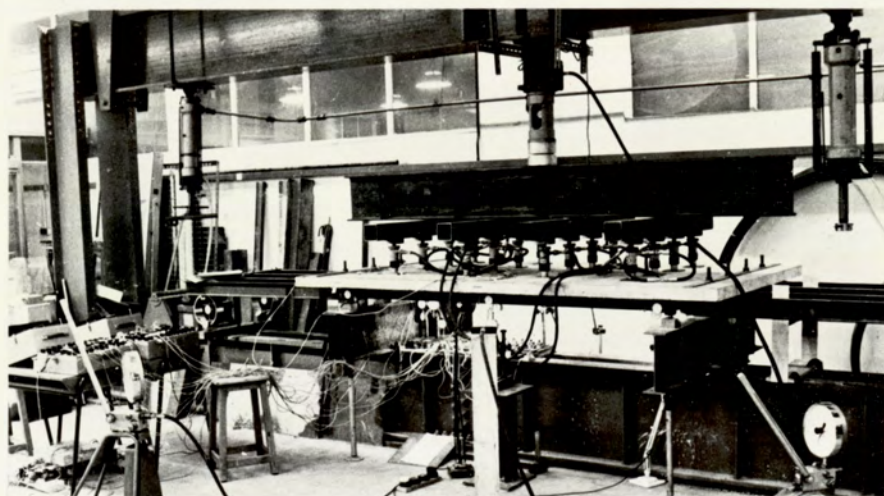


Plate 5. Experimental arrangement of test M_1 .

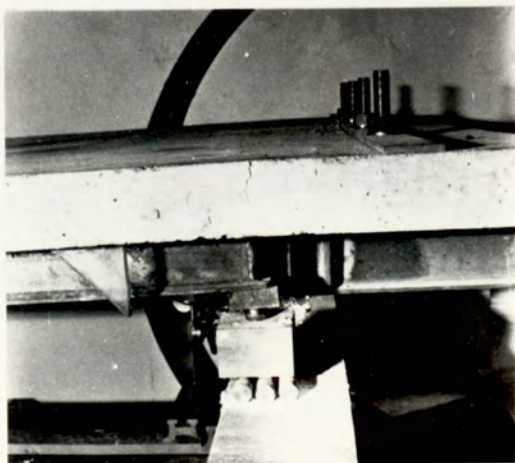


Plate 6. Ball joint arrangement at one of the corners of model M_1 .



Plate 7. Lever arm connection at the support to the secondary beam.

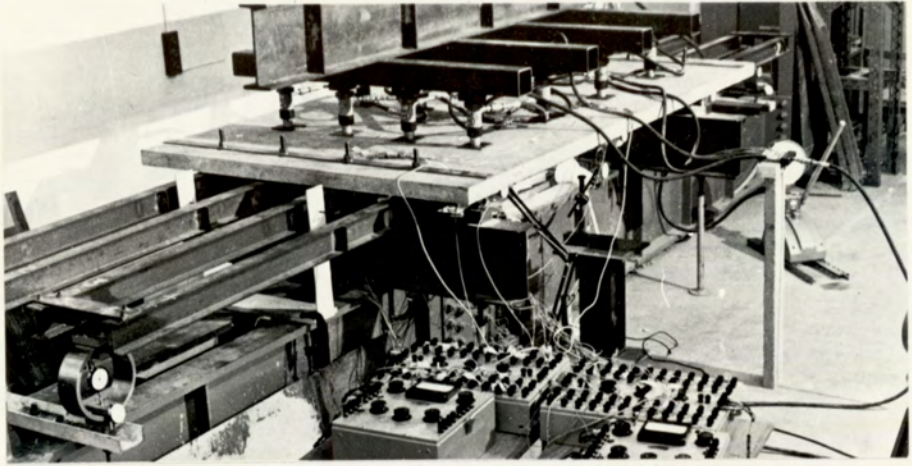


Plate 8. Details of lever arm system.

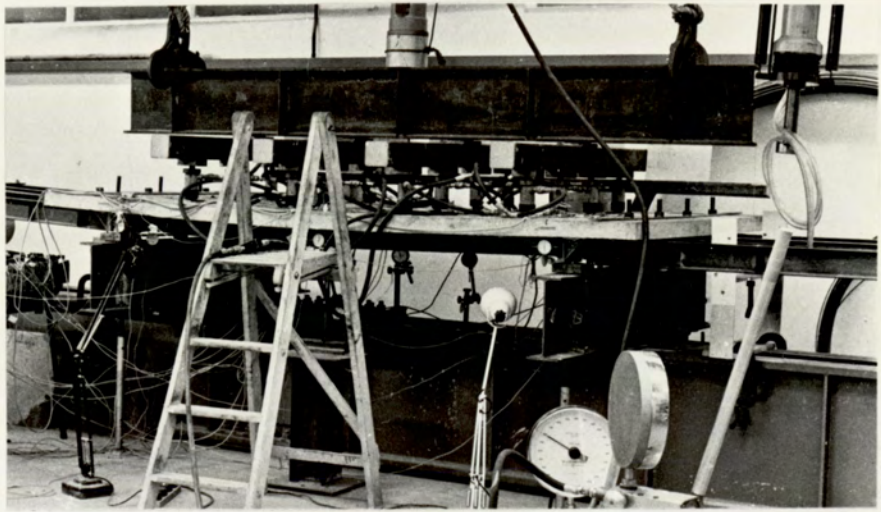


Plate 9. Experimental arrangement of test M_2 .

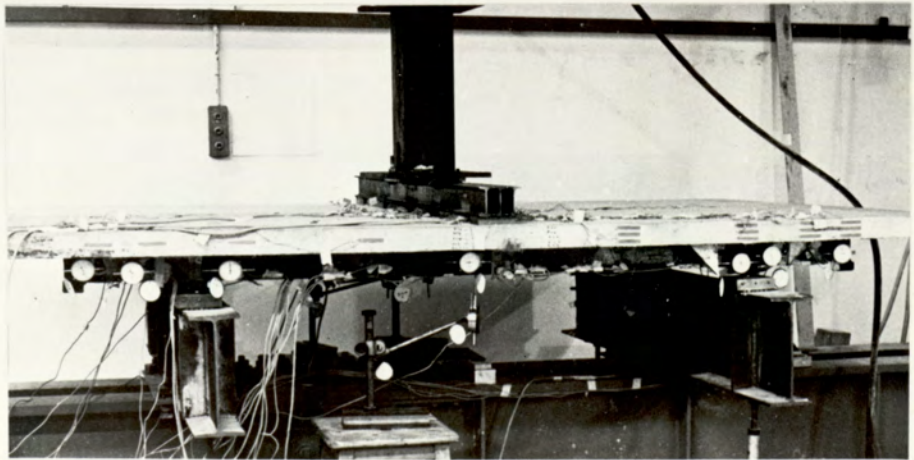


Plate 10. Experimental arrangement of test C_1 .

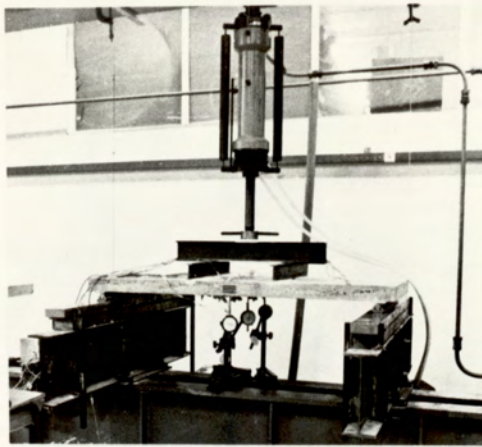


Plate 11. Experimental arrangement of slab strips S_1 and S_2 .

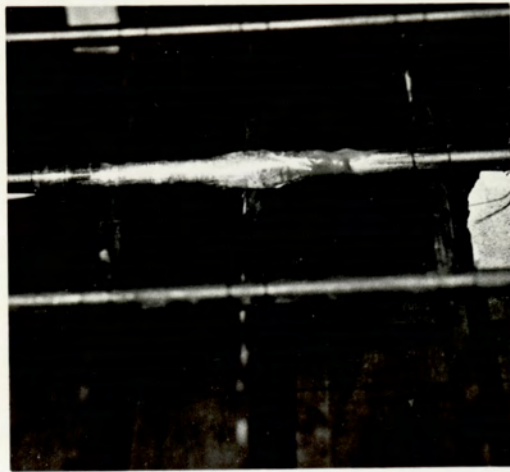


Plate 12. Waterproofing arrangement of electrical strain gauges attached to concrete reinforcement.

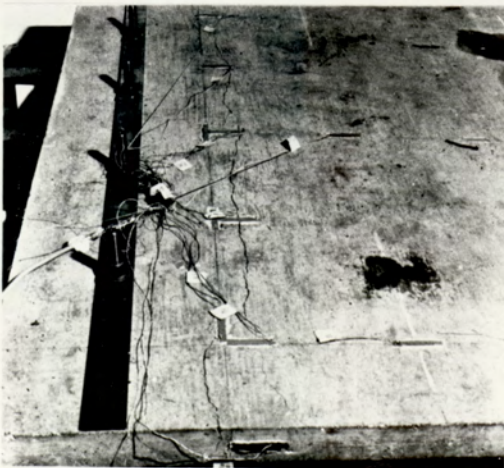


Plate 13

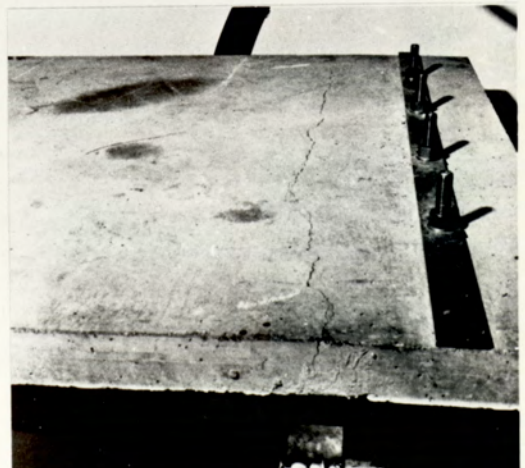


Plate 14

Tension cracks parallel to secondary beams. Test M_1 .

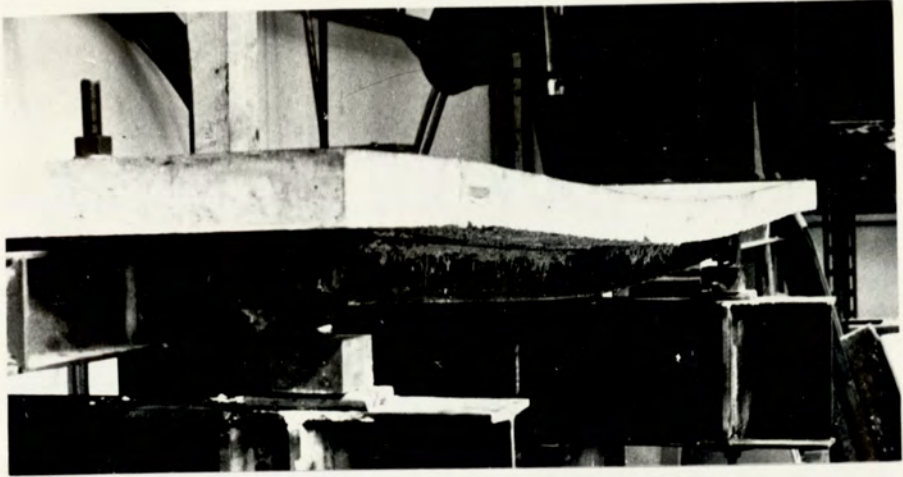


Plate 15. Final deflected shape of model M_1 after test.

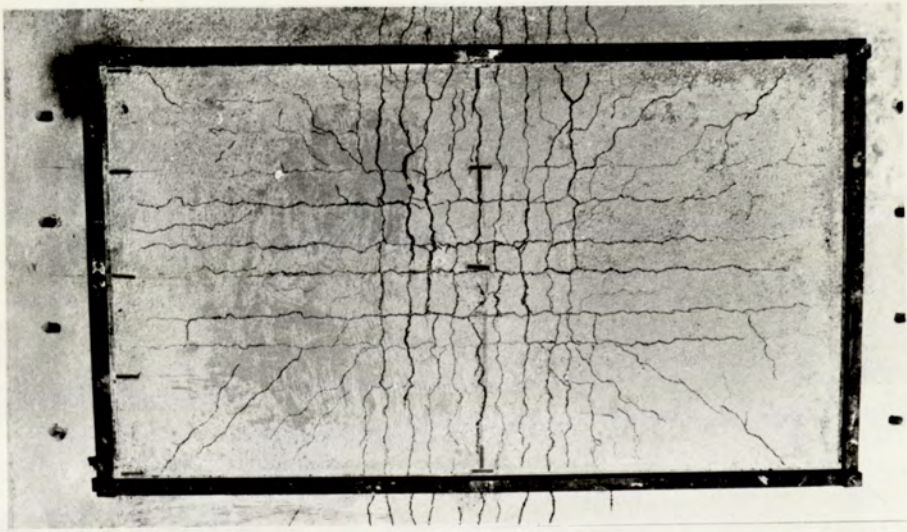


Plate 16. Pattern of cracks at lower slab surface of model M_1 after test.

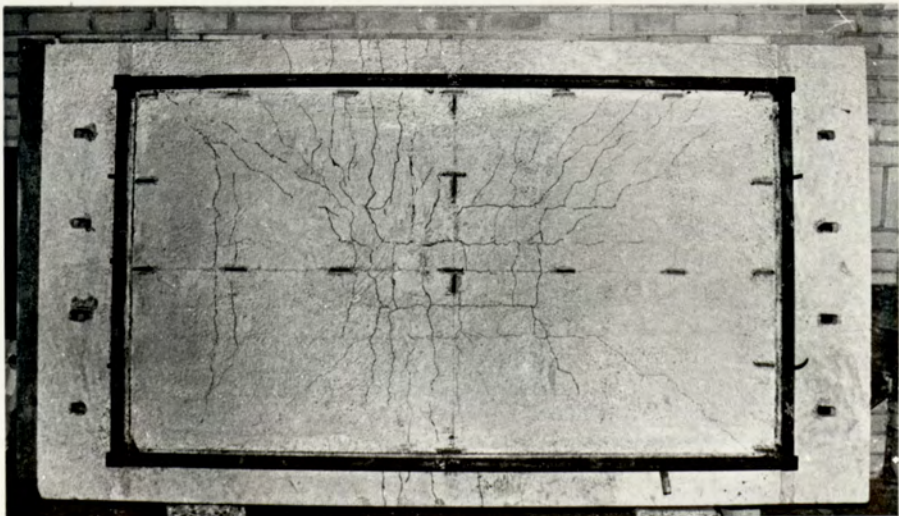


Plate 17. Pattern of cracks at lower slab surface of model M_2 after test.

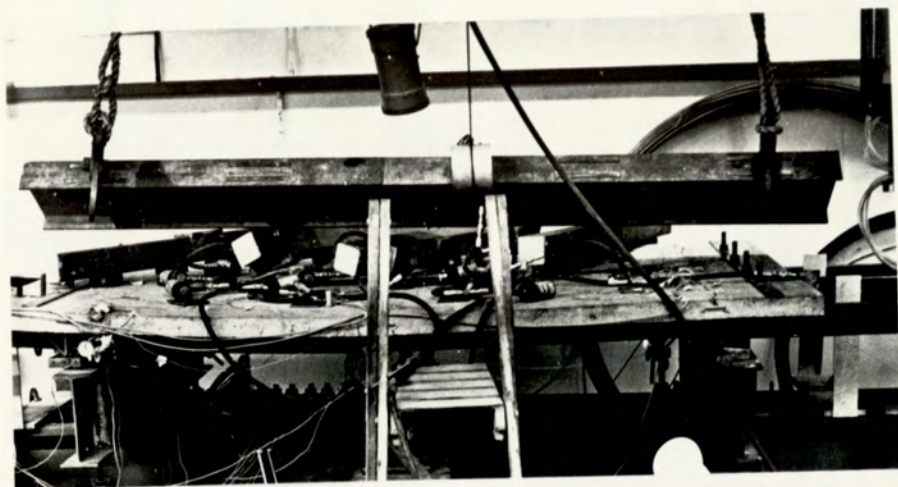


Plate 18. Model M_2 after collapse.

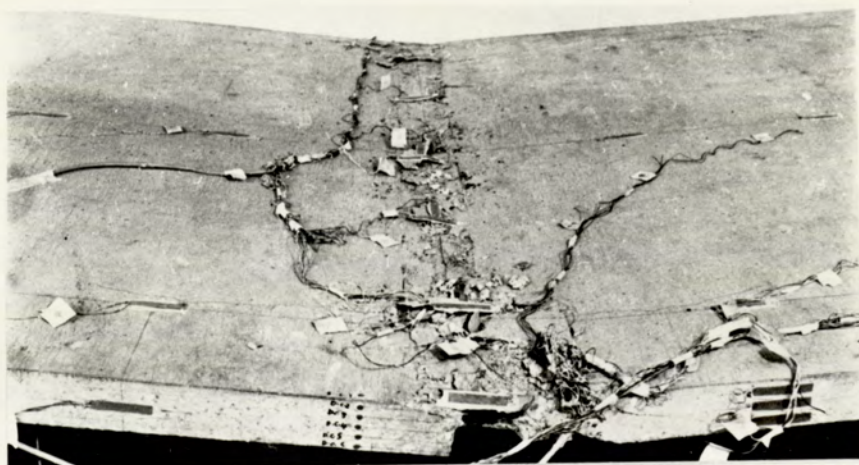


Plate 19. A crushing yield line across the full width of the slab after collapse of model M_3 in control test C_1 .



Plate 20. Formation of plastic composite hinges at mid-span of model M_3 after control test C_1 .

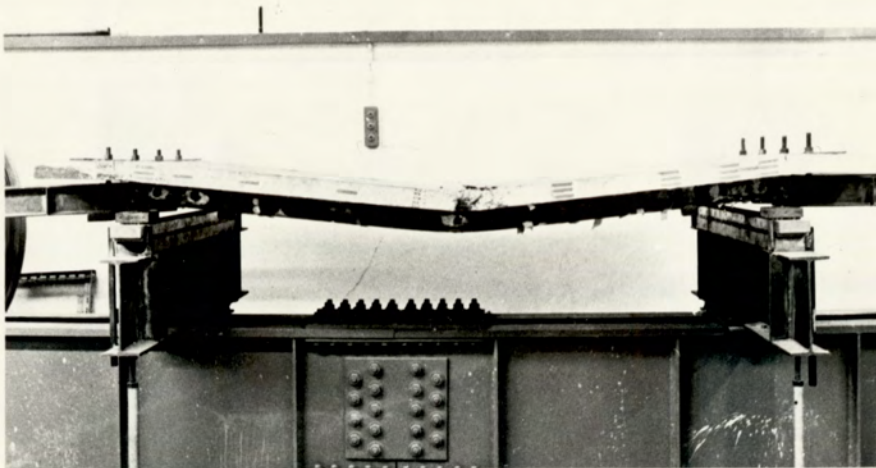


Plate 21. Model M_3 after collapse owing to the three control tests C_1 , C_2 and C_3 .

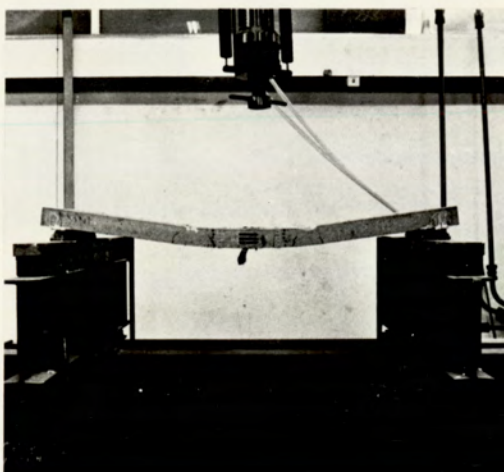


Plate 22. Slab strip S_1 after collapse.

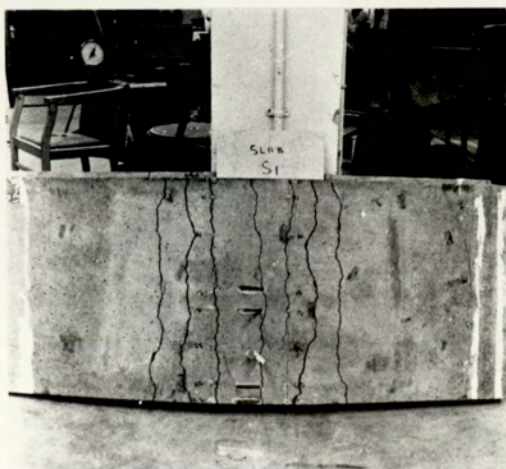


Plate 23

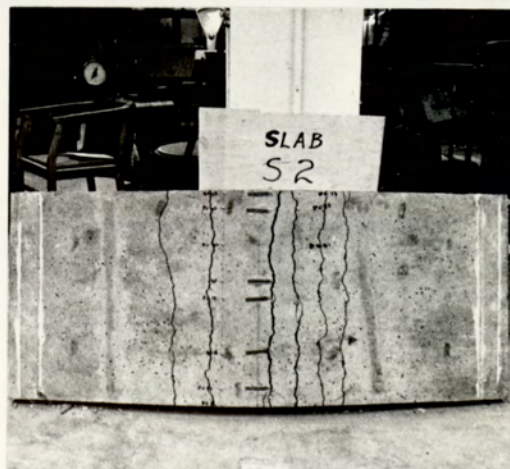


Plate 24

Formation of tension cracks in the constant bending moment zone after collapse of slab strips S_1 and S_2 .